



The  
University  
Of  
Sheffield.

Department  
Of  
Mechanical  
Engineering

## PhD Mechanical Engineering

### **Study of a low-cost, portable, and solar powered pump for improving income, food and energy security in Sub-Saharan Africa**

**Saeed MOHAMMED WAZED**

May 2021

**Professor William Nimmo**

**Professor Ben Richard Hughes**

Thesis submitted to the Department of Mechanical Engineering,  
University of Sheffield in partial fulfilment of the requirements for the  
degree of MPhil

# Dedication

---

To my parents, wife, and daughter  
Who never gave up on me

# Acknowledgement

---

I would like to express gratitude towards Professor Ben Richard Hughes, for entrusting me with this PhD role and believing in my capabilities. His hard work and determination are unparalleled and his self an inspiration to us all.

Secondly, I would like to thank Professor William Nimmo who took over the first supervisor duties during a crucial yet uncertain stage of my research and helping me to see it through to the submission of my thesis.

Thirdly, would like to thank Dr John Kaiser Calautit for guiding me through several phases of my research work, and would also like to thank fellow colleague Mohamed Elsakka who was crucial in my understanding of dynamic motion in computational analysis.

Special thanks to the Multidisciplinary Engineering Education team, Namely, Dr Andrew Garrad, Dr Robert Woolley and Dr Krys Bangert who were always there to lend me a helping hand. I greatly appreciate the help of the iForge staff and Energy 2050 Lab coordinator Dimitri for helping me through the experimental stages of my research work. I gathered a vast amount of knowledge while working under their guidance.

This research work has been a very humbling experience and through all the ups and downs I have had the support of my wife, Afia Tabassum, and my parents, Dr Mohammed Wazed Ali Mollah and Suraiya Perveen, who never gave up on me and pushed me to see through all the hardships, for believing in me even when I didn't believe in myself.

Lastly, I would like to welcome my daughter, Ameera Tabassum Saeed, to the world. It may seem like the worst right now, but trust in the resilience of Human beings. We will overcome this and everything that comes our way, we just need to see it through...

“When it's vain to try to dodge it,  
Do the best that you can do;  
You may fail, but you may conquer,  
See it through!”

- EDGAR ALBERT GUEST

# List of Publications

---

## Journal Publication:

- Mohammed Wazed S, Hughes BR, O'Connor D, Calautit JK. A Review of Sustainable Solar Irrigation Systems for Sub-Saharan Africa, *Renewable & Sustainable Energy Reviews*, 2017, Impact Factor 6.798

## Conference Proceedings:

- Calautit JK, Aquino AI, O'Connor D, Carbaneros S, Shahzad S, Mohammed Wazed S, Garwood TL, Hughes BR, Indoor environmental quality analysis of a low-energy windcatcher with horizontally-arranged heat transfer devices (HHTD), *International Conference on Applied Energy (ICAE)*, 2018, Impact Factor 5.746
- Mohammed Wazed S, Hughes BR, O'Connor D, Calautit JK. Solar Driven Irrigation Systems for Remote Rural Farms, *International Conference on Applied Energy (ICAE)*, 2018, Impact Factor 5.746
- Mohammed Wazed S, Hughes BR, O'Connor D, Calautit JK. Development of Stirling Pump mechanism for Irrigation in remote rural farms. Global Conference on Energy and Sustainable Development, 18-20 December 2018 (Published) WEENTECH Proceedings in Energy 5 (2019) 26-36

# Table of Contents

---

Dedication .....	1
Acknowledgement .....	2
List of Publications .....	3
Table of Contents .....	4
Chapter 1.....	15
1.1. Introduction .....	15
1.2. Research Aim and Objective .....	18
1.3. Research Methodology .....	18
Chapter 2.....	19
2.1. Introduction .....	19
2.2. PV Technologies .....	19
2.3. Solar Thermal Systems .....	27
2.4. Summary .....	36
Chapter 3.....	39
3.1. Introduction .....	39
3.2. Irrigation.....	39
3.3. Stirling Engine .....	44
3.3.1. Alpha Stirling Engine .....	44
3.3.2. Beta Stirling Engine .....	45
3.3.3. Gamma Stirling Engine .....	46
3.3.4. Free Piston Stirling Engine .....	47
3.4. CFD Analysis of Stirling Engines .....	48
3.5. Summary .....	49
Chapter 4.....	50
4.1. Introduction .....	50
4.2. Overview of low-cost, LTD Stirling engine .....	51
4.2.1. Kato Experiment.....	53
4.3. Experimental Equipment .....	55
4.3.1. Heating Plate .....	55
4.3.2. Pico Tech Thermocouple and Logger .....	55
4.3.3. Resistance Temperature Detector (RTD) Thermometer.....	57
4.3.4. Pressure Scanner.....	58

4.3.5.	Thermal Imaging Camera .....	60
4.4.	Experimental Set-up.....	61
4.5.	Experimental Procedure .....	62
4.6.	Temperature Calibration.....	64
4.6.1.	Impact of Sensor Location and Response Time .....	67
4.7.	Temperature Visualisation.....	68
4.8.	Pressure Recording .....	70
4.8.1.	Impact of Sensor Location and Response Time .....	71
4.9.	Rotational speed of the Stirling Engine.....	72
4.10.	Temperature difference across Displacer Cylinder.....	77
4.11.	Stirling Cycle Analysis.....	80
4.12.	Summary .....	88
Chapter 5.....		89
5.1.	Introduction .....	89
5.2.	Stirling Engine Simulation Study .....	90
5.2.1.	Motion Dynamics .....	91
5.2.2.	Modelling Parameters.....	91
5.2.3.	Result and Validation .....	93
5.3.	Simulation Replication .....	95
5.3.1.	2D model.....	95
5.3.2.	3D Model.....	98
5.4.	EMSE Simulation Study .....	102
5.4.1.	Mesh Quality.....	103
5.4.2.	Boundary Conditions.....	104
5.5.	Simulation Stabilisation .....	107
5.6.	Temperature Profile.....	111
5.6.1.	Temperature flow inside the displacer chamber.....	114
5.7.	Pressure Profiles .....	116
5.8.	Summary .....	120
Chapter 6.....		121
6.1.	Introduction .....	121
6.2.	The need for a cost focused solution.....	121
6.3.	Experimental Results .....	123
6.4.	CFD Results.....	124
6.5.	Future Work.....	125
Chapter 7.....		127

Chapter 8.....	136
8.1. Appendix 1 – User Defined Function .....	136
8.2. Appendix 2 – Profiles .....	139
8.3. Appendix 3 – Experimental Temperature Recordings .....	140
8.3.1. Inspected EMSE.....	140
8.3.2. DRILLED EMSE .....	189
8.3.3. Probed EMSE.....	213
8.3.4. Thermal Imaging Camera Recording.....	239
8.3.5. Temperature across plate .....	240
8.4. Appendix 4 – CFD Simulations .....	245
8.5. Appendix 5 – Publications.....	265
8.5.1. Review Paper .....	265
8.5.2. Conference Proceedings .....	266

# List of Figures

---

Fig. 1-1: a) Average Dietary energy supply b) GDP per capita of the population in Africa [2].....	15
Fig. 1-2: Ground water Resource in Africa [3].....	16
Fig. 1-3: a) Sub-Saharan Africa primary energy mix by sub-region Installed grid-based capacity by type and sub-region [1].....	b) 17
Fig. 1-4: Research Methodology .....	18
Fig. 2-1: Schematic of a simple PV irrigation set up for groundwater retrieval [10] .....	19
Fig. 2-2: Schematic diagram of micro-irrigation system powered by solar PV [14].....	20
Fig. 2-3: Schematic of proposed PV water pumping system for remote rural areas of Sub-Saharan Africa [27]	22
Fig. 2-4: A typical Rankine cycle solar thermal pumping system [12].....	27
Fig. 2-5: Solar Powered Organic Rankine Cycle system [35].....	28
Fig. 2-6: Solar Powered Low Temperature differential Stirling pump [40] .....	29
Fig. 2-7: Liquid piston pump design using diaphragms [34] .....	29
Fig. 2-8: Metal hydride based solar thermal water pumping system design [38] .....	30
Fig. 2-9: (a) Solar Stirling Water pump with dish [48] (b) SUNPULSE Stirling System [49] .....	32
Fig. 2-10: Schematic of proposed solar thermal water pumping system for remote rural areas of Sub-Saharan Africa [27] .....	33
Fig. 3-1: A typical Drip irrigation set-up [60].....	40
Fig. 3-2: Pressure (P) – Volume (V) and Temperature (T) – Entropy (S) diagram for Stirling Engine [44].....	44
Fig. 3-3: Alpha Stirling Engine Schematic.....	45
Fig. 3-4: Beta Stirling Engine Schematic .....	45
Fig. 3-5: Gamma Stirling Engine Schematic .....	46
Fig. 3-6: Free Piston Stirling Engine Schematic .....	47
Fig. 4-1: Educational model Stirling engine (EMSE).....	52
Fig. 4-2 : EMSE dimensions .....	52
Fig. 4-3: Kato Experiment set-up [83] .....	53
Fig. 4-4: Kato’s experimental findings [58] .....	54
Fig. 4-5: Indicated Diagrams of experiments conducted by Kato showing both series N and Series C results [58] .....	54
Fig. 4-6: MAPLELAB ceramic hotplate / stirrer .....	55
Fig. 4-7: Temperature logger and Thermocouple set-up .....	56
Fig. 4-8: Typical Thermal data .....	57
Fig. 4-9: Omega HH804 RTD thermometer with PT 100 probes connected to EMSE .....	58
Fig. 4-10: DSA3217 Pressure Scanner with port 1 connected to EMSE.....	59
Fig. 4-11: DSALink 4 pressure data acquisition software.....	60
Fig. 4-12: FLIR T650sc Thermal Imaging camera .....	61

Fig. 4-13: thermocouple and transducer set-up .....	61
Fig. 4-14: Typical temperature graph of EMSE test .....	65
Fig. 4-15: Typical recorded data for inspected EMSE.....	66
Fig. 4-16: Thermal image capture and interpretation. ....	68
Fig. 4-17: Thermal flow visualisation of EMSE operation. ....	69
Fig. 4-18: Thermal Imaging Camera (TIC) temperature data compared to similar test scenario using thermocouple (Thermo).....	70
Fig. 4-19: Typical pressure calibration based on volume change calculation .....	71
Fig. 4-20: Relation between the rotational speed and bottom surface temperature of various EMSE .....	76
Fig. 4-21: Temperature difference across displacer cylinder .....	78
Fig. 4-22 Cumulative temperature profile of EMSE .....	78
Fig. 4-23: Temperature relation at the hot end of the inspected EMSE.....	79
Fig. 4-24: Temperature relation at the cold end of the inspected EMSE .....	80
Fig. 4-25 Highlighting the difference in cycle speed across the test period.....	81
Fig. 4-26: Indicated work diagrams of Inspected EMSEs .....	84
Fig. 4-27: Indicated work diagrams of drilled EMSEs.....	85
Fig. 4-28: Indicated work diagrams of Probed EMSEs .....	86
Fig. 4-29: Work Done vs Temperature difference of modified EMSE.....	87
Fig. 5-1: Dimensions of Stirling engine derived from experiment .....	90
Fig. 5-2: Temperature contours across the whole engine at 10 different crank angles [56] .....	93
Fig. 5-3: Volume variation versus crank angle [56] .....	94
Fig. 5-4: USTREAM code validation [56] .....	94
Fig. 5-5: 2D Model Geometry and Mesh.....	95
Fig. 5-6: Dynamic Mesh Zone Set-up, all other zones (not indicated) are set to 'deforming' .....	97
Fig. 5-7: Temperature contours in the Stirling Engine at different crank angles, 2D model.....	97
Fig. 5-8: 3D Geometrical model of Stirling Engine .....	98
Fig. 5-9: 3D Model mesh generation .....	99
Fig. 5-10: Temperature contours in the Stirling Engine at different crank angles, 3D model.....	101
Fig. 5-11: Variation of volume against Crank angle in the compression and expansion chambers.....	102
Fig. 5-12 EMSE Geometry model .....	103
Fig. 5-13: Mesh Statistics based on various EMSE mesh sizes .....	103
Fig. 5-14: EMSE 3D mesh of the model.....	104
Fig. 5-15: Dynamic Mesh Set-up of EMSE .....	106
Fig. 5-16: Sample of Displacement and velocity profiles for piston and displacer of EMSE.....	106
Fig. 5-17: Starting engine cycle of the Stirling Engine – 0° to 360°.....	109
Fig. 5-18: Graphs showing how the engine goes from start to achieve stabilisation .....	109
Fig. 5-19: Engine Cycle once stabilisation has been achieved.....	110
Fig. 5-20: Temperature measurement locations from CFD results .....	111

<i>Fig. 5-21: comparison between experimental and CFD results.....</i>	<i>112</i>
<i>Fig. 5-22: Comparison of the Temperatures inside the displacer chamber .....</i>	<i>113</i>
<i>Fig. 5-23: Temperature profile inside the displacer chamber as a result of changing stroke. ....</i>	<i>115</i>
<i>Fig. 5-24 Temperature profile inside the displacer chamber as a result of changing displacer diameter .....</i>	<i>115</i>
<i>Fig. 5-25:Comparing the Stirling Cycle analysis as obtained by CFD vs Experiments .....</i>	<i>118</i>
<i>Fig. 5-26: Graph comparing the pressure profiles obtained by CFD analysis of the EMSE testing scenarios .....</i>	<i>119</i>
<i>Fig. 6-1: Conceptual model of the Stirling pump system. ....</i>	<i>126</i>

# List of Tables

---

<i>Table 2-1: PV cell efficiency at 25°C and 1000 W/m<sup>2</sup> [18]</i>	21
<i>Table 2-2: Environmental impact of different types of PV cell types [12]</i>	23
<i>Table 2-3: Review summary of Solar PV water pumping</i>	24
<i>Table 2-4: Range of temperature and ratio of concentration of various solar thermal systems [46]</i>	31
<i>Table 2-5: Review summary of solar thermal water pumping technology</i>	34
<i>Table 3-1 Small Farm Size, Sub-Saharan Africa [64]</i>	41
<i>Table 4-1: RTD Tolerance chart</i>	58
<i>Table 4-2: Rotational speeds for new EMSE</i>	72
<i>Table 4-3: Rotational speeds for Inspected EMSE</i>	73
<i>Table 4-4: Rotational speeds for drilled EMSE</i>	74
<i>Table 4-5: Rotational speeds for probed EMSE</i>	75
<i>Table 5-1: Grid Set-up</i>	93
<i>Table 5-2: Mesh Statistics 2D model</i>	96
<i>Table 5-3: Mesh Statistics 3D Model</i>	99
<i>Table 5-4: Material Properties for Stirling engine model</i>	105
<i>Table 5-5 time step size and number of time steps for CFD analysis</i>	107
<i>Table 5-6: Modified EMSE for CFD study</i>	114
<i>Table 6-1: Comparing various solar thermal technologies [87]</i>	122

# Abbreviations

---

AC	Alternating Current
AMRC	Advanced Manufacturing and Research Centre
ANN	Artificial Neural Network
BS	British Standard
CFD	Computational Fluid Dynamics
DC	Direct Current
EMSE	Education Model Stirling Engine
FAO	Food Agriculture Organisation
GDP	Gross Domestic Product
GHG	Green House Gas
ICAE	International Conference on Applied Energy
ID	Inner Diameter
LTD	Low Temperature Differential
MBGL	Meters Below Ground Level
NPV	Net Positive Value
PV	Photovoltaic
ORC	Organic Rankine Cycle
RSER	Renewable & Sustainable Energy Reviews
RTD	Resistance Temperature detection
Thermo	Thermocouple
TIC	Thermal Imaging Camera
TÜV	Technischer Überwachungsverein
UDF	User Defined Model

# Nomenclature

---

ET <sub>o</sub>	Evapotranspiration (mm/day)
K <sub>c</sub>	Crop Factor
ET Crop	Water required by crop (mm/day)
P <sub>e</sub>	Effective Rainfall (mm/day)
P	Pressure (Pa,kPa)
V	Volume (m <sup>3</sup> , cm <sup>3</sup> )
W	Work (J)
l <sub>1</sub> ,l <sub>2</sub> ,l <sub>3</sub> ,l <sub>4</sub>	Stirling engine miscellaneous height (mm)
L <sub>c1</sub> ,L <sub>c2</sub>	Crank drive height of Stirling engine (mm)
l <sub>d</sub>	Displacer height (mm)
l <sub>p</sub>	Piston height (mm)
z <sub>d</sub>	Height of displacer from datum (mm)
z <sub>p</sub>	Height of piston from datum (mm)
r <sub>1</sub>	Piston crank radius (mm)
r <sub>2</sub>	Displacer crank radius (mm)
R	Gas constant (287.0 J/kgK)
R <sub>1</sub>	Radius of piston cylinder (mm)
R <sub>2</sub>	Radius of Displacer cylinder (mm)
R <sub>d</sub>	Radius of displacer (mm)
θ	Crank angle of piston (°)
β	Crank angle of Displacer (°)
T <sub>h</sub>	Temperature at the bottom surface of the EMSE (K)
T <sub>c</sub>	Temperature at the top surface of the EMSE (K)
<i>P<sub>corr</sub></i>	corrected pressure (Pa)
<i>P<sub>avg</sub></i>	average pressure recorded (Pa)
<i>P<sub>h</sub></i>	Hydraulic Power (kW)

$P_s$	Shaft Power (kW)
$a$	Pressure amplitude (Pa)
$t$	Time step (sec)
$T$	Time Period (sec)
$TF$	Time factor that is adjusted to match the experimental results
$n$	Number of moles (mol)
$u,v,w$	Velocities (m/s)

# Abstract

---

The focus of this research was on Sub-Saharan Africa where a large portion of the poorer population is unable to receive their daily dietary supply, have a shortage of water and are frequently hit by famines. While being rich in energy resources, they are poor in energy supply. This research studies a system that has a potential to make use of the local resources efficiently, be of low-cost, utilise renewable energy and generate income in the region.

To narrow down the research criteria, emphasis has been put on independent remote rural farms in the Sub—Saharan Africa region. These farms are small scale and based on FAO statistics suggesting the average small farm size in the Sub-Saharan African region to be 1 hectare of land area. A literature review has been conducted to identify the various solar powered irrigation technologies and techniques that can be implemented. These are mainly in the form of solar photovoltaic (PV) technology and solar thermal technologies.

Based on the literature the most effective PV and solar thermal systems are presented for the irrigation of a small scare remote rural. Solar thermal technology for water pumping is lacking when compared to PV powered water pumping technologies especially in small scale operations. However, with the possibility of local production, low investment cost, easy maintenance and lower carbon footprint, solar thermal water pumping technologies have shown to be able to overcome the shortcomings of the PV technology that has stopped widespread use of the technology for irrigation applications in the region.

Experimental Analysis of a low temperature differential Stirling engine, EMSE, was conducted to map the temperature and pressure profile. Modifications made to the EMSE adversely affected the performance of the EMSE and a combination experimental scenario was utilised to validate the computational analysis of the Stirling Engine. The indicated work output remained consistent across the various scenarios to which the Stirling Engine was subjected, showing a threshold pressure based on the geometry and the construction of the engine. Low cost focus of the study is the Achilles' heel of the project. For an effective Stirling system, tighter tolerance is paramount but, very expensive to achieve.

# Chapter 1

## Introduction

### 1.1. Introduction

The global population is increasing, as a result of this, the demand for food, and in turn farming and irrigation is increasing as well. However, there is a severe lack of resources which mainly affects the poorer population of the world. In addition to this, there is also the issue of global warming which is a matter of international importance, it is not only necessary to produce more but to do so in a manner that protects the environment. This creates a need for the development of sustainable technologies that can be implemented to utilise the readily available local resources to drive the cost of the irrigation systems down.

The Sub-Saharan African region is marred by issues related to food, water and even though the region is rich in renewable energy resources, the supply is poor [1].

The Statistics presented by the FAO (Fig. 1-1) about the Sub-Saharan African region suggests that there is an adequate supply of food in the region with an average dietary supply of 110% [2]. However, 26% of the population still suffered from food insecurity issues. The reason for this is the dependency of many nations in the region on imported food, with almost 1/3 of the basic grains being imported [2]. As a result of this, the cost of the food is high making it unaffordable to the poorer population. This is clear from the GDP statistics provided showing the GDP of Sub-Saharan Africa to be just shy of US\$ 4,000 per capita [2].

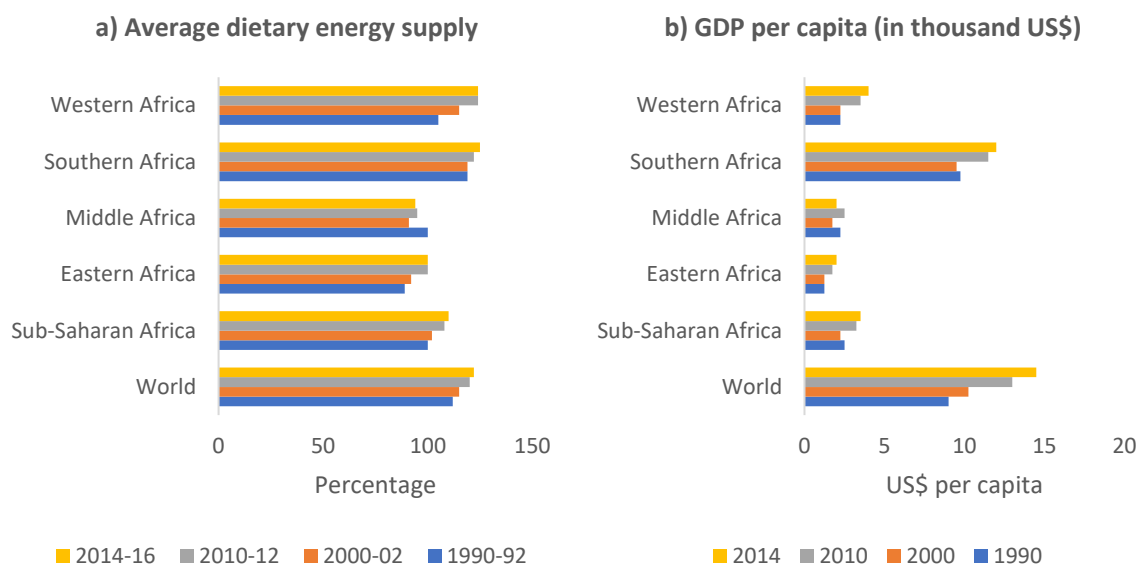


**Fig. 1-1: a) Average Dietary energy supply b) GDP per capita of the population in Africa [2]**

To overcome the cost of food, it has been suggested to produce the food locally. This will drive down the cost of food. However, that may not be as simple due the water issue.

Agriculture accounts for almost 70% of water use globally [3]. Securing the water in the Sub-Saharan African region for irrigation will be a difficult task considering there is a shortage of drinking water in the region. The water supply in the Sub-Saharan Africa region is inconsistent and often contaminated. The main water resources are surface water from open holes dug in sandy or dry river beds and these few wells are far and wide requiring people to travel many miles to obtain their supply of water. In addition to this, the Sub-Saharan Africa region is affected by long dry spells, just in February of 2017, the FAO declared Famine in Sudan and northern Nigeria which will affect over 30 million people [4]. All the above lead to 319 million people in the Sub-Saharan Africa region being without access to improved drinking water sources [5].

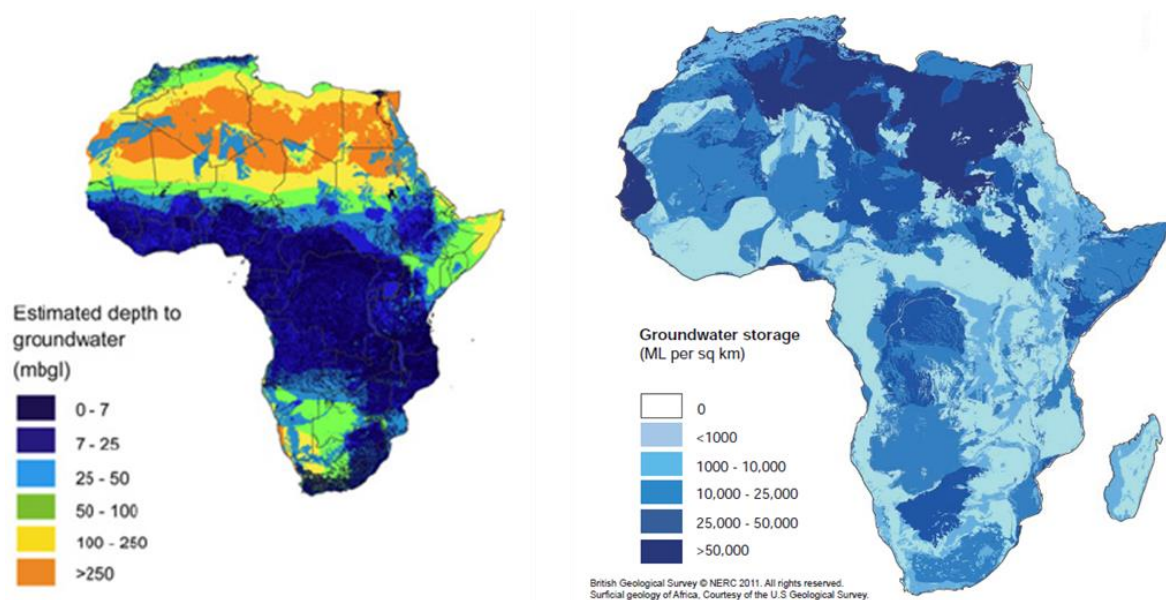


**Fig. 1-2: Ground water Resource in Africa [3]**

There is, however, an abundant reserve of ground water (Fig. 1-2) in the region but only 10% is currently harvested [6]. The issue here is, to harvest the ground water, energy is required. This cost of harvesting the ground reserves are very high. Not only is the initial investment high for purchasing generators and pumps but also the ongoing inflation in fuel costs leads to a consistent increase in operational and maintenance costs which are too high for the local population to instigate development [7].

The Sub-Saharan African region is very rich in energy resources but poor in its supply. The general population in the region uses bioenergy as fuel which includes fuelwood (animal waste and refuse), and charcoal. Almost 60% of the population do not have access to electricity [1]. Recently, however, there has been an increase in the demand and use of coal,

gas and oil with the help of governmental subsidies. While there are subsidies for using renewable technology, conventional fossil fuel technology is much more readily available and much cheaper and thus the preferred option (Fig. 1-3).

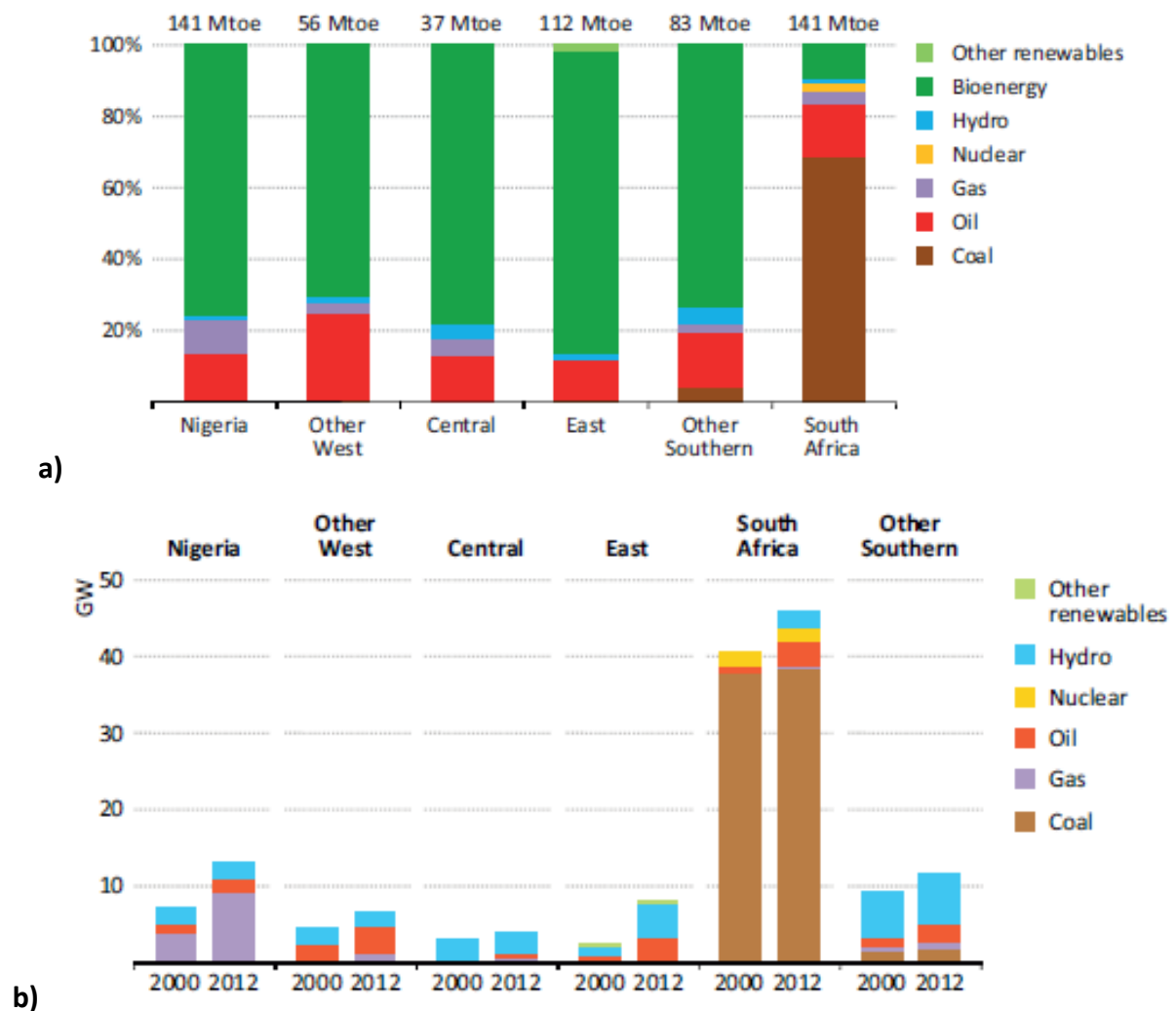


**Fig. 1-3: a) Sub-Saharan Africa primary energy mix by sub-region  
 b) Installed grid-based capacity by type and sub-region [1]**

Energy use is a matter of global importance and with effects of global warming being realised across the entire world, a conscience effort needs to be made to utilise renewable energy. However, the sub-Saharan African region is very much underdeveloped and to force them to implement costly renewable energy technologies would be inappropriate. The need is then to offer renewable energy at a low-cost than what is presently available.

Sub-Saharan Africa receives over 2000 kWh of global solar radiation annually, much greater than that received by the top countries implementing solar energy in the world [8]. Severe draught, lack of rain and long dry spells provides the opportunity for the utilisation of solar power in Sub-Saharan Africa, with both solar thermal and Photovoltaic (PV) technologies [3].

## 1.2. Research Aim and Objective

The aim of this research is to develop an independent, portable, low-cost solar powered irrigation system that assists in establishing a sustainable water-food-security nexus in developing nations. Stirling Engine powered irrigation technology, identified as the potential technology for this purpose, has been studied analytically as well as experimentally and compared to existing research to provide a better understanding of the technology. This research offers a larger data set and establishes key insights into low-cost Stirling engines that helps identify areas where the analysis and technology fails at addressing the viability of the technology. Finally, the study identifies key focus areas to meet the expectations of the research.

## 1.3. Research Methodology

Literature review will be utilized to establish the solar powered technology that will be investigated. Based on the Literature review, the solar powered technology will be analysed using Computational Fluid Dynamics (CFD) Modelling. The CFD model will then be validated using experimentation work. The key geometrical components of the system will be indicated and the performance optimised. Fig. 1-4 displays the project methodology.

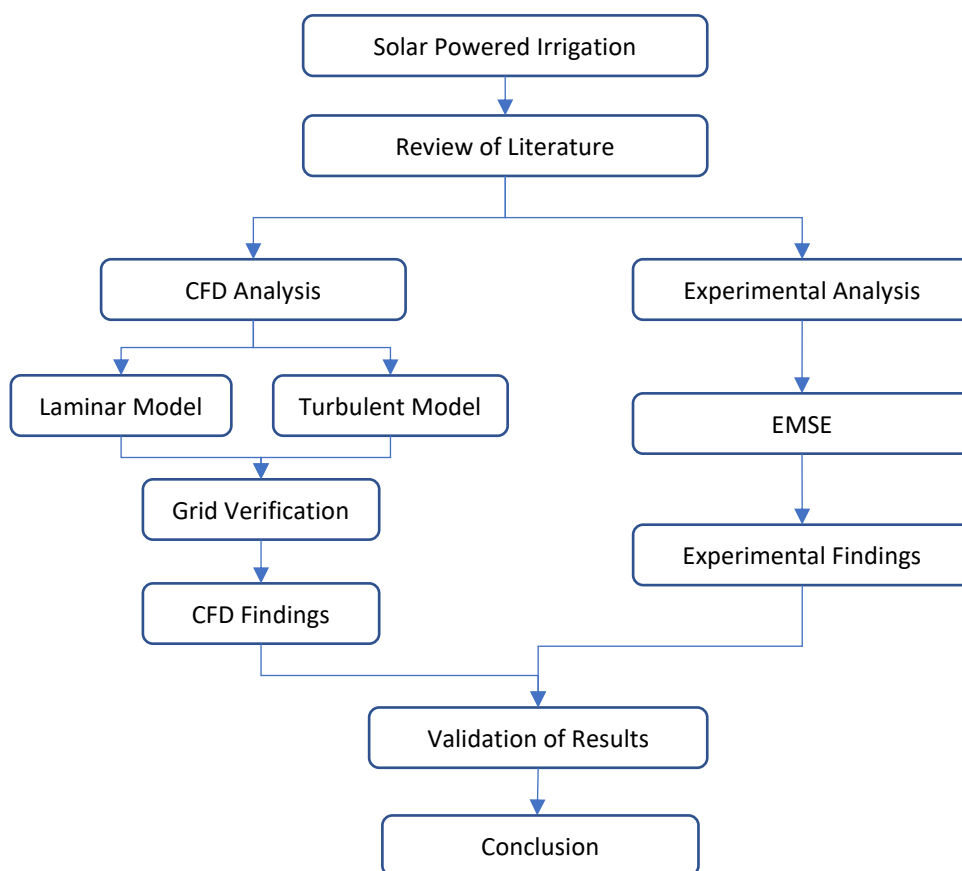


**Fig. 1-4: Research Methodology**

# Chapter 2

## Literature Review

### 2.1. Introduction

The following section contains review of literature containing various Solar powered technologies including solar photovoltaic (PV) and solar thermal technologies. While there is numerous researches on PV and Solar thermal technologies, the focus on this review is to study the implementation of the technology in irrigation.

A detailed Literature review has been published by the author and has been provided in Appendix 5.

### 2.2. PV Technologies

PV irrigation systems use PV panels to produce electricity from solar energy which is then used in conjunction with an electric motor to drive a pump. Fig. 2-1 depicts a typical PV irrigation set up. This system can be further enhanced depending on the output requirement, charge regulation based on the requirement of the pump (AC / DC) as well as the incorporation of a battery to counter the fluctuation of solar irradiation available throughout the day or even for irrigation at night, when lower water losses and higher irrigation uniformity is observed [9].

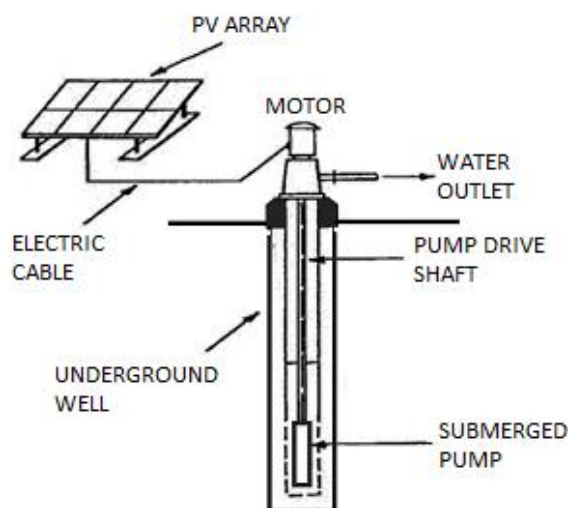
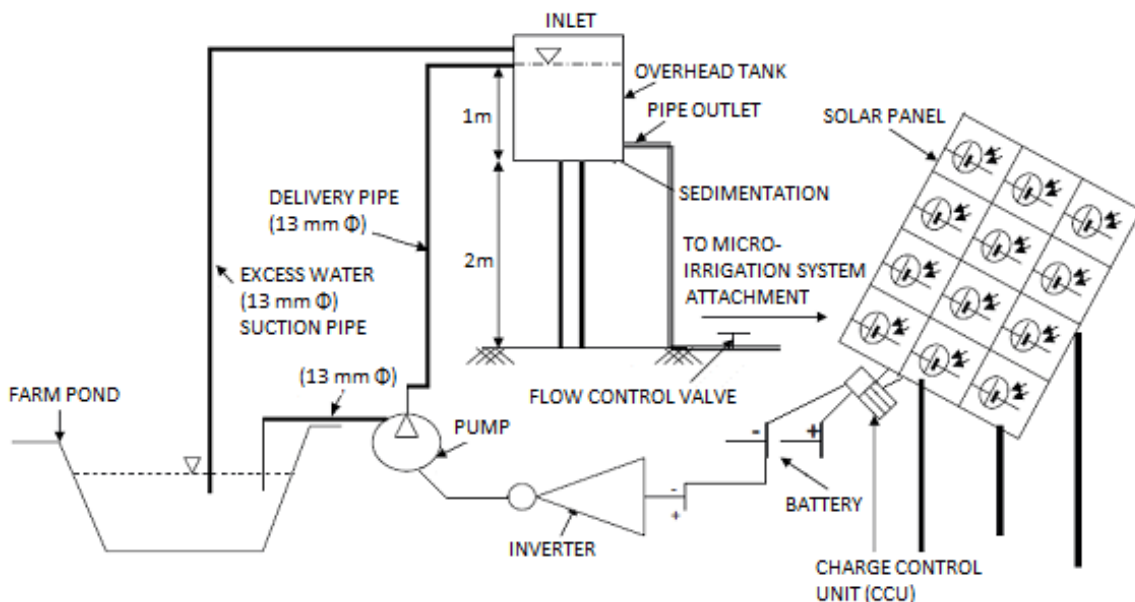


Fig. 2-1: Schematic of a simple PV irrigation set up for groundwater retrieval [10]

The water outlet from the irrigation system (depicted in Fig. 2-1) can be used either directly for irrigation or can be used to fill up a water storage tank. An advantage of the water storage tank is that it can be a substitute of the battery system, wherein the potential energy of the stored water can be utilised for drip irrigation.

Photovoltaic systems are generally very simple to implement, and an adequately designed system is efficient and can compete with other fossil fuel driven systems when operational and maintenance costs are considered. However, the initial investment is high and is one of the major issues making the technology inaccessible to the demographic in the Sub-Saharan Africa region [11].

While PV systems are easier to maintain than most other renewable energy systems, there are lots of factors that limit its use including, inconsistent solar irradiation, expensive tracking systems, reduction in efficiency due to overheating of panel systems, lower output due to energy conversion and one of the major issues identified in recent times is the large environmental impact in the production of PV panels [11–13]. Fig. 2-2 shows a systematic diagram of an irrigation system designed using PV panels.



**Fig. 2-2: Schematic diagram of micro-irrigation system powered by solar PV [14]**

A decrease in the cost of PV technology has meant many rural developments have been keen on utilising the technology. Because of this, a great amount of research has been conducted on solar PV technologies for water pumping in the recent years so much so that photovoltaic irrigation systems have become synonymous with solar-powered irrigation.

Multi-Junction PV panels are the most efficient form of PV panels but the environmental impact of these panels are higher than that of other renewable energy sources [12,15]. Table 2-1 shows the efficiencies of various PV cell types. Cadmium telluride cells are a better option with a module efficiency of 19.1%, with the least greenhouse gas emissions and quickest payback period [15,16]. In terms of cost, PV systems fare better in the lifetime cost analysis when compared to diesel [12,16,17]. The initial investment cost for PV panels are however too high in comparison to Diesel and other renewable energy systems such as solar thermal and wind [12]. However, a PV system can have a payback period of under 6 years [16], which is unmatched by other types of irrigation solutions in remote rural areas.

**Table 2-1: PV cell efficiency at 25°C and 1000 W/m<sup>2</sup> [18]**

<b>PV Cell Materials type</b>	<b>Efficiency (%)</b>	<b>PV Cell Materials type</b>	<b>Efficiency (%)</b>
<b>Silicon</b>		Dye mini module	10.7±0.4
<b>Si (crystalline)</b>	26.3±0.5	Thin-film chalcogenide	
<b>Si (multi-crystalline)</b>	21.3±0.6	CIGS (cell)	21.0±0.6
<b>Si (thin-film minimodule)</b>	10.5±0.3	CIGS (minimodule)	18.7± 0.6
<b>III–V cells</b>		CdTe(cell)	21.0 ±0.4
<b>GaAs (thin film)</b>	28.8±0.9	Multi-junction devices	
<b>GaAs (multi crystalline)</b>	18.4±0.5	Five-Junction Cell (bonded)	38.8±1.2
<b>InP (crystalline)</b>	22.1±0.7	InGaP/GaAs/InGaAs	37.9±1.2
<b>Dye sensitised</b>		a-Si/nc-Si/nc-Si (thin film)	14.0±0.4
<b>Dye</b>	11.9±0.4	Si (amorphous)	10.2±0.3

Based on research by R. López-Luque et al. [19], to irrigate 1 hectare of land less than 1 kW power is required and in such cases where the power system required is less than 5 kW, the DC motor system is preferred over AC motors. The study further indicates that permanent magnet DC motors provide the highest efficiency, torque and fastest response in comparison to other DC systems. The Positive displacement pump is shown to be beneficial for higher heads while for lower heads the diaphragm pump is better suited both providing efficiencies of 70% [13,16,20,21].

The use of battery is subject to the location and type of irrigation requirement, the costs of the systems also vary likewise. While an overhead tank may suffice in certain scenarios, others demand the use of battery for on demand use of electricity and a more consistent electricity supply [20,21]. Research by D. H. Muhsen et al. [11], on the other hand, proposed an aluminium foil reflector to boost the solar radiation.

The Power output and costs associated with PV systems vary depending on the irrigation scenarios [13,14,22–26]. To optimise the design of the PV system and the associated costs, it is important to understand the requirements of the crop by performing site surveys and analysing the working conditions. Considering the high solar potential in sub Saharan Africa and a case for drip irrigation, Fig. 2-3 shows the proposed solution for retrieving underground water for irrigation. The system provides 13.65% over all theoretical performance efficiency.

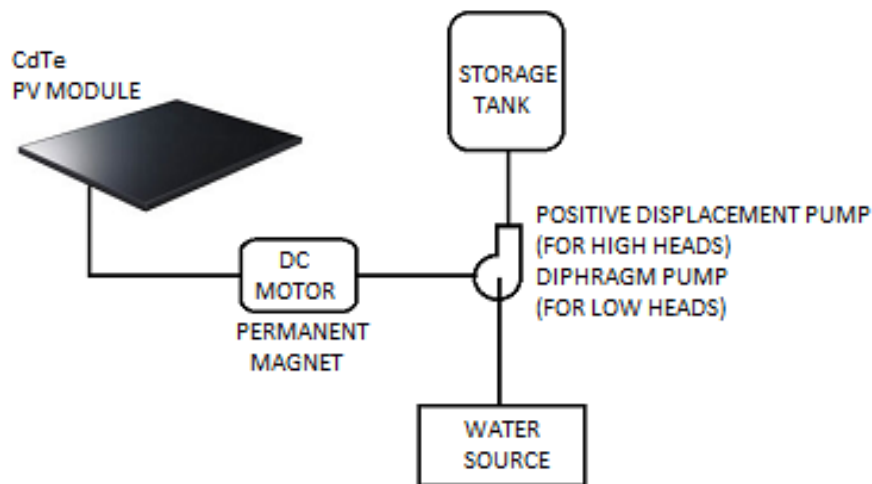


**Fig. 2-3: Schematic of proposed PV water pumping system for remote rural areas of Sub-Saharan Africa [27]**

Drawback of PV technologies include, the degradation of power of PV cells due to long term exposure is 0.8% per year [28]. At the elevated temperatures and humidity expected in sub-Saharan Africa the issue may be more prevalent. To compensate for this more intelligent system may have to be incorporated which will further increase the cost. Another issue with PV technology is that it's manufacture process poses a higher threat to the environment in comparison to other Renewable Energy Technologies and about 4 times more harmful than

Nuclear technology [12]. **Table 2-2** enlists the environmental impact of different PV cell types. Using batteries and the transportation further elevate the carbon footprint of the technology. Finally, accumulation of dust is another issue associated with PV technology.

**Table 2-2: Environmental impact of different types of PV cell types [12]**

Type of cell	Energy payback time* (Years)	Greenhouse Gas emissions (g-CO <sub>2</sub> -eq./kW h)	Lifetime (years)
<b>Mono crystalline</b>	2.5	50	N/A
<b>Multi crystalline</b>	2.0	43	N/A
<b>Cadmium telluride</b>	1.5	48	20
<b>Copper Indium selenide</b>	2.8	95	20
<b>Amorphous silicon</b>	3.2	34.3	20

\* Energy payback = energy used for manufacture and set up divided by energy produced.

The data from the reviews have been compiled and presented as per tabularised in **Table 2-3**. The Table focuses on the irrigation requirement of the system (including flowrate and pumping head), The PV module and power of the system utilised to meet the requirement, the area of the farm land and the cost of the technology.

**Table 2-3: Review summary of Solar PV water pumping**

Author	Location	Function	Flowrate	head	PV Panels	Power Out Avg	Battery	Farm Size	Cost
Deveci [20]	Turkey	Trees 2 hr irrigation	610 l/h	1m	2 x 10Wp	132 Wh	Yes	-	\$582 Investment
Campana [22]	Mongolia China	Alfaalfa	50 m <sup>3</sup> /ha	40m (TDH)	-	2.9 kWp	-	-	min - \$0.8 /Wp max - \$2.0 /Wp
Campana [23]	Mongolia China	Alfaalfa	3.9 m <sup>3</sup> /h	5m	6 x 0.96 kWp	-	-	-	\$2 /Wp
López-Luque [19]	Almeira Spain	Olive Trees	2 m <sup>3</sup> /h	40m 60m 80m	-	150 W/ha 250 W/ha 300 W/ha	-	250 trees /ha	\$2.14 /Wp
Chandel [16]	-	Orchard	3.4 - 3.8 l/h	-	-	900 Wp	-	-	-
	Madina Saudi Arabia	-	22 m <sup>3</sup> /day	-	24 Modules 8 series 3 parallel	-	-	-	-
	Gunung- kidul India	water Supply	0.4 - 0.9 l/s	1400 m	32 PV Panels	3200 Wp	-	-	-
	Spain	Orchard	161 m <sup>3</sup> /day	-	-	6 kWp	-	10 ha	-
	Algeria	-	60 m <sup>3</sup> /day	14.5m	-	-	-	-	\$0.04/m <sup>3</sup>
Chandel [28,29]	Himachal Pradesh India	Test	5500 l/h	-	12 mono-C-Si PV modules	396 Wp	Yes	-	-
Kumar [14]	Hyderabad India	-	900 l/h	4.5m	1.44 m <sup>2</sup>	148 W	Yes	2 ha	\$410 (full system)
Hossain [24]	Dhaka Bangladesh	Brinjal	100 l/min	33.5m	1050 Panels	1440 W	Yes	520 m <sup>2</sup>	\$5660
		Tomato			with tracking			520 m <sup>2</sup>	
		Wheat						496 m <sup>2</sup>	
		Rice						220 m <sup>2</sup>	

Table continued...

Author	Location	Function	Flowrate	head	PV Panels	Power Out Avg	Battery	Farm Size	Cost
Benghanem [30]	Saudi Arabia	Test	-	50m - 80m	PV array of 24 mono crystalline solar cells (8S x 3P)	1800 Wp	No	-	-
Treephak [21]	Thailand	Rice	15 m <sup>3</sup> /h	3.9m	250W x 6 AC	1500 W	No	0.5 ha	\$2800
					250 W x 4 DC	1000 W	No	0.5 ha	\$2000
					295 W x 4 AC	1180 W	Yes	0.5 ha	\$2800
					295 W x 3 DC	885 W	Yes	0.5 ha	\$2200
Yahyaoui [25]	Brazil	Tomato	200 m <sup>3</sup> /h	-	-	10 - 10000 W	Yes	10 ha	-
Reca [26]	Almeira Spain	Tomato	60000 l/h	40m	-	600 W/ha	No	1.9 ha	\$2.14 /Wp
Jones [17]	Jordan	Desalination	4000 - 15000 m <sup>3</sup> /ha/yr	25-100m	-	245 W	Yes	4-10 ha	\$1.25-\$4.30 /W
Sontake [13]	Nigeria	-	20 m <sup>3</sup> /day	-	60 WP x 28	-	Yes	-	-
	Germany	Portable water	-	5-125m	90 nos	180 kWp	-	-	-
	Bushland Texas	-	2-8 l/min	3-70m	-	160 W	-	-	-
	-	-	10-165 l/h	10-16m	2x45W	-	-	-	-
-	-	40 m <sup>3</sup> /day	10m	-	300-500 Wp	-	-	-	
Setiawan et al. [23]	Indonesia	Portable Water	0.2 – 0.9 l/s	218 m	32 x 100 Wp	3200 Wp	no	-	-
Muhsen [11]	Saudi Arabia	-	600 l/h	50m	-	0.98 kWp	-	-	-
	Egypt	-	150 m <sup>3</sup> /day	30	-	6.048 kWp	-	-	-
	Algeria	-	6 m <sup>3</sup> /day	-	(4Sx3P), (3Sx4P) BP Saturn	-	-	-	-

Table Continued...

Author	Location	Function	Flowrate	head	PV Panels	Power Out Avg	Batt-ery	Farm Size	Cost
Muhsen [11]	Kairouan Tunisia	-	6.5–30 m <sup>3</sup> /day	65-112 m	-	2.1 kWp	-	-	-
	Ghardaia Algeria	-	4-6 m <sup>3</sup> /day	19-35 m	-	-	-	-	-
	Madina Saudi Arabia	-	< 22 m <sup>3</sup> /day	80 m	(6S×3P), (12S×2P), (8S×3P), (6S×4P) ×75 Wp	-	-	-	-
	Oran Algeria	-	6-65 l/m	0.6 - 11 m	-	1.5 kWp	-	-	-
	Tall Hassan Jordan	-	45 m <sup>3</sup> /day	105 m	-	5.9 kWp	-	-	-
	Greece	-	20 m <sup>3</sup> /day	30 m	(2S×6P) ×51 Wp	-	-	-	-
	Turkey	-	18 m <sup>3</sup> /day	20 m	2 x 230 Wp	-	-	-	-
		-	52 m <sup>3</sup> /day		8 x 200 Wp				
	New Delhi India	-	38 m <sup>3</sup> /day	5 m	4S x 5P	-	-	-	-
	Purwodad Indonesia	-	1.44-3.24 m <sup>3</sup> /h	218.3 4 m	8S x 4P	3.2 kWp	-	-	-
	Louata Tunisia	-	7.7-14.7 m <sup>3</sup> /day	65 m	14S x 3P	2.1 kWp	-	-	-
	Madina Saudi Arabia	-	≤ 33 m <sup>3</sup> /day	50-80 m	8S x 3P	1.8 kWp	-	-	-
	Bejaia Algeria	-	43.66 - 27.91 l/min	11 m	6S x 3P	990Wp	-	-	-
Nigeria	-	10-30 m <sup>3</sup> /day	40 m	-	840-2520 Wp	-	-	-	
Tiwari and Kalamkar [31]	India	Domestic Use	20232 L/d		3S X2P	850	No	-	-
			23317 L/d		4S X 2P	1000			
			24374 L/d		5S X 2P	1020			
			22130 L/d		7S	1040			

Table continues...

Author	Location	Function	Flowrate	head	PV Panels	Power Out Avg	Batt-ery	Farm Size	Cost
Kabalci [32]	Turkey	Vineyard	400 m <sup>3</sup> /d	100 m	245 Wp Panels connected ((2P) X S) X2	2000 Wp	Yes	-	-
Sarkar [33]	Bangladesh	Farm land*	128 m <sup>3</sup> /d	12.8 m	Poly-crystalline Si	3.5 kW	Yes	-	\$ 1800 / kW
			373 m <sup>3</sup> /d	9.71 m		4 kW			
			740 m <sup>3</sup> /d	16 m		7.5 kW			
			645 m <sup>3</sup> /d	14.6 m		11 kW			
			300 m <sup>3</sup> /d	35 m		7.5 kW			

\* Only the Lowest and Highest range values have been identified in the table out of 108 installations

### 2.3. Solar Thermal Systems

Solar thermal systems obtain thermal energy from the sun via a solar collector or a solar concentrated surface. The energy is then transferred via a fluid or directly to either a Rankine, Brayton or Stirling Cycle engine which then converts the thermal energy into mechanical work. The mechanical work produced can be used directly to power pumps, converted to electrical energy for storage, or for powering an electrical pump. Fig. 2-4 shows a schematic of a solar thermal powered irrigation system. Direct utilisation of the mechanical power is desired; however, solar thermal technologies require consistent, direct solar irradiation to function adequately in the absence of such storage system may be required to be implemented. Storage of thermal energy is a much more difficult proposition when compared to the storage of electrical output.

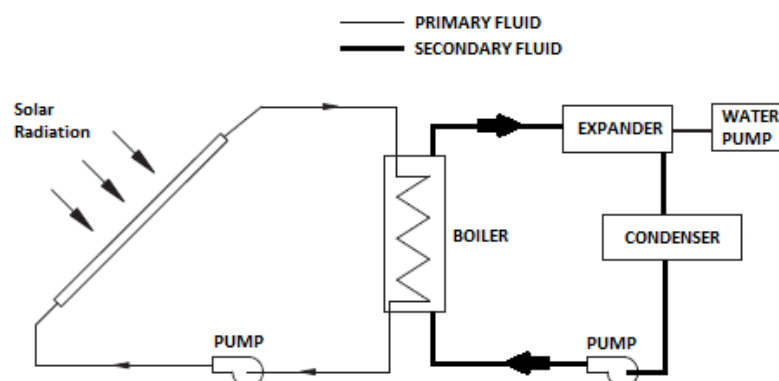
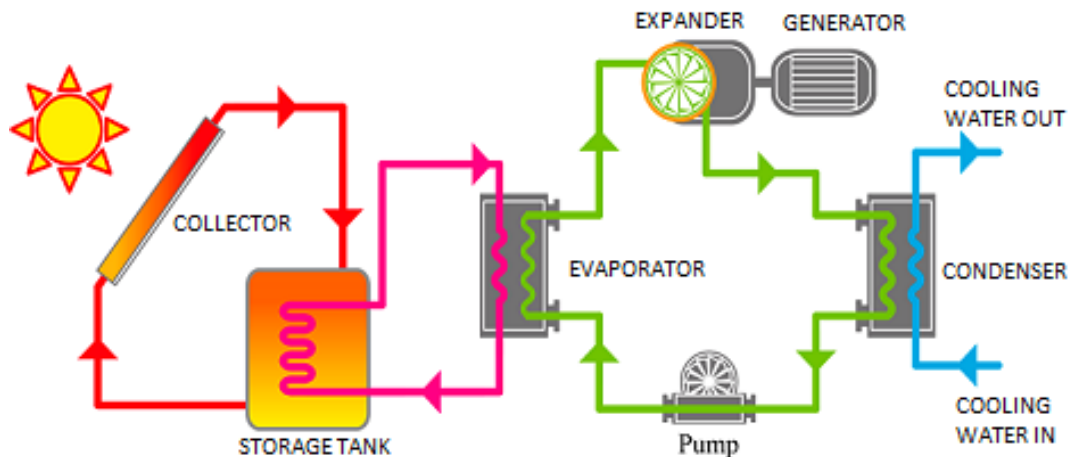


Fig. 2-4: A typical Rankine cycle solar thermal pumping system [12]

There are two types of solar thermal irrigation systems conventional technologies that use the Rankine cycle and unconventional systems that use vapour cycle liquid pistons or metal hydride systems to produce mechanical / electrical output [34].

Conventional systems are much larger and more complex in comparison to unconventional systems but is the most widely tested solar thermal systems [12]. Conventional systems require high investment costs, maintenance costs and have very low efficiencies (around 1%) and hence aren't considered for wide scale use for irrigation[13]. Instead conventional solar thermal irrigation may be undertaken in conjunction with desalination, or power generation [11,34]. Standalone, conventional systems are large, expensive and immobile in comparison to PV. Fig. 2-5 Shows a solar powered organic Rankine system.



**Fig. 2-5: Solar Powered Organic Rankine Cycle system [35]**

Unconventional technologies include Stirling Engine systems, Two stroke piston systems which are similar to Stirling systems [36,37] and metal hydride systems. Unconventional solar thermal technologies, generally have low pumping potential except for metal hydride systems that have flow of up to 2000 litres with a flat plate collector of just 1m<sup>2</sup> area. However, metal hydrides are expensive and not easily accessible in remote locations [12,34,38].

Stirling engines, are low cost systems, compact and easy to manufacture. Stirling engine irrigation systems are studied for low temperature operations 60 °C – 95 °C [34,39,40]. Due to the flexibility of Stirling systems in accommodating various heat sources and with the possibility of using better solar concentration techniques, higher temperature differences may be obtained which in turn will ensure a larger output from the system[34,37]. Fig. 2-6 shows a schematic of a Stirling cycle thermal powered irrigation system.

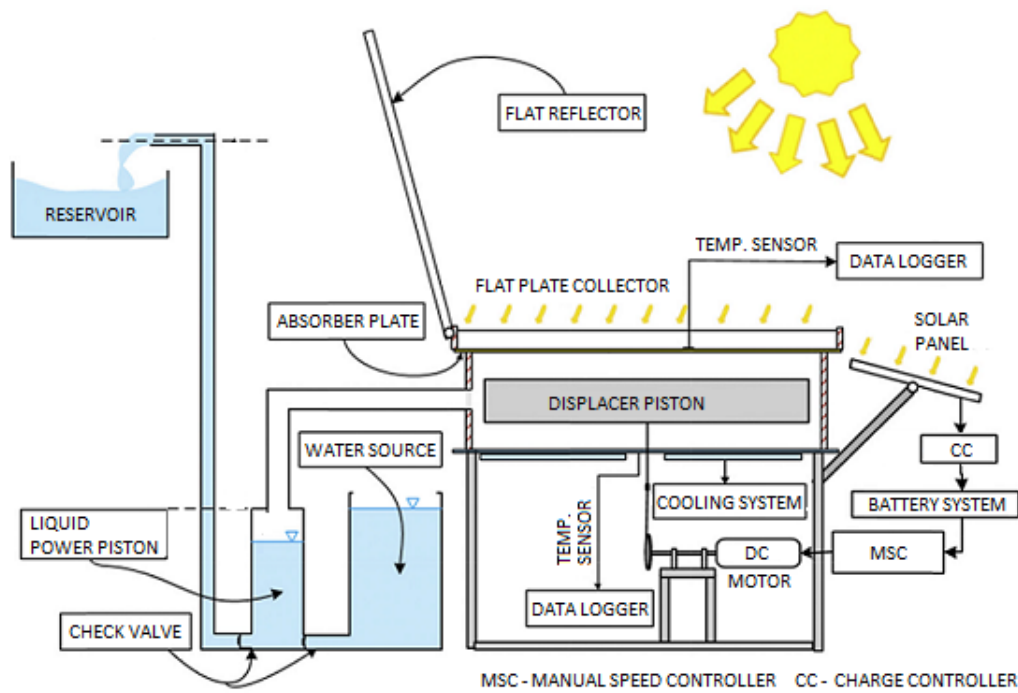


**Fig. 2-6: Solar Powered Low Temperature differential Stirling pump [40]**

A Stirling engine produces mechanical work by utilising cyclic compression and expansion of a working fluid (air, helium, hydrogen, nitrogen)[41] operating at different temperatures and enclosed in a fixed space [42]. The Stirling Engine can achieve the closest efficiency to the ideal Carnot cycle when compared to any other engines [43]. The efficiency of Stirling Engines are calculated to be between 30-40% for maximum operating temperatures up to 923-1073K at operating rates between 2000 – 4000 rpm [44].

Liquid pistons are a variation of free piston Stirling engines in which the solid pistons are replaced with liquid to allow lower levels of friction and air tightness, see Fig. 2-7 the fluidyne pump is an example of such a system where air is heated and cooled and causes a U-shape liquid column to oscillate and thus cause lifting and suction. In the laboratory, the fluidyne systems have been able to provide up to 3kW of power at a temperature difference of 95°C and pressure of 160kPa and giving 2m<sup>3</sup>/h pump capacity [39].

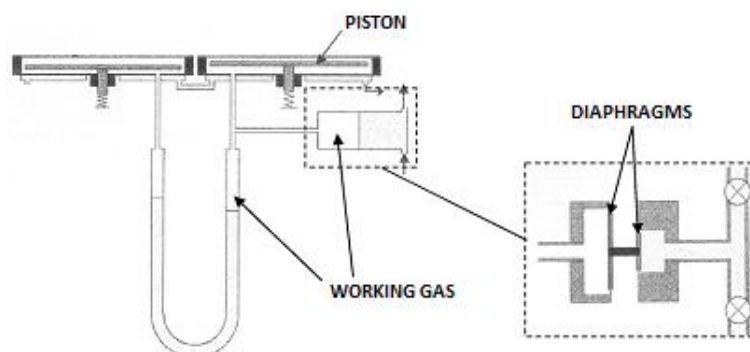


**Fig. 2-7: Liquid piston pump design using diaphragms [34]**

The final unconventional method discussed in the paper was using the metal hydride. In this system, metal hydride is subjected to heat causing release of hydrogen, as hydrogen is released the pressure is increased pressing down on the piston. Once the piston reaches the bottom of the cylinder, the metal hydride is then cooled, lowering the pressure and leading to the absorption of hydrogen. The system studied worked on the basis of heating and cooling of the metal hydride that could be controlled by a flat plate collector and the water flow generated by the pumping process respectively. A test on a metal hydride system was conducted in Kolkata in 2004 using a 1 m<sup>2</sup> flat collector at a tilt angle of 15°. On a clear day, a maximum of 2000 litres of water was pumped to a height of 15 m and on a cloudy day 500 litres of water was pumped. In terms of metal hydride use, on a clear day 240 l/day/kg of metal hydride is used while on a cloudy day it is about 60 l/day/kg [38]. The set-up of the system is shown in Fig. 2-8.

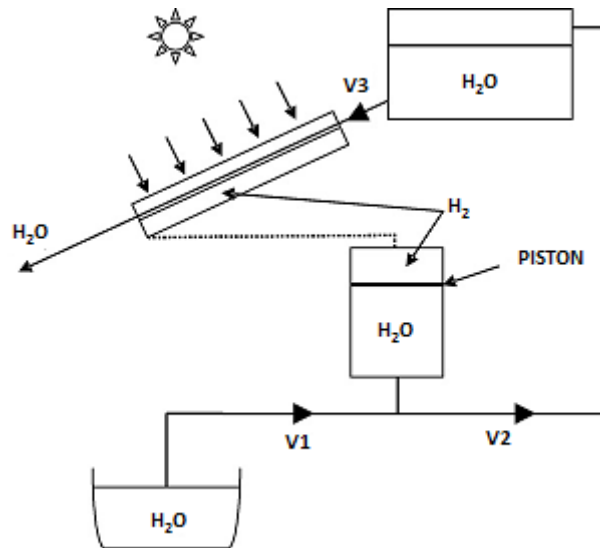


**Fig. 2-8: Metal hydride based solar thermal water pumping system design [38]**

In addition to the above, several novel 2 stroke systems have also been developed, by Kurhe et al. [45], Date and Akbarzadeh [36] and Sitranon et al. [37] which also work on a similar heating cooling cycle to drive a pumping mechanism.

The dish type solar concentrator is relatively cheap and the most commonly used solar concentration system used capable of providing concentration up to 500 °C with a single axis tracker. **Table 2-4** enlists different concentrator systems. Based on this system, cheaper and easier to manufacture concentration technologies have been designed such as the Linear Fresnel Reflector (400 °C concentration) [46]. Hence, the dish system is a good baseline for concentration technology that can be implemented with solar thermal irrigation systems. Local construction will further reduce the cost as well as carbon footprint of the system.

**Table 2-4: Range of temperature and ratio of concentration of various solar thermal systems**  
[46]

<b>Technology</b>	<b>T [°C]</b>	<b>Concentration Ratio</b>	<b>Tracking type</b>
<b>Air Collector</b>	0-50	1	-
<b>Pool Collector</b>	0-50	1	-
<b>Reflector Collector</b>	50-90	-	-
<b>Solar Pond</b>	70-90	1	-
<b>Solar Chimney</b>	20-80	1	-
<b>Flat Plate collector</b>	30-100	1	-
<b>Advanced Flat Plate Collector</b>	80-150	1	-
<b>Combined heat and power solar Collector</b>	80-150	8-80	1-axis
<b>Evacuated Tube Collector</b>	90-200	1	-
<b>Compound parabolic collector</b>	70-240	1-5	-
<b>Linear Fresnel Reflector</b>	100-400	8-80	1-axis
<b>Parabolic trough</b>	70-400	8-80	1-axis
<b>Heliostat field + Central Receiver</b>	500-800	600-1000	2-axis
<b>Dish Concentrators</b>	500-1200	800-8000	2-axis

The ease and accessibility of Stirling systems make it a viable option for testing and innovation. SUNORBIT, a company from Germany, have produced a concentrated solar system using the Stirling cycle capable of 500 Watts, 10 m head, 80,000 L/day known as the SUNPULSE [47], see Fig. 2-9.

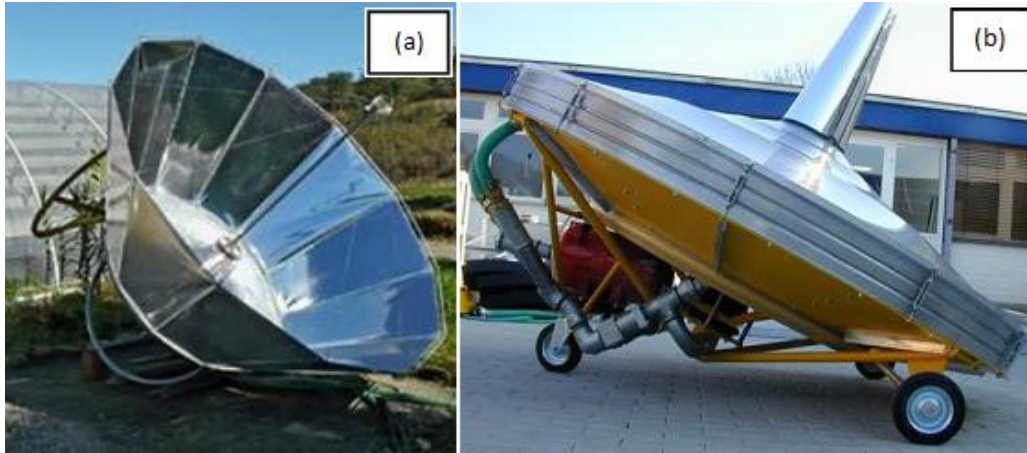


**Fig. 2-9: (a) Solar Stirling Water pump with dish [48] (b) SUNPULSE Stirling System [49]**

The system uses a foldable dish concentrator with a heat storage powering a  $\gamma$ -type Stirling engine. The pump has been tested across Europe, Africa, Asia and Australia and is estimated to cost US\$ 2,500. Tested by TÜV labs, the system is shown to meet the World Bank target of water cost for rural areas of 6 cents/m<sup>3</sup>. As per tests, the system designed can provide 2.4 cents/m<sup>3</sup>. Even though the technology is commercially available, it lacks formal research and analysis. The closest system to this was demonstrated by Jokar H, Tavakolpour-Saleh AR [40] who performed a mathematical analysis using MATLAB to demonstrate the work flow of the Stirling Engine.

Based on the research undertaken solar thermal technologies utilizing the Stirling engine provides the opportunity for small scale remote farms usage if the correct infrastructure is available for solar power concentration. Solar concentration technology that is cheap, effective and portable is essential to produce a feasible system. Parabolic concentrators and dish concentrators provide compact solutions; however, they can be expensive to purchase. Local alternatives utilising local materials to build concentration systems may be proposed, which will reduce the cost as well as carbon footprint of the system.

Utilising the technology to produce electricity is not viable, hence direct mechanical use for pumping is recommended in conjunction with a water storage tank is the optimal solution. Fig. 2-10 shows the proposed solution for retrieving underground water for irrigation in Sub Saharan Africa. A hybrid system comprising of Stirling pump with mechanical assist from an external system may be proposed to assist the displacer similar to work conducted by Jokar and Tavakolpour-Saleh [40].

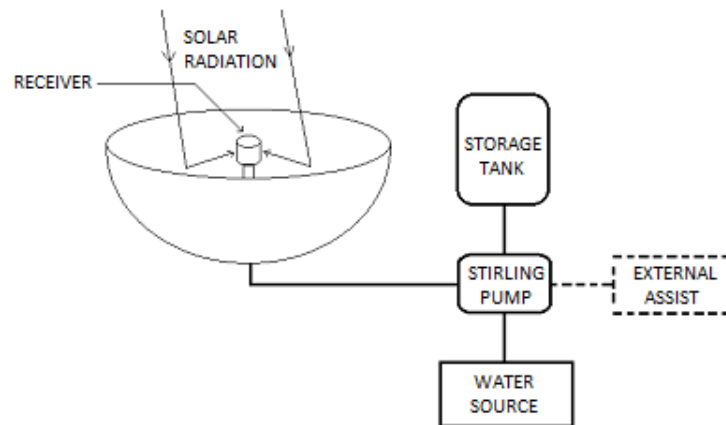


**Fig. 2-10: Schematic of proposed solar thermal water pumping system for remote rural areas of Sub-Saharan Africa [27]**

The data from the reviews of solar thermal technologies have been compiled and presented as per tabularised in **Table 2-5**. The data focuses on the irrigation attributes of the system including flowrate and pumping head, the thermal system and power output of the system utilised for irrigation and the cost of the technology. The reviews and data reveal a lack of real life testing to solar thermal technologies hence farm size data is not available for solar thermal technologies for comparison with PV technologies.

**Table 2-5: Review summary of solar thermal water pumping technology**

Author	Location	Flow-rate	head	Power Cycle	Collector Type	Temp Difference (°C)	Power Avg	Out	Cost
Mahkamov [39]	UK	-	-	Stirling	-	70 - 35	20 - 40 W	-	-
Delgado-Torrez [34]	Paris France	2.2 m <sup>3</sup> /h	-	Rankine	conical Reflector	-	-	-	-
	Paris France	7 l/min	3 m	Rankine	Parabolic 9.2 m <sup>2</sup>	-	-	-	-
	Pasadena US	5.3 m <sup>3</sup> /min	3.6 m	Rankine	Truncated cone 10m dia top 4.5m dia bottom	-	7.35	-	-
	-	-	-	Rankine	Flat Plate	-	14.7 kW	-	-
	Pensilvania US	-	-	Rankine	Solar Pond 11200 m <sup>2</sup>	-	2.57	-	-
	Pensilvania US	11.3-12 m <sup>3</sup> /min	10 m	Rankine	Wooden Boxes 1000 m <sup>2</sup>	-	10.29–11.76 kW	-	-
	Meadi Egypt	27 m <sup>3</sup> /min	-	Rankine	Parabolic Trough 60m x 4m	-	40.42 kW	-	-
	Mali Africa	11.3 m <sup>3</sup> /day	45.7 m	Rankine	-	-	-	-	-
	-	-	4.8 m	Ericsson	Parabolic	-	-	-	-
	Arizona US	38 m <sup>3</sup> /min	-	Rankine	Parabolic 554 m <sup>2</sup>	-	-	-	-
	New Mexico US	2.6 m <sup>3</sup> /min	34 m	Rankine	Parabolic 622.4 m <sup>2</sup>	-	-	-	-
	Guanajuato Mexico	1000 m <sup>3</sup> /day	-	Rankine	Flat Plate 2499 m <sup>2</sup>	-	-	-	-
	Dakar Senegal	8-10 l/min	13-14 m	Rankine	Flat Plate 6 m <sup>2</sup>	-	-	-	-
San Luis Mexico	2.5 m <sup>3</sup> /day	-	-	-	-	25kW	-	-	
Various	30 m <sup>3</sup> /day	20	-	Flat Plate 100 m <sup>2</sup>	-	-	-	-	
Mexico	-	-	Rankine	Parabolic Trough	-	1kW	-	-	

Author	Location	Flow-rate	head	Power Cycle	Collector Type	Temp Difference (°C)	Power Avg	Out	Cost
Delgado-Torrez [34]	Arizona US	-	-	Rankine	Parabolic Trough 2140 m <sup>2</sup>	-	-	-	-
	Egypt	-	-	Rankine	Flat Plate 384 m <sup>2</sup>	-	10 kW	-	-
	-	14.61 l/min	3 m	Rankine	4 x Flat Plate 1 m <sup>2</sup> each	-	-	-	-
	India	6.5 m <sup>3</sup> /day	11.2 m	Rankine	Flat Plate 7 m <sup>2</sup>	-	-	-	-
	India	-	-	Rankine	6 x Parabolic 9m dia	-	20 (500 °C Steam)	kW	-
	Iran	20 m <sup>3</sup> /day	-	Rankine	Flat Plate	-	-	-	-
	India	2 m <sup>3</sup> /day	6 m	Organic Rankine	Parabolic	-	-	-	-
	UK	0.5 - 2 m <sup>3</sup> /h	-	Liquid Piston	-	MAX Temp: 95	0.8-3 kW	-	-
Lakew [50]	Kolkata India	240 l/day	15 m	Metal Hydride	Flat Plate 1 m <sup>2</sup>	22-62	-	-	-
	-	-	-	Rankine	-	80 (plus 60°C Low level heat source)	2800 - 3750 kW	-	-
Tchanche [46]	UK	-	-	Organic Rankine	-	55	1.47 kW	-	\$ 30,000
	Sendai Japan	0.016 kg/s	-	-	-	-	350W	-	-
Date [36]	Australia	140 m <sup>3</sup> /day	35 m	2 Stroke Liquid Piston	Solar Pond 5200 m <sup>2</sup>	-	-	-	-
Kurhe [45]	India	20 L/hr	5 m	2 Stroke Diaphragm pump	Flat plate Collector	50-60	-	-	-
Baral [35]	Busan South Korea	-	-	Organic Rankine	Evacuated Tubes	65-95	0.4 kW - 1.38 kW	-	\$ 25,800
Jokar [40]	Iran	0.125 l/s	1.5 m	Stirling	Flat Plate Reflector 2x1m	100	1-2 W	-	-

Author	Location	Flow-rate	head	Power Cycle	Collector Type	Temp Difference (°C)	Power Avg	Out	Cost
Baral [51]	Nepal	2190-11100 m <sup>3</sup> /year	150 m	Organic Rankine	Evacuated Tubes 150-200 m <sup>2</sup>	60-100	1-5 kW		\$13,000 (1 kW) \$66,900 (5 kW)
Sitranon [37]	Thailand	60-95 l/h	2-6 m	Liquid Piston	-	70	-	-	-
Moonsri [52]	Thailand	192.2-218.8 l/day	1-5 m	Liquid Piston	Flat Plate	42.9-46.7	-	-	-
Bataineh [53]	Jordan	-	-	Rankine	Parabolic Trough 526 m <sup>2</sup>	-	30 kW		\$0.075/kWh

## 2.4. Summary

PV powered water pumping technologies are well developed, easily accessible and require almost no maintenance over the course of the lifetime of the technology. Studies suggest that the best way to optimise the cost and design of the PV powered system is to understand the requirements of the crop and perform extensive site survey to analyse the working conditions of the system. This is seen in relation to the use of a battery system where cost savings have been achieved in certain scenarios without using the battery while in other applications it was found that a battery in fact reduces costs.

While the cost of PV system, over the course of its lifetime, is much lower in comparison to diesel powered systems, the initial investment cost is much higher and often too much to bare for small scale rural farmers. Furthermore, if the purpose of solar panels is to reduce the impact on the environment, it falls short due to a substantial carbon footprint because of the manufacturing and transportation impacts of the technology.

This study identifies that there is a huge potential for solar thermal technology to meet the requirements of the small scale rural farmer by using a solar thermal water pumping system but the research on these systems are minimal, there is very few data available on the feasibility of these technologies especially for small scale purposes.

In terms of efficiency, solar thermal pumping systems can provide a maximum measured efficiency of 3% in comparison to 6% from photovoltaics. But the efficiency shouldn't be the

main priority in the selection of the appropriate technology, especially since the source is renewable. The main factors hence are a functional technology with low cost, local production capable and having low impact on the environment.

A locally produced solar thermal system would be more cost effective and environmentally friendly in comparison to PV panels, as far as initial investments are concerned for remote area irrigation. The issue with regards to solar thermal powered technologies is that, the amount of research undertaken on these irrigation systems is very low.

Based on the literature review, a Stirling pump system powered by a dish type solar concentrator may provide the necessary pump work to meet the requirements of the region. While there is a commercial system that matches this description is available there is no formal research material available on the unit and the cost of the system is high. Similar Stirling systems have been identified but require further development and analysis as in its present state they are unable to provide viable output.

The review of the existing literature and research covered solar PV and solar thermal powered irrigation systems. The review highlighted the prospects of utilising solar thermal technology, namely Stirling engine, for providing low-cost, portable technology that can be locally manufactured to provide income, food and energy security in developing nations. The following research gaps have been identified:

- While there is a commercial Stirling pump available, there is no formal research and analysis undertaken on the system.
- The cost of the SUNPULSE system is high considering the GDP of the region. Hence, a more affordable technology is required that will make the construction of the Stirling pump cheaper.
- More accurate multi-dimensional analysis of Stirling pumps is required, to analyse and optimise key geometrical components for the pump system.

This work will utilise simulation techniques to evaluate the possibility of using a low cost, low temperature differential Stirling Engine model as a Stirling pump. Several numerical models for the analysis of Stirling engines have been developed. However, one-dimensional mathematical models, demonstrated in the literature reviews, fall short of analysing the

working process. These short-comings can be partially overcome utilising more complex multi-dimensional analysis.

Computational Fluid Dynamics (CFD) modelling has shown to produce better accuracy [54] in demonstrating the working of Stirling engines and shall be utilised to simulate Stirling pumps. CFD modelling of Stirling engines is further discussed in Chapter 3.

In order to develop the Stirling pump, the following work will be carried out:

- Develop CFD model for Stirling pump based on models prepared for Stirling engines as demonstrated by Wen Lih-Chen et al. [55–57]
- Validation of CFD techniques using experimental methods similar to work conducted by Jokar and Tavakolpour-Saleh [40] and Kato [58]
- Assess the viability of the Stirling system to meet the requirements of small-scale independent farmers in the Sub-Saharan African Region.

# Chapter 3

## Background Theory

### 3.1. Introduction

The following section contains a framework of concepts and theories that will be utilised in this research work demonstrating the irrigation requirement, describing the Stirling engine systems and providing an insight into the analysis of Stirling engines using CFD.

In order to determine the irrigation requirement FAO statistics has been utilised to obtain the size of a typical farmland in sub-Saharan Africa and determine the flowrate required for the irrigation of the land. The source of water and the environmental impact of the water extraction is also discussed.

Background research has been carried out to summarize the different Stirling systems and determine which system is most likely to provide a suitable cost-effective solution for irrigation. Key research has been identified in order to build on the research towards obtaining a cost-effective solution for irrigation.

This section also provides background research on Analytical methods for the analysis of Stirling Engines focusing mainly on CFD as a tool in the analysis of the Stirling engine.

### 3.2. Irrigation

Presently the ground water reserves in shallow aquifers (under 50m depth) of Sub-Saharan Africa are a result of water collection for 20-70 years, hence are expected to withstand short term fluctuation of climate [59]. However, the resources are vastly underused presently, and the introduction of irrigation may stretch the capacities of the reserves. This entails a conscious effort that must be made to use the water resource responsibly.

The purpose of this research is not only to provide a pumping solution, but to also ensure the best practice for irrigation is incorporated. Hence, the drip irrigation method is considered to calculate the water flow requirements.

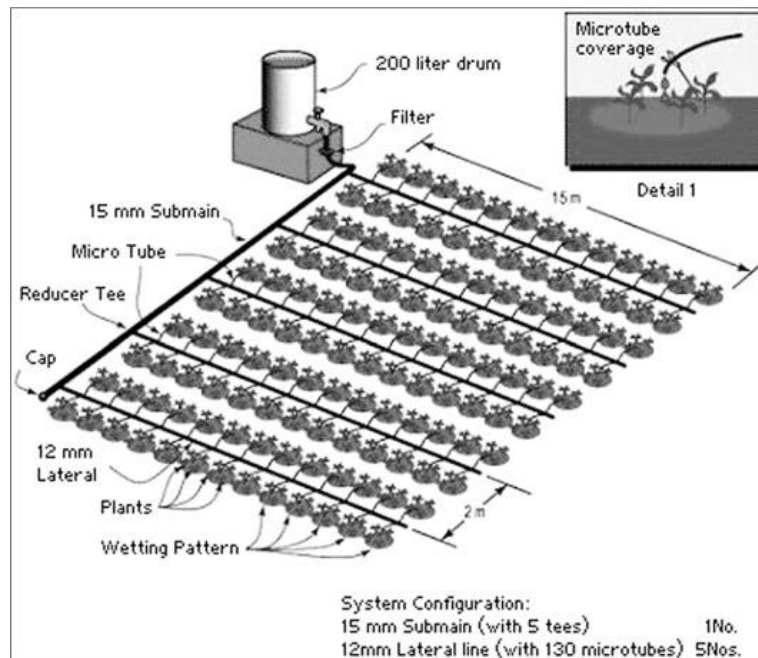


**Fig. 3-1: A typical Drip irrigation set-up [60]**

In the drip irrigation method, water from a storage tank is transported through a network of narrow pipes, valves and emitters to drip directly onto the root of the plants or on to the soil surface. Drip-irrigation also helps in controlling the amount of fertilizers used as, the fertiliser can be mixed with the water in the storage tank [61]. See a typical Drip irrigation arrangement in Fig. 3-1.

Drip irrigation is one of the most efficient methods of watering crops. Its field application efficiency can be as high as 90% compared to 60–80% for sprinkler and 50–60% for surface irrigation [62]. Drip irrigation method also have the lowest rate of soil evaporation of 7-10% of total water loss compared to 30% seen for fully wetted row crop irrigation methods [62].

Drip irrigation systems have already been implemented in regions of southern Africa for small-scale farmers. These systems generally use a reservoir ranging from 10–15 L bucket to 200-300L fuel drum reservoirs. Placed at a height of 1-2 m above the ground, the reservoirs can irrigate a small vegetable garden from 50 m<sup>2</sup> area up to 250-500 m<sup>2</sup> area. Presently the systems have not seen much success mainly due to the lack of access of water sources and improper implementation due to lack of proper education regarding the technology transferred to the farmers. The energy cost for the above systems are generally US\$ 500 to US\$ 700 per hectare which is just the labour cost associated with refilling the reservoirs [63].

For the purpose of this study, a 1 hectare land space is considered for irrigation based on the FAO statistics pertaining to small farm size in Sub-Saharan African region. The small farms are categorized between 0-10 hectares. The largest farm size seen in Niger with 6 hectares with an average of 2 hectares being the largest among the small farms. The smallest farms, however, average close to 0.01 hectares thus bringing the overall average small farm size to 1 hectare. See **Table 3-1** for Farm size data presented by the FAO.

The amount of water required to irrigate 1 hectare of land depends on the type of soil, the type of crop that will be harvested, the growth stage and the climate of the location. The Stirling pump design will be based on the worst-case scenario [11]. Since most of the imports in the region are for grains, crops in this criterion will be considered for the water requirement calculations. This may include rice, barley, lentils and wheat to name a few.

**Table 3-1 Small Farm Size, Sub-Saharan Africa [64]**

<b>Small Farms</b>			
<b>Country</b>	<b>min</b>	<b>max</b>	<b>avg</b>
<b>Kenya</b>	0.04	1.2	0.47
<b>Ethiopia</b>	0	2.3	1.01
<b>Malawi</b>	0.004	0.91	0.46
<b>Niger</b>	0.0002	6	2.63
<b>Nigeria</b>	0.00002	2.22	0.6
<b>Tanzania</b>	0.001	2.2	0.9
<b>Uganda</b>	0.004	1.6	0.7
<b>Average</b>	0.01	2.35	0.97

There are 6 steps to the calculation of irrigation water requirement:

- Step 1: Determine the reference crop evapotranspiration
- Step 2: Determine the crop factors

- Step 3: Calculate the crop water need
- Step 4: Determine the effective rainfall
- Step 5: Calculate the irrigation water need
- Step 6: Calculate the volume of water required

Reference crop evapotranspiration (ET<sub>o</sub>), expressed in mm/day is the amount of water needed by the various crops to grow optimally. For the ET<sub>o</sub> the worst-case scenario presents a hot, dry, windy and sunny day. Based on estimates provided by the FAO, in an arid location with temperatures above 25 °C the water needs in peak periods is 10mm/day for grains.

The Crop factor (K<sub>c</sub>) is the relationship between the reference grass crop and the crop being grown. For Grains such as Barley, oats and wheat the crop factor is highest in the Mid-Season measuring 1.15, while that of lentil is 1.1. Rice has the highest K<sub>c</sub> value of 1.35 also during its mid-season. Rice is a very water intensive crop and hence is not being considered.

The crop water needed (ET crop) is ET<sub>o</sub> x K<sub>c</sub>. Considering the crop factor for barley, oats and wheat, the ET crop value is 10 x 1.15 = 11.5 mm/day. Considering a dry day during the peak cultivation period, the effective rainfall (P<sub>e</sub>) is set to zero, the irrigation water requirement hence remains, ET crop – P<sub>e</sub> = 11.5 mm/day. For 1 hectare (10,000 m<sup>2</sup>) land space, the volume of water required = 10,000 (m<sup>2</sup>) x 0.0115 (m/day) = 115 m<sup>3</sup>/day = 115,000 litres of water per day. The Stirling engine is expected to work throughout the sunlight hours of the day. With a minimum of 6 hours of useable sunlight [65], the Stirling engine needs to be capable of a flowrate of **5.35 litres per second**.

The amount of hydraulic power (P<sub>h</sub> in kW) required to generate this flowrate can be calculated using the formula:

$$P_h = \frac{q\rho gh}{3.6 \times 10^6}$$

Where, 'q' is the flowrate (19.26 m<sup>3</sup>/h), 'ρ' is the density of water (considered to be 1000 kg/m<sup>3</sup>), 'g' is the acceleration due to gravity (estimated as 9.81 m/s<sup>2</sup>) and 'h' is the differential head considered to be 20m to allow transportation of the water from the underground reserve to a above ground tank to facilitate drip irrigation. Given the values, the power

required from the Stirling pump is 1.1 kW. Considering a pump efficiency of 60%, the Shaft power ( $P_s$  in kW) can be calculated using the formula:

$$P_s = P_h / \eta$$

Where,  $\eta$  is the pump efficiency. Thus, the Shaft power is 1.75 kW. Using 7 x 250 W commercially available solar panels PV technology can be used to generate the necessary power to run a pump. This arrangement will require approximately 11.2 m<sup>2</sup> for the panel installation area and would cost up to \$3,800 (USD) [66]. For solar thermal engine considering the example of the Sun Pulse system, with a hot side temperature of 150°C and a cold side temperature of 40°C, a mechanical efficiency of 13% is obtained. Using a 4 bar pressure loaded engine at 2 bar pressure, the Sun Pulse can provide an output of 2 kW at an estimated price of \$ 2,000 (USD) [67][47].

Both Solar PV irrigation [39] as well as solar thermal technologies using Rankine cycle systems [34] and in one case a theoretical set-up of 2-stroke date cycle systems [36] have been capable of achieving this target. The commercially produced SUNPULSE Stirling system is capable of 3.7 l/s at a 10 m head [47]. While attaining 5.3 litres per second is the preliminary goal, the target may be modified based on the capability of the Stirling engine based on the design that will be evaluated using Computational Fluid Dynamics.

### 3.3. Stirling Engine

The Stirling Engine is based on the Stirling cycle. This cycle consists of four main processes, Compression at constant temperature (T), Heat addition at constant volume (V), Expansion at constant temperature and constant volume heat removal [44], represented in Fig. 3-2.

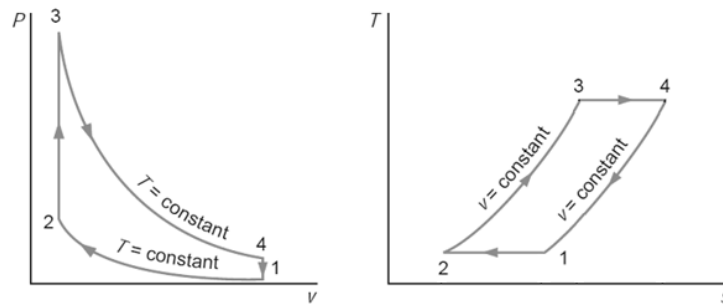


**Fig. 3-2: Pressure (P) – Volume (V) and Temperature (T) – Entropy (S) diagram for Stirling Engine [44]**

The Stirling engine consists of a hot side, a cold side and a regenerator. On the hot side, a heat exchanger obtains heat from a source, which can either be utilising fuel consumption or irradiative heat from the sun. The cold side, depending on the application, could either be exposed to atmospheric temperatures, a cold wall, or other liquid cooled systems.

The higher the difference in temperatures between the hot and cold sides, the better the efficiency of the system. The Regenerator is an area of heat storage that is generally connected between the hot and cold sides of the engine. This regenerator retains the heat that may otherwise have been lost to the surrounding environment and the space is also used to allow the working fluid to go from the cold side to the hot and vice versa.

There are Three major configurations of the Stirling Engines, Alpha, Beta and Gamma type:

#### 3.3.1. Alpha Stirling Engine

An alpha configuration Stirling Engine consists of two pistons contained in a hot and cold cylinder that are joined to a crankshaft at 90° phase angle to each other [44]. The cylinders are connected to each other with a Regenerator and the working Fluid is generally a gas. Fig. 3-3 depicts a simple alpha configuration schematic.

The Alpha Stirling Engines provide the highest power to volume conversion among the various types of Stirling Engines, however, durability of the seals of piston against the hot cylinder due to the requirement of close fit tolerance often creates technical problems [43].

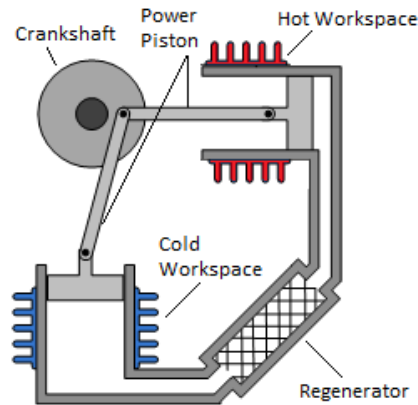


**Fig. 3-3: Alpha Stirling Engine Schematic**

### 3.3.2. Beta Stirling Engine

The Beta configuration Stirling Engine utilizes a displacer in conjunction with a power piston within one cylinder. The working fluid is navigated from the hot space to the cold space with the help of the displacer across the location of heat application, the regenerator and the cold workspace. The cold space houses the power piston which is used to compress the working fluid when the displacer brings the fluid to the cold workspace and expands when the fluid is taken to the heat application region [68]. Fig. 3-4 shows the schematic of a simple beta configuration.

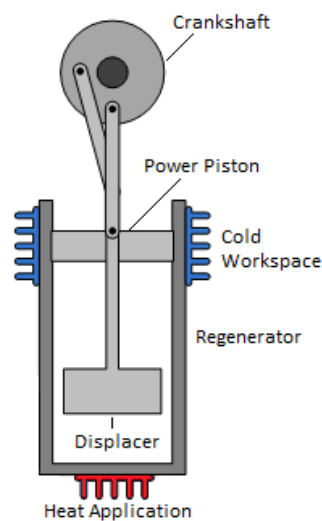


**Fig. 3-4: Beta Stirling Engine Schematic**

The Beta configuration has a compact set up and assists in eliminating the issue with the durability of the seal as faced in the alpha configuration in the hot workspace. However, because of the compact nature of the configuration, the surface area at the heat application is limited affecting the heat transfer from the source, leading to lower efficiency [43].

### 3.3.3. Gamma Stirling Engine

The functioning of the Gamma configuration Stirling Engine is similar to that of the Beta type Stirling Engine, however, in this configuration the power piston is mounted in a separate cylinder. This allows complete isolation of the power piston from the thermal reservoir. The Displacer can then be designed to a larger size to provide more swept area than both the alpha and beta configurations [69]. See Fig. 3-5 for schematic of a gamma configuration Stirling Engine.

A single Crankshaft connects the power piston and the displacer enabling the piston to compress as well as expand the working fluid. In this double acting piston arrangement, the gamma configuration Stirling Engine can provide the maximum possible mechanical efficiency, so long as the unit is designed vertically to reduce the friction due to bushing [70].

Since a higher mechanical efficiency is desirable for pumping systems, The Gamma Stirling Engine seems to be the most likely choice of Stirling engine to further investigate. Furthermore, the simplicity of the design of the gamma configuration has enabled wide range of research encompassing low temperature systems such as the Free Piston Stirling Engine.

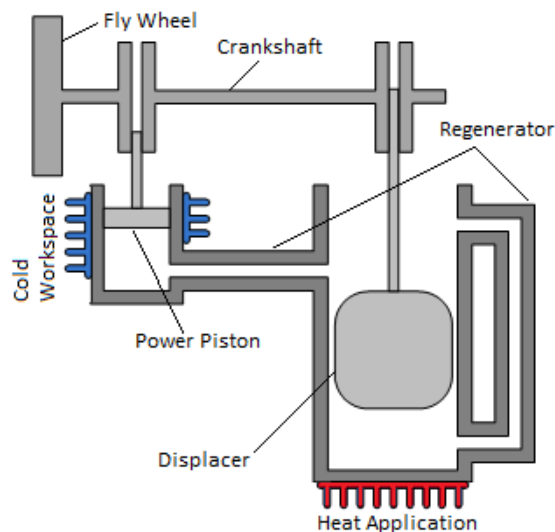
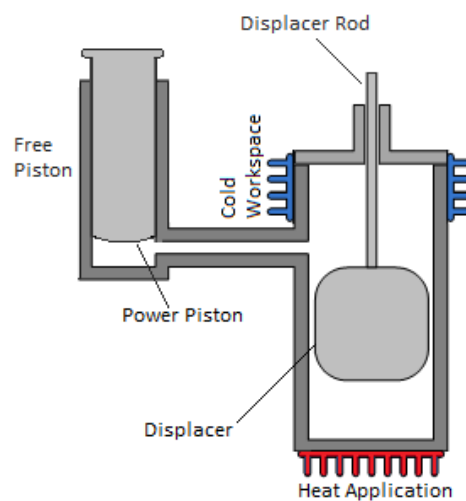


Fig. 3-5: Gamma Stirling Engine Schematic

### 3.3.4. Free Piston Stirling Engine

In a free piston Stirling engine, the power piston for a gamma type Stirling Engine is substituted with a free piston, a liquid piston or a diaphragm. Using a liquid piston or diaphragm drastically reduces the friction losses in the system, further improving the efficiency. There is no connection between the “piston” and displacer via a flywheel hence the mechanical work generated can be used as a pump [49]. Fig. 3-6 shows the schematic of a free piston Stirling engine. In this case Gravity is used to generate the compression stroke. There is no separate regenerator in the system, the narrow gap between the displacer and the cylinder containing it, act as the displacer.



**Fig. 3-6:** Free Piston Stirling Engine Schematic

The gamma type free piston Stirling pump is one of the simplest Stirling pumps in terms of construction and has been considered as the focus of this PhD thesis. To design an effective system, the irrigation requirement will be calculated based on the irrigation requirements the pump will be designed using CFD analysis. Concentrated solar thermal energy will be used as the heat source for the system and a liquid piston will provide the pump work required to pump water from the underground reserve to the storage tank. This system will be similar to the work done by Jokar and Tavakopour [40] (Fig. 2-6).

### 3.4. CFD Analysis of Stirling Engines

The analysis of Stirling Engine includes the complicated processes of heat and mass transfer due to the geometrical effects of the various multi-dimensional components of the engine. While Numerical methods have implemented to define the workings of the engine, an accurate representation of the performance is yet to be obtained. In such cases, advanced simulation approaches using CFD models can assist in mapping the geometrical features to accurately predict the heat and mass transfer of the system.

The first instance of successful application of 3D simulation of Stirling Engine is attributed to K. Mahkamov[54] in 2006. In his work, he developed a prototype of an alpha type biomass Stirling engine based on mathematical analysis. Upon testing the power output of the system was appreciably lower than that predicted. This prompted the use of advanced 3D CFD analysis which provided numerical results that closely replicate the experimental data.

With the application of CFD becoming more common in recent times, with CFD software becoming more accessible to researchers, numerous studies have been conducted covering both 2D and 3D simulations of Stirling engines. Due to the cyclic nature of the system, transient analysis is performed on a compressible fluid performing under the rules of the ideal gas.

Simulations made using 2D modelling are generally compiled within a short period of time when compared to 3D models. However, due to the non-uniform distribution temperature in Stirling Engines, the rate of heat transfer is not accurate. The same goes for fluid flow analysis in the Stirling engine. For both these parameters the geometry of the models need to be well defined and calls for a more complex 3D model analysis [71–73].

Both laminar and turbulent models for CFD analysis have been presented. To facilitate laminar flow conditions in the system the model prepared are very small [55–57,71,72,74,75]. Once again this is done to reduce the computational time and for the simulation of the Stirling engine but does not accurately represent the experimental parameters with which the results are compared. Furthermore, using a laminar flow model makes it difficult to obtain convergence as no unsteady term has been considered [76]. For an accurate representation of the fluid in the engine, turbulent modelling is required. In the research carried out, the k-epsilon turbulent model has been implemented for the analysis of the engine [54,73,76–79].

A number of softwares have been utilised for the production of the CFD models. Most of the early models were prepared using in-house softwares. While the principle of softwares are the same, accessibility is the major factor determining the use of software. Among the software used include, USTREAM mesh [56,57,71,74,75,80], FORTRAN77 [76,78], COMSOL Multiphysics [72,81] and ANSYS FLUENT [73,77,79,82].

In the context of this research, the desired Stirling pump system is required to have simple construction. Analysis by Wen-Lih Chen et al. [55,57] demonstrates a simple geometry while lacking detailed modelling of the regenerator and using laminar flow modelling and thus provides a baseline for further development. The model developed by Wen-Lih Chen et al. will be studied and further developed to demonstrate turbulent flow and a porous medium will be set-up in the displacer to demonstrate the regenerator. Subsequently the model will be adjusted to develop the Stirling pump system to pump water from an underground water reserve to a water storage tank for irrigation.

### **3.5. Summary**

Based on FAO statistics and the average land area for a small sized farm in the sub-Saharan Africa region is 1 hectare, and based on adverse conditions, the flowrate of water required to irrigate this land during the night is 5.35 litres per second, irrigated using drip irrigation method during the night time so as to allow maximum retention of liquid in the irrigated land.

In order to obtain the irrigation role in the most cost-effective way, the gamma type Stirling engine model has been selected based on the simplicity of the construction of the systems. In particular Free piston systems is the ideal choice since the frictional losses in these systems are reduced considerably due to the presence of liquid pistons.

3D CFD analysis has been identified as the preferred modelling tool for the analysis of the Stirling engines with the recent model produced by Weh-Lih Chen identified as being the model to be duplicated and thus be used to study the Stirling engine workflow.

# Chapter 4

## Experimental Results

### 4.1. Introduction

This chapter describes the components, experimental set-up and procedure that was implemented to study the working of the Educational Model Stirling Engine (EMSE); and the full-scale experimental results obtained using the Engine. The experimental investigation was undertaken to determine the temperatures achieved at the bottom and top surfaces of the displacer of the Stirling engine, the pressure recorded at the top section of the displacer chamber and the rotational speed of the Stirling engine. The temperature and the rotational speeds were utilised to set up the modelling parameters of the fluid analysis (CFD) using ANSYS Fluent. The resultant pressure from the model is then used to compare with the value recorded in the experiment to validate the model.

The Experiments utilised a low temperature differential (LTD) educational model Stirling engine (EMSE). Both qualitative and quantitative data analysis was carried out to determine the work done of the engine by measuring the pressure in the displacer cylinder and estimating the volume change in the cylinder based on the rotational speed of the Stirling Engine. A detailed experimental procedure has been established for the testing of the pressure and thermal properties of the Stirling engine.

°This chapter also outlines the devices used for data acquisition that were used for taking the measurements and recording the data captured. The DSA3217 Pressure Scanner was used to capture the pressure data connected to a laptop with the Scanivalve data logging software in order to record time-dependant pressure measurements. An Omega HH804 resistance temperature detector thermometer coupled with two self-adhesive thermocouples was used to collect and record time-dependant temperature measurements. A high-speed thermal camera was also used to visualise the temperature distribution across the displacer of the Stirling Engine.

Finally, the bottom surface of the EMSE has been set to reference temperatures to obtain specific temperature differences; between 293 -333 K between the two ends of the displacer chamber. This range of values have been selected to obtain a range of temperature differences to validate the working of the Stirling Engine simulation model and obtain a definitive model for performing design analysis of low-cost Stirling engines.

#### **4.2. Overview of low-cost, LTD Stirling engine**

The Stirling Engine utilised for the analysis is a low-temperature, gamma-type Stirling Engine often used for model making and generates miniscule amounts of energy in the order of 0.1-0.5 Watts, however, these systems are relatively cheaper to manufacture compared to Alpha and Beta type engines, functional and thus selected for further analysis for the development of the irrigation system. The two areas of interest for monitoring and recording is the piston and the displacer. A heating plate was used to generate a temperature difference between the bottom and top engine surfaces and to ensure consistent supply of heat being applied to the engine. The temperature was monitored using temperature gauges.

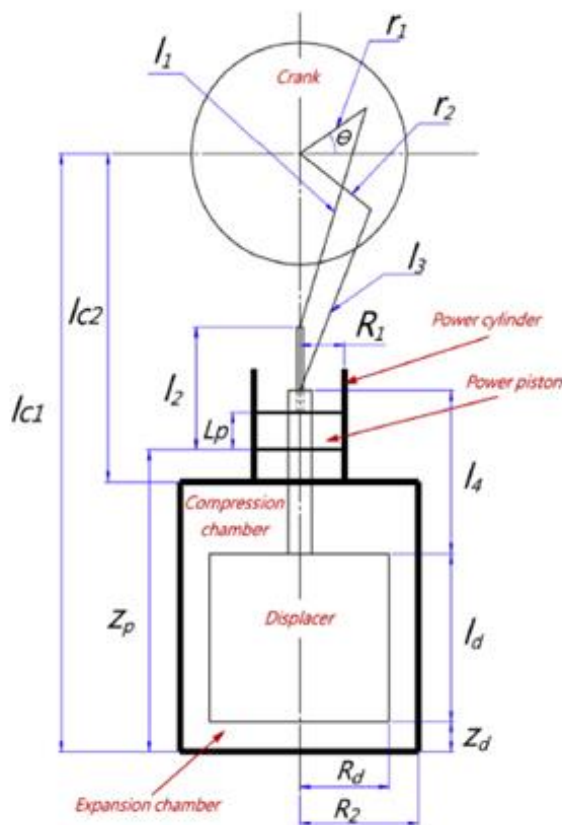
The purchased Educational Model Stirling Engine (EMSE) consists of two air-tight cylinders stacked on top of each other, the larger cylinder at the bottom is the displacer cylinder and the smaller cylinder on top being the piston cylinder. The displacer cylinder houses a displacer which allows for an annulus between itself and the displacer cylinder while the piston cylinder houses a piston fitting tight against the walls of the cylinder. The piston and the displacer are connected at 90 degrees to a flywheel. Air tightness is a crucial factor in ensuring the functionality of the engine and was the issue that was faced when building the models. A see-through displacer cylinder was implemented to clearly visualise the functioning of the engine. Air is the working fluid used in the Stirling engine.

The EMSE model is a lightweight engine weighing 300 g made of thin glass and stainless-steel components measuring a total height of 120 mm and a base circumference of 100mm. the engine is rated to a maximum speed of 180-200 rpm and the minimum temperature difference for it to function is 293 K. The piston of the engine comprises of two glass cylinders nestled within each other, while the displacer cylinder (similar to the built models) is made of foam material.

The EMSE is expected to be run on boiling water and is not meant to be exposed to direct flames, hence, the experimental temperature shall not exceed 373 K. Fig. 4-1 shows the Educational model Stirling engine. The dimensions of the engine are provided as per Fig. 4-2.



**Fig. 4-1: Educational model Stirling engine (EMSE)**



Length	Measurement
Lc1	85 mm
Lc2	65 mm
r1	4 mm
r2	4 mm
R1	7.85 mm
R2	45 mm
Rd	42 mm
l1	44 mm
l2	14.1822 mm
l3	44 mm
l4	26 mm
ld	9 mm
Lp	1.5 mm

**Fig. 4-2 : EMSE dimensions**

### 4.2.1. Kato Experiment

Yoshitaka Kato [83] designed, built and tested on a Low temperature differential, gamma-type Stirling Engine and presented indicated diagrams of Pressure-volume. Varying the heat source temperature between 75 to 95 degrees Celsius with air as the working fluid and no separate regenerator. While the exact dimensions of the engine tested is different, Kato's system is similar to the experiment undertaken in this research work and has been utilised to compare the relationships between the results obtained. Fig. 4-3 shows the Kato apparatus.

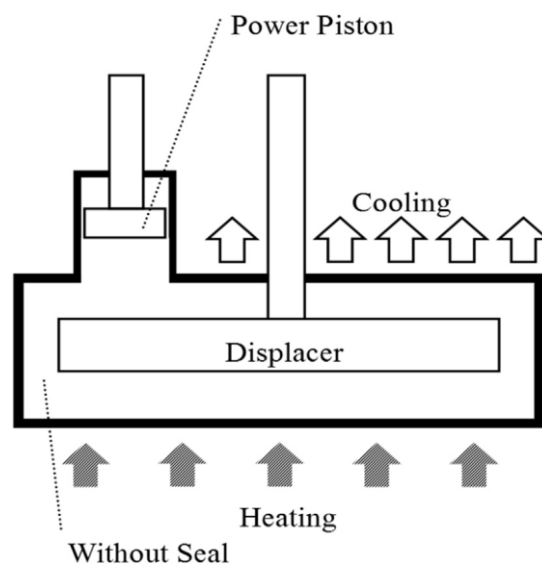


**Fig. 4-3: Kato Experiment set-up [83]**

Kato created two scenarios, one where the cold side temperature was controlled (Series C) and the other where the cold side temperature was not controlled (Series N). He noticed that for both the cases of controlled and uncontrolled cold side temperatures, the indicated work maintained an upward trajectory in relation to the hot side temperature. There were no differences identified in the indicated work on the basis of control or non-control of the cold side temperature. The cycle speeds observed were decreasing as the temperature in the hot side was increased. This was unexpected as the cycle speed is expected to increase as the temperature increases, unless components of the engine deformed somehow due to the increase in temperature leading to higher friction. The experimental findings for cycle speed and indicated work as obtained by Kato is demonstrated in Fig. 4-4.

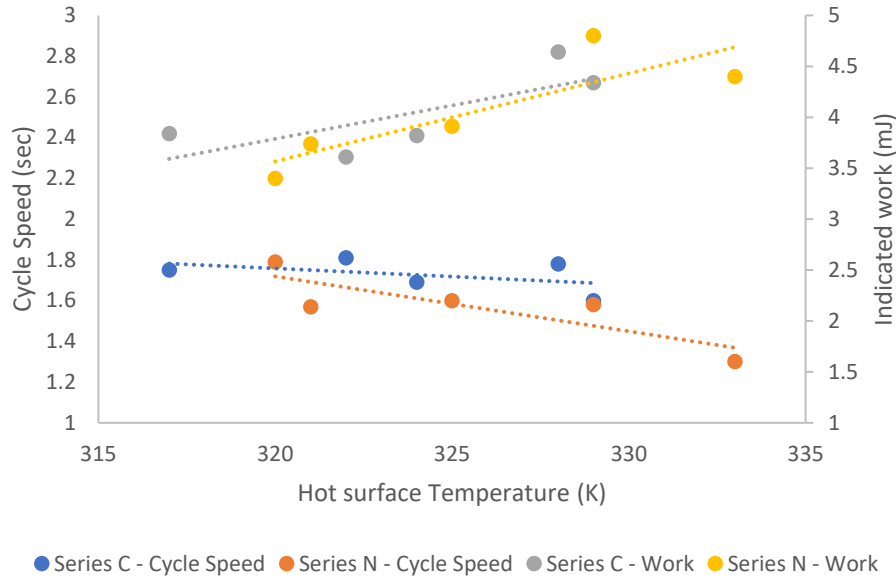


**Fig. 4-4: Kato's experimental findings [58]**

In most cases, there is no marked difference in the P-V diagram of the tested engines. Kato has provided only one cycle of the engine operation. Fig. 4-5 demonstrates the P-V diagram demonstrating the indicated work done by the Stirling Engine tested by Kato.

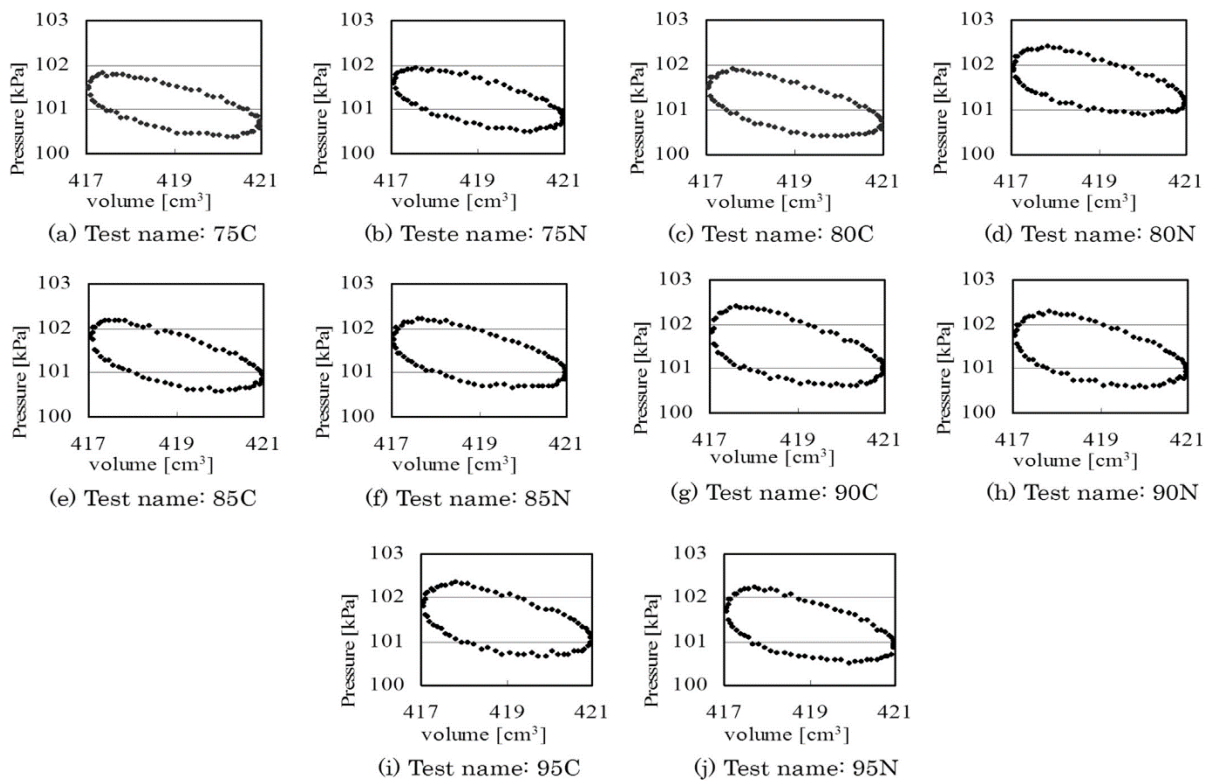


**Fig. 4-5: Indicated Diagrams of experiments conducted by Kato showing both series N and Series C results [58]**

### 4.3. Experimental Equipment

#### 4.3.1. Heating Plate

To provide heat to the Stirling engine the MAPLELAB ceramic hotplate / stirrer range SHC-1 was used. The device can generate heat from 293 K to 773 K and contains a feedback control to ensure that the plate doesn't overheat. There is a dial for controlling the temperature of the plate. The stirring function is not used for the device. Fig. 4-6 shows the hotplate.



**Fig. 4-6: MAPLELAB ceramic hotplate / stirrer**

The Maple ceramic hotplate is not calibrated, as a result, the EMSE was placed on a raised platform to allow a more controlled heat transfer to the bottom of the engine. Due to the small size of the EMSE and the requirement of the device to remain air tight, the temperature measurements are taken on the outer surfaces of the top and bottom plates of the engine and a single hole has been drilled on the top surface for the measurement of the pressure in the displacer chamber. The piston of the EMSE is made of glass and is very fragile, a trial hole on the measurement device caused the piston cylinder to shatter.

#### 4.3.2. Pico Tech Thermocouple and Logger

The temperature on the top and bottom surfaces were measured using type K, fibreglass insulated and exposed tip thermocouples and were recorded using USB TC-08 Thermocouple Data Logger. The measurement range of the device is between 240 K to 623 K with a

resolution of 0.001 K, temperature accuracy of Sum of  $\pm 0.2\%$  of reading and  $\pm 0.5$  K and voltage accuracy of the Sum of  $\pm 0.2\%$  of reading and  $\pm 10$   $\mu\text{V}$ . The maximum temperature during the testing was expected to reach 373 K based on the specifications of the EMSE, the error limits can be set to  $\pm 0.5$  K. In total, 6 thermocouples were used for the testing. 2 Thermocouples were mounted on the top plate and two at the bottom and a Further two thermocouples were placed inside the displacer cylinder; one curved to the top to take the temperature reading of the top section inside the displacer cylinder and the other curved towards the bottom to take measurements of the bottom section of the displacer cylinder. The thermocouples connected to the EMSE were SE001 Thermocouple made from Nickel Chrome/Nickel Aluminium (NiCr/NiAl) from Pico Tech with tolerances established to be 73 to +313 K:  $\pm 1.5$  K or  $\pm T \times 0.004$  as per IEC 60584-2:1993 / BS EN 60584-1:2013 under Tolerance class 1. An uncertainty of  $\pm 1.5$  K was added to the error range. Thus, the total uncertainty in the temperature reading was established to be  $\pm 2.0$  K. Fig. 4-7 shows the USB TC-08 data logger and the probe attachments.



**Fig. 4-7: Temperature logger and Thermocouple set-up**

The USB TC-08 Thermocouple Data Logger was connected to a laptop to record the temperature data using the proprietary data logging software PicoLog 6 which is a real-time data collection and display software. Temperature was recorded ever 100 ms. The data can then be exported as clipboard image, PDF and CSV. A typical reading of the Stirling Engine system is represented in Fig. 4-8.

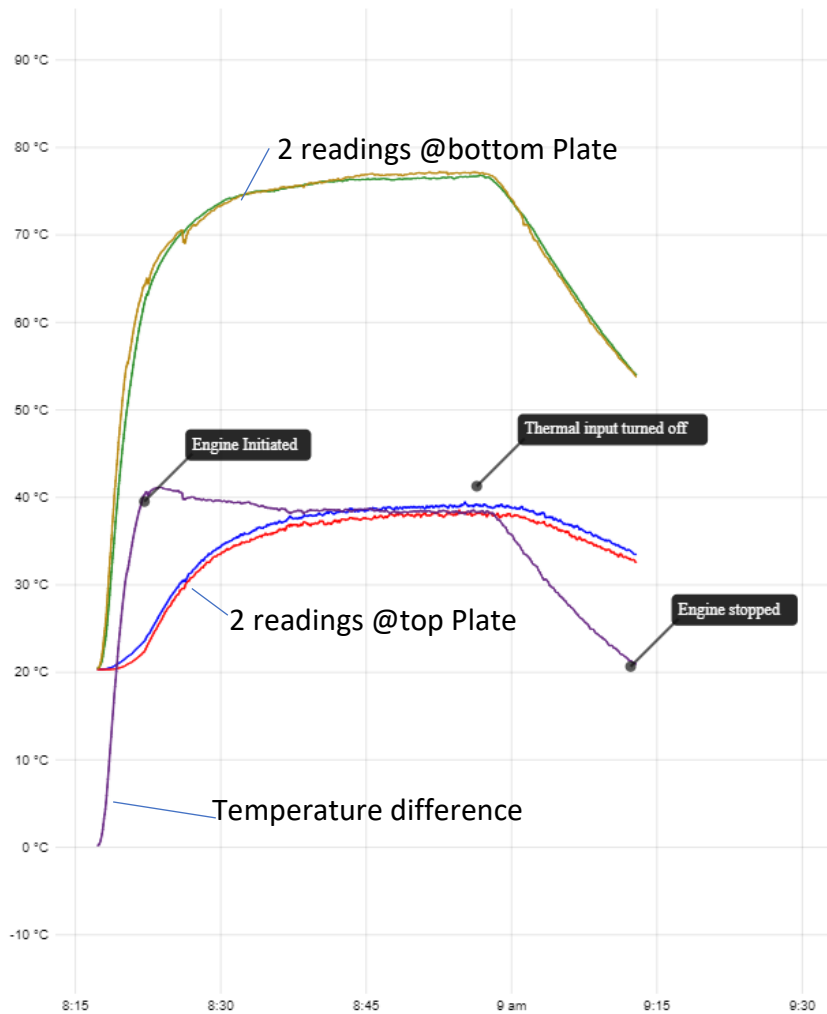


**Fig. 4-8: Typical Thermal data**

#### **4.3.3. Resistance Temperature Detector (RTD) Thermometer**

For the initial temperature measurements, the temperatures on the top and bottom surfaces of the EMSE was measured using thermocouples and recorded on the Omega HH804 resistance temperature detector (RTD) thermometer. The measurement range of the device is between 73 K to 1023 K with a resolution of 0.1K and an accuracy of  $\pm(0.05\% \text{ reading} + 0.2 \text{ K})$ . The maximum temperature during the testing was expected to reach 373 K based on the specifications of the EMSE, the error limits can be set to  $\pm 0.25 \text{ K}$ . The surface mounted, self-adhesive thermocouples connected to the device were PT100, SA1-RTD spec also from Omega and calibrated to between  $\pm 0.15 \text{ K}$  at 273 K and  $\pm 0.35 \text{ K}$  at 373 K DIN Class A. Since generally higher temperatures were being considered, an uncertainty of  $\pm 0.35 \text{ K}$  was added to the error range. Thus, the total uncertainty in the temperature reading was established to be  $\pm 0.65 \text{ K}$ .

The standard tolerances for Temperature and resistance of the self-adhesive backing for targeted Class A sensor elements on curved and flat surfaces are shown in Table 4-1. The IEC-751/BS EN60751 1996 standard tolerances for Pt 100  $\Omega$  RTD elements.

**Table 4-1: RTD Tolerance chart**

in K	$\pm K$	$\pm \Omega$
73	0.55	0.24
173	0.35	0.14
273	0.15	0.06
373	0.35	0.13
473	0.55	0.2

The Omega HH804 device was connected to a laptop to record the temperature data using the proprietary data logging software for the HH800 series of products. Fig. 4-9 shows the Omega HH804 RTD thermometer and PT 100 probe.



**Fig. 4-9: Omega HH804 RTD thermometer with PT 100 probes connected to EMSE**

#### 4.3.4. Pressure Scanner

The Pressure in the displacer chamber is measured using the Scanivalve DSA 3217 Pressure Scanner. The device contains 16 transducer pins for individual reference pressure monitoring with an outer diameter of 1.6 mm. plastic tubing of 1.4 mm ID was purchased and formed a connection between the device pin and the single hole drilled on the top plate of the EMSE. The software records the Pressure value of all the 16 ports and the reference values required for calibration of the transducers. At low pressure recordings, the accuracy of the transducer is  $\pm 0.12\%$ . Fig. 4-10 shows the Scanivalve DSA 3217 Pressure Scanner.



**Fig. 4-10: DSA3217 Pressure Scanner with port 1 connected to EMSE**

The temperature working range of the scanner is 273 K to 333 K. Which is another reason why the pressure measurement is only carried out on the top surface of the EMSE displacer cylinder and not the bottom. Based on initial experiments, the temperature of the scanner reached a maximum of 307 K with the temperature at the top of the displacer cylinder reaching a maximum of 314 K. The temperature at the bottom of the displacer cylinder reached in excess of 373 K in some cases. The Maximum thermal error at this scale is  $\pm 0.001\%$  of the full scale/K. Since the value is very small, no temperature compensation has been considered for the analysis.

The recording from the scanner saved using the Scanivalve proprietary software DSALink4. The DSA unit transfers data to the DSALink4 unit using an ethernet cable. The scan settings are applied to obtain a pressure recording in psi every 0.016 seconds taking 62.5 readings every second. The system was then calibrated using the CALZ button on the software. Calibration is carried out before each recording. The DSALink4 interface is demonstrated in Fig. 4-11.

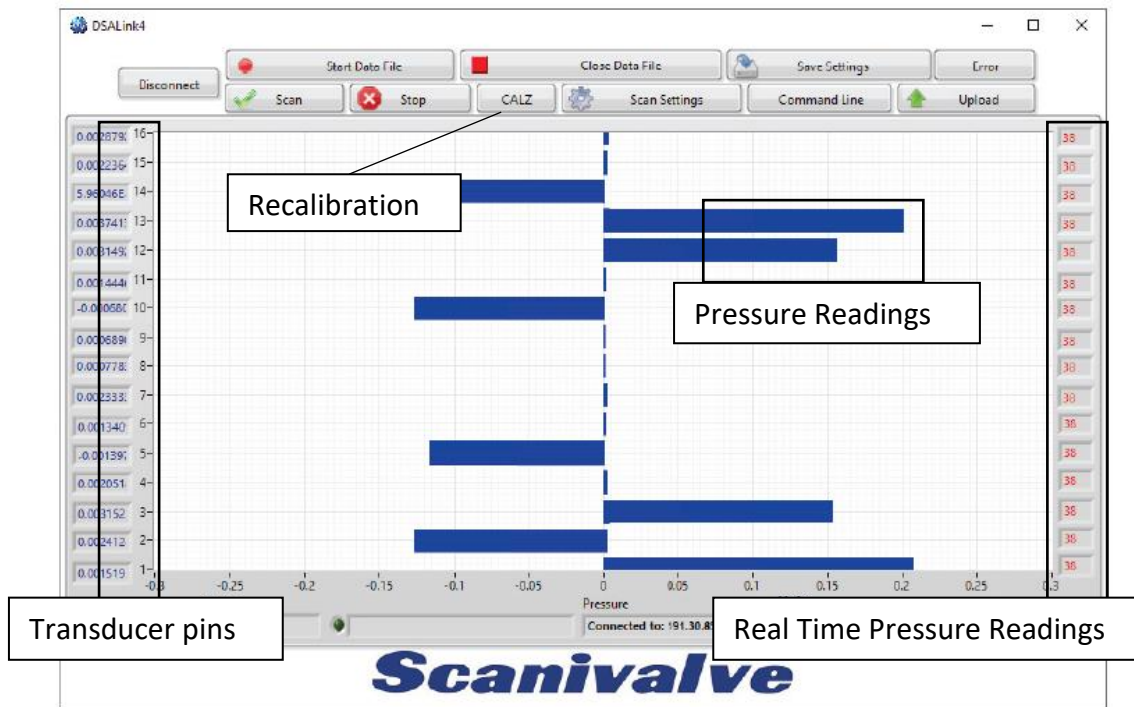


**Fig. 4-11: DSALink 4 pressure data acquisition software**

#### 4.3.5. Thermal Imaging Camera

The FLIR T650sc thermal imaging camera was utilised to visualise the temperature flow inside the displacer of the Stirling engine. The camera is capable of high-resolution video recording and the recording of temperature from a distance. The camera is adept to an accuracy of  $\pm 1$  K or  $\pm 1\%$  of temperature reading of an object within 278 K to 393 K which is a suitable range for the experiment. For uncertainty calculations,  $\pm 1$  K error range was considered for the calculations.

While relatively accurate, recordings using the FLIR thermal imaging camera produced files of size 1-2 GB and required a lot of storage space. Since more accurate measurements were possible using the RTD thermometers and no appreciable information was obtained using the visual recordings, only two recordings were taken using the thermal imaging camera. Fig. 4-12 shows the FLIR T650sc Thermal Imaging camera.

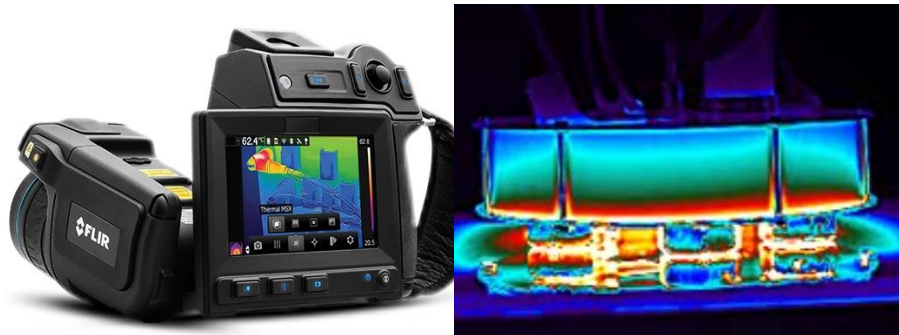


**Fig. 4-12: FLIR T650sc Thermal Imaging camera**

A demo version of FLIR Research Studio software was used to record the data on the computer at the rate of 30 readings per second. The software allows to analyse on both live and recorded data. Also allows flexible selection of temperature range to highlight the principal area of interest. The video captured and the data recorded can be exported from the software in MPEG4 and CSV formats.

#### **4.4. Experimental Set-up**

The tests were conducted in a closed Workshop at the owned by Free running Building at the Advanced Manufacturing Park, part of the Advanced Manufacturing and Research Centre (AMRC) of the University of Sheffield. The workshop maintained a room temperature of between 293 K and 297 K ensuring adequate conditions for the testing of the EMSE. The setting of the experiment is as Fig. 4-13.

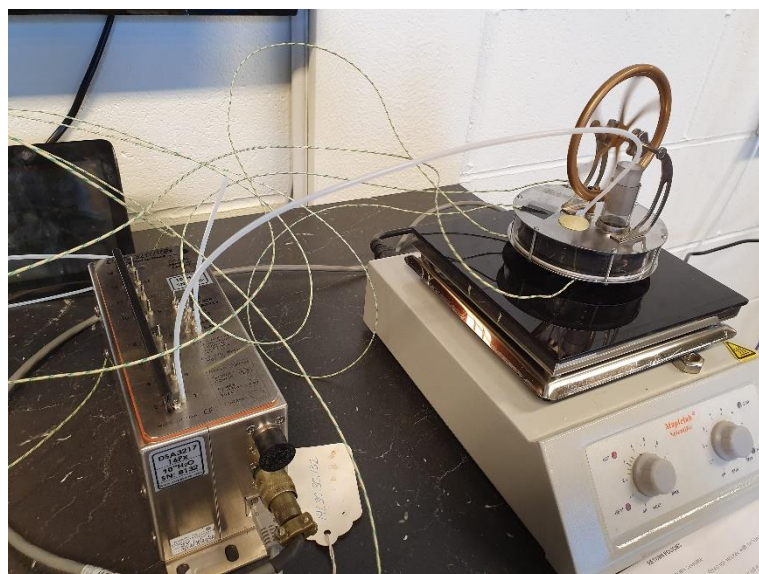


**Fig. 4-13: thermocouple and transducer set-up**

A 2mm hole is drilled on the top plate using a pillar drill by restricting the drive of the pillar drill such that it doesn't affect the displacer in the cylinder. After the hole has been drilled, a 2mm tube is forced into the hole and the connection is sealed using milliput epoxy resin. The epoxy resin ensures that a solid connection is formed and allows for reasonable mobility of the engine. The other end of the 2mm tube is connected to pin 1 of the pressure scanner.

Then 4 thermocouples are then connected on the top and bottom surfaces of the displacer cylinder (two on top, two at the bottom). The thermocouples are secured with electric tape. In order to stop the thermocouple wire at the bottom of the displacer cylinder the engine from touching the top surface of the heating plate, the wires need to be carefully guided along the base of the EMSE which is raised above the heater plate with the screw nuts securing the EMSE. The top thermocouples were connected to port 5 and 6 of the TC-08 logger, the bottom thermocouples were connected to ports 5 and 6 and the internal thermocouples were connected to ports 1 and 8.

It was ensured that all the engine mechanisms are functioning smoothly, there was no sliding noise as the displacer shaft oscillates through the top plate sealing the displacer, similarly it was ensured that there no such noise when the piston oscillates in the piston cylinder. This may be a result of growing friction at the contact points. In the case of such noises being observed, the areas were lubricated with pencil lead as per directed by the engine manufacturer. No oil-based lubricants could be used on the EMSE.

To calibrate the heating plate, an initial temperature analysis test was performed to assess the bottom surface temperature of the displacer chamber corresponding to the temperature as indicated on the heating plate. The heating plate dial is then marked to make the setting of the temperature quicker and so that there are no changes made to the set-up during the recording and all the changes that are recorded are because of the operation of the EMSE.

#### **4.5. Experimental Procedure**

Before starting off the recording process, it was ensured that the temperature of the top and bottom surfaces of the displacer chamber of the Stirling engine are similar and at the equilibrium temperature as expected at room temperature. In this case that temperature was between 293 K to 297 K. Between a resting time of 2 hours was required to allow for the

equipment to reach said equilibrium temperature. The DSALink 4 software is Calibrated by initiating the CALZ button.

The Heating plate is turned on, and the dial is set on the heating plate. Simultaneously, the recoding of the pressure scanner and the PICO TC-08 logger is initiated. This procedure is not time sensitive. The temperature of the system is allowed to rise and once the temperature difference between the top and bottom of the displacer cylinder has crossed 293 K, the flywheel of the Stirling engine is given a clockwise push to start the engine.

The thermal camera was utilised (initially) instead of the temperature probes to record the temperatures established at the top and bottom surfaces of the EMSE and in doing so provide a visual representation of the working process of the Stirling engine. Before initiating the heating plate, the camera is focused on the EMSE and two location identifying the top and bottom surfaces of the EMSE were mapped out in the FLIR research studio software. The recording is initiated, simultaneously with the heating plate and the pressure scanner.

As the temperature at the bottom surface reaches a desired based on the calibration of the heating plate. The engine was allowed to run for at least 10 minutes to let the engine stabilise between two temperature points across the top and bottom of the displacer chamber.

After 30 minutes of captured data, the heating plate is turned off and the recordings stopped to allow the engine to cool down and return to the equilibrium temperature. The recordings taken in this time allows for a stabilisation period after which the temperatures at the extremes of the displacer chambers have reached a no fluctuation point. Thus, obtaining a steady state based on which transient numerical analysis will be based upon.

Upon reaching this steady state, a video camera (smartphone camera) was used to record the working of the EMSE. This was done to measure the rotational speed of the EMSE at the stabilised differential temperatures. The Computational analysis will use the values of the top and bottom surface temperature and the rotational speed of the EMSE to generate a model. The pressure generated in the model will then be compared with the pressure recorded to validate the computational model.

The experiment is repeated to obtain recordings at a various temperature points of the bottom surface of the EMSE as well as different conditions of the EMSE. The conditions included:

1. **New EMSE** – These include testing of newly purchased EMSE model
2. **Inspected EMSE** – This includes testing of models that were opened, a hole has been drilled at the top of the EMSE and connected to a transducer to record the pressure.
3. **Drilled EMSE** – Holes were drilled into the displacer cylinder of this model for recording internal temperature data, however, no probes were placed
4. **Probed EMSE** – EMSE system including internal temperature recording with probes

Bottom surface temperatures were set between 313 K and 373 K. The results were then analysed and presented and compared to CFD analysis data to validate the CFD analysis.

#### **4.6. Temperature Calibration**

This section of the chapter describes how the temperature calibration is carried out on the recorded temperature readings taken from the test equipment used for conducting the experimental work. The difference in temperature between the top and the bottom surface of the Stirling Engine was monitored in order to determine the stabilisation period and thus indicate the stabilised time. Only the readings in the stabilised time will be considered for establishing the CFD parameters. The total recording time for the experiments spanned close to 30 minutes. Within 15 minutes, Stabilisation for most of the experiments was achieved, however, for a few of the experiments the EMSE was allowed to run to see if there are any changes in the stabilisation if the experiment would continue. Since the experimentation begins with both the top surface and the bottom surface at the same temperature requiring achieving the test temperature, the stabilisation time for each experiment is different. The temperature at the bottom surface of the engine begins to increase in temperature almost instantaneously with the temperature at the top surface increasing more gradually as seen in all the cases investigated. demonstrates the time dependent temperature readings recorded by the TC-08 logger for the different experimental scenarios. Fig. 4-14 shows the three regions of experiment including the stabilisation period, the region of data analysis and the shutdown for a typical EMSE. The shutdown procedure is not recorded for all the test recordings. Just

one of the tests was recorded in such manner for the purpose of demonstrating the three phases of the Test.

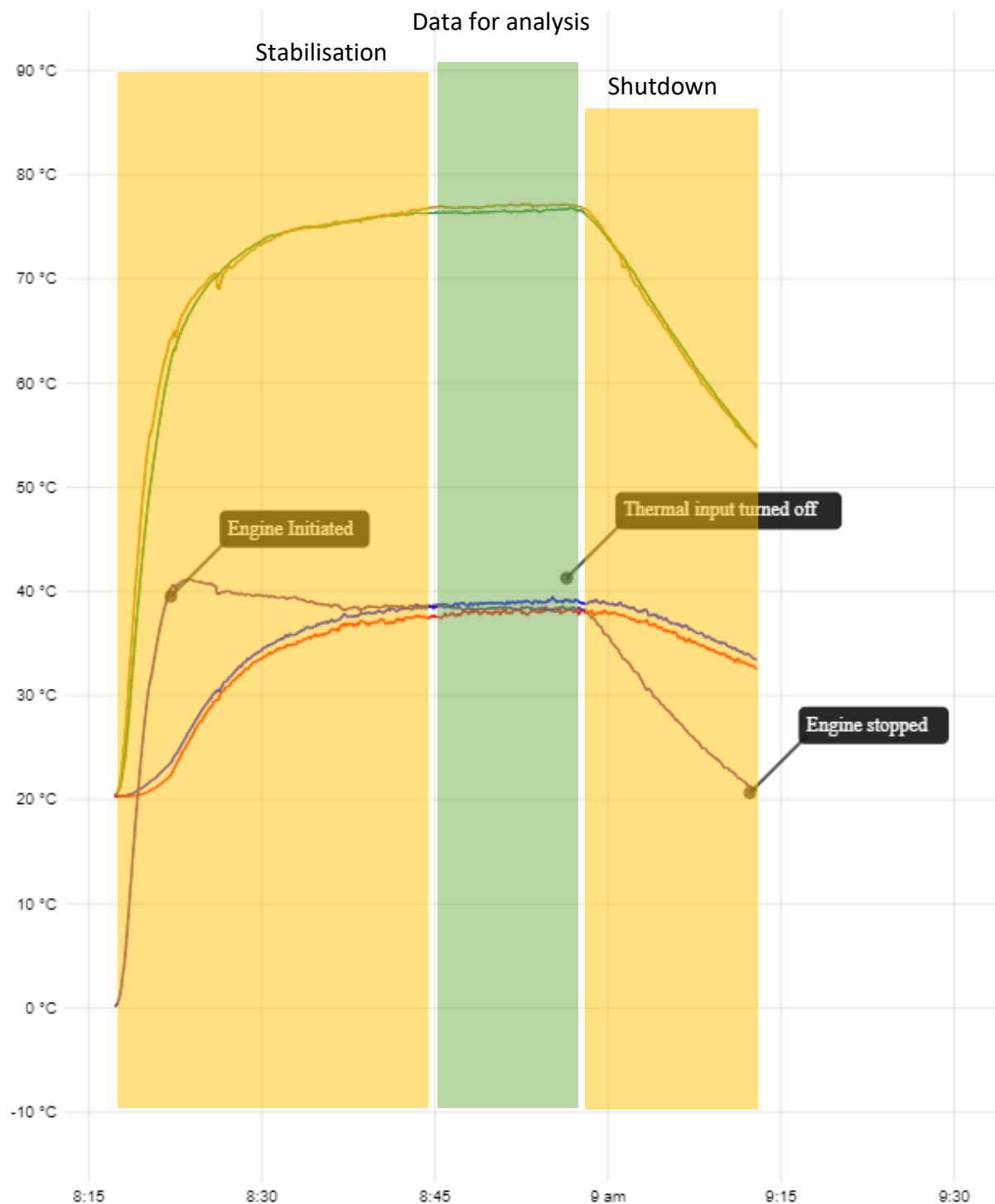


**Fig. 4-14: Typical temperature graph of EMSE test**

The stabilised temperature for the top and bottom surfaces of the Stirling engine is used to set-up the temperature profile of the computational analysis of the engine. The temperature

profiles of the four different test scenarios; new EMSE, Inspected EMSE, Drilled EMSE and Probed EMSE are similar to the graph shown in Fig. 4-14. However, for the probed EMSE two other graph lines will be included to demonstrate the temperature recordings inside the displacer cylinder as per shown in Fig. 4-15.

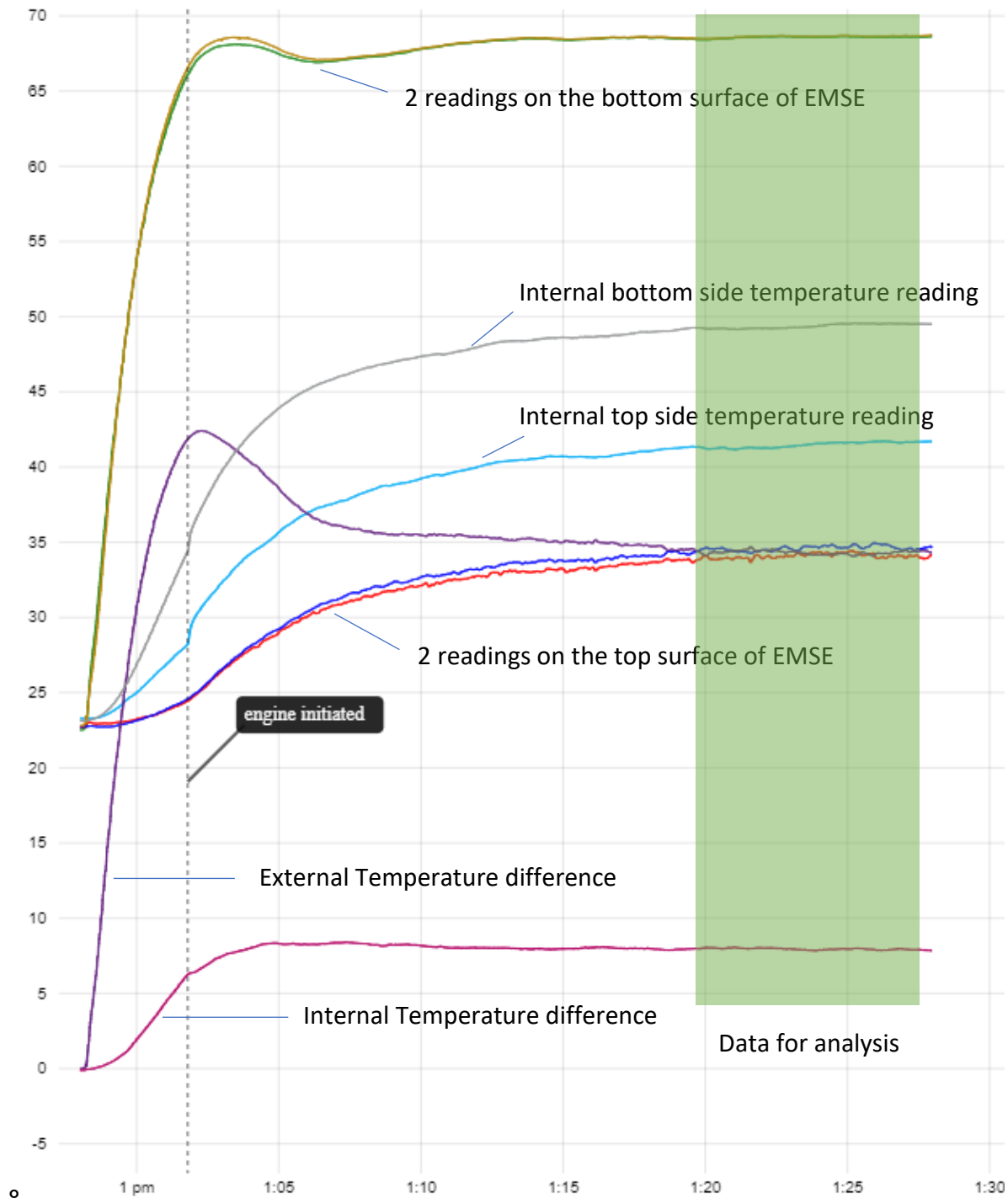


**Fig. 4-15: Typical recorded data for inspected EMSE**

Based on the pressure stabilisation only 10 seconds of the temperature data will be analysed.

#### **4.6.1. Impact of Sensor Location and Response Time**

In order to minimise intrusion onto the Stirling engine cylinder, 2 incisions have been made into the Stirling cylinder to measure the temperature one focusing on the top section of the Stirling Engine and the other focusing on the bottom section of the Stirling engine. Ideally more sensors were needed to obtain a larger coverage on the space, however, drilling holes into the cylinder is not ideal and therefore, a cylinder built to incorporate probes would be better suited for the study. The Feasibility of the number of intrusions and its impact on the performance of the engine is also not known and requires further investigation.

The conversion time of 100 - 200 ms from the data logger is a suitable response time for the experiment as an instantaneous time is not required for the purpose of the project, rather a stabilised temperature is more essential.

## 4.7. Temperature Visualisation

In this phase the temperature flow inside the displacer of the Stirling engine is visualised using a FLIR thermal recording camera. The average temperatures in two different regions were measured as shown in Fig. 4-16. The thermal camera was positioned such that it was able to clearly focus on the Stirling Engine.

The thermal gradient of the temperature has been visualised for an EMSE working scenario between 338K hot area and 310 cold area. The temperature data was recorded for one hour from the start when the hot plate was turned on, all the way to the end of the test. A gradual increase in the displacer chamber was identified as is indicated in Fig. 4-17. as per obtained from the image generated by the thermal imaging software, FLIR research studio. The full recording has been attached in the form of supplementary material.

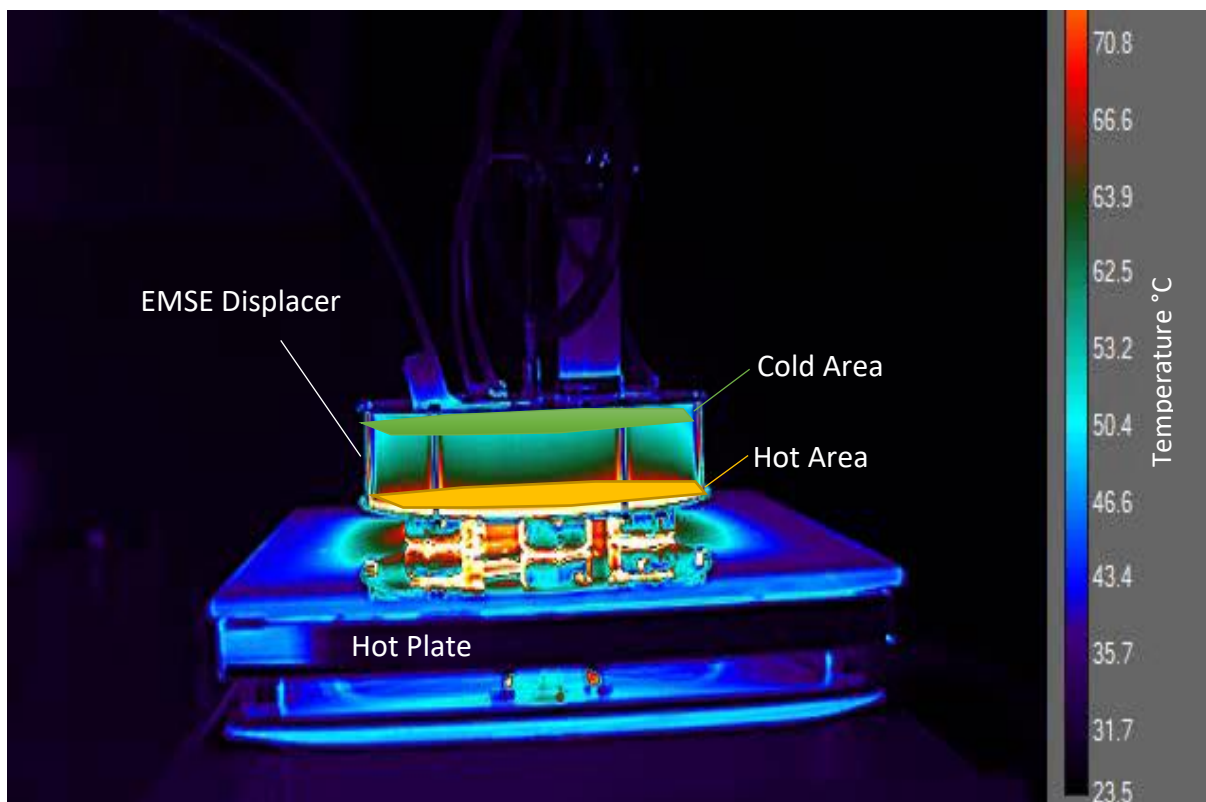
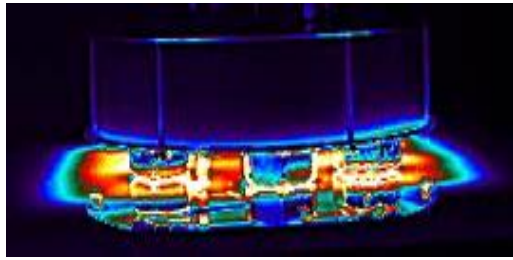
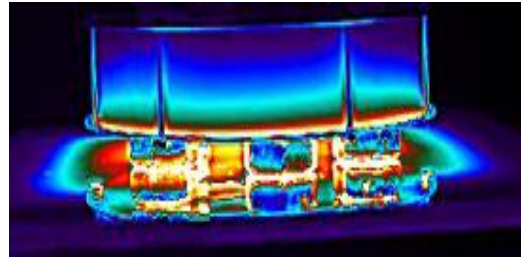


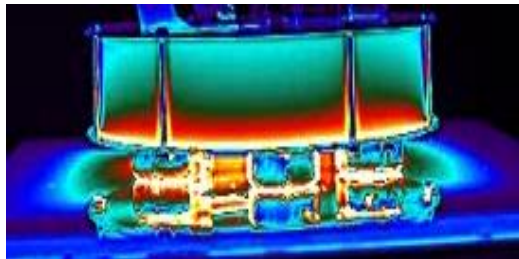
Fig. 4-16: Thermal image capture and interpretation.



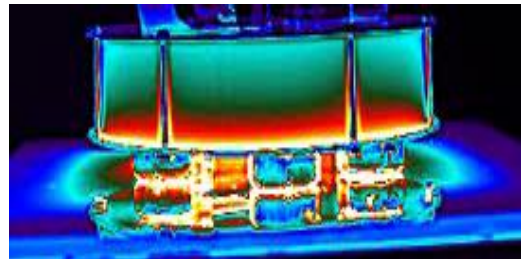
a. Start of test  $\Delta T = -0.02$  K



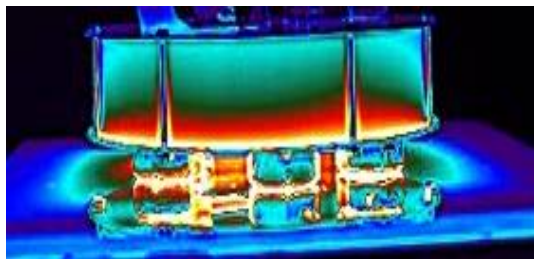
b. 5min into test  $\Delta T = 35.5$  K



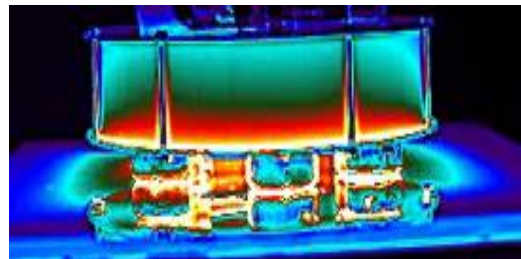
c. 10min into test  $\Delta T = 35.4$  K



d. 20min into test  $\Delta T = 35.4$  K



e. 30min (heat off)  $\Delta T = 35.4$  K



f. 40min  $\Delta T = 35.4$  K

**Fig. 4-17: Thermal flow visualisation of EMSE operation.**

Temperature data has also been captured using the thermal camera and has been presented as per shown in Fig. 4-18. This graph demonstrates relation between the temperature at the hot area and the cold area as obtained from the thermal imaging camera (TIC) and is compared against the thermocouple (Thermo) data for a similar temperature scenario.

The comparison demonstrates that there is an agreement between the temperatures in the two different scenarios. The temperature reading from the thermal imaging camera is based on a locked area that is set (see Fig. 4-16). The Heat plate is first allowed to reach the desired heating temperature and then the EMSE is placed on the heat plate for the thermal conduction to take place. This is the reason why the temperature is shown to rise faster in the Thermal imaging camera when compared to the thermocouple reading where the thermocouple is attached to the EMSE. As the test time progresses, the hot temperatures overlap. There is a slight difference in the temperature in the cold region which can be

attributed to difference in environmental conditions and further difference in the experimental set up for the two experiments.

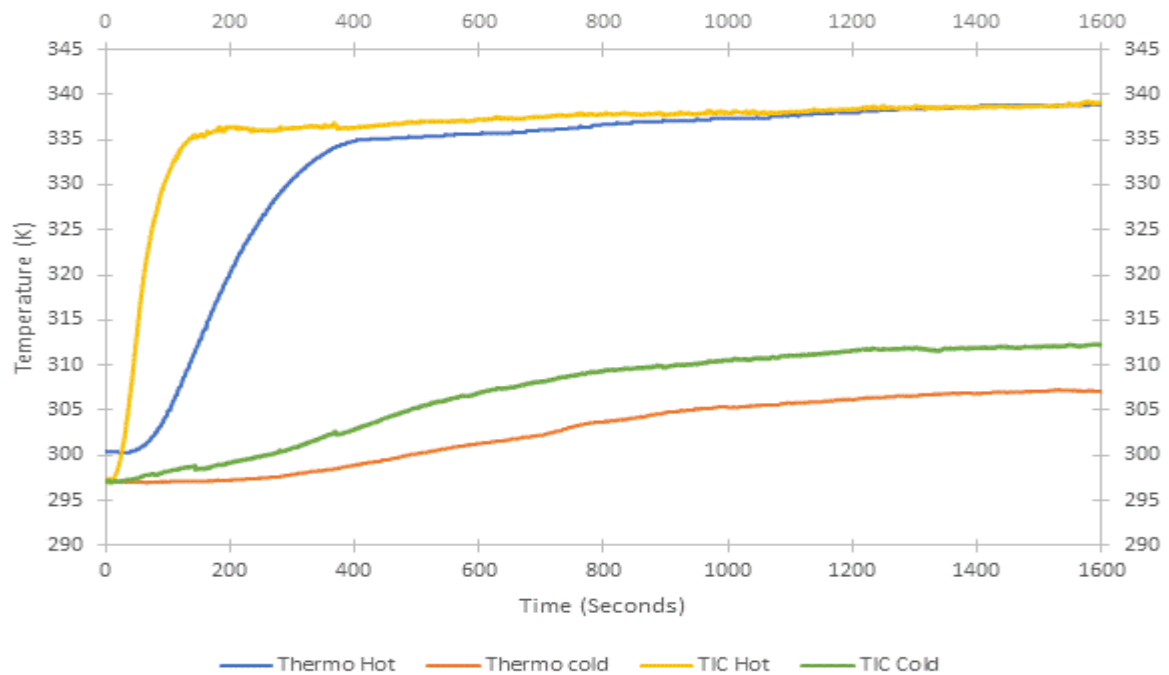


**Fig. 4-18: Thermal Imaging Camera (TIC) temperature data compared to similar test scenario using thermocouple (Thermo)**

Due to the agreement identified in the data between the thermal imaging camera and the data recorded using the thermocouple, it has been decided that thermo couples will be used for the remainder of the tests. Reducing the cost of the experiment. Furthermore, a more accurate measurement can be taken from inside the EMSE using the thermocouple when compared to the thermal imaging camera which measures the outer surfaces only.

#### **4.8. Pressure Recording**

This section of the chapter describes how the pressure recording was carried out on the recorded pressure data. Among the four sets of pressure data taken (for new, inspected, drilled and probed EMSE test scenarios), no pressure was recorded for the new EMSE. For the other types of tests performed, the pressure data is collected throughout the entire test time period. For analysis the pressure data was collected from the time period when the temperature was stabilised. The pressure data that has been collected oscillates at varying frequencies across the time period of the test. This is because the rotational speed of the engine is not consistent throughout the course of the test. 10 seconds of pressure data is

captured from the “data for analysis” region based on the inverse of the volume changes that have been calculated based on a set rotational speed of the EMSE. The rotational speed is set based on the frequency depicted in the recordings of the pressure data. Fig. 4-19 depicts a typical scenario of pressure calibration based on inverse volume and frequency calculations based on the oscillating frequency of the recorded pressure data.

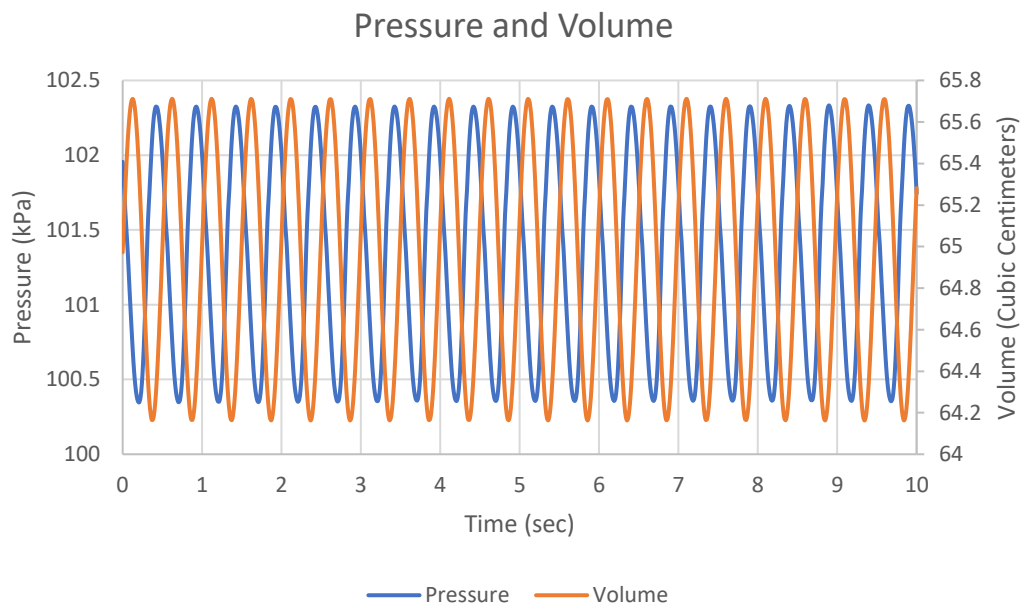


**Fig. 4-19: Typical pressure calibration based on volume change calculation**

#### **4.8.1. Impact of Sensor Location and Response Time**

In order to minimise intrusion onto the Stirling engine cylinder, 1 incision has been made into the Stirling cylinder to measure the pressure inside the cylinder. Ideally more sensors were needed to obtain a larger coverage on the space, however, drilling holes into the cylinder is not ideal and therefore, a cylinder built to incorporate probes would be better suited for the study. The Feasibility of the number of intrusions and its impact on the performance of the engine is also not known and requires further investigation.

The scan rate of 500 Hz from the data logger is a suitable response time for the experiment and assists in obtaining instantaneous pressure in order to map the full Stirling cycle.

#### 4.9. Rotational speed of the Stirling Engine

In this section, a relation between the rotational speed and the temperatures associated with the functioning of the Stirling engine are investigated. For the new EMSE, the rotational speeds of the Stirling engine were recorded based on video recording of the working of the Stirling engine. In order to record this data, the video play speed was reduced to 0.25 times of actual speed using VLC media player based on the video timeline and the rotation of the engine the values were recorded. VLC player addon Time V3.2 was used to obtain an accurate recording of the time to 1000<sup>th</sup> millisecond. The error factor for time is considered to be 0.25 milliseconds since the time jumps were larger than the smallest measurable time unit. For recording the number of rotations, the error consideration is  $\pm 0.25$  rotations. The rotational speeds of the new EMSE at various operating temperatures are as represented in Table 4-2.

**Table 4-2: Rotational speeds for new EMSE**

Test	Th (K)	Tc (K)	$\Delta T$	Rpm
21C_A	315.9	295.3	20.6	48
21C	317.8	297.0	20.8	42
27C_B	338.1	310.7	27.4	90
28C_B	335.0	307.4	27.6	90
31C_A	327.1	296.0	31.2	90
31C	338.1	306.8	31.2	87
39C	347.0	308.3	38.7	126
48C_A	347.1	299.0	48.1	156
48C	361.0	312.9	48.2	172.5
59C	376.1	316.6	59.5	196.5
62C_A	364.9	302.9	62.0	222

The temperature data for the new EMSE was obtained using Omega HH804 resistance temperature detector (RTD) thermometer with PT 100 probes and the data was logged using the Omega proprietary software.

For the Inspected EMSE, drilled EMSE and probed EMSE the rotational speeds are first recorded using the video method as described above, then the reading is fine tuned based on the frequency of the oscillations the pressure reading. This is done because, upon opening up the EMSE for inspection the rotational speed across the length of the tests were observed to be more uneven. In order to accurately record the rotational speed for the set pressure and temperature data the rotational speed had to be fined tuned to the data set. The rotational speeds of the inspected EMSE, drilled EMSE and probed EMSE are as per represented in Table 4-3 and Table 4-5 respectively.

**Table 4-3: Rotational speeds for Inspected EMSE**

Test	Th (K)	Tc (K)	$\Delta T$	Rpm
E6	343.5	309.5	34	118.1
E5	349.5	312	37.5	137.9
E4	350	311	39	101.8
E19	347.8	307.8	40	99.6
E20	348	308	40	90.1
E21	347.3	307.2	40.1	122.8
E17	348	307.8	40.3	101.9
E18	348.3	308	40.3	92.2
E24	352	310.5	41.5	123.6
E25	352.3	310.5	41.8	126.3
E26	352.5	310.6	41.9	127
E23	352	309.8	42.3	112.4

E22	352.8	309.5	43.3	128.1
E13	357	310	47	130
E14	357	310	47	120.4
E16	357	310	47	129
E12	357	309.5	47.5	121.1
E15	356.8	309	47.8	124
E7	362	314	48	142.8
E8	363	312	51	149

One of the earliest observations was that after inspection of the EMSE, it was unable to perform at lower temperature differences.

**Table 4-4: Rotational speeds for drilled EMSE**

Test	Th (K)	Tc (K)	$\Delta T$	Rpm
H12	349	310.1	38.9	106.1
H13	348.3	308.8	39.5	116.1
H14	348.8	309.7	39.1	111.6
H7	351.9	311	41	122
H5	353.6	311.4	42.2	128.3
H6	352.6	309.8	42.8	116.1
H11	354.8	311.5	43.3	138.1
H8	362.9	314.4	48.5	141.1
H9	362.1	313.4	48.8	157.7
H10	362	313.3	48.8	157.6

**Table 4-5: Rotational speeds for probed EMSE**

Test	Th (K)	Tc (K)	$\Delta T$	Rpm
HO14	341.6	307.3	34.3	62.1
HO9	344.7	307.3	37.4	69.9
HO10	344.7	307	37.7	66.2
HO12	352.7	310.4	42.3	75.2
HO13	352.8	310.1	42.6	73
HO11	352.4	309.6	42.8	70.9
HO2	361.1	311.9	49.2	62.7
HO3	362	312.4	49.6	72.8
HO4	361.3	311.5	49.8	69.8
HO15	363	312	51	78.5

The rotational speeds recorded were mapped against the temperature of the bottom surface of the EMSE (Th). While the rotational speed of the EMSE fluctuates for the inspected EMSE and subsequent modified EMSE, a general trendline can be observed between the values of the various models and the temperature. This trend is represented in Fig. 4-20.

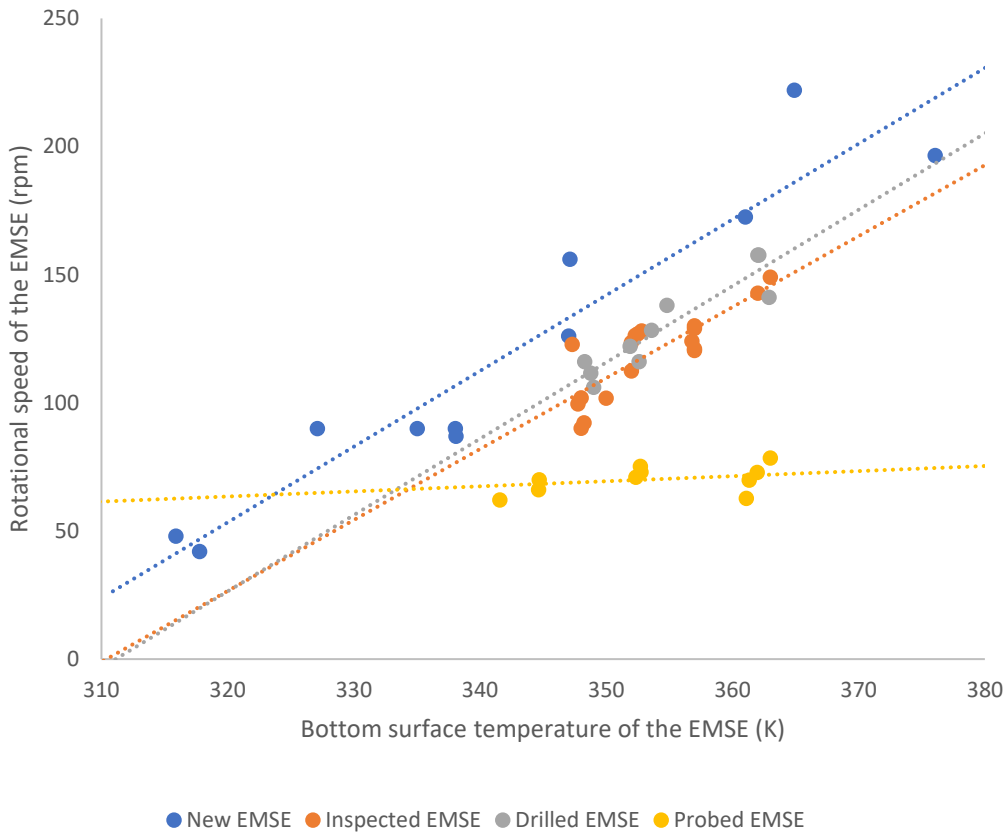


**Fig. 4-20: Relation between the rotational speed and bottom surface temperature of various EMSE**

As can be seen from the graph, the new EMSE (in general) demonstrates a higher rotational speed based on the temperature obtained at the bottom surface of the engine. Upon inspection of the engine, several factors could come into play including, the establishment of the hole for the pressure recording, tampering of the seal and slight miss alignments could occur that would reduce the capability of the engine. The slopes of new EMSE, inspected EMSE and the drilled EMSE are similar with a difference of 6% in the slope between the new EMSE and the inspected EMSE; and 1% difference in the slopes of the new EMSE and drilled EMSE.

The main difference in the relation comes for the case where the EMSE has been probed. In this case, since an external system was introduced inside the displacer chamber of the EMSE leading to two more holes that were required to be sealed and in this case the seal needed to be a pierced seal unlike the seal for the tubing of the connection to the transducer which was a protruding connection that could be sealed off better. As a result of this, the difference

between the slope of the new EMSE and the probed EMSE is 93%. The slope is slight (0.1983) and there is slight increase of rotational speed recorded with increase in the temperature.

Unlike the results presented by Kato[58], the results obtained in this experiment is more in tune with the expectations for the relation between the rotational speed and temperature to which the Stirling engine is subjected to.

#### **4.10. Temperature difference across Displacer Cylinder**

In this section the heat transfer between the bottom ( $T_h$ ) and top ( $T_c$ ) surfaces of the EMSE are investigated. This is done in order to observe if a definite relationship can be obtained between the top and bottom surfaces of the EMSE. The bottom surface of the displacer cylinder of the EMSE is subjected to heat from the heating plate which then heats up the top surface which is exposed to atmosphere as the engine runs. The general trend observed in this scenario is that, there is a definite separation between the two extremes of the cylinder that is consistently maintained as the EMSE functions after it has reached the stabilised position.

In order to make a fair judgement of the relation between the top and bottom surfaces of the EMSE, all tests are initiated with both the top and bottom surfaces at similar temperatures, at least within 5 K of each other. After inspection it was noticed that at lower temperatures the modified EMSEs didn't run., unlike the case with new EMSE tests. The new EMSE functioned for plate temperature differences between 20 K and 40 K, however, after inspection the EMSE failed to maintain continuous function at these temperatures. This may be attributed to the reduction in the sealing capabilities of the engine, alignment of the components and the increase in friction in the EMSE system.

The relation between the temperature of the hot surface and the cold surface is indicated in Fig. 4-21Fig. 4-21.

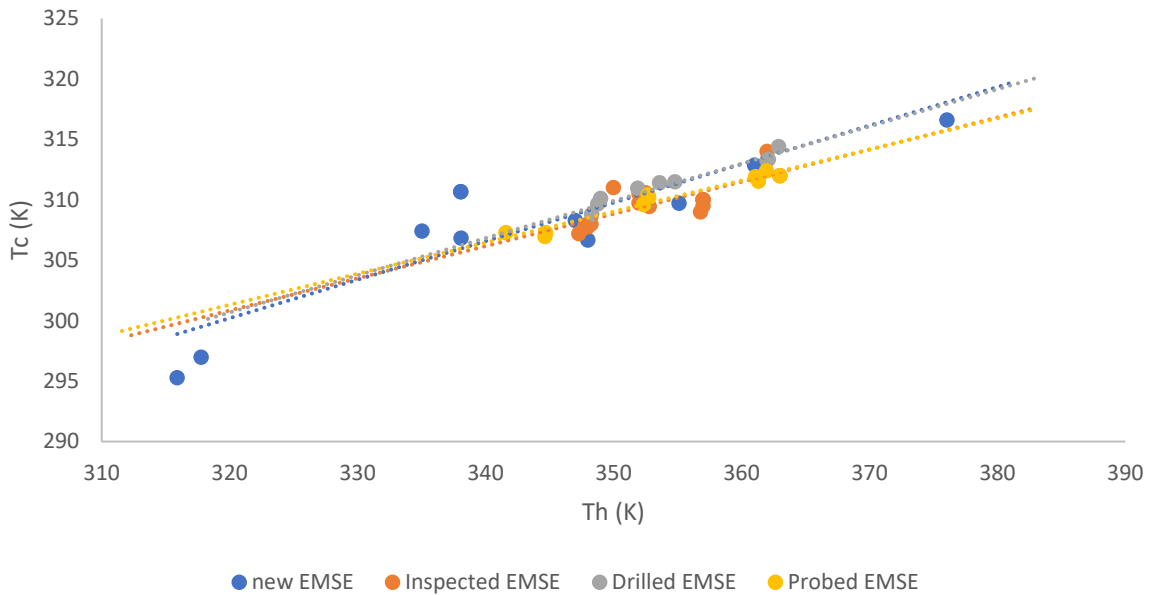


**Fig. 4-21: Temperature difference across displacer cylinder**

From the data, a general, linear trend is observed for all the EMSE case scenarios. In hot surface temperature range between 340 K and 365 K where all the EMSE were functioning, the linear expression derived from a standard linear trendline conforms to within 0.65% error and has a  $R^2$  value of 0.75. Fig. 4-22 demonstrates the cumulative graph showing a linear relation between all four stages of EMSE function for hot surface temperature between 338 K and 373 K.

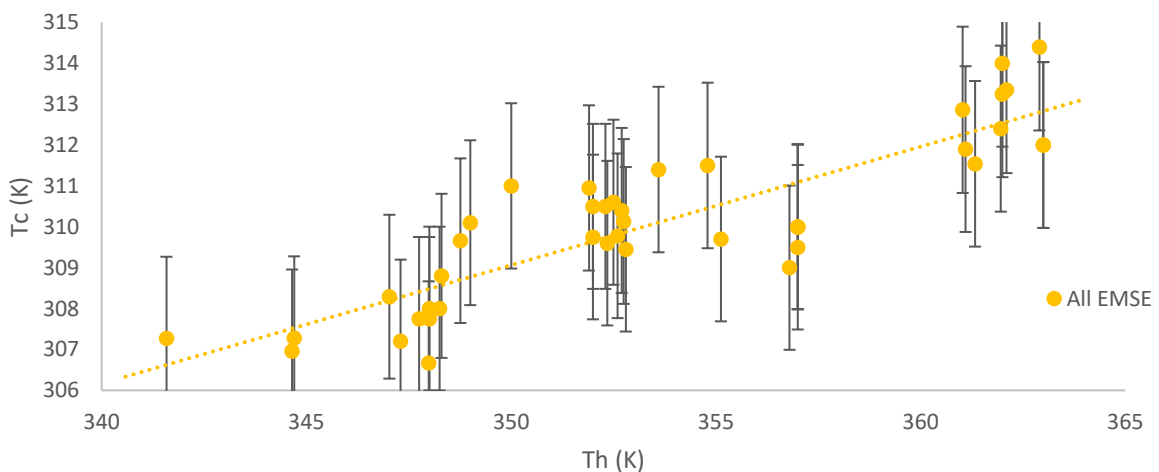


**Fig. 4-22 Cumulative temperature profile of EMSE**

Unlike The rotational speeds that showed a significant amount of deviation among the various modified EMSE, the temperature transmission between the bottom and top plates show a

more general linear trend. This indicates that the thermal transmission is not significantly affected due to the modifications made on the EMSE. Thermal transmission is solely based on the geometry of the Stirling engine.

For the inspected EMSE tests, temperature probes were installed inside the EMSE. Since it has been concluded that the temperature profile depends largely on the geometry of the Stirling engine, that temperatures recoded inside the Stirling Engine can be used to compare with the CFD data for validation. Since the top and bottom surfaces of the EMSE are made of an even layer of steel, there is a clear relation between the inside and outside of the EMSE. A graphical representation of the temperatures has been presented. Fig. 4-23 shows the relation between the temperatures of the inside and outer surface of the hot surface of the inspected EMSE and Fig. 4-24 shows the relation between the temperatures of the inside and outer surface of the cold side of the inspected EMSE.

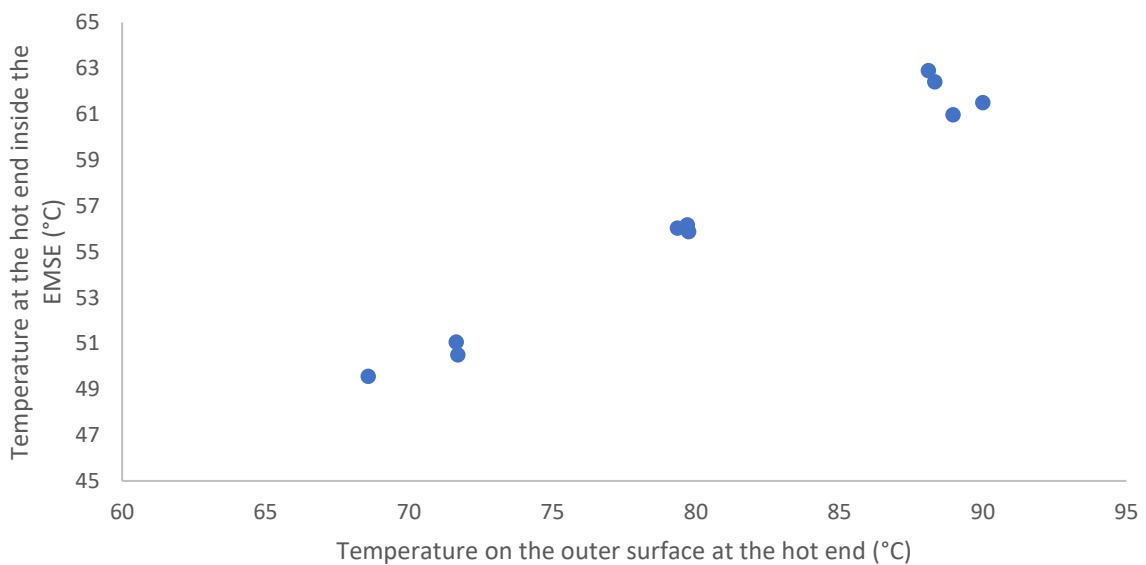


**Fig. 4-23: Temperature relation at the hot end of the inspected EMSE**

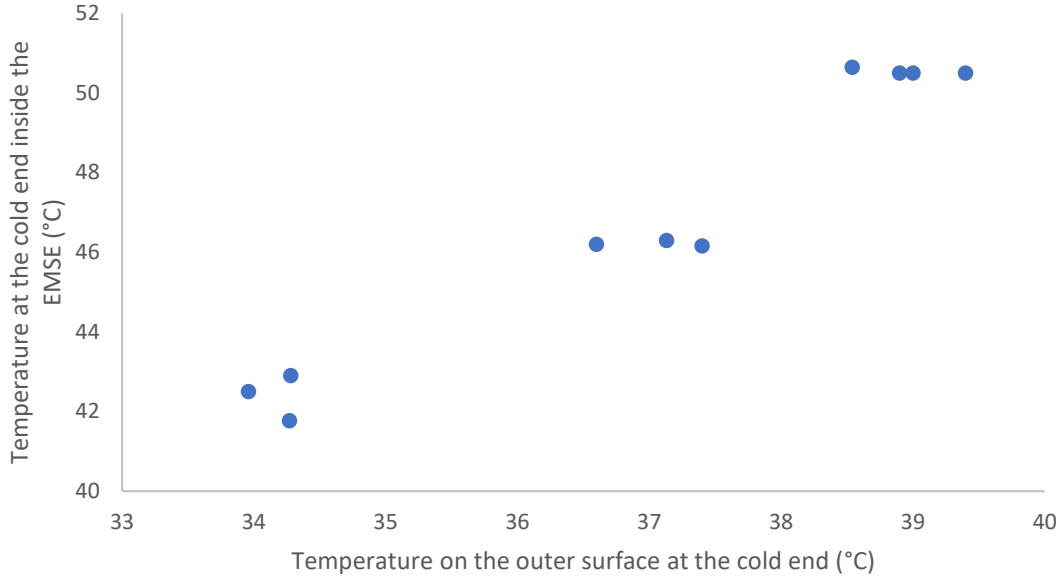


**Fig. 4-24: Temperature relation at the cold end of the inspected EMSE**

#### 4.11. Stirling Cycle Analysis

In this section the pressure recording is mapped against the volume of the Stirling engine. In order to map the pressure against the volume, first the volume is calculated based on the engine cycle speed at which the pressure has been recorded. Using motion dynamics as per established by Wen Lih Chen, The displacement of the Piston ( $z_p$ ) and displacer ( $z_d$ ) are represented below [56]:

$$z_p(\theta) = l_{c1} - \left( -r_1 \sin\theta + \sqrt{l_1^2 - r_1^2 \cos^2\theta} + l_2 \right) \quad \text{(Equation 1)}$$

$$z_d(\beta) = l_{c1} - \left( -r_2 \sin\beta + \sqrt{l_3^2 - r_2^2 \cos^2\beta} + l_4 + l_d \right) \quad \text{(Equation 2)}$$

The Velocities of the Piston ( $w_p$ ) and displacer ( $w_d$ ) are represented below [56]:

$$w_p(\theta) = r_1 \omega \cos\theta - \frac{r_1^2 \omega \cos\theta \sin\theta}{\sqrt{l_1^2 - r_1^2 \cos^2\theta}} \quad \text{Equation 3}$$

$$w_d(\beta) = r_2 \omega \cos\beta - \frac{r_2^2 \omega \cos\beta \sin\beta}{\sqrt{l_3^2 - r_2^2 \cos^2\beta}} \quad \text{Equation 4}$$

Where,

- $\theta$  is the starting crank angle determining the position of the power pistons
- $\beta = \theta - 90^\circ$  determining the position of the displacer. The piston and displacer are at  $90^\circ$  phase angle to each other.
- The rest of the factors are as described as per **Error! Reference source not found.**

The calculations are based on the crank angle of the engine, hence a reference list is created for each temperature scenario considering the a 10 degree change in crank angle. Two adjustments were made to ensure correlation between the experimental results and the calculated results. Firstly, since I did not have the means to continually measure the crank angle of the engine during the experimentation, the experimental results are then matched with the generated list by traversing the timeline of the experiment in order for the pressure recording from the experiment to match the inverse of the volume profile based on the calculated list. Secondly, the speed of rotation of the calculated list was adjusted to match the speed as per the experimental result. Adjusting the two factors assisted in obtaining two sets of graphs (experimental results and calculated results) overlapped and showed agreement.

It was observed that the cycle speed is not maintained at a constant rate throughout the length of the test. In some cases, the difference in the cycle speed is much larger than in other cases demonstrating over 20% deviation in the P-V cycle. Fig. 4- demonstrates two graphs to highlight the types of deviations observed during the testing of the inspected EMSEs. E7 test showed a maximum deviation of 7% while E10 showed a maximum deviation of 21%. A fluctuating system is much more difficult to model, as such this decision while provides a means to relate the results, it has high levels of error. Unfortunately, with LTD Stirling engines this is to be expected and thus only estimations can be expected for such models and is not a true depiction of the actual working of the engine due to the high error margins.

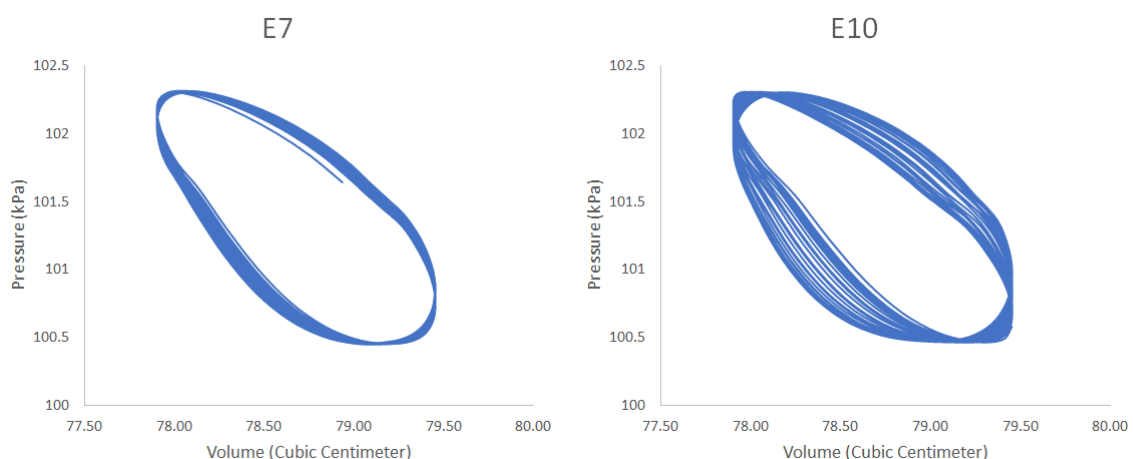


**Fig. 4-25 Highlighting the difference in cycle speed across the test period**

In order to obtain an average reading from the graph, a wave form equation was utilised to maintain a constant cycle speed and closely matching the P-V components. The cosine wave function to determine the Pressure is,

$$P_{corr} = P_{avg} + \left[ a \times \cos \left( \left( \frac{2\pi t}{T} \right) + TF \right) \right] \text{ (Equation 5)}$$

Where,

$P_{corr}$  is the corrected pressure

$P_{avg}$  is the average pressure recorded

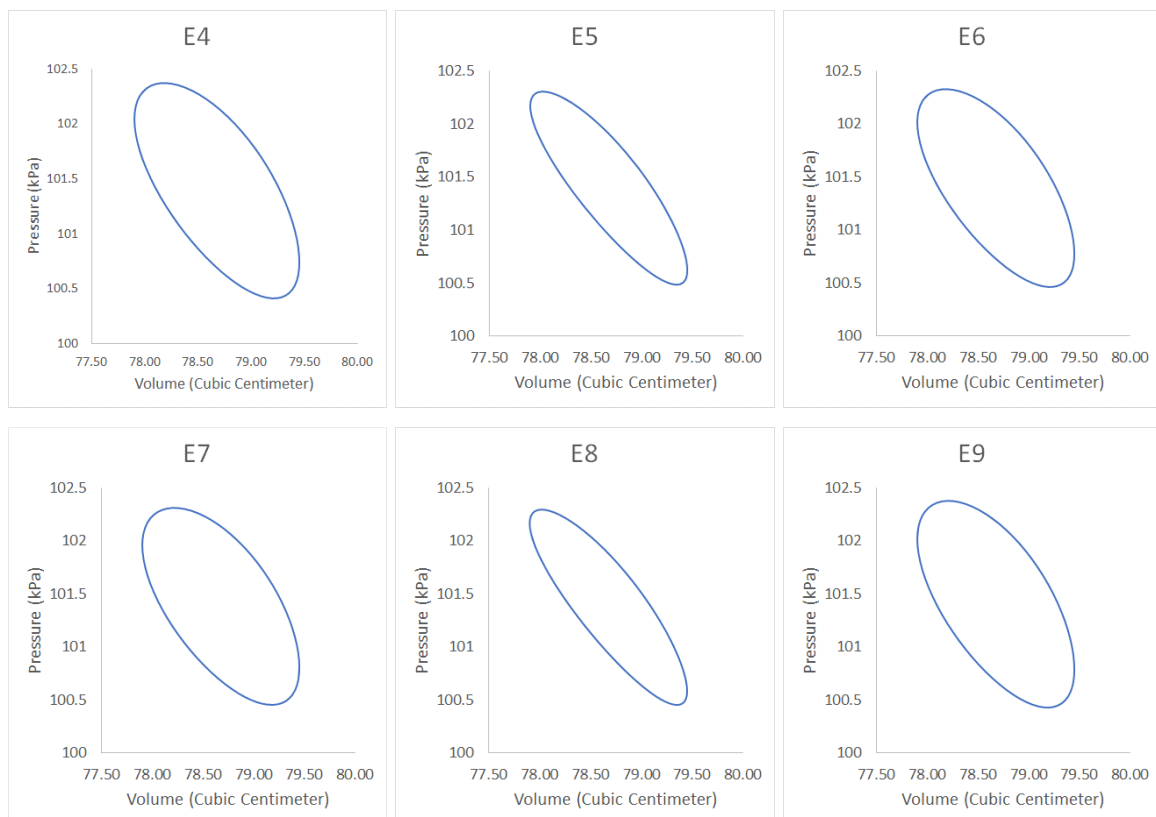
$a$  is the amplitude ( $a = \text{maximum pressure recorded} - \text{average pressure recorded}$ )

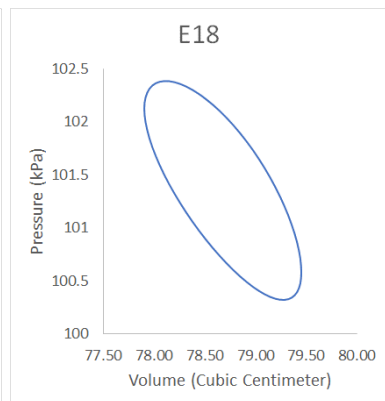
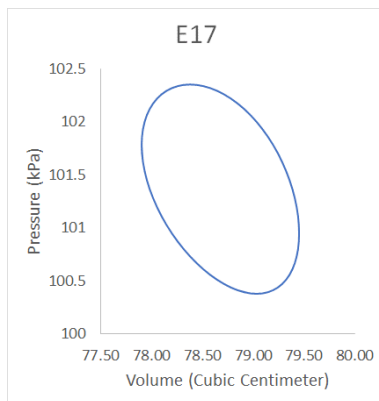
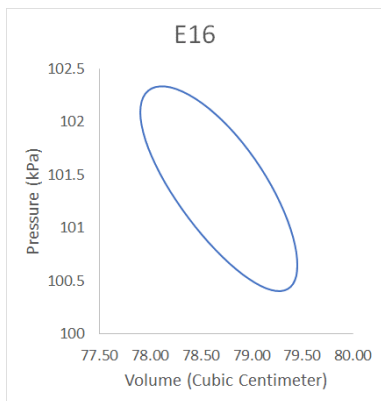
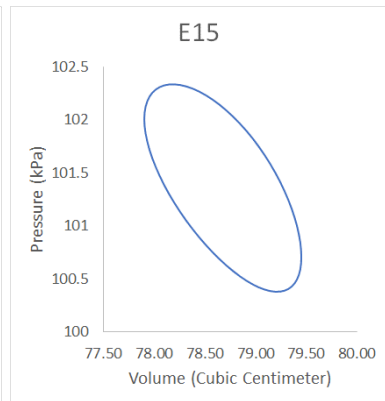
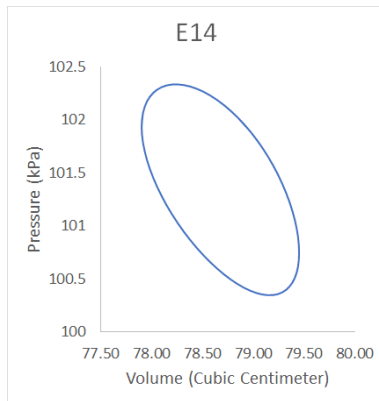
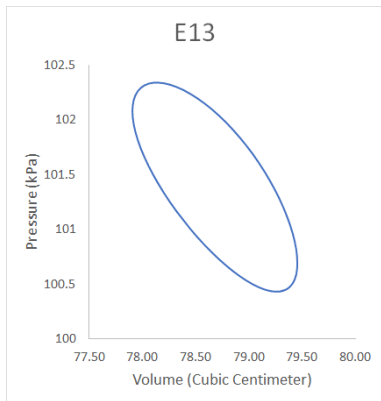
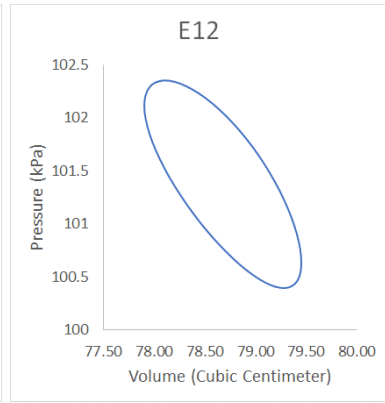
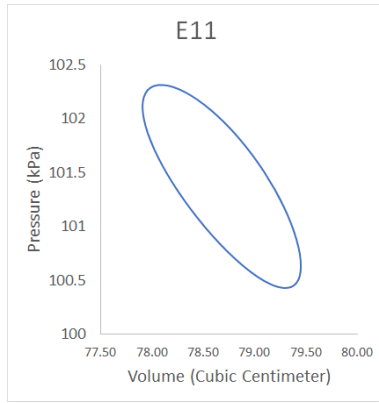
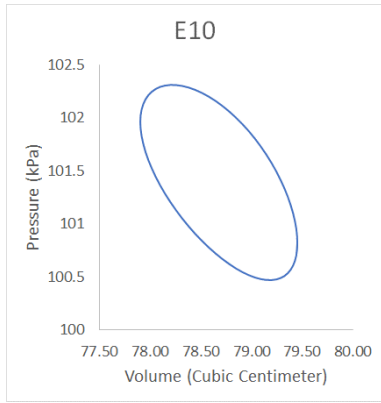
$t$  = time step of experiment

$T$  is the time period, and

$TF$  is the Time factor that is adjusted to match the experimental results

The averaged P-V diagrams demonstrating the indicated work is presented for inspected EMSE (Fig. 4-26), drilled EMSE (Fig. 4-27) and probed EMSE (Fig. 4-28).





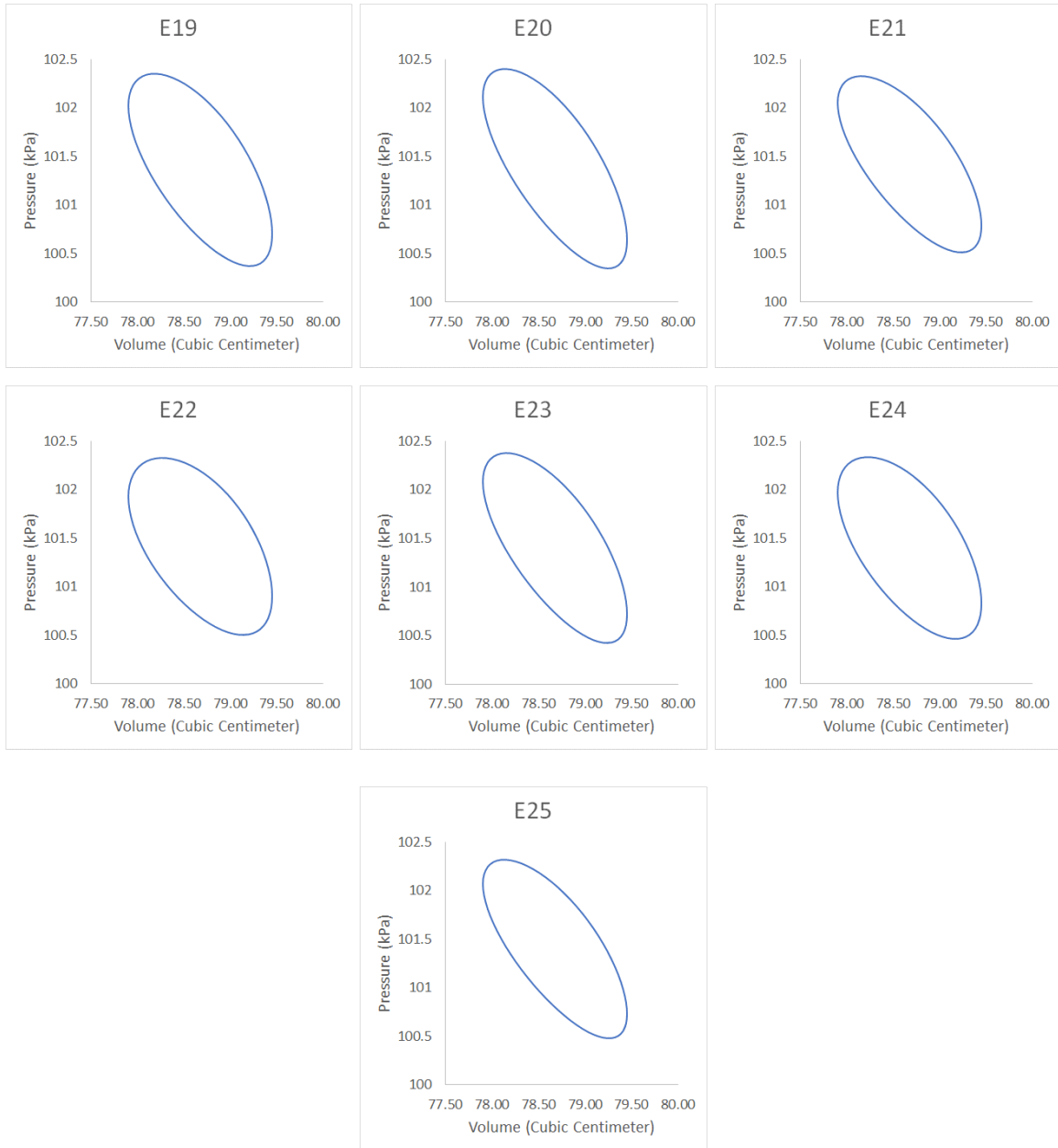


**Fig. 4-26: Indicated work diagrams of Inspected EMSEs**

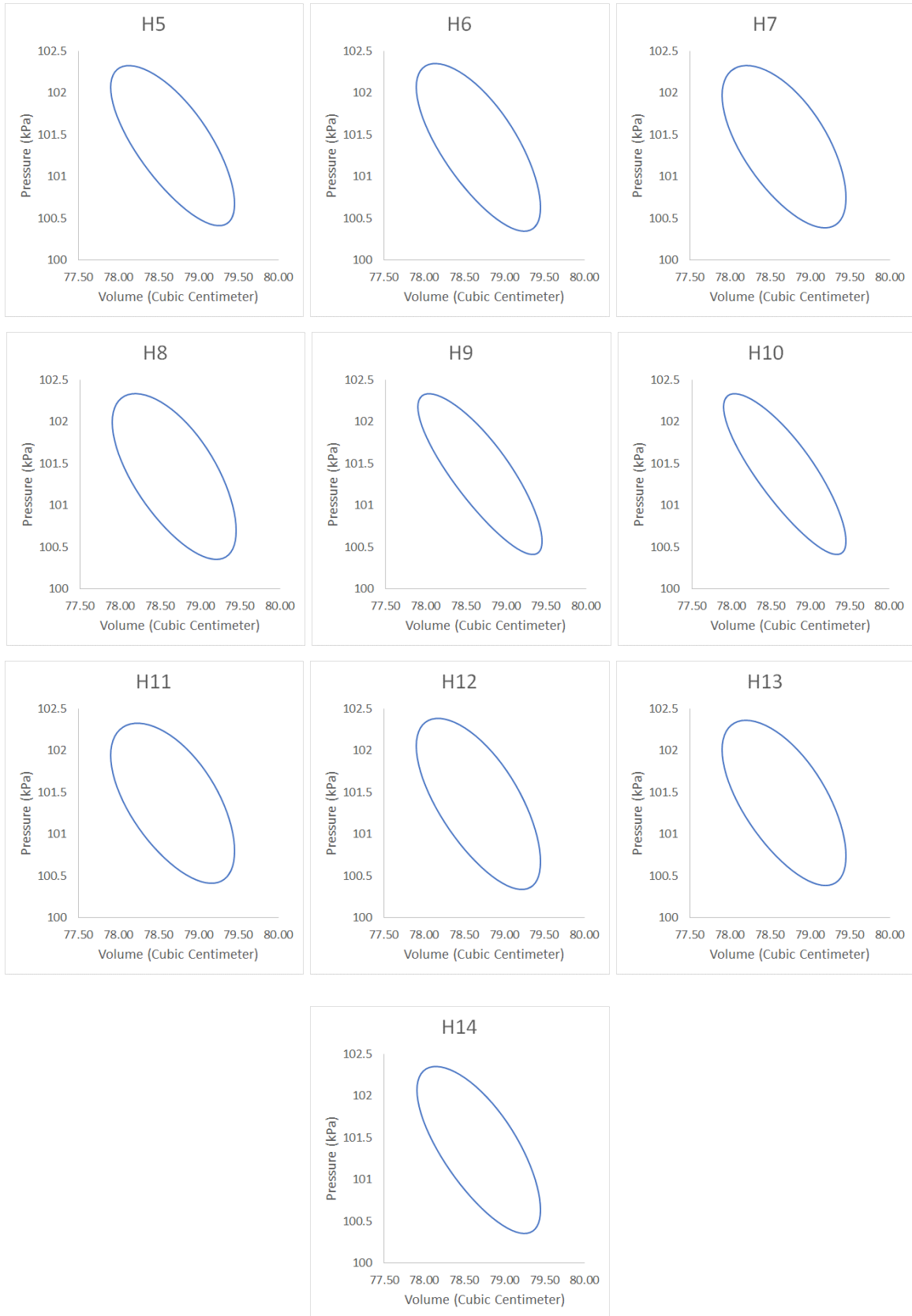


**Fig. 4-27: Indicated work diagrams of drilled EMSEs**

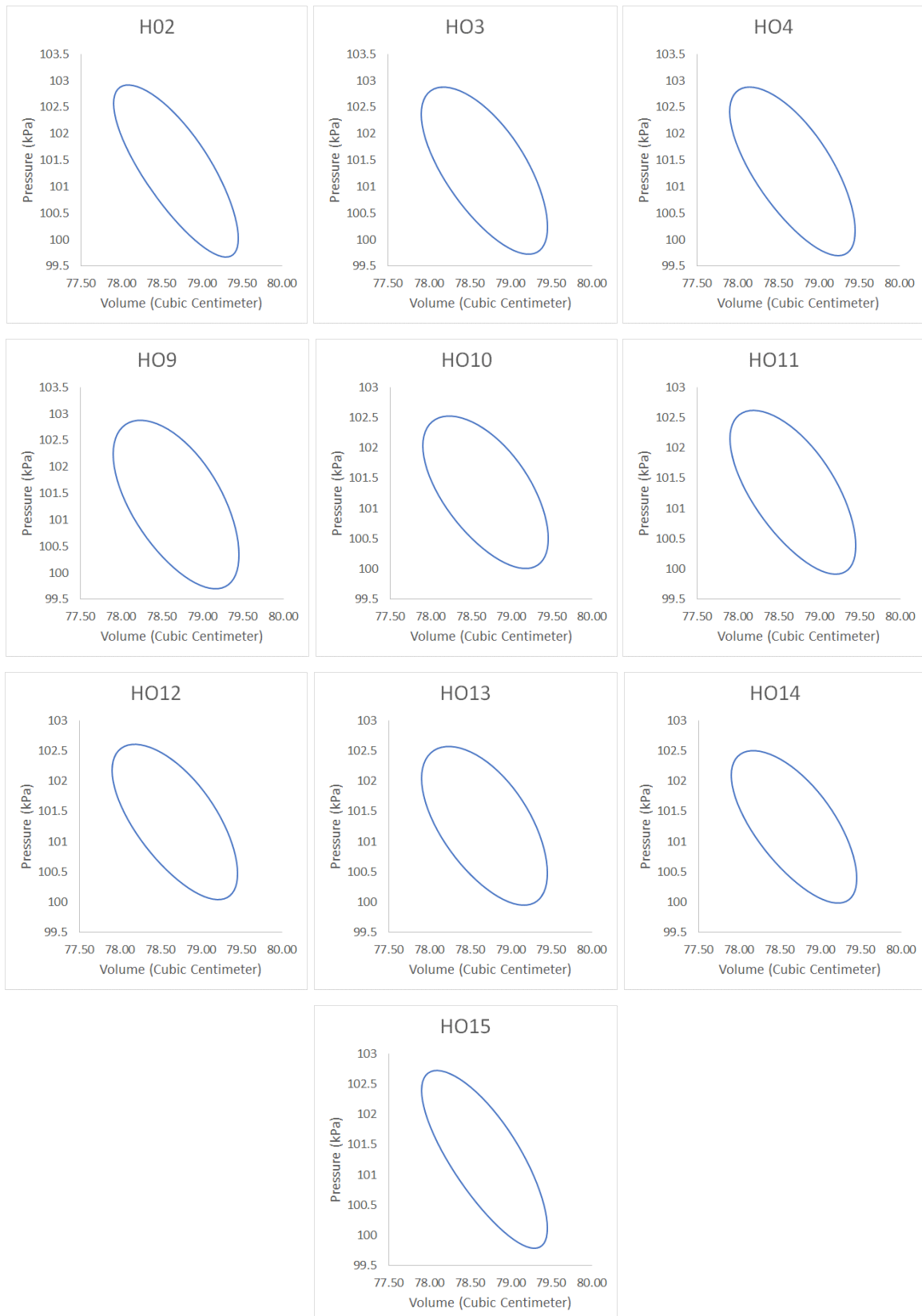


**Fig. 4-28: Indicated work diagrams of Probed EMSEs**

As demonstrated in Fig. 4-26, Fig. 4-27 and Fig. 4-28, there is no discernible differences that can be proposed between the inspected EMSE and the drilled EMSE with the Probed EMSE

showing the same cycle but with higher pressures recorded. This leads to conclude that as the rotational speed showed considerable decrease for the probed EMSE, that has led to the EMSE requiring to do more work and thus leading to an increase in pressure inside the EMSE.

Further comparison can be made using the work done analysis obtained from the area under the P-V Graph as represented in Fig. 4-29. The indicated work remains consistent across the various temperature differences the EMSE is subjected to in each case. As modifications are made on the EMSE, the indicated work increases. This is clearly observed as the inspected EMSE demonstrates a much lower indicated work value when compared to the drilled and probed EMSE. The probed EMSE demonstrates slightly higher indicated work than the drilled EMSEs.

The work done is expected to decrease as the temperature difference increases. However, the modified EMSEs produce a different result. This may be due the excess strain on the system due to the various modifications first reducing the air tightness and then further adding friction to the system with the introduction of probes for measurement.

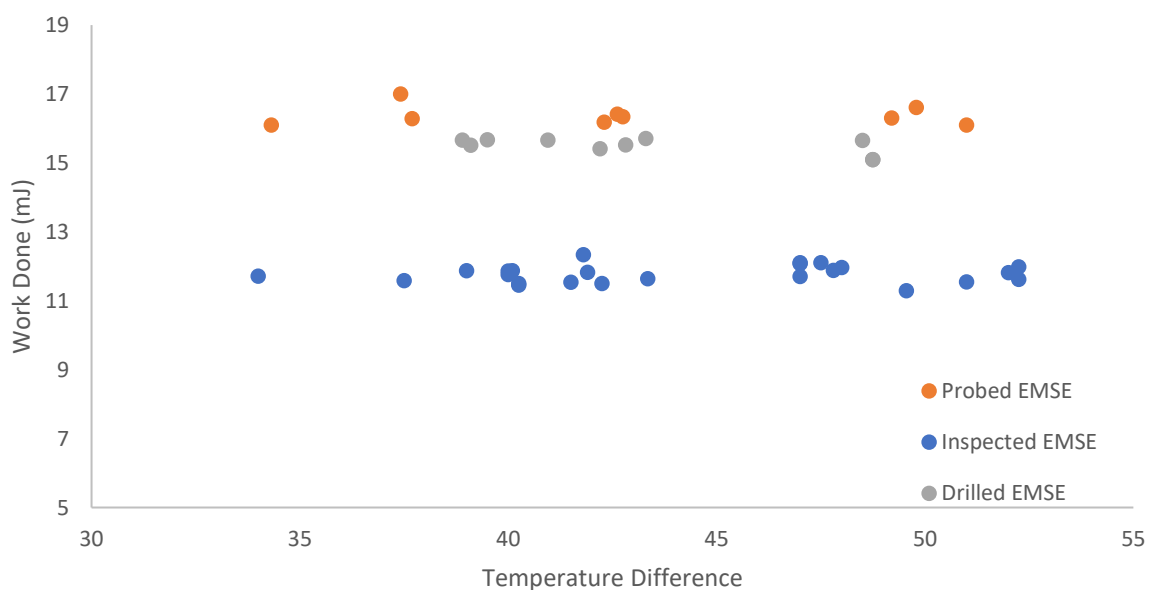


**Fig. 4-29: Work Done vs Temperature difference of modified EMSE**

Comparing with the results obtained by Kato[58], there is a much larger sample size of results presented in this research across a larger range of temperature. The general trend is better visualised in the results demonstrated in this work in comparison to the results demonstrated by Kato.

## 4.12. Summary

Research conducted by Kato [58] indicates contradicting results when compared to the results presented in this chapter. Considering a larger sample size presented here in comparison to Kato, the general trends established in this work offers a clearer insight into the working relationships of low cost, low temperature differential Stirling engines. Furthermore, Kato results indicate only one cycle of the engine operation for indicated work with no explanation or consideration of the cycle speed fluctuations observed especially for a simple, low cost engine build. This research demonstrates that up to 20% fluctuation in cycle speed is observed after stabilisation of the operation of the engine and to average the indicated work a wave function has been used to obtain a best fit cyclical indicated diagram.

The EMSE demonstrated directly proportional relationship between the rotational speed of the engine when compared to the increasing temperature of the hot surface. This contradicts the Kato findings where the relationship is inversely proportional. The P-V diagram is shown to have a similar cyclical pattern for all the tests conducted in both the Kato Indicated diagrams and the diagrams presented in this chapter. However, while Kato results demonstrated a general rise in indicated work as the hot side temperature was increased, the results in this chapter demonstrated more consistent indicated work across the various testing temperatures.

The rotational speeds obtained from the results of the inspected EMSE test has been utilised to develop CFD models. The temperature profiles and the indicated work diagrams have been used for verification of the CFD models as demonstrated in Chapter 5. The temperature profiles are a better set of result for the verification since the pressure is heavily impacted due to the various modification undertaken on the EMSE.

# Chapter 5

## Computational Analysis

### 5.1. Introduction

The analysis of Stirling Engine includes the complicated processes of heat and mass transfer due to the geometrical effects of the various multi-dimensional components of the engine. While Numerical methods have been implemented to define the workings of the engine, an accurate representation of the performance is yet to be obtained. In such cases, advanced simulation approaches using CFD models can assist in mapping the geometrical features to accurately predict the heat and mass transfer of the system. Utilising transient Computational Fluid Dynamics (CFD) modelling, a small-scale LTD Stirling engine was simulated demonstrating the internal workings of the engine. The CFD analysis in the form of temperature profiles show the initiation and normal operation of the Stirling Engine.

In order to create an accurate model, first, an existing verified research work was replicated. The model developed, was then used as the benchmark that is then modified to match the Educational Model Stirling Engine (EMSE) design. For the purpose of the study, the verified research work that was simulated is done by Wen Lih-Chen et al. [56]. They developed a Three-Dimensional CFD model simulating compressible flow to study the heat transfer characteristics of a gamma type Stirling engine containing two pistons.

While the authors of the verified simulation used an inhouse modelling software, ANSYS 16.1 simulation software will be used for preparing the model for this CFD analysis. Preparing the Stirling pump model is extremely complex, as it includes moving parts such as the piston and displacer with changing volumes. Moving meshes need to be set-up and codes are required to be established to simulate the motion of the piston and displacer. To assist in the learning process to model the moving mesh, first, a 2D model was created followed by a 3D model.

Upon finalising the model parameters of the Wen Lih-Chen model, the parameters were Implemented on the EMSE and the results obtained from the CFD analysis were compared against the results obtained from the experimental study presented In Chapter 4.

## 5.2. Stirling Engine Simulation Study

The design of the Stirling being studied is based on the experiment and numerical analysis by Wen-Lih Chen et al. [55,57], however, the dimensions of the model have been scaled down to half of the experimental model to retain a laminar flow inside the engine by reducing the Reynolds number. Furthermore, no regenerator has been added to the simulation of the system. The narrow gap between the displacer and the inner wall of the cylinder will act as the regenerative channel between the compression and expansion chambers.

The Stirling system studied is a gamma type Stirling Engine with two power pistons. The pistons and displacer are connected to a crank shaft. The pistons are at a 90-degree phase angle to the displacer. The CFD model developed only considers half the size of the original experimented research work to ensure laminar flow in the Stirling engine **Fig. 5-1** shows the dimensions of the Stirling engine that has been derived from the original experimentation work and numerical analysis by Wen Lih Chen et al.

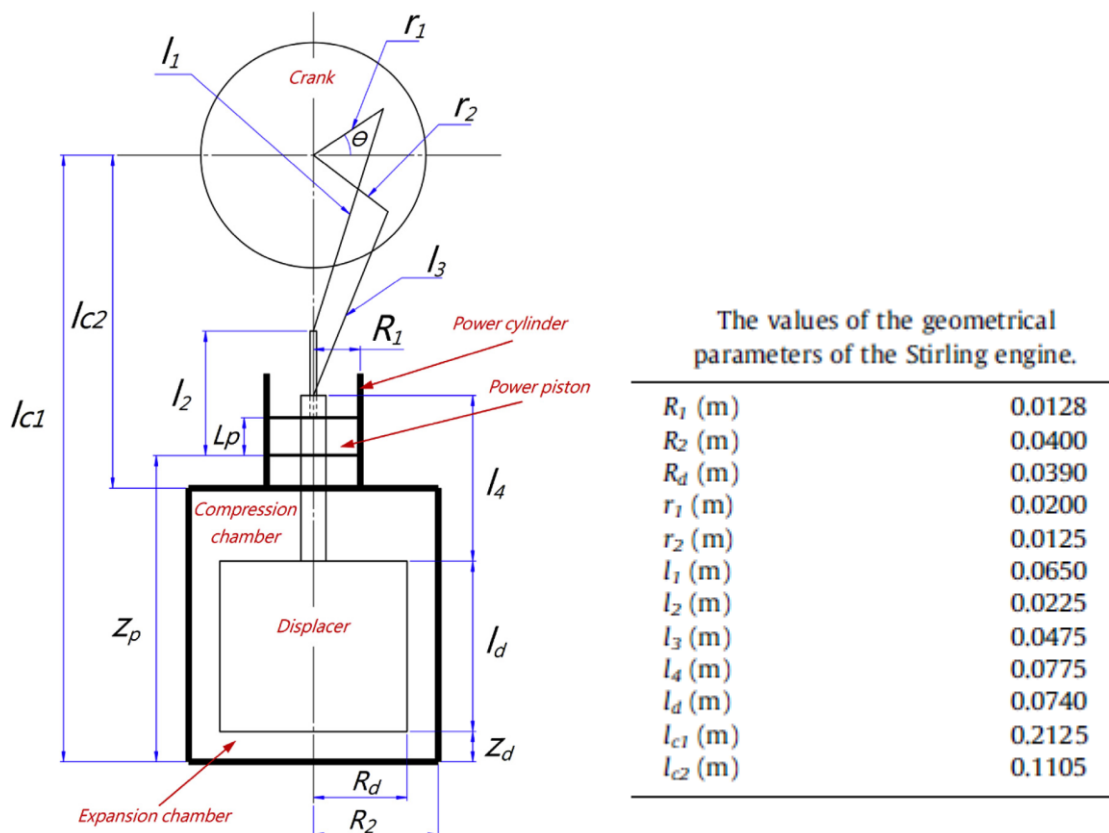


**Fig. 5-1: Dimensions of Stirling engine derived from experiment**

### 5.2.1. Motion Dynamics

The displacement of the Piston ( $z_p$ ) and displacer ( $z_d$ ) are represented below [56]:

$$z_p(\theta) = l_{c1} - \left( -r_1 \sin\theta + \sqrt{l_1^2 - r_1^2 \cos^2\theta} + l_2 \right) \quad \text{(Equation 6)}$$

$$z_d(\beta) = l_{c1} - \left( -r_2 \sin\beta + \sqrt{l_3^2 - r_2^2 \cos^2\beta} + l_4 + l_d \right) \quad \text{(Equation 7)}$$

The Velocities of the Piston ( $w_p$ ) and displacer ( $w_d$ ) are represented below [56]:

$$w_p(\theta) = r_1 \omega \cos\theta - \frac{r_1^2 \omega \cos\theta \sin\theta}{\sqrt{l_1^2 - r_1^2 \cos^2\theta}} \quad \text{Equation 8)}$$

$$w_d(\beta) = r_2 \omega \cos\beta - \frac{r_2^2 \omega \cos\beta \sin\beta}{\sqrt{l_3^2 - r_2^2 \cos^2\beta}} \quad \text{Equation 9)}$$

Where,

- $\theta$  is the starting crank angle determining the position of the power pistons
- $\beta = \theta - 90^\circ$  determining the position of the displacer. The piston and displacer are at 90 degree phase angle to each other.
- The rest of the factors are as described as per **Fig. 5-1**

### 5.2.2. Modelling Parameters

Wen-Lih Chen et al. has made the following assumptions:

- The fluid viscosity of all materials is constant
- Thermal properties of all materials are constant,
- Air is the working gas with properties defined by the ideal gas equation of state
- gas constant = 287.0 J/KgK
- Mechanical friction effects are ignored
- Thermal radiation effects are ignored.
- 3D Transient model
- Laminar Flow
- Flow is modelled using compressible Navier-Stokes equations
- Heat Transfer is modelled using the Energy Equation

- viscous dissipation effect has not been included

Pressure-based SIMPLEC finite volume code is used to conduct the simulation on the USTREAM platform. The dynamic mesh method implemented involves the changing of the geometry of the cells by expanding or compressing the volumes. In Ansys 16.1 this corresponds to smoothing and remeshing technique.

The following Boundary conditions have been implemented:

- $u$ ,  $v$  and  $w$  are velocity components in  $x$ ,  $y$  and  $z$  directions respectively.  $T_L$  is the Temperature at the cold surface,  $T_H$  is the Temperature at the Hot surface,  $\theta$  is the phase angle as per described in section 5.2.1.
- Engine Rotation speed,  $\omega = -120$  rpm (clockwise)
- Initial Conditions:  
 $\theta=0^\circ\text{C}$ ,  $u=v=w=0$ ,  $p=101.0$  kPa,  $T= T_L$   
 At the Hot End ( $z=0$ ):  
 $u=v=w=0$ ,  $T= T_H = 400$  K
- At the Cold End ( $z=l_{c1}-l_{c2}$ ):  
 $u=v=w=0$ ,  $T= T_L = 300$  K
- Surface of displacer (adiabatic):  
 $u=v=0$ ,  $w=w_d$ ,  $\frac{\delta T}{\delta n} = 0$  ( $n$  is the direction normal to the wall of displacer)
- Surface of Power Piston (adiabatic):  
 $u=v=0$ ,  $w=w_d$ ,  $\frac{\delta T}{\delta z} = 0$
- Lateral wall of the displacer cylinder:  
 $u=v=w=0$ ,  $T = T_L + \frac{z}{(l_{c1}-l_{c2})} (T_H - T_L)$

Since the design of the engine is symmetrical only a quarter of the engine will be simulated. Three grids were tested using three different time-step intervals with three time-step number cycles as per shown in **Table 5-1**. Four cycles were programmed to make the solution periodic. The paper discusses the solution obtained with the 110,569 grid at a time-step cycle of 200 times per cycle.

**Table 5-1: Grid Set-up**

Grid (number of cells)	Time-step Intervals (sec)	Time-Step / Cycle
80,566	$2.5 \times 10^{-3}s$	200
110,569	$1.667 \times 10^{-3}s$	300
141,438	$1.25 \times 10^{-3}s$	400

### 5.2.3. Result and Validation

The variations of the temperature within the Stirling engine is shown in **Fig. 5-2**

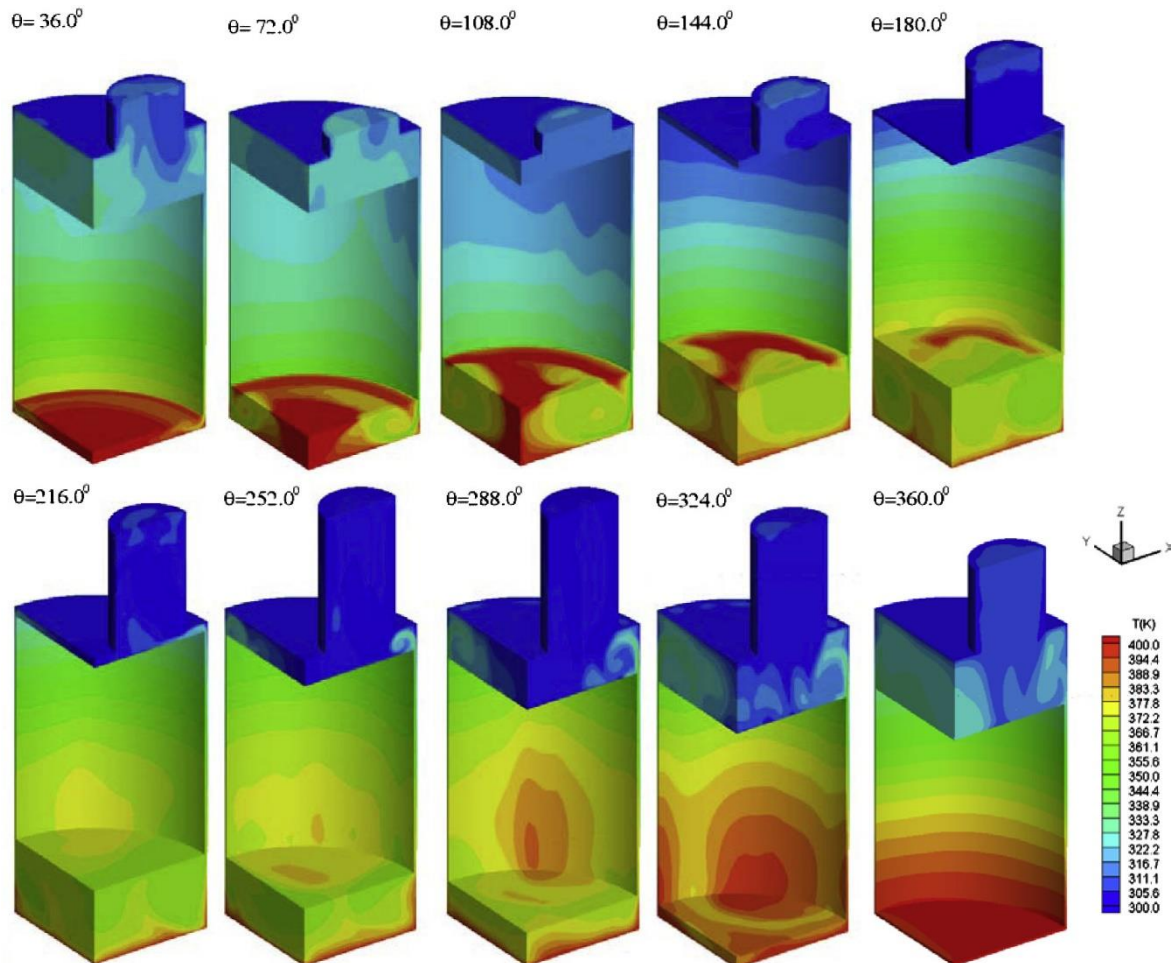


**Fig. 5-2: Temperature contours across the whole engine at 10 different crank angles [56]**

The variations of total ( $V_t$ ), expansion chamber ( $V_e$ ), and compression chamber ( $V_c$ ) volumes versus crank angle over an engine cycle is as per mapped in **Fig. 5-3**.

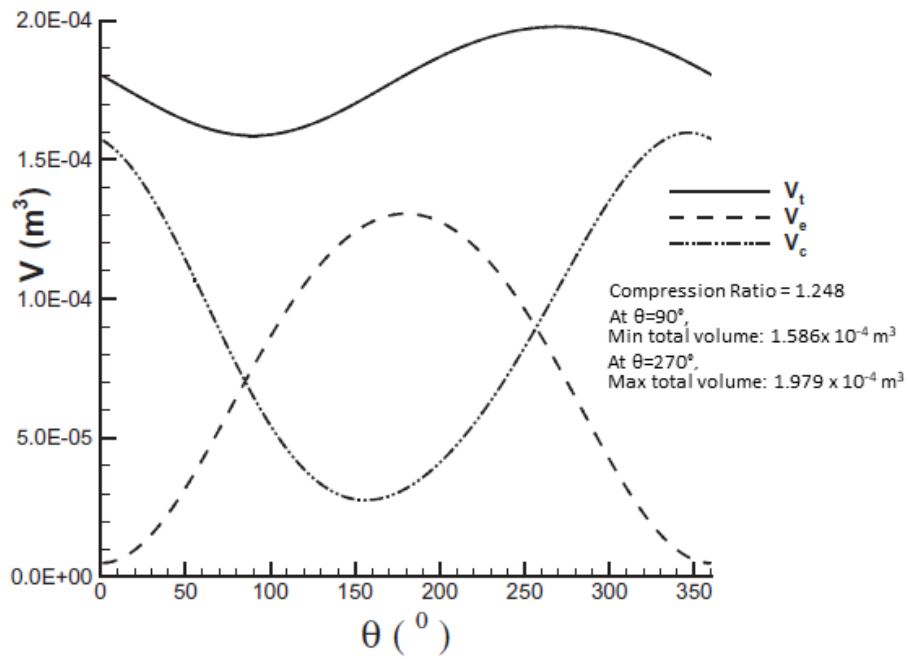


**Fig. 5-3: Volume variation versus crank angle [56]**

The USTREAM code is validated using an adiabatic cycle of the Stirling engine obtained from the simulation. The pressure average - Volume ( $P_{avg} - V$ ) graph of the engine cycle is mapped against the adiabatic relation between pressure and volume,  $PV^{1.4} = C$ , where  $C$  is constant. The relationship indicates that the USTREAM code results fit the relation, as shown in **Fig. 5-4**.

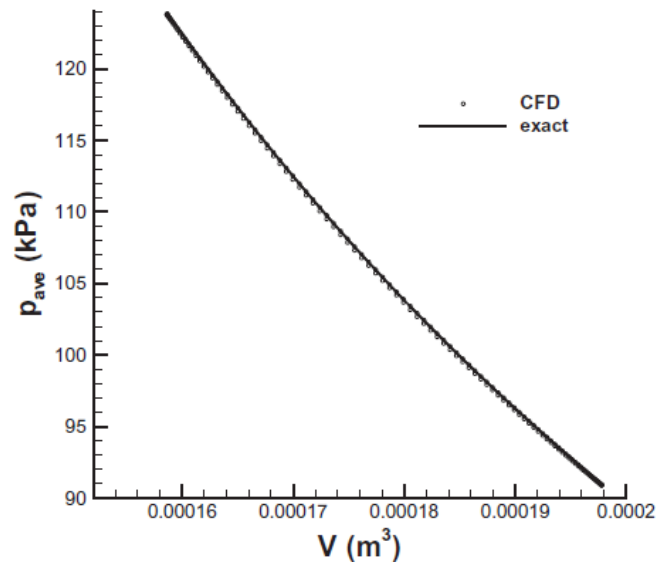


**Fig. 5-4: USTREAM code validation [56]**

### 5.3. Simulation Replication

The results obtained by Wen-Lih Chen et al. will be replicated using ANSYS 16.1 FLUENT simulation software. A 2D model will be first utilised to simply understand the moving mesh modelling in ANSYS. This model will then be translated into the 3D model. In order to simulate the motion of the displacer and piston, the motion dynamics was modelled using a user defined function (UDF) in C-programming using equations [1-4](#). The whole programme is presented in Appendix A. The C-programme takes up a lot of the computing power and makes the simulation very slow, hence based on the equations, profiles dictating the motion of the displacer were created. The profiles are a text file defining parameters of time and velocity as indicated in Appendix B.

#### 5.3.1. 2D model

A central cross-section has been modelled using the values listed in **Fig. 5-1** in geometry modeller and mesh was produced using the mesh modeller of ANSYS 16.1 see **Fig. 5-5**.

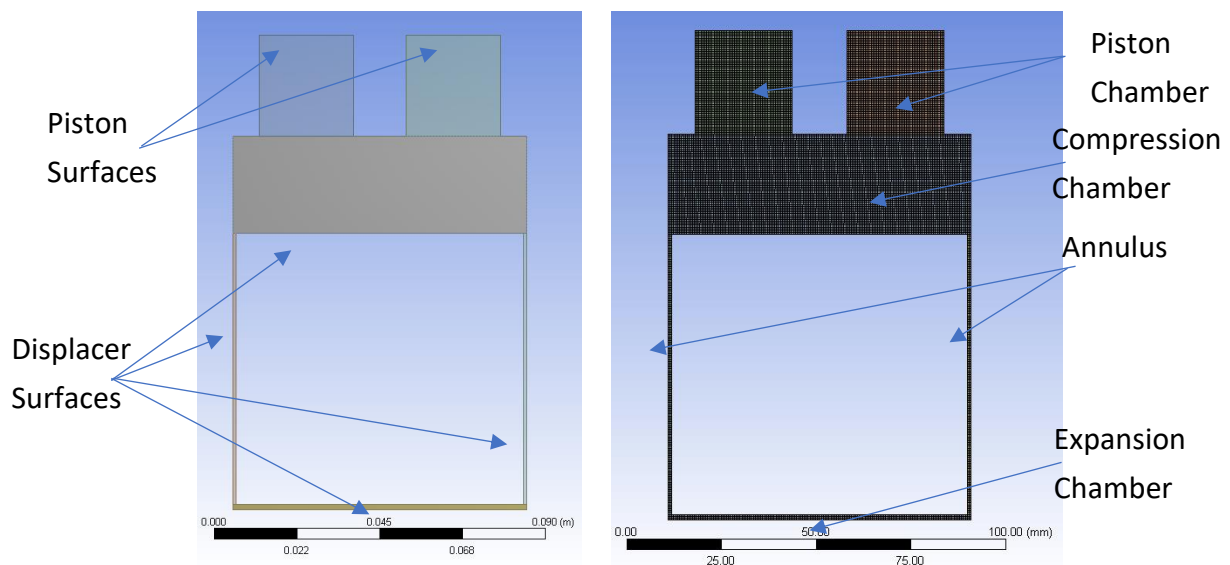


**Fig. 5-5: 2D Model Geometry and Mesh**

The geometry is separated into 6 sections, 2 pistons, a compression chamber, expansion chamber and the annulus of between the displacer and the inner surface of the Stirling engine shell. The sections were created to obtain an even quadrilateral mesh across the entirety of the Stirling cross-section. The interfaces of the intersections are grouped to ensure the entire model is considered as one continuous section for the CFD analysis. The Mesh is prepared

using Face Meshing using the quadrilaterals method and the face size has been set to 0.5mm. All the cell zones have been set to fluid, with a relevance factor of 100, Relevance centre to fine, high smoothing, slow transition and fine span angle. The statistics are as shown in **Table 5-2**.

**Table 5-2: Mesh Statistics 2D model**

<b>Nodes</b>	16158	<b>Max</b>	1.0415
<b>Elements</b>	15378	<b>Average</b>	1.0139
<b>Mesh Metric</b>	Aspect Ratio	<b>Standard Deviation</b>	5.6778e-003
<b>Min</b>	1.		

In FLUENT, the CFD model is then set-up in Transient mode, Laminar flow and the energy equation is turned on. In the material Properties, air is set as an Ideal gas, and boundary conditions are set for the Hot edge at the bottom at 400 K and the cold edge at the top including the pistons as 300 K as per noted in section 5.2.2. The UDF and the profiles for the piston and the displacer motion are then loaded using the FLUENT define function.

There are three types of dynamic mesh methods, Smoothing, Layering and Remeshing. The method used by Wen-Lih Chen et al. utilised smoothing and remeshing, however, using this method on ANSYS produced negative volumes and the simulation crashed. Hence, the layering method was used to conduct the simulation. The layering methods involves the adding and/or deleting cells to change the volume of the computational domain. A ratio based Layering method was implemented with a split and collapse factor of 0.2. The dynamic mesh zones have been defined by three parameters, rigid body, stationary body and deforming body. **Fig. 5-6** shows how each dynamic zone has been defined. The piston edges are assigned as pressure outlets.

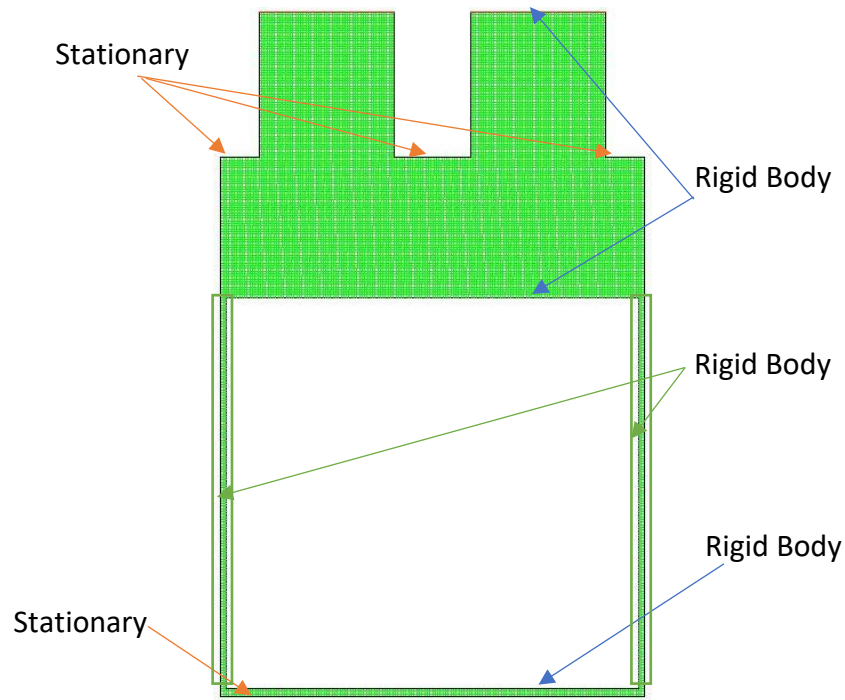


**Fig. 5-6: Dynamic Mesh Zone Set-up, all other zones (not indicated) are set to 'deforming'**

The time-step size utilised was 0.001733908 seconds with 576 steps dictating the number of steps required to complete 4 complete cycles of the Stirling engine. A maximum 20 iterations were set with a report being saved every 4 iterations. The mesh motion defined by both the UDF and the profile, returned the same results as per shown in **Fig. 5-7**. Using the UDF, the solution calculation took 30 minutes while with the profile it took 15 minutes.

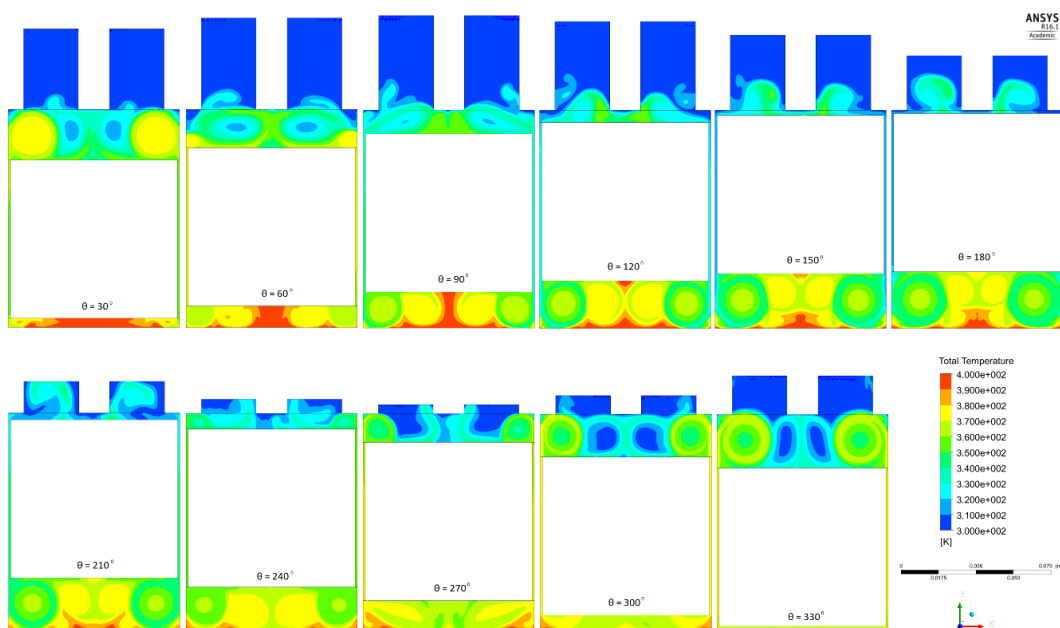


**Fig. 5-7: Temperature contours in the Stirling Engine at different crank angles, 2D model**

The motion of the piston and displacer are different when compared to the simulation by Wen-Lih Chen et al. because crank rotation is modelled clockwise (-120 rpm) while for this work, the rotation has been modelled in counter-clockwise direction (120 rpm). The Temperature profile however does seem similar to that of the model prepared by Wen-Lih Chen et al. However, the temperature modelling has not yet been performed on this model. This moving mesh model is then transferred to a 3D model, which will feature more zones that will require to be set-up during the dynamic modelling. 2D Simulation has been used to compare against 3D simulation for temperature profile analysis

### 5.3.2. 3D Model

The quarter section of the engine as seen in Wen-Lih Chen et al. is modelled using the geometry modeller in ANSYS using the dimensions in **Fig. 5-1**. Just like the 2D model, there are 4 major segments to the 3D model including, the compression chamber, the expansion chamber, the annulus and the piston. Only one piston is shown since only a quarter of the engine is modelled. The geometry has been further divided into 34 bodies, in order to generate a sweeping uniform quadrilateral mesh. The bodies are grouped so that they interact with the adjacent bodies for which the interfaces are set-up automatically by the ANSYS modeller. Since all the sections are connected, the mesh flows through from one body to the other, as such to maintain the uniformity. The segments created ensure this uniformity is maintained. See **Fig. 5-8**.

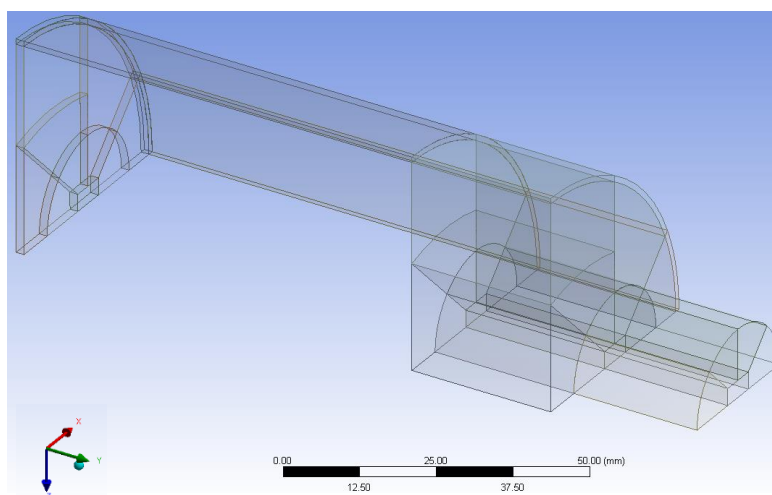


**Fig. 5-8: 3D Geometrical model of Stirling Engine**

The meshing for the 3D model is more complicated when compared to that of the 2D model, and has been generated manually. The number of divisions for each of the 34 bodies have been set so as to provide an even height of 0.5 mm for each element volume. The widths of volumes have been set in order to have a uniform mesh flow across the axis of the geometry. The constraint to the size of the mesh for the width is relaxed as the geometry is not symmetrical. Thus, the sweeping mesh grows from one end to the other. **Fig. 5-9** shows the generated mesh. All the cell zones have been set to fluid, with a relevance factor of 100, advanced size function is set on curvature, relevance centre is set to fine, high smoothing, slow transition and fine span angle. The statistics are as shown in **Table 5-3**.

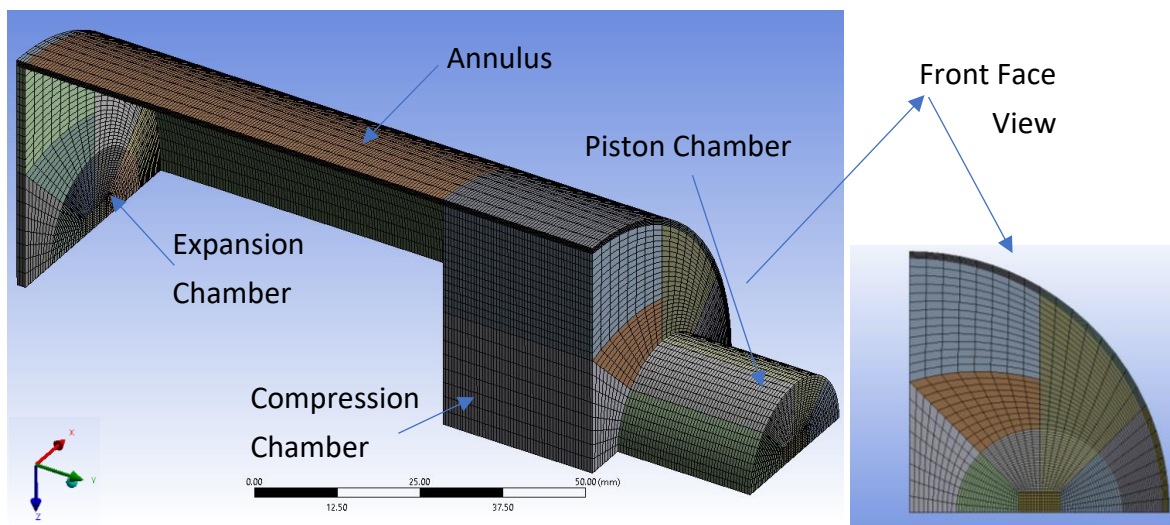


**Fig. 5-9: 3D Model mesh generation**

**Table 5-3: Mesh Statistics 3D Model**

<b>Nodes</b>	173090	<b>Average</b>	5.17476227272727
<b>Elements</b>	158400	<b>Standard Deviation</b>	5.2136092539616
<b>Mesh Metric</b>	Aspect Ratio	<b>Minimum Orthogonal Quality<sup>1</sup></b>	7.20906e-01
<b>Min</b>	1.25		
<b>Max</b>	18.631	<b>Maximum Ortho Skew<sup>2</sup></b>	2.79094e-01

<sup>1</sup> Orthogonal Quality ranges from 0 to 1, where values close to 0 correspond to low quality.

<sup>2</sup> Ortho Skew ranges from 0 to 1, where values close to 1 correspond to low quality.

Named sections have been created to combine the bodies of the major chambers to make the set-up of the dynamic mesh easier. This way the dynamic mesh properties can be assigned collectively to the 5 bodies that encompass the piston chamber, the 13 bodies of the compression and expansion chambers and the three bodies of the annulus. All the cut faces in the '-x' and 'z' directions have been set as symmetry to indicate that the model is a segment of the complete engine. The mesh quality reading shows high

In FLUENT, the CFD model is set-up in Transient mode, Laminar flow and the energy equation is turned on. In the material Properties, air is set as an Ideal gas, and boundary conditions are set for the Hot surface at the bottom at 400 K and the cold surface at the top including the pistons as 300K as per noted in section 5.2.2. The profiles for the piston and the displacer motion are then loaded using the FLUENT define function.

Like in the 2D model, the smoothing and remeshing model was attempted for the 3D model as well, however, similar to the 2D model the moving mesh failed due to the creation of negative volumes and hence the layering method was implemented. The layering of the 3D model is essentially the same as that of the 2D model. A ratio based Layering method was implemented with a split and collapse factor of 0.2.

The Dynamic mesh zones associated with the annulus are all set as rigid bodies, the bottom surface of the expansion chamber and the top surface of the compression chamber are set as stationary. The top of the pistons is set as rigid bodies and so is the top and bottom surfaces of the Expansion chamber and compression chamber respectively. All other zones have been set to deformation. The surface of the piston has been set as a pressure outlet.

The time-step size utilised was 0.001733908 seconds with 576 steps dictating the number of steps required to complete 4 complete cycles of the Stirling engine. A maximum 20 iterations were set with a report being saved every 4 iterations. The results obtained however were the same as per shown in **Fig. 5-10**.

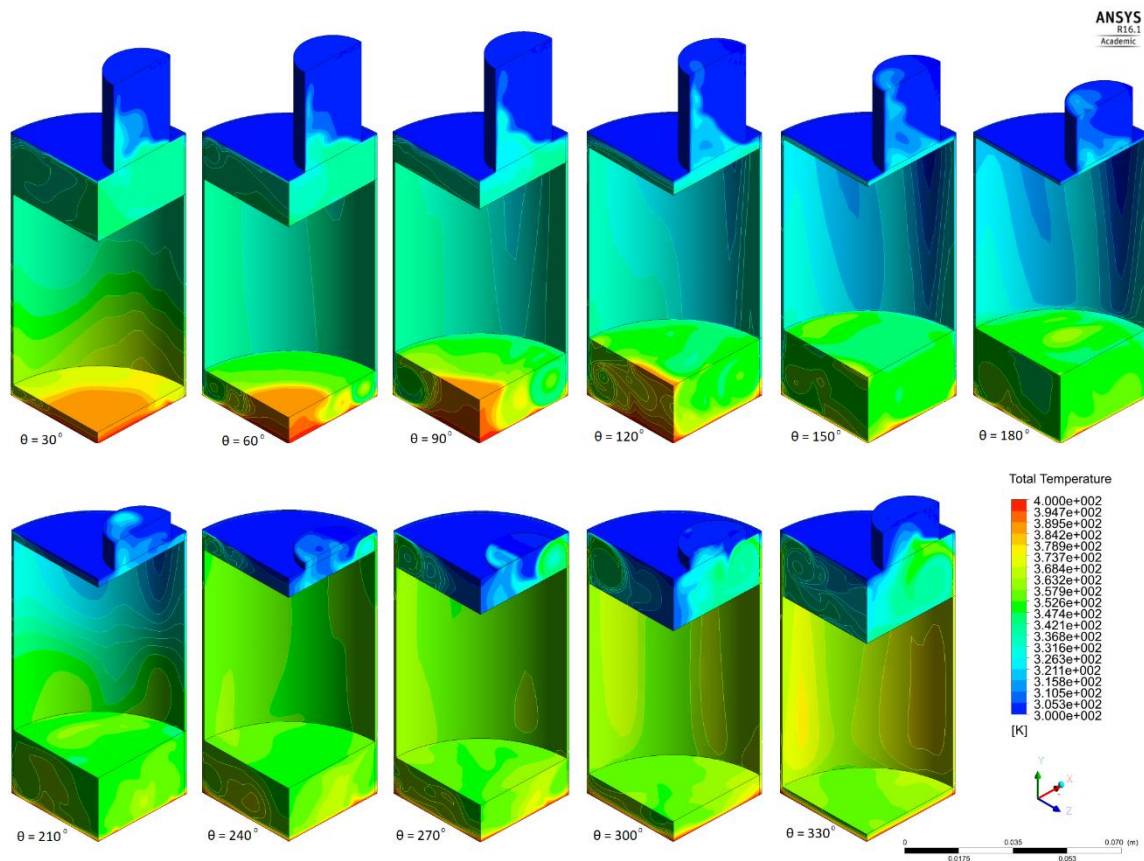


**Fig. 5-10: Temperature contours in the Stirling Engine at different crank angles, 3D model**

The 3D mesh motion has been generated and it is similar to that produced by Wen-Lih Chen et al. The only difference is that the crank rotation has been set in the anti-clockwise direction in this model compared to the model by Wen-Lih Chen et al. The temperature modelling has not been set-up in the model and hence does not produce the results shown in the original work. The Pressure profile obtained for the Stirling engine simulation indicates a max and minimum pressure of 6.5 Pa and -6.5 Pa respectively. There is an issue with the calculation since the initial pressure of the Stirling engine was set to 101 kPa. Both the temperature and pressure set-up needs to be further studied as the values for both these parameters are incorrect. This will require further development of the UDF and or creation of temperature profiles based on the boundary condition defined in section 5.2.2.

The chart for the volume variation and crank angle is demonstrated below in **Fig. 5-11**. The Graph obtained is a mirror image of the work by Wen-Lih Chen et al. since the rotation is considered as anti-clockwise, instead of clockwise as considered in the original work. The minimum and maximum values of the Total volume as obtained from the CFD analysis are:

$1.34 \times 10^{-4} \text{ m}^3$  ( $270^\circ$ ) and  $1.75 \times 10^{-4} \text{ m}^3$  ( $90^\circ$ ) respectively. This provides a compression ratio of 1.31.

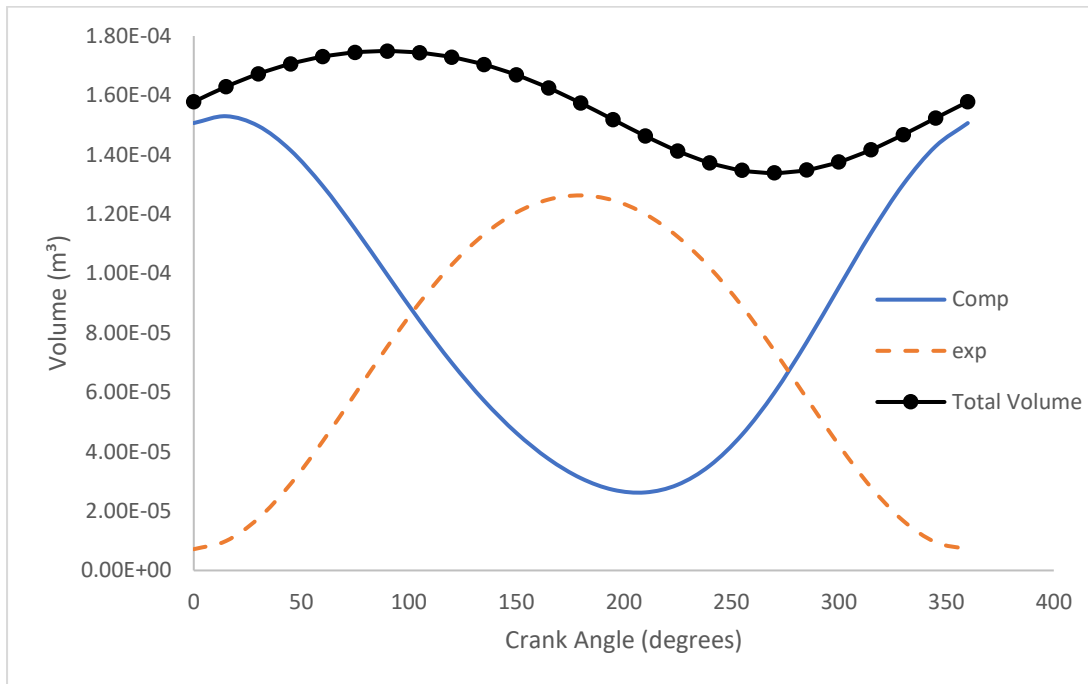


**Fig. 5-11: Variation of volume against Crank angle in the compression and expansion chambers**

The values obtained using the profile are similar to that generated by the original work by Wen-Lih Chen with minimum and maximum values of the Total volume as obtained from the CFD analysis are:  $1.586 \times 10^{-4} \text{ m}^3$  ( $90^\circ$ ) and  $1.979 \times 10^{-4} \text{ m}^3$  ( $270^\circ$ ) respectively with a compression ratio of 1.248. The model parameters have been utilised to study the EMSE.

#### 5.4. EMSE Simulation Study

The Educational Model Stirling Engine (EMSE) experimented on and discussed in Chapter 4 has been modelled to verify the CFD model presented in section 5.3.2. The dimensions for the EMSE are as provided in Fig. 4-2. The model generated in Design modeler contains the displacer chamber and piston Chamber with the location for the piston chamber translated to the center of the geometry, to simplify the meshing process. The translation of the location of the piston chamber does not affect the working process of the model. To further assist with the meshing the geometry has been divided into 35 parts of the fluid portion of the singular model body. Fig. 5-12 shows the EMSE model geometry prepared.

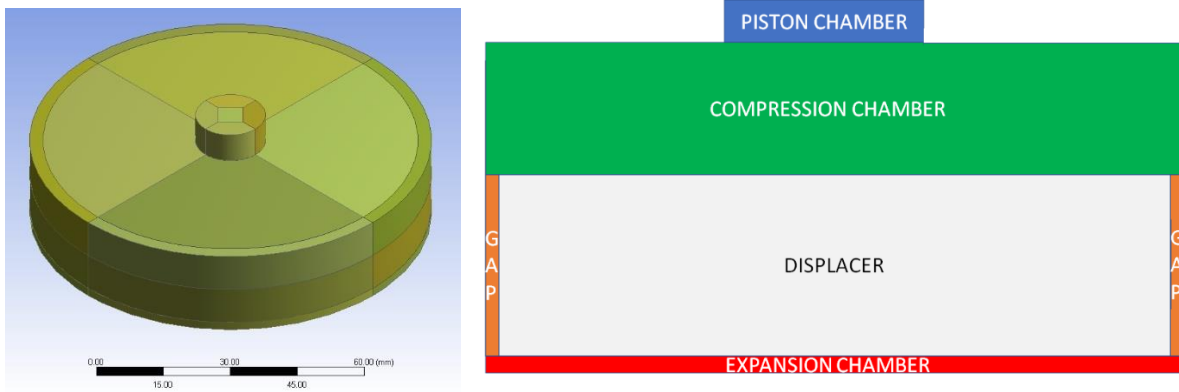


**Fig. 5-12 EMSE Geometry model**

### 5.4.1. Mesh Quality

Using the Fluent solver, Mesh was generated with a relevance factor of 100, using on curvature size functions, fine relevance centre, high smoothing and slow transition. To determine the appropriate size of the mesh, different size of meshes were created and the properties of the meshes including, minimum orthogonality quality, maximum orthogonal skew and maximum aspect ratios were noted. **Fig. 5-13** shows the values obtained from the meshes. Minimum orthogonal quality ranges from 0 to 1, where values close to 0 correspond to low quality. Maximum ortho skew ranges from 0 to 1, where values close to 1 correspond to low quality. Lower the maximum aspect ratio, the better the Mesh.

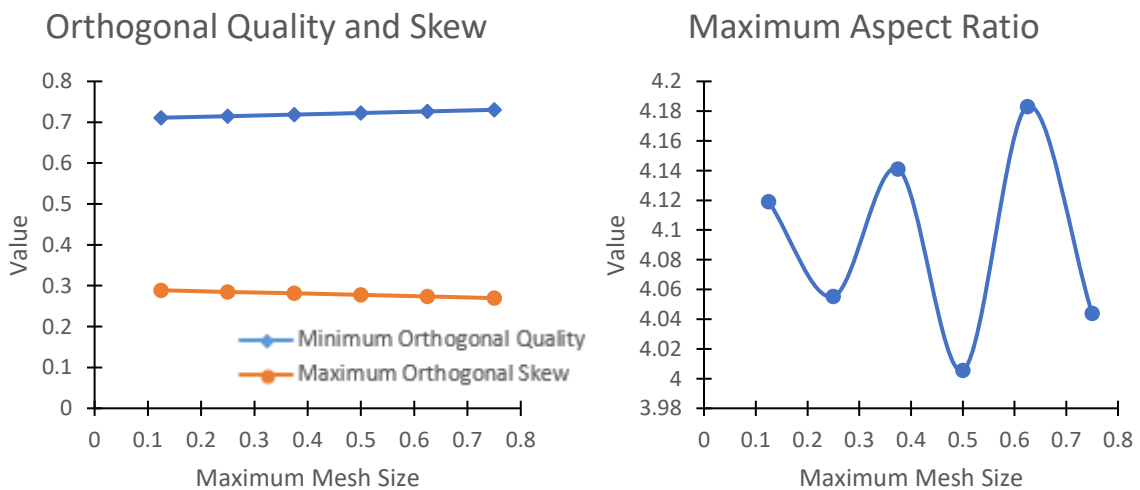


**Fig. 5-13: Mesh Statistics based on various EMSE mesh sizes**

Based on the data represented in **Fig. 5-13**, there is a minor difference in the minimum orthogonality quality and maximum orthogonal skew values from the mesh generated. These

values are seen to be tending to better quality as the mesh size increases. The maximum aspect ratio on the other hand shows better values for 0.5 mm mesh than the others. The maximum size of all the mesh edges have hence been specified as 0.5 mm. Leaving the rest of the parameters as the default value, the mesh generated is shown in Fig. 5-14.

The Mesh generated contains 430,624 nodes and 397,972 elements with maximum Aspect ratio 3.17428, minimum orthogonal quality is 0.745581 and maximum ortho skew is 0.254419.

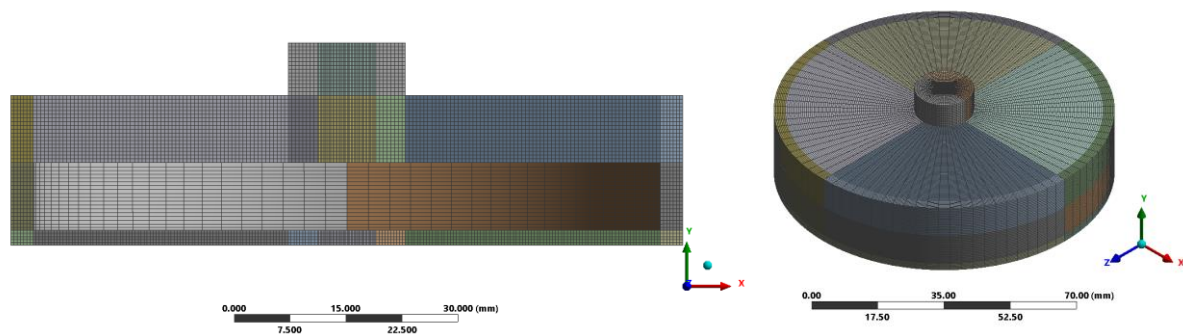


**Fig. 5-14: EMSE 3D mesh of the model**

Named sections were created to combine the bodies of the major chambers to make the set-up of the dynamic mesh. This method allows the dynamic mesh properties could be assigned collectively to the 5 bodies that encompass the piston chamber, the 13 bodies of the compression and 13 bodies making up expansion chambers and the 4 bodies of the annulus. The entire EMSE model is used for the simulation.

#### **5.4.2. Boundary Conditions**

The double precision Fluent solver working in transient mode was used to solve the model. The energy model was set up to calculate the enthalpy of the material and the flow of the fluids was set to standard k-epsilon model with standard wall functions. The material properties have been set up based on the materials that will be used to build the prototype. The materials and their properties have been listed in **Table 5-4**.

The boundary conditions based on the materials above was assigned to the walls. The outer wall of the expansion chamber was set to 400 K, while the operating temperature was set to 300 K (default room temperature). The pressure-velocity coupling scheme utilized was the SIMPLE scheme with an operating pressure of 101325 pascal.

**Table 5-4: Material Properties for Stirling engine model**

<b>Material</b>	<b>Density (kg/m<sup>3</sup>)</b>	<b>Specific Heat (j/kg-K)</b>	<b>Thermal Conductivity (W/m-K)</b>
Air* (Fluid)	Ideal	1006.43	0.0242
Brass [84] (Solid) – Piston	8860	380	233
Copper* (Solid) – Piston Cylinder	8978	381	387.6
Polystyrene [85] (Solid) - Displacer	1502	1995	0.161
Glass	2250	780	1.15
Acrylic [86] (Solid) – Displacer Cylinder	1160	1485	0.195
Aluminium* (Solid) – Top and Bottom of Displacer Cylinder	2719	871	202.4

\* Default material properties listed on ANSYS 16.1

The motion of the piston and displacer was simulated using a dynamic mesh generated by a User Defined Function (UDF) developed with C-Programming. The programme was formulated based on the motion dynamics equations of the piston and displacer. **Fig. 5-15** shows how each dynamic zone had been defined.

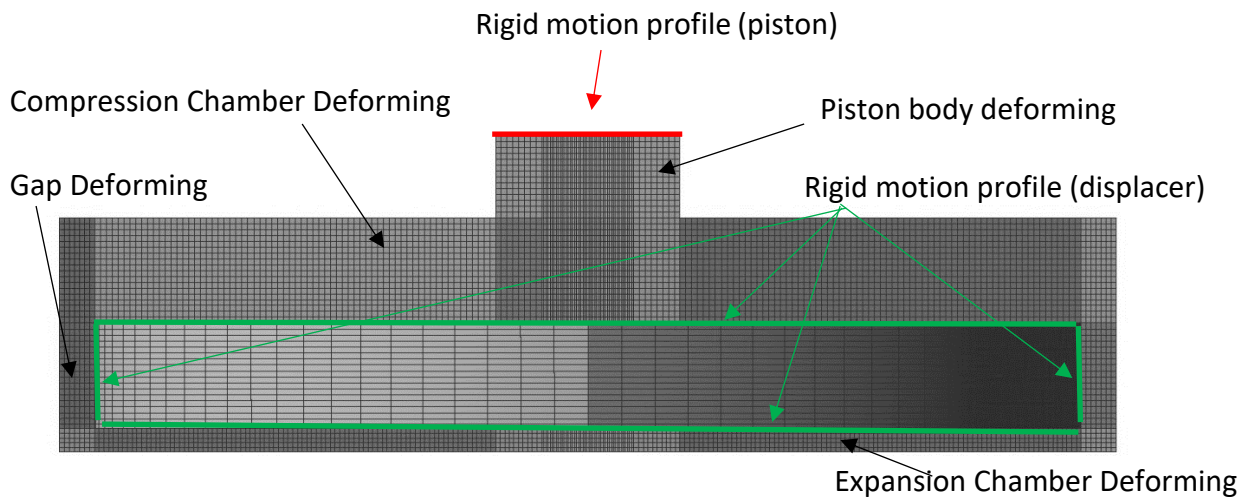


**Fig. 5-15: Dynamic Mesh Set-up of EMSE**

The piston and displacer are connected to a crank shaft. The pistons are at a 90-degree phase angle to the displacer. The motion of the power piston ( $z_p$ ) and displacer ( $z_d$ ) are dictated by the equations presented in section 5.2.1. Based on the dimensions of the Stirling Engine, the dynamic motion of the engine can be represented in graphical form as shown in Negative velocity indicates direction of movement. The graphical representation shown in Fig. 5-16 is for two full rotations of the crank shaft i.e. 720°.

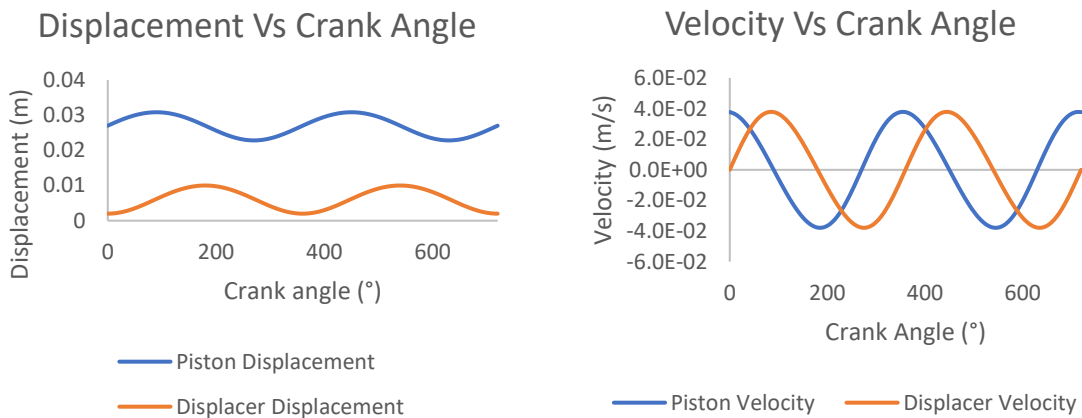


**Fig. 5-16: Sample of Displacement and velocity profiles for piston and displacer of EMSE**

The dynamic mesh method implemented involves the deleting and adding of cells from the mesh. In Ansys 16.1 this corresponds to the layering technique.

Over all 5 scenarios have been chosen for simulation based on the tests conducted in Chapter 4. These are Testing scenarios E6, E9, E16, E17 and E23 chosen to offer a range of temperature

difference between the displacer cylinder. Furthermore, the inspected EMSE tests have been considered for the CFD analysis because this is the closest to the original status of the EMSE. Further modifications to the EMSE added extra losses to the system.

Based on the rotational speeds recorded in the above scenarios, the time step sizes have been calculated so as to ensure no negative volumes are created during the dynamic simulation process. Each time step allowed a maximum 500 iterations to allow for convergence. Results are gathered every 2 time-steps which is equivalent to 10° crank shaft rotation. This set up allows of 20 cycles of the engine. This allows the simulation to achieve a stabilisation stage. Table 5-5 lists the time steps size and number of timesteps required for 40 cycles.

**Table 5-5 time step size and number of time steps for CFD analysis**

Test number (Simulation reference)	Time Step Size	Number of Time Steps
E06 (S06)	0.007056167	1419
E09 (S09)	0.005889282	1699
E16 (S16)	0.006459948	1549
E17 (S17)	0.008177952	1225
E23 (S23)	0.007413998	1350

## 5.5. Simulation Stabilisation

As the bottom of the Stirling Engine heats up, the temperature increases in the expansion chamber. An initial impetus is needed on the engine at this point to get it started. As the displacer moves up, the air in the expansion chamber expands and in turn compresses the air in the compression chamber. At the same time the piston is also pushed up due to the crankshaft motion and hence the Stirling engine cycle has been initiated. Test scenario E6 has been used to demonstrate the stabilisation process.

Fig. 5-17 demonstrates the first cycle of the Stirling engine from 0° crank rotation to 360°. As expected from the simulation, the air expands in the expansion chamber. We see a clear separation in the temperatures of the expansion chamber and the compression chamber.

There is some leakage of heat from the expansion chamber into the compression chamber through the gap between the displacer and the engine wall. This is also expected as the gap is expected to function as a regenerating channel working as a bridge between the chambers and temporarily storing heat. It has been observed that after 12 strokes the temperature profile stabilises. This is further elaborated in Fig. 5-18 where the average temperatures at 180-degree crank angle and 360 degree crank angles is seen to be consistent for both the hot chamber and cold chamber throughout the entirety of the simulation process after 12 strokes of CFD simulation.

From the graph it can be observed that once the Engine has stabilised, a difference is maintained in the temperature between the expansion and the compression chamber. The results show an average difference of 27 K between at the expansion and compression chambers at 180° crank angle and this difference is maintained at 360° crank angle.

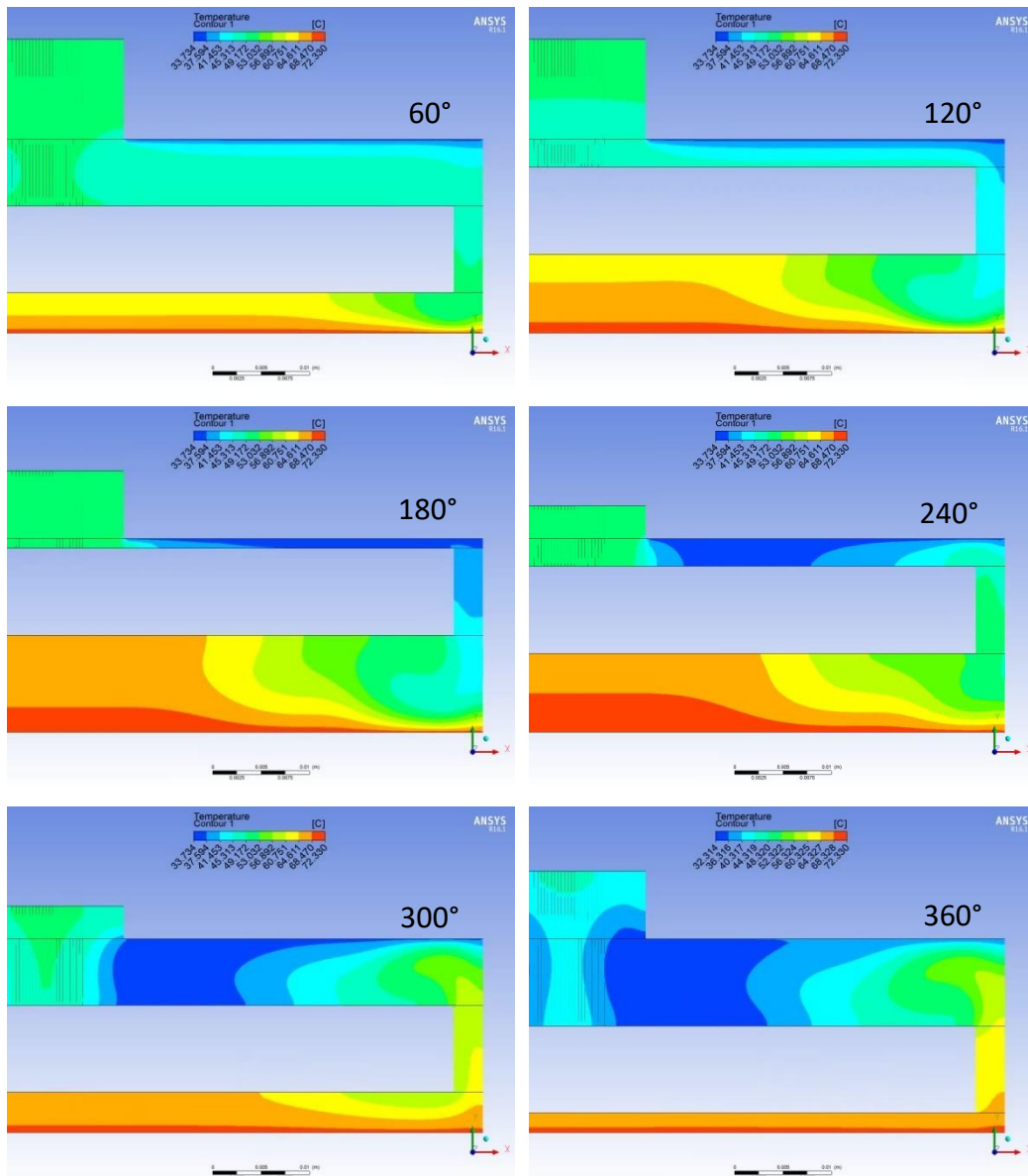


**Fig. 5-17: Starting engine cycle of the Stirling Engine – 0° to 360°.**

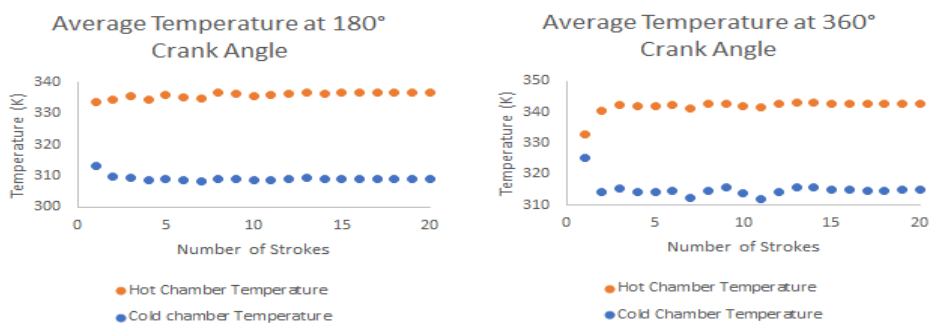


**Fig. 5-18: Graphs showing how the engine goes from start to achieve stabilisation**

The CFD results showing the temperature profiles for a stabilised engine function can thus be mapped as per Fig. 5-19 from 0° crank angle to 360° crank angle.

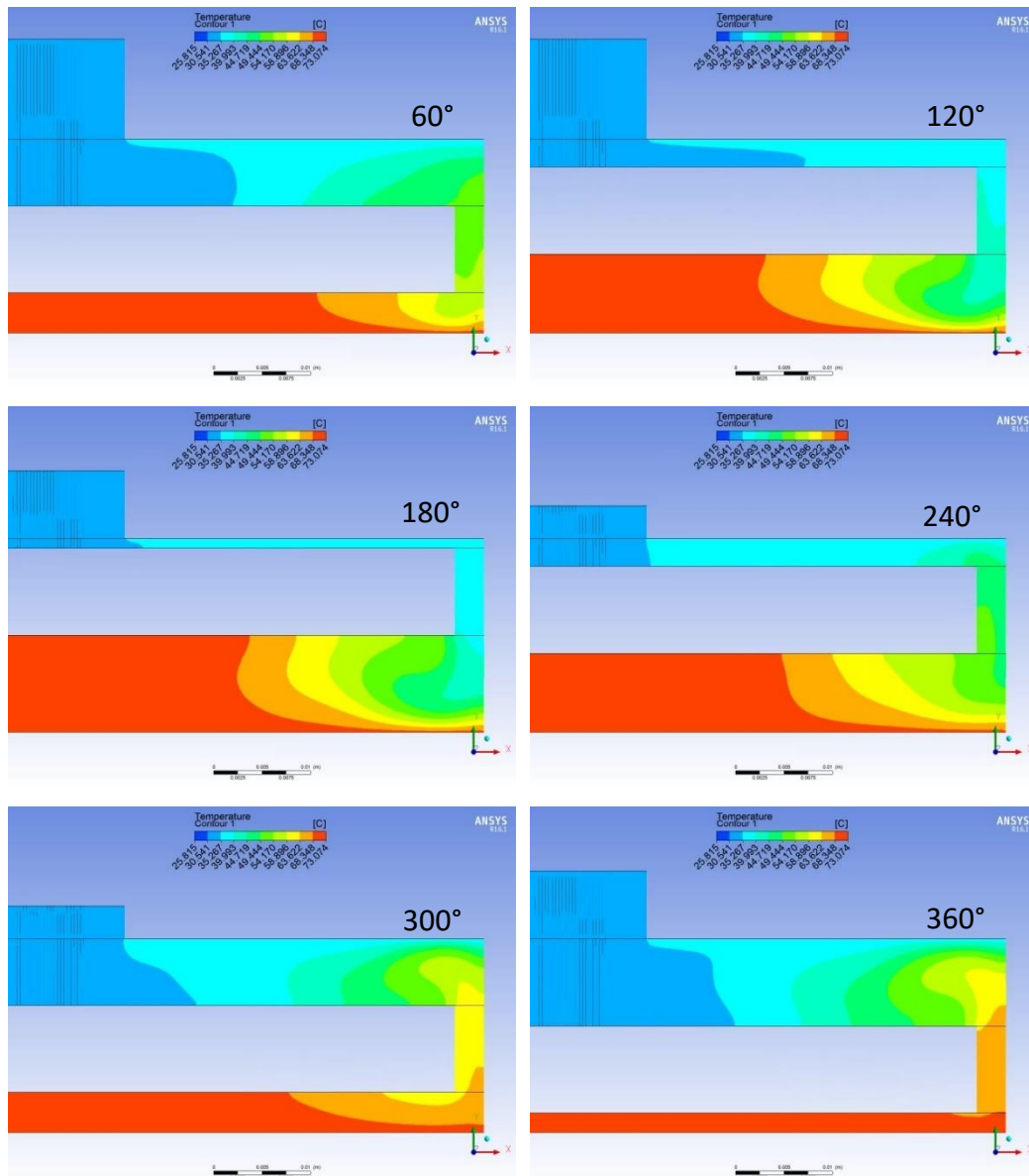


**Fig. 5-19: Engine Cycle once stabilisation has been achieved.**

Clear separation is seen between the temperature profiles of the expansion chamber and compression chamber further reinforcing the values represented above. The only region of mixing temperatures is the gap, however, since the gap is small it doesn't allow for total mixing between the expansion and compression chambers. This can be further improved by implementation of heat exchangers in the gap to act as a regenerator. This will allow for better temporary heat retaining at both the expansion and compression chambers.

## 5.6. Temperature Profile

The temperature profile recorded for the probed EMSE is compared to the Temperature profiles obtained using the CFD analysis. The CFD model has been developed based on the hot surface temperature, cold surface temperature and rotational speeds of the inspected EMSE test results, however, for the validation of the CFD model, the internal temperatures of the probed EMSE with a similar temperature profile has been used. The temperature profile in the probed EMSE is expected to have suffered a small losses when compared to the temperature profile inside an inspected EMSE due to the various modifications subjected onto the EMSE compared to the pressure inside the EMSE and frictional factor. Three such comparisons have been identified for the validation of the CFD results, including, S06 compared against HO10 (Scenario 1), S23 against HO13 (Scenario 2) and S09 against HO04 (Scenario 3). 2D CFD models were also generated for the above scenarios for comparison.

Temperature recording is observed at two locations of the CFD simulation. One at the top section of the displacer (Temp [1]), 0.018m from the bottom and the other 0.002 m from the bottom at the bottom section of the displacer (Temp [2]) as per shown in Fig. 5-20. The average of the temperature reading across one rotation is obtained and compared against the experimental results. The location of the points is as per measurements taken of the probes positioned inside of the displacer cylinder.

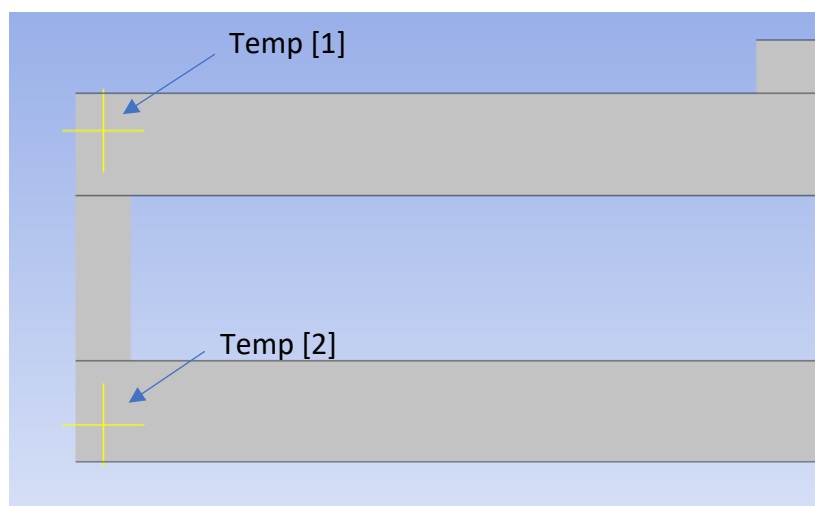


**Fig. 5-20: Temperature measurement locations from CFD results**

The comparison between experimental results and the results obtained from the 2D and 3D CFD analyses are represented in Fig. 5-21.

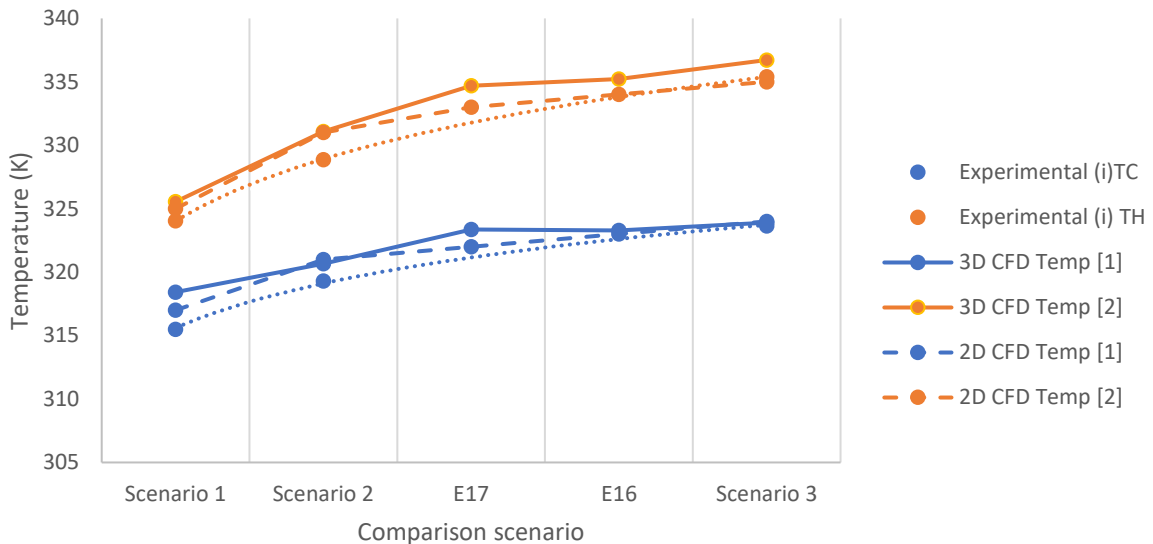


**Fig. 5-21: comparison between experimental and CFD results**

It can be seen that both 2D and 3D CFD analysis produce similar temperature profiles based on the measurements of Temp [1] and Temp [2].

As has been established previously, the testing scenarios are different to the actual CFD analysis. The EMSE tested is not large enough to accommodate a lot of modifications neither are Stirling engines very consistent in their operation. Therefore, for this study the relationships between the functional parameters of the EMSE are put into focus rather than the exact figures.

The Temperatures obtained from the CFD analysis are seen to be higher than those obtained from the experiments. There is, however, better agreement with the temperature on the cold side of the displacer chamber when compared to the hot side of the displacer chamber. The CFD Analysis in the hot section of the displacer chamber produces a maximum error of +1.3% when compared to +1% maximum error at the cold side. The slightly lower temperature may be a result of bleeding connection joints in the experiments which is reducing the temperatures associated with the EMSE.

The best way to negate the errors associated with the minor leaks would be to design and build an EMSE keeping in mind the experimental requirements and ensuring probe locations can be securely sealed without interfering EMSE operation. The higher the temperature the better the agreement between the experimental results and the CFD analysis.

With the low levels of error, it can be established that the temperature profile obtained from the CFD analysis is a valid representation of the EMSE temperature profile with an error percentage of  $\pm 1.3\%$ .

At lower temperatures the difference between the top and bottom sections inside the displacer chamber demonstrates smaller differences in temperature. This difference keeps increasing as the temperature tends higher. This demonstrates that while there is no regenerator in the EMSE, the gap between the displacer and the displacer cylinder possess a regenerative property which ensures re cycling of heat in the system.

The relationship between the temperatures at the top and bottom sections of the inside of the displacer chamber is further visualised as per Fig. 5-22.

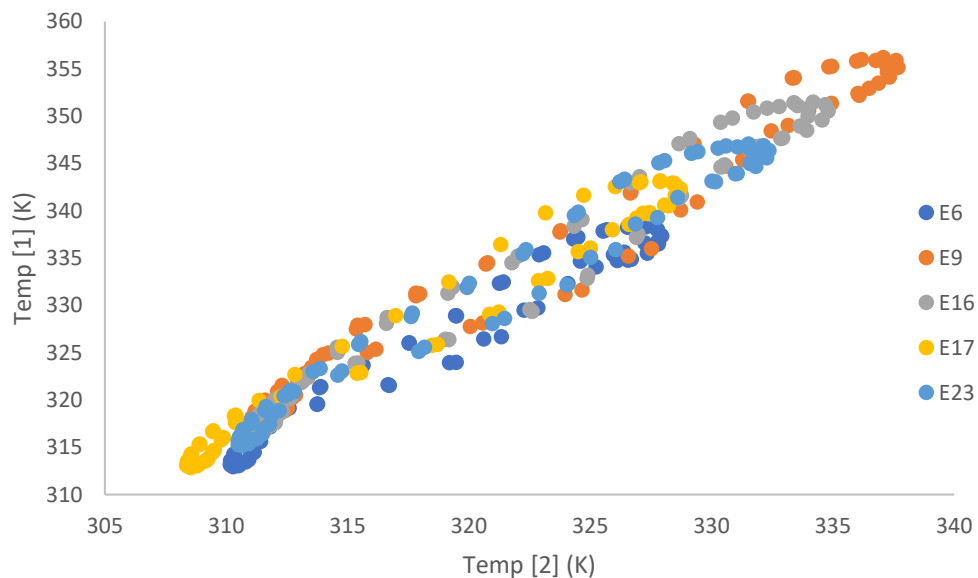


**Fig. 5-22: Comparison of the Temperatures inside the displacer chamber**

At any given point, there is a linear relationship between the temperatures at the top and bottom of the inside of the displacer. This relationship is consistent across all the temperatures that the EMSE has been subjected to. This is expected since the annulus between the displacer and the displacer cylinder does not change, neither does the stroke length. The cold side temperature remains fairly consistent (fluctuating within 2.5%) throughout the scenarios that have been analysed. However, the hot side shows a larger difference across the scenarios. Thus, as per the current setting of the EMSE, very little heat seeps into the cold side of the displacer.

### 5.6.1. Temperature flow inside the displacer chamber

To understand how the temperature flows inside the displacer chamber of the EMSE, the stroke and displacer diameter of the EMSE has been modified and studied with the help of CFD and noting the temperatures at the location points Temp[1] and Temp[2] of the new models as per indicated in Fig. 5-20.

Taking Simulation S23 as the base simulation the temperature profiles for two modifications have been analysed. The first case considering the size of the stroke (scenario T1 and T2) and the second case being the size of the displacer, namely the diameter (scenario T3 and T4). The measured parameters based on the experiments i.e. The hot side temperature, cold side temperature and the rotational speed of the EMSE under operation remains the same. The modifications are summarized below in Table 5-6.

**Table 5-6: Modified EMSE for CFD study**

Testing Scenario	Stroke	Displacer Diameter
S23	4 mm	-
T1	4.2 mm	-
T2	3.8 mm	84 mm
T3	-	86 mm
T4	-	82 mm

The change in the size of the stroke of the EMSE demonstrated minor changes in the temperature profile inside the displacer chamber. This change in in the temperature profile is noticeable as per shown in Fig. 5-23. A larger difference in the profile is identified when the stroke length is increased (T1), particularly when the displacer is halfway between the top and bottom of the stroke (average deviation of 0.2%). This indicates that for the EMSE, the transfer of temperature from the hot side to the cold side is reduced corresponding to a better performance of the EMSE, however, this increase is minor and negligible when compared to the overall performance of the EMSE.

With regards to the reduction of the stroke length (T2), the values are much more comparable (average deviation of 0.08%) to the original simulation scenario (S23) and the slope of the temperature profile closely matches that of S23.

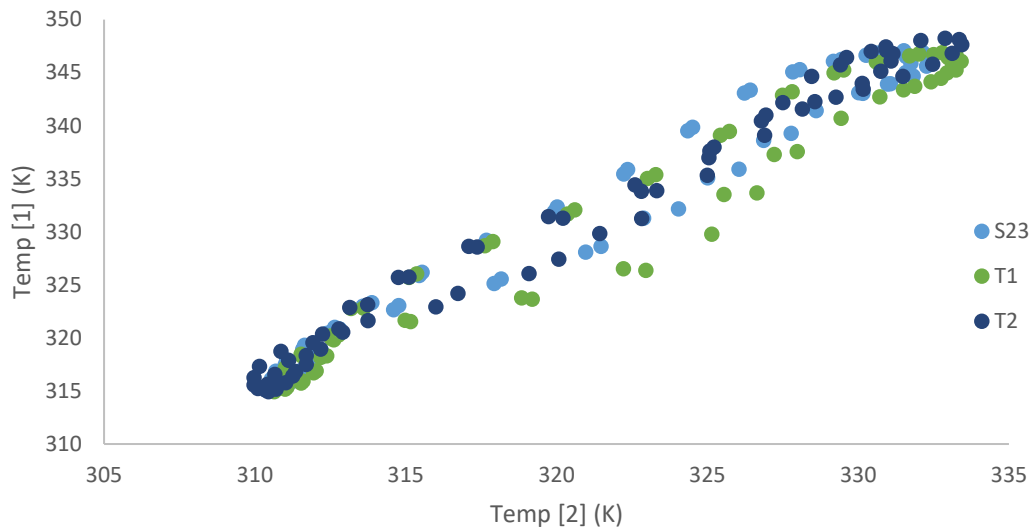


**Fig. 5-23: Temperature profile inside the displacer chamber as a result of changing stroke.**

A clearer indication of change in the performance in the EMSE can be demonstrated by changing the displacer diameter due to the larger scope of change. Fig. 5-24 shows the temperature profile as a result of the size change of the displacer.

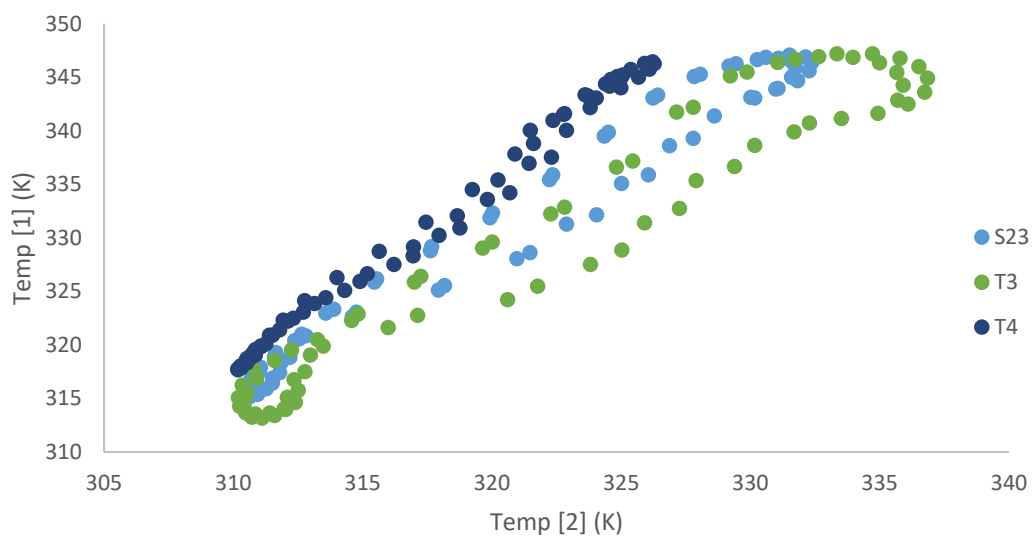


**Fig. 5-24 Temperature profile inside the displacer chamber as a result of changing displacer diameter**

A smaller displacer (scenario T4) reduces the fluctuation of temperature at the measurement points, however, the slope has increased, indicating a larger impact on the temperature at the cold side of the displacer cylinder from the hot end of the displacer cylinder. As expected, with the increase in the diameter of the displacer (Scenario T3), the transfer of temperature from the hot side to the cold side is reduced but this creates larger fluctuation at the measurement points.

The performance is thus better with a smaller annulus as indicated by a smaller slope in the temperature profile; however, the machining of the displacer becomes much more critical as the annulus decreases and the manufacturing tolerance needs to be reduced. The disorder in the cylinder is also seen to be increasing with the reduction in annulus size signified by a larger footprint of scenario T3 compared to scenario T4.

## 5.7. Pressure Profiles

The Pressure in the EMSE is obtained from the CFD analysis using a modified Schmidt equation. The Schmidt equation follows the isothermal analysis from which the pressure can be calculated using the equation:

$$p = nR \left( \frac{V_C}{T_k} + \frac{V_k}{T_k} + \frac{V_r}{T_r} + \frac{V_h}{T_a} + \frac{V_e}{T_a} \right)^{-1} \quad \text{(Equation 10)}$$

Where, ' $p$ ' is the pressure in Pascals, ' $n$ ' in the number of moles, ' $R$ ' is the gas constant with a value of 8.314462618 J/(K·mol), ' $V_C$ ' is the volume of the compression space in m<sup>3</sup>, ' $V_e$ ' is the volume of the expansion space in m<sup>3</sup>, ' $V_k$ ' is the volume of the rejector in m<sup>3</sup>, ' $V_h$ ' is the volume of the acceptor in m<sup>3</sup>, ' $V_r$ ' is the volume of the regenerator in m<sup>3</sup>, ' $T_k$ ' is the temperature at the rejector in K, ' $T_a$ ' is the temperature at the acceptor in K and ' $T_r$ ' is the regenerator temperature in K calculated using:

$$T_R = \frac{(T_a - T_k)}{\ln(T_a/T_k)} \quad \text{(Equation 11)}$$

The EMSE does not have a dedicated Regenerator section and the piston housing is connected directly with the displacer chamber. With the help of the CFD analysis the temperatures at each of the sections (including the compressor section, the expansion section and the annulus) are known at every point of the working cycle. Therefore the Schmidt equation is modified to:

$$p = nR \left( \frac{V_p}{T_p} + \frac{V_{PD}}{T_p} + \frac{V_c}{T_c} + \frac{V_{cD}}{T_c} + \frac{V_r}{T_r} + \frac{V_e}{T_e} + \frac{V_{eD}}{T_e} \right)^{-1} \quad \text{(Equation 12)}$$

Where, ' $V_p$ ' is the volume of the working space of the piston chamber in  $m^3$ , ' $V_{PD}$ ' is the volume of the dead space of the piston chamber in  $m^3$ , ' $V_{cD}$ ' is the volume of the dead space in the compression chamber in  $m^3$ , ' $V_{eD}$ ' is the volume of the dead space in the expansion chamber in  $m^3$ , ' $T_p$ ' is the Temperature in the piston chamber in K, ' $T_c$ ' is the temperature in the compression chamber in K and ' $T_e$ ' is the temperature in the expansion chamber in K.

The number of moles is calculated as per the initial conditions of the test with the pressure being atmospheric pressure (101325 Pa) and the room temperature (295 K). For each section volume (piston, compressor, expansion) the number of moles is calculated using the ideal gas law using the equation:

$$n = \frac{PV}{RT} \quad \text{(Equation 13)}$$

It has been considered that the number of moles does not change during the operation of the EMSE. Essentially establishing that there are no leaks in the system. The number of moles in each section is summed up to obtain the number of moles used to determine the pressure of the EMSE as per Equation 12.

The pressure profiles thus obtained from the CFD analysis and compared against the pressures obtained from the testing of the inspected EMSEs as per presented in section 4.11 in the form of Stirling cycle analysis. The comparison charts are presented as per Fig. 5-25.

The CFD analysis does not match the experimental results obtained. For each scenario analysed, the computational analysis demonstrates higher pressures and higher indicated work when compared to the experimental results. While the pressure profiles generated from the experimental results all map similar results regardless of the difference in temperature to which the EMSE is subjected. However, the CFD analysis results demonstrate a linear relationship where the indicated work, which increases with the increase in the temperature to which the EMSE is subjected.

The graphical comparison of the pressure profiles of the simulated EMSE as per the testing scenarios is shown in Fig. 5-26 demonstrating the Stirling cycle on the basis of no leaks in the EMSE system.

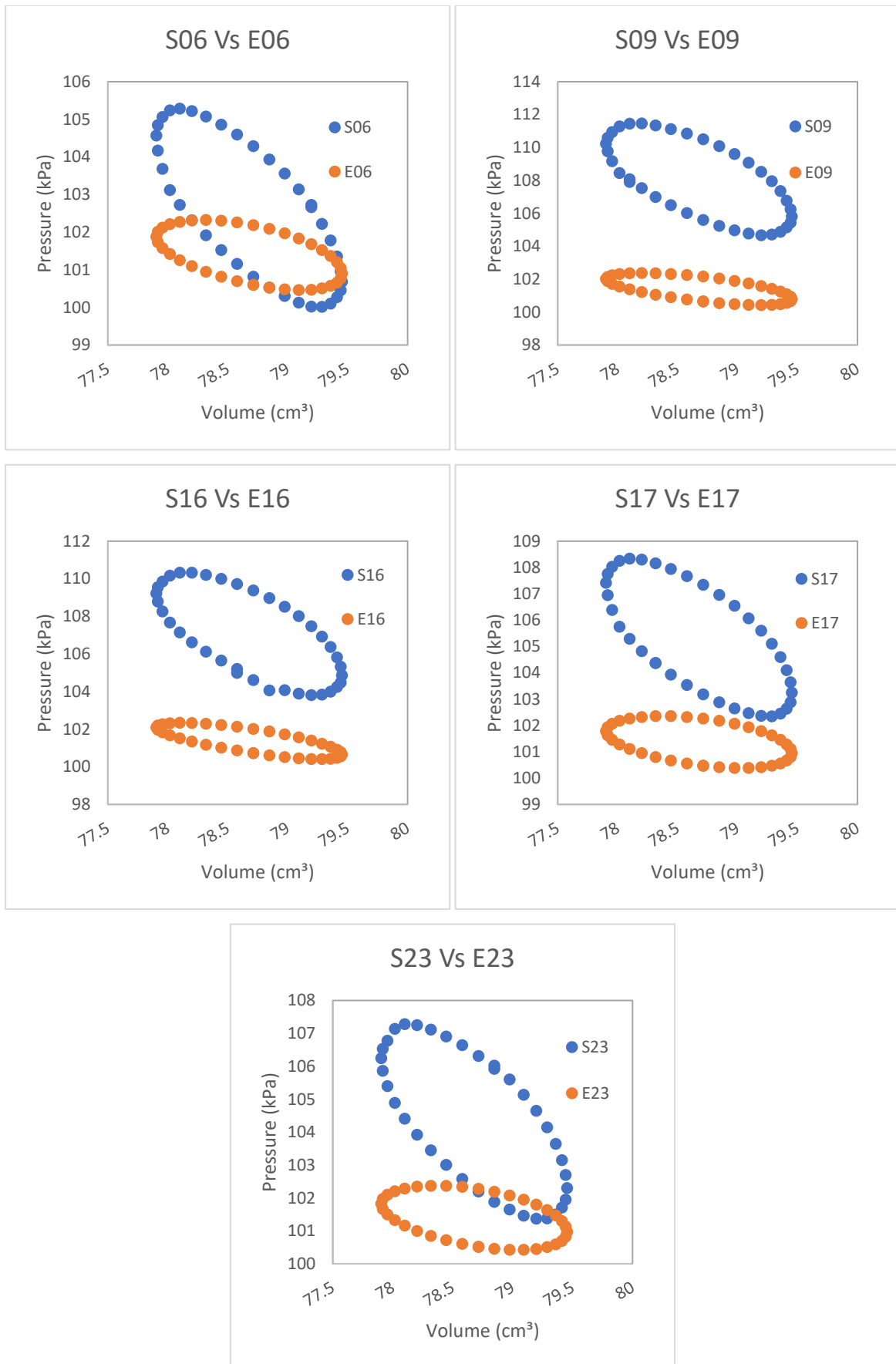


**Fig. 5-25: Comparing the Stirling Cycle analysis as obtained by CFD vs Experiments**

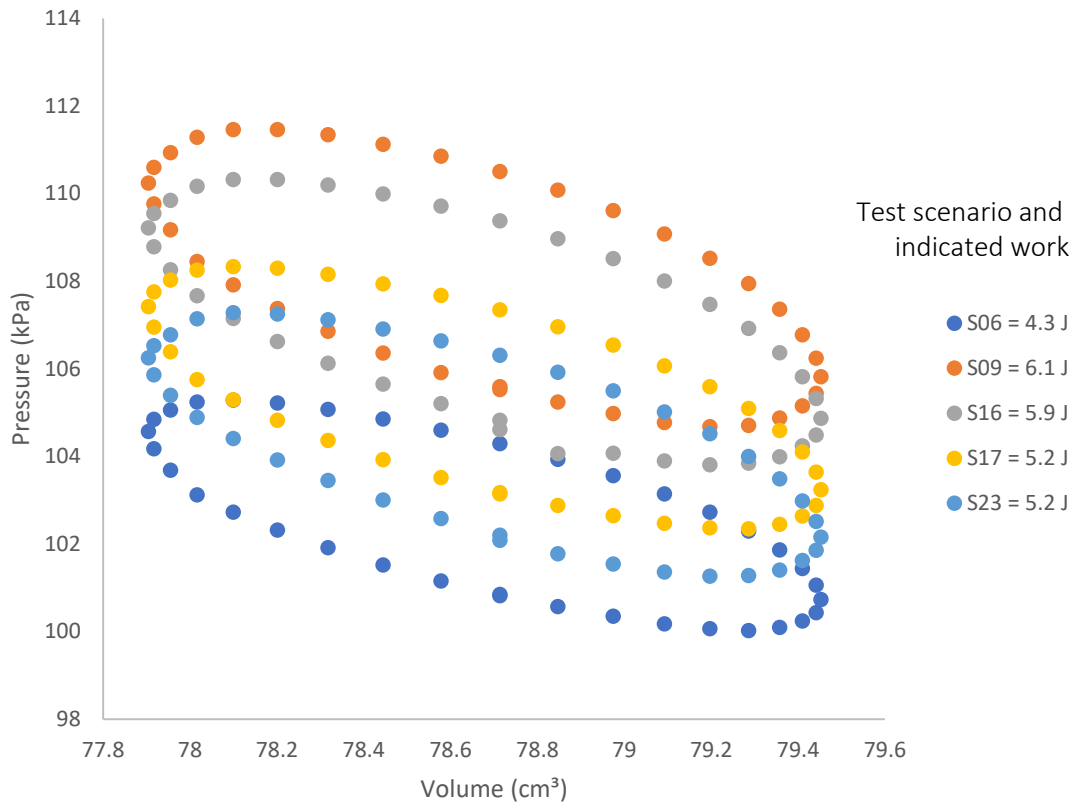


**Fig. 5-26: Graph comparing the pressure profiles obtained by CFD analysis of the EMSE testing scenarios**

The indicated work for the all the scenarios of inspected EMSE from the experimental results is  $0.012 \text{ J} \pm 0.01$ . The consistency in the PV diagram for the experimental results may be attributed to leaks in the EMSE displacer which occurs when the displacer chamber reaches a certain pressure point. This can be overcome with the help of better sealing and more accurate machining of the EMSE. This was also noticed in the Kato [58] experiments.

The maximum pressure retention capability, and subsequently the indicated work, of a Stirling engine will depend on its geometry and the quality of the manufacturing processes. Unless highly accurate manufacturing techniques are used ensuring very low tolerances, it is always going to be difficult to accurately predict the indicated work of the Stirling engine. As a result, it can be established that 3D computational analysis is not an essential tool for the designing of a low cost, low temperature Stirling engines such as the EMSE model that has been used in this research work.

Low cost solutions will always have to be physically tested as the error in indicated work is very high and differs based on the temperature to which the engine has been subjected.

## 5.8. Summary

In This chapter the computational analysis of a low cost, low temperature Stirling engine is presented. The work follows the parametric analysis presented by Wen Lih Chen [75] and uses the technique to simulate and analyse the EMSE.

The EMSE CFD model developed, utilises a full-scale 3D model in comparison to previous models developed ensuring no assumption of symmetry in the model. The model, however, lacks in the account of leaks In the EMSE system.

The temperature profile has been verified using the temperatures measured from the probed EMSE showing good agreement with 3D CFD analysis as well as 2D CFD analysis. However, the pressure profiles were not verified, because the relations between the pressure readings obtained from the experimental results differed greatly from what is obtained from the CFD analysis.

The results demonstrate that while there is minor difference in the temperature profile across the displacer chamber even after modifications on the EMSE, the pressures are impacted a lot more in comparison. This indicates that the construction of a Stirling engine is very crucial. For low cost, low temperature differential Stirling engines such as the EMSE, the materials used, the geometry of the engine and create several limitations on the pressure capability. Higher quality machining and materials significantly raises the cost of Stirling engines affecting the affordability of the pump system that is envisioned for this research work.

Assessing the pressure retention capabilities requires practical testing. As such, computational analysis is not an essential tool for the designing of a low cost, low temperature Stirling engine. Furthermore, there is good agreement between the temperature profiles generated from both the 2D simulated results as well as the 3D simulated results. If CFD analysis is proposed for analysis 2D simulation is sufficient.

# Chapter 6

## Conclusions

### 6.1. Introduction

This chapter summarises the findings of the research undertaken and provides insight in the following areas:

- Why a cost focused solution is required to ensure a feasible solution is obtained for irrigation in the sub-Saharan Africa region,
- Considering a cost-effective EMSE system, a summary of the experimental results and findings are presented, to determine the effectiveness of the system and analyse the practicality of such a device being used in the real-world scenario.
- A summary of the computational analysis and the comparison to the experimental results has been presented to identify the accuracy of CFD in analysis of the low-cost EMSE.
- Identifying key characteristics that can be analysed using CFD, a summary of models developed to further improve the efficiency of the EMSE have been presented.
- Finally based on the findings of the research, experimentation and analysis a future work objective has been set.

### 6.2. The need for a cost focused solution

The vast majority of the sub-Saharan African region is underdeveloped [87]. Severe draught, lack of rain and long dry spells means that the people in the region generally have to import food from other countries, increasing the cost of food. Almost 1/3 of the basic grains being imported [64]. Providing the residents of the region with a means to grow their own food is a strategic priority. In order to provide food security in the region, the available resources have been reviewed to ensure a sustainable system using suitable renewable technologies.

Solar thermal technologies provide the opportunity for small scale remote farms usage if the correct infrastructure is available for solar power concentration. Solar concentration technology that is cheap, effective and portable is essential to produce a feasible system.

Parabolic concentrators and dish concentrators provide compact solutions; however, an all-encompassing system is expensive to purchase. Local alternatives utilising local materials to build concentration systems may be proposed, which will reduce the cost as well as carbon footprint of the system. This has led to the proposal of using Stirling Engines which are compact relative to other forms of solar thermal technologies. Table shows how the solar thermal technologies have been compared for the purpose of low cost, irrigation system in the Sub-Saharan Africa region based on research by Wazed et. al. [87].

The focus of this research was to assist in the development of a Stirling engine system for irrigation that was affordable for the demographic in the Sub-Saharan Africa region for the empowerment of independent farmers. Hence, the cost of the technology was a major factor dictating the type of Stirling systems that have been investigated. This ensured that the materials used, and the manufacturing techniques opted for the Stirling Engine Is easily accessible to the demographic.

**Table 6-1: Comparing various solar thermal technologies [87]**

<b>Property</b>	<b>Rankine Cycle System</b>	<b>Stirling Engine</b>	<b>Metal Engine</b>	<b>Hydride Piston Pump</b>	<b>Liquid Piston Pump</b>
<b>Size</b>	Large	Small	Small		Small
<b>Locally sourced materials</b>	No	Yes	No		No
<b>Mobility</b>	No	Yes	Yes		Yes
<b>Cost</b>	High	Less	High		Less

Low temperature differential, gamma-type Stirling engine was selected for the investigation because of the relative ease of manufacture. However, low cost systems Investigated were generally very small in size, such as, that tested by Kato [78] and the EMSE tested in this Investigation.

### 6.3. Experimental Results

Experiments were conducted on a Low temperature differential Education Model Stirring Engine (EMSE) to study the working of the engine across the various modification stages to internal temperature readings of the EMSE.

1. Experimental tests were divided into 4 different types including, new EMSE, Inspected EMSE, Drilled EMSE and Probed EMSE. Temperature of the outer bottom and top surfaces of the displacer chamber and the pressure inside the displacer chamber is measured for the Inspected EMSE and drilled EMSE. The Probed EMSE also measures the temperatures inside the displacer chamber using two probes, one in the top section of the displacer chamber and one in the bottom section of the displacer chamber. Just the top and bottom surface temperatures of the new EMSE is measured. The temperature ratio between the top and bottom surface of the EMSE remained consistent throughout all the testing scenarios within difference percentage of 0.65% and  $R^2$  value of 0.75; which insists that the modifications on the EMSE does not have any impact on the temperature profile. The P-V Diagram and consequently the indicated work remains consistent across the individual testing scenarios regardless of the temperatures the scenarios are subjected to. However, the work done increases from Inspected EMSE to Drilled EMSE by 24% to and from inspected EMSE to Probed EMSE respectively by 28%. These results parallel that of Kato [78] indicating a restricting pressure capability of the EMSE which depends on the geometry and the quality of fabrication of the EMSE. This result is different from theoretical estimations which indicate increasing work with increasing temperature difference.
2. Temperature visualization from a Thermal Imaging showed good agreement for the temperature profile across the hot surface of the displacer chamber with a slight difference in the values of the temperature at the cold surface of the displacer. The rate at which the hot side temperature increases is different when compared between the Thermal imaging camera and the thermocouple. Using thermocouples reduces the cost of the experiments and also ensures more accurate measurement of temperatures inside the EMSE, since thermal imaging cameras only measure the outer surface temperatures hence instantaneous temperatures are less accurate.

3. Graphing the temperature at the bottom surface of the Stirling Engine to the rotational speeds demonstrates a linear relationship the slope of which decreases with modifications made to the EMSE. The slope is severely affected on the Probed EMSE with a slope of 0.1983 and 95% difference when compared with the new EMSE.
4. A large discrepancy is apparent between the experimental results of pressure and the results obtained using theoretical estimations. The researcher is circumspect of the Pressure sensing device with regards to its accuracy. Since due to the pandemic validation of the pressure recordings was not possible it is one of the areas where the experimental results are wanting. Add to this the high levels of friction and leakages in the system due to the low precision construction further added to the issue of erroneous results that had to undergo a lot of processing in order to make a comparison with the theoretical results.

#### **6.4. CFD Results**

Computational Analysis of the EMSE is conducted based on the principles demonstrated by Wen Lih Chen [56]. A full-scale 3D model was simulated and analysed to negate any symmetry related errors. The CFD analysis allows the simulation to run for 10 seconds to allow for stabilization period such that the temperatures in the EMSE reaches a stable range and a clear separation is observed between the top and bottom surface temperatures. Finally, a 1 second time period (9s-10s simulation time) is considered to conduct the analysis. 2D CFD model was also generated for experimentation scenarios E06, E09 and E23.

1. Measuring temperatures at two points on the inner region of the EMSE simulation (Temp [1] and Temp [2]) mirroring the experimental scenario, both the 2D and 3D simulations show good agreement with the experimental results. With a maximum error difference of +1.3% at the hot plate and a maximum of +1% error at the cold plate.
2. At lower temperatures the difference between the top and bottom sections inside the displacer chamber demonstrates smaller differences in temperature. This difference keeps increasing as the temperature tends higher. This demonstrates that while there is no regenerator in the EMSE, the gap between the displacer and the displacer cylinder possess a regenerative property which ensures re cycling of heat in the system.

3. The temperature profile remained consistent across the change in the stroke length in the EMSE. Due to a short displacer height, there was little impact expected, however, it is clear that halfway between the stroke a larger variance in temperature values were presented due to change in stroke length. Since, larger changes could be administered to the displacer diameter a more clear indication of the change in performance of the EMSE was identified. A smaller displacer (scenario T4) reduces the fluctuation of temperature at the measurement points, however, the slope has increased, indicating a larger impact on the temperature at the cold side of the displacer cylinder from the hot end of the displacer cylinder.
4. The CFD analysis does not match the experimental results obtained for the pressure readings of the EMSE. the computational analysis demonstrates higher pressures and higher indicated work when compared to the experimental results. The indicated work for the all the scenarios of inspected EMSE from the experimental results is  $0.012 \text{ J} \pm 0.1$ .
5. 3D computational analysis is not necessary in estimating the functioning of a Stirling Engine. 2D and 3D analysis both offer good estimation of the temperature profile of the EMSE, however, the pressure profile does not match that of the experiments. This has been attributed to material and construction factors that limit the pressure capabilities of the Stirling Engine which is difficult to quantify. Therefore, while CFD is a convenient tool for quickly carrying out the analysis, it is no more accurate than any other numerical methods especially for low cost products which feature cheaper materials. Low cost Stirling Engines need to be practically tested to accurately evaluate it's properties.

## **6.5. Future Work**

This research was based on the fundamental understanding of the working process of a low-cost, low temperature differential Stirling engine using a readily available Stirling model. The ideal way to more accurately study this would be by custom building Stirling engine models of varying geometrical and special features to establish a more solid data base. Furthermore, research is required in various types of materials that could be used to build the engine to satisfy the low cost while maintain the functionality of the engine. Air tightness is one of the major factors that affects the effectivity of the Stirling Engine.

Further practical experimentation is required on pump configurations to ensure adequate pumping capabilities to meet the irrigation requirements. Analysis of the utilisation of Solar power is necessary, whether it used just solar thermal energy or a combination of Solar thermal and solar PV or other renewable sources available in the sub-Saharan Africa region. Environmental and economic impact study of technology is also an important analysis required for today's climate.

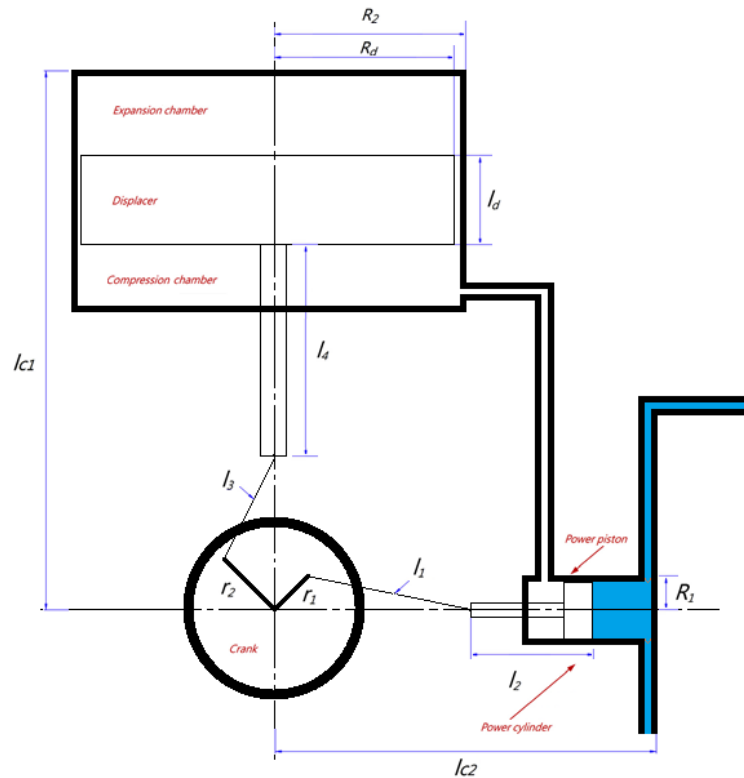


**Fig. 6-1: Conceptual model of the Stirling pump system.**

# Chapter 7

## REFERENCES

- [1] Iea. Africa Energy Outlook: A Focus on Prospects in Sub-Saharan Africa 2014:1–242.
- [2] FAO. REGIONAL OVERVIEW OF FOOD SECURITY AND NUTRITION. FAO; 2016.
- [3] Knox J, Hess T, Daccache A, Ferguson IM, Maxwell RM. assessment Quantitative maps of groundwater resources in Africa n.d. doi:10.1088/1748-9326/7/2/024009.
- [4] FAO. FAO - News Article: Famine hits parts of South Sudan 2017. <http://www.fao.org/news/story/en/item/471251/icode/> (accessed June 4, 2017).
- [5] UNICEF. 2015 Update and MDG Assessment 2015.
- [6] Kashaigili JJ. Ground water Availability and Use in Sub-Saharan Africa. Srilanka: International Water Management Institute; 2012. doi:10.5337/2012.213.
- [7] Pavelic P, Villholth KG, Shu Y, Rebelo L-M, Smakhtin V. Smallholder groundwater irrigation in Sub-Saharan Africa: country-level estimates of development potential. *Water Int* 2013;38:392–407. doi:10.1080/02508060.2013.819601.
- [8] Quansah DA, Adaramola MS, Mensah LD. Solar Photovoltaics in sub-Saharan Africa – Addressing Barriers , Unlocking Potential. *Energy Procedia* 2016;106:97–110. doi:10.1016/j.egypro.2016.12.108.
- [9] Cavero J, Faci JM, Martínez-Cob A. Relevance of sprinkler irrigation time of the day on alfalfa forage production. *Agric Water Manag* 2016;178:304–13. doi:10.1016/j.agwat.2016.10.008.
- [10] Ramos JS, Ramos HM. Solar powered pumps to supply water for rural or isolated zones: A case study. *Energy Sustain Dev* 2009;13:151–8. doi:10.1016/j.esd.2009.06.006.
- [11] Muhsen DH, Khatib T, Nagi F. A review of photovoltaic water pumping system designing methods, control strategies and field performance. *Renew Sustain Energy Rev* 2017;68:70–86. doi:10.1016/j.rser.2016.09.129.

- [12] Gopal C, Mohanraj M, Chandramohan P, Chandrasekar P. Renewable energy source water pumping systems - A literature review. *Renew Sustain Energy Rev* 2013;25:351–70. doi:10.1016/j.rser.2013.04.012.
- [13] Sontake VC, Kalamkar VR. Solar photovoltaic water pumping system - A comprehensive review. *Renew Sustain Energy Rev* 2016;59:1038–67. doi:10.1016/j.rser.2016.01.021.
- [14] Kumar M, Reddy KS, Adake R V., Rao CVKN. Solar powered micro-irrigation system for small holders of dryland agriculture in India. *Agric Water Manag* 2015;158:112–9. doi:10.1016/j.agwat.2015.05.006.
- [15] Martin A. Green, Keith Emery, Yoshihiro Hishikawa WW and EDD. Solar cell efficiency tables (Version 45). *Prog Photovolt Res Appl* 2007;23:659–76. doi:10.1002/pip.2573.
- [16] Chandel SS, Nagaraju Naik M, Chandel R. Review of solar photovoltaic water pumping system technology for irrigation and community drinking water supplies. *Renew Sustain Energy Rev* 2015;49:1084–99. doi:10.1016/j.rser.2015.04.083.
- [17] Jones MA, Odeh I, Haddad M, Mohammad AH, Quinn JC. Economic analysis of photovoltaic (PV) powered water pumping and desalination without energy storage for agriculture. *Desalination* 2016;387:35–45. doi:10.1016/j.desal.2016.02.035.
- [18] Green M., Emery K, Hishikawa Y, Warta W, Dunlop ED, Levi DH, et al. Solar cell efficiency tables (version 49) Martin. *Prog PHOTOVOLTAICS Res Appl* 2017;25:3–13. doi:10.1002/pip.1160.
- [19] López-Luque R, Reca J, Martínez J. Optimal design of a standalone direct pumping photovoltaic system for deficit irrigation of olive orchards. *Appl Energy* 2015;149:13–23. doi:10.1016/j.apenergy.2015.03.107.
- [20] Deveci O, Onkol M, Unver HO, Ozturk Z. Design and development of a low-cost solar powered drip irrigation system using Systems Modeling Language. *J Clean Prod* 2015;102:529–44. doi:10.1016/j.jclepro.2015.04.124.
- [21] Treephak K, Thongpron J, Somsak D, Saelao J, Patcharaprakiti N. An economic evaluation comparison of solar water pumping system with engine pumping system for rice cultivation. *Jpn J Appl Phys* 2015;54:08KH01.

- [22] Campana PE, Li H, Yan J. Techno-economic feasibility of the irrigation system for the grassland and farmland conservation in China: Photovoltaic vs. wind power water pumping. *Energy Convers Manag* 2015;103:311–20. doi:10.1016/j.enconman.2015.06.034.
- [23] Campana PE, Li H, Zhang J, Zhang R, Liu J, Yan J. Economic optimization of photovoltaic water pumping systems for irrigation. *Energy Convers Manag* 2015;95:32–41. doi:10.1016/j.enconman.2015.01.066.
- [24] Hossain MA, Hassan MS, Mottalib MA, Ahmmed S. Technical and economic feasibility of solar pump irrigations for eco-friendly environment. *Procedia Eng* 2015;105:670–8. doi:10.1016/j.proeng.2015.05.047.
- [25] Yahyaoui I, Tadeo F, Vieira M. Energy and water management for drip-irrigation of tomatoes in a semi- arid district. *Agric Water Manag* 2016. doi:10.1016/j.agwat.2016.08.003.
- [26] Reca J, Torrente C, López-Luque R, Martínez J. Feasibility analysis of a standalone direct pumping photovoltaic system for irrigation in Mediterranean greenhouses. *Renew Energy* 2016;85:1143–54. doi:10.1016/j.renene.2015.07.056.
- [27] Mohammed Wazed S, Hughes BR, O’Connor D, Calautit JK. A Review of Sustainable Solar Irrigation Systems for Developing Countries. 2017.
- [28] Chandel SS, Nagaraju Naik M, Sharma V, Chandel R. Degradation analysis of 28 year field exposed mono-c-Si photovoltaic modules of a direct coupled solar water pumping system in western Himalayan region of India. *Renew Energy* 2015;78:193–202. doi:10.1016/j.renene.2015.01.015.
- [29] Merino, G.G. Lagos, L.O. Gontupil JE. Monitoring and Evaluation of a Direct Coupled Photovoltaic Pumping System. *Appl Eng Agric* 2008;24:277–84. doi:10.13031/2013.24495.
- [30] Benghanem M, Daffallah KO, Alamri SN, Joraid AA. Effect of pumping head on solar water pumping system. *Energy Convers Manag* 2014;77:334–9. doi:10.1016/j.enconman.2013.09.043.

- [31] Tiwari AK, Kalamkar VR. Performance investigations of solar water pumping system using helical pump under the outdoor condition of Nagpur, India. *Renew Energy* 2016;97:737–45. doi:10.1016/j.renene.2016.06.021.
- [32] Kabalci Y, Kabalci E, Canbaz R, Calpbinici A. Design and implementation of a solar plant and irrigation system with remote monitoring and remote control infrastructures. *Sol Energy* 2016;139:506–17. doi:10.1016/j.solener.2016.10.026.
- [33] Sarkar MNI, Ghosh HR. Techno-economic analysis and challenges of solar powered pumps dissemination in Bangladesh. *Sustain Energy Technol Assessments* 2017;20:33–46. doi:10.1016/j.seta.2017.02.013.
- [34] Delgado-Torres AM. Solar thermal heat engines for water pumping: An update. *Renew Sustain Energy Rev* 2009;13:462–72. doi:10.1016/j.rser.2007.11.004.
- [35] Baral S, Kim D, Yun E, Kim K. Experimental and Thermoeconomic Analysis of Small-Scale Solar Organic Rankine Cycle (SORC) System. *Entropy* 2015;17:2039–61. doi:10.3390/e17042039.
- [36] Date A, Akbarzadeh A. Theoretical study of a new thermodynamic power cycle for thermal water pumping application and its prospects when coupled to a solar pond. *Appl Therm Eng* 2013;58:511–21. doi:10.1016/j.applthermaleng.2013.05.004.
- [37] Sitranon J, Lertsatitthanakorn C, Namprakai P, Prathinthong N, Suparos T, Roonprasang N. Performance Enhancement of Solar Water Heater with a Thermal Water Pump. *J Energy Eng* 2015;141:04014036. doi:10.1061/(ASCE)EY.1943-7897.0000216.
- [38] Das D, Ram Gopal M. Studies on a metal hydride based solar water pump. *Int J Hydrogen Energy* 2004;29:103–12. doi:10.1016/S0360-3199(03)00044-2.
- [39] Mahkamov K, Orda EP. Solar thermal water pumps: A preliminary analysis of the working process. *J Sol Energy Eng Trans ASME* 2005;127:29–36. doi:10.1115/1.1767191.
- [40] Jokar H, Tavakolpour-Saleh AR. A novel solar-powered active low temperature differential Stirling pump. *Renew Energy* 2015;81:319–37. doi:10.1016/j.renene.2015.03.041.

- [41] Ferreira AC, Nunes ML, Teixeira JC, Martins LB, Teixeira SFCF. Thermodynamic and Economic Optimization of a Solar-powered Stirling engine for Micro- Cogeneration Purposes. *Proc Ecos 2015 - 28Th Int Conf Effic Cost, Optim Simul Environ Impact Energy Syst* 2015;111:13 pgs.
- [42] Felix A. Farret MGS. Appendix C the Stirling Engine. 2006. doi:10.1002/0471755621.
- [43] Bagheri A, Bostanci H, Foster PR. Preliminary analysis of an innovative rotary displacer stirling engine. *ASME Int Mech Eng Congr Expo Proc* 2015;6A-2015. doi:10.1115/IMECE2015-52455.
- [44] Ahmadi MH, Ahmadi M-A, Pourfayaz F. Thermal models for analysis of performance of Stirling engine: A review. *Renew Sustain Energy Rev* 2017;68:168–84. doi:10.1016/j.rser.2016.09.033.
- [45] Kurhe N, Funde A, Gokhale P, Jadkar S, Ghaisas S, Date A. Development of Low Temperature Heat Engine for Water Pumping Application. *Energy Procedia* 2017;110:292–7. doi:10.1016/j.egypro.2017.03.142.
- [46] Tchanche BF, Lambrinos G, Frangoudakis A, Papadakis G. Low-grade heat conversion into power using organic Rankine cycles - A review of various applications. *Renew Sustain Energy Rev* 2011;15:3963–79. doi:10.1016/j.rser.2011.07.024.
- [47] Sunvention Sunpulse. Sunvention Stirling Machine. vol. 0. n.d.
- [48] Coen Reith. Solar Stirling Engine Water Pump. JOVOTO 2013. [https://uploads1.jovo.to/idea\\_attachments/579121/solar-stirling-common-waterpump-1\\_big.jpg?1448775192](https://uploads1.jovo.to/idea_attachments/579121/solar-stirling-common-waterpump-1_big.jpg?1448775192) (accessed January 20, 2017).
- [49] S VC. Beginners Guide to Stirling engines. Vineeth C S; 2011.
- [50] Lakew AA, Bolland O, Ladam Y. Theoretical thermodynamic analysis of Rankine power cycle with thermal driven pump. *Appl Energy* 2011;88:3005–11. doi:10.1016/j.apenergy.2011.03.029.
- [51] Baral S, Kim KC. Stand-alone solar organic Rankine cycle water pumping system and its economic viability in Nepal. *Sustain* 2016;8:1–18. doi:10.3390/su8010018.
- [52] Moonsri P, Kunchornrat J, Namprakai P. Hybrid Energy Thermal Water Pump for

- Producing Hot Water from a Shallow Well in Thailand. *J Energy Eng* 2015;04015023:04015023. doi:10.1061/(ASCE)EY.1943-7897.0000278.
- [53] Bataineh KM. Optimization analysis of solar thermal water pump. *Renew Sustain Energy Rev* 2016;55:603–13. doi:10.1016/j.rser.2015.10.146.
- [54] Mahkamov K. Design Improvements to a Biomass Stirling Engine Using Mathematical Analysis and 3D CFD Modeling 2013;128. doi:10.1115/1.2213273.
- [55] Chen WL, Wong KL, Chen HE. An experimental study on the performance of the moving regenerator for a  $\gamma$ -type twin power piston Stirling engine. *Energy Convers Manag* 2014;77:118–28. doi:10.1016/j.enconman.2013.09.030.
- [56] Chen W-L, Wong K-L, Chang Y-F. A computational fluid dynamics study on the heat transfer characteristics of the working cycle of a low-temperature-differential  $\gamma$ -type Stirling engine. *Int J Heat Mass Transf* 2014;75:145–55. doi:10.1016/j.ijheatmasstransfer.2014.03.055.
- [57] Chen WL, Wong KL, Po LW. A numerical analysis on the performance of a pressurized twin power piston gamma-type Stirling engine. *Energy Convers Manag* 2012;62:84–92. doi:10.1016/j.enconman.2012.02.035.
- [58] Kato Y. Indicated diagrams of low temperature differential Stirling engines with channel-shaped heat exchangers Heat exchanger Magnification. *Renew Energy* 2017;103:30–7. doi:10.1016/j.renene.2016.11.026.
- [59] MacDonald, A. M., H. C. Bonsor, R. C. Calow, R. G. Taylor, D. J. Lapworth, L. Maurice, J. Tucker and BEOD. Groundwater resilience to climate change in Africa. *Groundw Sci Program* 2011:32.
- [60] Venot JP. A Success of Some Sort: Social Enterprises and Drip Irrigation in the Developing World. *World Dev* 2016;79:69–81. doi:10.1016/j.worlddev.2015.11.002.
- [61] Katherine Martinko. How drip irrigation can save the world : TreeHugger. *Tree Hugger* 2016. <https://www.treehugger.com/sustainable-agriculture/how-drip-irrigation-can-save-world.html> (accessed June 13, 2017).
- [62] Karlberg L, Vries FWTP De. Exploring potentials and constraints of low-cost drip

- irrigation with saline water in sub-Saharan Africa 2004;29:1035–42. doi:10.1016/j.pce.2004.08.004.
- [63] FAO. Irrigation Techniques for Small-scale Farmers. 2016.
- [64] FAO. Farm size | FAO | Food and Agriculture Organization of the United Nations 2012. <http://www.fao.org/family-farming/data-sources/dataportrait/farm-size/en/>.
- [65] Solargis. Download free solar resource maps | Solargis. Dolargis 2010. <http://solargis.com/products/maps-and-gis-data/free/download/africa-and-middle-east> (accessed June 17, 2017).
- [66] Irena. Solar Pv in Africa: Costs and market. 2016.
- [67] Paccoud O, Kleinwächter J, Genkinger P. Stirling engine and method of using a Stirling engine. DE112016001342T5, 2016.
- [68] Kreith F, Goswami DY. The CRC handbook of Mechanical Engineering. Second. Washington DC: CRC Press LLC; 2005.
- [69] Hooshang M, Askari Moghadam R, AlizadehNia S. Dynamic response simulation and experiment for gamma-type Stirling engine. Renew Energy 2016;86:192–205. doi:10.1016/j.renene.2015.08.018.
- [70] Kongtragool B, Wongwiset S. A review of solar-powered Stirling engines and low temperature differential Stirling engines. Renew Sustain Energy Rev 2003;7:131–54. doi:10.1016/S1364-0321(02)00053-9.
- [71] Leon J, Chen W. A computational fluid dynamics study on the heat transfer characteristics of the working cycle of a  $\beta$ -type Stirling engine. Energy Convers Manag 2014;88:177–88. doi:10.1016/j.enconman.2014.08.040.
- [72] Alfarawi S, Mahmoud S. Influence of phase angle and dead volume on gamma-type Stirling engine power using CFD simulation. Energy Convers Manag 2016;124:130–40. doi:10.1016/j.enconman.2016.07.016.
- [73] Cheng C, Chen Y. Numerical simulation of thermal and flow fields inside a 1-kW  $\beta$ -type Stirling engine. Appl Therm Eng 2017;121:554–61. doi:10.1016/j.applthermaleng.2017.04.105.

- [74] Chen W, Wong K, Chang Y. International Journal of Heat and Mass Transfer A numerical study on the effects of moving regenerator to the performance of a  $\beta$ -type Stirling engine. *Int J Heat Mass Transf* 2015;83:499–508. doi:10.1016/j.ijheatmasstransfer.2014.12.035.
- [75] Chen W, Yang Y, Leon J. A CFD parametric study on the performance of a low-temperature-differential  $\gamma$ -type Stirling engine. *Energy Convers Manag* 2015;106:635–43. doi:10.1016/j.enconman.2015.10.007.
- [76] Kato Y, Saitoh S, Ishimatsu K, Iwamoto M. Effect of geometry and speed on the temperatures estimated by CFD for an isothermal model of a gamma configuration low temperature differential Stirling engine with Flat-shaped heat exchangers. *Appl Therm Eng* 2017;115:111–22. doi:10.1016/j.applthermaleng.2016.12.070.
- [77] Xiao G, Sultan U, Ni M, Peng H, Zhou X, Wang S, et al. Design optimization with computational fluid dynamic analysis of  $\beta$ -type Stirling engine. *Appl Therm Eng* 2017;113:87–102. doi:10.1016/j.applthermaleng.2016.10.063.
- [78] Kato Y. Indicated diagrams of low temperature differential Stirling engines with channel-shaped heat exchangers Heat exchanger Magnification. *Renew Energy* 2017;103:30–7. doi:10.1016/j.renene.2016.11.026.
- [79] Tongdee N, Jandakaew M, Dolwichai T. Thermodynamics analysis for optimal geometrical parameters and influence of heat sink temperature of Gamma-configuration Stirling engine. *Energy Procedia* 2017;105:1782–8. doi:10.1016/j.egypro.2017.03.516.
- [80] Chen W. A study on the effects of geometric parameters in a low-temperature-differential  $\gamma$ -type Stirling engine using CFD. *Int J Heat Mass Transf* 2017;107:1002–13. doi:10.1016/j.ijheatmasstransfer.2016.11.007.
- [81] Almajri AK, Mahmoud S, Al-dadah R. Modelling and parametric study of an efficient Alpha type Stirling engine performance based on 3D CFD analysis. *Energy Convers Manag* 2017;145:93–106. doi:10.1016/j.enconman.2017.04.073.
- [82] Abuelyamen A, Abualhamayel H, Mokheimer EMA. Parametric study on beta-type Stirling engine. *Energy Convers Manag* 2017;145:53–63.

- doi:10.1016/j.enconman.2017.04.098.
- [83] Kato Y. Indicated diagrams of a low temperature differential Stirling engine using flat plates as heat exchangers. *Renew Energy* 2016;85:973–80. doi:10.1016/j.renene.2015.07.053.
- [84] MATWEB. Overview of materials for Brass. MATWEB n.d. <http://www.matweb.com/search/DataSheet.aspx?MatGUID=d3bd4617903543ada92f4c101c2a20e5> (accessed July 26, 2018).
- [85] MATWEB. Overview of materials for Polystyrene, Impact Modified. MATWEB n.d. <http://www.matweb.com/search/datasheet.aspx?matguid=be2fb354bdd54f4ba07710a547e1cb02&n=1> (accessed July 26, 2018).
- [86] MATWEB. Overview of materials for Acrylic, Extruded. MATWEB n.d. <http://www.matweb.com/search/datasheet.aspx?matguid=632572aeef2a4224b5ac8fbd4f1b6f77&n=1> (accessed July 26, 2018).
- [87] Mohammed Wazed S, Hughes BR, O'Connor D, Kaiser Calautit J. A review of sustainable solar irrigation systems for Sub-Saharan Africa. *Renew Sustain Energy Rev* 2018;81:1206–25. doi:10.1016/j.rser.2017.08.039.

# Chapter 8

## APPENDICES

### 8.1. Appendix 1 – User Defined Function

```
#include "udf.h"
#include "math.h"
#include "dynamesh_tools.h"

#define RADIANS(deg) (M_PI*(deg)/180.0)
#define rpm 120 /* clockwise */
#define start_angle 0 /* start angle of Piston in degrees */
#define lc1 0.2125 /* Crank to base of Cylinder */

/* Piston Parameters */
#define r1 0.0200 /* Piston Stroke */
#define l1 0.0650 /* Piston Connecting Rod */
#define l2 0.0225 /* Length of Piston + Piston Rod */

/* Displacer Parameters */
#define r2 0.0125 /* Displacer Stroke */
#define l3 0.0475 /* Displacer Connecting Rod */
#define l4 0.0775 /* Displacer Rod */
#define ld 0.0740 /* Displacer Length */

DEFINE_CG_MOTION(piston, dt, vel, omega, time, dtime)
{
    real z_piston, angle_p, w_p;

    /* compute current angle at t = time
    note: crank-rpm is in units of RPM
    crank-start-angle is in units of degree */
    angle_p = start_angle + (time * (rpm / 60) * 360);
    angle_p = RADIANS(angle_p);
```

```

/* converting RPM to Radians per sec */
w_p = rpm * 2 * M_PI / 60;

/* compute current z_piston (=0 at tdc, angle = 0) */
/* z_piston = L + (A / 2 * (1 - cos(angle))) - (sqrt((L * L) - (((A * A) / 4) *
(sin(angle) * sin(angle)))); */
z_piston = lc1 - ((-r1 * sin(angle_p)) + sqrt((l1*l1) -
(r1*r1*cos(angle_p)*cos(angle_p)) + l2);

/* re-set velocities */
NV_S(vel, = , 0.0);
NV_S(omega, = , 0.0);

/* compute velocity formula, Motion in Y axis */
vel[0] = 0;
vel[1] = (r1*w_p*cos(angle_p)) - ((r1*r1*w_p*cos(angle_p)*sin(angle_p)) /
sqrt((l1*l1) - (r1*r1*cos(angle_p)*cos(angle_p))));
vel[2] = 0;

/* Print Message */
Message("\ntime = %f, piston = %f, angle_p = %f, vel[1] = %f", time, z_piston,
(angle_p * 180 / M_PI), vel[1]);
}

```

```

DEFINE_CG_MOTION(displacement, dt, vel, omega, time, dtime)
{
    real z_disp, angle_d, w_d;

    /* compute current angle at t = time
    note: crank-rpm is in units of RPM
    crank-start-angle is in units of degree */
    angle_d = start_angle - 90 + (time * (rpm / 60) * 360);
    angle_d = RADIANS(angle_d);

    /* converting RPM to Radians per sec */

```

```

w_d = rpm * 2 * M_PI / 60;

/* compute current z_piston (=0 at tdc, angle = 0) */
/* z_piston = L + (A / 2 * (1 - cos(angle))) - (sqrt((L * L) - (((A * A) / 4) *
(sin(angle) * sin(angle)))); */
z_disp = lc1 - ((-r2 * sin(angle_d)) + sqrt((l3*l3) -
(r2*r2*cos(angle_d)*cos(angle_d)) + l4 + ld);

/* re-set velocities */
NV_S(vel, = , 0.0);
NV_S(omega, = , 0.0);

/* compute velocity formula, Motion in Y axis */
vel[0] = 0;
vel[1] = (r2*w_d*cos(angle_d)) - ((r2*r2*w_d*cos(angle_d)*sin(angle_d)) /
sqrt((l3*l3) - (r2*r2*cos(angle_d)*cos(angle_d))));
vel[2] = 0;

/* Print Message */
Message("\ntime = %f, disp = %f, angle_d = %f, vel[1] = %f", time, z_disp,
(angle_d * 180 / M_PI), vel[1]);
}

```

## 8.2. Appendix 2 – Profiles

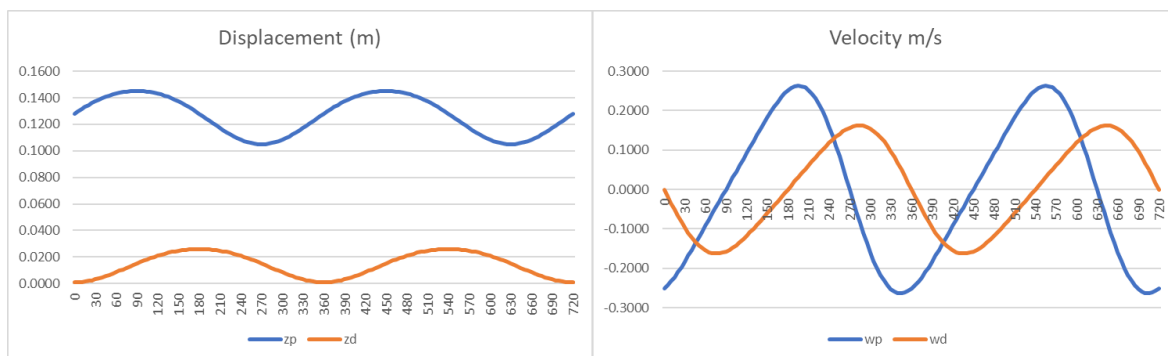
Using equations [1-4](#) profiles were created using excel. A Sample of the calculations has been shown below:

Piston Angle	0
Piston Displacement	
lc1	0.2125 m
r1	0.02 m
theta	0 deg
sin theta	0
cos theta	1
l1	0.065 m
l2	0.0225 m
r1*sin theta	0
l1^2	0.004225
r1^2	0.0004
cos theta ^2	1
r1^2 x cos theta^2	0.0004
<b>zp</b>	<b>0.128153416 m</b>

Displacer Displacement	
lc1	0.2125 m
r2	0.0125 m
beta	-90 deg
sin beta	-1
cos beta	0
l3	0.0475 m
l4	0.0775 m
ld	0.074 m
r2*sin beta	-0.0125
l3^2	0.00225625
r2^2	0.00015625
cos beta ^2	0
r2^2 x cos beta ^2	0
<b>zd</b>	<b>0.001 m</b>

Piston Velocity	
r1	0.02 m
omega	-12.56637061 rad/s
theta	0 deg
sin beta	0
cos beta	1
l1	0.065 m
r1*omega*cos theta	-0.251327412
r1^2	0.0004
r1^2*omega*cos theta*sin theta	0
l1^2	0.004225
Cos theta ^2	1
r1^2 * Cos theta^2	0.0004
SQRT((l1^2-r1^2*cos theta^2)	0.061846584
<b>Wp</b>	<b>-0.251327412 m/s</b>

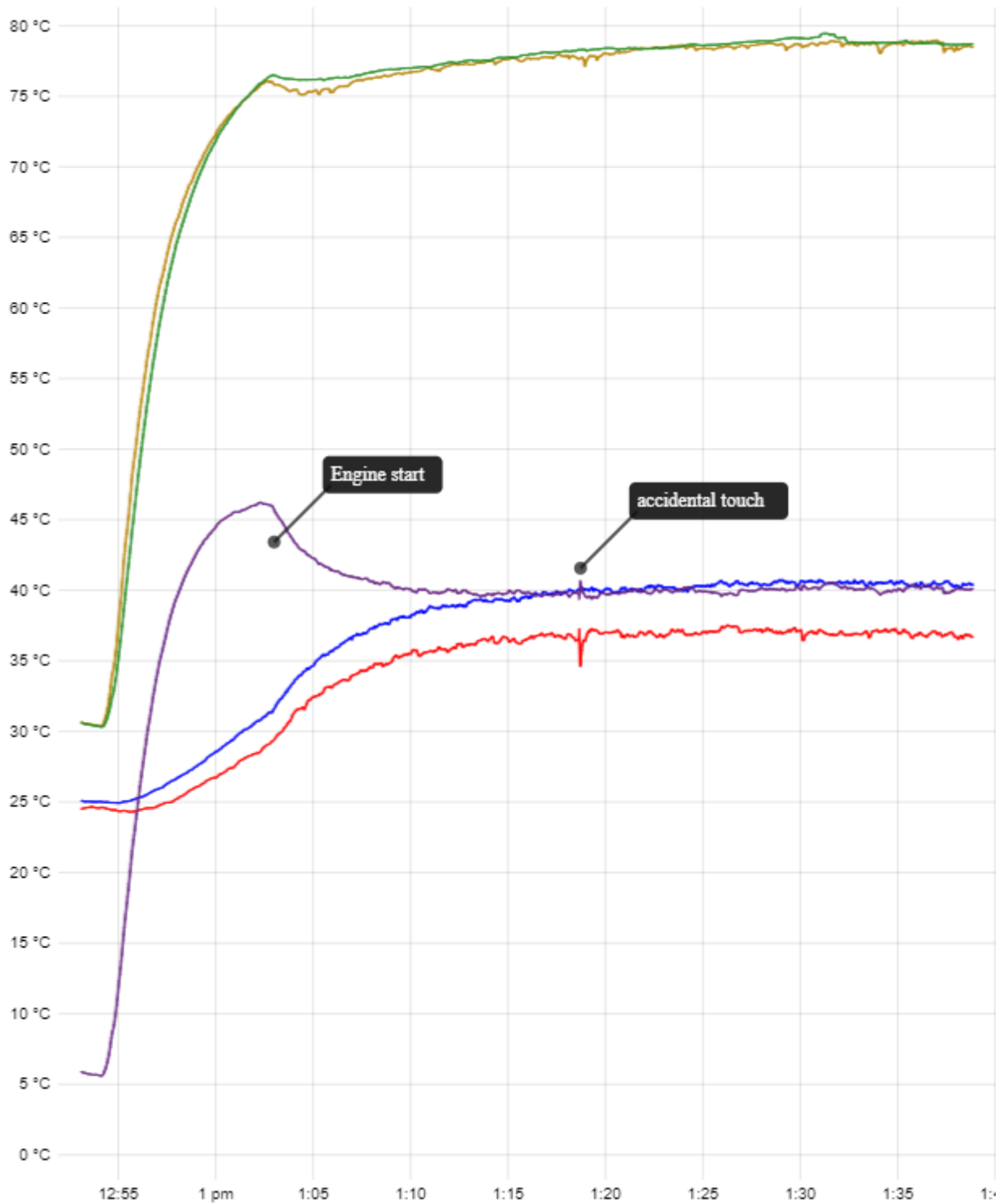
Displacer Velocity	
r2	0.0125
omega	-12.56637061 rad/s
beta	-90 deg
sin beta	-1
cos beta	0
l3	0.0475 m
r2*omega*cos beta	0
r2^2	0.00015625
r2^2*omega*cos beta*sin beta	0
l3^2	0.00225625
Cos beta ^2	0
r2^2 * Cos beta^2	0
SQRT((l3^2-r2^2*cos beta^2)	0.0475
<b>Wd</b>	<b>0 m/s</b>



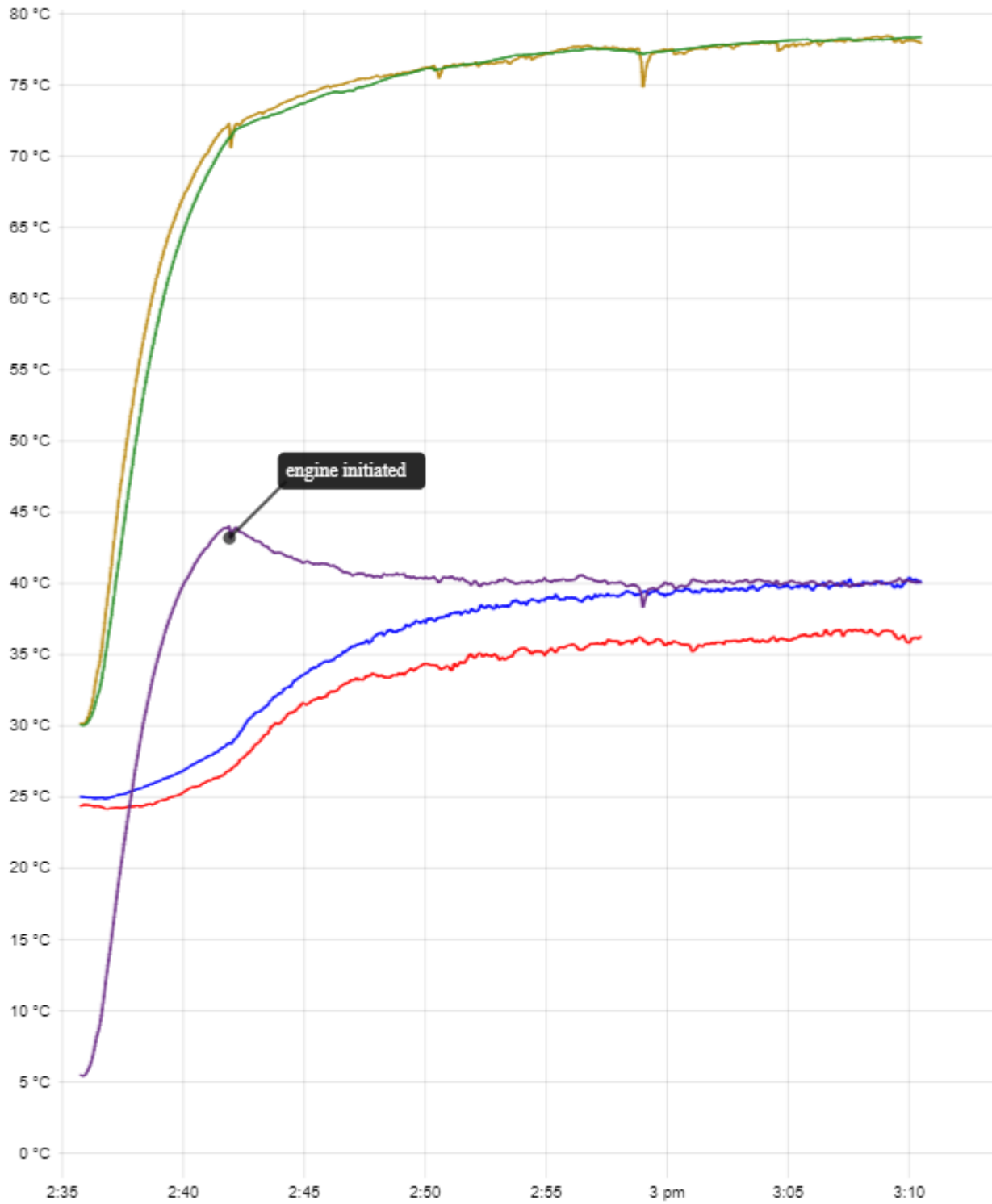
### 8.3. Appendix 3 – Experimental Temperature Recordings

#### 8.3.1. Inspected EMSE

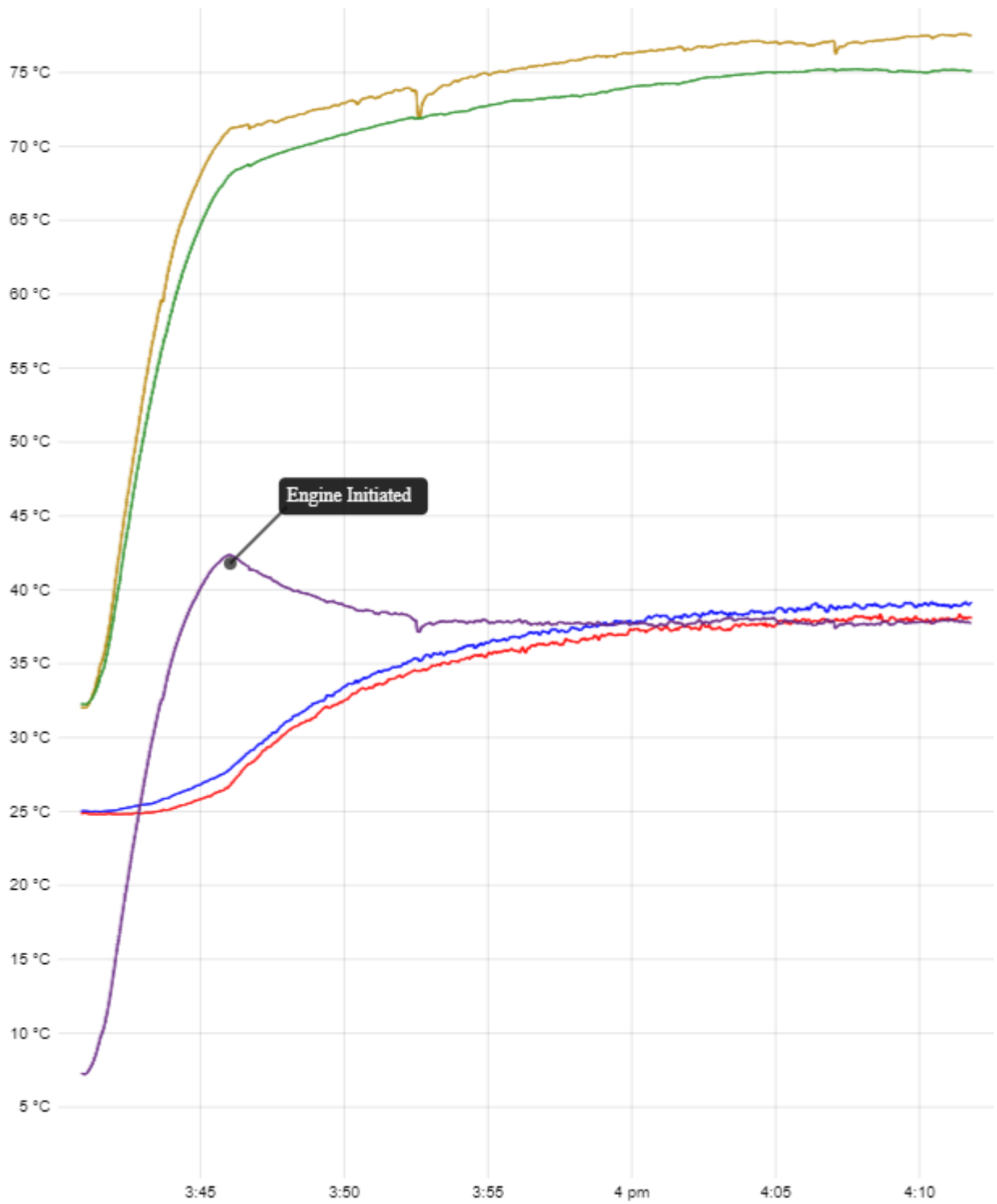
E1



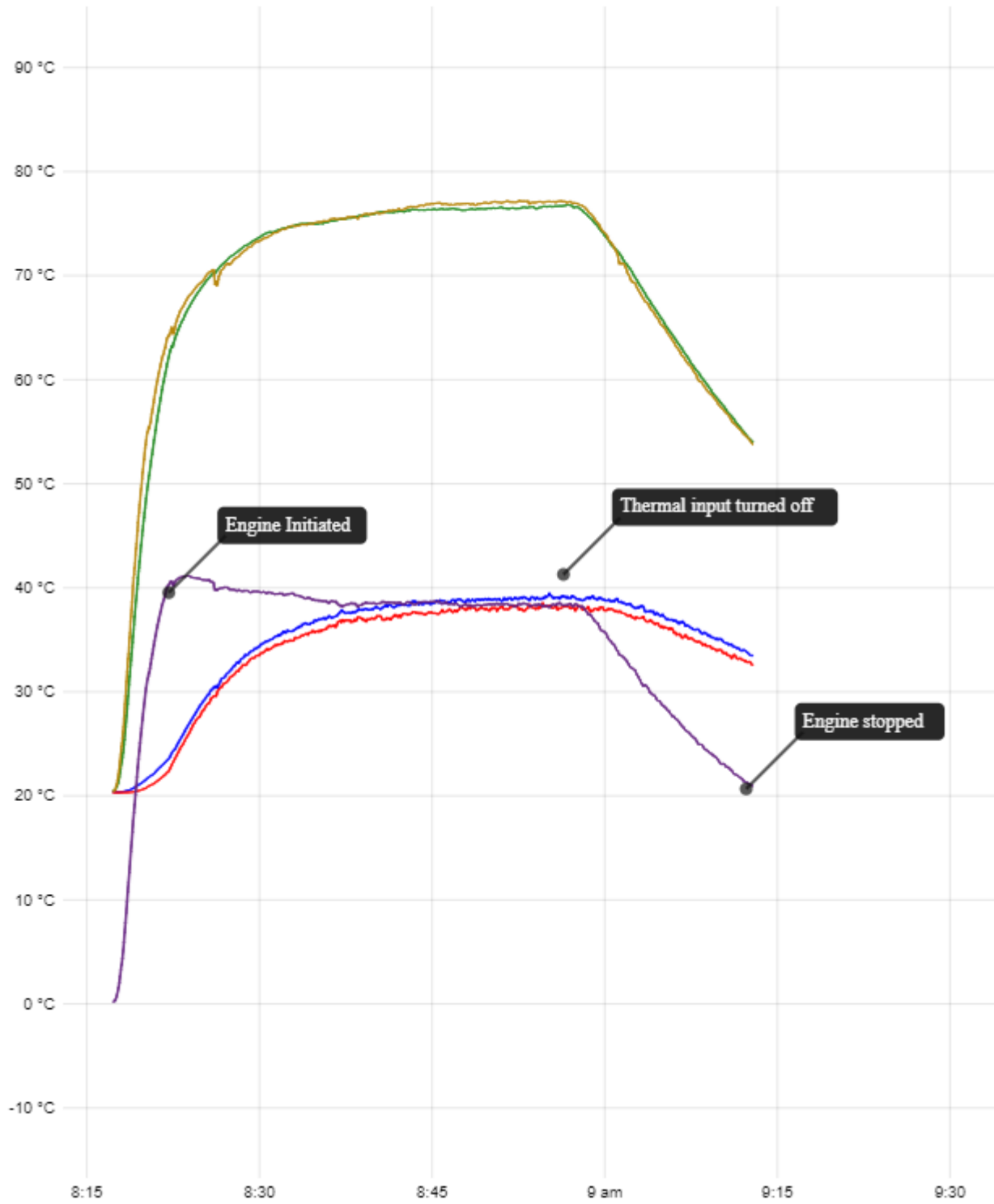
## E2

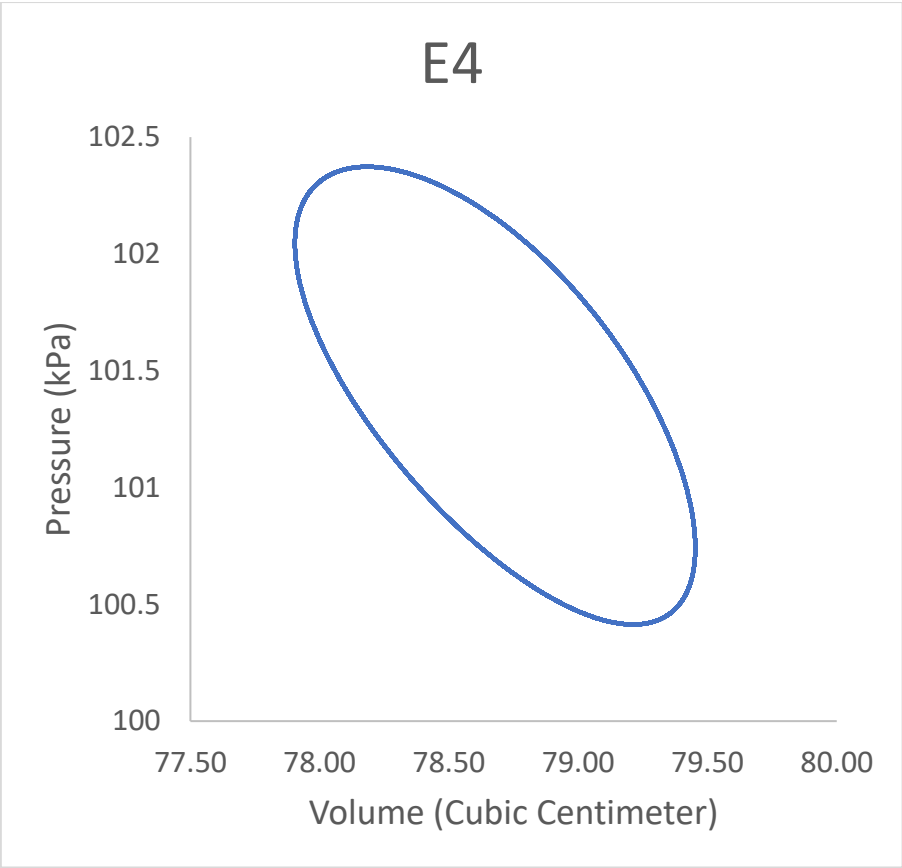


### E3

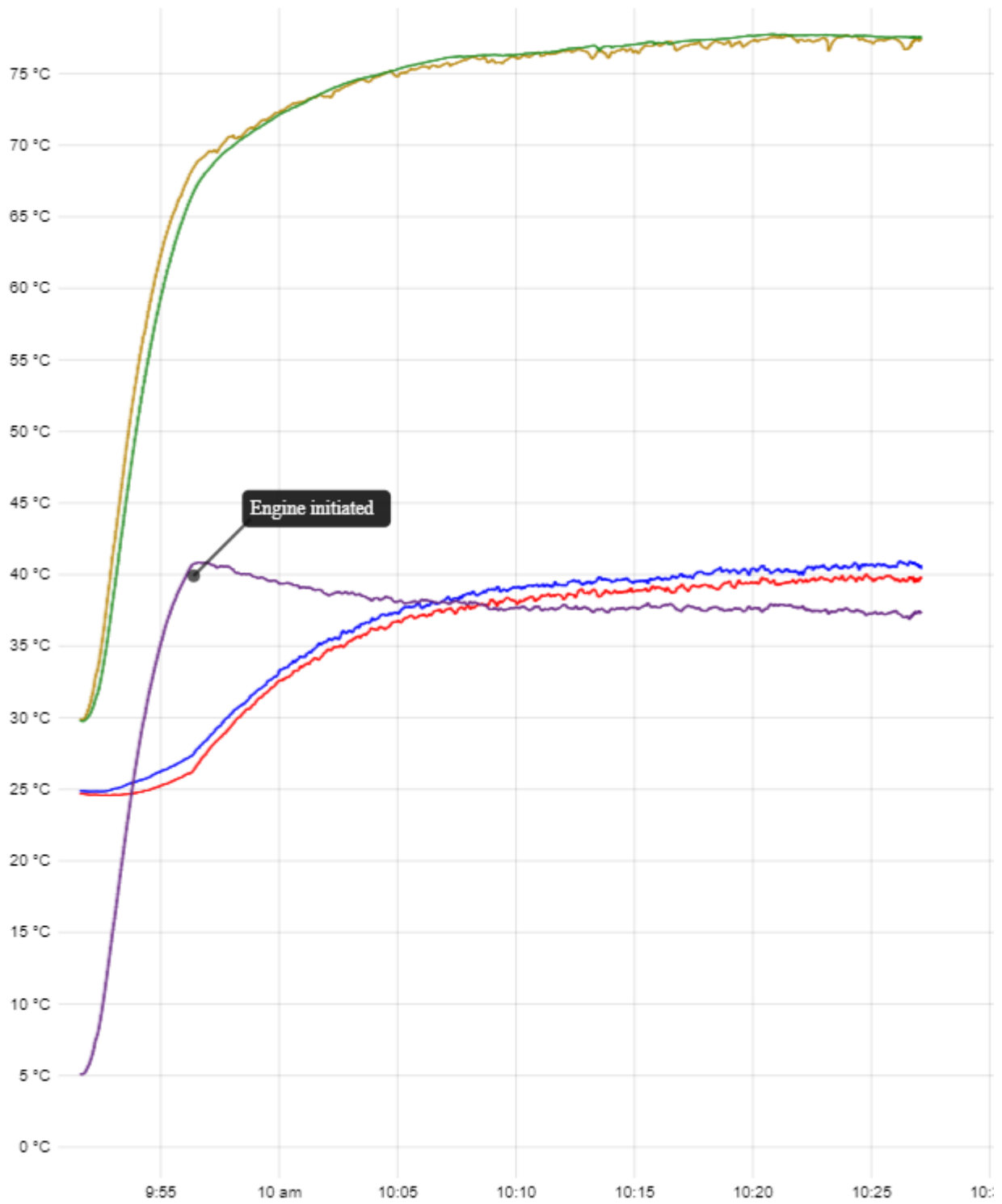


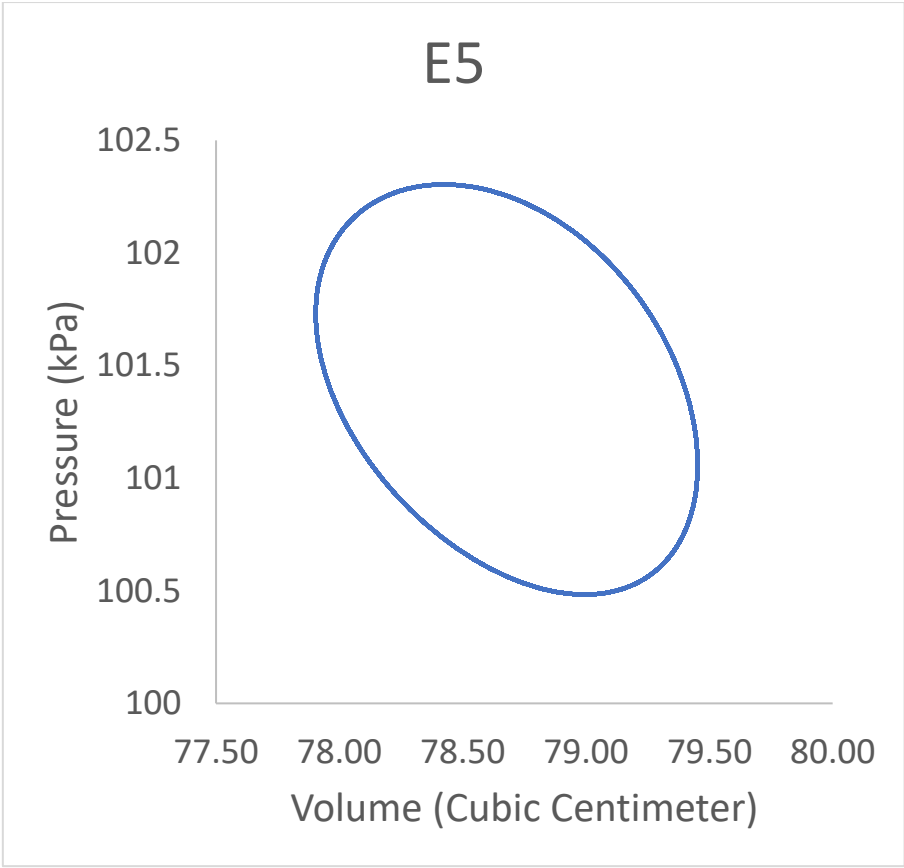
# E4



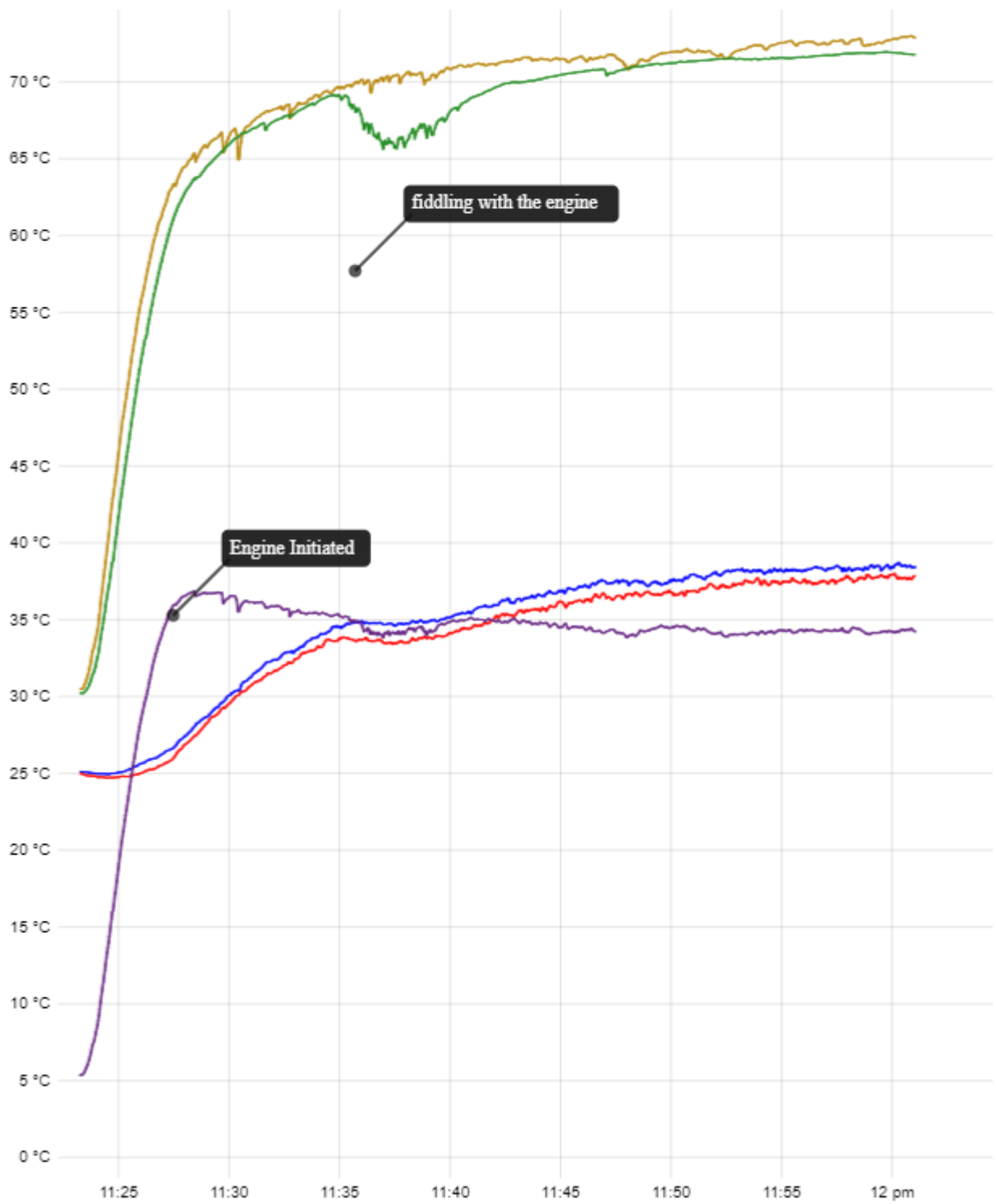


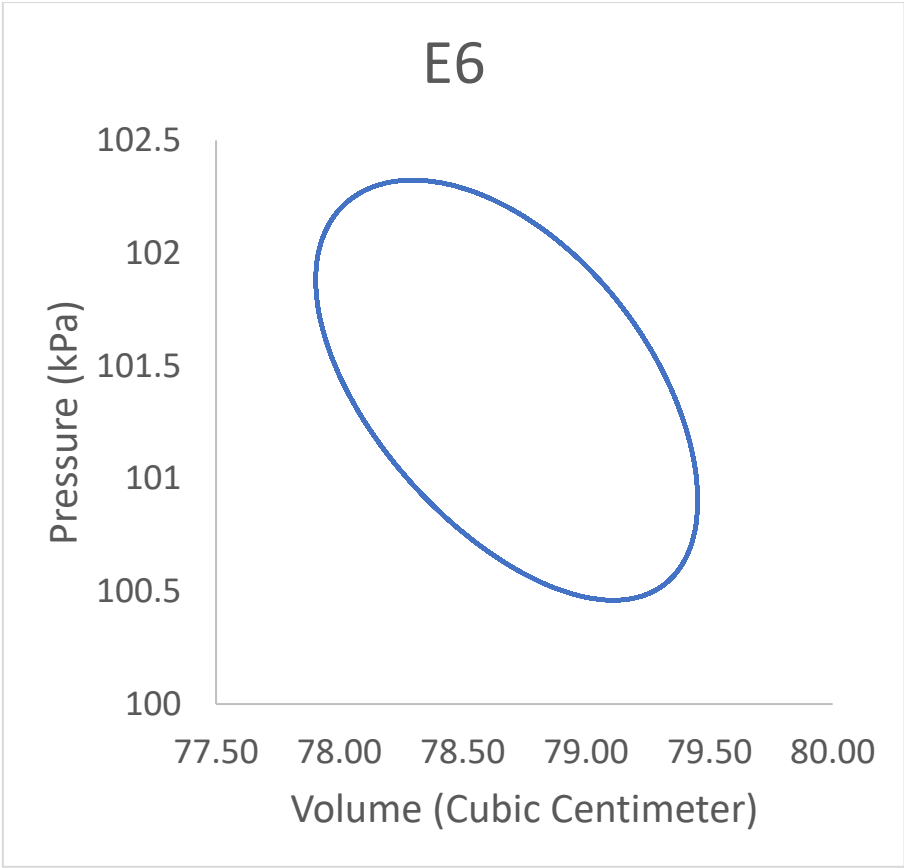
# E5



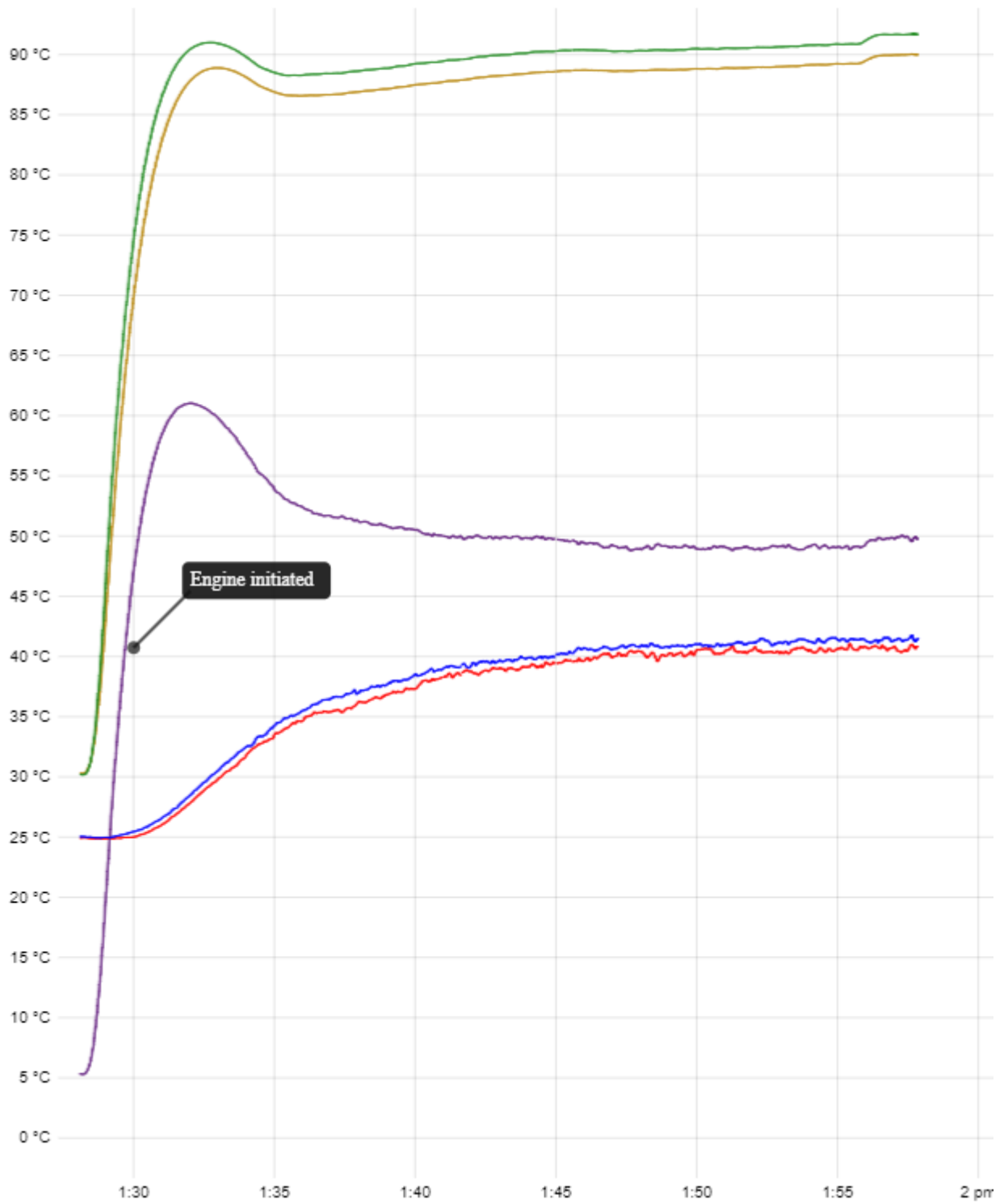


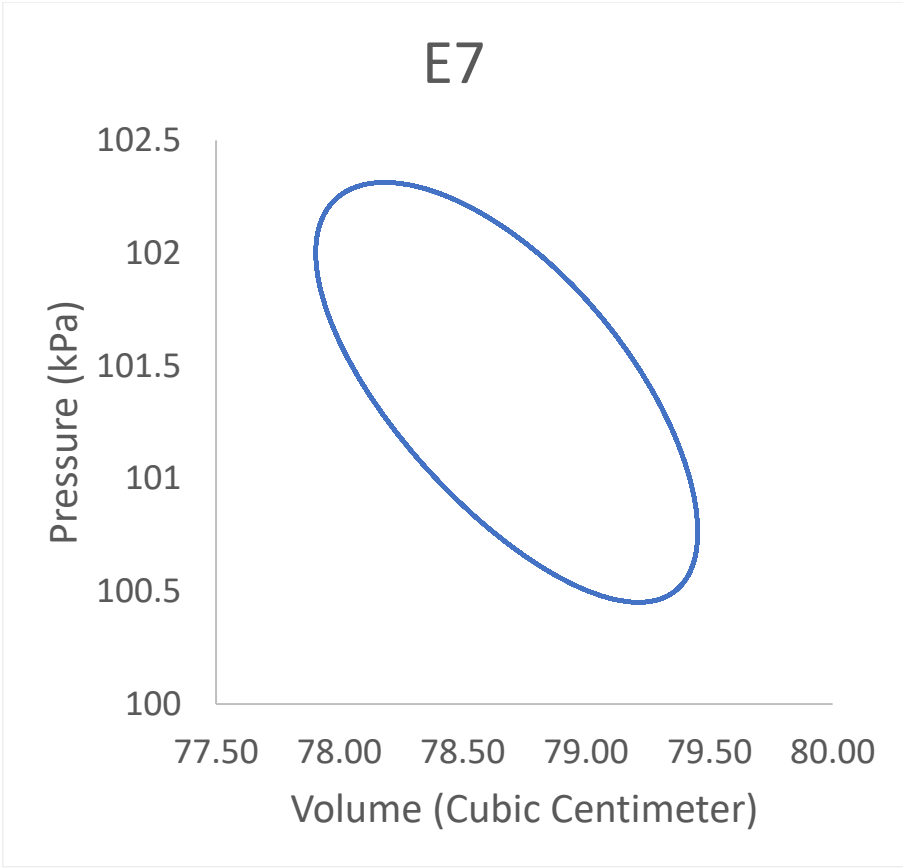
# E6



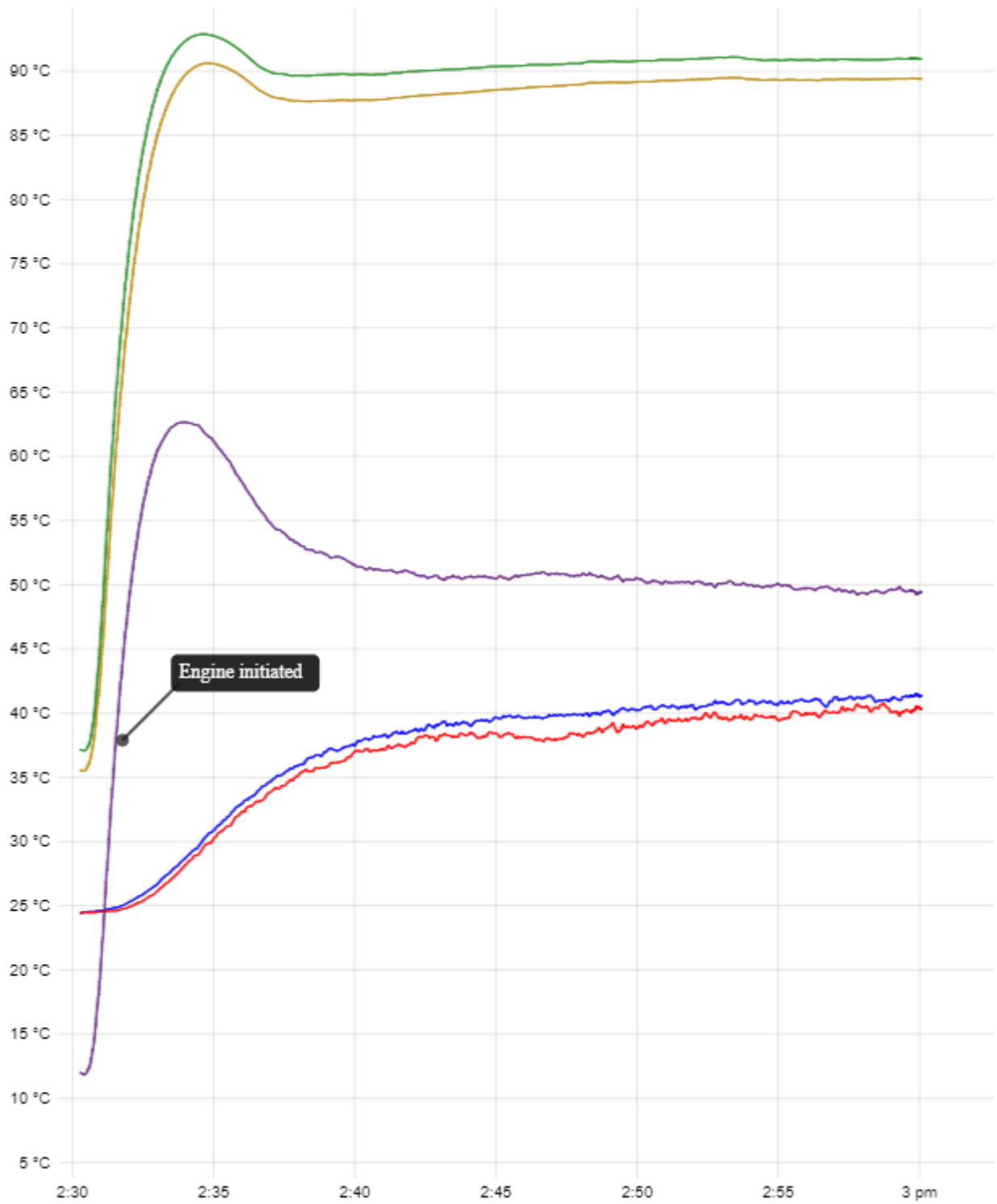


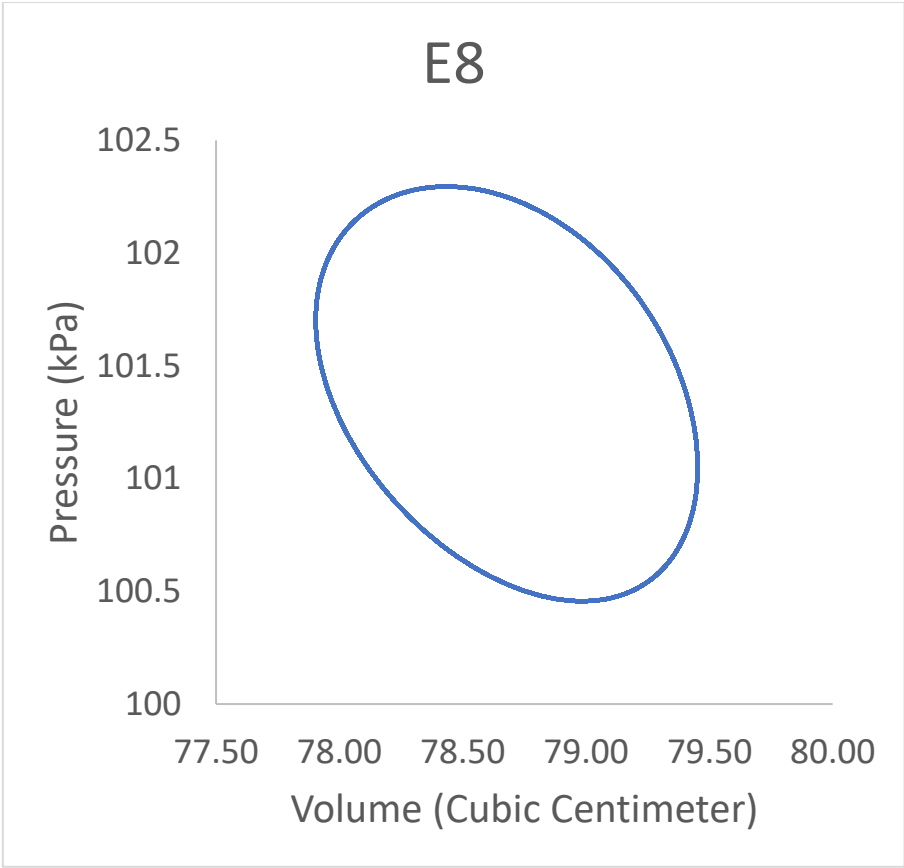
# E7



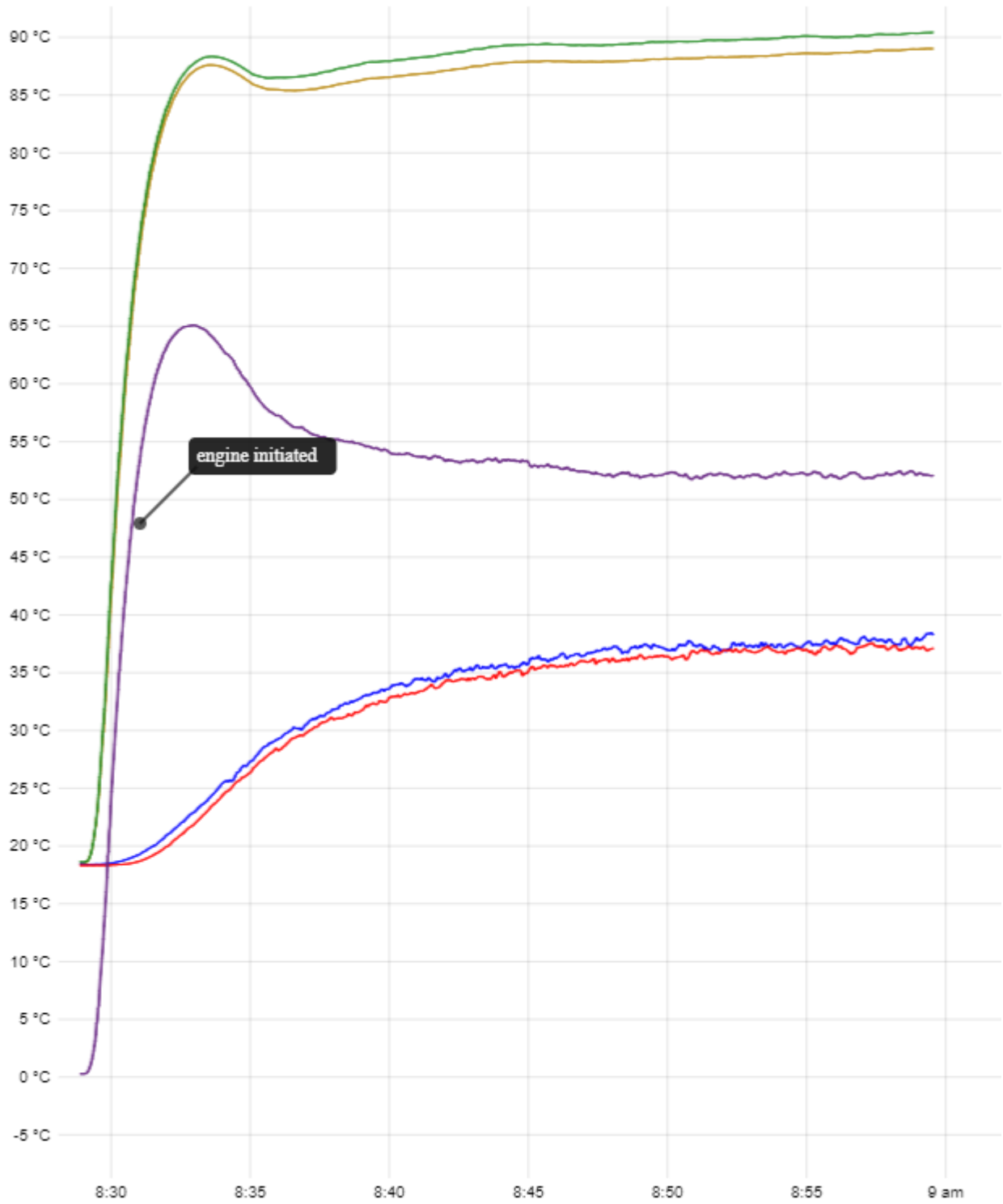


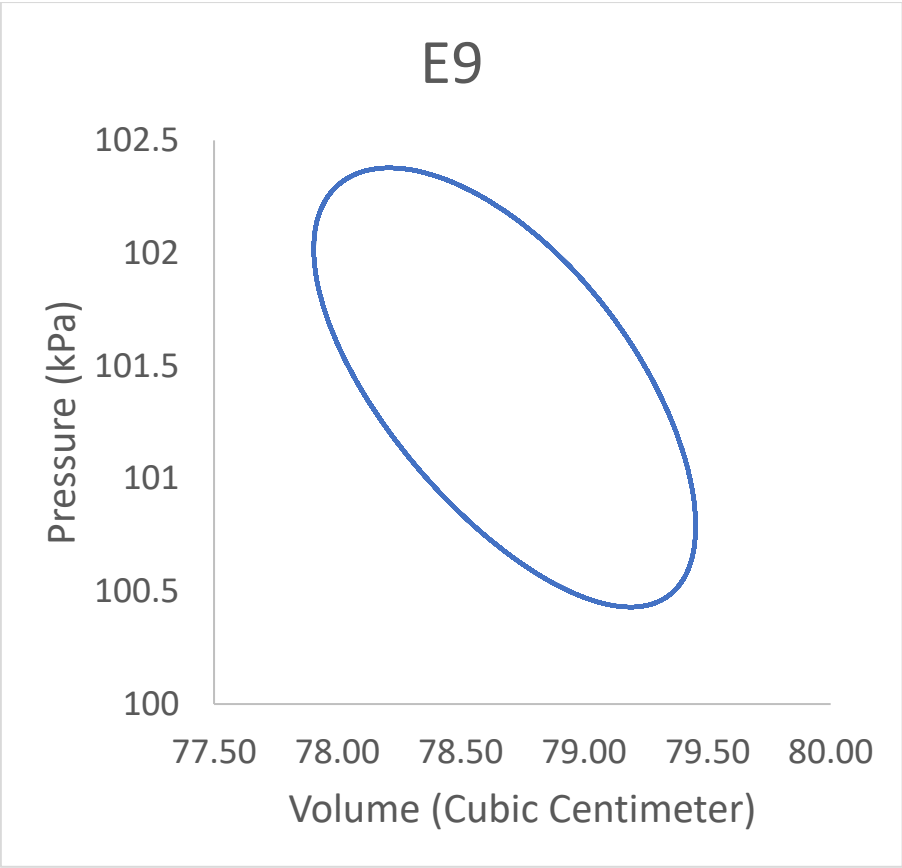
# E8



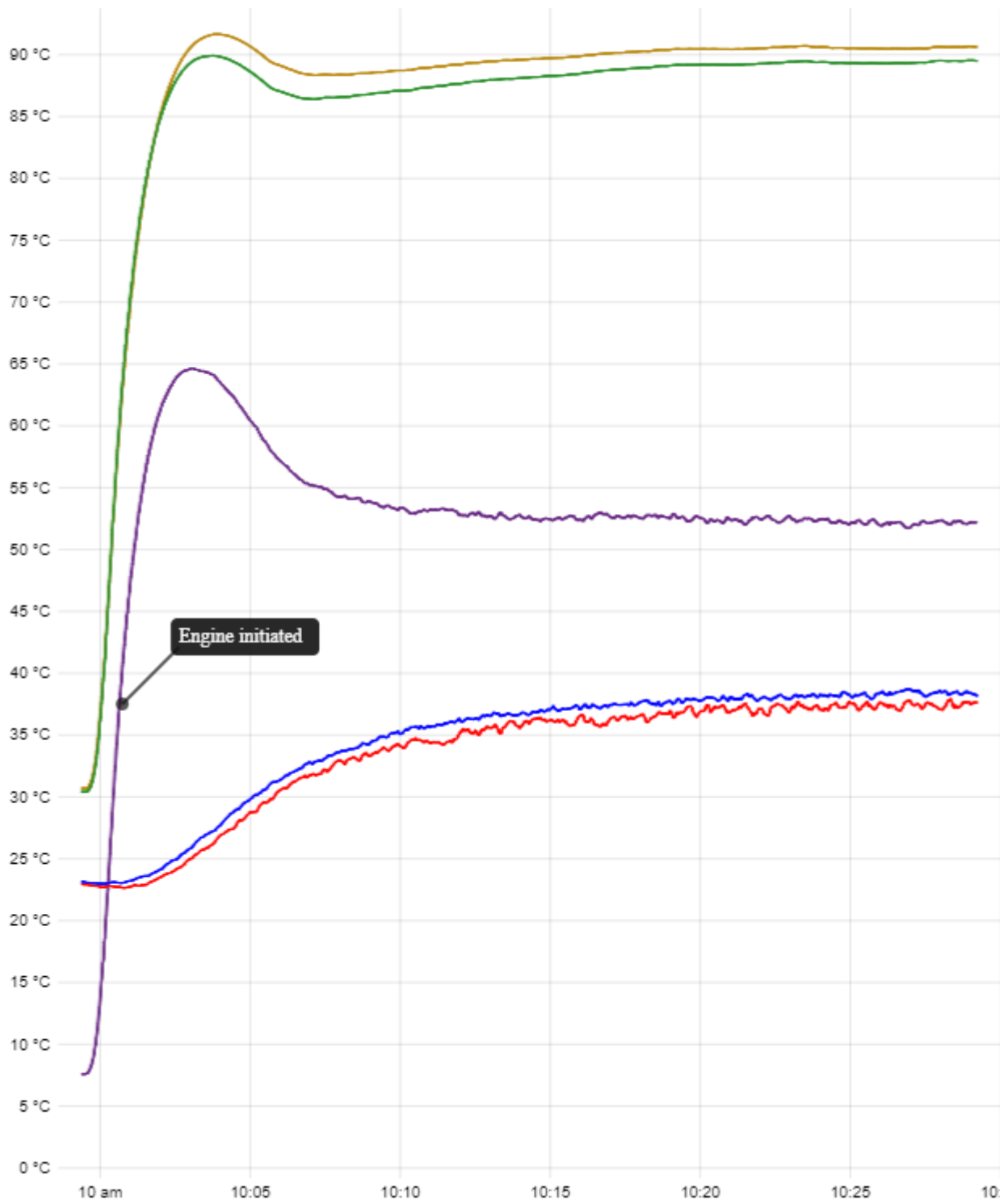


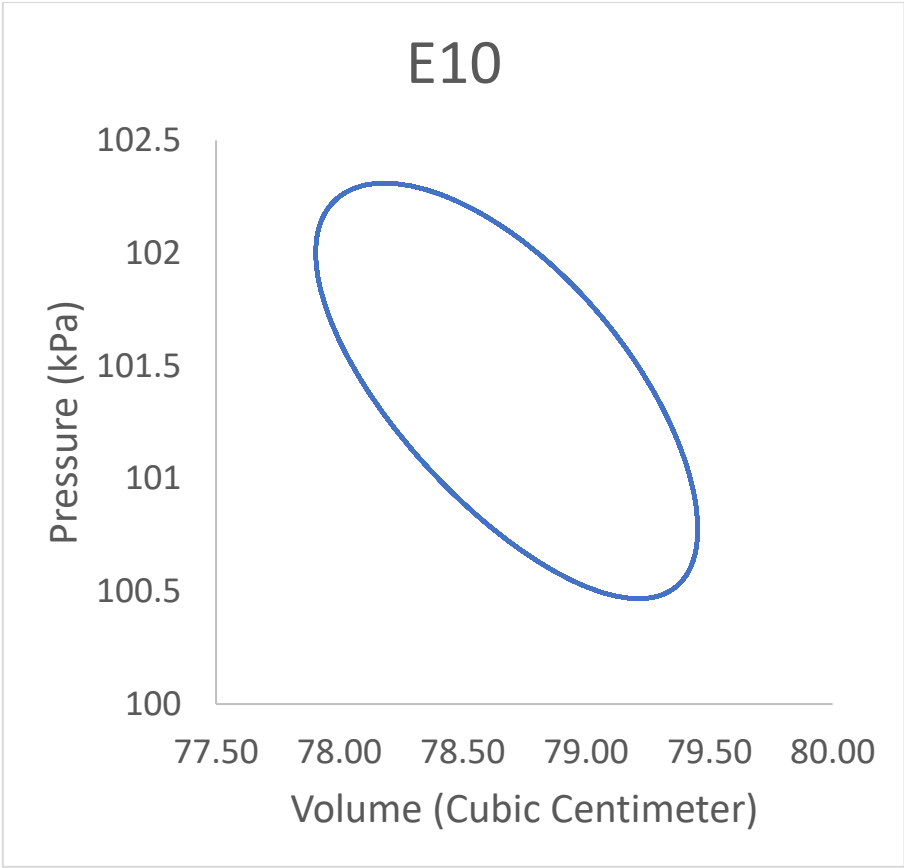
# E9



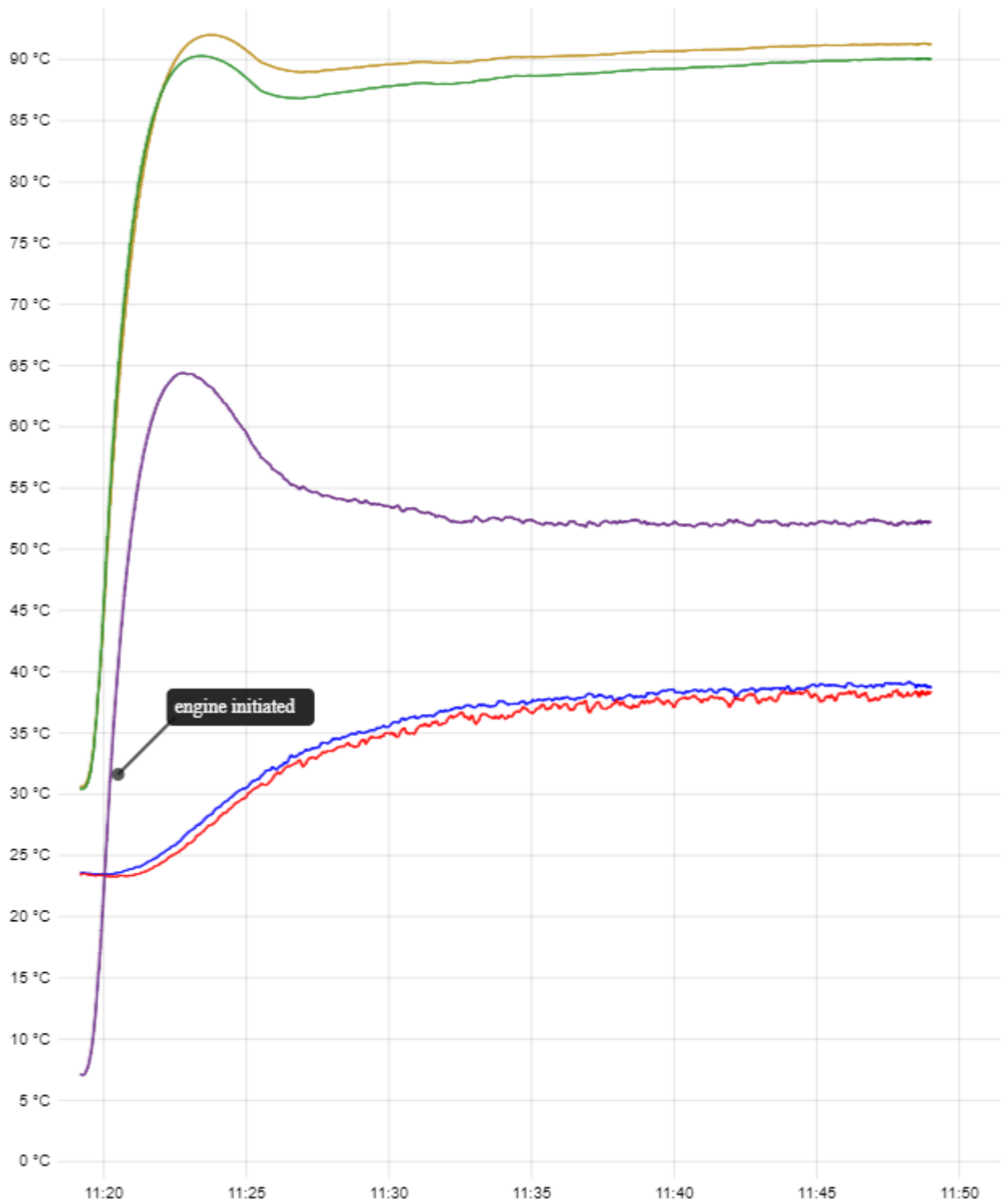


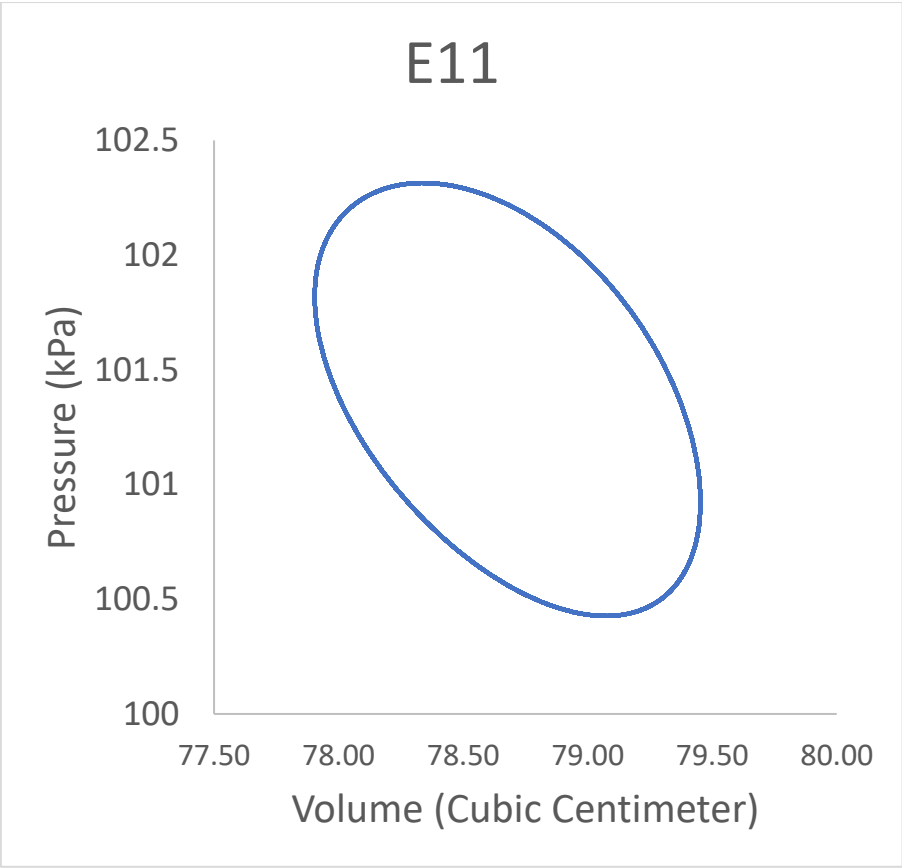
# E10



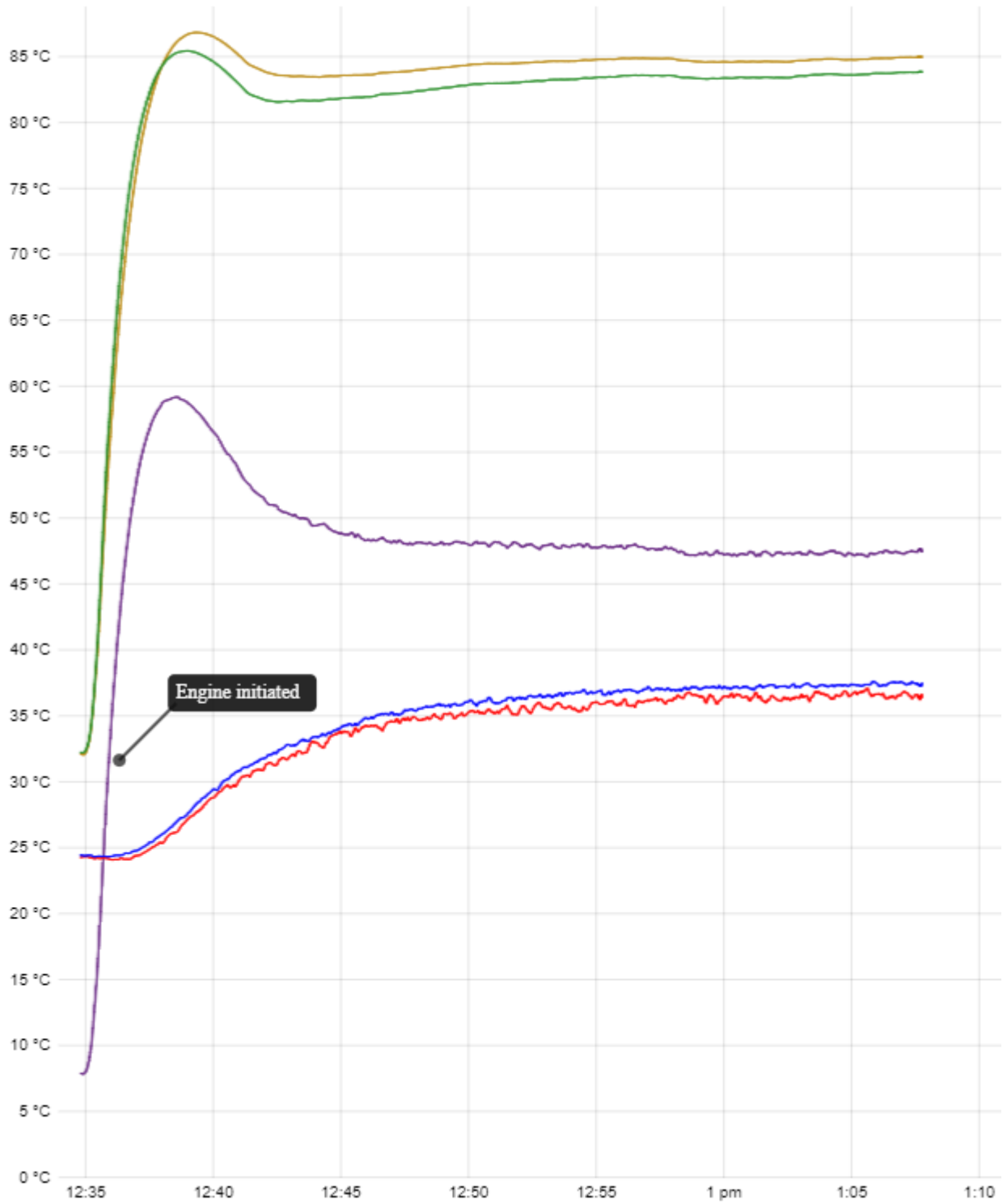


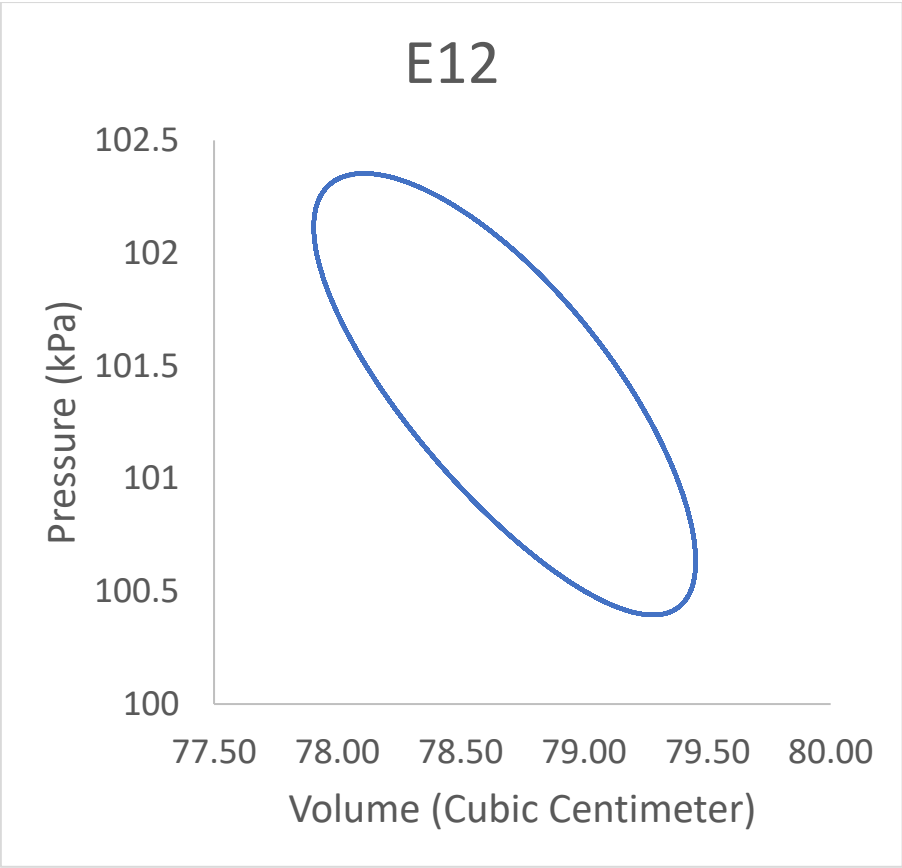
# E11



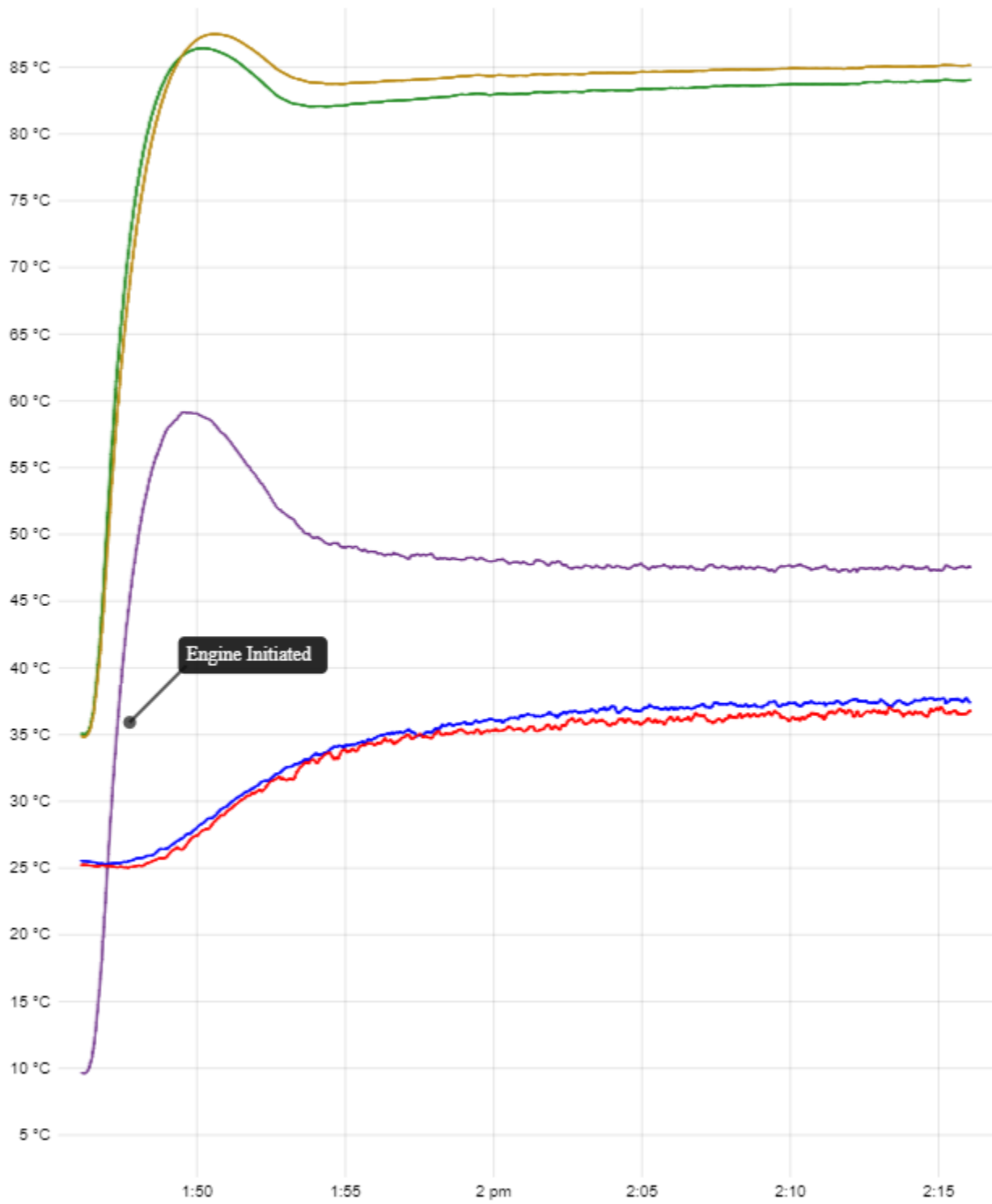


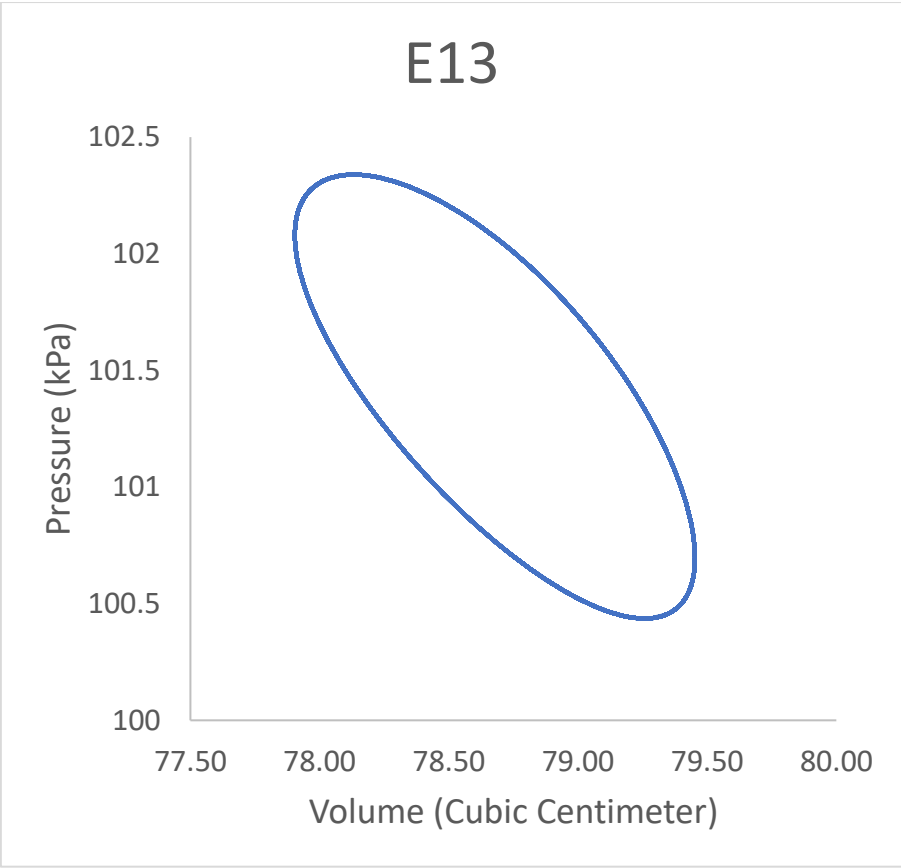
# E12



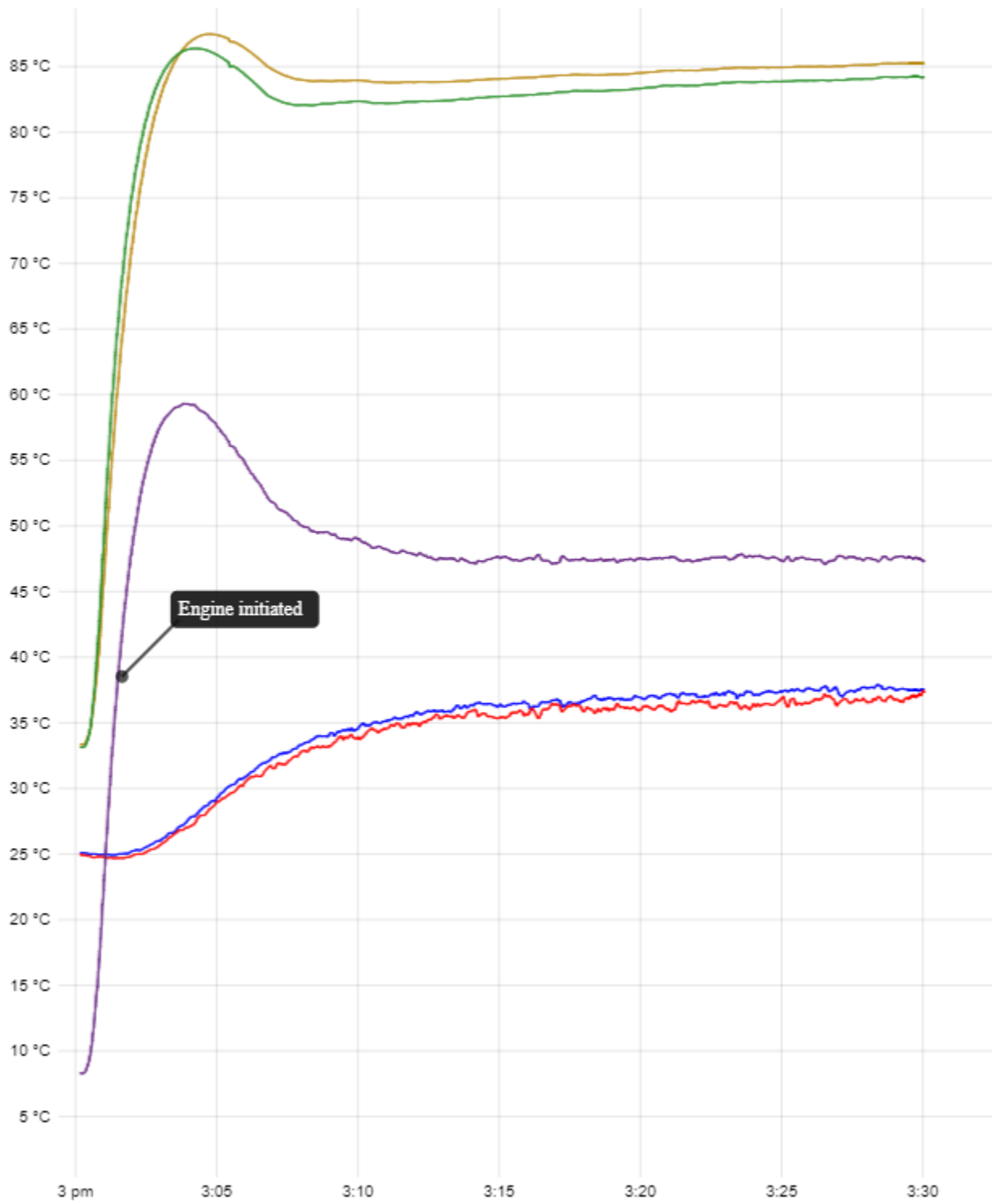


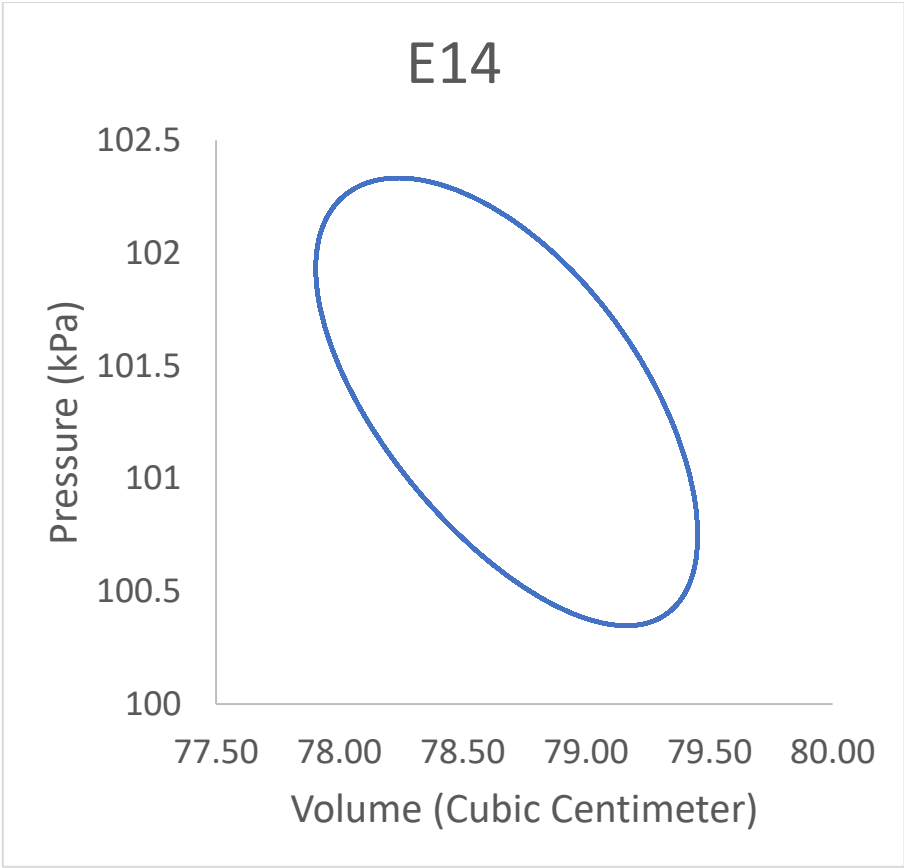
# E13



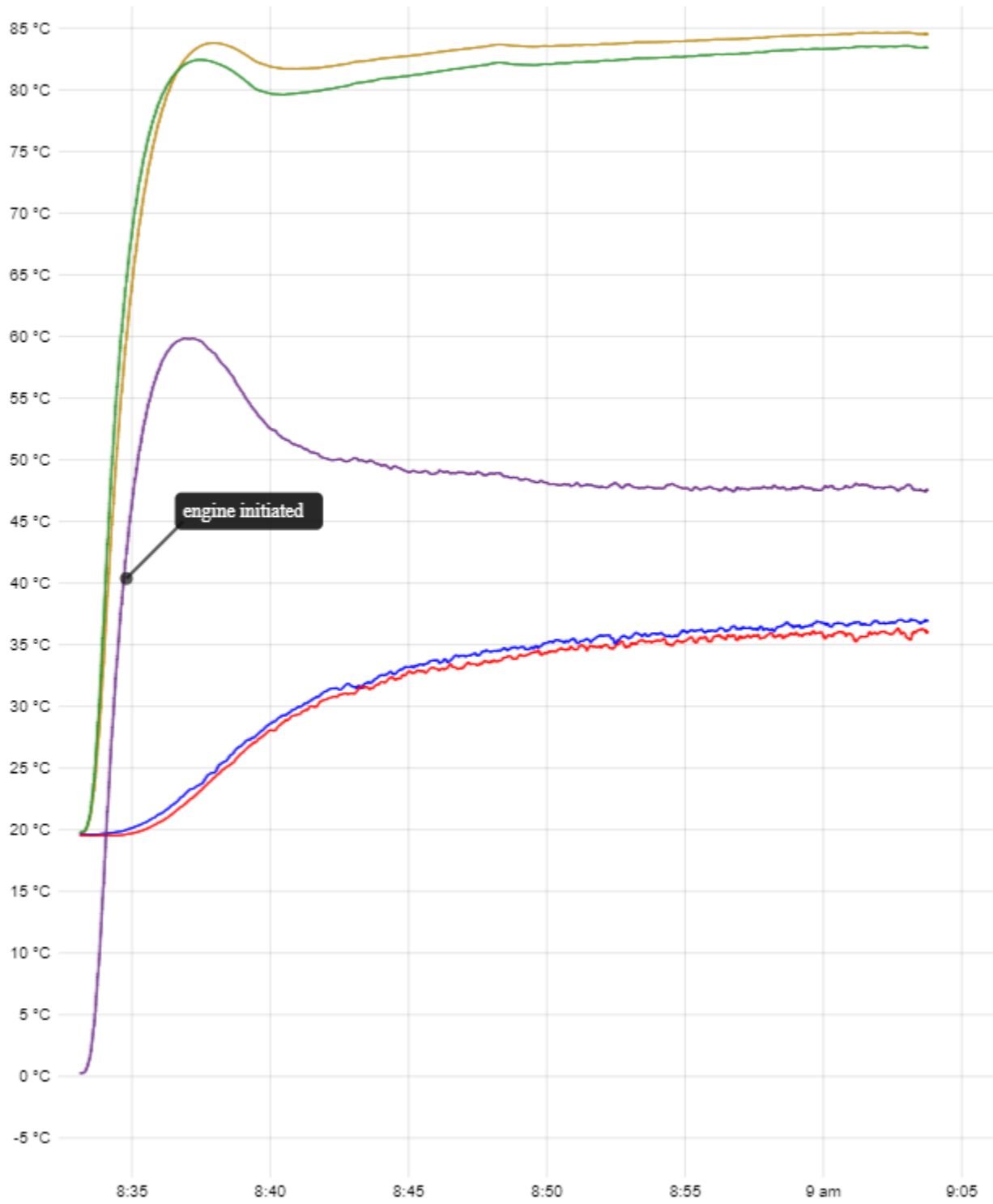


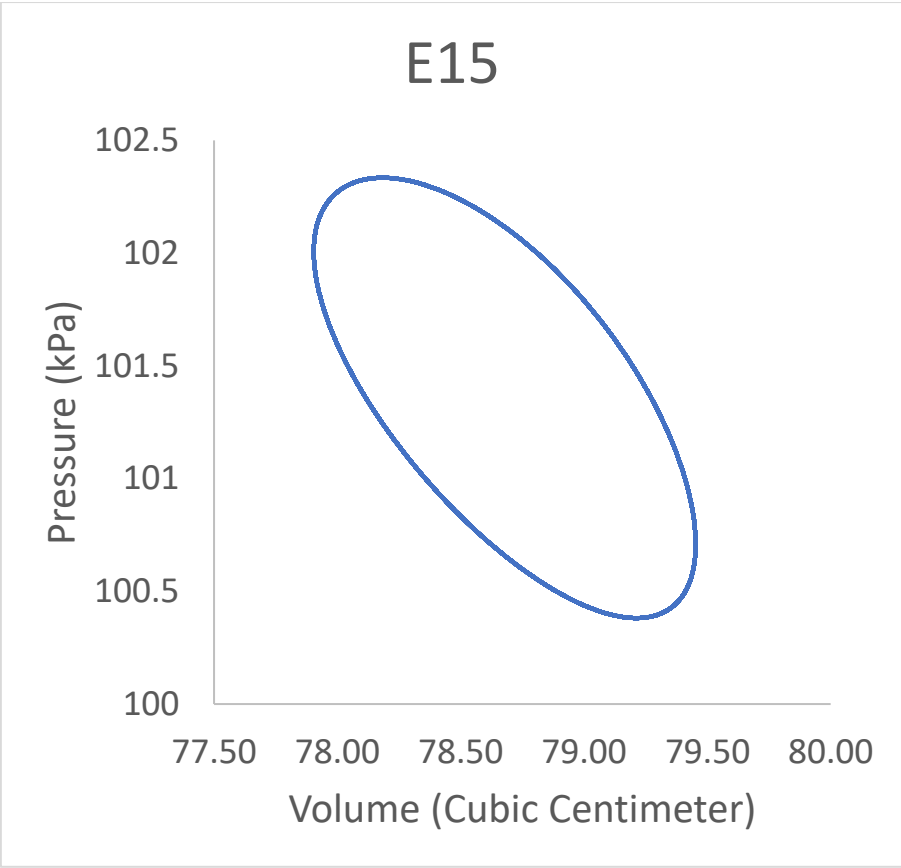
# E14



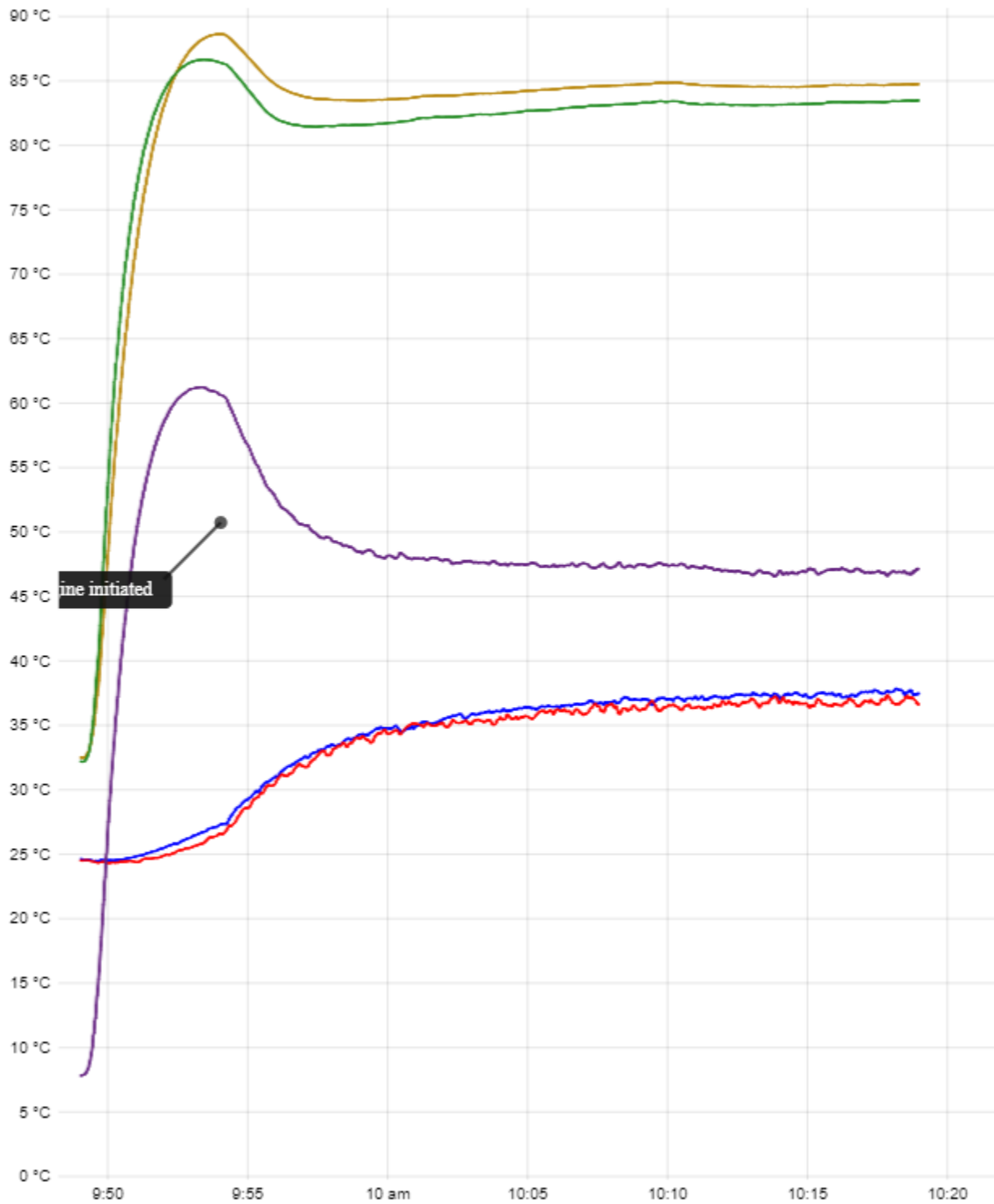


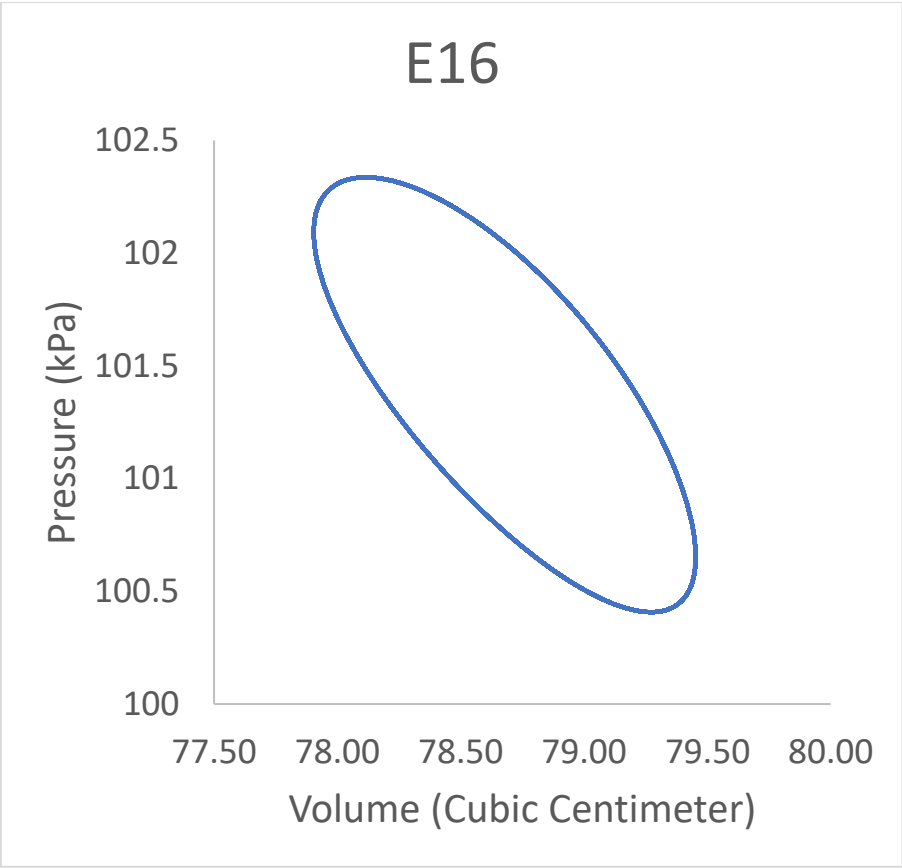
# E15



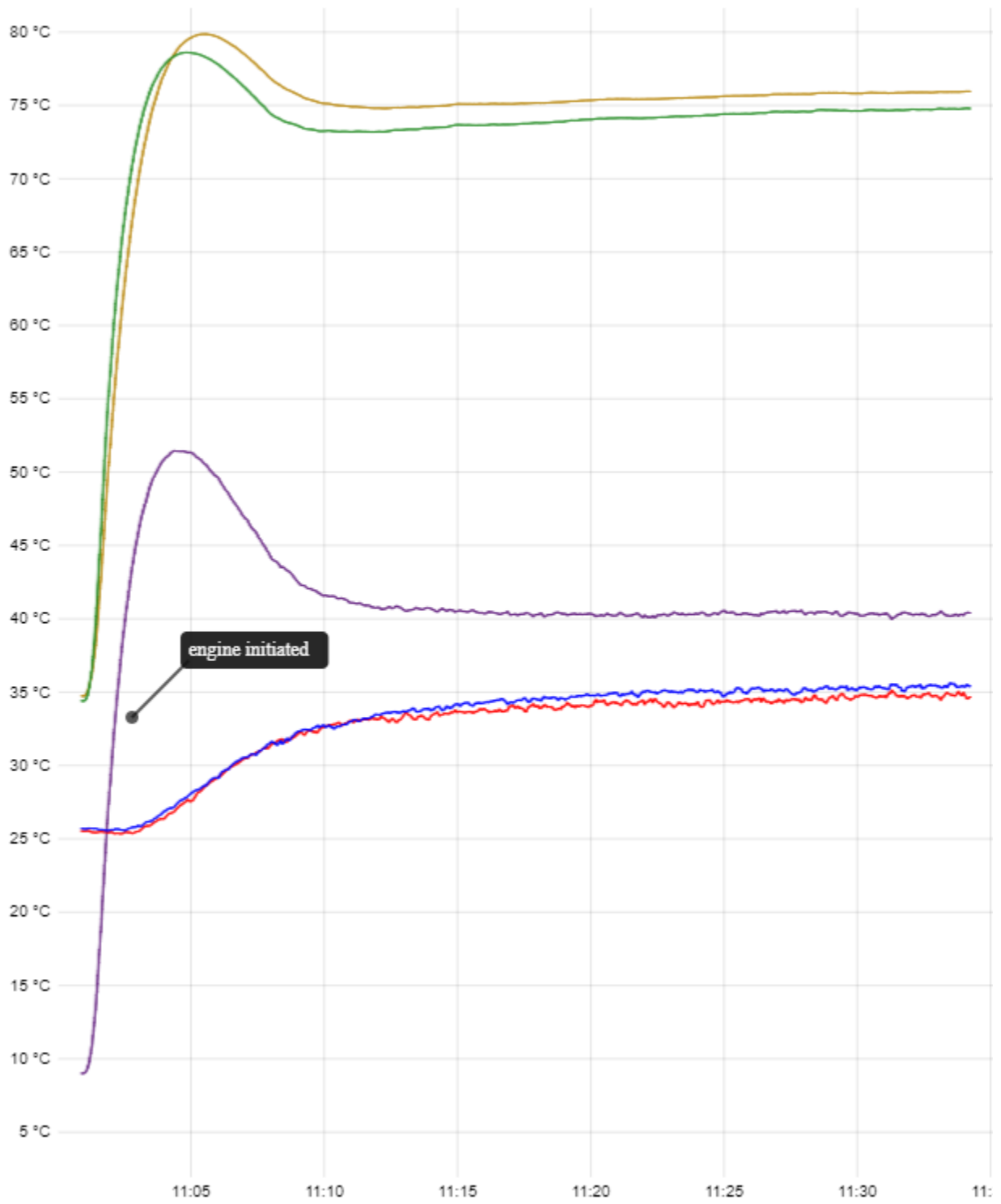


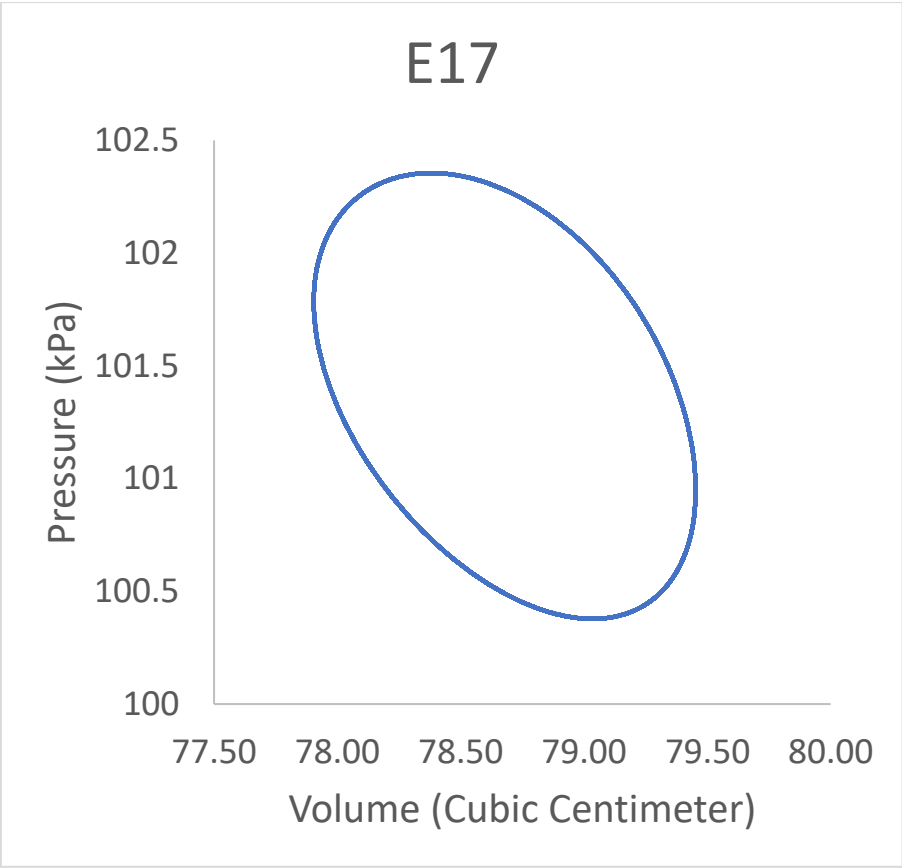
# E16



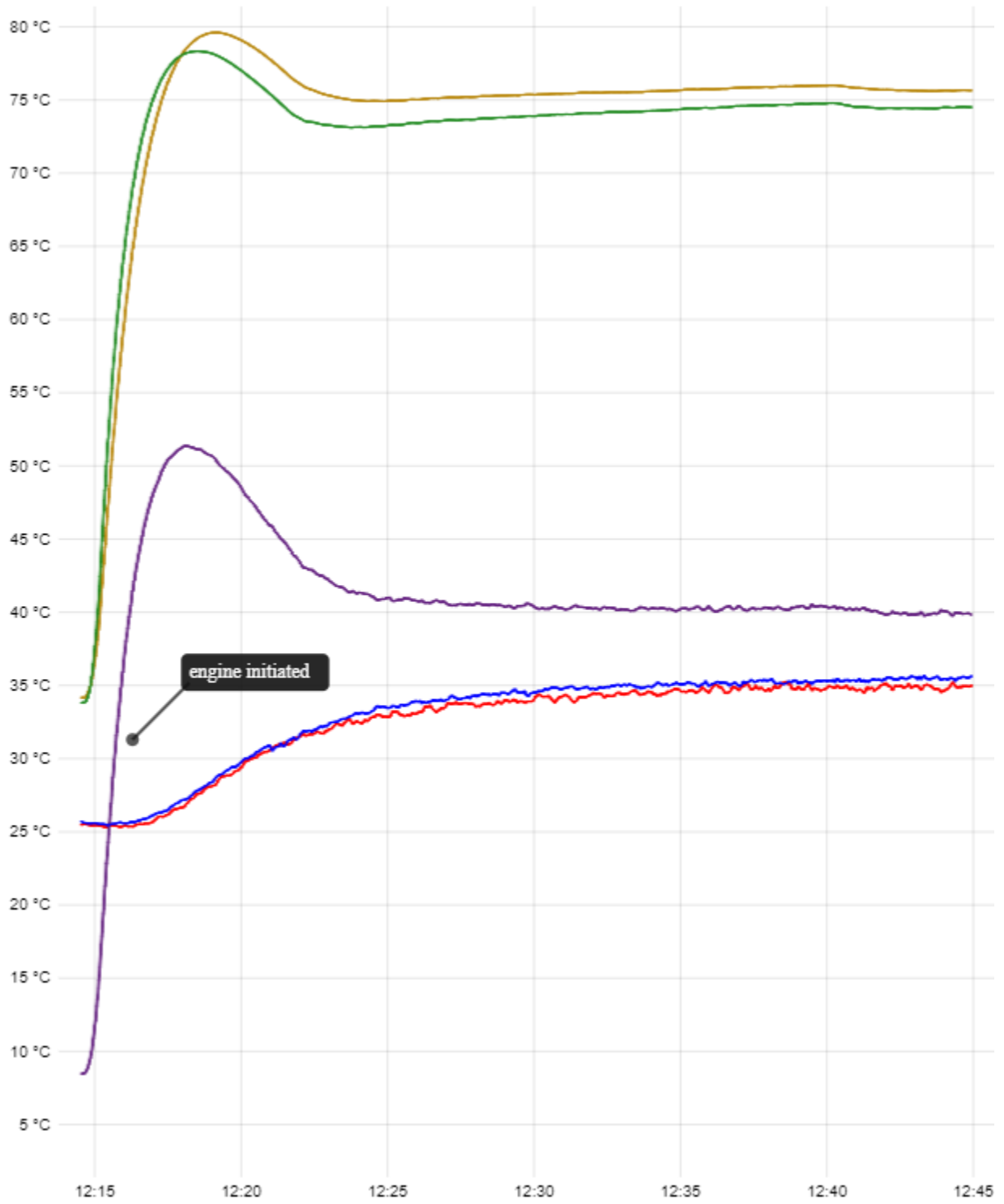


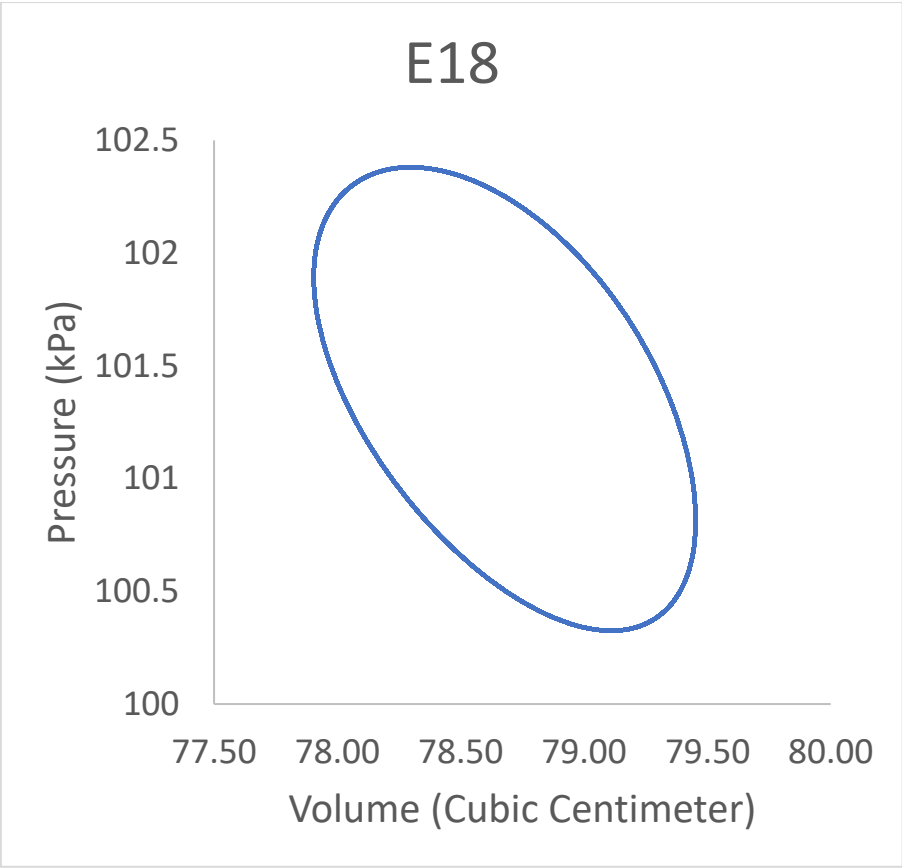
# E17



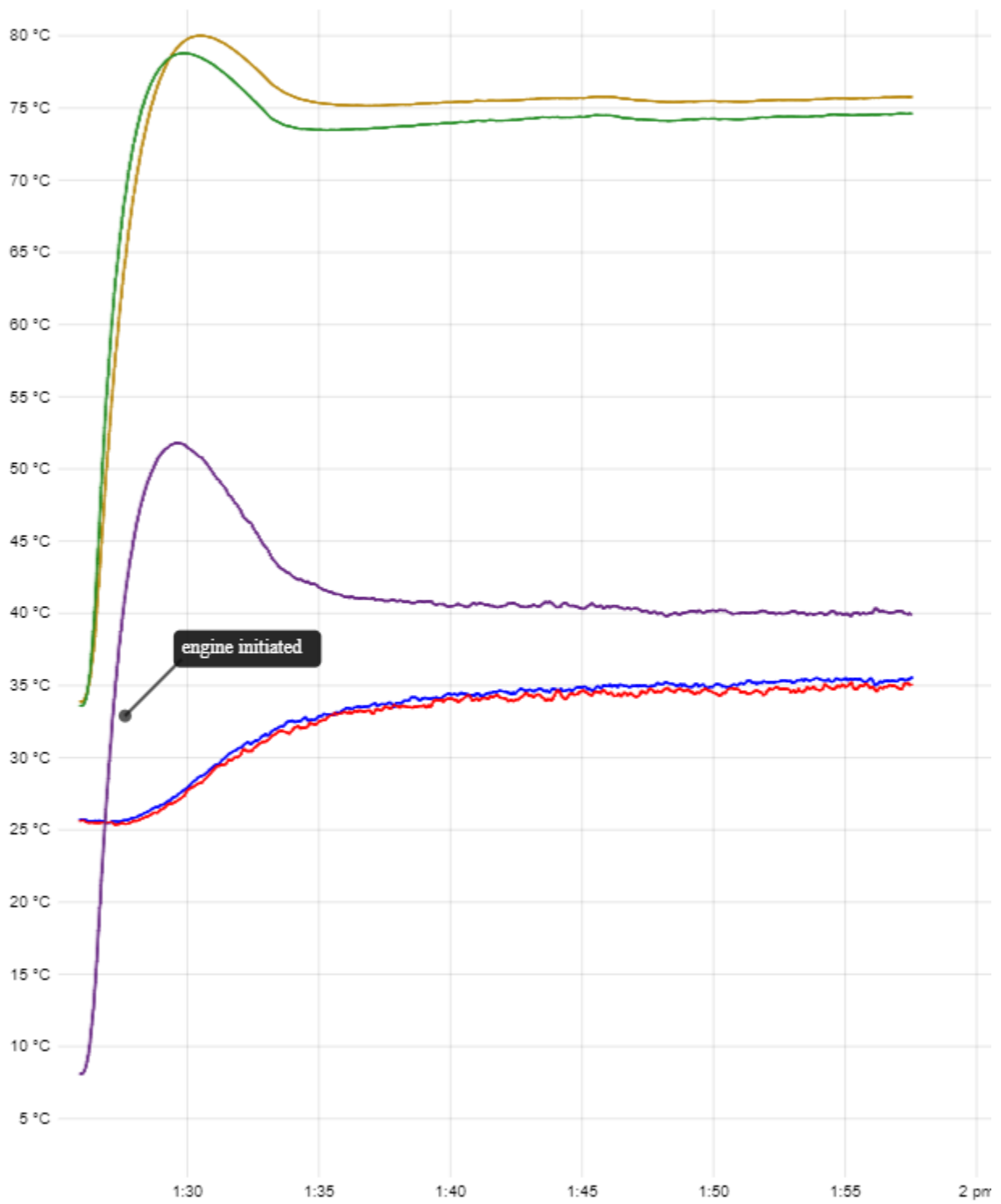


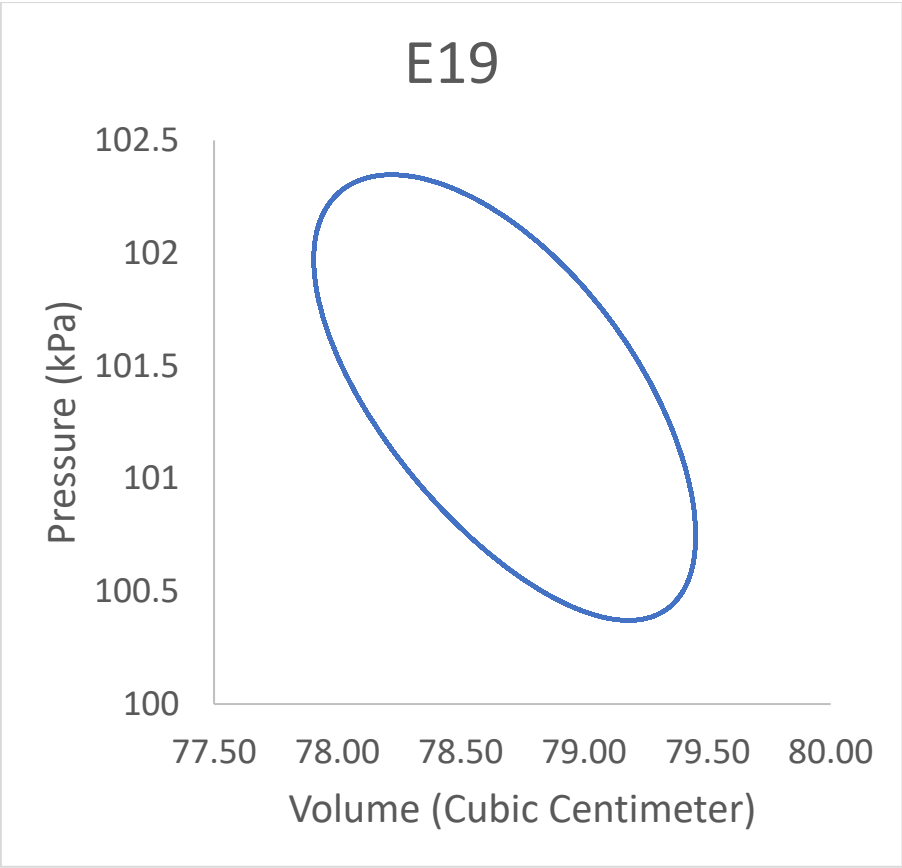
# E18



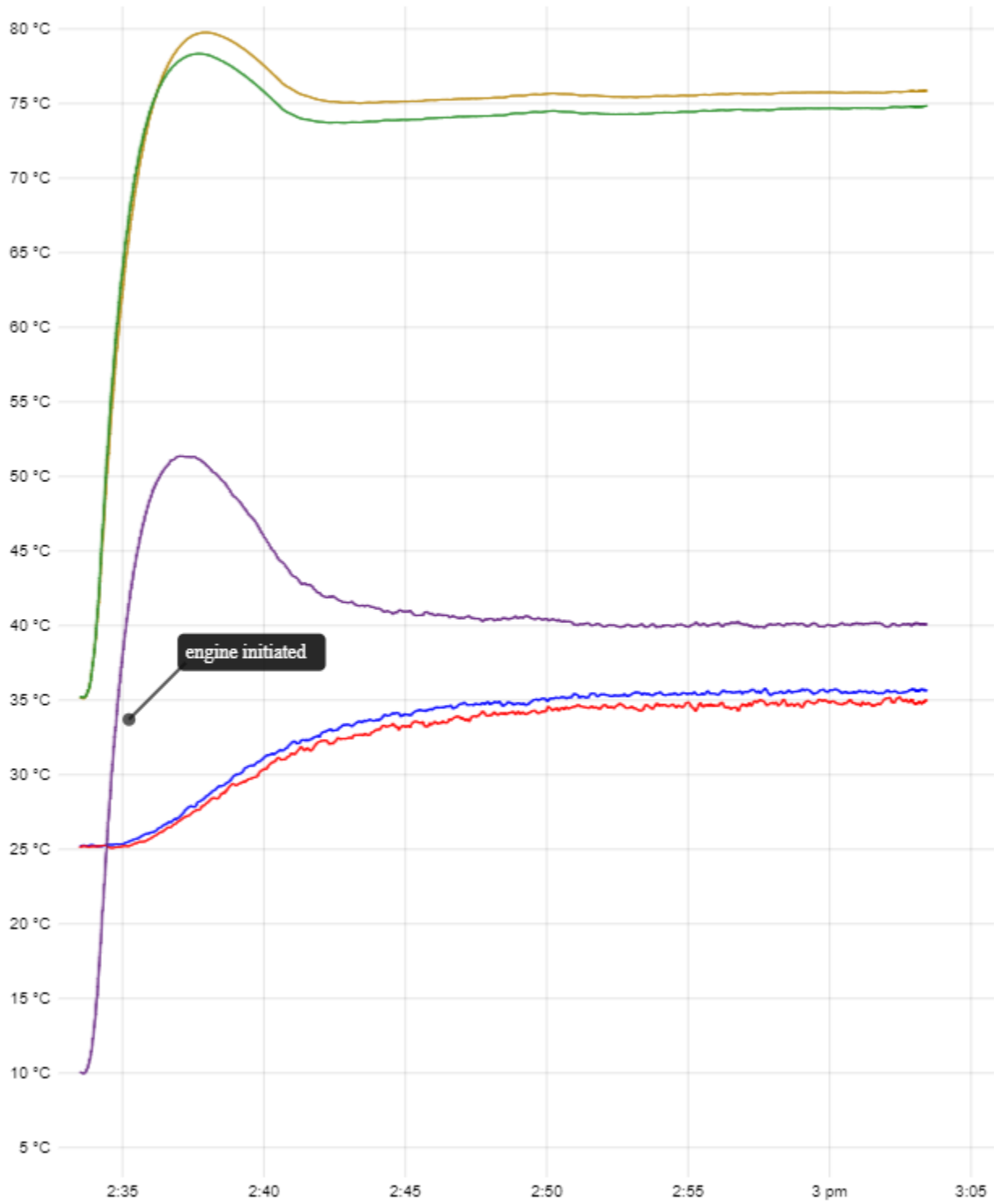


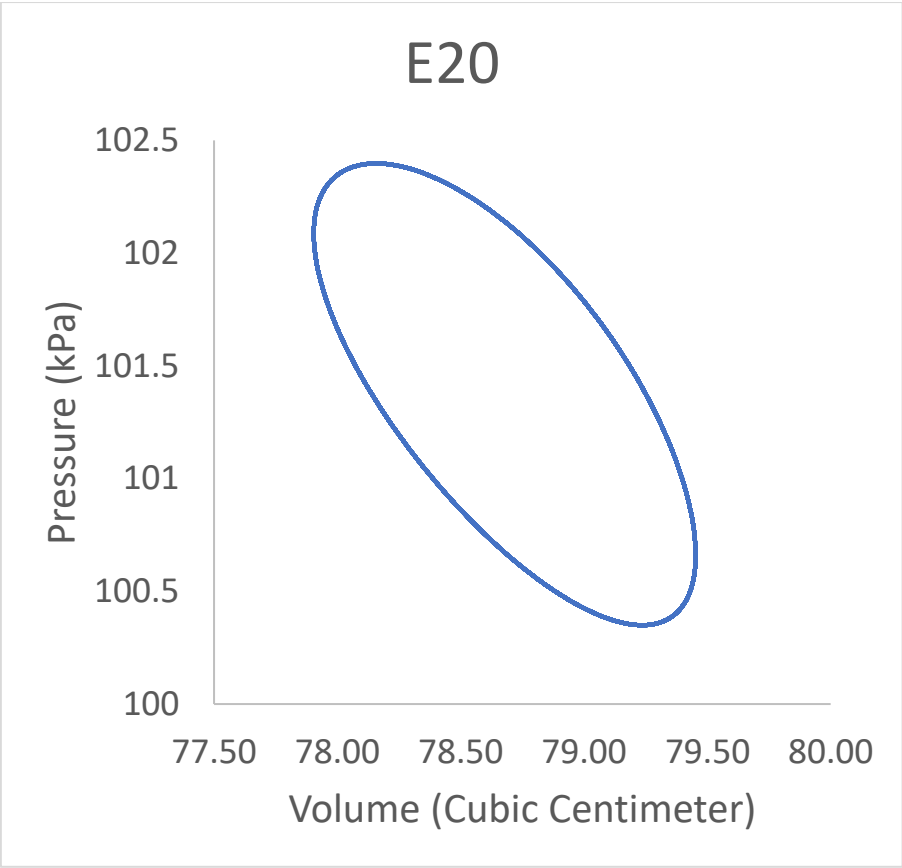
# E19



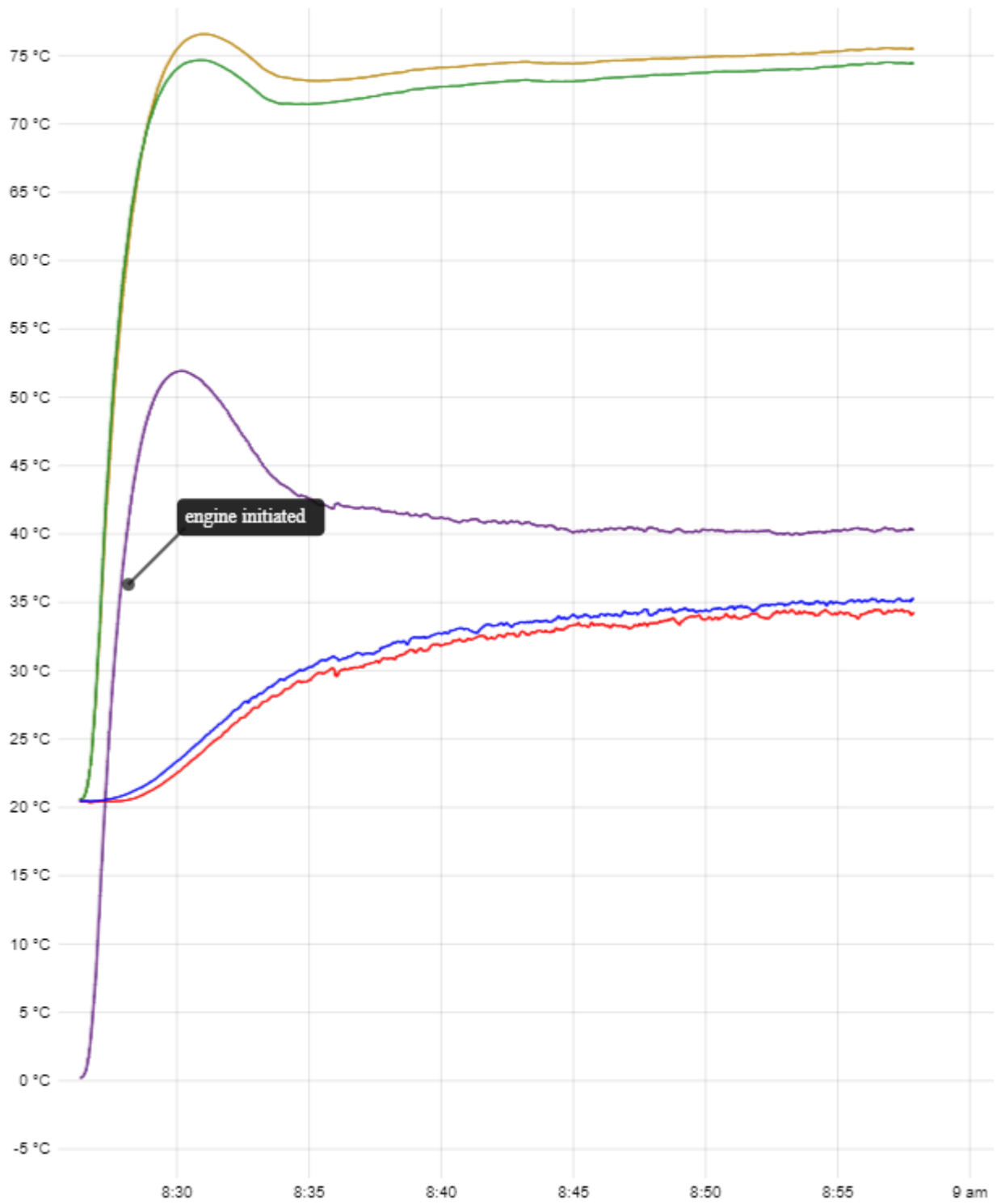


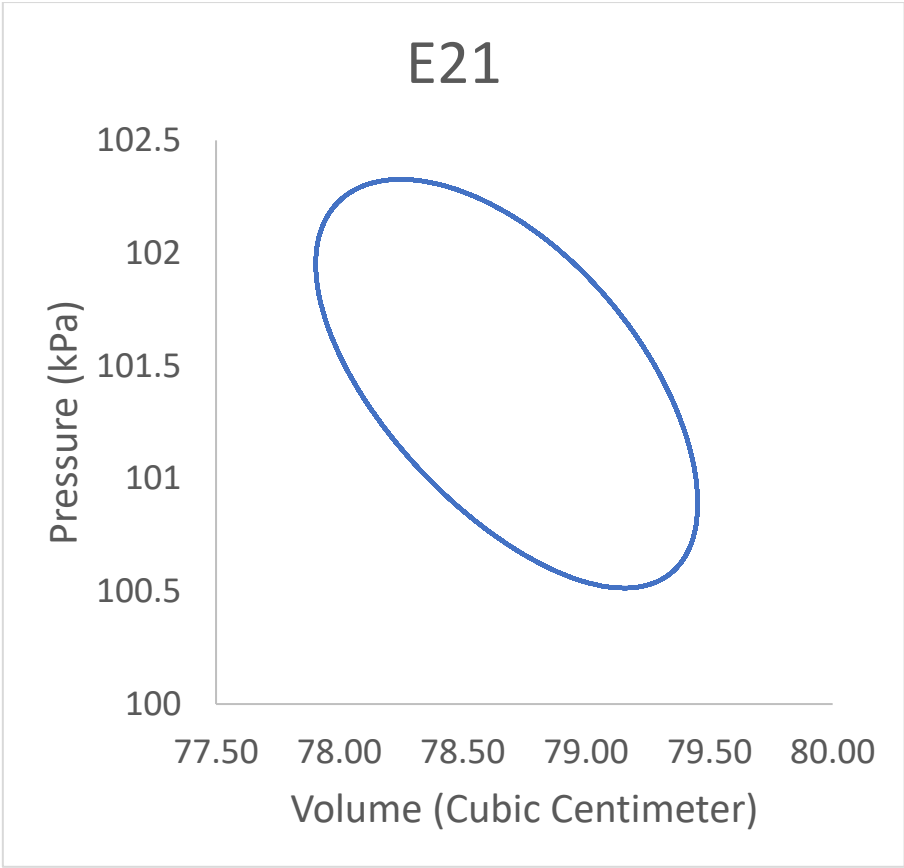
## E20



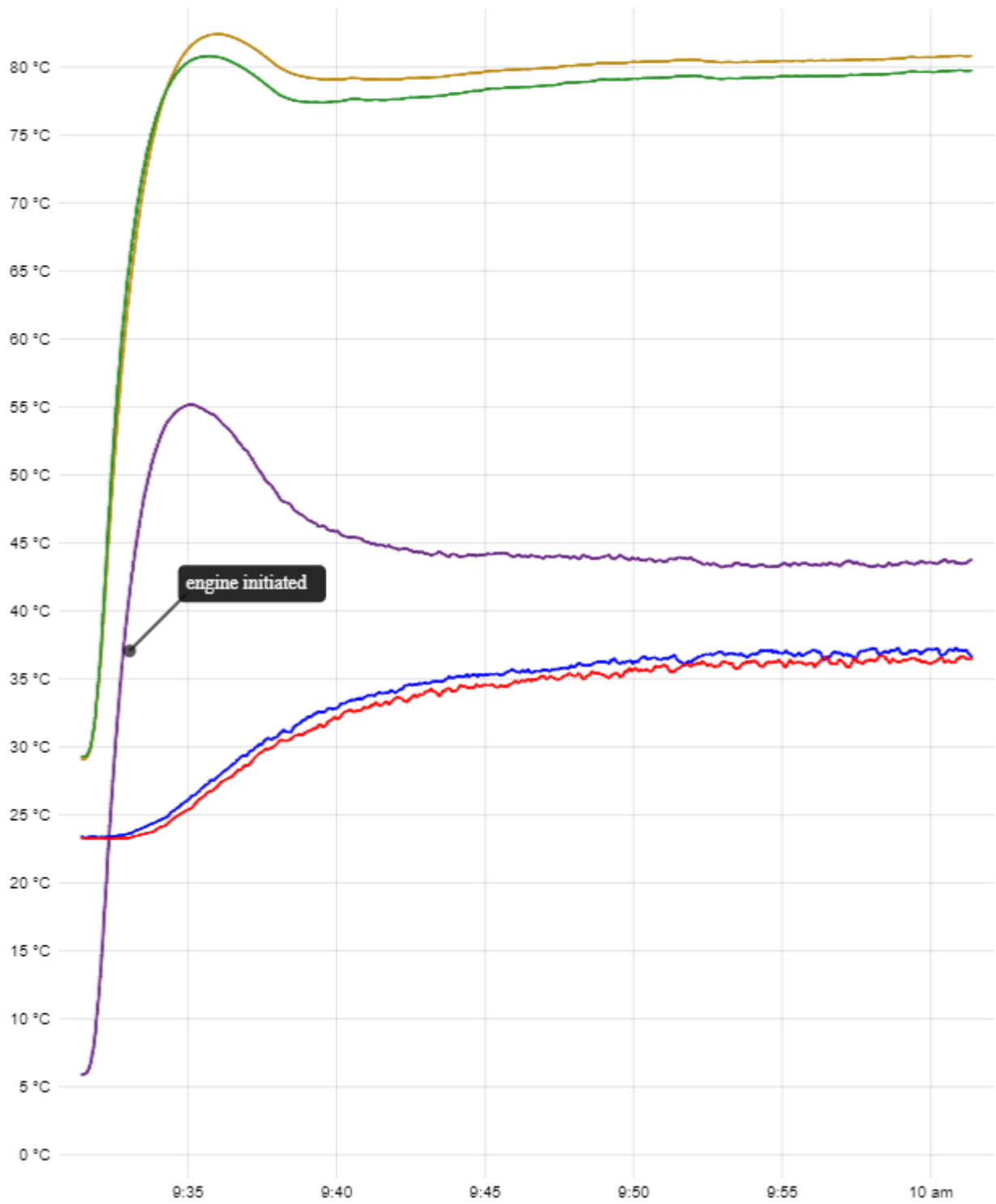


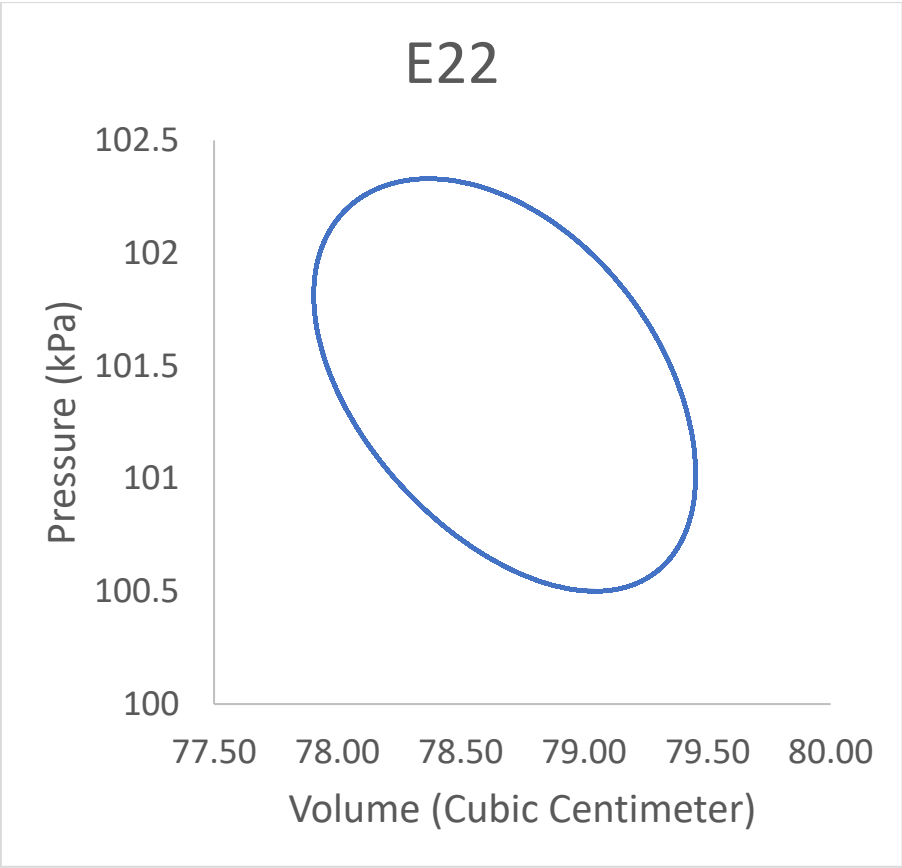
# E21



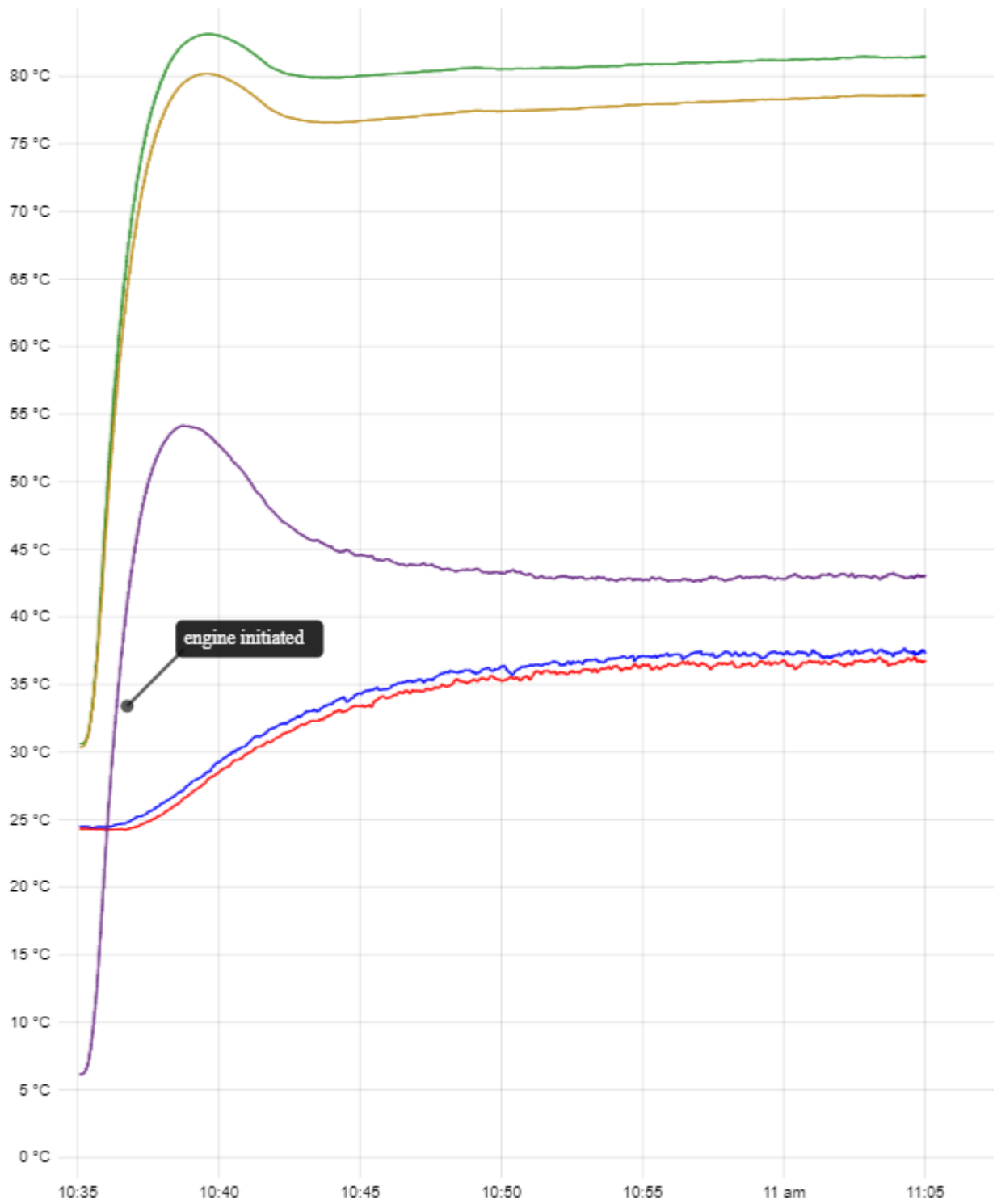


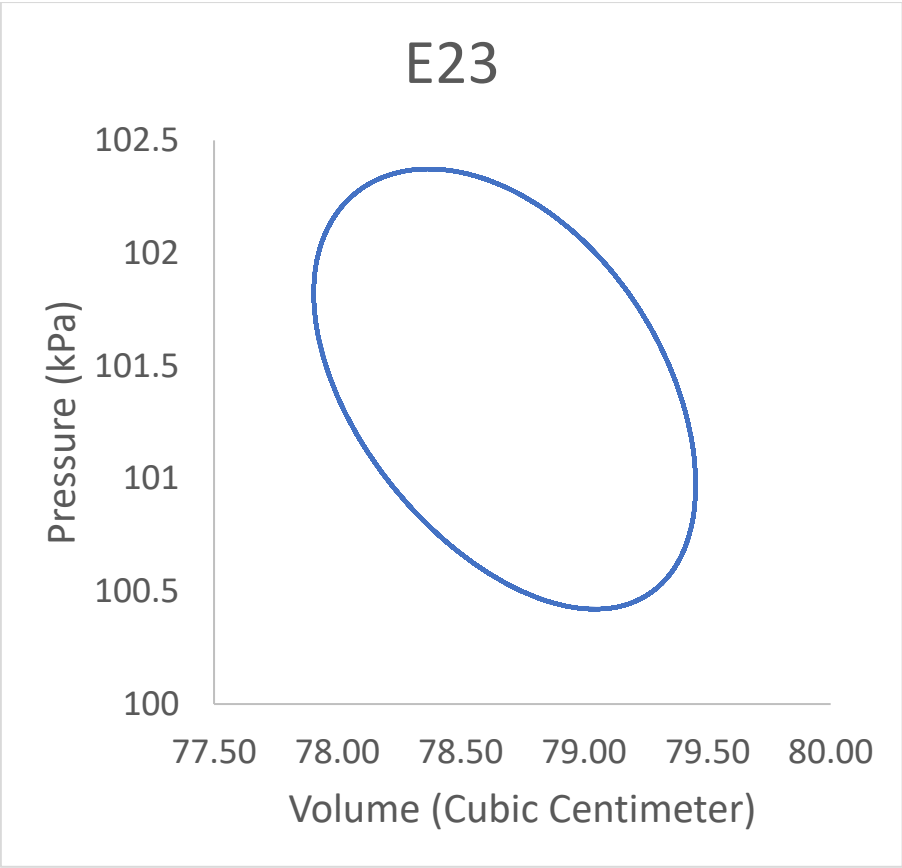
## E22



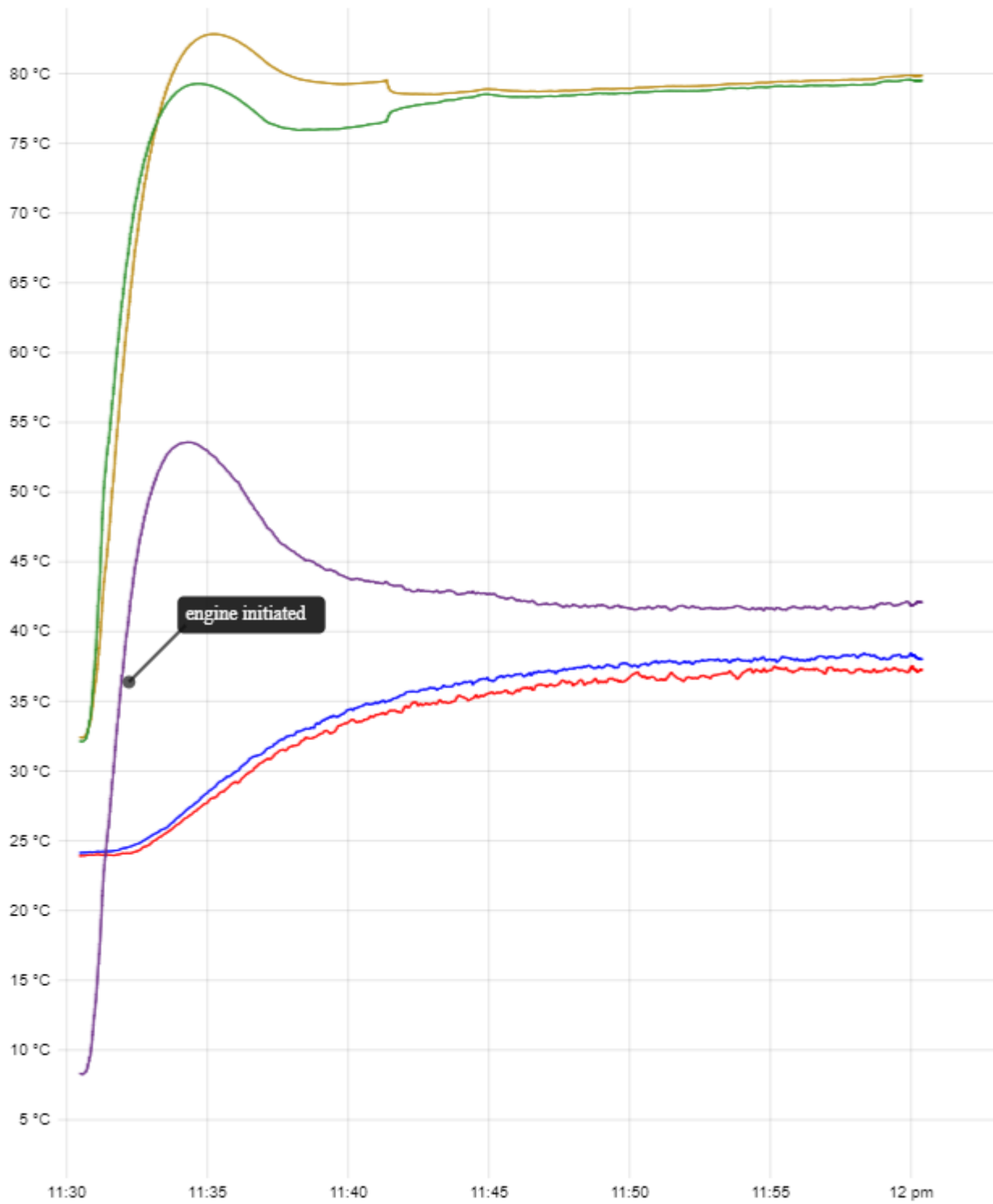


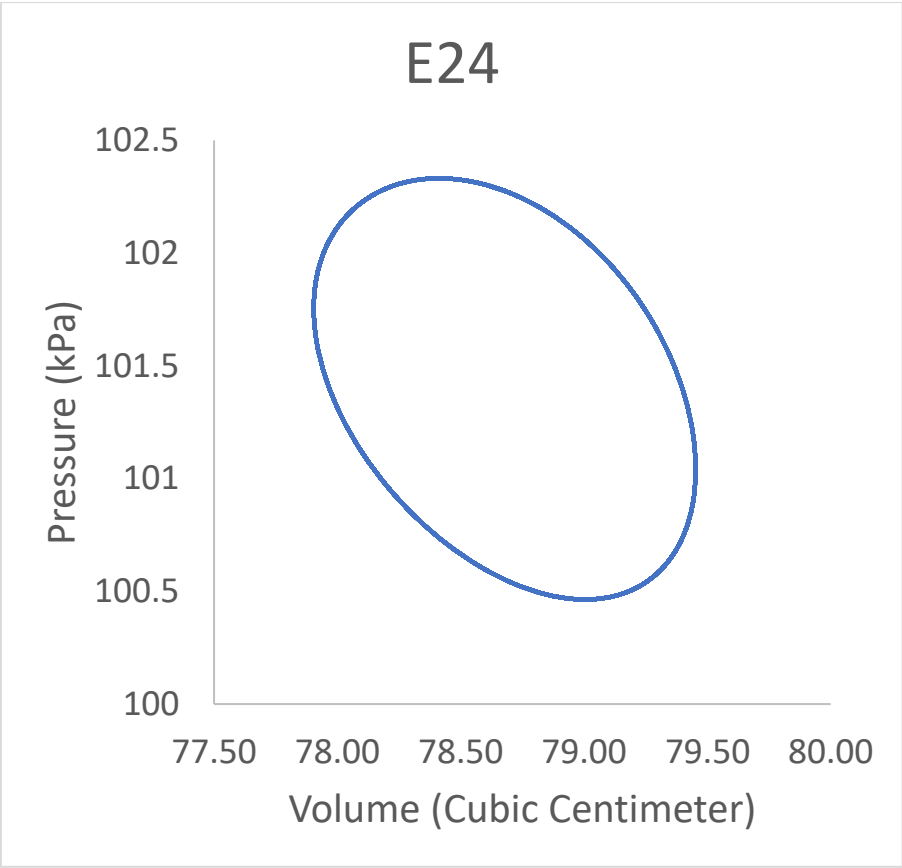
# E23



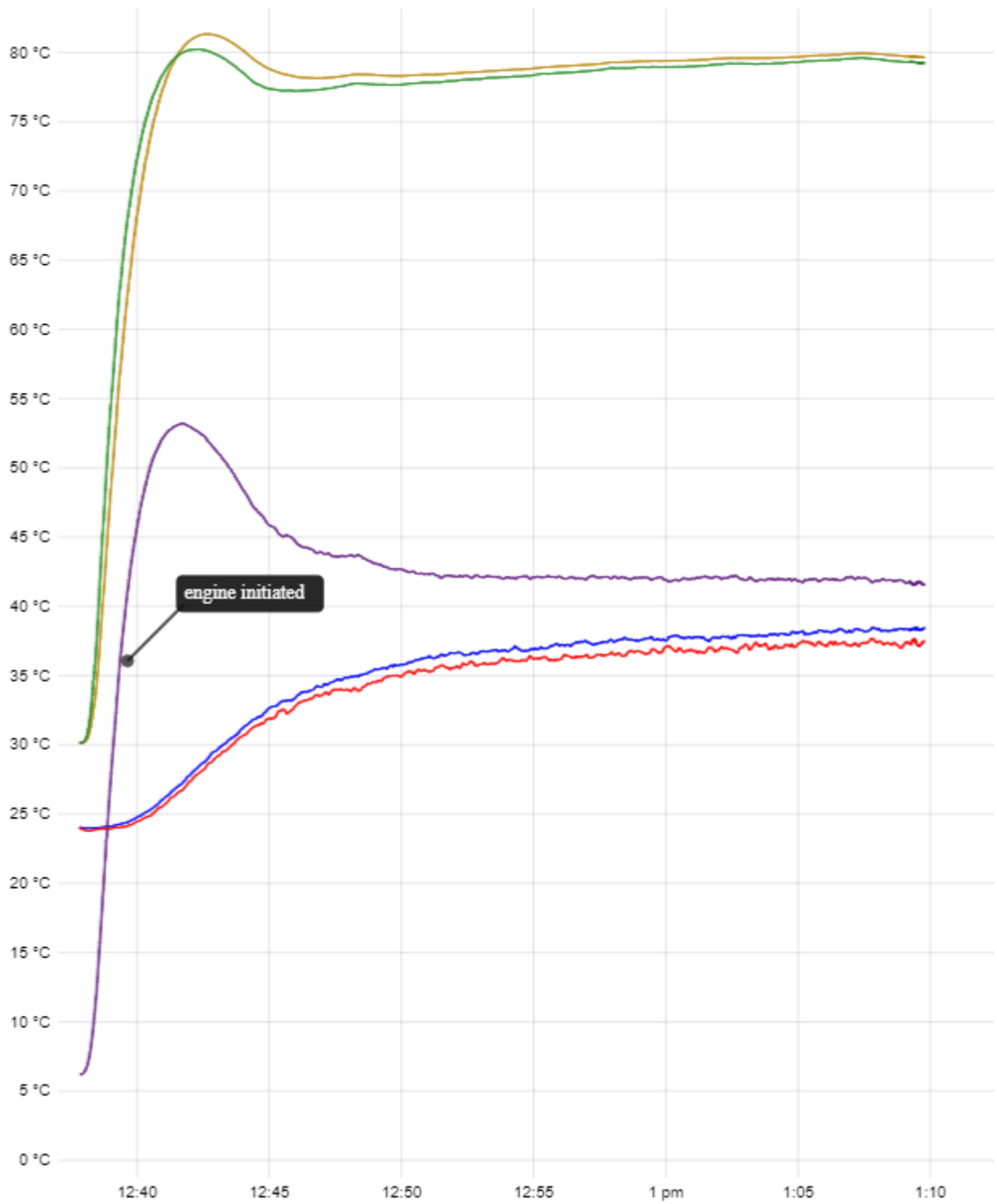


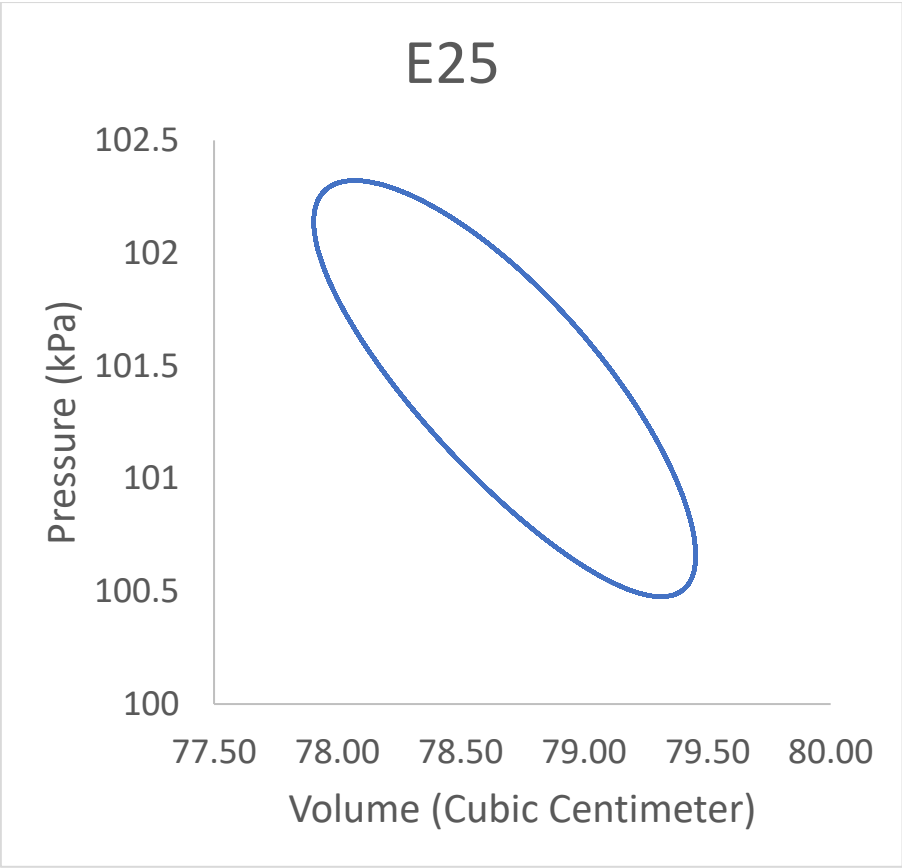
# E24



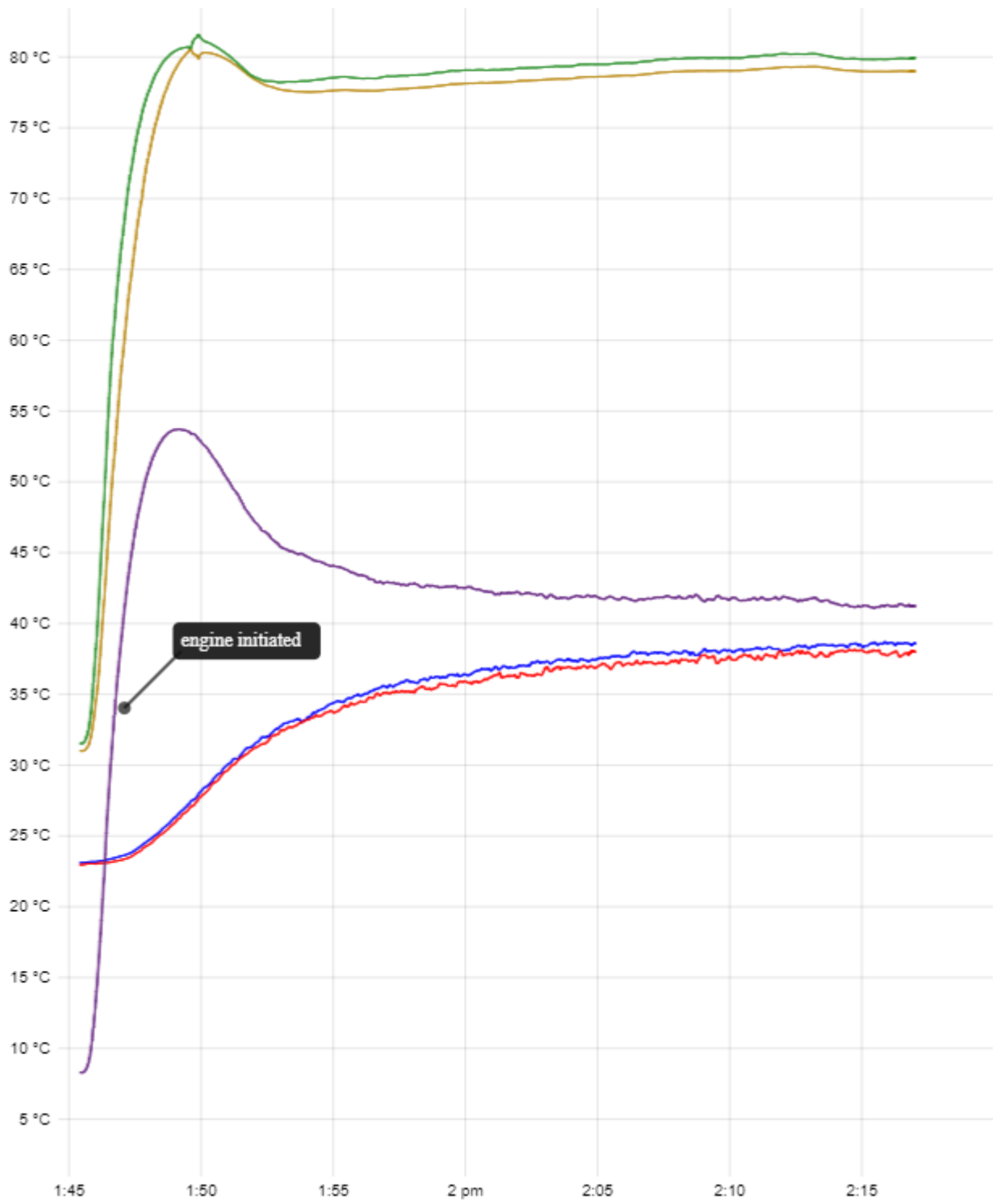


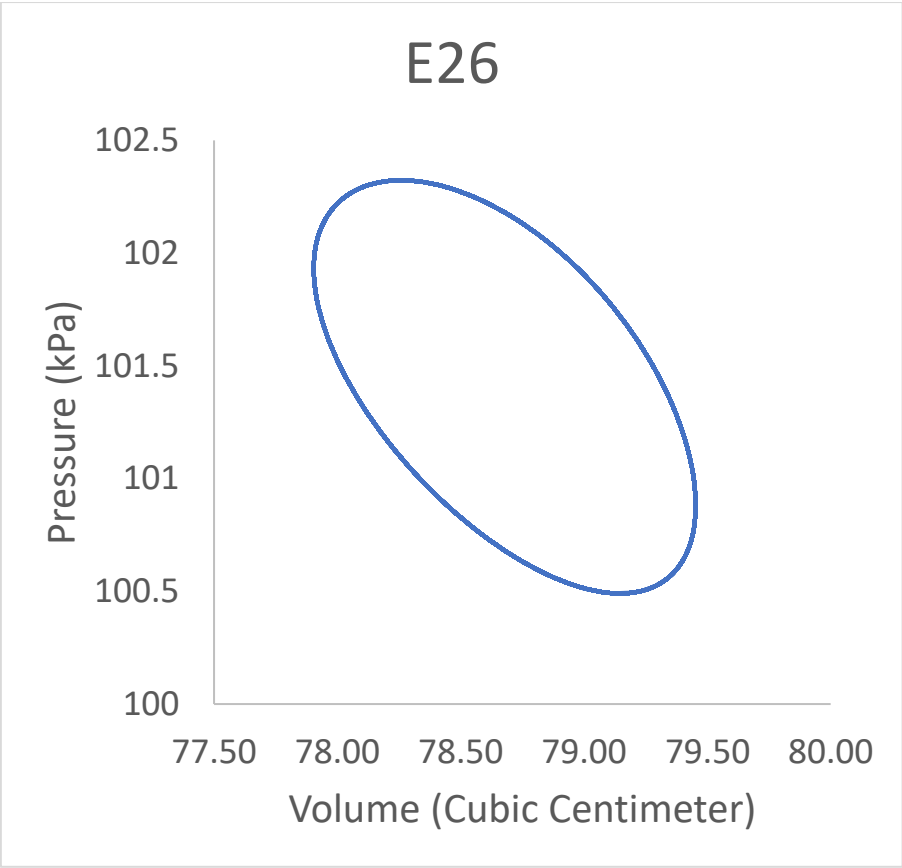
# E25





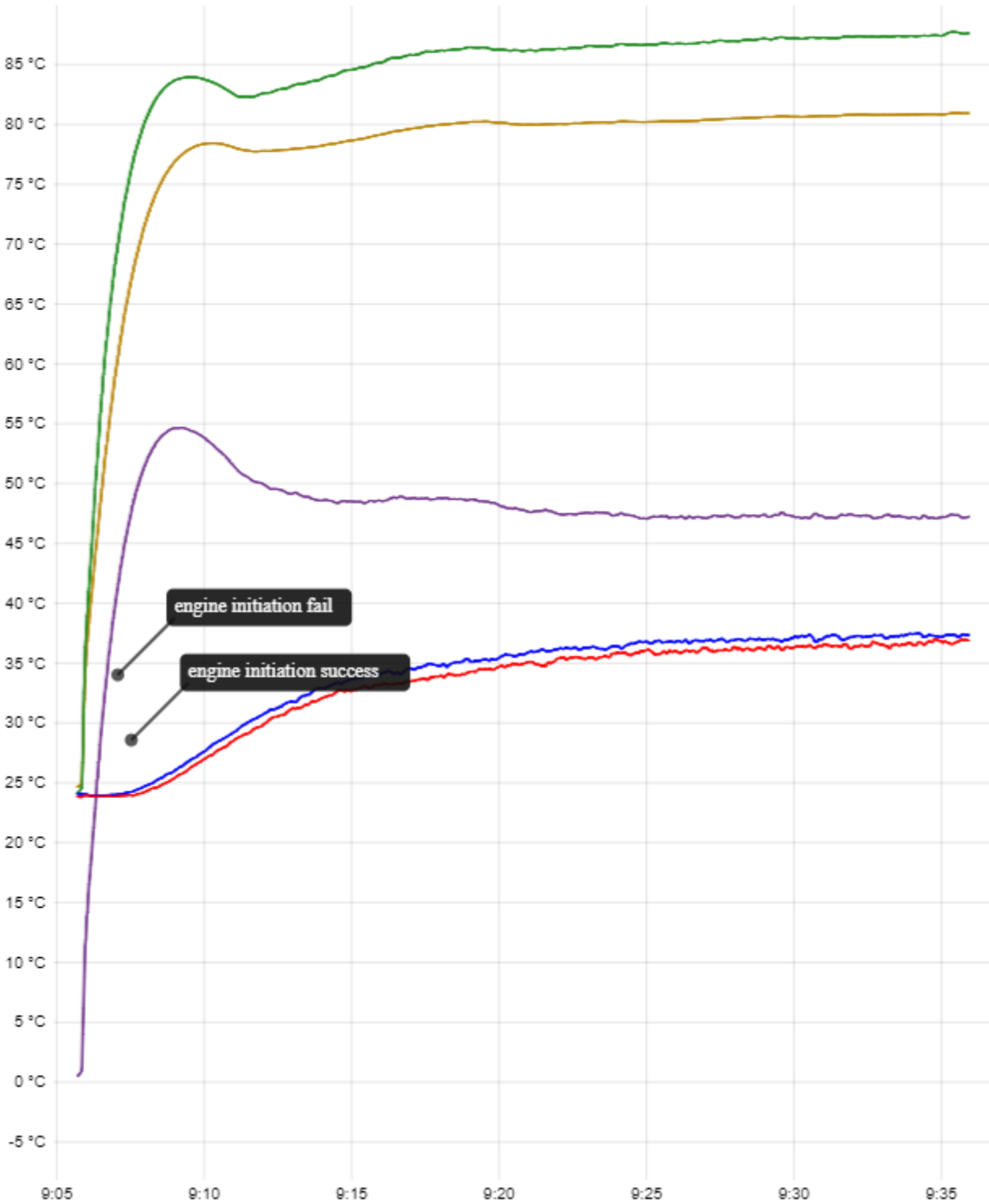
# E26



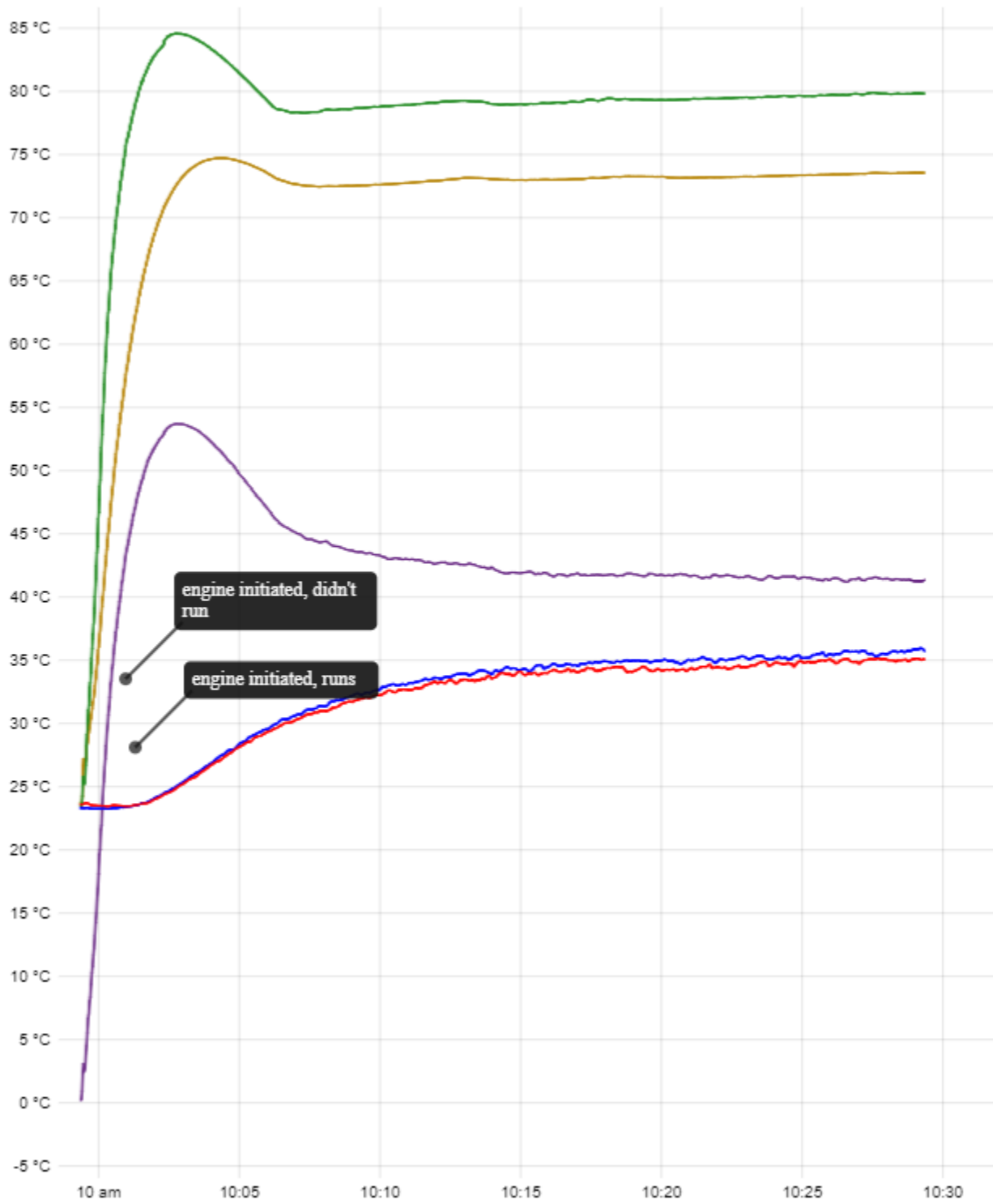


8.3.2. DRILLED EMSE

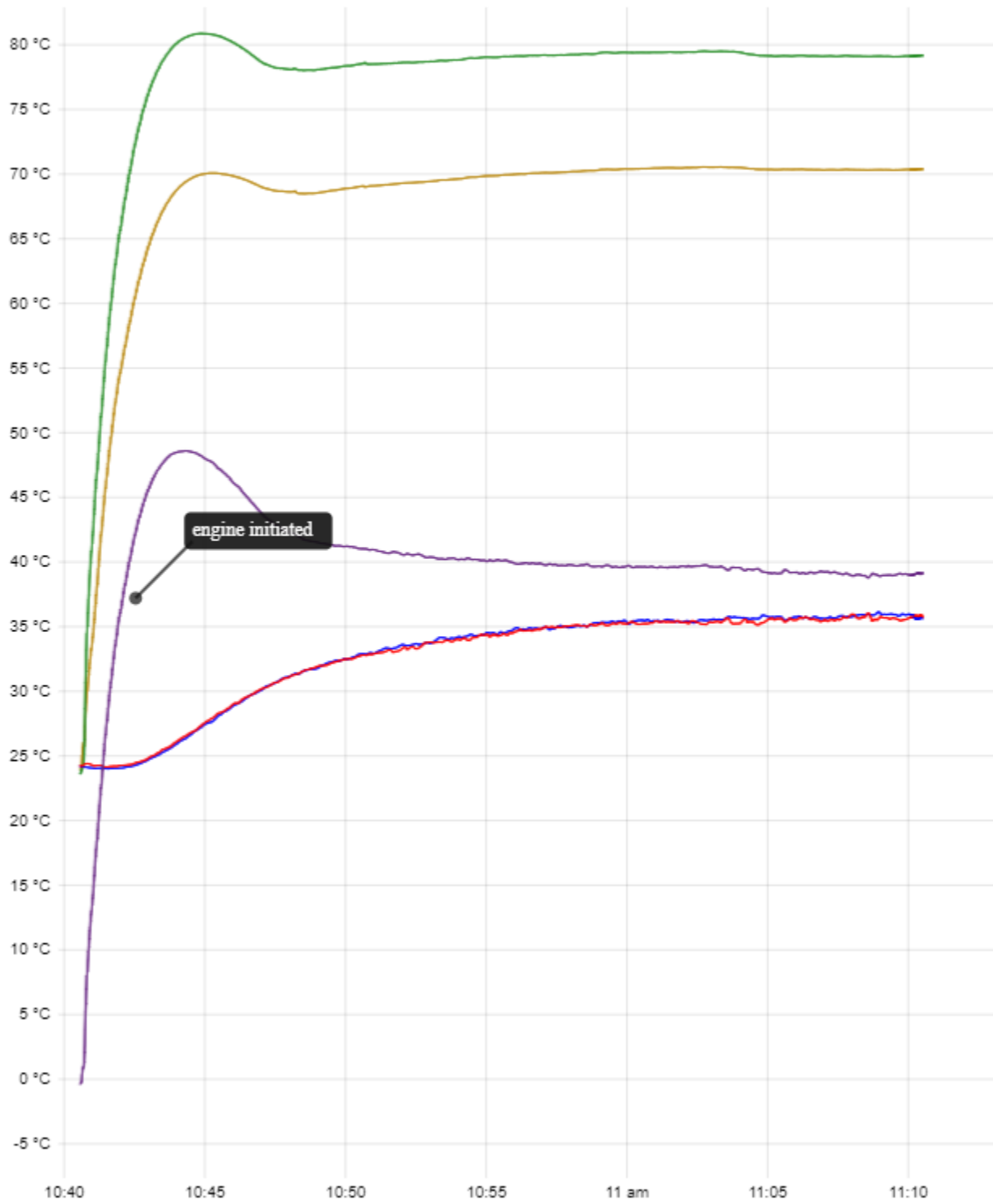
H1



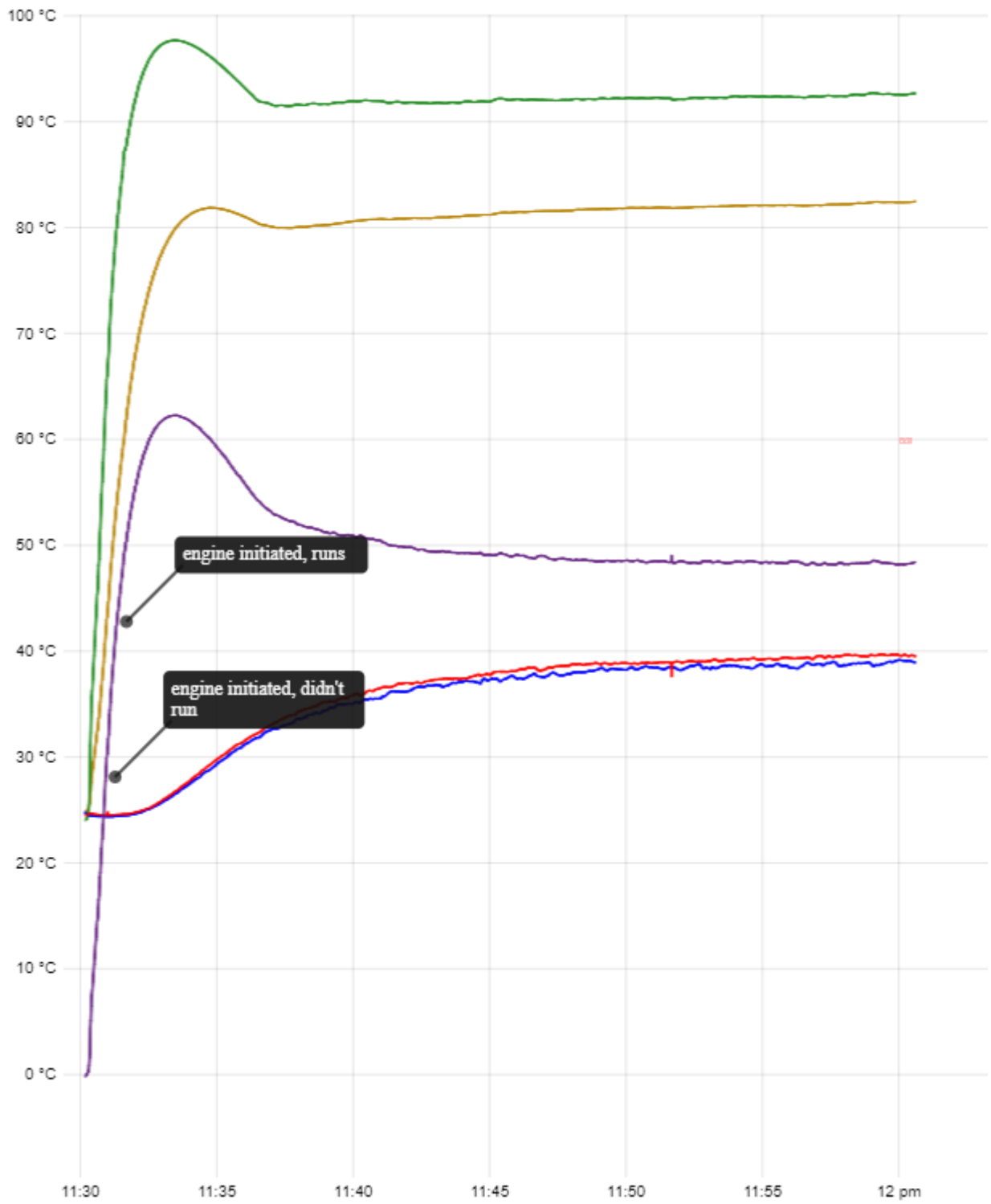
H2



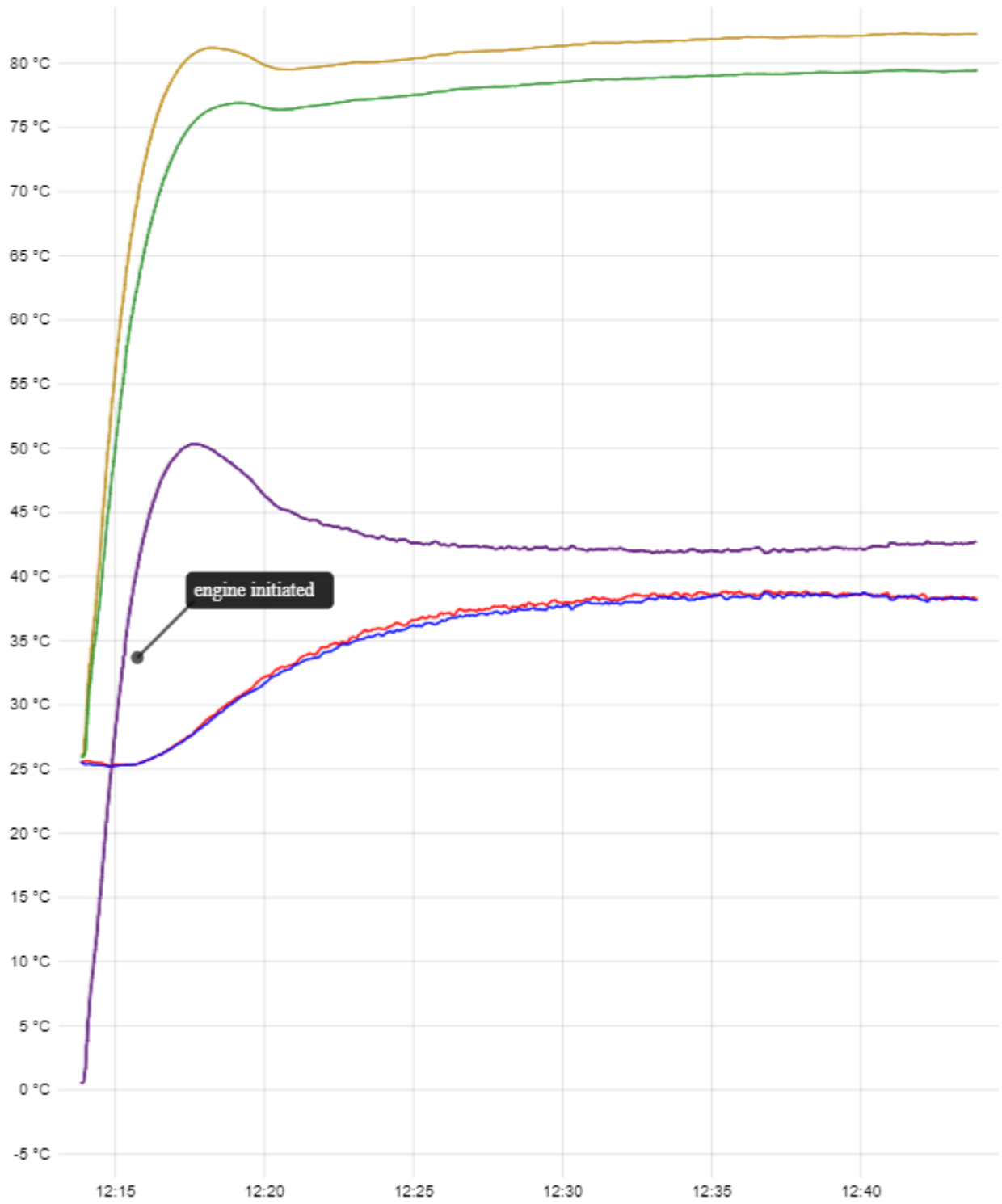
H3

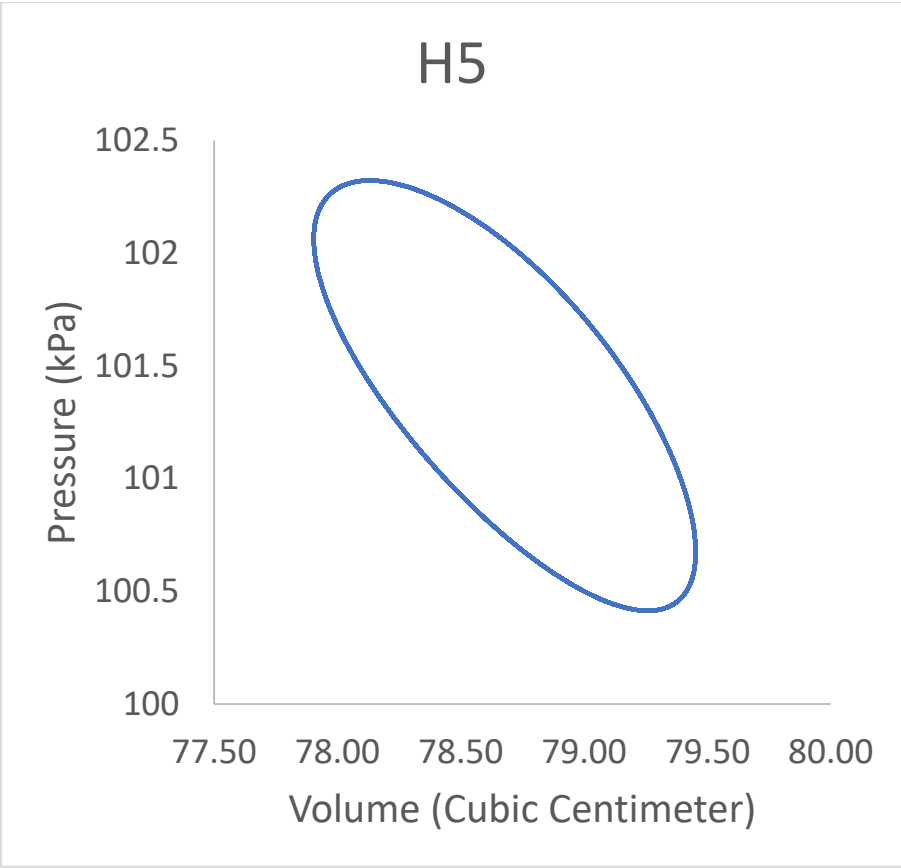


H4

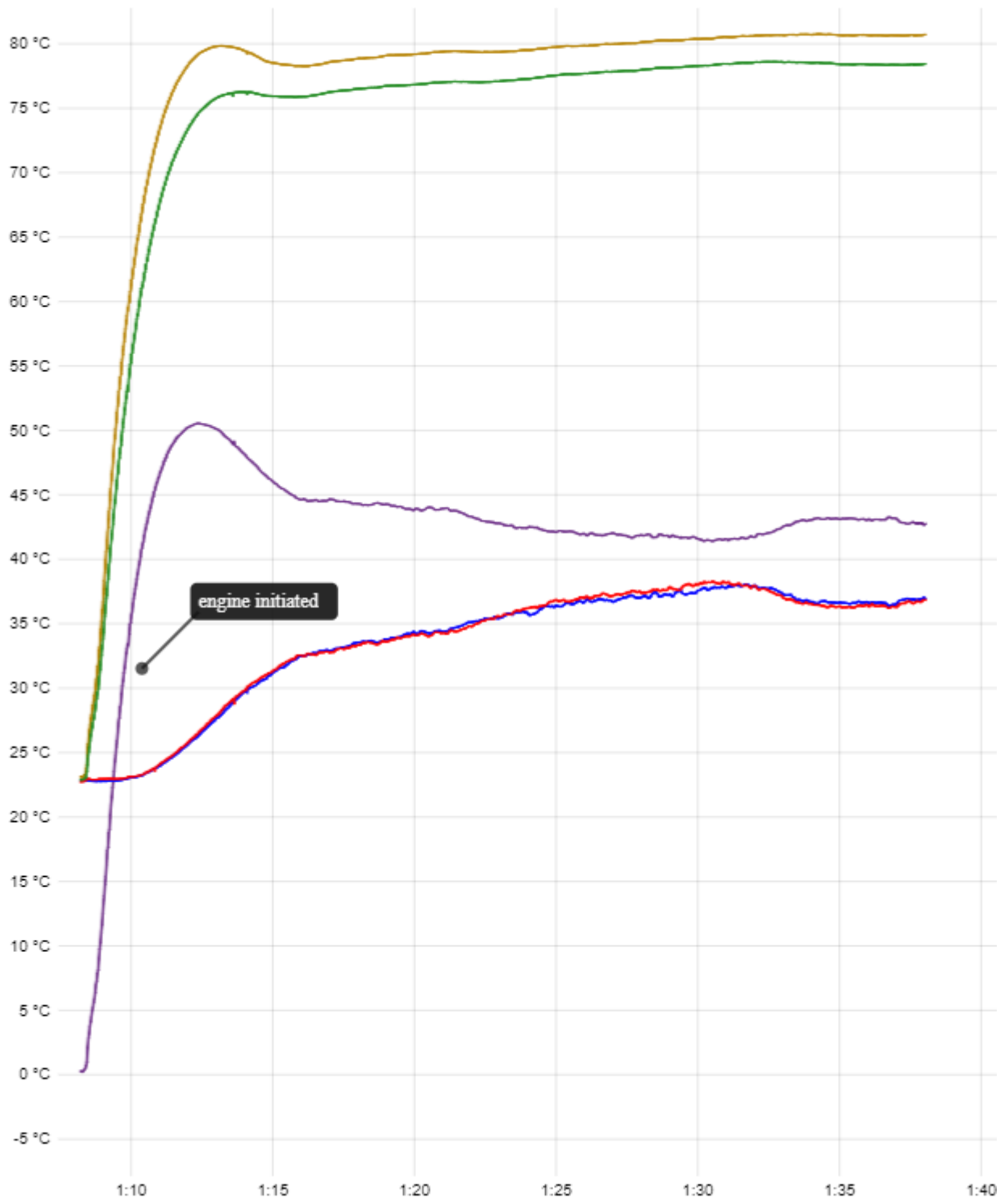


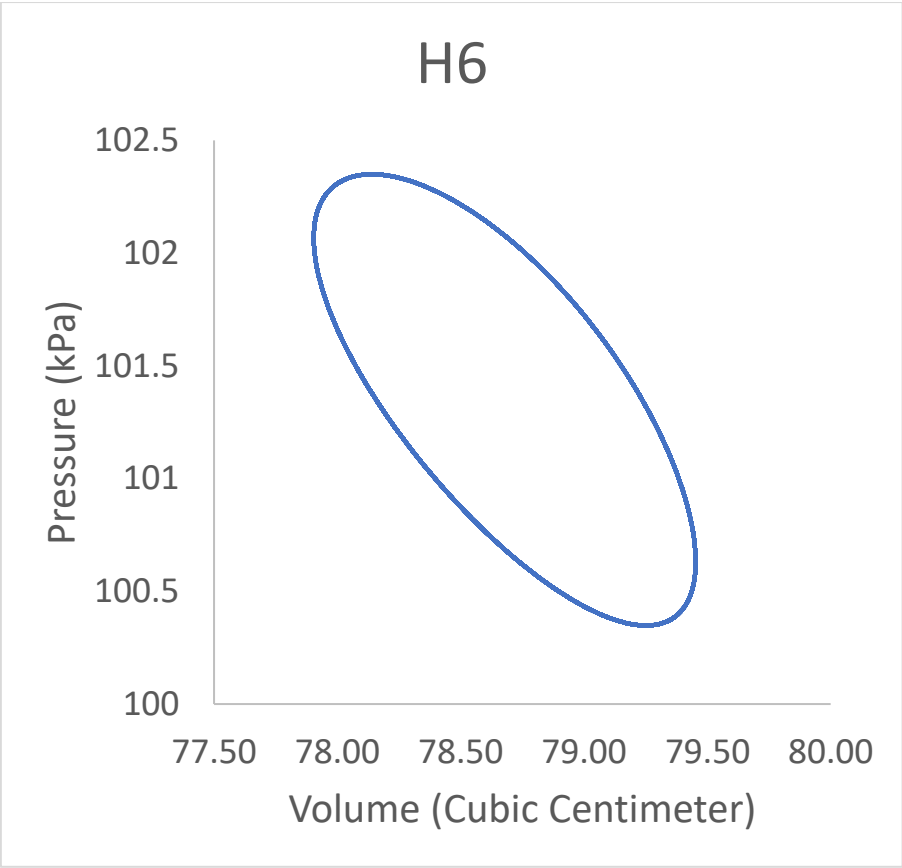
H5



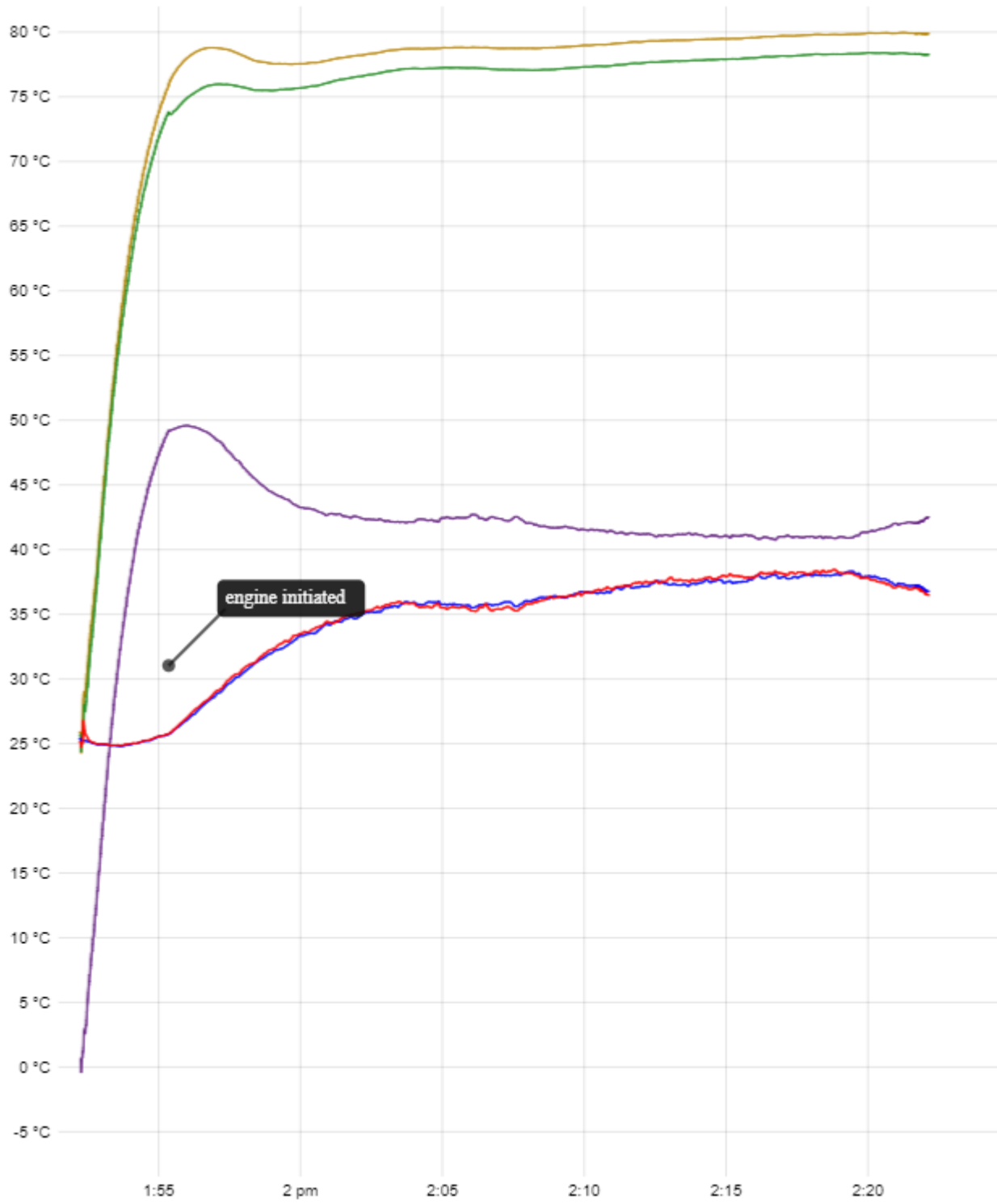


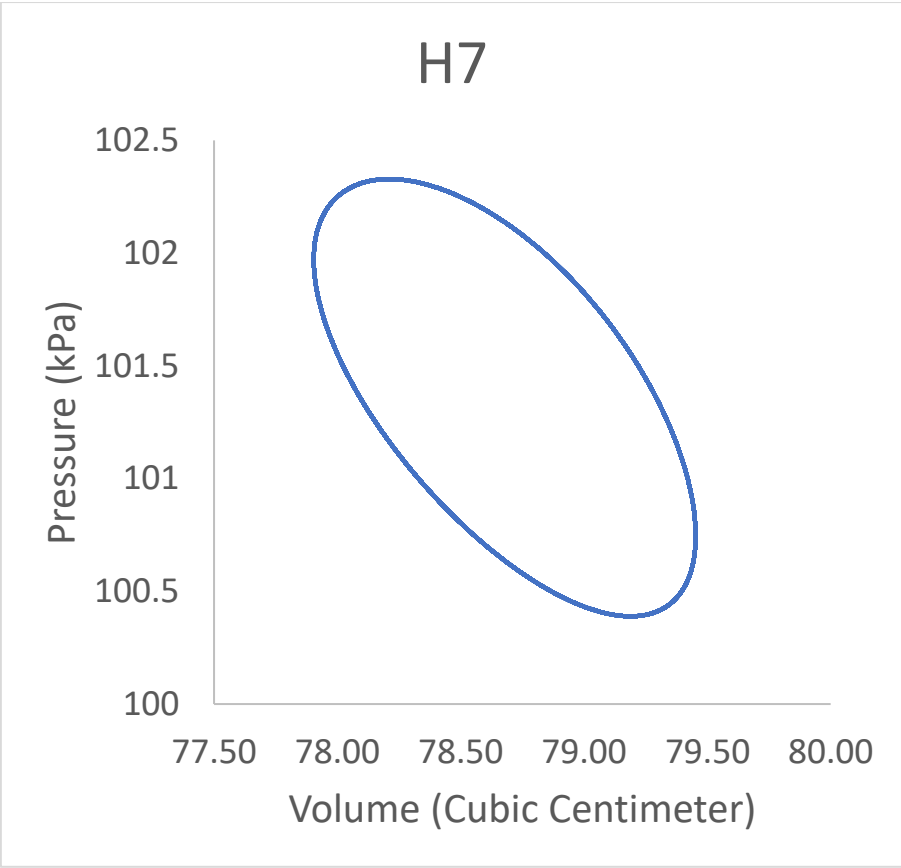
# H6



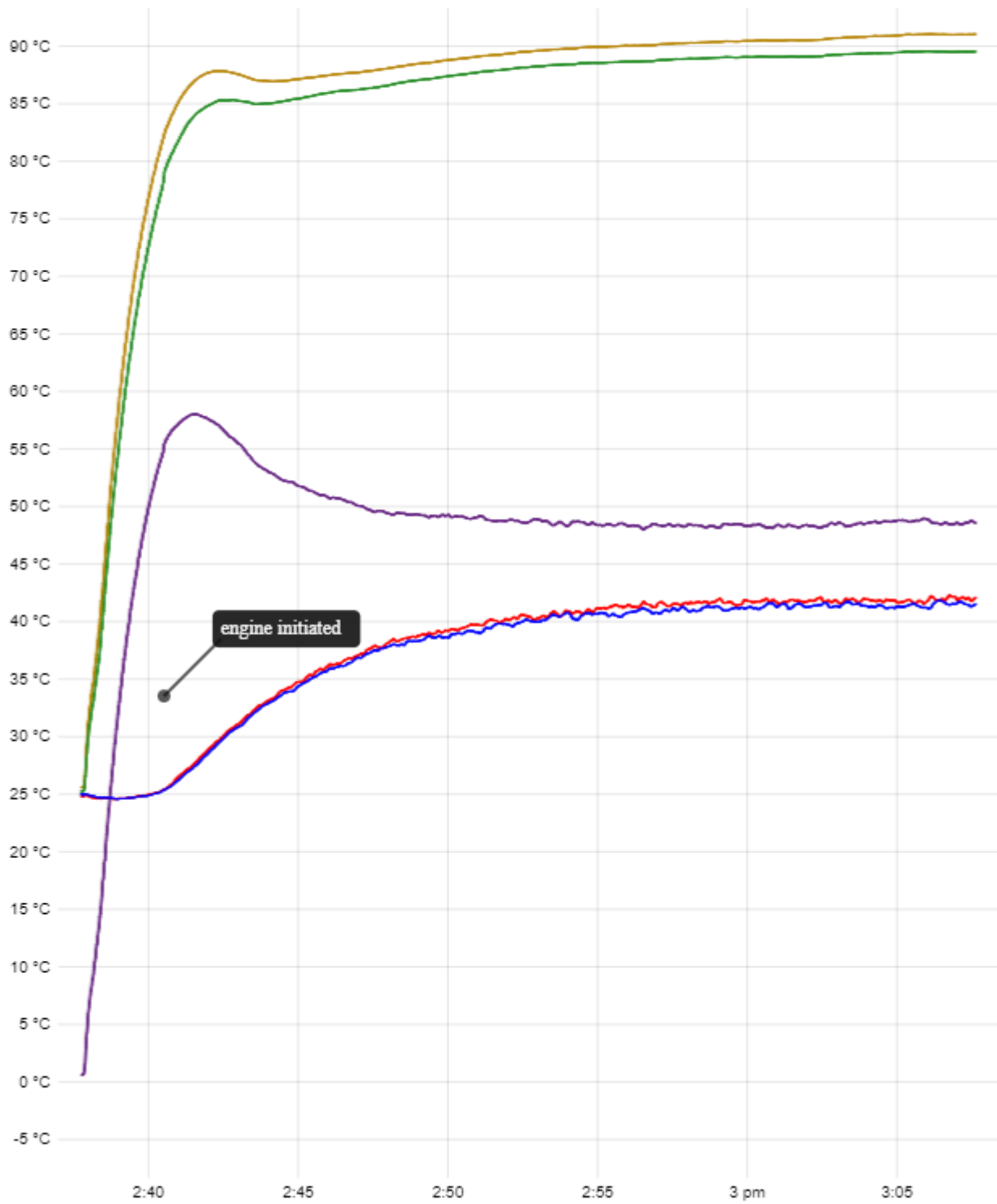


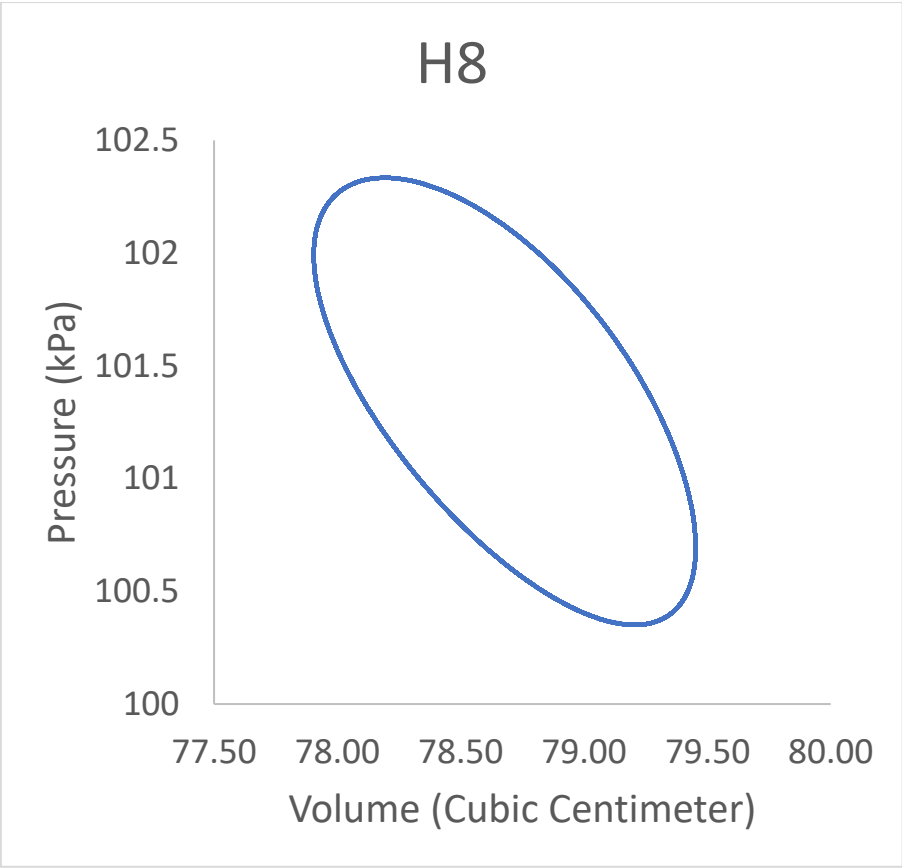
# H7



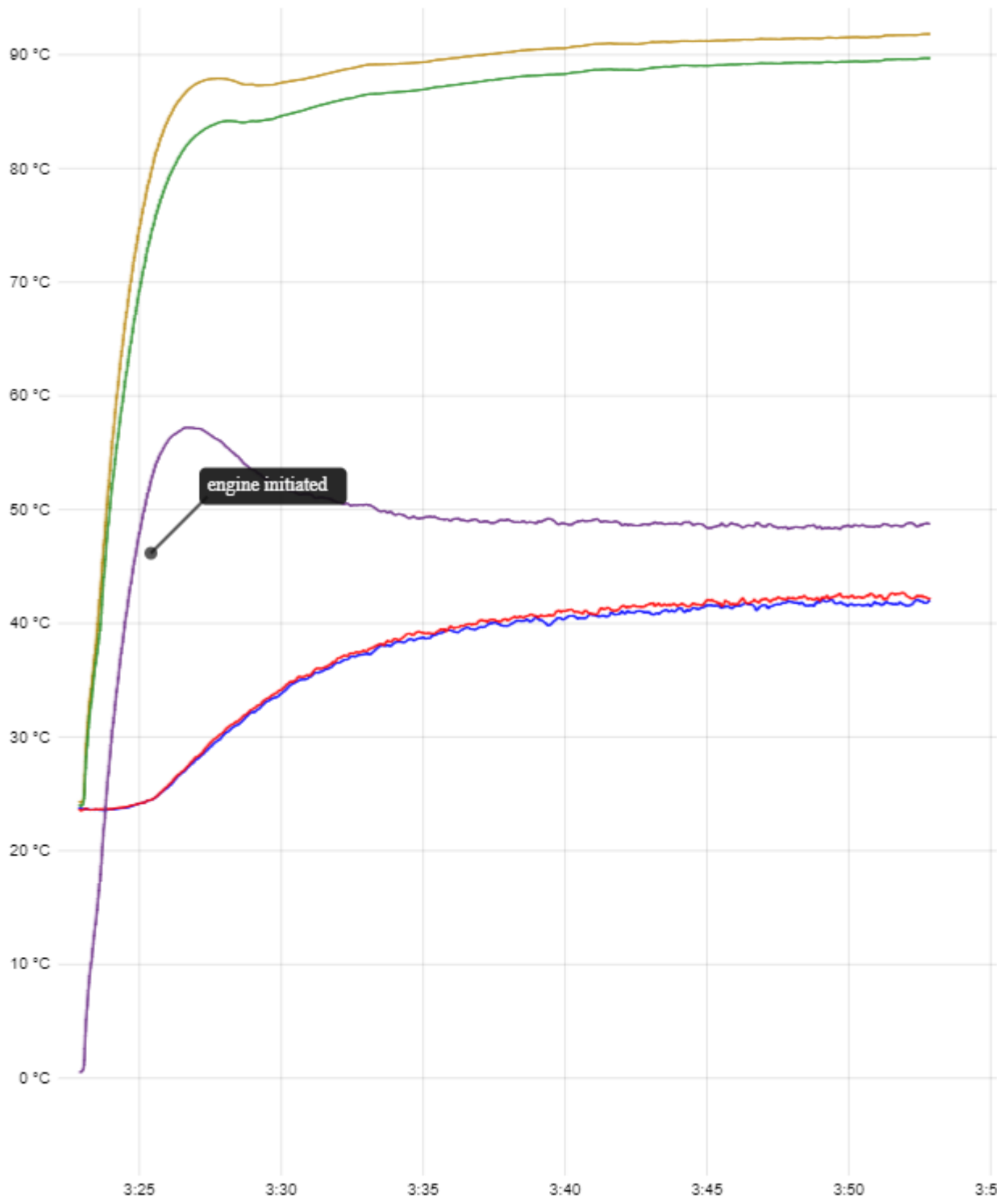


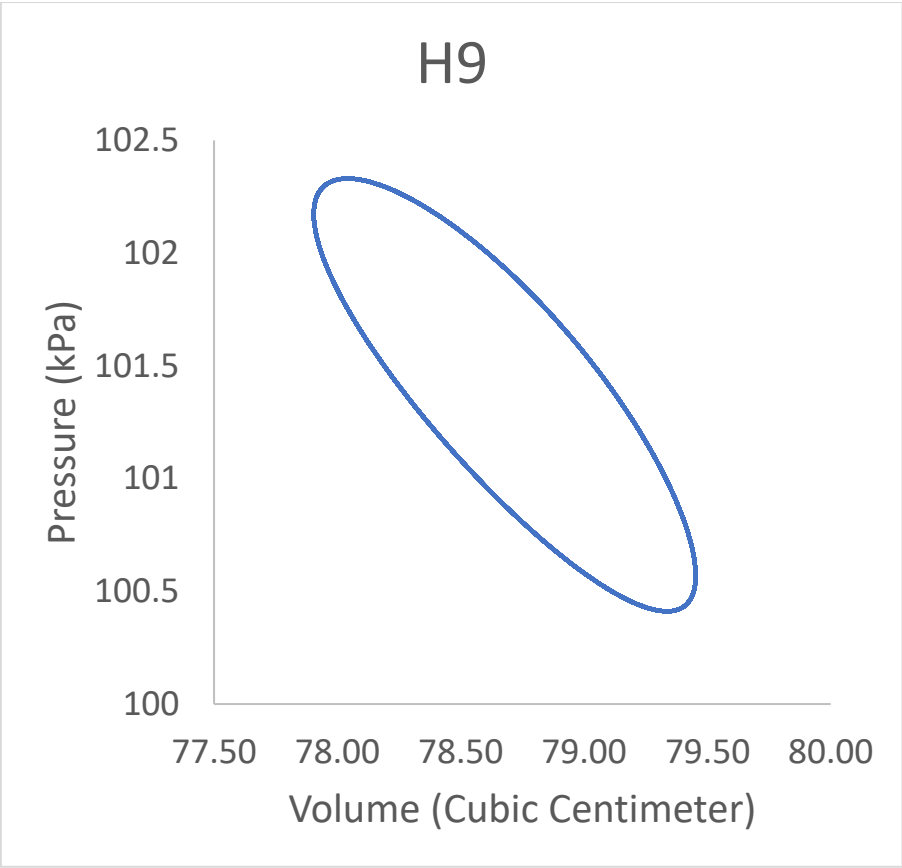
# H8



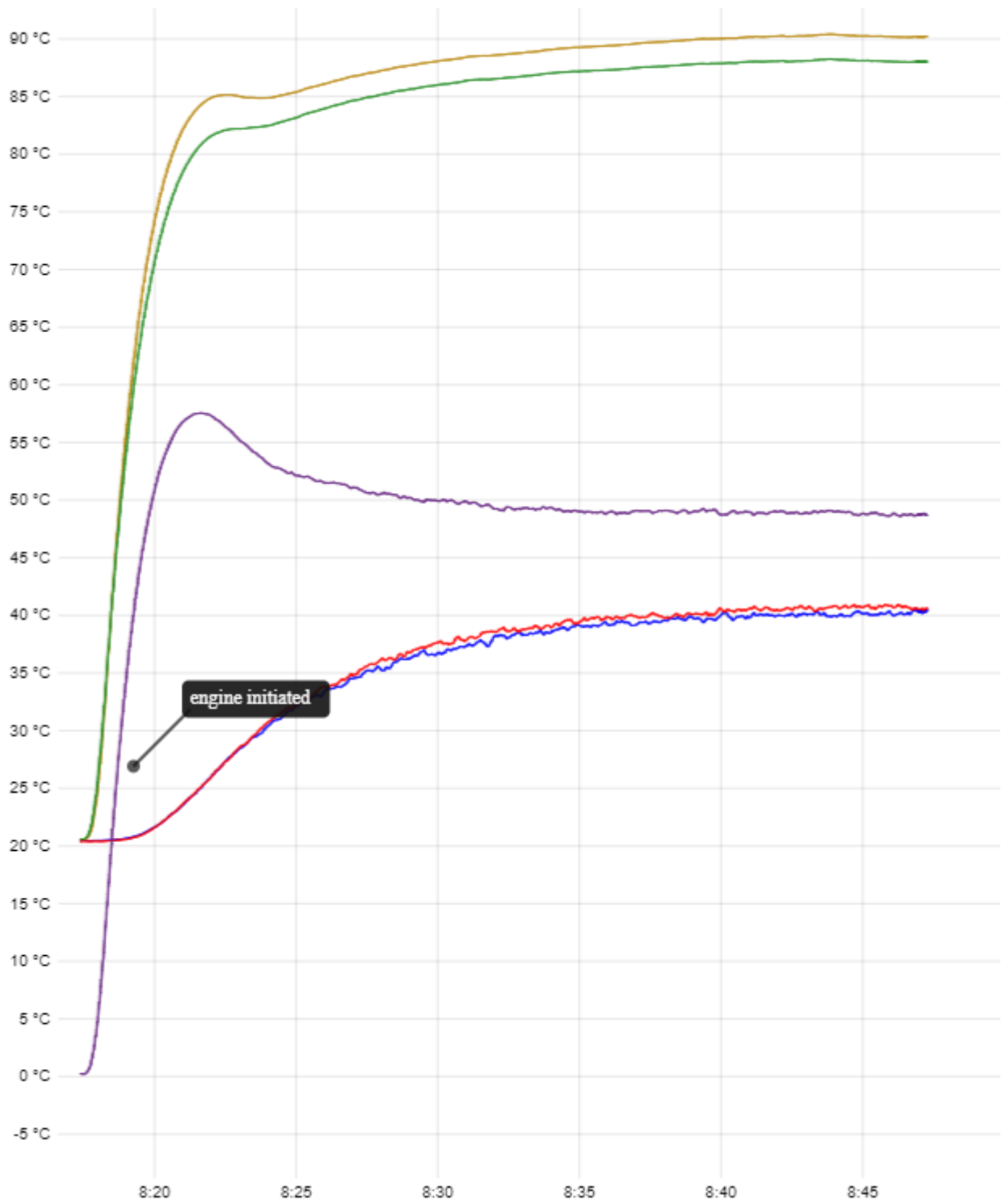


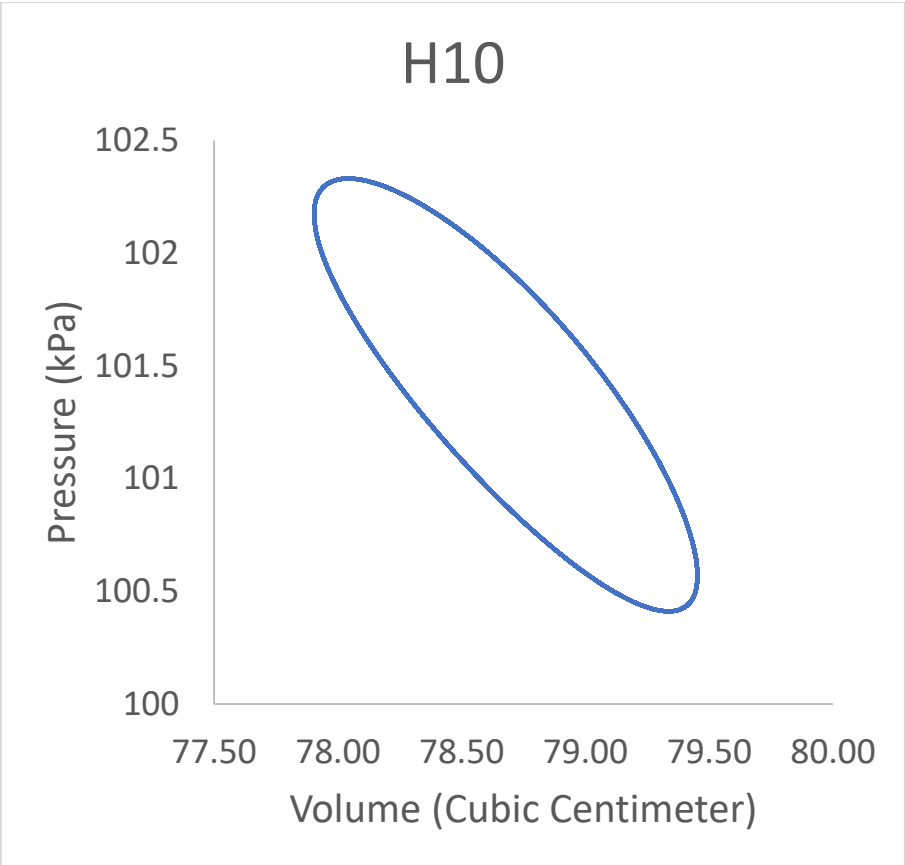
# H9



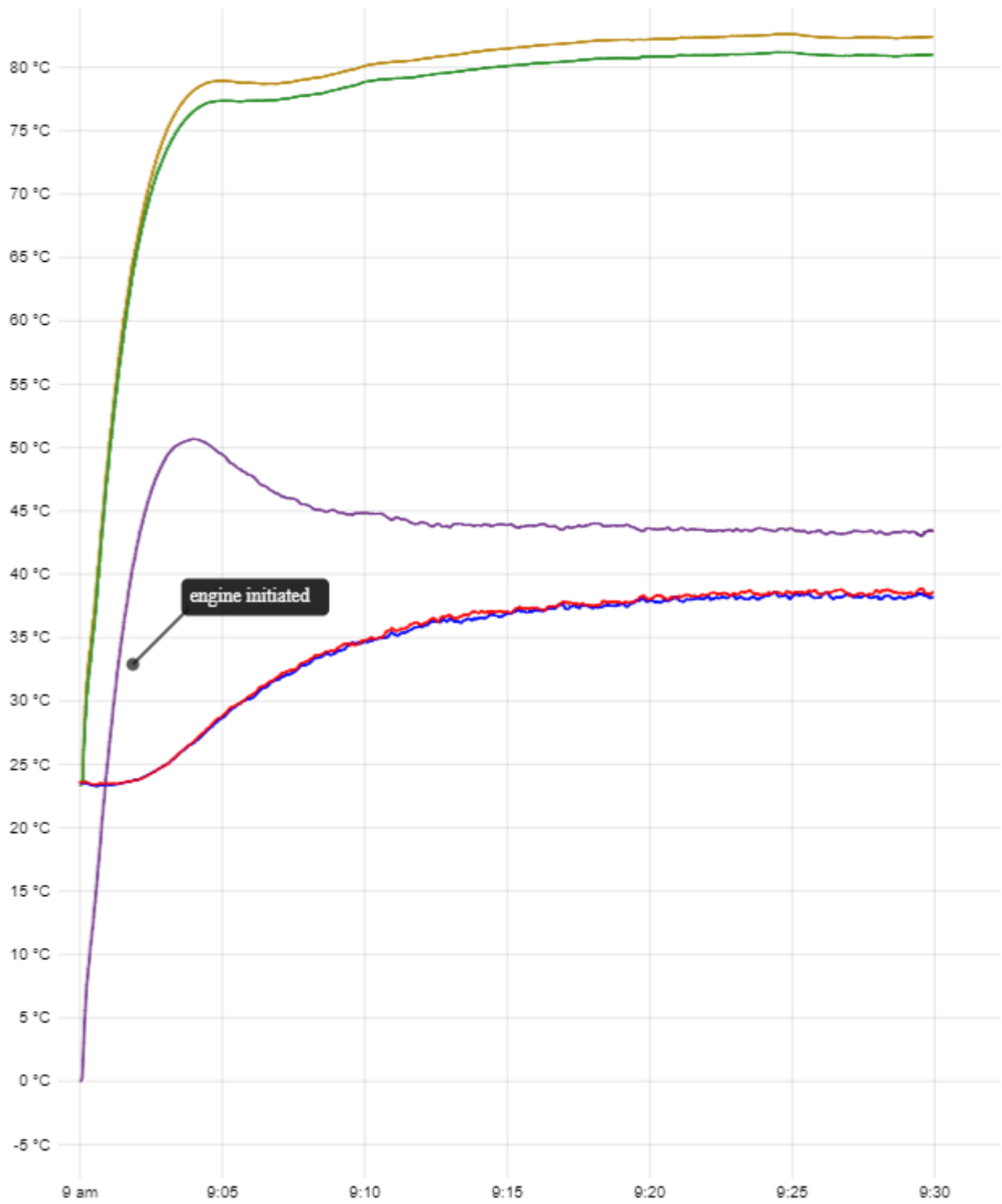


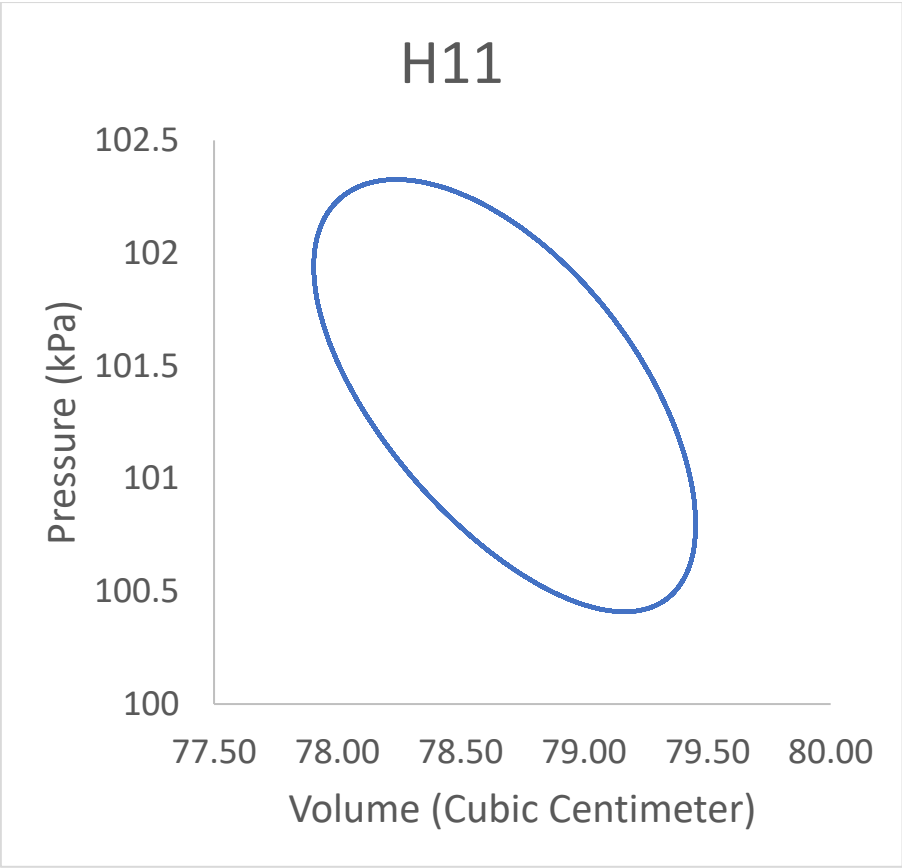
# H10



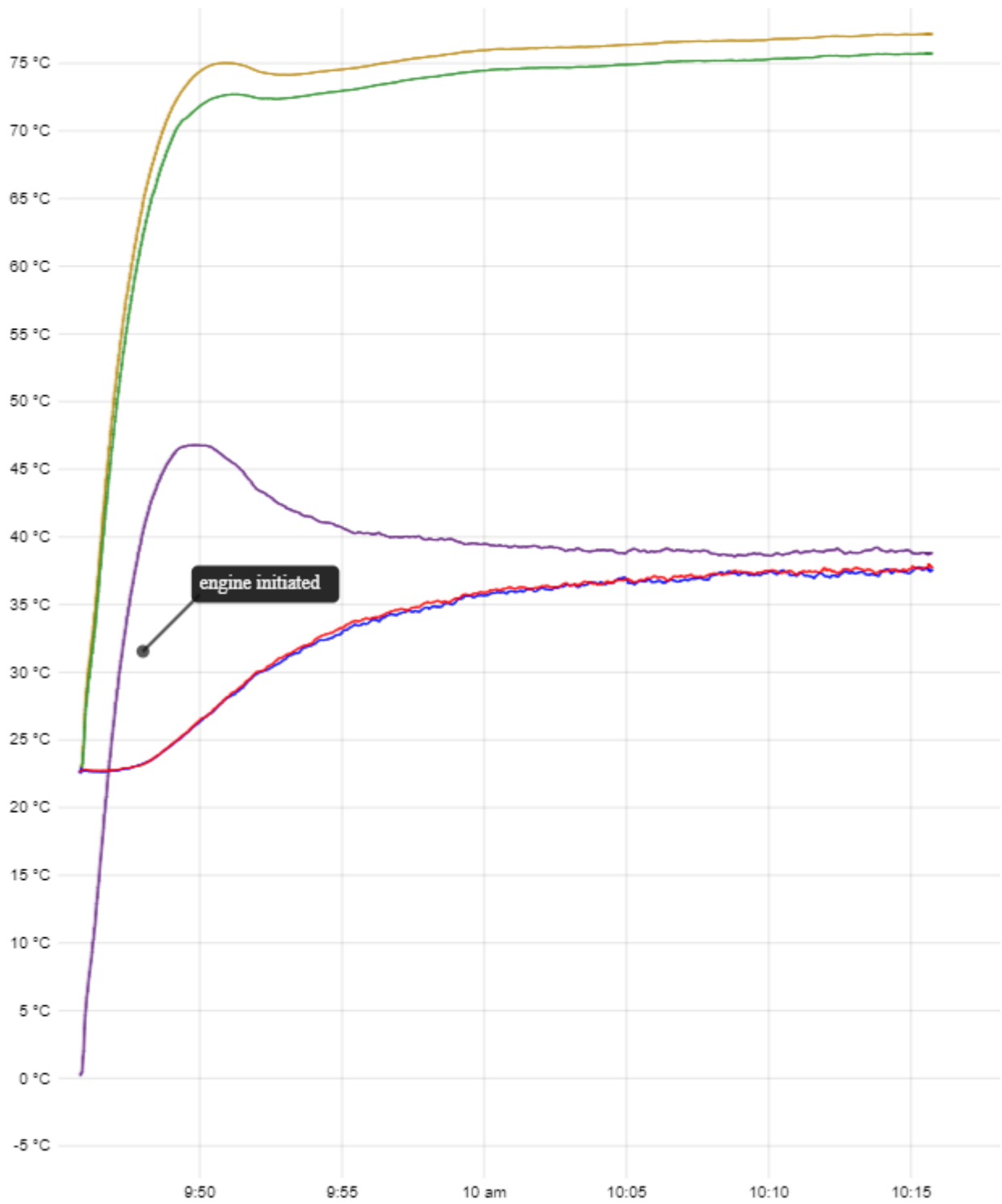


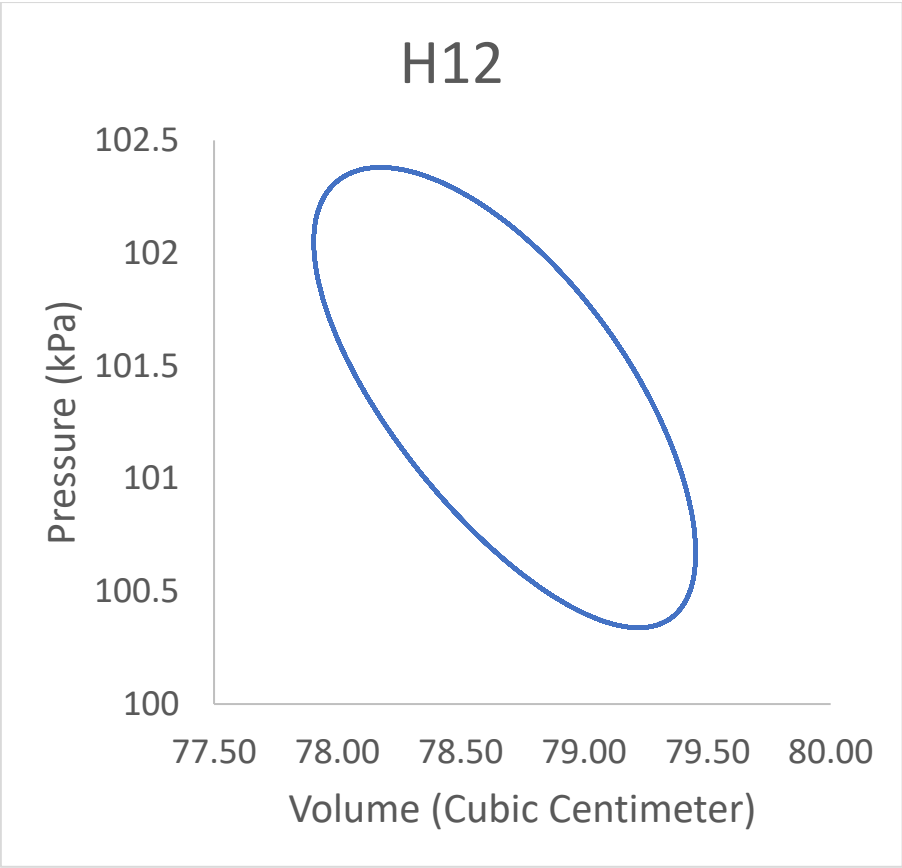
# H11



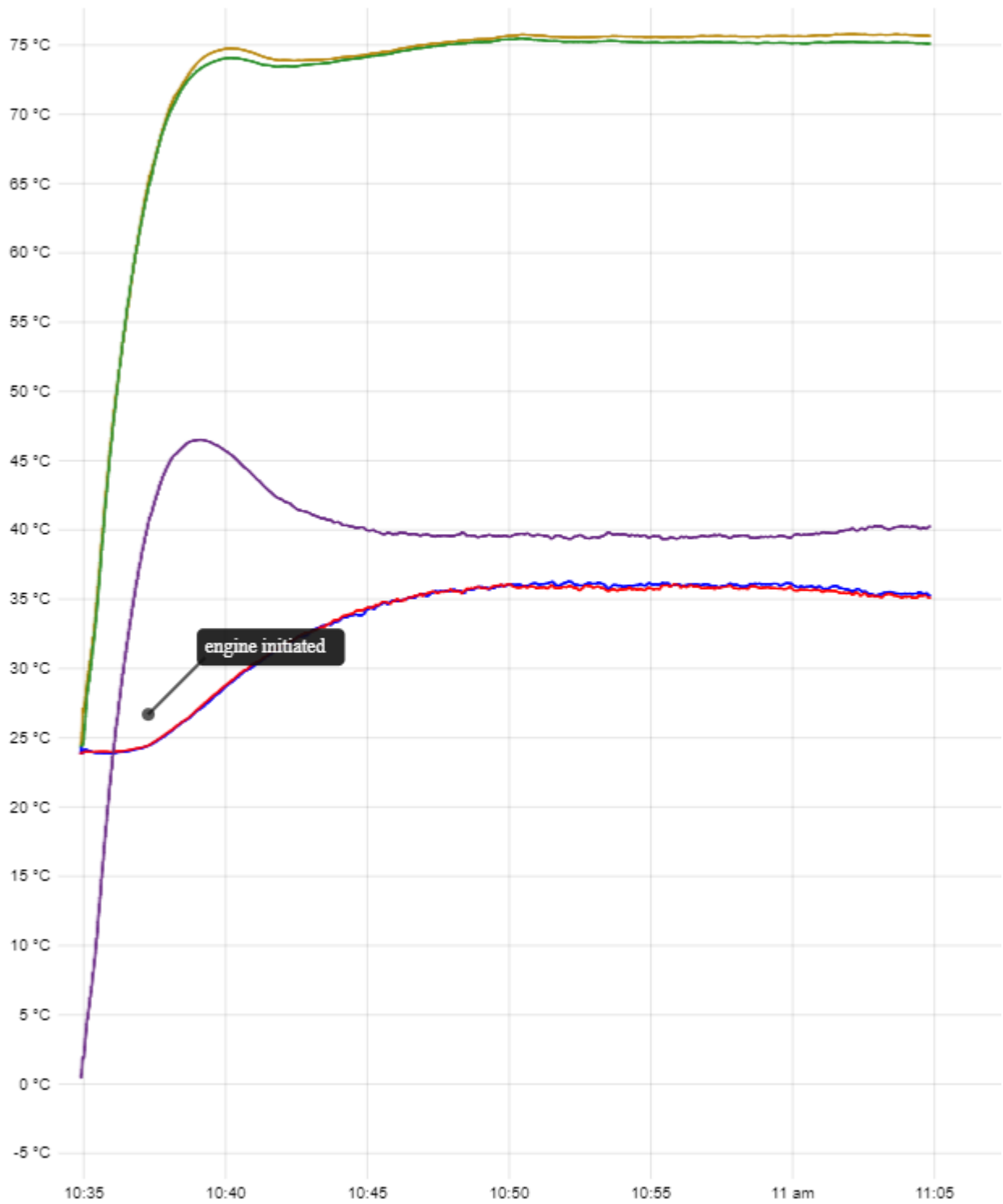


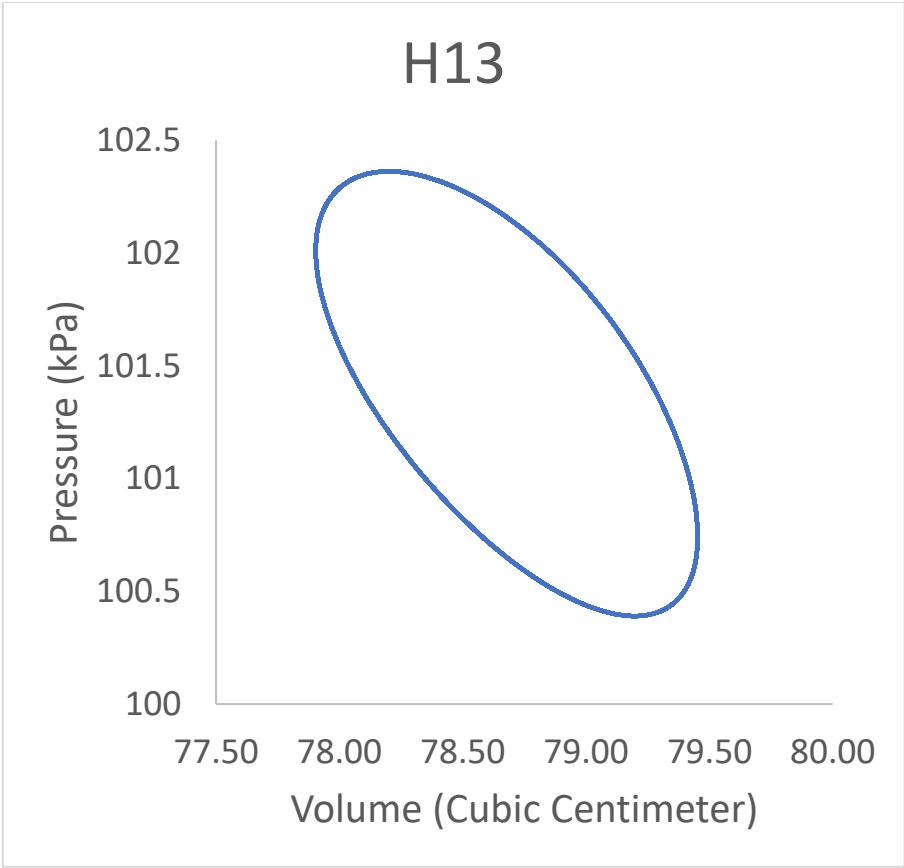
# H12



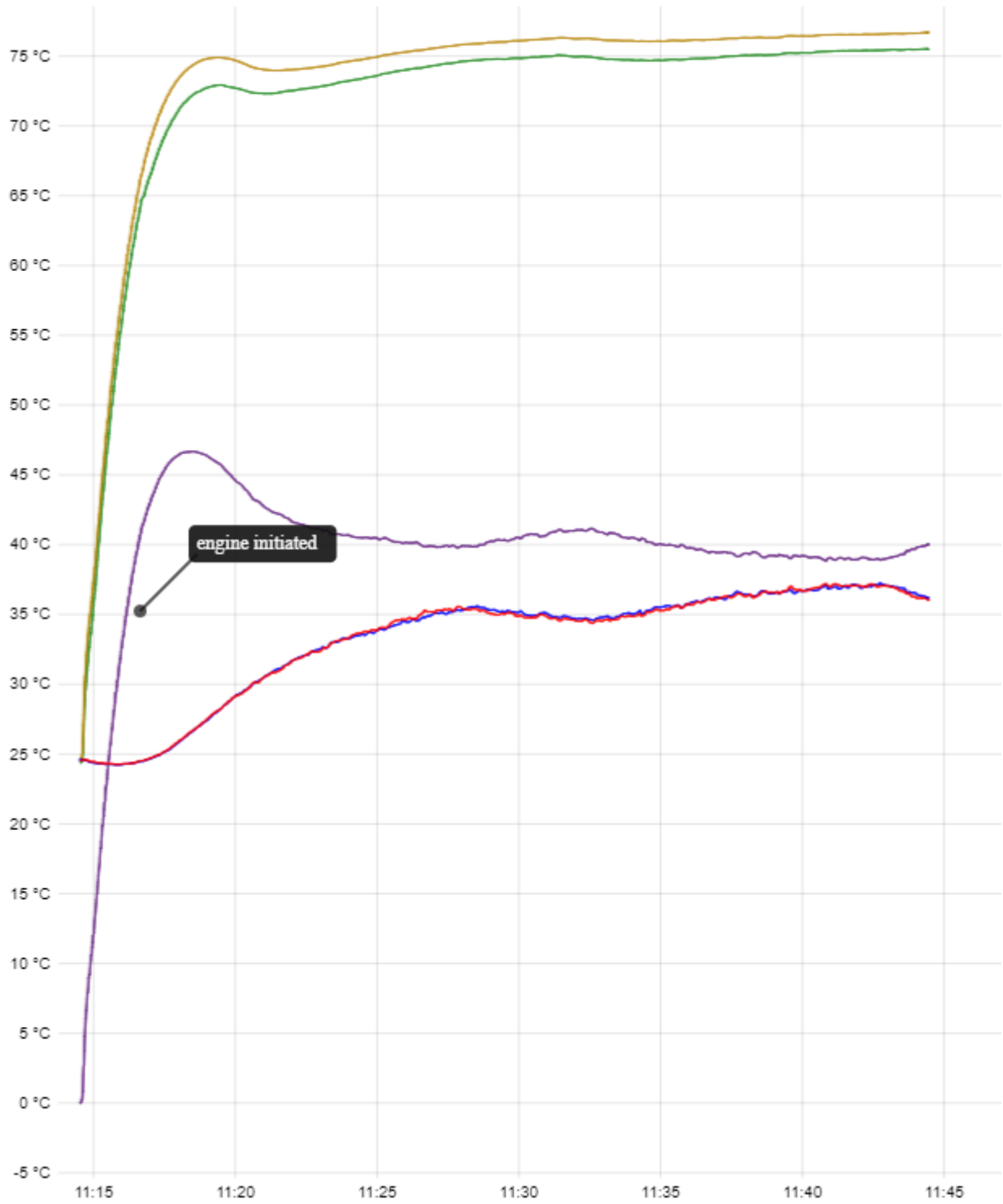


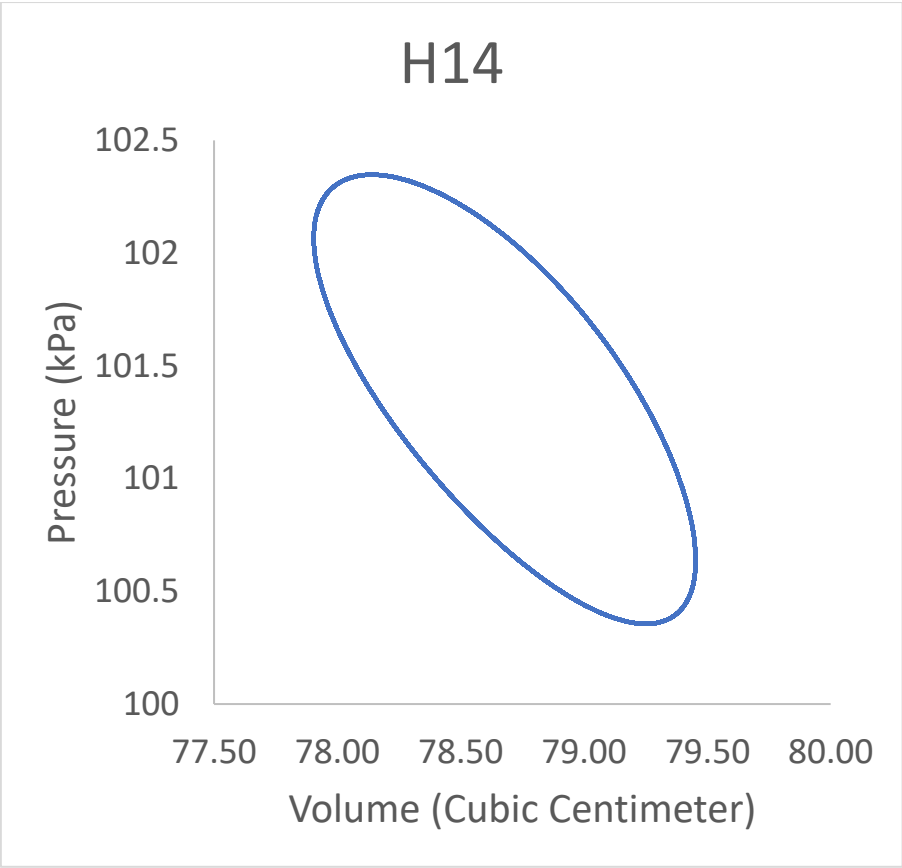
### H13





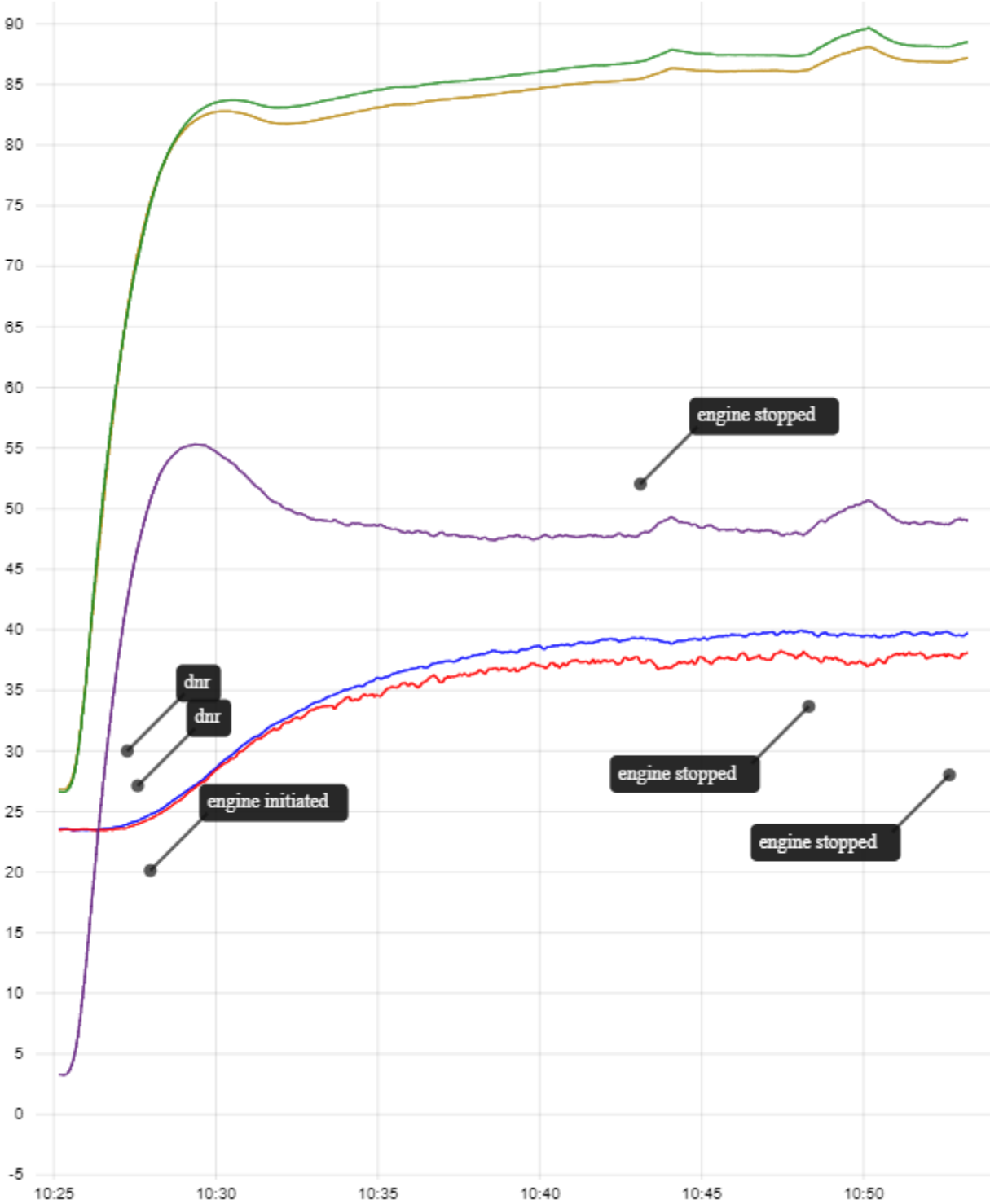
# H14



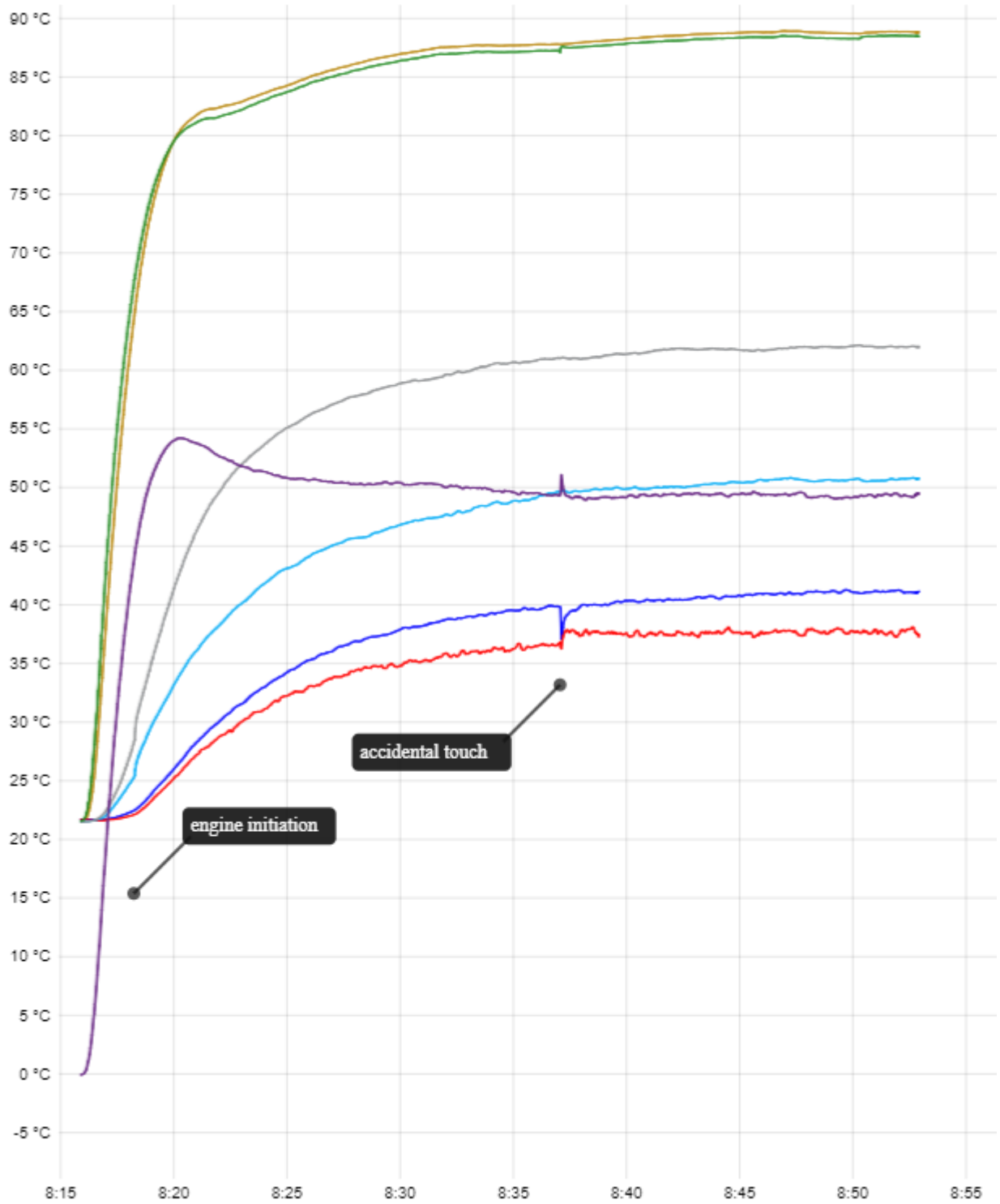


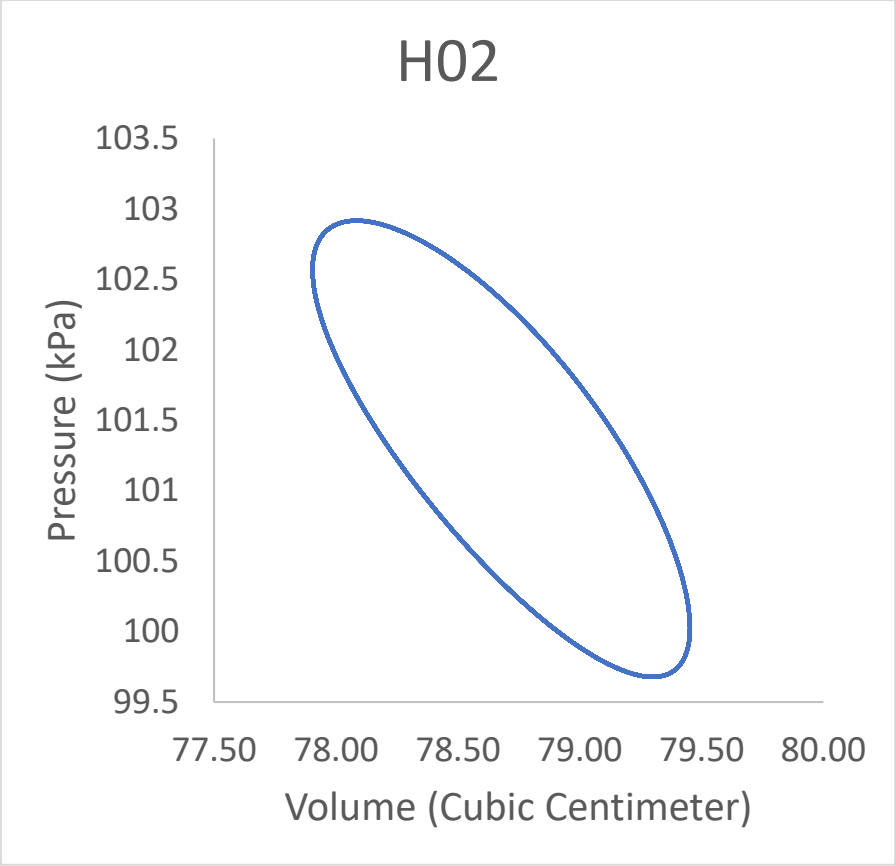
8.3.3. Probed EMSE

HO1

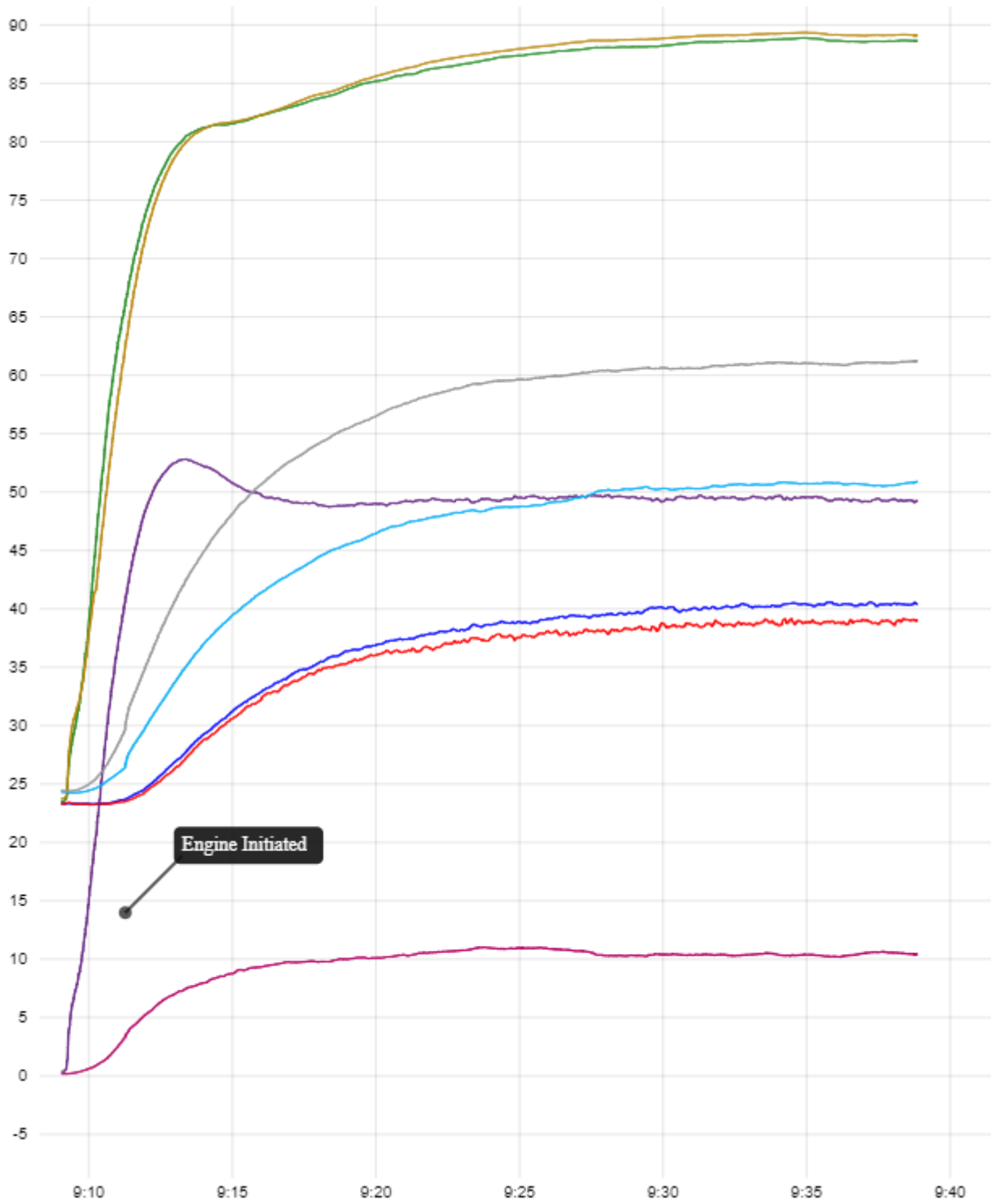


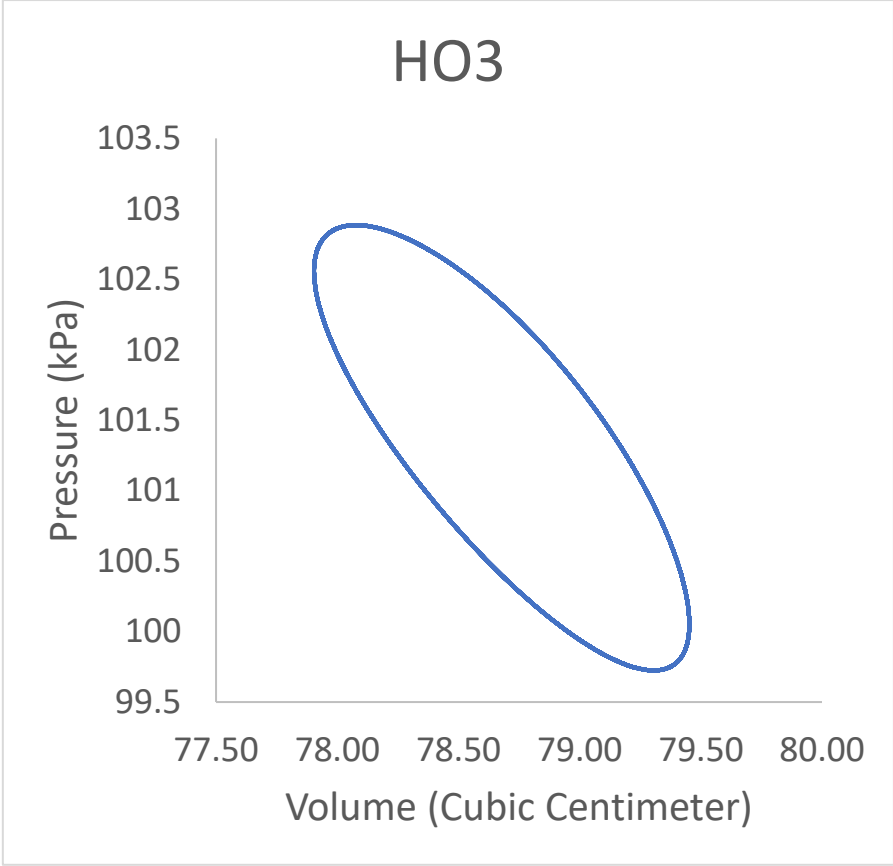
HO2



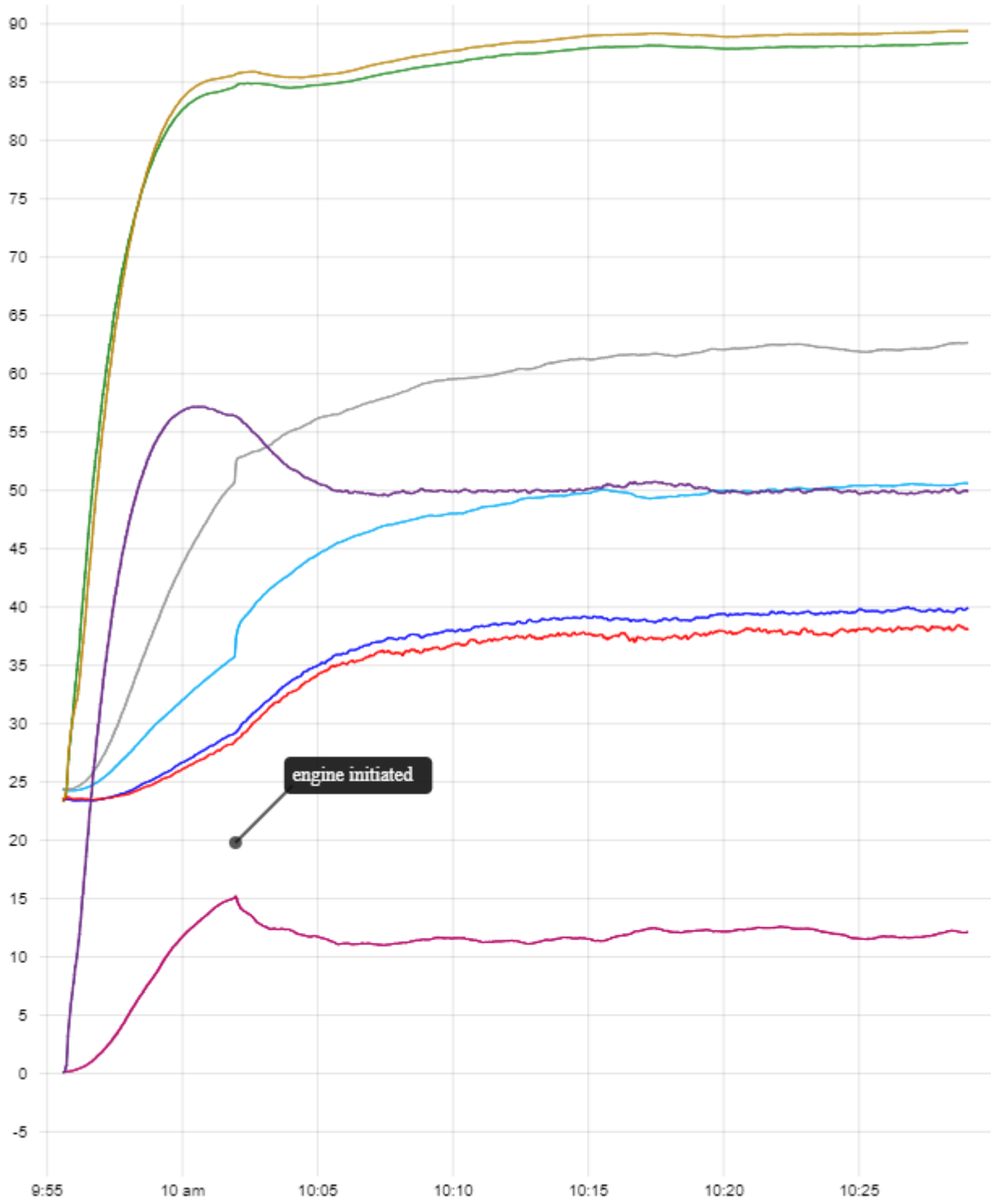


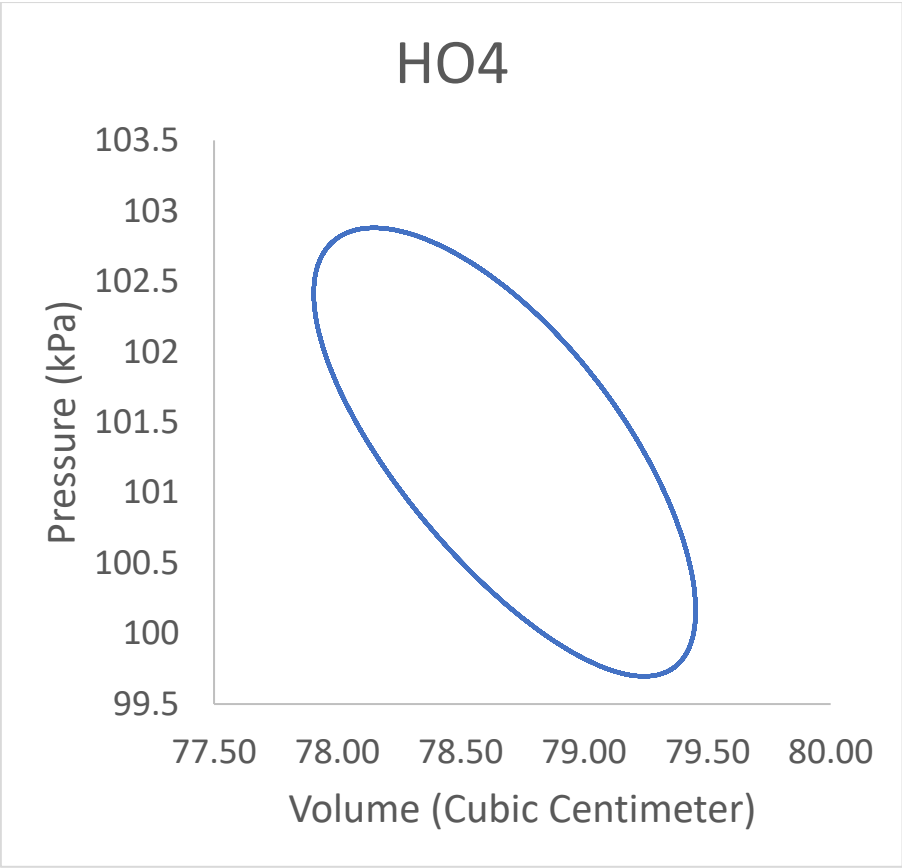
### H03



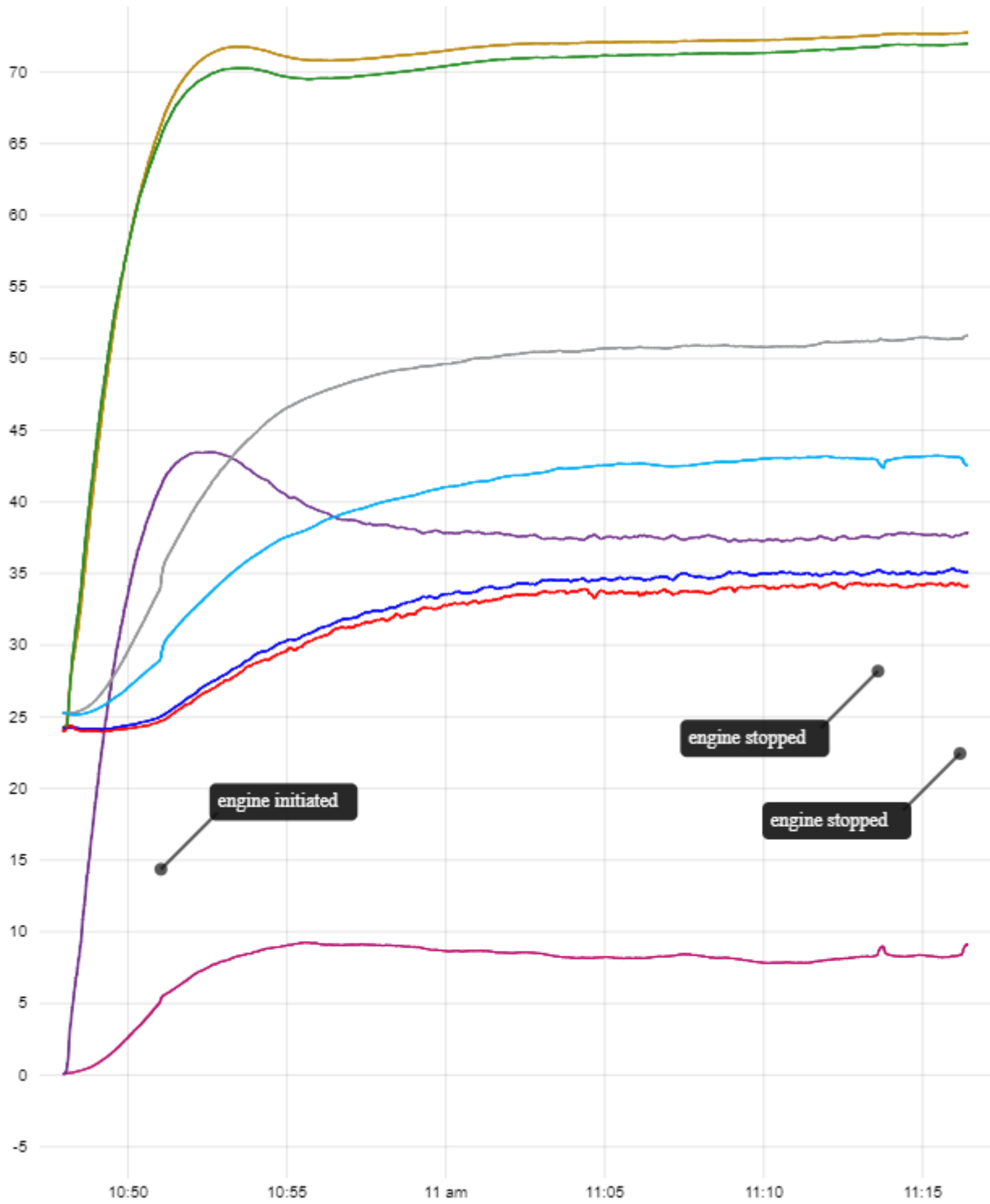


# HO4

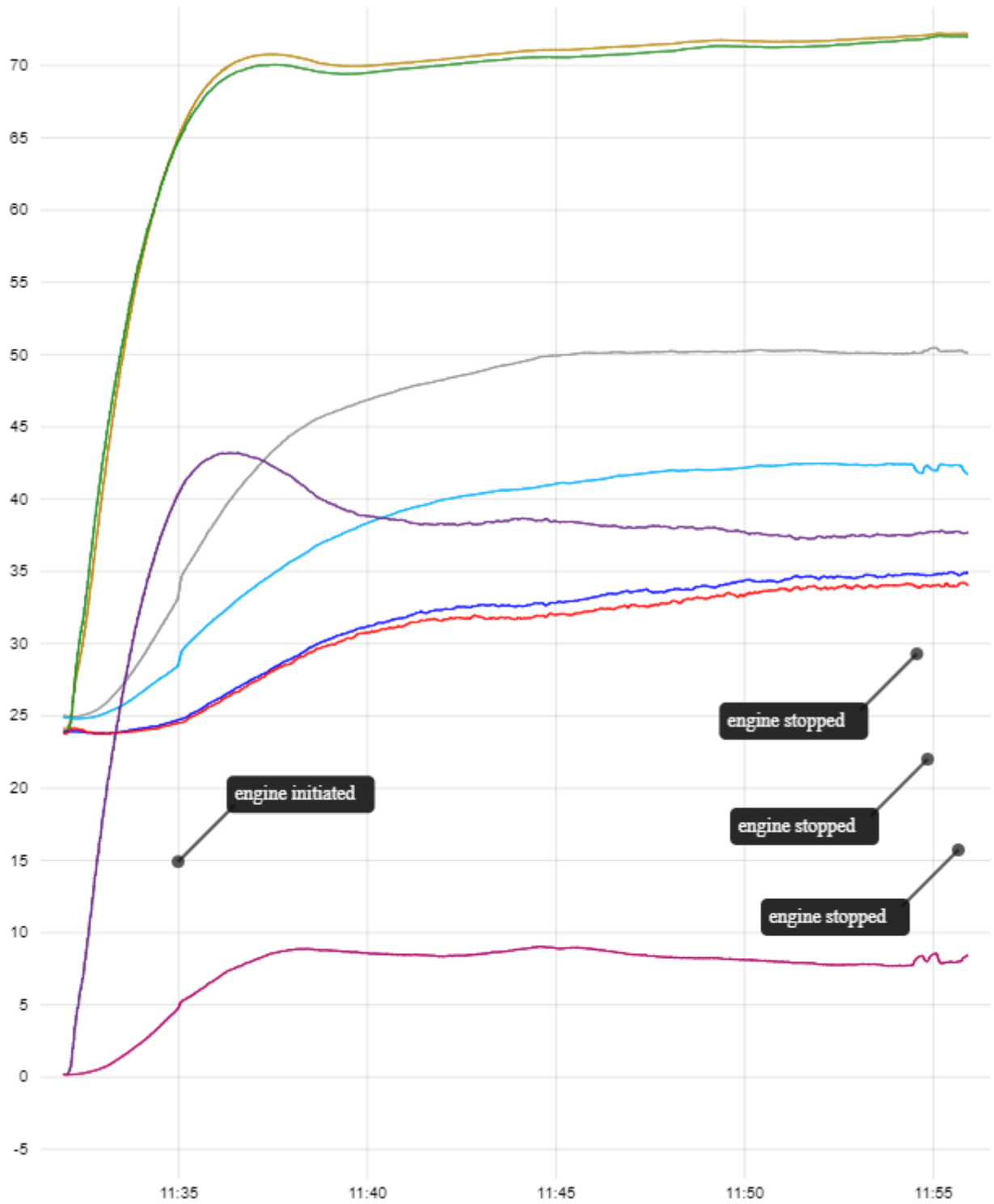




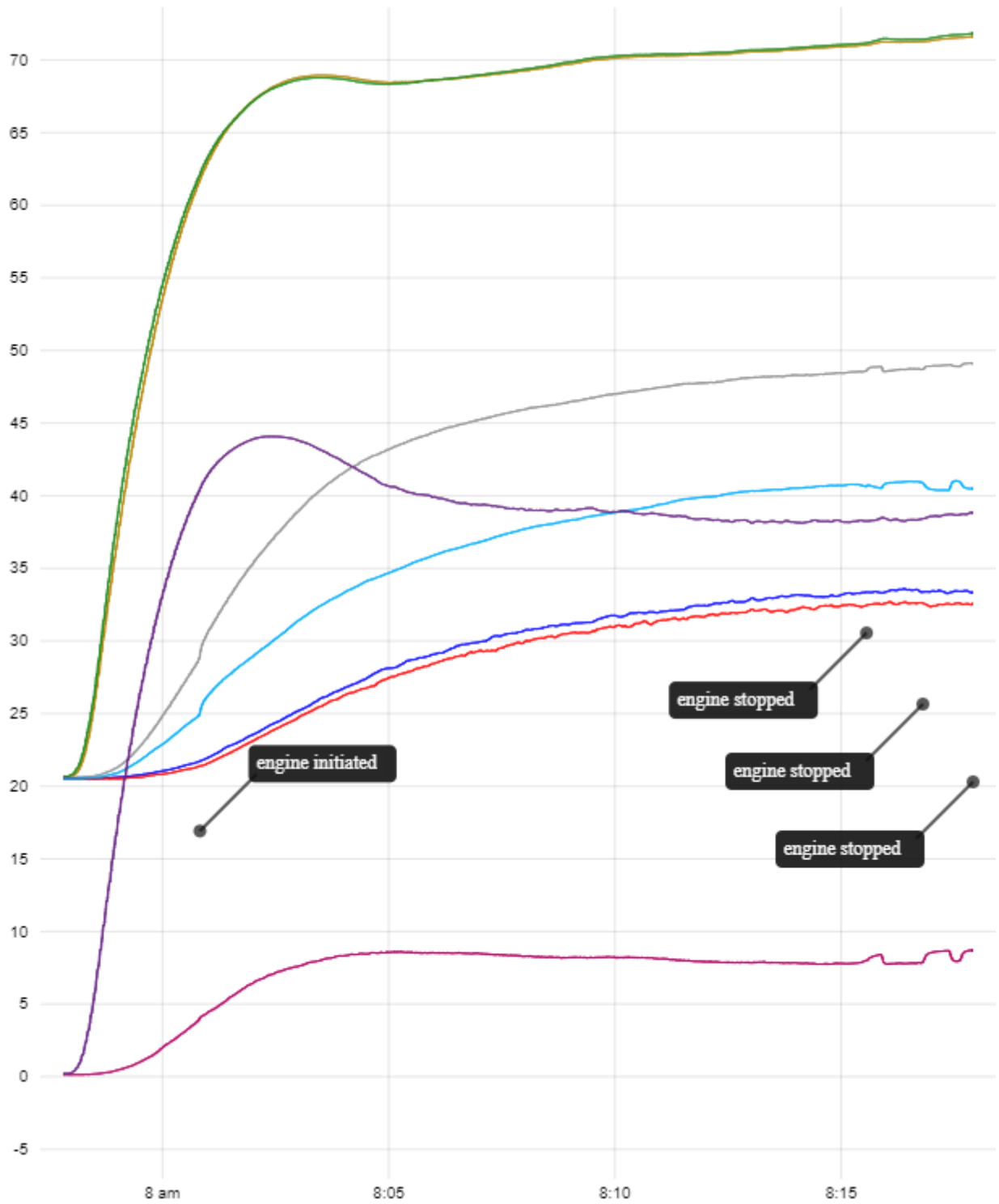
# H05



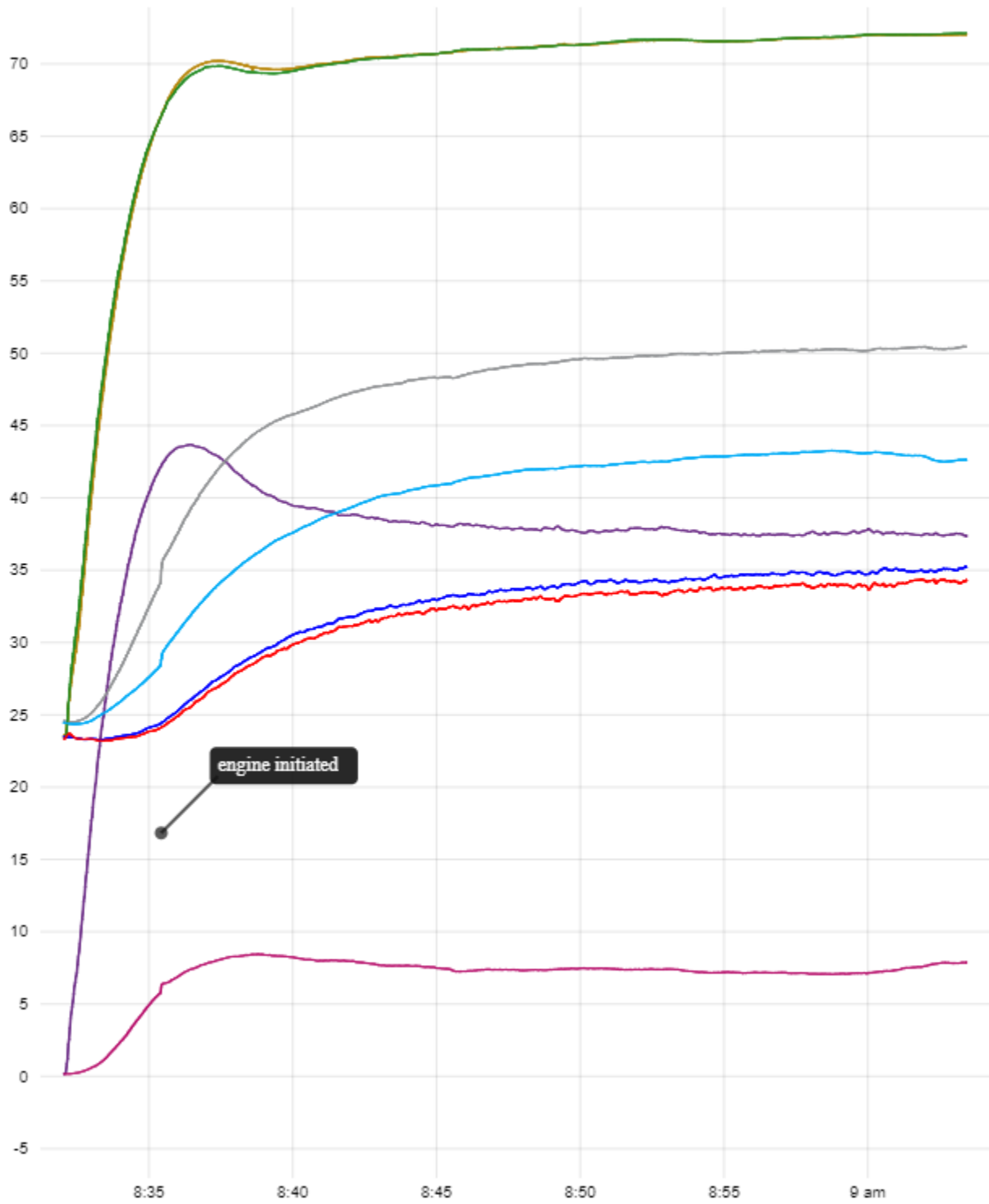
# H06

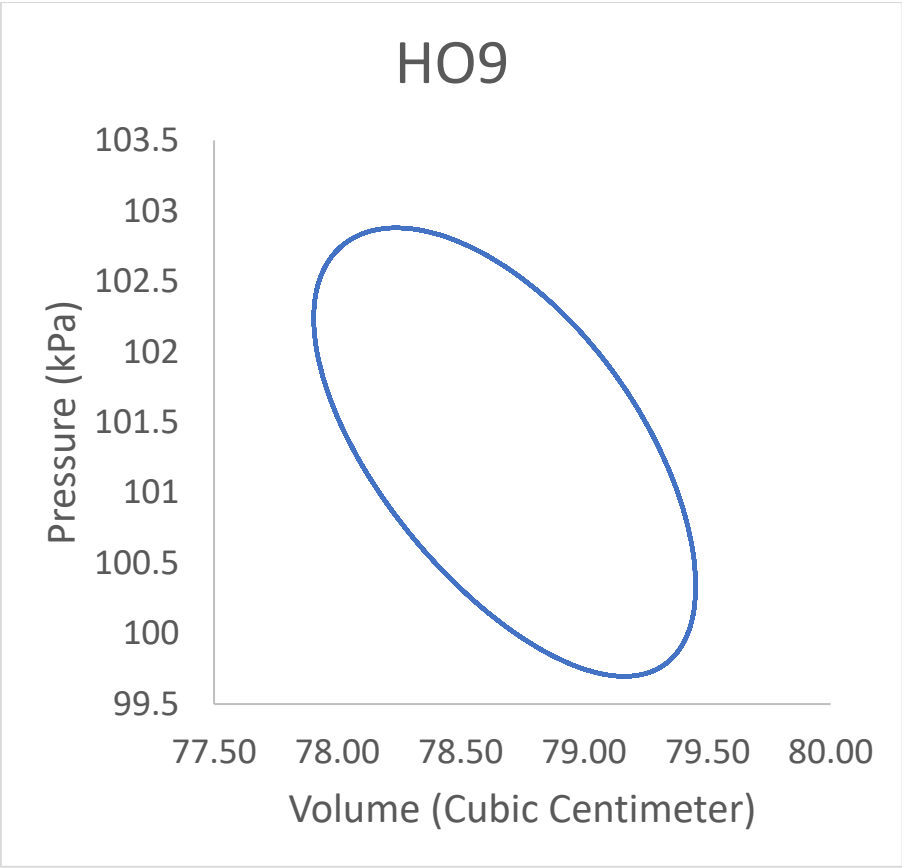


H08

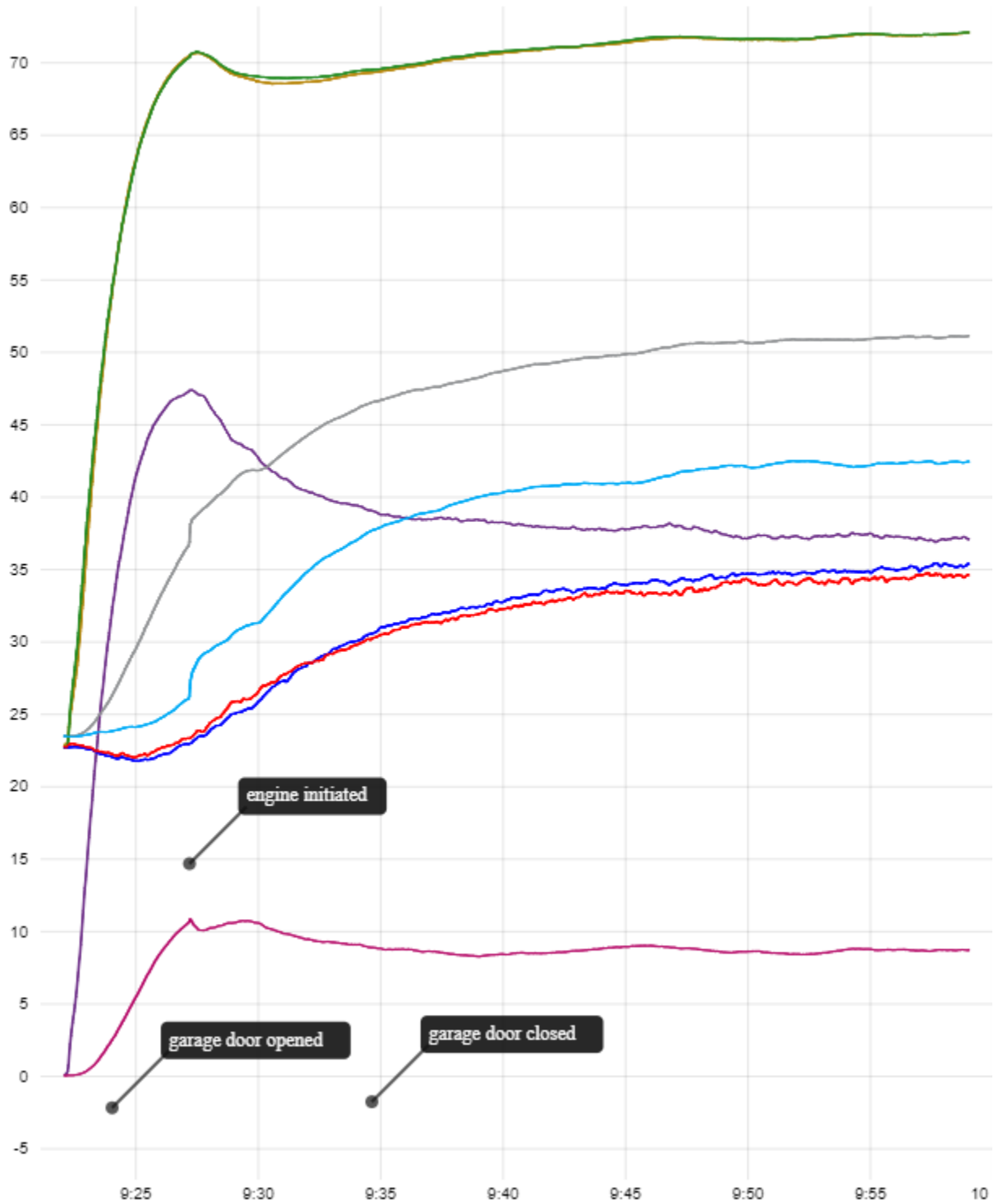


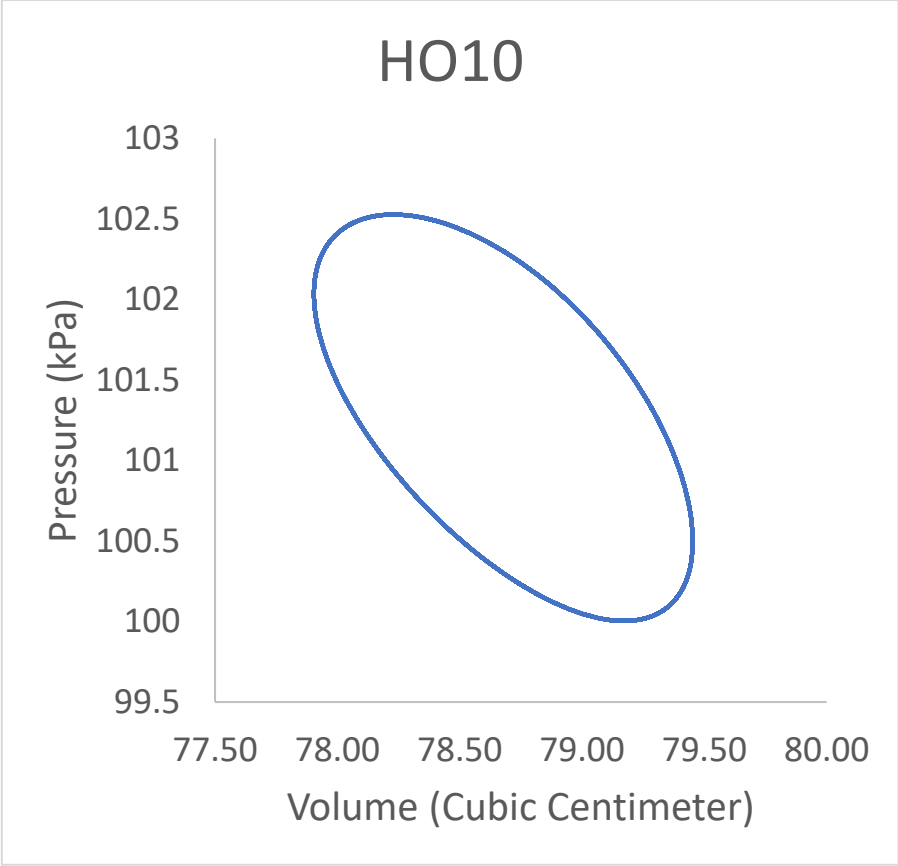
H09



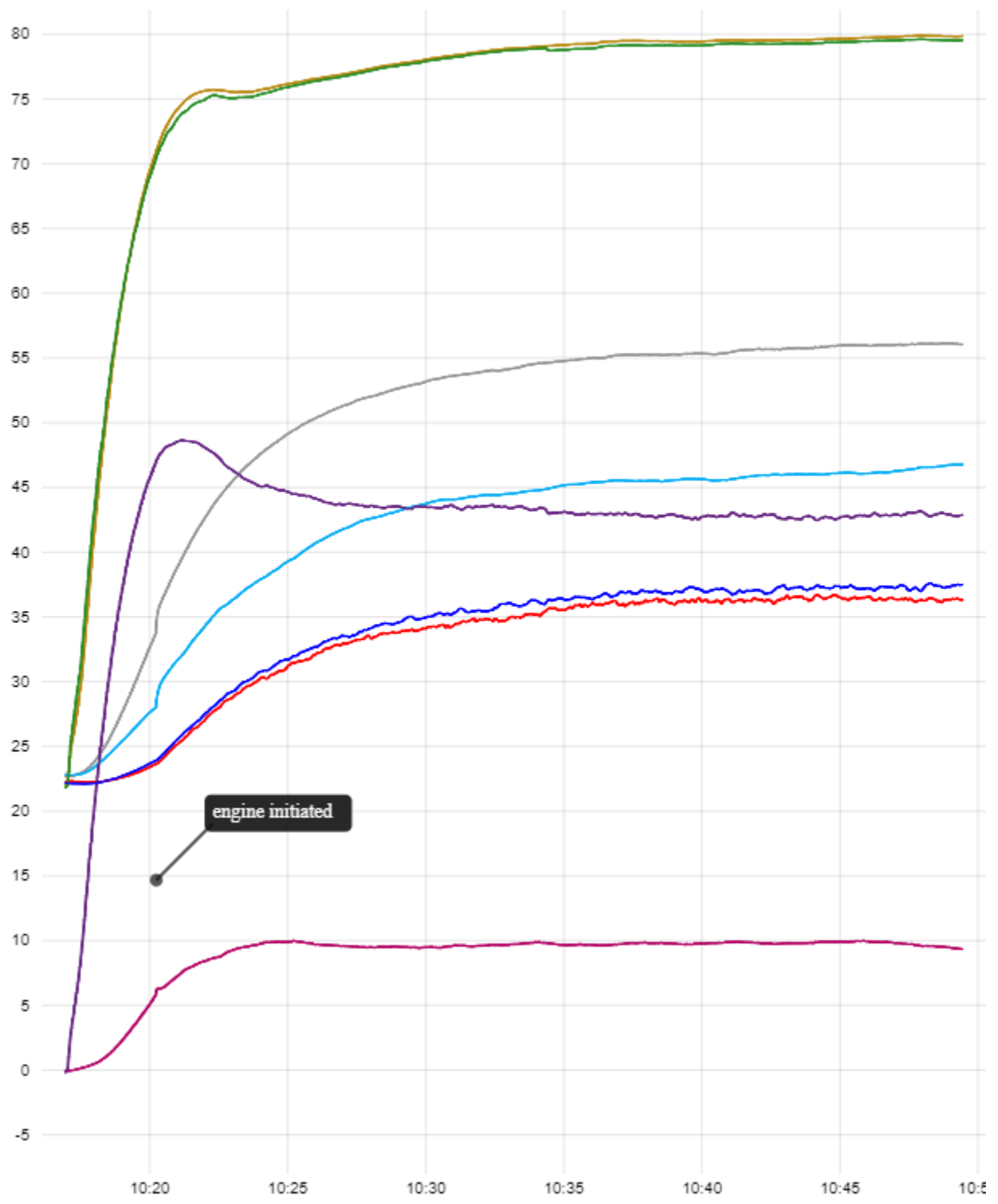


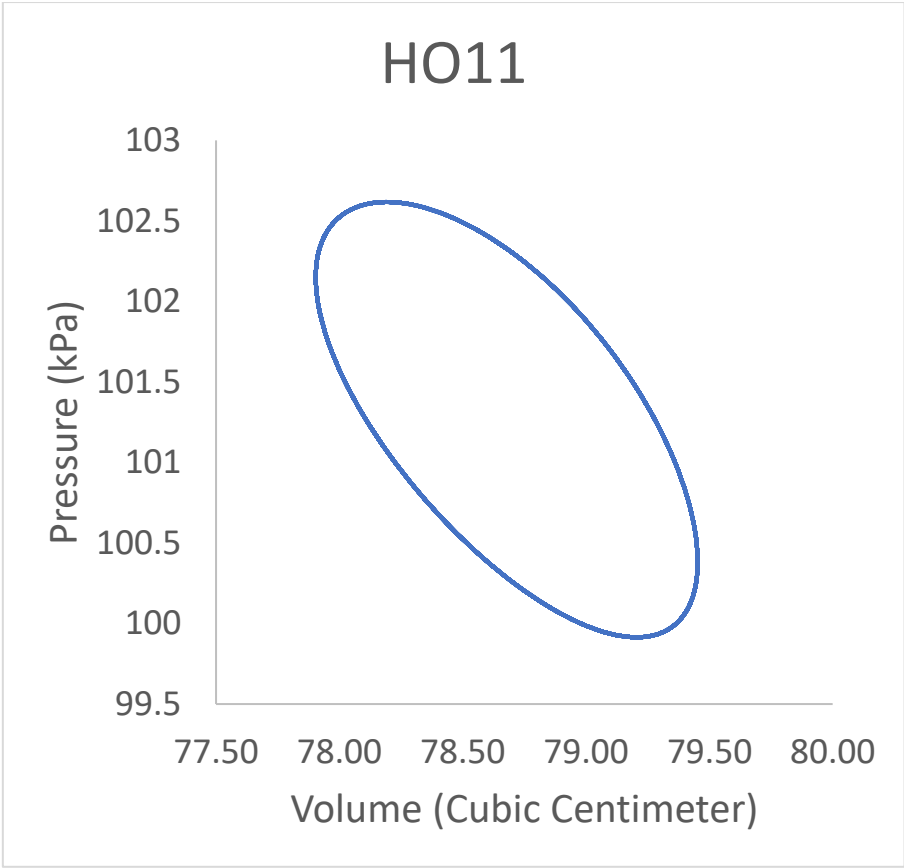
# HO10



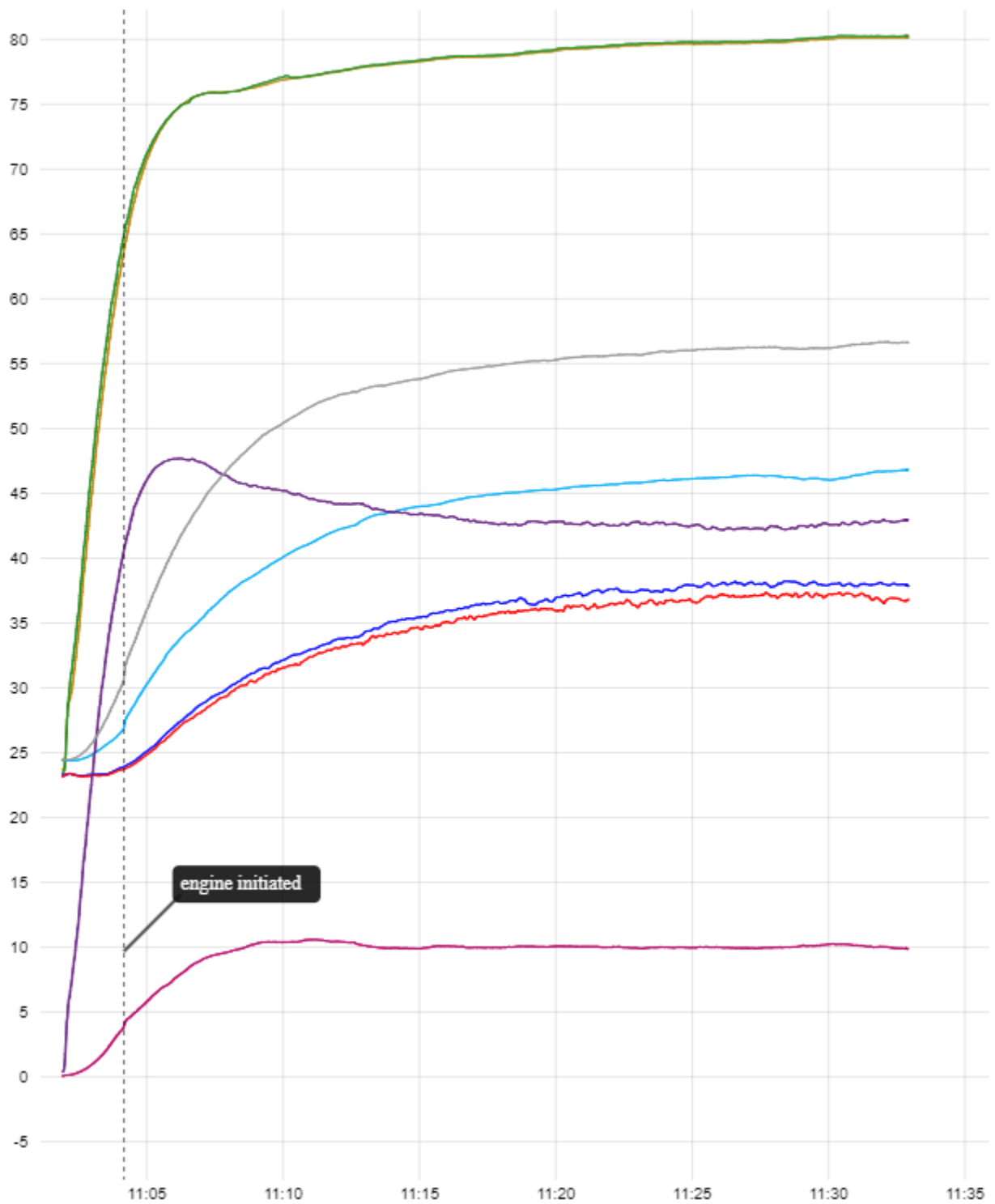


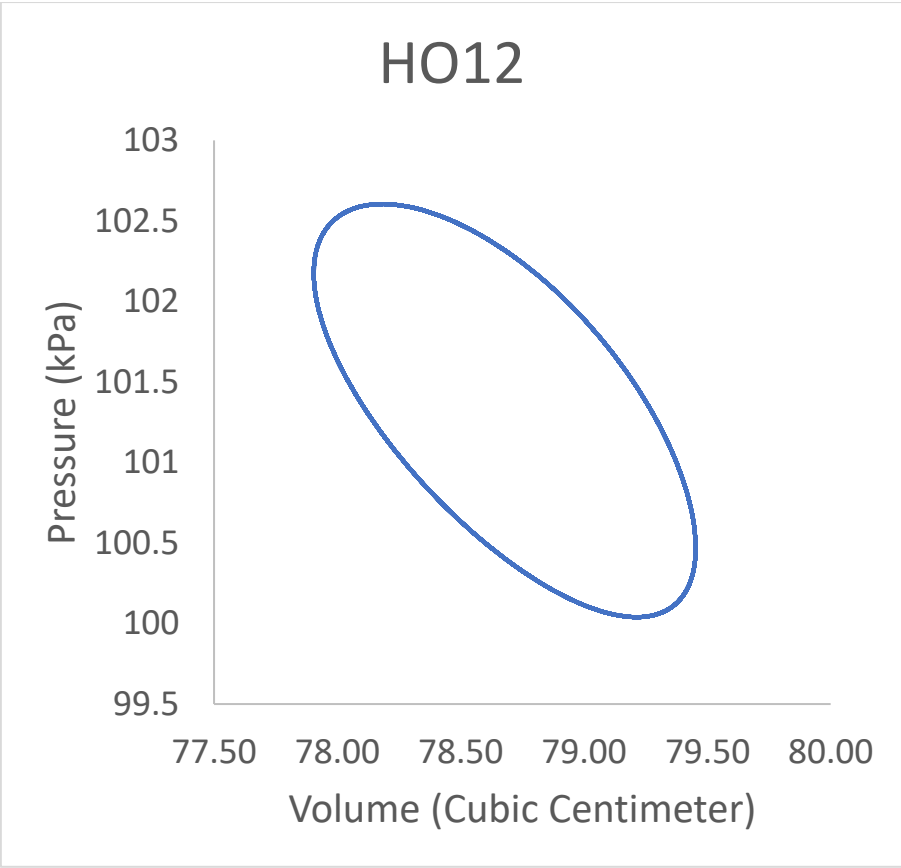
# HO11



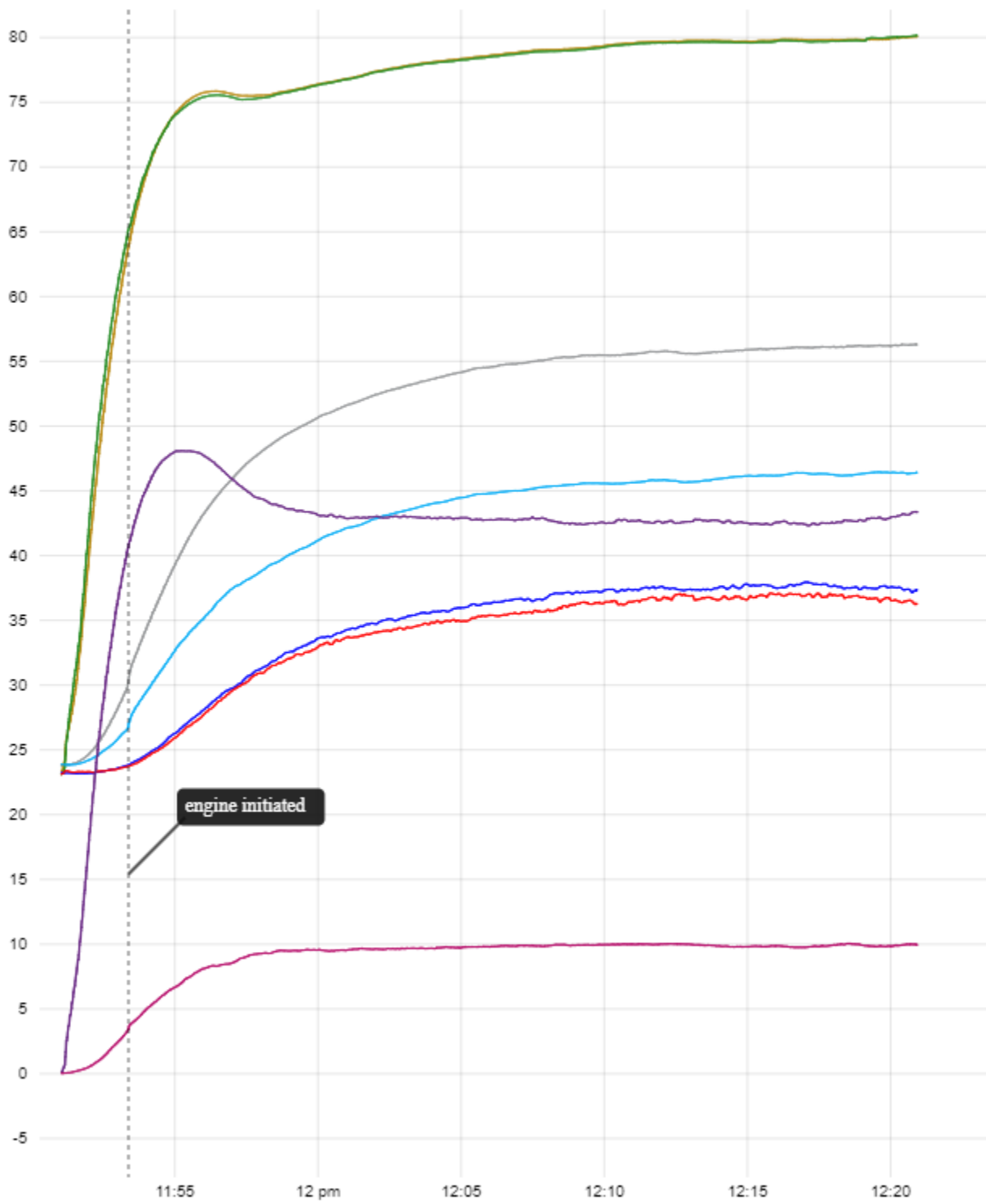


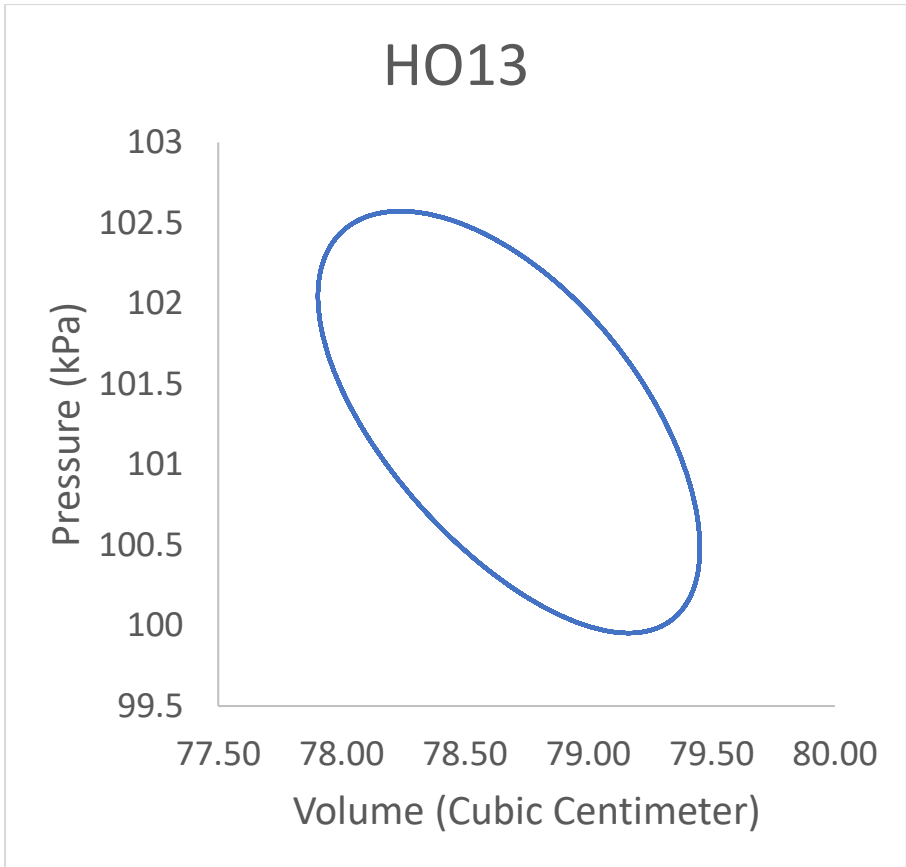
# HO12



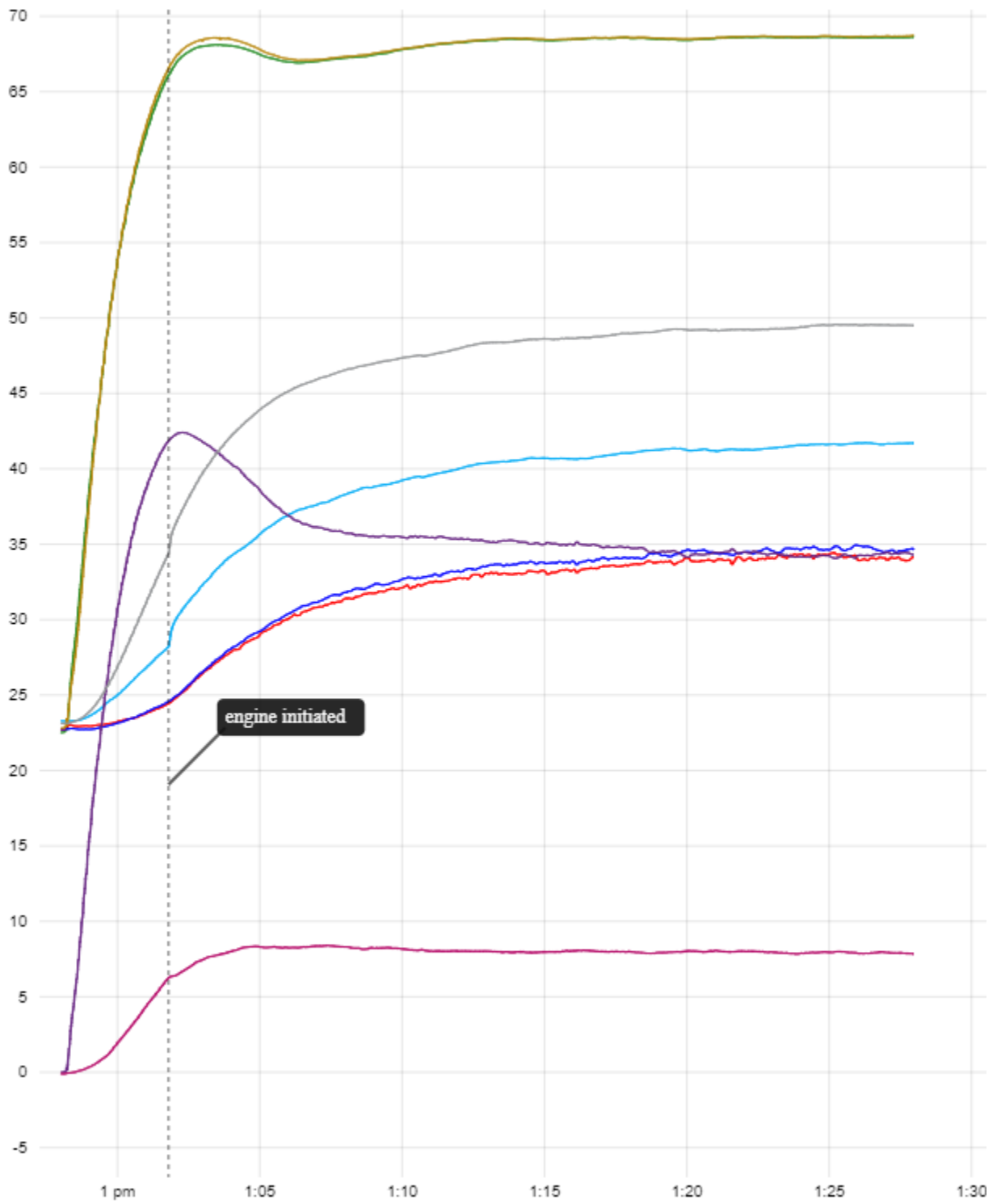


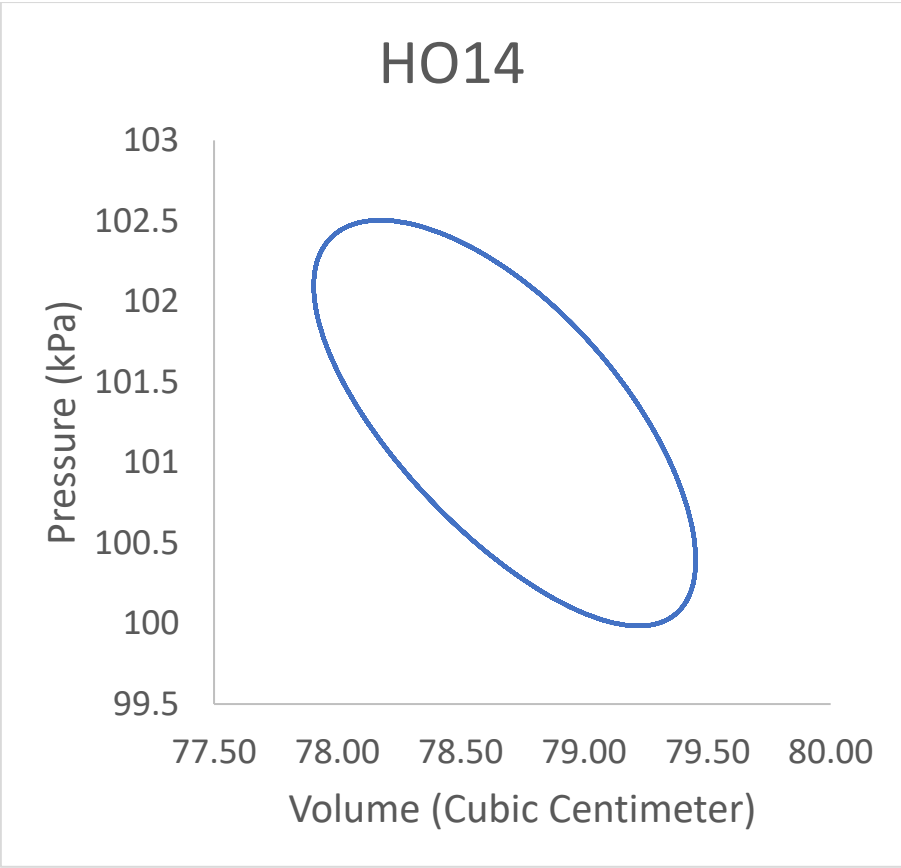
# HO13



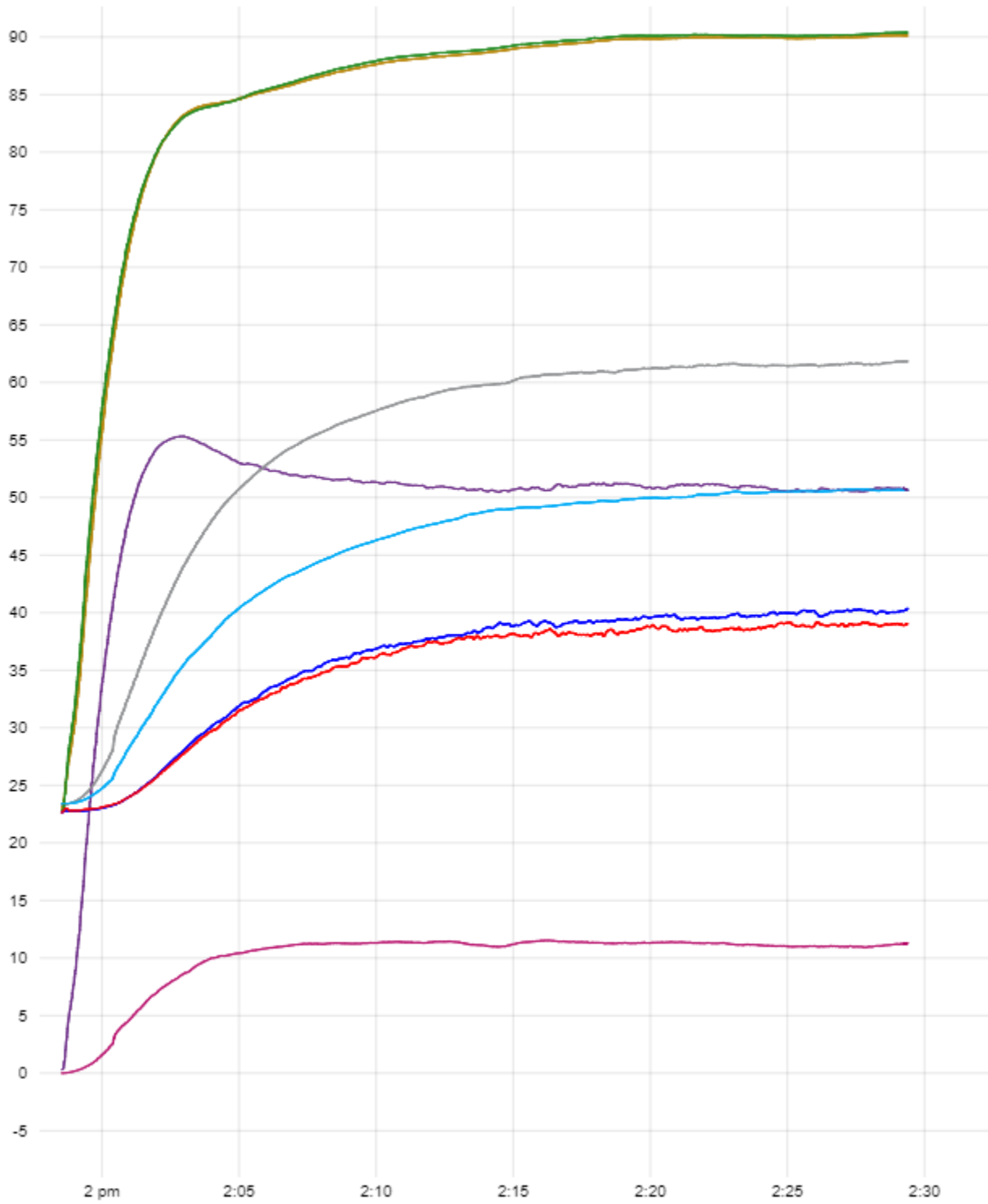


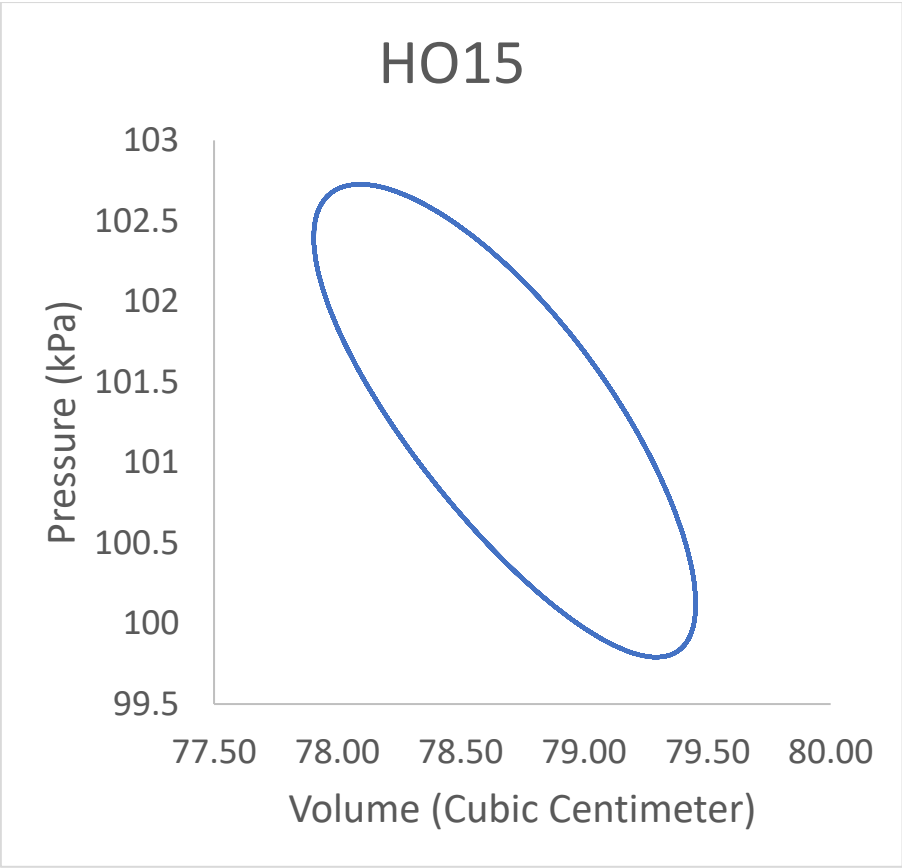
# HO14





# HO15





## INSPECTED EMSE

Exp (E)	$\Delta T$	TH (°C)	TC (°C)	$\omega$	Work (mJ)
6	34	343.5	309.5	118.1	11.72185
5	37.5	349.5	312	137.9	11.58467
4	39	350	311	101.8	11.87991
19	40	347.75	307.75	99.6	11.76394
20	40	348	308	90.1	11.87103
21	40.1	347.3	307.2	122.8	11.87459
17	40.25	348	307.75	101.9	11.45405
18	40.25	348.25	308	92.2	11.50818
24	41.5	352	310.5	123.6	11.5426
25	41.8	352.3	310.5	126.3	12.34349
26	41.9	352.5	310.6	126.95	11.83252
23	42.25	352	309.75	112.4	11.5029
22	43.35	352.8	309.45	128.1	11.64612
13	47	357	310	130	12.0812
14	47	357	310	120.4	11.70662
16	47	357	310	129	12.10952
12	47.5	357	309.5	121.1	12.11226
15	47.8	356.8	309	124	11.88103
7	48	362	314	142.8	11.97048
8	51	363	312	149	11.54822
9	52	362	310	141.5	11.82114
10	52.25	363	310.75	157.8	11.99013
11	52.25	363	310.75	146.8	11.62238

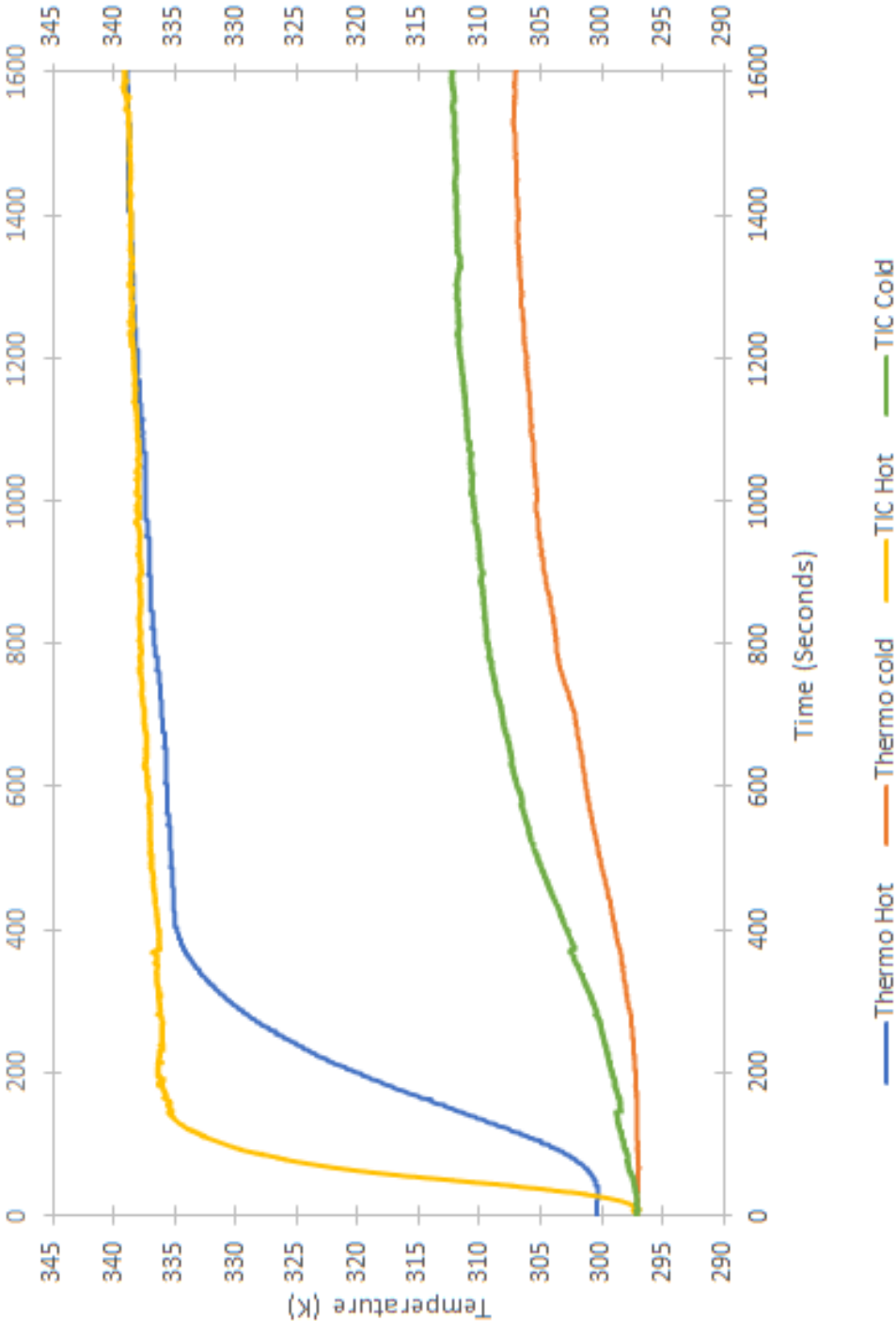
### Drilled EMSE

Exp (H)	$\Delta T$	TH (°C)	TC (°C)	$\omega$	Work (mJ)	
5	42.2	353.6	311.4	128.3	15.41935	
6	42.82	352.6	309.78	116.1	15.52544	
7	40.95	351.9	310.95	122	15.66458	
8	48.5	362.9	314.4	141.1	15.65936	
9	48.75	362.1	313.35	157.7	15.09528	
10	48.75	362	313.25	157.6	15.09528	
11	43.3	354.8	311.5	138.1	15.70951	
12	38.9	349	310.1	106.1	15.66846	
13	39.5	348.3	308.8	116.1	15.67714	
14	39.1	348.76	309.66	111.6	15.51782	

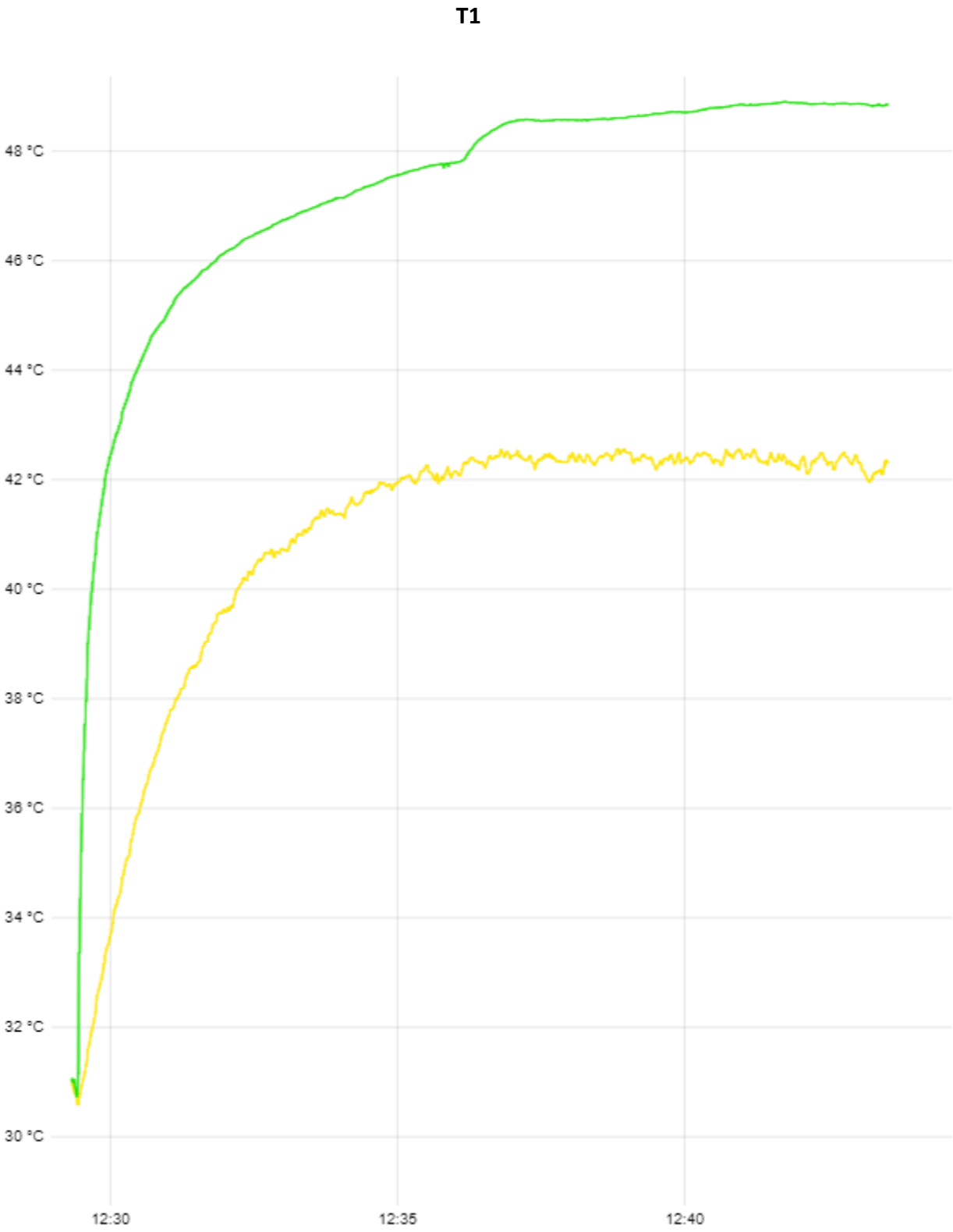
### Probed EMSE

Exp (HO)	$\Delta T$	TH (°C)	TC (°C)	(i)TH (°C)	(i)TC (°C)	DT (i)	$\omega$	Work (mJ)
2	49.2	361.1	311.9	62.9	50.5	12.4	62.7	16.30920052
3	49.56	361.96	312.4	60.97	50.5	10.47	72.8	11.28573045
4	49.79	361.33	311.54	62.4	50.65	11.75	69.8	16.61558705
9	37.42	344.7	307.28	50.5	42.9	7.6	69.9	16.9998852
10	37.69	344.65	306.96	51.05	42.5	8.55	66.15	16.29128502
11	42.75	352.35	309.6	56.03	46.2	9.83	70.9	16.34706898
12	42.3	352.7	310.4	56.16	46.16	10	75.2	16.189633
13	42.62	352.75	310.13	55.87	46.3	9.57	73	16.4174486
14	34.31	341.58	307.27	49.56	41.77	7.79	62.1	16.10430233
15	51	363	312	61.5	50.5	11	78.45	16.10508363

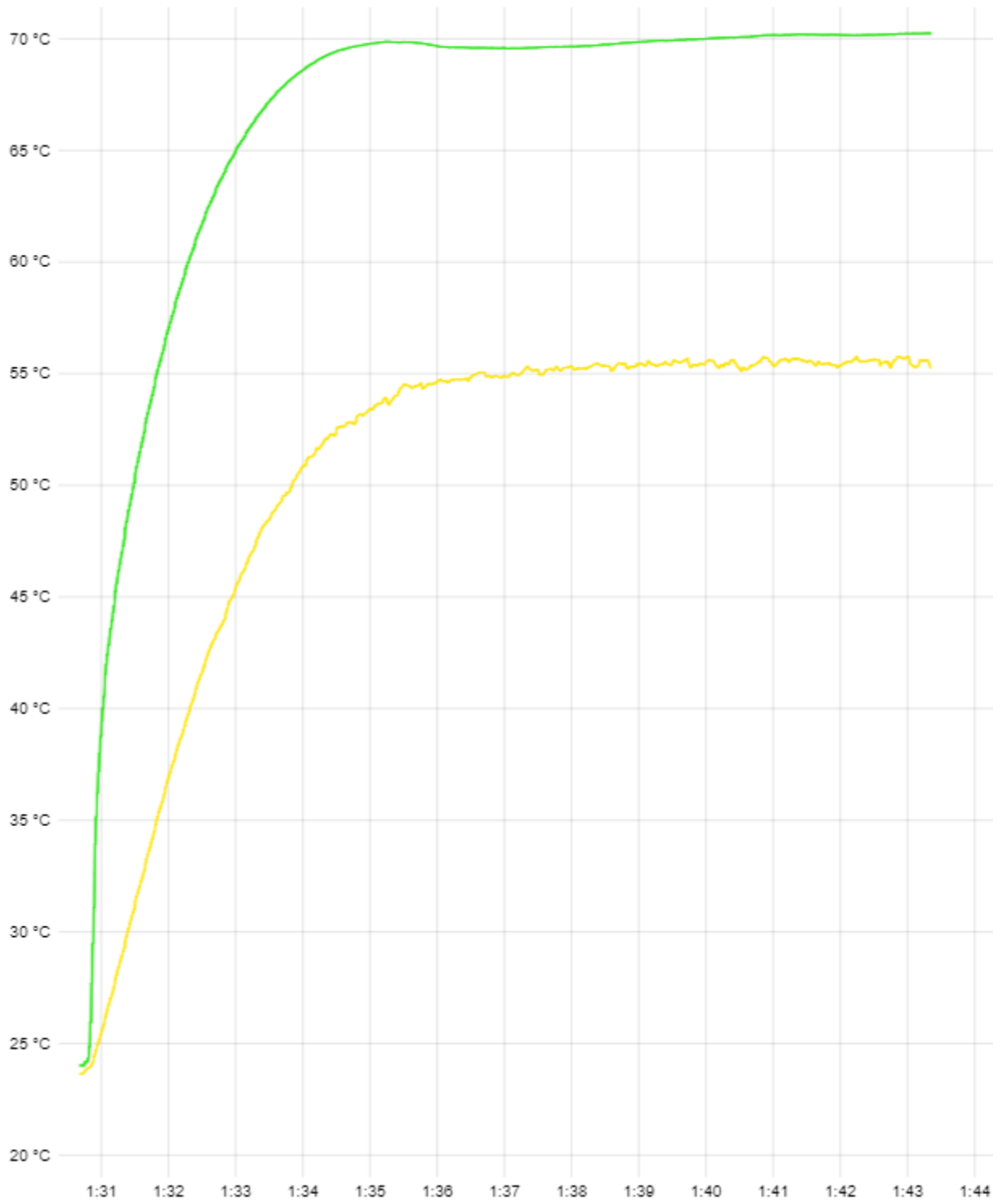
8.3.4. Thermal Imaging Camera Recording



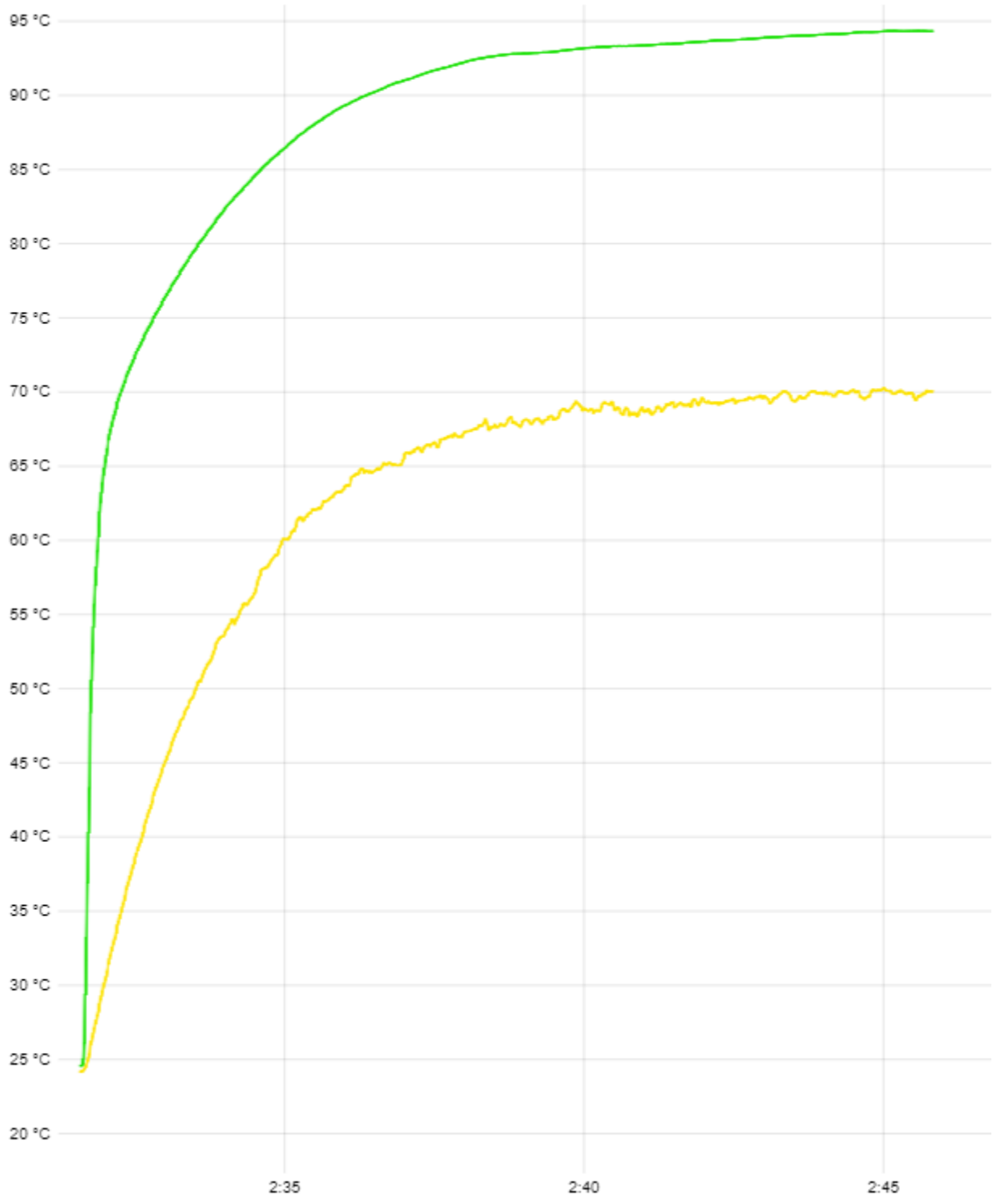
8.3.5. Temperature across plate



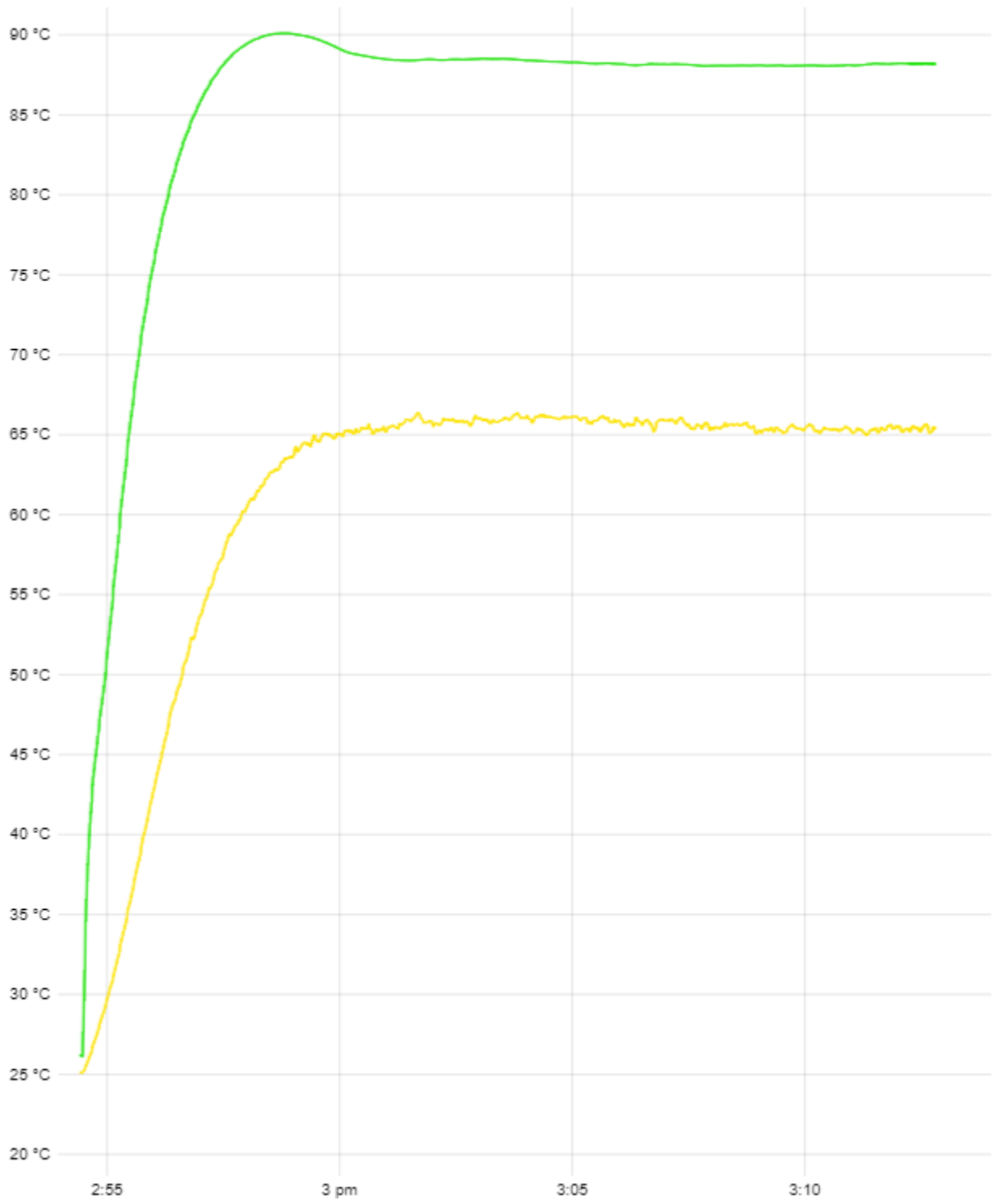
**T2**



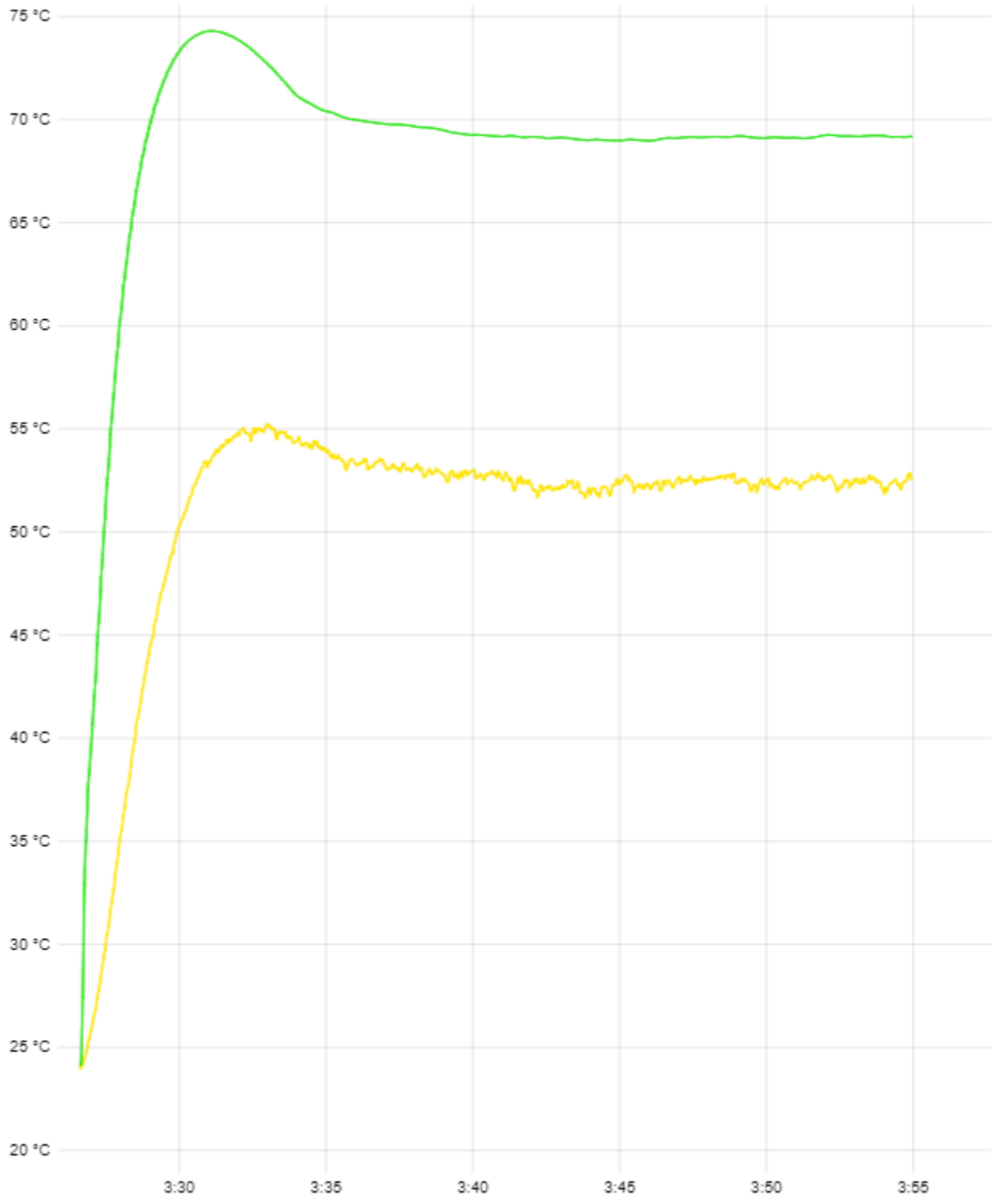
T3



T4



T5



## 8.4. Appendix 4 – CFD Simulations

### 3D CFD Results of E6 Experimental Scenario

Time	Theta	Temp [C]	Temp [R]	Temp [E]	Temp [P]	Vol [C]	Vol [R]	Vol [E]	Vol [P]	T Vol	
8.00169	8.00169	313.401	329.449	342.124	307.655	3.06E-05	7.38E-06	3.93E-05	5.46E-07	7.79E-05	77.90
8.01581	8.01581	314.072	332.231	342.508	307.624	3.51E-05	7.38E-06	3.49E-05	5.58E-07	7.79E-05	77.92
8.02992	8.02992	314.306	334.263	342.429	307.175	3.95E-05	7.38E-06	3.05E-05	5.96E-07	7.80E-05	77.95
8.04403	8.04403	313.871	335.093	341.843	306.028	4.37E-05	7.38E-06	2.63E-05	6.58E-07	7.80E-05	78.02
8.05814	8.05814	314.432	336.714	342.149	305.951	4.75E-05	7.38E-06	2.25E-05	7.41E-07	7.81E-05	78.10
8.07226	8.07226	314.821	337.921	342.344	305.852	5.08E-05	7.38E-06	1.92E-05	8.43E-07	7.82E-05	78.20
8.08637	8.08637	315.042	338.81	342.482	305.742	5.36E-05	7.38E-06	1.64E-05	9.59E-07	7.83E-05	78.32
8.10048	8.10048	315.093	339.395	342.506	305.583	5.56E-05	7.38E-06	1.44E-05	1.09E-06	7.84E-05	78.44
8.11459	8.11459	314.959	339.666	342.617	305.46	5.68E-05	7.38E-06	1.31E-05	1.22E-06	7.86E-05	78.58
8.1287	8.1287	314.665	339.561	342.641	305.335	5.73E-05	7.38E-06	1.27E-05	1.36E-06	7.87E-05	78.71
8.14282	8.14282	314.23	338.91	342.647	305.167	5.68E-05	7.38E-06	1.31E-05	1.49E-06	7.88E-05	78.85
8.15693	8.15693	313.692	337.374	342.607	305.047	5.56E-05	7.38E-06	1.44E-05	1.62E-06	7.90E-05	78.97
8.17104	8.17104	313.045	334.713	342.379	304.92	5.36E-05	7.38E-06	1.64E-05	1.73E-06	7.91E-05	79.09
8.18515	8.18515	312.325	331.442	341.969	304.779	5.08E-05	7.38E-06	1.92E-05	1.84E-06	7.92E-05	79.20
8.19927	8.19927	311.509	328.414	341.298	304.592	4.75E-05	7.38E-06	2.25E-05	1.93E-06	7.93E-05	79.29
8.21338	8.21338	310.797	325.863	340.587	304.519	4.37E-05	7.38E-06	2.63E-05	2.00E-06	7.94E-05	79.36
8.22749	8.22749	310.121	323.212	339.808	304.443	3.95E-05	7.38E-06	3.05E-05	2.05E-06	7.94E-05	79.41
8.2416	8.2416	309.469	320.382	338.935	304.448	3.51E-05	7.38E-06	3.49E-05	2.08E-06	7.94E-05	79.44
8.25572	8.25572	309.092	317.775	338.249	304.532	3.06E-05	7.38E-06	3.93E-05	2.09E-06	7.95E-05	79.45
8.26983	8.26983	308.815	315.641	337.522	304.642	2.63E-05	7.38E-06	4.37E-05	2.08E-06	7.94E-05	79.44
8.28394	8.28394	308.574	314.037	336.97	304.775	2.21E-05	7.38E-06	4.79E-05	2.05E-06	7.94E-05	79.41
8.29805	8.29805	308.479	312.884	336.529	304.962	1.82E-05	7.38E-06	5.18E-05	2.00E-06	7.94E-05	79.36
8.31216	8.31216	308.471	312.06	336.215	305.166	1.48E-05	7.38E-06	5.52E-05	1.93E-06	7.93E-05	79.29
8.32628	8.32628	308.532	311.456	336.004	305.323	1.18E-05	7.38E-06	5.81E-05	1.84E-06	7.92E-05	79.20
8.34039	8.34039	308.66	311.048	335.908	305.525	9.48E-06	7.38E-06	6.05E-05	1.73E-06	7.91E-05	79.09
8.3545	8.3545	308.825	310.872	336.013	305.747	7.76E-06	7.38E-06	6.22E-05	1.62E-06	7.90E-05	78.97
8.36861	8.36861	308.967	310.864	336.195	305.961	6.71E-06	7.38E-06	6.33E-05	1.49E-06	7.88E-05	78.85
8.38273	8.38273	309.072	311.054	336.536	306.183	6.36E-06	7.38E-06	6.36E-05	1.36E-06	7.87E-05	78.71
8.39684	8.39684	309.173	311.555	336.993	306.441	6.71E-06	7.38E-06	6.33E-05	1.22E-06	7.86E-05	78.58
8.41095	8.41095	309.314	312.64	337.527	306.661	7.76E-06	7.38E-06	6.22E-05	1.09E-06	7.84E-05	78.44
8.42506	8.42506	309.475	314.669	338.146	306.881	9.48E-06	7.38E-06	6.05E-05	9.59E-07	7.83E-05	78.32
8.43918	8.43918	309.782	317.505	338.792	307.049	1.18E-05	7.38E-06	5.81E-05	8.43E-07	7.82E-05	78.20
8.45329	8.45329	310.316	320.345	339.471	307.192	1.48E-05	7.38E-06	5.52E-05	7.41E-07	7.81E-05	78.10
8.4674	8.4674	310.996	322.517	340.137	307.275	1.82E-05	7.38E-06	5.18E-05	6.58E-07	7.80E-05	78.02
8.48151	8.48151	311.614	324.271	340.689	307.209	2.21E-05	7.38E-06	4.79E-05	5.96E-07	7.80E-05	77.95
8.49563	8.49563	312.318	326.489	341.292	307.237	2.63E-05	7.38E-06	4.37E-05	5.58E-07	7.79E-05	77.92
8.50974	8.50974	313.006	329.074	341.83	307.124	3.06E-05	7.38E-06	3.93E-05	5.46E-07	7.79E-05	77.90
8.52385	8.52385	313.479	331.663	342.039	306.887	3.51E-05	7.38E-06	3.49E-05	5.58E-07	7.79E-05	77.92
8.53796	8.53796	313.771	333.771	342.021	306.474	3.95E-05	7.38E-06	3.05E-05	5.96E-07	7.80E-05	77.95
8.55207	8.55207	313.851	335.161	341.895	305.817	4.37E-05	7.38E-06	2.63E-05	6.58E-07	7.80E-05	78.02
8.56619	8.56619	314.399	336.774	342.165	305.748	4.75E-05	7.38E-06	2.25E-05	7.41E-07	7.81E-05	78.10

Time	Theta	Temp [C]	Temp [R]	Temp [E]	Temp [P]	Vol [C]	Vol [R]	Vol [E]	Vol [P]	T Vol	
8.5803	8.5803	314.784	337.977	342.346	305.661	5.08E-05	7.38E-06	1.92E-05	8.43E-07	7.82E-05	78.20
8.59441	8.59441	315.003	338.855	342.481	305.564	5.36E-05	7.38E-06	1.64E-05	9.59E-07	7.83E-05	78.32
8.60852	8.60852	315.053	339.431	342.505	305.415	5.56E-05	7.38E-06	1.44E-05	1.09E-06	7.84E-05	78.44
8.62264	8.62264	314.889	339.66	342.597	305.276	5.68E-05	7.38E-06	1.31E-05	1.22E-06	7.86E-05	78.58
8.63675	8.63675	314.556	339.504	342.601	305.127	5.73E-05	7.38E-06	1.27E-05	1.36E-06	7.87E-05	78.71
8.65086	8.65086	314.084	338.799	342.594	304.93	5.68E-05	7.38E-06	1.31E-05	1.49E-06	7.88E-05	78.85
8.66497	8.66497	313.522	337.22	342.551	304.794	5.56E-05	7.38E-06	1.44E-05	1.62E-06	7.90E-05	78.97
8.67909	8.67909	312.872	334.539	342.327	304.669	5.36E-05	7.38E-06	1.64E-05	1.73E-06	7.91E-05	79.09
8.6932	8.6932	312.182	331.29	341.945	304.563	5.08E-05	7.38E-06	1.92E-05	1.84E-06	7.92E-05	79.20
8.70731	8.70731	311.477	328.364	341.367	304.489	4.75E-05	7.38E-06	2.25E-05	1.93E-06	7.93E-05	79.29
8.72142	8.72142	310.794	325.839	340.669	304.451	4.37E-05	7.38E-06	2.63E-05	2.00E-06	7.94E-05	79.36
8.73553	8.73553	310.176	323.243	339.935	304.441	3.95E-05	7.38E-06	3.05E-05	2.05E-06	7.94E-05	79.41
8.74965	8.74965	309.514	320.418	339.042	304.442	3.51E-05	7.38E-06	3.49E-05	2.08E-06	7.94E-05	79.44
8.76376	8.76376	308.933	317.605	338.148	304.308	3.06E-05	7.38E-06	3.93E-05	2.09E-06	7.95E-05	79.45
8.77787	8.77787	308.504	315.266	337.256	304.221	2.63E-05	7.38E-06	4.37E-05	2.08E-06	7.94E-05	79.44
8.79198	8.79198	308.31	313.683	336.729	304.361	2.21E-05	7.38E-06	4.79E-05	2.05E-06	7.94E-05	79.41
8.8061	8.8061	308.249	312.578	336.304	304.554	1.82E-05	7.38E-06	5.18E-05	2.00E-06	7.94E-05	79.36
8.82021	8.82021	308.274	311.81	336.003	304.763	1.48E-05	7.38E-06	5.52E-05	1.93E-06	7.93E-05	79.29
8.83432	8.83432	308.399	311.29	335.837	304.956	1.18E-05	7.38E-06	5.81E-05	1.84E-06	7.92E-05	79.20
8.84843	8.84843	308.596	310.975	335.802	305.22	9.48E-06	7.38E-06	6.05E-05	1.73E-06	7.91E-05	79.09
8.86255	8.86255	308.777	310.838	335.931	305.46	7.76E-06	7.38E-06	6.22E-05	1.62E-06	7.90E-05	78.97
8.87666	8.87666	308.934	310.863	336.14	305.699	6.71E-06	7.38E-06	6.33E-05	1.49E-06	7.88E-05	78.85
8.89077	8.89077	309.041	311.07	336.5	305.938	6.36E-06	7.38E-06	6.36E-05	1.36E-06	7.87E-05	78.71
8.90488	8.90488	309.136	311.568	336.959	306.197	6.71E-06	7.38E-06	6.33E-05	1.22E-06	7.86E-05	78.58
8.91899	8.91899	309.275	312.634	337.496	306.418	7.76E-06	7.38E-06	6.22E-05	1.09E-06	7.84E-05	78.44
8.93311	8.93311	309.436	314.621	338.119	306.637	9.48E-06	7.38E-06	6.05E-05	9.59E-07	7.83E-05	78.32
8.94722	8.94722	309.74	317.4	338.77	306.803	1.18E-05	7.38E-06	5.81E-05	8.43E-07	7.82E-05	78.20
8.96133	8.96133	310.242	320.178	339.43	306.923	1.48E-05	7.38E-06	5.52E-05	7.41E-07	7.81E-05	78.10
8.97544	8.97544	310.766	322.197	339.956	306.859	1.82E-05	7.38E-06	5.18E-05	6.58E-07		
8.98956	8.98956	311.011	323.604	340.152	306.416	2.21E-05	7.38E-06	4.79E-05	5.96E-07		
9.00367	9.00367	311.817	325.997	340.836	306.498	2.63E-05	7.38E-06	4.37E-05	5.58E-07		

## 2D CFD Results of E6 experimental scenario

Time	Theta	Temp [C]	Temp [R]	Temp [E]	Temp [P]
8.00169	8.00169	312.8572154	328.7738678	341.2345537	307.31281
8.01581	8.01581	313.1319451	331.6010695	341.6193243	307.3899885
8.02992	8.02992	313.6652802	334.2027476	341.7919696	306.8578584
8.04403	8.04403	313.2587749	334.4090905	341.7667118	305.389826
8.05814	8.05814	314.2887223	336.658577	341.9281105	305.8047061
8.07226	8.07226	313.9021676	337.2091017	342.0541927	305.5284827
8.08637	8.08637	314.5771695	338.4835201	342.2653602	305.3380573
8.10048	8.10048	314.4227703	339.297861	341.6044954	305.169003
8.11459	8.11459	314.0407635	339.0249438	342.2284795	305.1556511
8.1287	8.1287	313.9027117	339.5567382	342.12642	305.0967843
8.14282	8.14282	313.9812131	338.5076866	342.1753431	305.0928781
8.15693	8.15693	312.8725819	336.815821	342.3175248	304.528686
8.17104	8.17104	312.7061494	334.3565394	342.2918955	304.3679393
8.18515	8.18515	312.0661459	331.1745701	341.4363264	304.6457062
8.19927	8.19927	310.5377359	327.4486482	340.9713397	303.820765
8.21338	8.21338	310.7238901	325.2822298	340.3200313	303.5536549
8.22749	8.22749	309.9385353	322.7095753	339.4505649	303.7106422
8.2416	8.2416	308.8889214	320.0025825	338.8652139	303.877447
8.25572	8.25572	308.3421013	317.5137833	337.3947708	304.4213023
8.26983	8.26983	308.3304992	315.1739286	337.4636084	304.4204679
8.28394	8.28394	308.1547023	313.0904717	336.8386327	304.4220079
8.29805	8.29805	307.6154363	312.5671675	336.2506245	304.8789469
8.31216	8.31216	307.8642187	312.0305277	335.6334131	304.6602979
8.32628	8.32628	307.6330941	311.1577285	335.8872808	305.0191233
8.34039	8.34039	308.2940493	310.1262627	335.8526753	305.1502863
8.3545	8.3545	308.7727207	310.104833	335.1899107	305.617036
8.36861	8.36861	308.917398	310.8111872	335.5043452	305.7447367
8.38273	8.38273	308.1198429	310.1346842	336.1914031	305.4344833
8.39684	8.39684	308.3511221	311.2731569	336.3498009	306.4328241
8.41095	8.41095	309.1113539	311.8942471	336.7331999	305.9168646
8.42506	8.42506	308.8369411	314.3244278	337.759237	306.0621742
8.43918	8.43918	309.3529517	316.967635	337.8068146	306.1030085
8.45329	8.45329	309.4916118	319.9008793	339.2374376	307.0541547
8.4674	8.4674	310.0774352	321.530046	339.2111517	306.8585734
8.48151	8.48151	310.9440185	324.1826198	339.9812161	306.8419664
8.49563	8.49563	311.3987761	326.1239916	340.4497791	306.338761
8.50974	8.50974	312.056544	328.9600685	341.0047705	306.8090483
8.52385	8.52385	312.9700915	330.6662332	341.9841909	306.7331298
8.53796	8.53796	313.4773976	333.2669785	341.5761136	306.1245311
8.55207	8.55207	313.5988846	334.5867491	341.802533	305.1275738
8.56619	8.56619	314.1856815	336.0410025	341.4186816	305.5230045
8.5803	8.5803	314.2216928	337.9448956	341.6408948	305.1506144
8.59441	8.59441	314.813445	338.4042278	341.9342262	304.7740333

Time	Theta	Temp [C]	Temp [R]	Temp [E]	Temp [P]
8.60852	8.60852	314.5055889	338.992336	342.2625751	304.7942247
8.62264	8.62264	313.918699	338.7918645	341.7722392	305.0963666
8.63675	8.63675	313.8462569	338.9312359	342.5432385	304.1274492
8.65086	8.65086	313.5516137	338.180425	342.1136735	304.7553288
8.66497	8.66497	312.6259479	337.1919726	341.9376545	304.5768756
8.67909	8.67909	312.8529935	333.8156582	342.0464491	304.6346096
8.6932	8.6932	311.1977703	330.4453334	341.6174434	304.1186049
8.70731	8.70731	311.4241888	328.2770291	340.6595815	303.6442865
8.72142	8.72142	309.8537262	325.3271387	340.3835255	304.051917
8.73553	8.73553	309.18665	322.5433527	339.3043827	303.4638753
8.74965	8.74965	309.3950028	320.3650091	338.425368	304.2029529
8.76376	8.76376	308.1152012	317.2313021	337.162653	303.3493717
8.77787	8.77787	308.453655	314.9708669	336.2717408	303.7161722
8.79198	8.79198	307.5072168	313.0053227	336.6487785	303.5207622
8.8061	8.8061	308.0406491	312.1088819	335.4678186	303.6988417
8.82021	8.82021	307.4691026	311.1600617	335.3802519	304.2024098
8.83432	8.83432	308.0101053	310.625934	335.0003449	304.3987866
8.84843	8.84843	307.6519956	310.7154372	335.299274	305.2074968
8.86255	8.86255	308.2272356	310.5430724	335.3450837	305.0124174
8.87666	8.87666	308.4710478	310.5638494	336.0971006	305.6582502
8.89077	8.89077	308.7423572	310.2466393	335.7367843	304.9521624
8.90488	8.90488	308.722094	311.2832613	336.0227285	305.9038489
8.91899	8.91899	308.5023789	312.4665637	337.0330755	306.3455735
8.93311	8.93311	309.180033	314.3104974	337.5683321	305.8576336
8.94722	8.94722	309.5017325	317.215732	337.9887188	305.854944

### 3D CFD Results of E9 Experimental Scenario

Time	Theta	Temp [C]	Temp [R]	Temp [E]	Temp [P]	Vol [C]	Vol [R]	Vol [E]	Vol [P]	T Vol	
8.00169	8.00169	313.401	329.449	342.124	307.655	3.51E-05	7.38E-06	3.49E-05	2.08E-06	7.94E-05	79.44
8.01581	8.01581	314.072	332.231	342.508	307.624	3.06E-05	7.38E-06	3.93E-05	2.09E-06	7.95E-05	79.45
8.02992	8.02992	314.306	334.263	342.429	307.175	2.63E-05	7.38E-06	4.37E-05	2.08E-06	7.94E-05	79.44
8.04403	8.04403	313.871	335.093	341.843	306.028	2.21E-05	7.38E-06	4.79E-05	2.05E-06	7.94E-05	79.41
8.05814	8.05814	314.432	336.714	342.149	305.951	1.82E-05	7.38E-06	5.18E-05	2.00E-06	7.94E-05	79.36
8.07226	8.07226	314.821	337.921	342.344	305.852	1.48E-05	7.38E-06	5.52E-05	1.93E-06	7.93E-05	79.29
8.08637	8.08637	315.042	338.81	342.482	305.742	1.18E-05	7.38E-06	5.81E-05	1.84E-06	7.92E-05	79.20
8.10048	8.10048	315.093	339.395	342.506	305.583	9.48E-06	7.38E-06	6.05E-05	1.73E-06	7.91E-05	79.09
8.11459	8.11459	314.959	339.666	342.617	305.46	7.76E-06	7.38E-06	6.22E-05	1.62E-06	7.90E-05	78.97
8.1287	8.1287	314.665	339.561	342.641	305.335	6.71E-06	7.38E-06	6.33E-05	1.49E-06	7.88E-05	78.85
8.14282	8.14282	314.23	338.91	342.647	305.167	6.36E-06	7.38E-06	6.36E-05	1.36E-06	7.87E-05	78.71
8.15693	8.15693	313.692	337.374	342.607	305.047	6.71E-06	7.38E-06	6.33E-05	1.22E-06	7.86E-05	78.58
8.17104	8.17104	313.045	334.713	342.379	304.92	7.76E-06	7.38E-06	6.22E-05	1.09E-06	7.84E-05	78.44
8.18515	8.18515	312.325	331.442	341.969	304.779	9.48E-06	7.38E-06	6.05E-05	9.59E-07	7.83E-05	78.32
8.19927	8.19927	311.509	328.414	341.298	304.592	1.18E-05	7.38E-06	5.81E-05	8.43E-07	7.82E-05	78.20
8.21338	8.21338	310.797	325.863	340.587	304.519	1.48E-05	7.38E-06	5.52E-05	7.41E-07	7.81E-05	78.10
8.22749	8.22749	310.121	323.212	339.808	304.443	1.82E-05	7.38E-06	5.18E-05	6.58E-07	7.80E-05	78.02
8.2416	8.2416	309.469	320.382	338.935	304.448	2.21E-05	7.38E-06	4.79E-05	5.96E-07	7.80E-05	77.95
8.25572	8.25572	309.092	317.775	338.249	304.532	2.63E-05	7.38E-06	4.37E-05	5.58E-07	7.79E-05	77.92
8.26983	8.26983	308.815	315.641	337.522	304.642	3.06E-05	7.38E-06	3.93E-05	5.46E-07	7.79E-05	77.90
8.28394	8.28394	308.574	314.037	336.97	304.775	3.51E-05	7.38E-06	3.49E-05	5.58E-07	7.79E-05	77.92
8.29805	8.29805	308.479	312.884	336.529	304.962	3.95E-05	7.38E-06	3.05E-05	5.96E-07	7.80E-05	77.95
8.31216	8.31216	308.471	312.06	336.215	305.166	4.37E-05	7.38E-06	2.63E-05	6.58E-07	7.80E-05	78.02
8.32628	8.32628	308.532	311.456	336.004	305.323	4.75E-05	7.38E-06	2.25E-05	7.41E-07	7.81E-05	78.10
8.34039	8.34039	308.66	311.048	335.908	305.525	5.08E-05	7.38E-06	1.92E-05	8.43E-07	7.82E-05	78.20
8.3545	8.3545	308.825	310.872	336.013	305.747	5.36E-05	7.38E-06	1.64E-05	9.59E-07	7.83E-05	78.32
8.36861	8.36861	308.967	310.864	336.195	305.961	5.56E-05	7.38E-06	1.44E-05	1.09E-06	7.84E-05	78.44
8.38273	8.38273	309.072	311.054	336.536	306.183	5.68E-05	7.38E-06	1.31E-05	1.22E-06	7.86E-05	78.58
8.39684	8.39684	309.173	311.555	336.993	306.441	5.73E-05	7.38E-06	1.27E-05	1.36E-06	7.87E-05	78.71
8.41095	8.41095	309.314	312.64	337.527	306.661	5.68E-05	7.38E-06	1.31E-05	1.49E-06	7.88E-05	78.85
8.42506	8.42506	309.475	314.669	338.146	306.881	5.56E-05	7.38E-06	1.44E-05	1.62E-06	7.90E-05	78.97
8.43918	8.43918	309.782	317.505	338.792	307.049	5.36E-05	7.38E-06	1.64E-05	1.73E-06	7.91E-05	79.09
8.45329	8.45329	310.316	320.345	339.471	307.192	5.08E-05	7.38E-06	1.92E-05	1.84E-06	7.92E-05	79.20
8.4674	8.4674	310.996	322.517	340.137	307.275	4.75E-05	7.38E-06	2.25E-05	1.93E-06	7.93E-05	79.29
8.48151	8.48151	311.614	324.271	340.689	307.209	4.37E-05	7.38E-06	2.63E-05	2.00E-06	7.94E-05	79.36
8.49563	8.49563	312.318	326.489	341.292	307.237	3.95E-05	7.38E-06	3.05E-05	2.05E-06	7.94E-05	79.41
8.50974	8.50974	313.006	329.074	341.83	307.124	3.51E-05	7.38E-06	3.49E-05	2.08E-06	7.94E-05	79.44
8.52385	8.52385	313.479	331.663	342.039	306.887	3.06E-05	7.38E-06	3.93E-05	2.09E-06	7.95E-05	79.45
8.53796	8.53796	313.771	333.771	342.021	306.474	2.63E-05	7.38E-06	4.37E-05	2.08E-06	7.94E-05	79.44
8.55207	8.55207	313.851	335.161	341.895	305.817	2.21E-05	7.38E-06	4.79E-05	2.05E-06	7.94E-05	79.41
8.56619	8.56619	314.399	336.774	342.165	305.748	1.82E-05	7.38E-06	5.18E-05	2.00E-06	7.94E-05	79.36
8.5803	8.5803	314.784	337.977	342.346	305.661	1.48E-05	7.38E-06	5.52E-05	1.93E-06	7.93E-05	79.29
8.59441	8.59441	315.003	338.855	342.481	305.564	1.18E-05	7.38E-06	5.81E-05	1.84E-06	7.92E-05	79.20

Time	Theta	Temp [C]	Temp [R]	Temp [E]	Temp [P]	Vol [C]	Vol [R]	Vol [E]	Vol [P]	T Vol	
8.60852	8.60852	315.053	339.431	342.505	305.415	9.48E-06	7.38E-06	6.05E-05	1.73E-06	7.91E-05	79.09
8.62264	8.62264	314.889	339.66	342.597	305.276	7.76E-06	7.38E-06	6.22E-05	1.62E-06	7.90E-05	78.97
8.63675	8.63675	314.556	339.504	342.601	305.127	6.71E-06	7.38E-06	6.33E-05	1.49E-06	7.88E-05	78.85
8.65086	8.65086	314.084	338.799	342.594	304.93	6.36E-06	7.38E-06	6.36E-05	1.36E-06	7.87E-05	78.71
8.66497	8.66497	313.522	337.22	342.551	304.794	6.71E-06	7.38E-06	6.33E-05	1.22E-06	7.86E-05	78.58
8.67909	8.67909	312.872	334.539	342.327	304.669	7.76E-06	7.38E-06	6.22E-05	1.09E-06	7.84E-05	78.44
8.6932	8.6932	312.182	331.29	341.945	304.563	9.48E-06	7.38E-06	6.05E-05	9.59E-07	7.83E-05	78.32
8.70731	8.70731	311.477	328.364	341.367	304.489	1.18E-05	7.38E-06	5.81E-05	8.43E-07	7.82E-05	78.20
8.72142	8.72142	310.794	325.839	340.669	304.451	1.48E-05	7.38E-06	5.52E-05	7.41E-07	7.81E-05	78.10
8.73553	8.73553	310.176	323.243	339.935	304.441	1.82E-05	7.38E-06	5.18E-05	6.58E-07	7.80E-05	78.02
8.74965	8.74965	309.514	320.418	339.042	304.442	2.21E-05	7.38E-06	4.79E-05	5.96E-07	7.80E-05	77.95
8.76376	8.76376	308.933	317.605	338.148	304.308	2.63E-05	7.38E-06	4.37E-05	5.58E-07	7.79E-05	77.92
8.77787	8.77787	308.504	315.266	337.256	304.221	3.06E-05	7.38E-06	3.93E-05	5.46E-07	7.79E-05	77.90
8.79198	8.79198	308.31	313.683	336.729	304.361	3.51E-05	7.38E-06	3.49E-05	5.58E-07	7.79E-05	77.92
8.8061	8.8061	308.249	312.578	336.304	304.554	3.95E-05	7.38E-06	3.05E-05	5.96E-07	7.80E-05	77.95
8.82021	8.82021	308.274	311.81	336.003	304.763	4.37E-05	7.38E-06	2.63E-05	6.58E-07	7.80E-05	78.02
8.83432	8.83432	308.399	311.29	335.837	304.956	4.75E-05	7.38E-06	2.25E-05	7.41E-07	7.81E-05	78.10
8.84843	8.84843	308.596	310.975	335.802	305.22	5.08E-05	7.38E-06	1.92E-05	8.43E-07	7.82E-05	78.20
8.86255	8.86255	308.777	310.838	335.931	305.46	5.36E-05	7.38E-06	1.64E-05	9.59E-07	7.83E-05	78.32
8.87666	8.87666	308.934	310.863	336.14	305.699	5.56E-05	7.38E-06	1.44E-05	1.09E-06	7.84E-05	78.44
8.89077	8.89077	309.041	311.07	336.5	305.938	5.68E-05	7.38E-06	1.31E-05	1.22E-06	7.86E-05	78.58
8.90488	8.90488	309.136	311.568	336.959	306.197	5.73E-05	7.38E-06	1.27E-05	1.36E-06	7.87E-05	78.71
8.91899	8.91899	309.275	312.634	337.496	306.418	5.68E-05	7.38E-06	1.31E-05	1.49E-06	7.88E-05	78.85
8.93311	8.93311	309.436	314.621	338.119	306.637	5.56E-05	7.38E-06	1.44E-05	1.62E-06	7.90E-05	78.97
8.94722	8.94722	309.74	317.4	338.77	306.803	5.36E-05	7.38E-06	1.64E-05	1.73E-06	7.91E-05	79.09
8.96133	8.96133	310.242	320.178	339.43	306.923	5.08E-05	7.38E-06	1.92E-05	1.84E-06	7.92E-05	79.20
8.97544	8.97544	310.766	322.197	339.956	306.859	4.75E-05	7.38E-06	2.25E-05	1.93E-06		
8.98956	8.98956	311.011	323.604	340.152	306.416	4.37E-05	7.38E-06	2.63E-05	2.00E-06		
9.00367	9.00367	311.817	325.997	340.836	306.498	3.95E-05	7.38E-06	3.05E-05	2.05E-06		

## 2D CFD Results of E9 Experimental Scenario

Time	Theta	Temp [C]	Temp [R]	Temp [E]	Temp [P]
8.00169	8.00169	312.4922213	329.0196151	341.6500469	307.6099683
8.01581	8.01581	313.578258	331.7792547	341.532034	306.689364
8.02992	8.02992	313.6181281	333.8639873	342.4157132	306.7770485
8.04403	8.04403	312.9575145	334.1483946	341.3375073	305.4568513
8.05814	8.05814	313.5853574	336.68634	342.0502291	305.1648345
8.07226	8.07226	314.0054559	337.2660314	341.7465923	305.3721575
8.08637	8.08637	314.4922646	337.8986421	342.00641	305.7297486
8.10048	8.10048	314.9499545	338.5474374	341.6531398	305.5461574
8.11459	8.11459	314.8606624	339.2656889	342.0824156	305.2256398
8.1287	8.1287	314.4170055	339.3047512	342.4343765	304.9899304
8.14282	8.14282	313.2624686	338.3223002	342.146562	304.5202953
8.15693	8.15693	313.6689283	337.1144806	342.1061627	304.0715176
8.17104	8.17104	312.2149539	334.1916201	342.0887921	304.0938661
8.18515	8.18515	312.0597665	331.3542028	341.5125501	303.7941577
8.19927	8.19927	310.5475297	328.1531833	340.6813604	304.2268729
8.21338	8.21338	310.6241381	325.3003371	339.6346133	303.5207985
8.22749	8.22749	309.7602781	322.7956633	338.8450274	303.9862471
8.2416	8.2416	309.078323	320.0658661	338.3867059	303.4686327
8.25572	8.25572	308.9739521	317.7720027	337.9901879	303.7435437
8.26983	8.26983	307.8360608	315.1546244	336.7656466	303.7761005
8.28394	8.28394	308.1008078	313.6607802	336.6460022	304.2078886
8.29805	8.29805	307.8993086	312.6336797	335.9389903	304.9568042
8.31216	8.31216	307.6408673	311.1892272	335.9783577	304.8023607
8.32628	8.32628	308.2896601	310.964325	335.6814355	305.0748157
8.34039	8.34039	308.2975094	310.148996	335.3221707	305.0228845
8.3545	8.3545	308.7514425	310.3328061	335.5651475	305.7091074
8.36861	8.36861	308.6908201	310.5977976	335.3758434	305.3518163
8.38273	8.38273	308.3218444	310.0845628	335.560082	306.1568377
8.39684	8.39684	308.2290854	310.6141385	336.7588421	305.8103494
8.41095	8.41095	308.7000585	312.029725	337.1350218	306.6020813
8.42506	8.42506	308.7847983	313.7125746	337.2866769	306.635315
8.43918	8.43918	309.5228277	316.8775067	338.0595571	306.8203642
8.45329	8.45329	309.9473506	320.0415445	338.9217728	307.0829285
8.4674	8.4674	310.3548169	321.9794688	339.6364078	307.1169693
8.48151	8.48151	310.8276792	323.4573657	340.6779502	306.4854586
8.49563	8.49563	311.6173935	326.1770908	340.4906485	307.1243938
8.50974	8.50974	312.7887896	328.0982105	340.8688551	306.8301561
8.52385	8.52385	312.6613537	330.9443361	341.7683561	306.2818816
8.53796	8.53796	312.8329516	333.0566023	341.6329916	305.4747414
8.55207	8.55207	313.0764489	334.5348704	341.8106152	304.9999049
8.56619	8.56619	314.2972083	336.4936579	341.991313	305.1436133
8.5803	8.5803	314.281893	337.677361	341.7570598	304.8708519
8.59441	8.59441	314.9221987	338.6751685	341.6513727	305.0741968

Time	Theta	Temp [C]	Temp [R]	Temp [E]	Temp [P]
8.60852	8.60852	314.4856117	339.0118069	341.9957684	305.2759218
8.62264	8.62264	314.0485483	339.4442405	342.1612991	304.8518169
8.63675	8.63675	314.2587702	339.1431452	342.1932404	304.5816983
8.65086	8.65086	313.5277427	338.3987343	342.1187627	304.1392796
8.66497	8.66497	313.4693834	336.3384579	342.3053541	303.8556564
8.67909	8.67909	312.325458	334.017798	342.1338192	304.1892359
8.6932	8.6932	311.4255565	331.2147123	341.3749183	304.3249579
8.70731	8.70731	310.4884079	328.2079024	341.1386411	304.0062479
8.72142	8.72142	310.0866373	325.5258442	339.9028291	303.8233189
8.73553	8.73553	309.7444151	322.9256737	339.3220246	303.4778936
8.74965	8.74965	308.8669999	319.9944952	338.2250915	304.2718167
8.76376	8.76376	308.3883633	316.7380735	337.6546207	303.7260719
8.77787	8.77787	308.1881042	314.7060205	336.2720188	303.7422176
8.79198	8.79198	308.2192992	313.6209671	336.4722657	303.915852
8.8061	8.8061	307.744086	312.1483447	335.90692	304.0214756
8.82021	8.82021	307.4028933	311.7327141	335.2600294	304.3736661
8.83432	8.83432	308.1926955	311.0691516	335.0622461	304.8380522
8.84843	8.84843	307.8910506	310.0901385	335.5473033	304.6553675
8.86255	8.86255	308.0909449	310.4402193	335.8182944	305.2977808
8.87666	8.87666	308.0027106	310.6643755	335.4432095	305.1226401
8.89077	8.89077	308.5104996	310.1918365	336.2903112	305.4748033
8.90488	8.90488	308.8881408	310.8886324	336.3743923	305.2821858
8.91899	8.91899	308.5423194	312.1677034	337.4107913	305.5281893
8.93311	8.93311	308.9886254	314.047822	338.0018596	305.670917
8.94722	8.94722	308.9717933	316.4822296	338.7275439	306.2239628
8.96133	8.96133	309.6672139	319.6124328	339.3973954	306.5999834

### 3D CFD Results of E16 Experimental Scenario

Time	Theta	Temp [C]	Temp [R]	Temp [E]	Temp [P]	Vol [C]	Vol [R]	Vol [E]	Vol [P]	T Vol	
8.00169	8.00169	313.401	329.449	342.124	307.655	1.82E-05	7.38E-06	5.18E-05	2.00E-06	7.94E-05	79.36
8.01581	8.01581	314.072	332.231	342.508	307.624	1.48E-05	7.38E-06	5.52E-05	1.93E-06	7.93E-05	79.29
8.02992	8.02992	314.306	334.263	342.429	307.175	1.18E-05	7.38E-06	5.81E-05	1.84E-06	7.92E-05	79.20
8.04403	8.04403	313.871	335.093	341.843	306.028	9.48E-06	7.38E-06	6.05E-05	1.73E-06	7.91E-05	79.09
8.05814	8.05814	314.432	336.714	342.149	305.951	7.76E-06	7.38E-06	6.22E-05	1.62E-06	7.90E-05	78.97
8.07226	8.07226	314.821	337.921	342.344	305.852	6.71E-06	7.38E-06	6.33E-05	1.49E-06	7.88E-05	78.85
8.08637	8.08637	315.042	338.81	342.482	305.742	6.36E-06	7.38E-06	6.36E-05	1.36E-06	7.87E-05	78.71
8.10048	8.10048	315.093	339.395	342.506	305.583	6.71E-06	7.38E-06	6.33E-05	1.22E-06	7.86E-05	78.58
8.11459	8.11459	314.959	339.666	342.617	305.46	7.76E-06	7.38E-06	6.22E-05	1.09E-06	7.84E-05	78.44
8.1287	8.1287	314.665	339.561	342.641	305.335	9.48E-06	7.38E-06	6.05E-05	9.59E-07	7.83E-05	78.32
8.14282	8.14282	314.23	338.91	342.647	305.167	1.18E-05	7.38E-06	5.81E-05	8.43E-07	7.82E-05	78.20
8.15693	8.15693	313.692	337.374	342.607	305.047	1.48E-05	7.38E-06	5.52E-05	7.41E-07	7.81E-05	78.10
8.17104	8.17104	313.045	334.713	342.379	304.92	1.82E-05	7.38E-06	5.18E-05	6.58E-07	7.80E-05	78.02
8.18515	8.18515	312.325	331.442	341.969	304.779	2.21E-05	7.38E-06	4.79E-05	5.96E-07	7.80E-05	77.95
8.19927	8.19927	311.509	328.414	341.298	304.592	2.63E-05	7.38E-06	4.37E-05	5.58E-07	7.79E-05	77.92
8.21338	8.21338	310.797	325.863	340.587	304.519	3.06E-05	7.38E-06	3.93E-05	5.46E-07	7.79E-05	77.90
8.22749	8.22749	310.121	323.212	339.808	304.443	3.51E-05	7.38E-06	3.49E-05	5.58E-07	7.79E-05	77.92
8.2416	8.2416	309.469	320.382	338.935	304.448	3.95E-05	7.38E-06	3.05E-05	5.96E-07	7.80E-05	77.95
8.25572	8.25572	309.092	317.775	338.249	304.532	4.37E-05	7.38E-06	2.63E-05	6.58E-07	7.80E-05	78.02
8.26983	8.26983	308.815	315.641	337.522	304.642	4.75E-05	7.38E-06	2.25E-05	7.41E-07	7.81E-05	78.10
8.28394	8.28394	308.574	314.037	336.97	304.775	5.08E-05	7.38E-06	1.92E-05	8.43E-07	7.82E-05	78.20
8.29805	8.29805	308.479	312.884	336.529	304.962	5.36E-05	7.38E-06	1.64E-05	9.59E-07	7.83E-05	78.32
8.31216	8.31216	308.471	312.06	336.215	305.166	5.56E-05	7.38E-06	1.44E-05	1.09E-06	7.84E-05	78.44
8.32628	8.32628	308.532	311.456	336.004	305.323	5.68E-05	7.38E-06	1.31E-05	1.22E-06	7.86E-05	78.58
8.34039	8.34039	308.66	311.048	335.908	305.525	5.73E-05	7.38E-06	1.27E-05	1.36E-06	7.87E-05	78.71
8.3545	8.3545	308.825	310.872	336.013	305.747	5.68E-05	7.38E-06	1.31E-05	1.49E-06	7.88E-05	78.85
8.36861	8.36861	308.967	310.864	336.195	305.961	5.56E-05	7.38E-06	1.44E-05	1.62E-06	7.90E-05	78.97
8.38273	8.38273	309.072	311.054	336.536	306.183	5.36E-05	7.38E-06	1.64E-05	1.73E-06	7.91E-05	79.09
8.39684	8.39684	309.173	311.555	336.993	306.441	5.08E-05	7.38E-06	1.92E-05	1.84E-06	7.92E-05	79.20
8.41095	8.41095	309.314	312.64	337.527	306.661	4.75E-05	7.38E-06	2.25E-05	1.93E-06	7.93E-05	79.29
8.42506	8.42506	309.475	314.669	338.146	306.881	4.37E-05	7.38E-06	2.63E-05	2.00E-06	7.94E-05	79.36
8.43918	8.43918	309.782	317.505	338.792	307.049	3.95E-05	7.38E-06	3.05E-05	2.05E-06	7.94E-05	79.41
8.45329	8.45329	310.316	320.345	339.471	307.192	3.51E-05	7.38E-06	3.49E-05	2.08E-06	7.94E-05	79.44
8.4674	8.4674	310.996	322.517	340.137	307.275	3.06E-05	7.38E-06	3.93E-05	2.09E-06	7.95E-05	79.45
8.48151	8.48151	311.614	324.271	340.689	307.209	2.63E-05	7.38E-06	4.37E-05	2.08E-06	7.94E-05	79.44
8.49563	8.49563	312.318	326.489	341.292	307.237	2.21E-05	7.38E-06	4.79E-05	2.05E-06	7.94E-05	79.41
8.50974	8.50974	313.006	329.074	341.83	307.124	1.82E-05	7.38E-06	5.18E-05	2.00E-06	7.94E-05	79.36
8.52385	8.52385	313.479	331.663	342.039	306.887	1.48E-05	7.38E-06	5.52E-05	1.93E-06	7.93E-05	79.29
8.53796	8.53796	313.771	333.771	342.021	306.474	1.18E-05	7.38E-06	5.81E-05	1.84E-06	7.92E-05	79.20
8.55207	8.55207	313.851	335.161	341.895	305.817	9.48E-06	7.38E-06	6.05E-05	1.73E-06	7.91E-05	79.09
8.56619	8.56619	314.399	336.774	342.165	305.748	7.76E-06	7.38E-06	6.22E-05	1.62E-06	7.90E-05	78.97
8.5803	8.5803	314.784	337.977	342.346	305.661	6.71E-06	7.38E-06	6.33E-05	1.49E-06	7.88E-05	78.85
8.59441	8.59441	315.003	338.855	342.481	305.564	6.36E-06	7.38E-06	6.36E-05	1.36E-06	7.87E-05	78.71

Time	Theta	Temp [C]	Temp [R]	Temp [E]	Temp [P]	Vol [C]	Vol [R]	Vol [E]	Vol [P]	T Vol	
8.60852	8.60852	315.053	339.431	342.505	305.415	6.71E-06	7.38E-06	6.33E-05	1.22E-06	7.86E-05	78.58
8.62264	8.62264	314.889	339.66	342.597	305.276	7.76E-06	7.38E-06	6.22E-05	1.09E-06	7.84E-05	78.44
8.63675	8.63675	314.556	339.504	342.601	305.127	9.48E-06	7.38E-06	6.05E-05	9.59E-07	7.83E-05	78.32
8.65086	8.65086	314.084	338.799	342.594	304.93	1.18E-05	7.38E-06	5.81E-05	8.43E-07	7.82E-05	78.20
8.66497	8.66497	313.522	337.22	342.551	304.794	1.48E-05	7.38E-06	5.52E-05	7.41E-07	7.81E-05	78.10
8.67909	8.67909	312.872	334.539	342.327	304.669	1.82E-05	7.38E-06	5.18E-05	6.58E-07	7.80E-05	78.02
8.6932	8.6932	312.182	331.29	341.945	304.563	2.21E-05	7.38E-06	4.79E-05	5.96E-07	7.80E-05	77.95
8.70731	8.70731	311.477	328.364	341.367	304.489	2.63E-05	7.38E-06	4.37E-05	5.58E-07	7.79E-05	77.92
8.72142	8.72142	310.794	325.839	340.669	304.451	3.06E-05	7.38E-06	3.93E-05	5.46E-07	7.79E-05	77.90
8.73553	8.73553	310.176	323.243	339.935	304.441	3.51E-05	7.38E-06	3.49E-05	5.58E-07	7.79E-05	77.92
8.74965	8.74965	309.514	320.418	339.042	304.442	3.95E-05	7.38E-06	3.05E-05	5.96E-07	7.80E-05	77.95
8.76376	8.76376	308.933	317.605	338.148	304.308	4.37E-05	7.38E-06	2.63E-05	6.58E-07	7.80E-05	78.02
8.77787	8.77787	308.504	315.266	337.256	304.221	4.75E-05	7.38E-06	2.25E-05	7.41E-07	7.81E-05	78.10
8.79198	8.79198	308.31	313.683	336.729	304.361	5.08E-05	7.38E-06	1.92E-05	8.43E-07	7.82E-05	78.20
8.8061	8.8061	308.249	312.578	336.304	304.554	5.36E-05	7.38E-06	1.64E-05	9.59E-07	7.83E-05	78.32
8.82021	8.82021	308.274	311.81	336.003	304.763	5.56E-05	7.38E-06	1.44E-05	1.09E-06	7.84E-05	78.44
8.83432	8.83432	308.399	311.29	335.837	304.956	5.68E-05	7.38E-06	1.31E-05	1.22E-06	7.86E-05	78.58
8.84843	8.84843	308.596	310.975	335.802	305.22	5.73E-05	7.38E-06	1.27E-05	1.36E-06	7.87E-05	78.71
8.86255	8.86255	308.777	310.838	335.931	305.46	5.68E-05	7.38E-06	1.31E-05	1.49E-06	7.88E-05	78.85
8.87666	8.87666	308.934	310.863	336.14	305.699	5.56E-05	7.38E-06	1.44E-05	1.62E-06	7.90E-05	78.97
8.89077	8.89077	309.041	311.07	336.5	305.938	5.36E-05	7.38E-06	1.64E-05	1.73E-06	7.91E-05	79.09
8.90488	8.90488	309.136	311.568	336.959	306.197	5.08E-05	7.38E-06	1.92E-05	1.84E-06	7.92E-05	79.20
8.91899	8.91899	309.275	312.634	337.496	306.418	4.75E-05	7.38E-06	2.25E-05	1.93E-06	7.93E-05	79.29
8.93311	8.93311	309.436	314.621	338.119	306.637	4.37E-05	7.38E-06	2.63E-05	2.00E-06	7.94E-05	79.36
8.94722	8.94722	309.74	317.4	338.77	306.803	3.95E-05	7.38E-06	3.05E-05	2.05E-06	7.94E-05	79.41
8.96133	8.96133	310.242	320.178	339.43	306.923	3.51E-05	7.38E-06	3.49E-05	2.08E-06	7.94E-05	79.44
8.97544	8.97544	310.766	322.197	339.956	306.859	3.06E-05	7.38E-06	3.93E-05	2.09E-06		
8.98956	8.98956	311.011	323.604	340.152	306.416	2.63E-05	7.38E-06	4.37E-05	2.08E-06		
9.00367	9.00367	311.817	325.997	340.836	306.498	2.21E-05	7.38E-06	4.79E-05	2.05E-06		

## 2D CFD Results of E16 Experimental Scenario

Time	Theta	Temp [C]	Temp [R]	Temp [E]	Temp [P]
8.00169	8.00169	314.0878565	329.8305289	342.3157362	308.2972334
8.01581	8.01581	314.6435288	332.4418004	342.957314	308.1698948
8.02992	8.02992	314.7133046	334.7246155	342.5539314	308.1042572
8.04403	8.04403	313.9324509	335.6619965	342.390574	306.1533163
8.05814	8.05814	314.9604221	337.4092051	342.7728288	306.9479992
8.07226	8.07226	315.6613691	338.7129881	342.8967736	305.88215
8.08637	8.08637	315.4794686	339.2005753	342.6540682	306.7368268
8.10048	8.10048	315.5387219	339.4936873	343.2694211	306.145939
8.11459	8.11459	315.6473251	340.200781	343.0859994	306.3813796
8.1287	8.1287	315.0987819	339.9790175	343.4206119	305.9359621
8.14282	8.14282	314.7364371	339.6316245	342.7654787	305.949966
8.15693	8.15693	314.5782693	338.2993752	343.0476901	305.807947
8.17104	8.17104	313.1235701	335.1035133	342.8611147	305.3823692
8.18515	8.18515	312.882025	331.9629423	342.3908783	305.2087154
8.19927	8.19927	311.9735641	329.2844029	341.6150175	305.283931
8.21338	8.21338	311.5726656	326.3375297	340.6728634	305.043912
8.22749	8.22749	310.364483	323.3528193	339.8804692	304.8228501
8.2416	8.2416	309.866089	321.2357518	339.5352894	304.6728302
8.25572	8.25572	309.8056502	318.3456134	338.5808962	304.9236116
8.26983	8.26983	308.9852009	316.1532056	337.7142382	305.1527525
8.28394	8.28394	308.7938871	314.5838826	337.2543572	305.4145561
8.29805	8.29805	308.6791441	313.4308511	337.4529887	305.2246341
8.31216	8.31216	309.4140058	312.7608531	336.2712442	305.7201032
8.32628	8.32628	309.4994339	311.8478555	336.4319669	305.4634292
8.34039	8.34039	309.5165687	311.0895722	336.0293172	306.5238329
8.3545	8.3545	309.043004	311.7670852	336.1983282	306.2235754
8.36861	8.36861	309.8392718	311.1505817	336.2574777	306.3028708
8.38273	8.38273	309.4969533	311.8789992	336.7079194	306.8947972
8.39684	8.39684	309.4728029	311.8587588	337.0017439	306.4689214
8.41095	8.41095	309.7817028	312.9168887	337.9701852	307.5685328
8.42506	8.42506	310.3906733	315.6374129	338.6695692	307.5453383
8.43918	8.43918	310.376332	317.7305288	339.6773176	307.807865
8.45329	8.45329	311.2943587	321.2303154	339.5026627	308.1488312
8.4674	8.4674	311.5659019	323.4768149	340.8730255	307.5499607
8.48151	8.48151	312.6016031	324.6441875	341.2831827	308.0378836
8.49563	8.49563	312.6676501	326.5598831	341.8929944	308.180066
8.50974	8.50974	313.7856011	329.2115182	342.624587	307.5040045
8.52385	8.52385	314.3808126	332.1411714	342.8245102	307.000168
8.53796	8.53796	314.6867684	334.7236077	342.1869783	306.4816545
8.55207	8.55207	313.9217265	335.4527998	341.9212057	305.906877
8.56619	8.56619	314.5175782	337.054353	343.153397	306.6904933
8.5803	8.5803	315.3811313	338.5025291	343.2066224	305.9833076
8.59441	8.59441	315.7955125	339.8068118	342.9764138	305.9349041

Time	Theta	Temp [C]	Temp [R]	Temp [E]	Temp [P]
8.60852	8.60852	315.3236817	339.8064006	343.5033168	306.1231579
8.62264	8.62264	315.8702211	340.0190825	342.9011086	306.0958373
8.63675	8.63675	315.2642276	339.8503636	343.5771531	306.1137264
8.65086	8.65086	314.2943681	339.4569051	343.5631051	305.7565778
8.66497	8.66497	313.8009724	338.064043	342.9166914	305.566352
8.67909	8.67909	313.6567847	335.3868908	342.5287011	304.8065072
8.6932	8.6932	312.7964094	331.5912483	342.6225428	305.561414
8.70731	8.70731	312.3471992	328.3716603	341.7932915	304.7040508
8.72142	8.72142	311.4955029	325.8739523	340.9661938	304.7315043
8.73553	8.73553	310.4139076	323.7825813	340.4161385	304.5974308
8.74965	8.74965	309.5571688	321.0300564	339.3965117	305.376435
8.76376	8.76376	309.2102174	317.9743387	338.6549524	304.8635195
8.77787	8.77787	308.851709	316.0927255	337.4802969	304.5338408
8.79198	8.79198	308.8494645	314.2661831	336.9328019	305.0539827
8.8061	8.8061	309.1484473	313.3033357	337.0955301	305.4931502
8.82021	8.82021	308.7029879	312.5491799	336.3336376	305.0353359
8.83432	8.83432	308.6160851	311.8254675	336.2771982	305.4022919
8.84843	8.84843	309.481273	311.1720486	335.928621	305.7965766
8.86255	8.86255	308.8187338	311.3899115	336.7946875	305.5415412
8.87666	8.87666	309.7403403	310.9979984	337.0384238	306.5825721
8.89077	8.89077	309.9106978	311.3279463	337.4876244	306.0322761
8.90488	8.90488	309.9099174	311.8063592	337.1514343	306.8126774
8.91899	8.91899	310.2074427	313.3469935	337.8282658	307.207179
8.93311	8.93311	309.4703729	315.4386161	338.8864479	307.0178855
8.94722	8.94722	310.5322446	318.0727601	339.4966718	307.7223048
8.96133	8.96133	310.586049	320.2339123	340.3561431	307.7656198

### 3D CFD Results of E17 Experimental Scenario

Time	Theta	Temp [C]	Temp [R]	Temp [E]	Temp [P]	Vol [C]	Vol [R]	Vol [E]	Vol [P]	T Vol	
8.00169	8.00169	313.401	329.449	342.124	307.655	2.63E-05	7.38E-06	4.37E-05	2.08E-06	7.94E-05	79.44
8.01581	8.01581	314.072	332.231	342.508	307.624	2.21E-05	7.38E-06	4.79E-05	2.05E-06	7.94E-05	79.41
8.02992	8.02992	314.306	334.263	342.429	307.175	1.82E-05	7.38E-06	5.18E-05	2.00E-06	7.94E-05	79.36
8.04403	8.04403	313.871	335.093	341.843	306.028	1.48E-05	7.38E-06	5.52E-05	1.93E-06	7.93E-05	79.29
8.05814	8.05814	314.432	336.714	342.149	305.951	1.18E-05	7.38E-06	5.81E-05	1.84E-06	7.92E-05	79.20
8.07226	8.07226	314.821	337.921	342.344	305.852	9.48E-06	7.38E-06	6.05E-05	1.73E-06	7.91E-05	79.09
8.08637	8.08637	315.042	338.81	342.482	305.742	7.76E-06	7.38E-06	6.22E-05	1.62E-06	7.90E-05	78.97
8.10048	8.10048	315.093	339.395	342.506	305.583	6.71E-06	7.38E-06	6.33E-05	1.49E-06	7.88E-05	78.85
8.11459	8.11459	314.959	339.666	342.617	305.46	6.36E-06	7.38E-06	6.36E-05	1.36E-06	7.87E-05	78.71
8.1287	8.1287	314.665	339.561	342.641	305.335	6.71E-06	7.38E-06	6.33E-05	1.22E-06	7.86E-05	78.58
8.14282	8.14282	314.23	338.91	342.647	305.167	7.76E-06	7.38E-06	6.22E-05	1.09E-06	7.84E-05	78.44
8.15693	8.15693	313.692	337.374	342.607	305.047	9.48E-06	7.38E-06	6.05E-05	9.59E-07	7.83E-05	78.32
8.17104	8.17104	313.045	334.713	342.379	304.92	1.18E-05	7.38E-06	5.81E-05	8.43E-07	7.82E-05	78.20
8.18515	8.18515	312.325	331.442	341.969	304.779	1.48E-05	7.38E-06	5.52E-05	7.41E-07	7.81E-05	78.10
8.19927	8.19927	311.509	328.414	341.298	304.592	1.82E-05	7.38E-06	5.18E-05	6.58E-07	7.80E-05	78.02
8.21338	8.21338	310.797	325.863	340.587	304.519	2.21E-05	7.38E-06	4.79E-05	5.96E-07	7.80E-05	77.95
8.22749	8.22749	310.121	323.212	339.808	304.443	2.63E-05	7.38E-06	4.37E-05	5.58E-07	7.79E-05	77.92
8.2416	8.2416	309.469	320.382	338.935	304.448	3.06E-05	7.38E-06	3.93E-05	5.46E-07	7.79E-05	77.90
8.25572	8.25572	309.092	317.775	338.249	304.532	3.51E-05	7.38E-06	3.49E-05	5.58E-07	7.79E-05	77.92
8.26983	8.26983	308.815	315.641	337.522	304.642	3.95E-05	7.38E-06	3.05E-05	5.96E-07	7.80E-05	77.95
8.28394	8.28394	308.574	314.037	336.97	304.775	4.37E-05	7.38E-06	2.63E-05	6.58E-07	7.80E-05	78.02
8.29805	8.29805	308.479	312.884	336.529	304.962	4.75E-05	7.38E-06	2.25E-05	7.41E-07	7.81E-05	78.10
8.31216	8.31216	308.471	312.06	336.215	305.166	5.08E-05	7.38E-06	1.92E-05	8.43E-07	7.82E-05	78.20
8.32628	8.32628	308.532	311.456	336.004	305.323	5.36E-05	7.38E-06	1.64E-05	9.59E-07	7.83E-05	78.32
8.34039	8.34039	308.66	311.048	335.908	305.525	5.56E-05	7.38E-06	1.44E-05	1.09E-06	7.84E-05	78.44
8.3545	8.3545	308.825	310.872	336.013	305.747	5.68E-05	7.38E-06	1.31E-05	1.22E-06	7.86E-05	78.58
8.36861	8.36861	308.967	310.864	336.195	305.961	5.73E-05	7.38E-06	1.27E-05	1.36E-06	7.87E-05	78.71
8.38273	8.38273	309.072	311.054	336.536	306.183	5.68E-05	7.38E-06	1.31E-05	1.49E-06	7.88E-05	78.85
8.39684	8.39684	309.173	311.555	336.993	306.441	5.56E-05	7.38E-06	1.44E-05	1.62E-06	7.90E-05	78.97
8.41095	8.41095	309.314	312.64	337.527	306.661	5.36E-05	7.38E-06	1.64E-05	1.73E-06	7.91E-05	79.09
8.42506	8.42506	309.475	314.669	338.146	306.881	5.08E-05	7.38E-06	1.92E-05	1.84E-06	7.92E-05	79.20
8.43918	8.43918	309.782	317.505	338.792	307.049	4.75E-05	7.38E-06	2.25E-05	1.93E-06	7.93E-05	79.29
8.45329	8.45329	310.316	320.345	339.471	307.192	4.37E-05	7.38E-06	2.63E-05	2.00E-06	7.94E-05	79.36
8.4674	8.4674	310.996	322.517	340.137	307.275	3.95E-05	7.38E-06	3.05E-05	2.05E-06	7.94E-05	79.41
8.48151	8.48151	311.614	324.271	340.689	307.209	3.51E-05	7.38E-06	3.49E-05	2.08E-06	7.94E-05	79.44
8.49563	8.49563	312.318	326.489	341.292	307.237	3.06E-05	7.38E-06	3.93E-05	2.09E-06	7.95E-05	79.45
8.50974	8.50974	313.006	329.074	341.83	307.124	2.63E-05	7.38E-06	4.37E-05	2.08E-06	7.94E-05	79.44
8.52385	8.52385	313.479	331.663	342.039	306.887	2.21E-05	7.38E-06	4.79E-05	2.05E-06	7.94E-05	79.41
8.53796	8.53796	313.771	333.771	342.021	306.474	1.82E-05	7.38E-06	5.18E-05	2.00E-06	7.94E-05	79.36
8.55207	8.55207	313.851	335.161	341.895	305.817	1.48E-05	7.38E-06	5.52E-05	1.93E-06	7.93E-05	79.29
8.56619	8.56619	314.399	336.774	342.165	305.748	1.18E-05	7.38E-06	5.81E-05	1.84E-06	7.92E-05	79.20
8.5803	8.5803	314.784	337.977	342.346	305.661	9.48E-06	7.38E-06	6.05E-05	1.73E-06	7.91E-05	79.09
8.59441	8.59441	315.003	338.855	342.481	305.564	7.76E-06	7.38E-06	6.22E-05	1.62E-06	7.90E-05	78.97

Time	Theta	Temp [C]	Temp [R]	Temp [E]	Temp [P]	Vol [C]	Vol [R]	Vol [E]	Vol [P]	T Vol	
8.60852	8.60852	315.053	339.431	342.505	305.415	6.71E-06	7.38E-06	6.33E-05	1.49E-06	7.88E-05	78.85
8.62264	8.62264	314.889	339.66	342.597	305.276	6.36E-06	7.38E-06	6.36E-05	1.36E-06	7.87E-05	78.71
8.63675	8.63675	314.556	339.504	342.601	305.127	6.71E-06	7.38E-06	6.33E-05	1.22E-06	7.86E-05	78.58
8.65086	8.65086	314.084	338.799	342.594	304.93	7.76E-06	7.38E-06	6.22E-05	1.09E-06	7.84E-05	78.44
8.66497	8.66497	313.522	337.22	342.551	304.794	9.48E-06	7.38E-06	6.05E-05	9.59E-07	7.83E-05	78.32
8.67909	8.67909	312.872	334.539	342.327	304.669	1.18E-05	7.38E-06	5.81E-05	8.43E-07	7.82E-05	78.20
8.6932	8.6932	312.182	331.29	341.945	304.563	1.48E-05	7.38E-06	5.52E-05	7.41E-07	7.81E-05	78.10
8.70731	8.70731	311.477	328.364	341.367	304.489	1.82E-05	7.38E-06	5.18E-05	6.58E-07	7.80E-05	78.02
8.72142	8.72142	310.794	325.839	340.669	304.451	2.21E-05	7.38E-06	4.79E-05	5.96E-07	7.80E-05	77.95
8.73553	8.73553	310.176	323.243	339.935	304.441	2.63E-05	7.38E-06	4.37E-05	5.58E-07	7.79E-05	77.92
8.74965	8.74965	309.514	320.418	339.042	304.442	3.06E-05	7.38E-06	3.93E-05	5.46E-07	7.79E-05	77.90
8.76376	8.76376	308.933	317.605	338.148	304.308	3.51E-05	7.38E-06	3.49E-05	5.58E-07	7.79E-05	77.92
8.77787	8.77787	308.504	315.266	337.256	304.221	3.95E-05	7.38E-06	3.05E-05	5.96E-07	7.80E-05	77.95
8.79198	8.79198	308.31	313.683	336.729	304.361	4.37E-05	7.38E-06	2.63E-05	6.58E-07	7.80E-05	78.02
8.8061	8.8061	308.249	312.578	336.304	304.554	4.75E-05	7.38E-06	2.25E-05	7.41E-07	7.81E-05	78.10
8.82021	8.82021	308.274	311.81	336.003	304.763	5.08E-05	7.38E-06	1.92E-05	8.43E-07	7.82E-05	78.20
8.83432	8.83432	308.399	311.29	335.837	304.956	5.36E-05	7.38E-06	1.64E-05	9.59E-07	7.83E-05	78.32
8.84843	8.84843	308.596	310.975	335.802	305.22	5.56E-05	7.38E-06	1.44E-05	1.09E-06	7.84E-05	78.44
8.86255	8.86255	308.777	310.838	335.931	305.46	5.68E-05	7.38E-06	1.31E-05	1.22E-06	7.86E-05	78.58
8.87666	8.87666	308.934	310.863	336.14	305.699	5.73E-05	7.38E-06	1.27E-05	1.36E-06	7.87E-05	78.71
8.89077	8.89077	309.041	311.07	336.5	305.938	0.00E+00	0.00E+00	0.00E+00	0.00E+00	0.00E+00	0.00
8.90488	8.90488	309.136	311.568	336.959	306.197	0.00E+00	0.00E+00	0.00E+00	0.00E+00	0.00E+00	0.00
8.91899	8.91899	309.275	312.634	337.496	306.418	0.00E+00	0.00E+00	0.00E+00	0.00E+00	0.00E+00	0.00
8.93311	8.93311	309.436	314.621	338.119	306.637	0.00E+00	0.00E+00	0.00E+00	0.00E+00	0.00E+00	0.00
8.94722	8.94722	309.74	317.4	338.77	306.803	0.00E+00	0.00E+00	0.00E+00	0.00E+00	0.00E+00	0.00
8.96133	8.96133	310.242	320.178	339.43	306.923	0.00E+00	0.00E+00	0.00E+00	0.00E+00	0.00E+00	0.00
8.97544	8.97544	310.766	322.197	339.956	306.859	0.00E+00	0.00E+00	0.00E+00	0.00E+00		
8.98956	8.98956	311.011	323.604	340.152	306.416	0.00E+00	0.00E+00	0.00E+00	0.00E+00		
9.00367	9.00367	311.817	325.997	340.836	306.498	0.00E+00	0.00E+00	0.00E+00	0.00E+00		

## 2D CFD Results of E17 Experimental Scenario

Time	Theta	Temp [C]	Temp [R]	Temp [E]	Temp [P]
8.00169	8.00169	313.8826147	328.9607735	342.8659193	307.1195325
8.01581	8.01581	314.3465691	332.4846809	342.791375	308.0669678
8.02992	8.02992	315.0350677	334.8970334	343.0374635	307.8702046
8.04403	8.04403	314.7896899	336.0907435	342.2038424	307.0086961
8.05814	8.05814	315.0467612	336.8768318	342.8252877	306.560276
8.07226	8.07226	315.2019417	338.3900439	343.051216	306.8185308
8.08637	8.08637	315.1316015	339.4773153	342.4984036	306.2640917
8.10048	8.10048	315.9010178	339.4501294	342.5588115	306.1249133
8.11459	8.11459	315.0770229	339.7277562	343.549602	306.1085718
8.1287	8.1287	315.3604867	340.3850648	343.1426818	305.9008483
8.14282	8.14282	314.9412499	339.6135954	342.6705462	305.7380099
8.15693	8.15693	314.3843331	337.9456031	343.3205087	305.1944775
8.17104	8.17104	313.641622	335.511044	343.2376579	305.7679281
8.18515	8.18515	312.4321501	331.9300645	342.9565383	304.7903514
8.19927	8.19927	311.7893055	329.2127065	342.0456928	305.3088042
8.21338	8.21338	311.2112952	326.4259947	340.792851	304.6755234
8.22749	8.22749	310.1427357	324.0794563	340.2932659	305.0978974
8.2416	8.2416	310.210928	321.3740821	339.8455737	304.7219094
8.25572	8.25572	309.3120748	318.6591816	338.3358054	305.1899466
8.26983	8.26983	309.4342831	315.8978354	337.5275635	305.2551803
8.28394	8.28394	309.239314	314.6404375	337.4626946	304.8162855
8.29805	8.29805	309.421121	313.153163	337.0252415	305.584708
8.31216	8.31216	309.2871961	313.0532182	336.3756557	305.5027629
8.32628	8.32628	309.5298556	311.7213698	336.2341058	305.7793063
8.34039	8.34039	308.8274355	311.5703986	336.0639634	306.4215033
8.3545	8.3545	308.8890739	311.2335285	336.148558	306.6984591
8.36861	8.36861	309.7367832	311.3980918	336.4398935	306.0285838
8.38273	8.38273	309.3850571	311.5920592	337.3462376	306.7686503
8.39684	8.39684	309.2496074	312.5097338	337.0974118	306.5101181
8.41095	8.41095	310.0309937	312.7867903	337.8071483	307.0798129
8.42506	8.42506	310.1642557	315.4475861	339.0974055	307.2441122
8.43918	8.43918	310.4481191	317.5202907	339.0218522	307.2220021
8.45329	8.45329	310.8558519	321.0294525	339.8342505	308.1170513
8.4674	8.4674	311.3297416	323.0503695	340.6737987	307.5375738
8.48151	8.48151	312.3816609	324.3650126	341.015656	307.4198871
8.49563	8.49563	313.2431409	326.9638668	341.3163131	308.21321
8.50974	8.50974	313.3157217	329.2556957	342.4893652	308.0226287
8.52385	8.52385	313.9193481	332.5471118	342.7701387	307.2905294
8.53796	8.53796	314.3046412	334.6596763	342.7477806	307.1221286
8.55207	8.55207	314.0981112	335.786202	342.8733284	306.6654915
8.56619	8.56619	314.6666016	337.7276623	342.3076817	306.3541426
8.5803	8.5803	315.4825551	338.6767329	342.4325126	306.6210707
8.59441	8.59441	315.4633064	338.8678973	343.3303157	305.7526806

Time	Theta	Temp [C]	Temp [R]	Temp [E]	Temp [P]
8.60852	8.60852	315.4541203	339.5014124	343.3650653	306.0355741
8.62264	8.62264	314.9964251	340.3390114	342.8145331	305.306861
8.63675	8.63675	314.7066932	339.8908874	343.1992804	305.9006543
8.65086	8.65086	315.0722064	339.4717165	343.4352359	304.9362759
8.66497	8.66497	314.2161625	337.663614	343.3571999	305.1430949
8.67909	8.67909	313.7280122	334.9113027	342.8823058	305.2769987
8.6932	8.6932	312.9997076	331.6138051	342.8234811	304.6605999
8.70731	8.70731	311.9633986	329.351444	341.8128101	304.986616
8.72142	8.72142	310.8744453	326.3456105	340.7306291	305.1695034
8.73553	8.73553	310.2773455	323.6411268	340.896441	304.9252666
8.74965	8.74965	310.402433	320.7474269	339.1868095	304.8672326
8.76376	8.76376	308.9907813	317.7754019	339.1294077	304.9848768
8.77787	8.77787	309.4562881	315.6105949	337.748463	304.5107369
8.79198	8.79198	309.2639637	313.807828	337.3765013	304.4594648
8.8061	8.8061	308.5814343	312.7897727	337.2320875	304.901683
8.82021	8.82021	308.8793016	311.9170376	336.3074464	305.5202494
8.83432	8.83432	308.4920995	311.4473547	336.3770667	305.3976726
8.84843	8.84843	309.1849354	311.6579802	336.5919778	305.7163596
8.86255	8.86255	308.9014813	311.4850694	336.9254803	306.4450844
8.87666	8.87666	309.3614163	310.9214784	336.5731483	306.057098
8.89077	8.89077	309.997123	311.708921	337.2536995	306.5183683
8.90488	8.90488	309.5763439	311.7830407	337.7432528	306.1989487
8.91899	8.91899	310.0386261	313.2538802	338.0327894	306.9466562
8.93311	8.93311	309.7597956	315.2914546	338.5403138	307.2877183
8.94722	8.94722	309.7757641	317.5894872	339.4277533	307.5298901
8.96133	8.96133	310.6597128	320.8370919	340.019656	307.244077

### 3D CFD Results of E23 Experimental Scenario

Time	Theta	Temp [C]	Temp [R]	Temp [E]	Temp [P]	Vol [C]	Vol [R]	Vol [E]	Vol [P]	T Vol	
8.00169	8.00169	313.401	329.449	342.124	307.655	4.37E-05	7.38E-06	2.63E-05	6.58E-07	7.80E-05	78.02
8.01581	8.01581	314.072	332.231	342.508	307.624	4.75E-05	7.38E-06	2.25E-05	7.41E-07	7.81E-05	78.10
8.02992	8.02992	314.306	334.263	342.429	307.175	5.08E-05	7.38E-06	1.92E-05	8.43E-07	7.82E-05	78.20
8.04403	8.04403	313.871	335.093	341.843	306.028	5.36E-05	7.38E-06	1.64E-05	9.59E-07	7.83E-05	78.32
8.05814	8.05814	314.432	336.714	342.149	305.951	5.56E-05	7.38E-06	1.44E-05	1.09E-06	7.84E-05	78.44
8.07226	8.07226	314.821	337.921	342.344	305.852	5.68E-05	7.38E-06	1.31E-05	1.22E-06	7.86E-05	78.58
8.08637	8.08637	315.042	338.81	342.482	305.742	5.73E-05	7.38E-06	1.27E-05	1.36E-06	7.87E-05	78.71
8.10048	8.10048	315.093	339.395	342.506	305.583	5.68E-05	7.38E-06	1.31E-05	1.49E-06	7.88E-05	78.85
8.11459	8.11459	314.959	339.666	342.617	305.46	5.56E-05	7.38E-06	1.44E-05	1.62E-06	7.90E-05	78.97
8.1287	8.1287	314.665	339.561	342.641	305.335	5.36E-05	7.38E-06	1.64E-05	1.73E-06	7.91E-05	79.09
8.14282	8.14282	314.23	338.91	342.647	305.167	5.08E-05	7.38E-06	1.92E-05	1.84E-06	7.92E-05	79.20
8.15693	8.15693	313.692	337.374	342.607	305.047	4.75E-05	7.38E-06	2.25E-05	1.93E-06	7.93E-05	79.29
8.17104	8.17104	313.045	334.713	342.379	304.92	4.37E-05	7.38E-06	2.63E-05	2.00E-06	7.94E-05	79.36
8.18515	8.18515	312.325	331.442	341.969	304.779	3.95E-05	7.38E-06	3.05E-05	2.05E-06	7.94E-05	79.41
8.19927	8.19927	311.509	328.414	341.298	304.592	3.51E-05	7.38E-06	3.49E-05	2.08E-06	7.94E-05	79.44
8.21338	8.21338	310.797	325.863	340.587	304.519	3.06E-05	7.38E-06	3.93E-05	2.09E-06	7.95E-05	79.45
8.22749	8.22749	310.121	323.212	339.808	304.443	2.63E-05	7.38E-06	4.37E-05	2.08E-06	7.94E-05	79.44
8.2416	8.2416	309.469	320.382	338.935	304.448	2.21E-05	7.38E-06	4.79E-05	2.05E-06	7.94E-05	79.41
8.25572	8.25572	309.092	317.775	338.249	304.532	1.82E-05	7.38E-06	5.18E-05	2.00E-06	7.94E-05	79.36
8.26983	8.26983	308.815	315.641	337.522	304.642	1.48E-05	7.38E-06	5.52E-05	1.93E-06	7.93E-05	79.29
8.28394	8.28394	308.574	314.037	336.97	304.775	1.18E-05	7.38E-06	5.81E-05	1.84E-06	7.92E-05	79.20
8.29805	8.29805	308.479	312.884	336.529	304.962	9.48E-06	7.38E-06	6.05E-05	1.73E-06	7.91E-05	79.09
8.31216	8.31216	308.471	312.06	336.215	305.166	7.76E-06	7.38E-06	6.22E-05	1.62E-06	7.90E-05	78.97
8.32628	8.32628	308.532	311.456	336.004	305.323	6.71E-06	7.38E-06	6.33E-05	1.49E-06	7.88E-05	78.85
8.34039	8.34039	308.66	311.048	335.908	305.525	6.36E-06	7.38E-06	6.36E-05	1.36E-06	7.87E-05	78.71
8.3545	8.3545	308.825	310.872	336.013	305.747	6.71E-06	7.38E-06	6.33E-05	1.22E-06	7.86E-05	78.58
8.36861	8.36861	308.967	310.864	336.195	305.961	7.76E-06	7.38E-06	6.22E-05	1.09E-06	7.84E-05	78.44
8.38273	8.38273	309.072	311.054	336.536	306.183	9.48E-06	7.38E-06	6.05E-05	9.59E-07	7.83E-05	78.32
8.39684	8.39684	309.173	311.555	336.993	306.441	1.18E-05	7.38E-06	5.81E-05	8.43E-07	7.82E-05	78.20
8.41095	8.41095	309.314	312.64	337.527	306.661	1.48E-05	7.38E-06	5.52E-05	7.41E-07	7.81E-05	78.10
8.42506	8.42506	309.475	314.669	338.146	306.881	1.82E-05	7.38E-06	5.18E-05	6.58E-07	7.80E-05	78.02
8.43918	8.43918	309.782	317.505	338.792	307.049	2.21E-05	7.38E-06	4.79E-05	5.96E-07	7.80E-05	77.95
8.45329	8.45329	310.316	320.345	339.471	307.192	2.63E-05	7.38E-06	4.37E-05	5.58E-07	7.79E-05	77.92
8.4674	8.4674	310.996	322.517	340.137	307.275	3.06E-05	7.38E-06	3.93E-05	5.46E-07	7.79E-05	77.90
8.48151	8.48151	311.614	324.271	340.689	307.209	3.51E-05	7.38E-06	3.49E-05	5.58E-07	7.79E-05	77.92
8.49563	8.49563	312.318	326.489	341.292	307.237	3.95E-05	7.38E-06	3.05E-05	5.96E-07	7.80E-05	77.95
8.50974	8.50974	313.006	329.074	341.83	307.124	4.37E-05	7.38E-06	2.63E-05	6.58E-07	7.80E-05	78.02
8.52385	8.52385	313.479	331.663	342.039	306.887	4.75E-05	7.38E-06	2.25E-05	7.41E-07	7.81E-05	78.10
8.53796	8.53796	313.771	333.771	342.021	306.474	5.08E-05	7.38E-06	1.92E-05	8.43E-07	7.82E-05	78.20
8.55207	8.55207	313.851	335.161	341.895	305.817	5.36E-05	7.38E-06	1.64E-05	9.59E-07	7.83E-05	78.32
8.56619	8.56619	314.399	336.774	342.165	305.748	5.56E-05	7.38E-06	1.44E-05	1.09E-06	7.84E-05	78.44
8.5803	8.5803	314.784	337.977	342.346	305.661	5.68E-05	7.38E-06	1.31E-05	1.22E-06	7.86E-05	78.58
8.59441	8.59441	315.003	338.855	342.481	305.564	5.73E-05	7.38E-06	1.27E-05	1.36E-06	7.87E-05	78.71

Time	Theta	Temp [C]	Temp [R]	Temp [E]	Temp [P]	Vol [C]	Vol [R]	Vol [E]	Vol [P]	T Vol	
8.60852	8.60852	315.053	339.431	342.505	305.415	5.68E-05	7.38E-06	1.31E-05	1.49E-06	7.88E-05	78.85
8.62264	8.62264	314.889	339.66	342.597	305.276	5.56E-05	7.38E-06	1.44E-05	1.62E-06	7.90E-05	78.97
8.63675	8.63675	314.556	339.504	342.601	305.127	5.36E-05	7.38E-06	1.64E-05	1.73E-06	7.91E-05	79.09
8.65086	8.65086	314.084	338.799	342.594	304.93	5.08E-05	7.38E-06	1.92E-05	1.84E-06	7.92E-05	79.20
8.66497	8.66497	313.522	337.22	342.551	304.794	4.75E-05	7.38E-06	2.25E-05	1.93E-06	7.93E-05	79.29
8.67909	8.67909	312.872	334.539	342.327	304.669	4.37E-05	7.38E-06	2.63E-05	2.00E-06	7.94E-05	79.36
8.6932	8.6932	312.182	331.29	341.945	304.563	3.95E-05	7.38E-06	3.05E-05	2.05E-06	7.94E-05	79.41
8.70731	8.70731	311.477	328.364	341.367	304.489	3.51E-05	7.38E-06	3.49E-05	2.08E-06	7.94E-05	79.44
8.72142	8.72142	310.794	325.839	340.669	304.451	3.06E-05	7.38E-06	3.93E-05	2.09E-06	7.95E-05	79.45
8.73553	8.73553	310.176	323.243	339.935	304.441	2.63E-05	7.38E-06	4.37E-05	2.08E-06	7.94E-05	79.44
8.74965	8.74965	309.514	320.418	339.042	304.442	2.21E-05	7.38E-06	4.79E-05	2.05E-06	7.94E-05	79.41
8.76376	8.76376	308.933	317.605	338.148	304.308	1.82E-05	7.38E-06	5.18E-05	2.00E-06	7.94E-05	79.36
8.77787	8.77787	308.504	315.266	337.256	304.221	1.48E-05	7.38E-06	5.52E-05	1.93E-06	7.93E-05	79.29
8.79198	8.79198	308.31	313.683	336.729	304.361	1.18E-05	7.38E-06	5.81E-05	1.84E-06	7.92E-05	79.20
8.8061	8.8061	308.249	312.578	336.304	304.554	9.48E-06	7.38E-06	6.05E-05	1.73E-06	7.91E-05	79.09
8.82021	8.82021	308.274	311.81	336.003	304.763	7.76E-06	7.38E-06	6.22E-05	1.62E-06	7.90E-05	78.97
8.83432	8.83432	308.399	311.29	335.837	304.956	6.71E-06	7.38E-06	6.33E-05	1.49E-06	7.88E-05	78.85
8.84843	8.84843	308.596	310.975	335.802	305.22	6.36E-06	7.38E-06	6.36E-05	1.36E-06	7.87E-05	78.71
8.86255	8.86255	308.777	310.838	335.931	305.46	6.71E-06	7.38E-06	6.33E-05	1.22E-06	7.86E-05	78.58
8.87666	8.87666	308.934	310.863	336.14	305.699	7.76E-06	7.38E-06	6.22E-05	1.09E-06	7.84E-05	78.44
8.89077	8.89077	309.041	311.07	336.5	305.938	9.48E-06	7.38E-06	6.05E-05	9.59E-07	7.83E-05	78.32
8.90488	8.90488	309.136	311.568	336.959	306.197	1.18E-05	7.38E-06	5.81E-05	8.43E-07	7.82E-05	78.20
8.91899	8.91899	309.275	312.634	337.496	306.418	1.48E-05	7.38E-06	5.52E-05	7.41E-07	7.81E-05	78.10
8.93311	8.93311	309.436	314.621	338.119	306.637	1.82E-05	7.38E-06	5.18E-05	6.58E-07	7.80E-05	78.02
8.94722	8.94722	309.74	317.4	338.77	306.803	2.21E-05	7.38E-06	4.79E-05	5.96E-07	7.80E-05	77.95
8.96133	8.96133	310.242	320.178	339.43	306.923	2.63E-05	7.38E-06	4.37E-05	5.58E-07	7.79E-05	77.92
8.97544	8.97544	310.766	322.197	339.956	306.859	3.06E-05	7.38E-06	3.93E-05	5.46E-07		
8.98956	8.98956	311.011	323.604	340.152	306.416	0.00E+00	0.00E+00	0.00E+00	0.00E+00		
9.00367	9.00367	311.817	325.997	340.836	306.498	0.00E+00	0.00E+00	0.00E+00	0.00E+00		

## 2D CFD Results of E23 Experimental Scenario

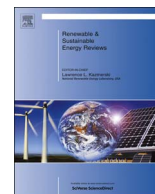
Time	Theta	Temp [C]	Temp [R]	Temp [E]	Temp [P]
8.00169	8.00169	313.1060587	330.2410442	341.4984351	308.6071071
8.01581	8.01581	313.6875885	332.6303687	342.3961742	308.0381025
8.02992	8.02992	313.4504197	334.9193281	342.0324808	307.5502237
8.04403	8.04403	313.3274343	335.8885703	341.0762989	306.8368181
8.05814	8.05814	314.1132402	337.0575651	341.8678311	306.3373686
8.07226	8.07226	314.2739627	338.3884908	341.4380105	306.1707823
8.08637	8.08637	314.5489493	339.1123008	342.0493634	306.1600669
8.10048	8.10048	314.9699654	340.1113481	342.2372942	306.2837474
8.11459	8.11459	314.0579976	340.5617313	342.5344334	306.3542364
8.1287	8.1287	314.5390162	340.3795797	341.7564207	306.1115201
8.14282	8.14282	314.2010649	339.8012316	342.3247983	305.3658819
8.15693	8.15693	312.8971412	337.9393526	341.6619466	305.712793
8.17104	8.17104	312.9903387	335.6848269	342.2441093	305.075755
8.18515	8.18515	311.4595898	332.1194093	341.5870563	305.0227786
8.19927	8.19927	310.8515251	329.4103064	341.2911251	305.0948743
8.21338	8.21338	310.0304206	326.2888933	340.1524832	305.2443113
8.22749	8.22749	309.3533754	323.3733844	339.4560794	305.3498297
8.2416	8.2416	308.7551729	321.1211325	338.5399923	304.9474789
8.25572	8.25572	308.2375986	318.2250181	337.545262	304.981133
8.26983	8.26983	308.1440085	316.1114873	337.119371	304.6973193
8.28394	8.28394	307.6726806	314.7864433	336.2215387	305.6111954
8.29805	8.29805	308.4659462	313.2153938	335.96796	305.7668384
8.31216	8.31216	307.6185702	312.5003005	335.5516187	305.8849171
8.32628	8.32628	308.222307	311.6554714	335.3683146	305.7015498
8.34039	8.34039	307.8760979	311.6922095	335.9005238	306.1135231
8.3545	8.3545	307.9083973	311.1593916	335.7238641	305.8607231
8.36861	8.36861	308.7632486	311.610379	336.0001624	305.9860356
8.38273	8.38273	308.2125825	311.9567735	336.129152	306.4609528
8.39684	8.39684	308.6257964	312.3004812	336.9167012	306.7415544
8.41095	8.41095	308.8027492	312.9090284	337.2446824	307.2304486
8.42506	8.42506	309.3049736	315.4659683	337.8706456	307.7649544
8.43918	8.43918	309.235238	317.515997	337.8915333	307.1589755
8.45329	8.45329	309.5849203	320.6366793	339.3486561	307.417529
8.4674	8.4674	310.9534814	323.4885365	340.0414426	307.4347642
8.48151	8.48151	311.4864306	324.8410854	340.4746474	308.0825748
8.49563	8.49563	311.390639	327.1139291	340.6636588	308.0235166
8.50974	8.50974	312.8031727	329.8217981	341.3396108	307.6449776
8.52385	8.52385	312.8496647	332.5424948	341.8096774	307.6451641
8.53796	8.53796	313.4745193	334.4861754	341.0330627	306.5682698
8.55207	8.55207	312.9293267	335.934819	340.9163734	306.2927794
8.56619	8.56619	313.9617292	337.7285785	341.3191357	306.224166
8.5803	8.5803	313.8063623	338.0937171	341.9101738	306.3670918
8.59441	8.59441	314.4619872	339.4294472	341.6951353	305.6417871

Time	Theta	Temp [C]	Temp [R]	Temp [E]	Temp [P]
8.60852	8.60852	314.4485487	340.0524402	342.4160029	306.1984308
8.62264	8.62264	314.4531826	339.979207	342.4405011	305.3591678
8.63675	8.63675	314.1941174	340.0035323	342.0733639	306.029597
8.65086	8.65086	313.6321423	339.6983301	341.7124927	305.7894303
8.66497	8.66497	312.9247647	337.8064492	342.171652	305.6109936
8.67909	8.67909	312.5261101	335.2278658	341.460062	305.5239344
8.6932	8.6932	311.2609151	331.9552233	340.9524955	304.5970709
8.70731	8.70731	310.5549315	328.7902528	341.1068199	304.9805723
8.72142	8.72142	310.6254543	326.749584	340.5561772	304.5793873
8.73553	8.73553	310.0520373	324.1280664	339.3452046	304.5316706
8.74965	8.74965	309.2564474	320.7500686	338.806963	305.2858472
8.76376	8.76376	308.8469793	318.3461827	337.7852083	304.789629
8.77787	8.77787	308.4593318	315.5672069	336.744653	304.7418376
8.79198	8.79198	307.7547298	314.6605371	335.9006199	305.3180589
8.8061	8.8061	307.6028599	312.9640114	335.9573267	305.0362502
8.82021	8.82021	308.0717617	312.2711021	335.0163592	304.8582582
8.83432	8.83432	307.4749077	311.3210727	335.7729315	305.7263058
8.84843	8.84843	307.9721364	311.6610449	335.5797596	305.7029037
8.86255	8.86255	308.6338492	311.0222115	335.88551	305.5904614
8.87666	8.87666	308.8932074	310.9358828	335.23672	306.567849
8.89077	8.89077	308.738751	311.6675384	336.3260088	306.3480246
8.90488	8.90488	308.4916037	312.0225569	336.0869033	306.5338882
8.91899	8.91899	308.5540108	313.1808	336.950567	306.74278
8.93311	8.93311	308.4854047	314.9885632	337.7923951	307.0906797
8.94722	8.94722	309.480437	317.9044337	337.8085087	306.9122665
8.96133	8.96133	310.021185	320.6531177	338.8659723	307.3474968

## **8.5. Appendix 5 – Publications**

### **8.5.1. Review Paper**

Mohammed Wazed S, Hughes BR, O'Connor D, Calautit JK. A Review of Sustainable Solar Irrigation Systems for Sub-Saharan Africa, *Renewable & Sustainable Energy Reviews*, 2017, Impact Factor 6.798



## A review of sustainable solar irrigation systems for Sub-Saharan Africa



Saeed Mohammed Wazed<sup>a,\*</sup>, Ben Richard Hughes<sup>a</sup>, Dominic O'Connor<sup>a</sup>, John Kaiser Calautit<sup>b</sup>

<sup>a</sup> Energy2050, Mechanical Engineering, Faculty of Engineering, University of Sheffield, Sheffield, South Yorkshire S10 2TN, United Kingdom

<sup>b</sup> Department of Architecture and Built Environment, University of Nottingham, Nottingham NG7 2RD, United Kingdom

### ARTICLE INFO

#### Keywords:

Solar energy  
Solar water pumping  
Photovoltaics  
Concentrated solar thermal  
Stirling engine  
Irrigation

### ABSTRACT

This investigation focused on the research undertaken on solar photovoltaic (PV) and solar thermal technologies for pumping water generally for irrigation of remote rural farms specifically considering the Sub-Saharan African region. Solar PV systems have been researched extensively for irrigation purposes due to the rise in Oil prices and the upscaling in commercialisation of PV technology. Based on the literature the most effective PV system is presented for the irrigation of a small scale remote rural farm with respect to the cost, pumping capacity and system efficiency. Similarly, solar thermal systems are reviewed and the most effective system described. Unlike PV technology, solar thermal technology for water pumping is lacking especially in small scale operations. However, with the possibility of local production, low investment cost, easy maintenance and lower carbon footprint, solar thermal water pumping technologies may be able to overcome the shortcomings of the PV technology that has stopped widespread use of the technology for irrigation applications. Taking into consideration recent developments in concentrated solar technologies using the Stirling engine, novel solar thermal water pumping systems may be developed. This review also highlighted the different methodologies such as modelling, used to investigate and optimise the performance of solar powered systems.

### 1. Introduction

Population growth and food insecurity necessitates an increase in farming and irrigation all over the world. The focus here is not only to produce more but to do so in a manner that protects the environment. Moreover, the impact on poorer nations, which are already struggling with food shortage, is far more adverse than others as more land and energy is required to meet the requirements of the future. This creates a need for the development of sustainable technologies that can be implemented to utilise the readily available local resources to drive the cost of the irrigation systems down.

The Sub-Saharan region in Africa is one such region that is marred by inconsistent supply of safe water supplies. Contaminated ground water and long dry spells means that the main source of water in these regions are the rich groundwater reserves. Only 10% of this region utilises groundwater and most of this stems from the lack of economic incentives [1]. The cost of harvesting the reserves are very high. Not only is the initial investment high for purchasing generators and pumps but also the ongoing inflation in fuel costs leads to a consistent increase in operational and maintenance costs [2]. Such costs are extremely high for remote small scale independent farmers to bear.

The focus of this review is to investigate affordable irrigation systems that will be portable and utilise the local resources for

manufacture and maintenance. Emphasis is also provided on the use of renewable energy resources to negate the requirement of fossil fuel driven motors (generally diesel powered) and pumps to further reduce the running cost of irrigation. Severe draught, lack of rain and long dry spells provides the opportunity for the utilisation of solar power in Sub-Saharan Africa, with both solar thermal and Photovoltaic (PV) technologies [3], and hence, is considered the focus of this review.

In the review, solar thermal and PV technologies will be compared on the basis of cost, power output and flow generated. The above parameters have been selected in order to design a system that will be viable for the independent farmer for irrigation of remote small scale farms in the Sub-Saharan African region with average small scale farm size of 1 ha according to the Food and Agriculture Organisation (FAO) [4].

The research on solar thermal power has not been as prominent as PV panels in recent times for water pumping applications. However, major development in solar thermal technologies incorporating Stirling Engines warrants a review of solar thermal systems for irrigation because of its potential to work at low temperatures and relatively simple construction. This review paper highlights major technological developments made in PV irrigation systems, solar thermal irrigation systems and new developments in solar thermal technology that could be utilised in irrigation, with focus on medium to low powered Stirling

\* Corresponding author.

E-mail address: [SMohammedWazed1@sheffield.ac.uk](mailto:SMohammedWazed1@sheffield.ac.uk) (S. Mohammed Wazed).

cycle engines. The findings are summarised and the performance of the systems are compared to identify the key advantages and disadvantages of each technology.

## 2. Research methodology

A literature review is performed on PV and solar thermal irrigation systems. While there is numerous research on PV and Solar thermal technologies, the focus on this review is to study the implementation of the technology in irrigation. To obtain the research material for this literature review, keyword search has been utilised incorporating, “solar water pumps”, “solar irrigation”, “PV irrigation”, “solar thermal irrigation”, “PV water pumping systems”, “Stirling pumps”, “Rankine Cycle water pumps”, “ORC water pumps”, “ORC irrigation” and “Stirling Irrigation”. No location bias has been set. The University of Sheffield’s “StarPlus Library Discovery” search tool, “Science-Direct” search engine and the “Google” search engine has been utilised.

PV system reviews have been divided in 4 sections:

- PV irrigation technology reviews – Contains reviews of papers which enlists the various PV technologies that have been studied in the years prior to the publication.
- PV irrigations systems – Contains reviews of papers which describe unique irrigation systems design.
- PV irrigation systems performance – Contains reviews of papers that discuss technologies and control systems that can be used to optimise PV irrigation systems
- PV irrigation technology in comparison to other technologies – Contains reviews of papers that compare PV irrigation technologies against other technologies including Diesel generated pump systems and Renewable energy generated pump systems.

Solar Thermal system reviews have been divided in 3 sections:

- Solar thermal irrigation technology reviews – Contains reviews of papers which enlists the various solar thermal technologies that have been studied in the years prior to the publication.
- Conventional solar thermal technologies – Contains reviews of papers discussing solar thermal technologies based on the Rankine cycle.
- Unconventional solar thermal technologies – Contains reviews of papers discussing solar thermal technologies based on Stirling cycle and other two stroke systems.

After the literature review was performed each solar powered technology (PV and Solar Thermal) is then individually analysed. A summary table of all the technology systems reviewed is presented and the best irrigation set-up has been established. Following this the future of solar irrigation technology is discussed.

## 3. PV irrigation systems

PV Technologies convert solar energy into electrical energy and then coupled with an electric motor is used to drive an electric pump. Fig. 1 depicts a typical PV irrigation set up. This system can be further enhanced depending on the output requirement, charge regulation based on the requirement of the pump (AC/DC) as well as the incorporation of a battery to counter the fluctuation of solar irradiation available throughout the day or even for irrigation at night, when lower water losses and higher irrigation uniformity is observed [5].

The water outlet from the irrigation system (depicted in Fig. 1) can be used either directly for irrigation or can be used to fill up a water storage tank. An advantage of the water storage tank is that it can be a substitute of the battery system, wherein the potential energy of the stored water can be utilised for drip irrigation.

Photovoltaic systems are generally very simple to implement, and an adequately designed system is efficient and can compete with other

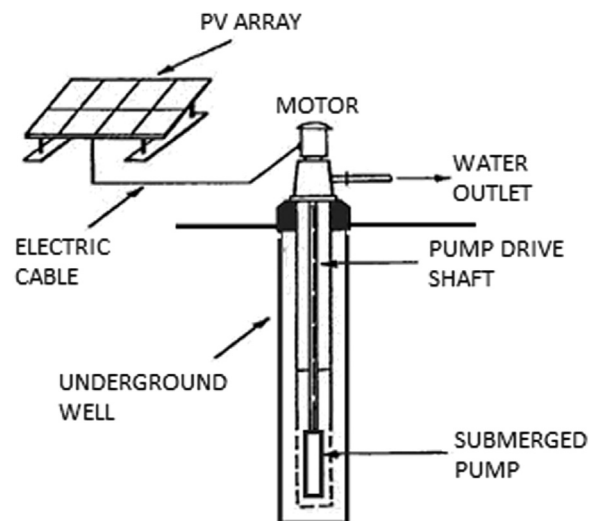


Fig. 1. Schematic of a simple PV irrigation set up for groundwater retrieval [6].

systems when operational and maintenance costs are considered. However, the initial investment is often identified as a major turn off [7]. While PV systems are easier to maintain than most other renewable energy systems, there are lots of factors that limit its use including, inconsistent solar irradiation, expensive tracking systems, reduction in efficiency due to overheating of panel systems, lower output due to energy conversion and one of the major issues identified in recent times is the large environmental impact in the production of PV panels [7–9].

A decrease in the cost of PV technology has meant many rural developments have been keen on utilising the technology because of this, a great amount of research has been conducted on solar PV technologies for water pumping in the recent years so much so that photovoltaic irrigation systems have become synonymous with solar-powered irrigation. Significant research has been conducted on performance, feasibility and economic viability of various PV systems as detailed below.

### 3.1. PV irrigation technology reviews

Chandel et al. [10] reviewed technologies for irrigation and supply of drinking water to communities that utilises solar PV technology. The study focussed on new technology updates, efficiency, analysis of the performance, efficient sizing of panels, degradation of supplying power to the pump from the PV panels and the economic and environmental aspects of utilising PV technology. In comparison to diesel / conventional electric system, PV systems were identified to be more economically viable in urban and remote rural areas with a payback time of 4–6 years achieved. For shallow wells (10–20 m deep), AC motor pump systems showed similar water output levels when compared to DC motor pump systems, however, at higher depths (30–50 m) DC motor systems provide higher flowrates. The efficiency of different types of solar cells are as per indicated in Table 1 (as tabularised by Green et al. [11]) with Multijunction five-junction cells demonstrating the highest efficiency of almost 39%. Thin film CdTe cells, which are widely available commercially, are rated at an efficiency of 21%.

The efficiency of the system can be further improved using positive displacement pumps, diaphragm pumps and progressing cavity pumps were capable of pumping efficiencies of up to 70%. A Maximum Power Point Tracking [12] system could be utilised for further increasing the efficiency of the PV water pumping system by converting the high voltage from the DC output of the PV panels to a lower voltage for charging of batteries. The power degradation in PV modules was established to be 0.8% per year as a result of prolonged field exposure and requires further research [13]. While automatic tracking helped in increasing the efficiency, the cost was too high; instead double axis

**Table 1**  
PV cell efficiency at 25 °C and 1000 W/m<sup>2</sup> [11].

PV cell materials type	Efficiency (%)	PV cell materials type	Efficiency (%)
<b>Silicon</b>		Dye mini module	10.7 ± 0.4
Si (crystalline)	26.3 ± 0.5	<b>Thin-film chalcogenide</b>	
Si (multi-crystalline)	21.3 ± 0.6	CIGS (cell)	21.0 ± 0.6
Si (thin-film minimodule)	10.5 ± 0.3	CIGS (minimodule)	18.7 ± 0.6
<b>III–V cells</b>		CdTe(cell)	21.0 ± 0.4
GaAs (thin film)	28.8 ± 0.9	<b>Multi-junction devices</b>	
GaAs (multi crystalline)	18.4 ± 0.5	Five-Junction Cell (bonded)	38.8 ± 1.2
InP (crystalline)	22.1 ± 0.7	InGaP/GaAs/InGaAs	37.9 ± 1.2
<b>Dye sensitised</b>		a-Si/nc-Si/nc-Si (thin film)	14.0 ± 0.4
Dye	11.9 ± 0.4	<b>Si (amorphous)</b>	10.2 ± 0.3

manual tracking systems were suggested to be implemented which helped improve the system efficiency by 20% and were relatively cheaper. The main factors affecting PV panels were dust accumulation, over heating of PV modules and fluctuation of solar irradiation. To counter the inconsistency in solar irradiation carefully modelled battery systems were suggested to be implemented to ensure economic viability, spraying with water assisted in both dust clearance and cooling of the modules.

Sontake and Kalamkar [9] conducted a comprehensive review of PV water pumping systems encompassing literature from various fields of engineering between the years 1975–2014. The review breaks down the different types of technologies based on site specific designs, site specific performance, performance of the solar pump using different motors, different ratings of PV panels and investigating implement MPPT models. Cost reduction methods were also investigated, and it was found that 60% of the cost could be reduced by manufacturing PV panels locally. The study also discussed new concepts and design ideas that could be utilised to enhance the effectiveness of the PV panels, reducing the complexity as well as reducing the costs focusing on low capacity PV pumps.

In the review, regions in Africa showed great promise, especially northern and Sub-Saharan African regions, in both Sudan and Egypt PV water pumps was seen to be able to efficiently pump water and provided low operating costs. In Nigeria, the pump performance was seen to be satisfactory providing 20 m<sup>3</sup>/day [14]. Research in Algeria also provided positive results concluding that PV water pumps could sufficiently pump water for small scale farm sized under 2 ha [15]. That said, site specific research was proposed, as the performance of pumps was seen to be 10–25% less than that claimed by the manufacturer [16]. The Various parameters that influence PV pumping technology has been summarised as per Fig. 2.

The research estimates a range of optimal power output that can be produced at a solar radiation of 1000 W/m<sup>2</sup>, wherein, 1 m<sup>2</sup> panel area could produce 100 W, and 17 m<sup>2</sup> area could produce 900 W output. It was also proposed that diaphragm pumps with DC motor be used for small capacity pumps while centrifugal pumps with induction motor would be preferable for higher capacity pumps [9]. Helical pumps were also shown to be suitable for high heads of over 50–150 m with Grundfos 6SQF-2 pump showing no loss after 3 years' performance [18]. DC motors has been the preference for 80% of the research conducted showing the highest efficiencies with 10% research showing AC motors providing higher efficiencies for higher capacity pumps, however, the increase in efficiency is minimal. Development in DC motors such as Permanent Magnet Synchronous Motors which are brushless motors and use permanent magnets instead of winding rotors compared to conventional DC motors, further elevates the

potential of DC motors.

Research has shown that because of the losses incurred on PV systems, 16% of the work potential of the PV panels are lost [19]. Few ways to reduce this loss has been proposed including the implementation of tracking, cleaning of panels and cooling of the panels as at higher temperatures the panels show lower efficiencies. Furthermore, computer assisted design has been proposed to optimise the various components of the PV water pump system. Optimisation by implementing MPPT for pumps is shown to increase efficiency by 35% [20] and water pumped quantity was increased by 7.4% [21].

Though overheating is an issue boosting with reflectors during days of lower radiation can enhance the power output of the PV system as observed in Fig. 3.

### 3.2. PV irrigation systems

Deveci et al. [22] designed and developed a drip irrigation system that utilises solar PV power for a project in Turkey covering 1000 m<sup>2</sup> and containing over 100 trees, it was considered that it would require 1450 l of water/day. From June to October, the site was irrigated 2 h a day with the help of an automatic timer. The PV panels (generating 132 Wh/day using two 10 W PV panels to generate 12 VDC) charged a battery (14 Ah, 12 VDC) buffer throughout the day during available sunlight using Maximum Power Point Tracker (MMPT) to increase the PV conversion efficiency to operate at the maximum power point of the I-V curve. The DC pump was powered by the batteries providing consistent voltage and hence optimal performance of the pump. While other research considers using of the battery to drive the cost, Deveci et al. argued that utilising the battery ensures that the overall cost of the system decreases by 63%, thus ensuring better payback and hence making the system cheaper overall. This could allow the use of cheaper PV technology. To better understand of the system characteristics, a context diagram is presented in Fig. 4.

Setiawan et al. [23] designed a PV powered water pumping system to supply water in a village in Indonesia. The systems consisted of 32 panels that produced 3200 Wp and operated 2 submersible pumps (Lorentz PS1800 HR-05HL) to provide a flowrate between 0.4–0.9 l/s and a total head of 218.34 m. The system consisted of 4 stacks of 8 solar cells connected in series, with 2 stack connected in parallel feeding each pump. The pumps are in turn connected in parallel to provide the ultimate head. The Project was funded by Ministry of Research and Technology Republic of Indonesia in conjunction with the Ministry of Public Works however, the costs associated with the system are not indicated. The system designed was optimal in providing clean water to the village where previously the inhabitants would use stored rainwater for survival.

Campana et al. [24] devised a novel optimisation process by which PV water pumping systems could be economically optimised for irrigational purposes. A simulation considering the availability of groundwater, water supply, the investment costs, and the revenue from the crop sale has been developed. To prove the effectiveness of this approach, the simulation is applied to an existing PV water pumping system with the results showed positive impact guaranteeing continuous operation, reducing PV array size and thus reducing the investment and thus lowering the payback period. Nine PV modules, positioned at a tilt angle of 42° and –32° surface Azimuth angle, were proposed to produce 1.44 kWp powering a 1.1 kW Centrifugal AC pump. However, as per the simulation, due to the low rate of replenishment of the ground water resource, the specifications of the system had to be downgraded to produce 0.96 kWp, which in turn decreased 18.8% of the investment capital. The study enforced the use of natural groundwater level replenishment so that the cost of foraging for water source can be reduced as well as protect the groundwater source from being over used. Fig. 5 demonstrates the relation between annual profits and pump capacity at US\$ 1/Wp and US\$ 2/Wp and establishes that with adherence to the ground water level constraints,

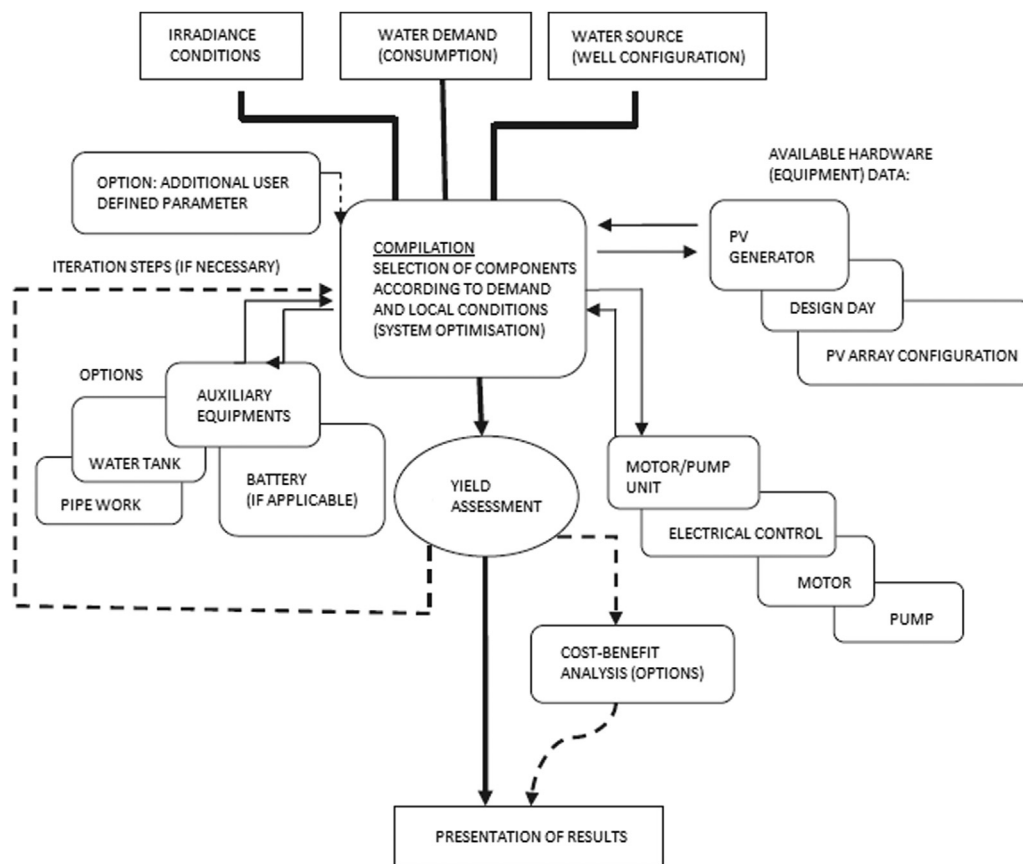


Fig. 2. Parameters that influence PV water pump design [17].

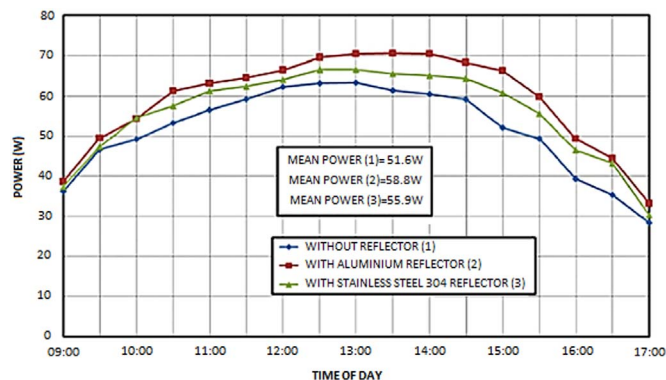


Fig. 3. Power output comparison with and without solar irradiation boost [9].

the most feasible solution is a PV water pump just shy of 1 kWp at US\$ 1/Wp.

López-Luque et al. [25] proposed a standalone design for a direct pumping PV system for the irrigation of olive orchards optimised with the help of a simulation model for “deficit irrigation” leading to reduction of cost and water savings. The model simulates, the power of the PV system, the balance between energy and water of the irrigation system and the yield of the crop. Using this, the cost of operation of the system and the profit margin was evaluated. The system allowed for a certain level of water stress on the crops if the yield of the crop was not affected. The demand was reduced and thus the system implemented could be cheaper while at the same time saving water. On evaluating a case study in Spain, the optimal power requirement was evaluated as 150 W/ha for 40 m head, 250 W/ha for 60 m head and 300 W/ha for 80 m head for “deficit irrigation” wherein, the plants are irrigated lower than the prescribed amount which

requires a thorough understanding of the plant's yield response. For full irrigation, the results were 300 W/ha for 40 m head, 400 W/ha for 60 m head and 600 W/ha for 80 m head. The system was found to be feasible for “deficit irrigation” but not full irrigation. “Deficit irrigation” tactics also provided 4–6% of water saving.

Hossain et al. [26] studied the suitability of utilising solar powered irrigation in Bangladesh for the cultivation of Rice, brinjal (eggplant), tomato and wheat both in the technical and economic sense. Pumps were stationed in 4 different places and the performance of the pumps were tested measuring the solar radiation, voltage and current generated, flowrate and the head. The drip and furrow methods were implemented in the research. Eggplant and tomatoes were tested using both drip and furrow method while wheat was tested using just the furrow method, the method used for rice cultivation was not specified in the study. Around 0.5 ha land was considered for all crops except for rice which was cultivated in a 0.2 ha land. The pump was powered by Solar panel providing between 1050 and 1440 Wp. Considering all four locations, the lifetime profit to cost ratio of utilising the PV powered irrigation system was determined for each crop with tomato, brinjal and wheat shown to be between 2.22–2.34, however, rice was merely 0.31. This is as per pump cost of US\$ 5700, a life of 20 years and an average discharge of 100 l/minute. 50% of water was saved using drip irrigation of tomatoes and brinjal. Rice cultivation, however, was not seen as economically viable using PV powered irrigation system method due to the low yield, high water requirement (3 times that of the other products).

Kumar et al. [27] conducted field experiments and testing of a gravity-fed type drip irrigation system powered by solar PV for a small land of 18 m × 6 m area. The study was conducted in Central India. Water from a pond was pumped to a storage tank (1000 L) and applied for irrigation as per the Star Configuration irrigation system which contains four micro tube emitters joined at a central connector

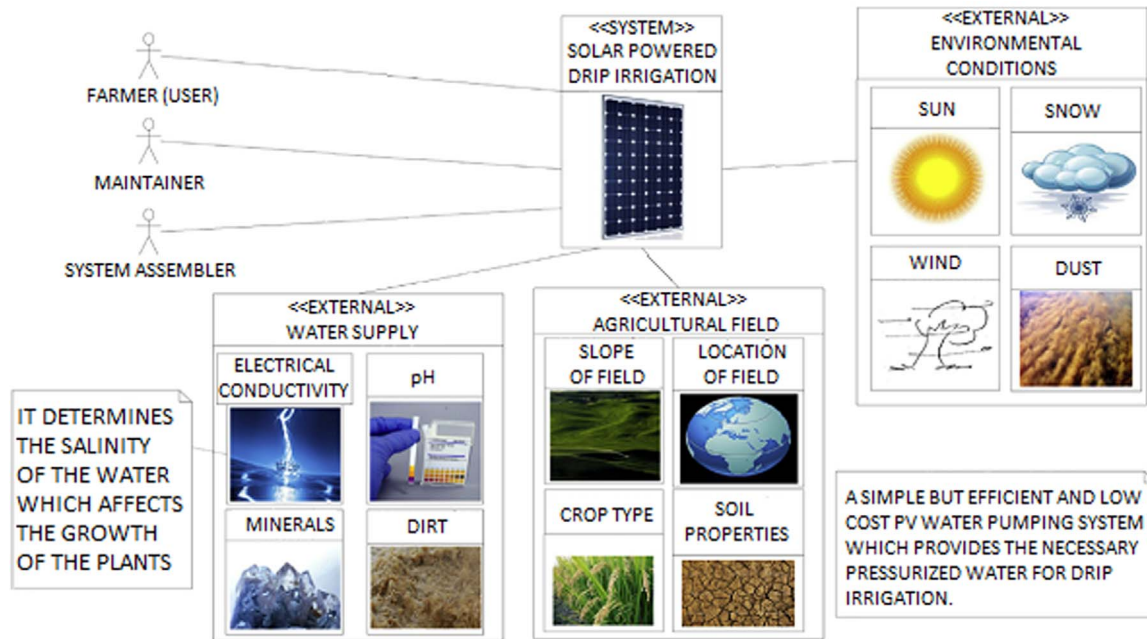


Fig. 4. Context diagram representing drip irrigation system powered by PV [22].

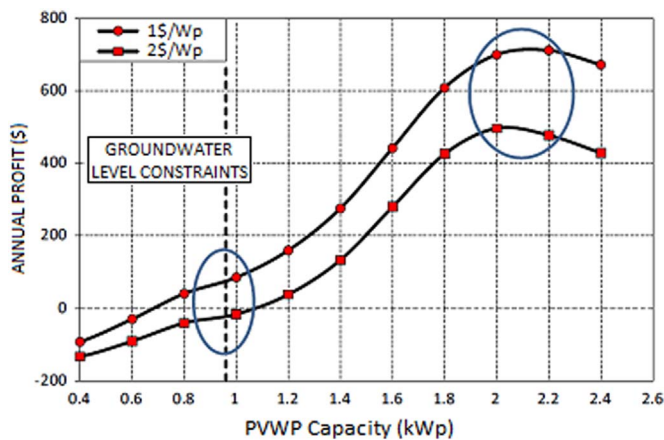


Fig. 5. Pump capacity vs annual profits with constrained groundwater levels [24].

accessing water from the sub main through another connecting microtube [28]. The pumping system consisted of 148 W solar panel and a minimum power voltage of 15 V, power current 4% A, fitted with

a 12 V battery with a capacity of 10 A for 5 h, an AC type inverter powering an AC pump of 60 W drive, input power of 110 W and discharging at 15 l/min. The overall cost of the set-up was US \$410 including the cost of solar panels, solar charge control unit, battery with accessories, inverter, pump, overhead tank and civil works. See Fig. 6 for the schematic diagram of the set-up. It was established that this system would be enough to irrigate 0.2 ha of land. As a very small test area was considered, the overall head loss during the conveyance of the water from the storage tank to the crops was almost negligible. The system was recommended to be run between the times of 11 a.m. and 3 p.m. when maximum irradiation could be used and that would be enough for the irrigation needs for a day.

Reca et al. [29] conducted a feasibility analysis of the profitability of a direct pumping PV system that would work standalone and be used for irrigation in Spanish greenhouses (18 °C and 3000–3600 sun hours per year, 0.75 ha/greenhouse, drip irrigation, required 3 l/hour, 40 m pump head, 8720 W/ha), see Fig. 7. A simulated model comprised of PV power generation, pumping management, and irrigational water requirements was prepared. Several sectors were considered and two strategies of management of irrigational services were established either to irrigate each sector one by one or to group irrigate sectors.

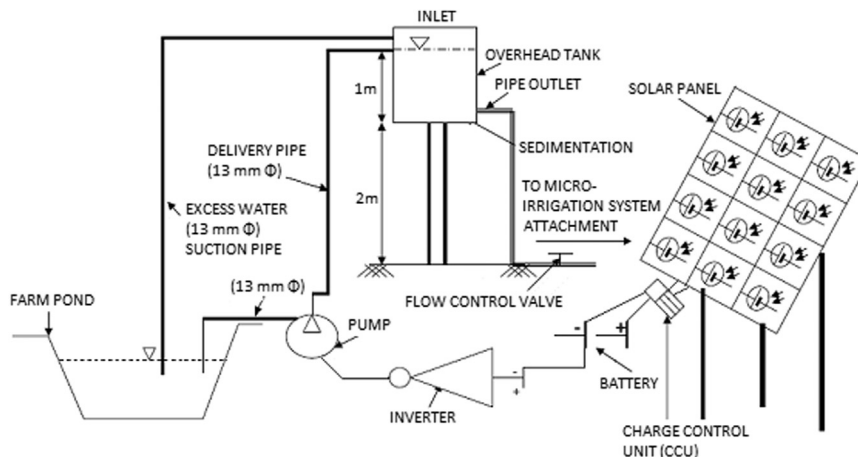


Fig. 6. Schematic diagram of micro-irrigation system powered by solar PV [27].

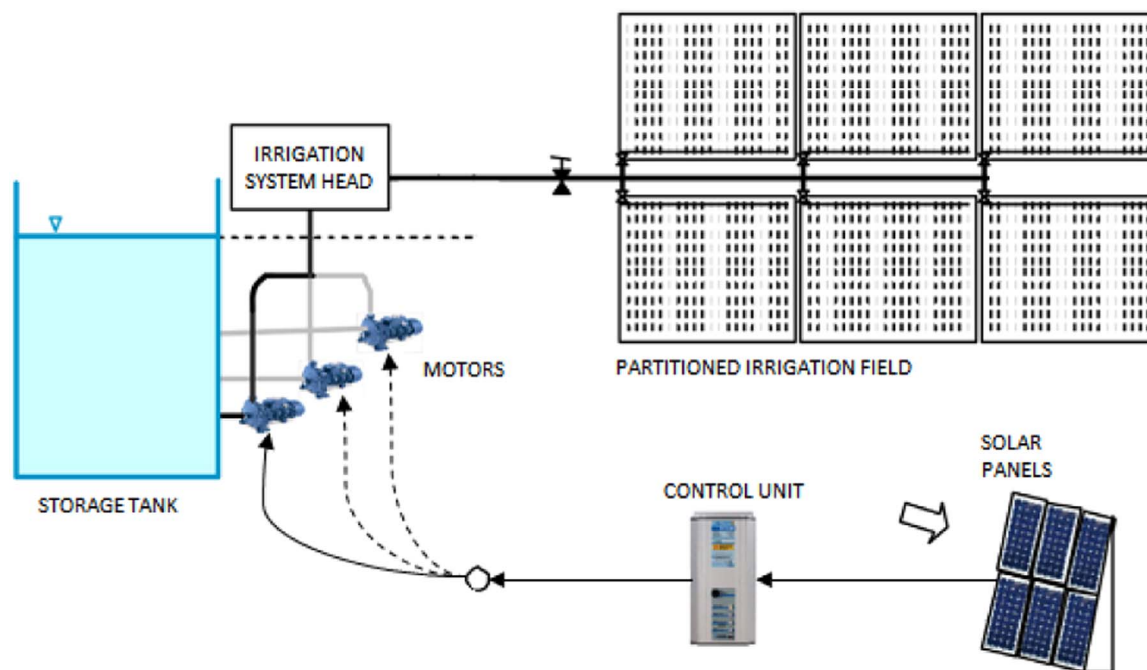


Fig. 7. PV irrigation system management layout [29].

The simulation proposed that irrigation of one sector at a time was more profitable than group irrigation, as that would require bigger and more expensive pumps. Profit was obtained by assigning 4 sectors in a hectare, however, the profit margin and efficiency of the system was still low with the highest Net Positive Value (NPV) obtained with 6 sectors, after which the NPV decreased. The profitability of the system could be improved if, the excess produced electricity from the PV panels could be used for other purposes.

### 3.3. PV irrigation systems performance

Chandel et al. [30] published the analysis of degradation of a mono-C-Si PV module (33 W rated, 1 m × 0.38 m) that had been exposed in the field for 28 years in the western Himalayan region of India. The PV module was used for a direct coupled PV water pump and the study's main objective was to identify the impact on the water pump caused due to the PV degradation. Visually the defects identified by the study were discolouration, oxidation of anti-reflective coating and the grid fingers and bubble formation causing delamination in the back sheet. Using a 1 m × 0.38 m sized PV panel producing 373 W, a head of 10 m was obtained with a discharge of 5500 l/h. The degradation for this system was measured to be 1.4% per year using visual, thermal imaging and indoor I-V characteristic measurements of modules under a sun simulator. The results coincided with studies undertaken previously, however, the results showed increase in open current voltage which was expected to reduce, this aspect requires further investigative study.

Yahyaoui et al. [31] modelled the management of an autonomous watering system using “Fuzzy Logic” [32] for energy and water for drip irrigation in a semi-arid district for production of tomatoes supported by PV panels and batteries. The water volume needed by tomatoes was first evaluated during the production cycle across March - July, then the PV panels, batteries and water pumps would be controlled based on the energy availability. The algorithm considered the semi-arid conditions depicted in Tunisia for the irrigation of 10 ha land at 200 m<sup>3</sup>/h before sunrise. Based on the study only 20% of the required power came from the battery, while 80% from the PV panels with a control system regulated the usage of power and helped elevate the battery life and increased the overall efficiency of the system.

Rawat et al. [33] reviewed the different ways of modelling and

optimisation of size and design methodologies of standalone and grid connected PV water pumping systems in India. A PV system including an array of PV cells, converter, inverter and a battery storage system is considered. To ensure that the PV system performs optimally, equations have been developed for modelling and design methodologies. The study concludes that PV systems are better sized when long term data of the site is available, numerical methods for sizing the PV systems are as good as the data available. In the case of inferior data, more intelligent systems need to be implemented to for better optimisation, such as “fuzzy logic”, however these techniques are more complex and would require more expenses. The other factors to efficiently size PV systems are the efficiency curve of inverters, Load management and the motor torque.

Jones et al. [34] analysed the economics behind the use of PV water pumping at variable speeds in conjunction with a desalination system without the use of energy storage for agriculture. See Fig. 8 for various configurations suggestions of a desalinated water irrigation pump system. For comparison, the PV system was put up against diesel systems and systems utilising energy from the grid. The study was conducted in Jordan and focuses on 15–120 kW size for desalination of water salinity range of 1500–7500 ppm and at depths of 25–100 m. The study found that using large system sizes greatly reduces the price of desalination with a 15 kW system costing US\$ 1.55 /m<sup>3</sup> while a 111 kW system costing at US\$ 0.7 /m<sup>3</sup>. PV technology was seen to be less economical than grid-powered systems but more economical than diesel powered systems. Furthermore, PV systems was shown to be more profitable for crops that provide high returns and low water consumption, shallow groundwater levels and low salinity levels.

Muhsen et al. [7] examined water pumping systems utilising photovoltaic technology featuring the modelling, design procedures, control strategies, field performance, reliability and feasibility of PV systems. Based on the review conducted, the highest system efficiency of 7% was observed for a system using helical pumps providing 0–8.4 l/min of flowrate in the Amarillo Texas region [35]. The highest average flowrate of 2600 l per hour was quoted to be generated for a 990 Wp system in Algeria with 11 m head giving a productivity of 9498.030 m<sup>3</sup>/kWp per year, the efficiency of the system was 1.299% without shading and 0.83% with shading [36]. The most extensive research was conducted on a 3–5% efficient system with a size of 2kWp

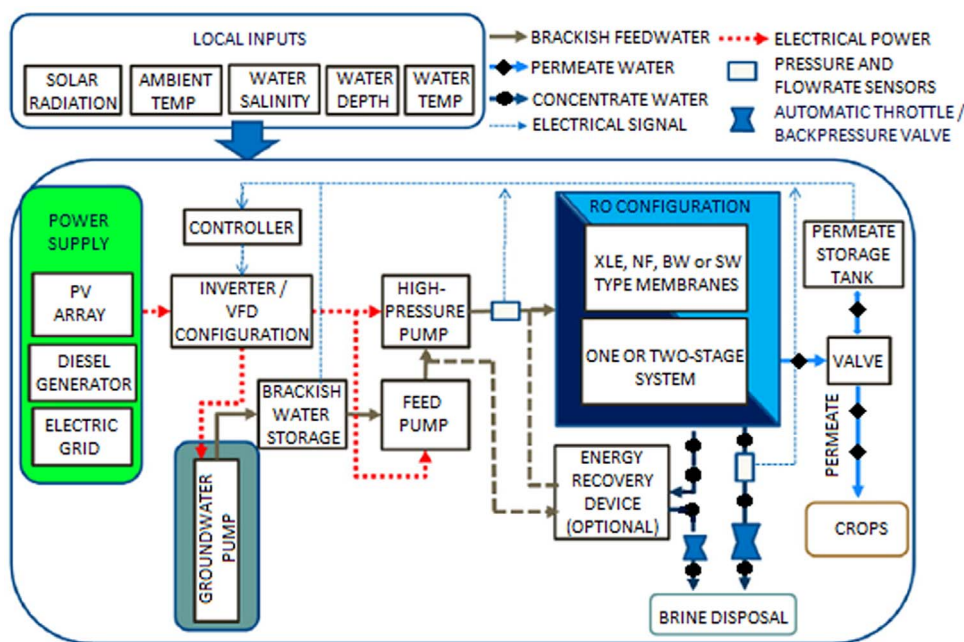


Fig. 8. Various configurations for set up of desalinated water pumping system [34].

capable of water head of 5–125 m and was conducted in seven different countries however, this research was done 20 years ago [37]. On average, the overall efficiency of systems is about 3.4% with an average annual water pumped being 6580.611 m<sup>3</sup>/kWp. The study highlighted that the most effective way to size the PV modules is using numerical sizing and control works utilising traditional MPPT.

Campana et al. [38] Investigated the most suitable locations in China where PV water pumping systems could be implemented for irrigation of grasslands. The assessment was made using an optimisation model of renewable energy systems that was spatially explicit based on overall minimisation of cost of the supply chain. The study demonstrated that PV water pumping systems provide a high potential for the improvement of forage productivity to meet the local demand. Land area of 1 ha was considered for a micro irrigation system and a hydraulic head of 20 m was established powered by a 1.44 kWp PV panels [39]. It was established that an increase of 25% in the yield of forage from grasslands resulted in 300% increase in the production of forage using PV water pump irrigation systems.

Elkholy and Fathy [40] developed an Artificial Neural Network (ANN) trained by a Teaching Learning Based Optimisation Algorithm (TBOA) [41] to obtain maximum power from solar panels by regulating the inverter voltage and frequency. The TBOA is an algorithm designed on the basis of the teacher-student relationship of learning to solve continuous and nonlinear functions to find a global optimal solution. The authors modelled an irrigation system that consisted of a PV array (116 × 71.3271 W connected in series) with a three-phase induction motor that drives a centrifugal pump (220/380 V, 1.1 kW, 50 Hz) for pumping water on MATLAB and Simulink. Based on the simulations undertaken, the efficiency of the system incorporating the ANN-TLBO method was higher than the voltage-frequency control method between 100 and 500 W power generation, however, over 600 W generation, the efficiencies of methods were closer.

Closas and Rap [42] investigated the impacts, opportunities and limitations of PV powered water pumping systems that utilise ground water reserves. The authors show that most projects overlook the true financial and economic costs of the technology and the use of the water resources which adversely affects the environment negatively. The study insists that link between water, energy and food must be balanced and this can only be possible when accurate data is provided. Monitoring of Ground water is deemed paramount so that the sustainability goals of the

technology is met and the livelihood of the future inhabitants are not threatened. The data obtained would be used not only to design the adequate irrigation system, but also can assist in regulation of subsidies and thus avoid “market distortions”. The paper has adequately described key aspects often overlooked when new irrigation technology is being developed this is true for every irrigation system, however, the authors have focused only on PV powered systems.

#### 3.4. PV irrigation technology in comparison to other technologies

Campana et al. [43] discussed the technological and economic feasibility of renewable energy systems for irrigation and conservation of farmlands in China, comparing PV water pumping technology to wind powered water pumping systems. Based on the irrigation water requirement (calculated as per FAO [44]), a model was developed to calculate the size of PV and wind powered systems based on varying solar irradiation and wind speeds respectively. A storage system or battery was considered as they are shown to impact adversely to the cost. The alfalfa plant was considered for the simulation model which has a plant density of 75,000 plants per hectare, 90% canopy cover, growing between May to September (140 days). The PV system produced a capacity of 2.9 kWp (at 2 \$/Wp) while wind power generated 2.6 kWp (at 5.5 \$/Wp) to power a 2.2 kW pump with the PV water pump irrigated land having higher produce than that irrigated with wind power. The study established that depending on the site wind powered systems can compete with PV systems, however, PV systems overall have more potential and better performance.

Treephak et al. [45] conducted an economic evaluation to compare PV powered and gasoline powered water pumping systems for irrigation and cultivation of rice. A 1.6 acre of land irrigated for 25 years was considered for the analysis and the fuel cost required for the pumping of water for the cultivation of rice is considered. With the same conditions, PV powered systems consisting of PV panels along with four different configurations are analysed including, AC motor without battery (S1), DC motor without battery (S2), AC motor with battery (S3) and DC motor with battery (S4). See Table 2.

Treephak et al. shows that stirring away from a gasoline powered system, the solar panels would save US \$280 every year of fuel cost. From the analysis, a DC motor system without battery provides the highest economic value.

**Table 2**  
Economic analysis of different PV systems [45].

Scenario	Motor size (W)		Battery	Inverter (W)	Solar panel	Estimated cost	Payback period (years)
	AC	DC					
S1	750	–	–	1500	250 W (× 6)	\$2800	10.1
S2	–	500	–	–	250 W (× 4)	\$2000	7
S3	375	–	85 Ah (× 4)	1200	295 W (× 4)	\$2800	13.5
S4	–	250	60 Ah (× 4)	–	295 W (× 3)	\$2200	9.3

Sarkar and Ghosh [46] presented a techno-economic analysis of solar powered pumps in Bangladesh. They also provided a list of 108 functioning solar PV pump systems across Bangladesh as an initiative by Infrastructure Development Company Limited (IDCOL). The authors compared PV technology with diesel generators. For a PV system between 0.1 and 20 kW the PV array cost will be US\$ 1000/kW, Inverter cost of US\$ 500/kW and Battery cost of US\$ 300/kW compared to US\$ 600/kW for Diesel. For maintenance, the study suggests that the diesel generator system would cost US\$ 438/year compared to US\$ 80/year for the PV system. The payback period of the PV system was calculated to be 9.33 years producing a benefit to cost ratio of 1.08. The authors have not provided a parallel calculation for the Payback period of a diesel system which may have shown a better comparison, however, a greenhouse gasses (GHG) reduction analysis has been conducted showing that there is a net reduction of 0.865237 t of CO<sub>2</sub> using a PV powered system when compared to diesel system. The GHG analysis however only considers operational emission hence sighting GHG emissions of Solar PV system to be zero.

Gopal et al. [8] conducted a review encompassing different renewable energy source water pumping systems for water pumping including solar PV, solar thermal, wind energy, biomass and hybrid renewable energy systems. The paper describes the limitations of each system and identifies further research that can be undertaken.

With respect to PV technology, a payback period of 6 years was calculated, sustainable for domestic applications up to “medium head” requirements. In drip irrigation applications, it was observed that PV technologies was more effective especially in rural areas, for grassland conversation and small scale irrigation applications. The potential of PV panels to be able to considerably reduce the CO<sub>2</sub> emissions over its 25 years of operation is also envisaged [47].

The main issues that plague PV technology are its affinity to be affected by the intensity of solar radiation, the change in temperature and the velocity of water flow. Energy storage costs are also identified to be very high however, use of a storage tank boosts the performance. One fact the review admits that needs to be addressed is the environmental impact that PV panel manufacture process has, which would be higher for systems using battery for storage. The environmental impact is measured by energy payback time and greenhouse gas emissions. See Table 3.

**Table 3**  
Environmental impact of different types of PV cell types [8].

Type of cell	Energy payback time <sup>a</sup> (years)	Greenhouse Gas emissions (g-CO <sub>2</sub> -eq./kW h)	Lifetime (years)
Mono crystalline	2.5	50	N/A
Multi crystalline	2.0	43	N/A
Cadmium telluride	1.5	48	20
Copper Indium selenide	2.8	95	20
Amorphous silicon	3.2	34.3	20

<sup>a</sup> Energy payback = energy used for manufacture and set up divided by energy produced.

Cadmium telluride PV cells have been shown to have the best environmental impact with the smallest carbon footprint and payback period in comparison to all solar PV technologies [48] with the highest module efficiency of 19.6% [49]. In comparison PV technology is seen 10 times safer than coal fired plants but 4 times higher in comparison to Nuclear and wind turbine power plants [8]. The average Global warming Potential for 1 kWh of electricity is seen consistently higher as calculated from previous literature is 0.078 kgCO<sub>2</sub>-eq for PV technology, whereas both Nuclear and Wind produce 0.02 kgCO<sub>2</sub>-eq [50].

Solar thermal technology, on the other hand, had very less research undertaken and not commercialised due to its low conversion efficiency. Two types of technologies were discussed including, one using vapour power cycles (Rankine Cycle) and the methyl hydride systems. The system efficiencies of vapour powered cycles were very poor ranging from between 0.12% to a maximum of 3% for a 1 m<sup>2</sup> flat collector aperture area working between heads of 6–15 m pumping between 170 l per day to 1400 l per day with the highest operation values observed for lower heads during the summer using R113 as the working fluid [51].

Water pumping systems using Methyl Hydride could provide higher output at 2000 l per day using a 1 m<sup>2</sup> solar collector up to 15 m, but even then, the efficiency was 1.5% [52]. The authors establish that due to the low conversion efficiencies, high costs and environmentally unsafe working fluids; solar thermal technologies fall short of PV irrigation technologies.

Gopal et al. identifies that PV, wind and a hybrid system utilising PV and wind will best suit conditions in India when compared with Diesel technologies. Even though the initial investment for PV hybrid is 9 times more than that of Diesel, the Operational and maintenance costs of diesel is 80 times more than that of PV technologies making it economically feasible for the region [8].

#### 4. Solar thermal systems

Solar thermal systems obtain thermal energy from the sun via a solar collector or a solar concentrated surface. The energy is then transferred via a fluid or directly to either a Rankine, Brayton or Stirling Cycle engine which then converts the thermal energy into mechanical work. The mechanical work produced can be used directly to power pumps, converted to electrical energy for storage, or for powering an electrical pump. Fig. 9 shows a schematic of a solar thermal powered irrigation system. Obviously, direct utilisation of the mechanical power is desired, however, storage of thermal energy is a much more difficult proposition when compared to the storage of electrical output.

Most of the research on solar thermal powered irrigation system utilises the Rankine Cycle system or variations of the same. In this system, a working fluid is circulated through a system of boilers, expanders and condenser. The fluid is initially evaporated at the boiler by obtaining heat from a source, in this case solar thermal energy, it then passes through an expansion device (for example a turbine) which generates the power output and then is condensed to complete the cycle [8]. Rankine cycle systems have demonstrated very low thermal efficiencies (around 1%) and high cost associated with initial investment, maintenance and working fluids [9]. Furthermore these systems

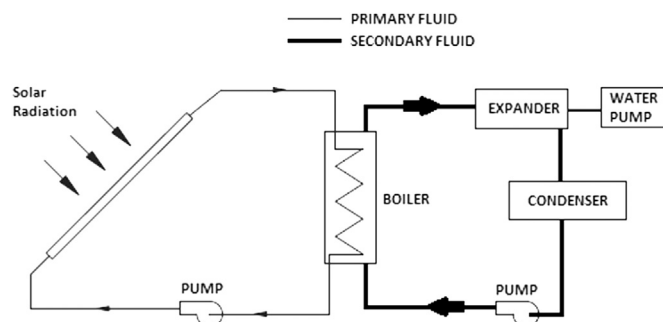


Fig. 9. A typical Rankine cycle solar thermal pumping system [8].

require a significantly larger land space to work with and is very difficult to leakproof the system [8]. These issues have affected solar thermal irrigation research in the recent years, especially as more and more emphasis is being given to the irrigation of smaller farm spaces making this technology unfeasible.

Recently, however, research on medium to low temperature Stirling engines coupled with commercial interest due to the simple construction of Stirling systems has been successful in elevating the technology. Fig. 10. shows a schematic of a Stirling cycle thermal powered irrigation system. A Stirling engine produces mechanical work by utilising cyclic compression and expansion of a working fluid (air, helium, hydrogen, nitrogen) [53] operating at different temperatures and enclosed in a fixed space [54]. The Stirling Engine can achieve the closest efficiency to the ideal Carnot cycle when compared to any other engines [55]. The efficiency of Stirling Engines are calculated to be between 30–40% for maximum operating temperatures up to 923–1073 K at operating rates between 2000 and 4000 rpm [56].

There are three major types of Stirling Engines,  $\alpha$ ,  $\beta$  and  $\gamma$  type differentiated by its configuration. The  $\alpha$ -type engine has two pistons contained in hot and cold cylinders, the  $\beta$ -type engine has 1 cylinder containing a power piston and a diaphragm while the  $\gamma$ -type engine is similar to the  $\beta$ -type engine but houses the power piston separately.  $\gamma$ -type systems have the highest thermal efficiency when compared to the other two systems. Variations of the  $\gamma$ -type engine are the free piston

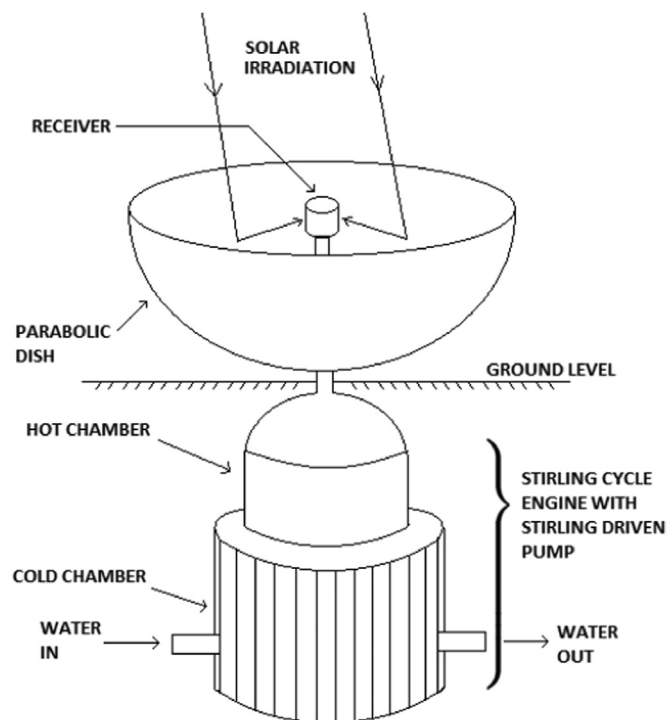


Fig. 10. An example of a Stirling cycle thermal power irrigation system.

engine and the Fluidyne pump [55].

Unlike PV technology, solar thermal technologies for pumping water has not been widely researched in the last 10 years. In fact, no papers were found between 2006 to 2008.

#### 4.1. Solar thermal irrigation technology reviews

Delgado-Torres [57] provided a review of solar thermal heat engines for water pumping. He classified the technologies into two types, conventional and unconventional. Solar energy was first converted into Mechanical energy either by a power cycle or the adsorption/desorption cycle, the mechanical energy was then either converted into electrical energy to be used for a conventional pump or used directly with an unconventional pump design. Among the conventional methods, the Rankine cycle systems were discussed. Rankine systems generally used water as the working fluid, but as time went on various other fluids were used either on their own or sometimes in conjunction. The working fluids tested included, water, sulphur dioxide, ether, chlorobenzene, R11, R113 and HT-43. Flat plate and parabolic collectors were the preferred collector systems as per the research undertaken, however there was also research undertaken on conical reflectors, truncated cones, and wooden boxes with reflector plates.

The largest Parabolic trough collector project was in Egypt in 1913 that used a 60 m long and 4 m wide parabolic trough to pump 27 m<sup>3</sup>/min and delivered 40.42 kW maximum power output [58]. In 1976, in Mexico, a flat plate collector spanning about 2.5 ha included a vapour powered turbine that was used to generate electricity to produce 1000 m<sup>3</sup>/day [59]. The largest parabolic dish installation was made in India in 1987 that used 6 collectors with 9 m diameter each to produce steam at 500 °C at 7 MPa to drive a steam engine rated at 20 kW which was then connected to an irrigation system [60]. The wooden box with reflector plates was also an interesting project, that spanned over 1000 m<sup>2</sup> (1 ha) land area and produced a mean daily power output between 10.29–11.76 kW and a maximum power output of 17.64–23.52 kW generating a discharge of 11.3–12 m<sup>3</sup>/min across a head of 10 m [58]. Among the smaller systems, included a truncated cone with 10 m diameter at the top and 4.5 m diameter at the bottom which could provide 7.35 kW driving a pump to discharge at 6.4 m<sup>3</sup>/min of power by generating steam at 1.03 MPa from a 5 m depth [58].

Most of the conventional systems discussed were too large in size and required a big financial investment. Moreover, the Rankine systems is very complex and would require a lot of maintenance dealing with intricate pipe work, boiler and turbines. The author discussed three distinct alternative methods that could be used to make the technology viable for small scale use. Among the unconventional methods for water pumping, the author discusses three distinct categories which are, vapour cycle systems, liquid piston systems and metal hydride systems. Vapour cycle systems use a simple displacement pump with the water being displaced by steam/ethyl/pentane vapour. A 1 m<sup>2</sup> area flat plate solar collector using such a vapour cycle was able to provide a flow of 336 l/day at 6 m head, 250 l/day at 8 m head and 17 l/day at 10 m head [61].

Liquid pistons is a variation of free piston Stirling engines in which the solid pistons is replaced with liquid to allow lower levels of friction and air tightness, see Fig. 11. The Fluidyne pump is an example of such a system where air is heated and cooled and causes a U-shape liquid column to oscillate and thus cause lifting and suction. In the laboratory, the Fluidyne systems have been able to provide up to 3 kW of power at a temperature difference of 95 °C and pressure of 160kPa and giving 2 m<sup>3</sup>/h pump capacity [62].

The final unconventional method discussed in the paper was using the metal hydride. In this system, metal hydride is subjected to heat causing release of hydrogen, as hydrogen is released the pressure is increased pressing down on the piston. Once the piston reaches the bottom of the cylinder, the metal hydride is then cooled, lowering the pressure and leading to the absorption of hydrogen. The system studied

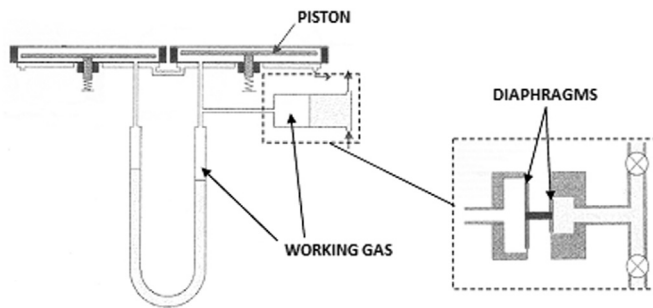


Fig. 11. Liquid Piston pump design using diaphragms [57].

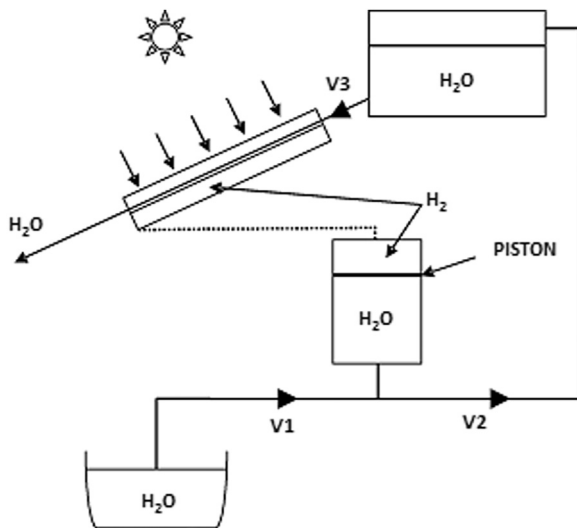


Fig. 12. Metal hydride based solar thermal water pumping system design [52].

worked on the basis of heating and cooling of the metal hydride that could be controlled by a flat plate collector and the water flow generated by the pumping process respectively. A test on a metal hydride system was conducted in Kolkata in 2004 using a 1 m<sup>2</sup> flat collector at a tilt angle of 15°. On a clear day, a maximum of 2000 l of water was pumped to a height of 15 m and on a cloudy day 500 l of water was pumped. In terms of metal hydride use, on a clear day 240 l/day/kg of metal hydride is used while on a cloudy day it is about 60 l/day/kg [52]. The set-up of the system is shown in Fig. 12

The issue with unconventional systems is that the power output of the systems is much lower than those systems using the conventional methods. Added to this the operational costs of metal hydride systems is high as well. However, unconventional systems have the advantage of being used in difficult to access rural areas and the relatively smaller scale systems. This could allow even small scale farmers can benefit from a feasible and viable technology. The classification of conventional and unconventional technologies as established by Delgado-Torrez shall be followed in this paper.

#### 4.2. Conventional solar thermal technologies

Lakew et al. [63] conducted a thermodynamic analysis of a low temperature (60 °C) heat source Rankine cycle functioning in conjunction with a thermal driven pump with supercritical carbon dioxide as the working fluid. A shell and tube heat exchanger (diameter = 5 mm) functioned as the thermal pump removing the need of a mechanical driven pump and thus reducing the maintenance. A continuous source of heat was required for this system. The study showed that a Rankine cycle operating with a thermal driven pump had higher power generation capability than conventional Rankine cycle but an additional low temperature heat source was required for this process.

Table 4

Range of temperature and ratio of concentration of various solar thermal systems [64].

Technology	T [°C]	Concentration ratio	Tracking type
Air Collector	0–50	1	–
Pool Collector	0–50	1	–
Reflector Collector	50–90	–	–
Solar Pond	70–90	1	–
Solar Chimney	20–80	1	–
Flat Plate collector	30–100	1	–
Advanced Flat Plate Collector	80–150	1	–
Combined heat and power solar Collector	80–150	8–80	1-axis
Evacuated Tube Collector	90–200	1	–
Compound parabolic collector	70–240	1–5	–
Linear Fresnel Reflector	100–400	8–80	1-axis
Parabolic trough	70–400	8–80	1-axis
Heliostat field + Central Receiver	500–800	600–1000	2-axis
Dish Concentrators	500–1200	800–8000	2-axis

Hence in this method, there was a requirement for a heat source for the boiler (100 °C) as well as a heat source (60 °C) for the pump. While the heat source for the boiler was the same in both the thermal pump driven Rankin cycle and the mechanical pump driven Rankine cycle, the thermal pump did not require maintenance, had lower noise levels and vibration and maintained a lower rate of efficiency deterioration when compared to mechanical pumps. However, in terms of cost it was more expensive due to the requirement of heat exchangers.

Tchanche et al. [64] reviewed the various applications of using organic Rankine cycles for generating power from low-grade heat. The study considers co-generation systems, water heat recovery systems, desalination systems as well as solar thermal power systems. Organic Rankine cycles utilised refrigerants and hydrocarbons as the working fluid instead of water as Rankine cycles using water were more complex and utilised expensive turbines which are also at high risk of erosion. Furthermore, water needs to be superheated so that during expansion the water does not condense which in turn means there is excess pressure in the evaporator. The authors listed the temperature ranges and concentration ratios of different collector systems as per Table 4. Dish concentrators provided the highest temperatures with the least footprint. Without a tracking system Evacuated tube collectors and parabolic collectors are shown to have the highest concentration ratios.

One of the more comprehensive systems discussed in the study included an Organic Rankine Cycle system consisting of a 60 kW propane boiler, compact brazed heat exchanger, air compressed diaphragm pump, radial flow turbine at 65,000 rpm and a high-speed actuator working at relatively low temperatures between 93 °C in the inlet (81 °C at the evaporator) and 38 °C at the condenser with n-Pentane as the working fluid producing a mass flowrate of 0.1 kg/s, power output of 1.44 kWe and costing US \$25,880 with 37% of the cost attributed to the cost of the turbine-generator [65]. The other systems discussed, used different mid to high range collector systems and tested various types of working fluids. Hybrid systems with collectors and gas/diesel burner systems were also considered.

Solar Ponds were also discussed with large to medium size power plants shown to be constructed and operated in Israel, Australia and the USA. Systems working on the principal of Organic Rankine Cycle for pumping of water for desalination and distribution were also studied but the size of these systems were large for consideration for small scale irrigation.

Low grade conversion systems investigated in this paper were investigated specifically for ocean thermal energy conversion to function offshore at low temperatures and function as a total resource

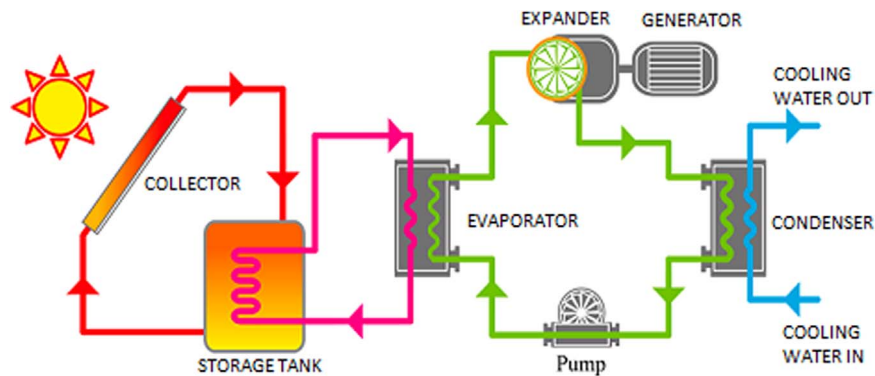


Fig. 13. Solar powered organic Rankine cycle system [66].

system. These systems are good for off the grid power solutions for remote areas, however, the size and costs associated with the systems will be viable only if the technology is implemented on a community level and not individual level.

Baral et al. [66] performed a thermo-economic analysis and experimentation of a small-scale organic Rankine cycle system that was powered by solar energy for power generation in rural areas. The power output from the designed system ranged between 400 W and 1.38 kW during the year with the maximum output in April. The system is a typical organic Rankine cycle system using refrigerant R245fa as the working fluid and 15 evacuated tube solar collectors would provide hot water 90 °C to 120 °C. see Fig. 13. The selling cost for the technology was found to be US\$ 0.68 and at that price the payback period is 19 years for operational components most of which have a life time of 20 years. This has been calculated as per the prototype tested, however, a subsidised development programme can assist in fine tuning the technology and thus reducing the cost of the technology. Even then, the technology would not be suitable for independent small scale farmers.

Baral and Kim [67] analysed the economic viability of a standalone organic Rankine cycle system that functions on solar thermal energy to pump water for drip irrigation in rural Nepalese area. The authors performed experiments based on a prototype and analysed the economic viability of the system based on the solar radiation data described in Fig. 13. Economic assessments were carried out for 1 kW and 5 kW systems and the cost of hot water (at 40 °C) was shown to be between US\$ 1.86/m<sup>3</sup> and US\$ 2.47/m<sup>3</sup> for a 1 kW system and 150 m pumping head pumping 2190 m<sup>3</sup> per year, while the 5 kW system pumped 11,100 m<sup>3</sup> per year. Increasing the size of the system and decreasing the pumping head was shown to reduce the cost generating a profit index of 1.6 with a payback period of 8 years at the above costs of selling water. Such a system is viable for a rural community service but not for independent small scale farmers.

Moonsri et al. [68] designed a thermal water pump functioning on hybrid energy input for pumping water from a shallow well to produce hot water in Thailand. The systems consisted of a 2.1 m<sup>2</sup> solar collector at an inclination of 14° made of copper plates and tubes and a 2000 W electric heater to work in conjunction with the solar collector to produce steam coupled with a system described in Fig. 17 based on research conducted by Sitranon et al. [69]. The system could pump 215 l of water up to 3 m height working on 6.5 MJ of power from the hybrid system. The study compares the system with a solar PV powered system. Though the comparison was not conclusive, it identifies various maintenance issues with the hybrid system including the erosion of rubber seals, valves and heat loss. PV systems disadvantages are highlighted in terms of performance loss at high temperatures, expensive battery and the environmental impact of producing PV panels.

Bataineh [70] investigated the performance of a water pumping systems powered by solar thermal energy. Recent developments in

solar thermal systems were also presented and methodologies to further enhance the energy conversion were proposed. Set in Jordan, a system working on the principal of the Rankine cycle in conjunction with parabolic trough collector was studied using mathematically simulate models. Considering a 526 m<sup>2</sup> collector area, producing 30 kW energy, 20 years of operational life of the system, 6% maintenance cost per year, US\$ 250/m<sup>2</sup> being the cost of the solar field and US\$ 60,000 the cost of the steam turbines, the cost of solar energy amounts to US\$ 0.075/kWh which in comparison to diesel is 0.082/kWh. While the technology is more cost effective than diesel generated, it is still more expensive than PV and requires a large area. The investment cost is also very high making it unsuitable for rural areas.

#### 4.3. Unconventional solar thermal technologies

Mahkamov and Orda [62] performed a preliminary analysis of the working process of solar thermal water pumps designed similar to a free-piston Stirling Engine. The system uses a fluid piston that claims to overcome issues of instability that were faced by conventional fluid piston pumps by including a new diaphragm setting and reducing the dead space in the hot cylinder, cold cylinder and regenerator. They discussed in their paper that solar thermal water pumps were low maintenance and low cost systems that could provide pumping capacities of 0.2–1 m<sup>3</sup>/h and a dynamic head of 1.5–5 m with an air-steam mixture as the working fluid. The study proposed a mathematical model to simulate the internal processes associated with liquid piston engine. The mathematical model was then compared with a laboratory prototype and the parameters were mostly within 5–10% of the predicted models but compressor volume was recorded over 20% higher than that predicted.

Kurhe et al. [71] designed a heat engine using organic working fluid (acetone) to provide 20 L/h of water per stroke and an operating head of 5 m. The thermal water pump cycle functioned at a working temperature of 85 °C to produce a system efficiency of 0.25–0.5%. The engine used a chemical inert membrane that was displaced due to the pressure developed by the working fluid to pump water. The pressure of the working fluid was regulated using a heat exchanger where hot and cold water was pumped into the evaporate and condense the working fluid respectively. See Fig. 14. The efficiency of the system was low due the loss of heat through the membrane at the water interface. The need for work input necessitates the use of a separate power source.

Jokar and Tavakolpour-Saleh [72] introduced a novel active low temperature differential pump that is powered predominantly by solar thermal energy and operates on the basis of the Stirling cycle. The proposed system works with a liquid piston to provide effective sealing while reducing friction generally associated with solid power pistons and the cylinder encasing the piston. A flat plate solar collector with a reflecting surface is the heat source while the heat sink is a water-cooled surface and air is the working fluid in the main chamber that

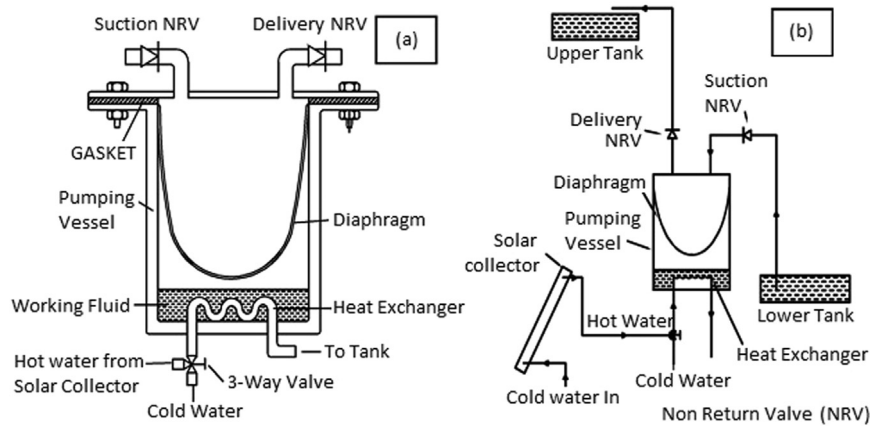


Fig. 14. (a) Pumping vessel assembly (b) Full system schematic [71].

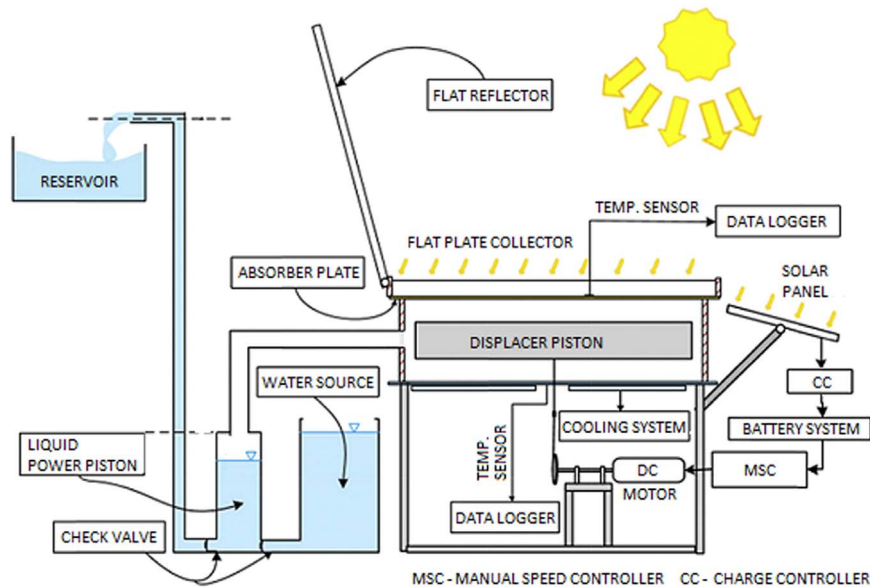


Fig. 15. Solar powered low temperature differential stirling pump [72].

houses a displacer. A DC motor powered by a small battery and PV system controls the motion of the displacer piston to allow for adjustment of the working frequency to account for the pressure variation of the working fluid. For more controlled system, pressurised helium is recommended as a working fluid. The PV system also assists in initiating the displacer piston, as displayed in Fig. 15.

A mathematical model was prepared and compared with small scale experimental results with the model results closely matching the experimental data. This is a novel idea of assisting the displacer piston, however, using the PV module and battery makes it very expensive.

Date and Akbarzadeh [73] conducted a theoretical study of a water pumping system powered by a solar pond and implementing a novel thermodynamic power cycle. The study proposed the system as an alternative to electrical pumps used in salt farms, that works at a temperature difference of 60 °C and acetone as the working fluid. The study introduced a two-stroke thermal powered pump cycle that extracts the work at the same time the working fluid is evaporated at a constant temperature while during the condensation the water that is being pumped adds the work on the working fluid.

The study proposes a hybrid system where the pump is thermally powered and all the auxiliary power for sensors, valves and the working fluid pump comes from a battery and PV system. The condenser and heat exchangers are contained within the solar pond system, as shown in Fig. 16. The analysis proposes that at 10% heat extraction of the annual average

global solar radiation, a head of 22 m can be anticipated for operation up to 338 days of the year pumping 0.53 m<sup>3</sup> of water per m<sup>2</sup> of solar pond area per day. The research goes on to establish that with a floor area of 5200 m<sup>2</sup> of solar pond 2800 m<sup>3</sup>/day of salt water could be pumped from depths between 2–10 m. For this, a 20 L stroke volume will be required in conjunction with 0.01 m<sup>2</sup> heat exchanger and 0.1 m<sup>2</sup> condenser.

The thermal pump proposed can theoretically replace electrical pumps, however, the costs and practicality associated with the technology required experimentation work and further study.

Sitranon et al. [69] conducted a parametric study of the suction head assembly of a thermal water pump with steam as the working fluid and discussed its applications. The study analysed the amount of air that is required to be added to the steam working fluid and looked to shorten the cooling time by employing direct contact cooling. A 2-stroke liquid piston powered by an electrical heater was used to provide consistent heat source to the heating tank to transfer water from a well to a storage tank, as shown in Fig. 17. The study suggests that using air in conjunction with steam as the working fluid will lower the working temperature and thus make it more suitable for solar thermal use. Tests were conducted in Thailand and the results matched that of the simulation model used. At a temperature difference of about 60 °C, 123.9 L of water was pumped requiring 19.73 MJ of energy to provide a mean suction head of 6 m and a discharge head of 1 m.



**Table 5**  
Review summary of Solar PV water pumping.

Author	Location	Function	Flowrate	Head	PV panels	Power out avg	Battery	Farm size	Cost
Deveci [22]	Turkey	Trees 2 h irrigation	610 l/h	1 m	2 × 10 Wp	132 Wh	Yes	–	\$582
Campana [43]	Mongolia China	Alfaalfa	50 m <sup>3</sup> /ha	40 m (TDH)	–	2.9 kWp	–	–	Investment min - \$0.8/Wp max - \$2.0/Wp
Campana [24]	Mongolia China	Alfaalfa	3.9 m <sup>3</sup> /h	5 m	6 × 0.96 kWp	–	–	–	\$2/Wp
López-Luque [25]	Almeira Spain	Olive Trees	2 m <sup>3</sup> /h	40 m 60 m 80 m	–	150 W/ha 250 W/ha 300 W/ha	–	250 trees /ha	\$2.14/Wp
Chandel [10]	– Madina Saudi Arabia	Orchard –	3.4–3.8 l/h 22 m <sup>3</sup> /day	–	– 24 Modules 8 series 3 parallel	900 Wp –	– –	– –	– –
	Gunung-kidul India	water Supply	0.4–0.9 l/s	1400 m	32 PV Panels	3200 Wp	–	–	–
	Spain Algeria	Orchard –	161 m <sup>3</sup> /day 60 m <sup>3</sup> /day	– 14.5 m	– –	6 kWp –	– –	10 ha –	– \$0.04 /m <sup>3</sup>
Chandel [30,74]	Himachal Pradesh India	Test	5500 l/h 4929 l/d <sup>a</sup>	–	12 mono-C-Si PV modules	396 Wp 235 Wp <sup>a</sup>	Yes –	– –	– –
Kumar [27]	Hyderabad India	–	900 l/h	4.5 m	1.44 m <sup>2</sup>	148 W	Yes	2 ha	\$410 (full system)
Hossain [26]	Dhaka Bangladesh	Brinjal Tomato Wheat Rice	100 l/min	33.5 m	1050 Panels with tracking	1440 W	Yes	520 m <sup>2</sup> 520 m <sup>2</sup> 496 m <sup>2</sup> 220 m <sup>2</sup>	\$5660
Bengh-anem [75]	Saudi Arabia	Test	–	50–80 m	PV array of 24 mono crystalline solar cells (8S × 3P)	1800 Wp	No	–	–
Treephak [45]	Thailand	Rice	15 m <sup>3</sup> /h	3.9 m	250 W × 6 - AC 250 W × 4 - DC 295 W × 4 - AC 295 W × 3 - DC	1500 W 1000 W 1180 W 885 W	No No Yes Yes	0.5 ha 0.5 ha 0.5 ha 0.5 ha	\$2800 \$2000 \$2800 \$2200
Yahyaoui [31]	Brazil	Tomato	200 m <sup>3</sup> /h	–	–	10–10,000 W	Yes	10 ha	–
Reca [29]	Almeira Spain	Tomato	60,000 l/h	40 m	–	600 W/ha	No	1.9 ha	\$2.14 /Wp
Jones [34]	Jordan	Desalination	4000– 15,000 m <sup>3</sup> /ha/ yr	25–100 m	–	245 W	Yes	4–10 ha	\$1.25–\$4.30 /W
Sontake [9]	Nigeria	–	20 m <sup>3</sup> /day	–	60 WP × 28	–	Yes	–	–
	Germany	Portable water	–	5–125 m	90 nos	180 kWp	–	–	–
	Bushland Texas	–	2–8 l/min	3–70 m	–	160 W	–	–	–
	–	–	10–165 l/h	10–16 m	2 × 45 W	–	–	–	–
	–	–	40 m <sup>3</sup> /day	10 m	–	300–500 Wp	–	–	–
Setiawan et al. [23]	Indone-sia	Portable Water	0.2–0.9 l/s	218 m	32 × 100 Wp	3200 Wp	no	–	–
Muhsen [7]	Saudi Arabia	–	600 l/h	50 m	–	0.98 kWp	–	–	–
	Egypt	–	150 m <sup>3</sup> /day	30	–	6.048 kWp	–	–	–
	Algeria	–	6 m <sup>3</sup> /day	–	(4S × 3P), (3S × 4P) BP Saturn	–	–	–	–
	Kairouan Tunisia	–	6.5–30 m <sup>3</sup> /day	65–112 m	–	2.1 kWp	–	–	–
	Ghardaia Algeria	–	4–6 m <sup>3</sup> /day	19–35 m	–	–	–	–	–
	Madina Saudi Arabia	–	< 22 m <sup>3</sup> /day	80 m	(6S × 3P), (12S × 2P), (8S × 3P), (6S × 4P) × 75 Wp	–	–	–	–
	Oran Algeria	–	6–65 l/m	0.6–11 m	–	1.5 kWp	–	–	–
	Tall Hassan Jordan	–	45 m <sup>3</sup> /day	105 m	–	5.9 kWp	–	–	–
	Greece	–	20 m <sup>3</sup> /day	30 m	(2S × 6P) × 51 Wp	–	–	–	–
	Turkey	–	18 m <sup>3</sup> /day 52 m <sup>3</sup> /day	20 m	2 × 230 Wp 8 × 200 Wp	–	–	–	–
	New Delhi India	–	38 m <sup>3</sup> /day	5 m	4S × 5P	–	–	–	–
	Purwodad Indonesia	–	1.44–3.24 m <sup>3</sup> / h	218.34 m	8S × 4P	3.2 kWp	–	–	–
	Louata Tunisia	–	7.7–14.7 m <sup>3</sup> / day	65 m	14S × 3P	2.1 kWp	–	–	–
	Madina Saudi Arabia	–	≤ 33 m <sup>3</sup> /day	50–80 m	8S × 3P	1.8 kWp	–	–	–
	Bejaia	–	43.66–	11 m	6S × 3P	990 Wp	–	–	–

(continued on next page)

Table 5 (continued)

Author	Location	Function	Flowrate	Head	PV panels	Power out avg	Battery	Farm size	Cost
Tiwari and Kalamkar [76]	Algeria	Domestic Use	27.91 l/min	40 m	–	840–2520 Wp	–	–	–
	Nigeria		10–30 m <sup>3</sup> /day						
	India		20,232 L/d						
			23,317 L/d						
			24,374 L/d						
Kabaleci [77]	Turkey	Vineyard	22,130 L/d	100 m	5S × 2P	1020	Yes	–	–
			400 m <sup>3</sup> /d		7S	1040			
					245 Wp Panels connected ((2P) × S) × 2	2000 Wp			
Sarkar [46]	Bangladesh	Farm land <sup>b</sup>	128 m <sup>3</sup> /d	12.8 m	Poly-crystalline Si	3.5 kW	Yes	–	\$ 1800/kW
			373 m <sup>3</sup> /d	9.71 m		4 kW			
			740 m <sup>3</sup> /d	16 m		7.5 kW			
			645 m <sup>3</sup> /d	14.6 m		11 kW			
			300 m <sup>3</sup> /d	35 m		7.5 kW			

<sup>a</sup> Values recorded after 28 years of exposure. Initial value based on capacity.

<sup>b</sup> Only the Lowest and Highest values have been identified in the table out of 108 installations.

Several other studies quote varying values of power output and costs, hence, the conclusion from these studies is that the best way to optimise the cost and design of the PV powered system is to understand the requirements of the crop and perform extensive site survey to analyse the working conditions of the system. The more data available the more efficient the design of the system and thus lower the costs. It is often due to the lack of data that PV systems costs increase as more complex and intelligent systems are integrated into the system. One of the major reasons for the use of the battery is the functionality of the pump. Inconsistent irradiation and thus power output from the PV panels may vary restricting the time of operation of the pumps.

Based on the literature reviews, and considering the case for drip irrigation, the simplest, most cost effective solar PV system is one consisting of cadmium telluride PV module at 19.5% efficiency. The panel combines with a permanent magnet DC motor driven pumps (positive displacement pump for higher heads or diaphragm pump for lower heads) capable of providing 70% pump system efficiency. Using a storage tank instead of battery, this system provides an overall theoretical system efficiency of 13.65%, as shown in Fig. 18. The system will function when solar radiation is available and water from the storage tank can be used for drip irrigational purposes.

That brings us to the drawbacks of the PV technology, one of the major issues with Solar PV technologies is the degradation of power of PV cells due to long term exposure. Generally, the degradation is measured to be 0.8% per year as per climatic conditions in India [30], however, elevated temperatures and humidity in Sub-Saharan Africa may pose further challenge to PV technology. The issue here is that, it is a parameter that has not been extensively studied, hence in pursuit to compensate for the loss of degradation more intelligent systems (such as ANN, MPPT and Fuzzy Logic based controllers) may have to be incorporated and that will drive the cost up. Furthermore, any maintenance or modifications of the system will be expensive if

resources such as replacement cells are not readily available in the region in case of shipping or operational misuse.

Implementing PV technology is costly enough for Farmers. Weak knowledge-exchange and lack of incentives further creates further difficulty for innovative practices [78].

While PV technology is 10 times less harmful to the environment than coal it is still 4 times more harmful than Nuclear and wind turbine power plants [8,50]. Furthermore, the carbon footprint of transportation is also required to be considered for the Sub-Saharan African region as PV panels are not produced in this region.

Accumulation of dust on the Panels, overheating during energy conversion and functioning at higher temperatures are some of the other main issues associated with the reduction of performance of solar panels.

### 5.2. Solar thermal technologies

The data from the reviews of solar thermal technologies have been compiled and presented as per tabularised in Table 6. The data focuses on the irrigation attributes of the system including flowrate and pumping head, the thermal system and power output of the system utilised for irrigation and the cost of the technology. The reviews and data reveal a lack of real life testing to solar thermal technologies hence farm size data is not available for solar thermal technologies for comparison with PV technologies.

Solar thermal powered water pumping technologies can be categorised into two types, conventional pumps and unconventional. Conventional Technologies generally utilise the Rankine Cycle whereas unconventional systems make us of the vapour cycle, metal hydride systems or liquid pistons. Conventional systems are shown to produce more power in comparison to unconventional systems however, conventional systems are generally very large and complex. Because of this and the low efficiency the conventional systems do not pose to be an effective solution. Unconventional technologies on the other hand generally pose lower pumping potential or in the case of Metal hydride solutions, pose high costs.

The most compact type of solar concentrators are dish concentrators which in conjunction with a double axis tracking mechanism can provide up to 1200 °C which is also on the high cost side. At low costs the options include the flat plate / reflector collectors capable to provide up to 100 °C temperatures. In the median Liner Fresnel collectors provide both a low cost and high temperature potential of up to 400 °C. The most frequently used collector technology however is the Parabolic trough collectors shown in the studies capable of providing temperatures up to 500 °C with a single axis tracking mechanism [64].

The organic Rankine cycle systems are the most common form of

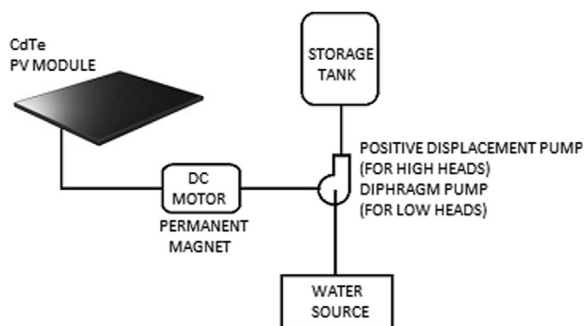


Fig. 18. Schematic of the most effective Solar PV water pumping system for remote rural areas based on literature reviews.

**Table 6**  
Review summary of solar thermal water pumping technology.

Author	Location	Flowrate	Head	Power cycle	Collector type	Temp difference (°C)	Power out avg	Cost
Mahkamov [62] Delgado- Torrez [57]	UK	–	–	Stirling	–	70–35	20–40 W	–
	Paris	2.2 m <sup>3</sup> /h	–	Rankine	Conical Reflector	–	–	–
	France	7 l/min	3 m	Rankine	Parabolic 9.2 m <sup>2</sup>	–	–	–
	France	–	–	–	–	–	–	–
	Pasadena US	5.3 m <sup>3</sup> /min	3.6 m	Rankine	Truncated cone 10 m dia top 4.5 m dia bottom	–	7.35	–
	–	–	–	Rankine	Flat Plate	–	14.7 kW	–
	Pensilvania US	–	–	Rankine	Solar Pond 11,200 m <sup>2</sup>	–	2.57	–
	Pensilvania US	11.3–12 m <sup>3</sup> /min	10 m	Rankine	Wooden Boxes 1000 m <sup>2</sup>	–	10.29–11.76 kW	–
	Meady Egypt	27 m <sup>3</sup> /min	–	Rankine	Parabolic Trough 60 m × 4 m	–	40.42 kW	–
	Mali Africa	11.3 m <sup>3</sup> /day	45.7 m	Rankine	–	–	–	–
	–	–	4.8 m	Ericsson	Parabolic	–	–	–
	Arizona US	38 m <sup>3</sup> /min	–	Rankine	Parabolic 554 m <sup>2</sup>	–	–	–
	New Mexico US	2.6 m <sup>3</sup> /min	34 m	Rankine	Parabolic 622.4 m <sup>2</sup>	–	–	–
	Guanajuato Mexico	1000 m <sup>3</sup> /day	–	Rankine	Flat Plate 2499 m <sup>2</sup>	–	–	–
	Dakar Senegal	8–10 l/min	13–14 m	Rankine	Flat Plate 6 m <sup>2</sup>	–	–	–
	San Luis Mexico	2.5 m <sup>3</sup> /day	–	–	–	–	25 kW	–
	Various	30 m <sup>3</sup> /day	20	–	Flat Plate 100 m <sup>2</sup>	–	–	–
	Mexico	–	–	Rankine	Parabolic Trough	–	1 kW	–
	Arizona US	–	–	Rankine	Parabolic Trough 2140 m <sup>2</sup>	–	–	–
	Egypt	–	–	Rankine	Flat Plate 384 m <sup>2</sup>	–	10 kW	–
–	14.61 l/min	3 m	Rankine	4 × Flat Plate 1 m <sup>2</sup> each	–	–	–	
India	6.5 m <sup>3</sup> /day	11.2 m	Rankine	Flat Plate 7 m <sup>2</sup>	–	–	–	
Delgado- Torrez [57]	India	–	–	Rankine	6 × Parabolic 9 m dia	–	20 kW (500 °C Steam)	–
	Iran	20 m <sup>3</sup> /day	–	Rankine	Flat Plate	–	–	–
	India	2 m <sup>3</sup> /day	6 m	Organic Rankine	Parabolic	–	–	–
	UK	0.5–2 m <sup>3</sup> /h	–	Liquid Piston	–	MAX Temp: 95	0.8–3 kW	–
Lakew [63]	Kolkata India	240 l/day	15 m	Metal Hydride Rankine	Flat Plate 1 m <sup>2</sup>	22–62	–	–
	–	–	–	–	–	80 (plus 60 °C Low level heat source)	2800–3750 kW	–
Tchanche [64]	UK	–	–	Organic Rankine	–	55	1.47 kW	\$ 30,000
	Sendai Japan	0.016 kg/s	–	–	–	–	350 W	–
Date [73]	Australia	140 m <sup>3</sup> /day	35 m	2-Stroke Liquid Piston	Solar Pond 5200 m <sup>2</sup>	–	–	–
Kurhe [71]	India	20 L/h	5 m	2-Stroke Diaphragm pump	Flat plate Collector	50–60	–	–
Baral [66]	Busan South Korea	–	–	Organic Rankine	Evacuated Tubes	65–95	0.4 kW–1.38 kW	\$ 25,800
Jokar [72]	Iran	0.125 l/s	1.5 m	Stirling	Flat Plate Reflector 2×1 m	100	1–2 W	–
Baral [67]	Nepal	2190–11100 m <sup>3</sup> /year	150 m	Organic Rankine	Evacuated Tubes 150–200 m <sup>2</sup>	60–100	1–5 kW	\$13,000 (1 kW) \$66,900 (5 kW)
Sitranon [69]	Thailand	60–95 l/h	2–6 m	Liquid Piston	–	70	–	–
Moonsri [68]	Thailand	192.2–218.8 l/day	1–5 m	Liquid Piston	Flat Plate	42.9–46.7	–	–
Bataineh [70]	Jordan	–	–	Rankine	Parabolic Trough 526 m <sup>2</sup>	–	30 kW	\$0.075/kWh

concentrated solar thermal power generation system utilised for irrigation. These systems are generally multi facet as they would be highly inefficient for the sole purpose for irrigation. Most systems with this technology undertakes irrigation in conjunction with either desalination or rural power generation. Small systems are shown to generate between 1.5 kW power with a payback period of 20 years, while larger systems are capable of a maximum 40 kW to provide a pumping capacity of 27 m<sup>3</sup>/min. These systems may be favourable for investment by a group of farmers in a village. However, as a standalone system it is very large and immobile in comparison to PV panels while the investment costs are similar.

Stirling cycle systems are also used for irrigational purposes. These systems generate lower power; however, they are compact and are easy to manufacture. The Stirling cycle based technology systems are investigated mostly to reduce the cost, thus the research undertaken investigated medium to low power solar collection / temperatures with a difference of 60–95 °C. Higher temperatures should be able to provide better outputs. The systems investigated in this paper provide relatively low head losses and flows; however, provisions are shown to add more heat into the system or inject mechanical assistance to further elevate the technology to provide a bigger output. The main advantage with the Stirling cycle system is that any heat source may be used to provide the thermal energy and hence may be suitable for use in a hybrid system. Liquid piston systems pump water directly which is then collected in a storage tank to irrigate fields using the drip irrigation method.

Two stroke piston systems have also been proposed that function like the Stirling cycle systems. Metal hydride systems have shown the best results in this providing the largest pumping head and flow of up to 2000 l using just a 1 m<sup>2</sup> flat plate collector. However, the use of metal hydrides makes this technology inaccessible to remote locations and farmers.

Based on the research undertaken solar thermal technologies utilising the Stirling engine holds the highest potential for small scale remote farms usage if the correct infrastructure is available for solar power concentration. Solar concentration technology that is cheap, effective and portable is required for this. Parabolic concentrators and dish concentrators provide compact solutions; however, they can be expensive to purchase. Local alternatives utilising local materials to build concentration systems may be proposed, which will reduce the cost as well as carbon footprint of the system. Utilising the technology to produce electricity is not viable, hence direct mechanical use for pumping is recommended in conjunction with a water storage tank is the optimal solution, this can be seen in Fig. 19.

A hybrid system may be proposed that combines the Stirling pump with and external mechanical system assist for the displacer in the case of inadequate solar irradiation like that proposed by Jokar and Tavakolpour-Saleh [72]; however, their use of solar panel and battery system defeats the investment cost aspect. Other external assistance solutions such as wind power may be investigated based on local resources availability.

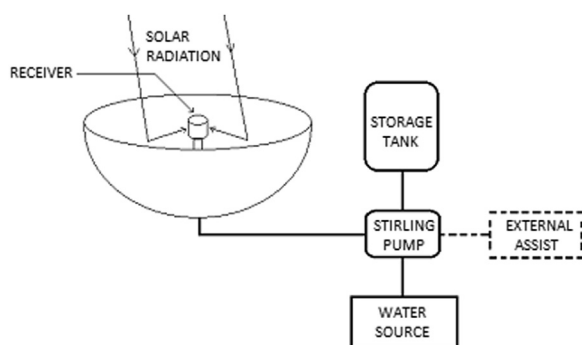


Fig. 19. Schematic of the most effective solar thermal water pumping system for remote rural areas based on literature reviews.

## 6. Future of solar powered water pumping systems

In terms of efficiency, solar thermal pumping systems conjure a maximum measured efficiency of 3% in comparison to 6% from photovoltaics. But the efficiency shouldn't be the main priority in the selection of the appropriate technology, especially since the source is renewable. The main factors hence are Cost and the impact on the environment.

A locally produced solar thermal system would be more cost effective and environmentally friendly in comparison to PV panels, as far as initial investments are concerned for remote area irrigation. The issue with regards to solar thermal powered technologies is that, the amount of research undertaken on these irrigation systems is very low; however, commercial technology exists that utilise thermal energy, but have not been studied critically.

The ease and accessibility of Stirling systems make it a viable option for testing and innovation, take for instance, SUNORBIT, a company from Germany, have produced a concentrated solar system capable of 500 W, 10 m head, 80,000 L/day known as the SUNPULSE [79]. See Fig. 20. The system uses a foldable dish concentrator with a heat storage powering a  $\gamma$ -type Stirling engine. The pump has been tested across Europe, Africa, Asia and Australia and is estimated to cost US\$ 2500.

Tested by TÜV labs, the system is shown to meet the World Bank target of water cost for rural areas of 6 cents/m<sup>3</sup>. As per tests, the system designed can provide 2.4 cents/m<sup>3</sup>.

Similar systems have been researched recently however, most of the research conducted focus on the potential of the Stirling cycle for the generation of electricity. These systems tend to be more expensive including dual axis solar tracking and large concentrators. Barreto and Canhoto [82] modelled a Stirling engine including a dish solar concentrator system, thermal receiver, and functioned as per three cycles, thermal cycle, mechanical ( $\beta$ -type Stirling engine) and electric energy conversion. The global efficiency of the system was recorded to be 10.4%. Combine that a 70% efficient pumping system, a pumping system efficiency of 7.28% available.

Based on the concentration factor, the efficiency was mapped as per shown in Fig. 21. There is a definite loss by converting mechanical energy to electrical energy in this system. Furthermore, a  $\beta$ -type Stirling engine is not the most efficient Stirling engine.

Using the basis of the study performed by Barreto and Canhoto [82], and understanding the SUNPULSE technology will help develop a model based on theoretical and real life results to help design systems that best matches the scenarios presented for remote rural irrigation and thus develop apposite solar thermal water pumping technology to match the performance of solar PV solutions, while keeping overall costs down and being more environmental friendly.

## 7. Conclusions

PV powered water pumping technologies are well developed, easily accessible and require almost no maintenance over the course of the lifetime of the technology. Studies suggest that the best way to optimise the cost and design of the PV powered system is to understand the requirements of the crop and perform extensive site survey to analyse the working conditions of the system. This is seen in relation to the use of a battery system where cost savings have been achieved in certain scenarios without using the battery while in other applications it was found that a battery in fact reduces costs. While the cost of PV system, over the course of its lifetime, is much lower in comparison to diesel powered systems, the initial investment cost is much higher and often too much to bare for small scale rural farmers. Furthermore, if the purpose of solar panels is to reduce the impact on the environment, it falls short due to a substantial carbon footprint because of the manufacturing and transportation impacts of the technology.

This study identifies that there is a huge potential for solar thermal

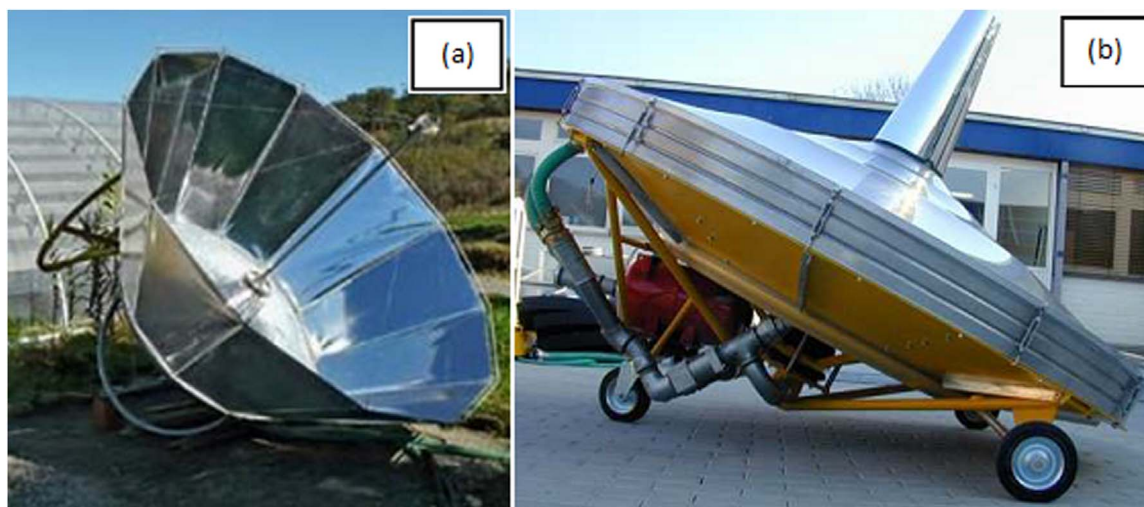


Fig. 20. (a) Solar Stirling water pump with dish [80] (b) SUNPULSE Stirling system [81].

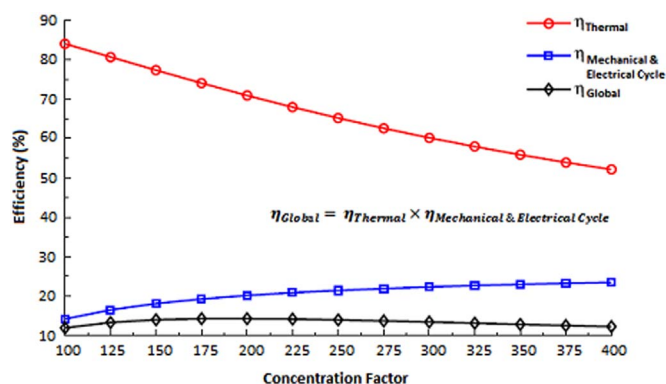


Fig. 21. Solar concentration factor and its effect on efficiency [82].

technology to meet the requirements of the small scale rural farmer by using a solar thermal water pumping system but the research on these systems are minimal, there is very few data available on the feasibility of these technologies especially for small scale purposes. Organic Rankine Cycle systems are the most common form of concentrated solar thermal power generation systems utilised for irrigation, however, these systems are feasible only on a large scale. That said, commercial technologies and studies in recent development in Stirling engines positively depict solar thermal water pumping capabilities keeping costs to a minimum and appreciably reducing the carbon footprint through the utilisation of local resources and local manufacture while matching the performance of PV technology.

## Acknowledgement

The Authors are grateful to the Grantham Centre for Sustainable Futures working in conjunction with the University of Sheffield (Charity number: X1089) for their support in sponsoring the PhD research program.

## References

- [1] Kashaigili JJ. Ground water Availability and Use in Sub-Saharan Africa. Srilanka: International Water Management Institute; 2012. <http://dx.doi.org/10.5337/2012.213>.
- [2] Pavelic P, Villholth KG, Shu Y, Rebelo L-M, Smakhtin V. Smallholder groundwater irrigation in Sub-Saharan Africa: country-level estimates of development potential. *Water Int* 2013;38:392–407. <http://dx.doi.org/10.1080/02508060.2013.819601>.
- [3] International Renewable Energy Agency (IRENA). Africa 2030: Roadmap for a renewable energy future. REmap 2030 Program; 2015. <http://dx.doi.org/10.1017/CBO9781107415324.004>.
- [4] FAO. Farm size|FAO|Food and Agriculture Organization of the United Nations; 2012. (<http://www.fao.org/family-farming/data-sources/dataportrait/farm-size/en/>).
- [5] Cavero J, Faci JM, Martínez-Cob A. Relevance of sprinkler irrigation time of the day on alfalfa forage production. *Agric Water Manag* 2016;178:304–13. <http://dx.doi.org/10.1016/j.agwat.2016.10.008>.
- [6] Ramos JS, Ramos HM. Solar powered pumps to supply water for rural or isolated zones: a case study. *Energy Sustain Dev* 2009;13:151–8. <http://dx.doi.org/10.1016/j.esd.2009.06.006>.
- [7] Muhsen DH, Khatib T, Nagi F. A review of photovoltaic water pumping system designing methods, control strategies and field performance. *Renew Sustain Energy Rev* 2017;68:70–86. <http://dx.doi.org/10.1016/j.rser.2016.09.129>.
- [8] Gopal C, Mohanraj M, Chandramohan P, Chandrasekar P. Renewable energy source water pumping systems – a literature review. *Renew Sustain Energy Rev* 2013;25:351–70. <http://dx.doi.org/10.1016/j.rser.2013.04.012>.
- [9] Sontake VC, Kalamkar VR. Solar photovoltaic water pumping system – a comprehensive review. *Renew Sustain Energy Rev* 2016;59:1038–67. <http://dx.doi.org/10.1016/j.rser.2016.01.021>.
- [10] Chandel SS, Nagaraju Naik M, Chandel R. Review of solar photovoltaic water pumping system technology for irrigation and community drinking water supplies. *Renew Sustain Energy Rev* 2015;49:1084–99. <http://dx.doi.org/10.1016/j.rser.2015.04.083>.
- [11] Green M, Emery K, Hishikawa Y, Warta W, Dunlop ED, Levi DH, et al. Solar cell efficiency tables (version 49) Martin. *Prog Photovolt Res Appl* 2017;25:3–13. <http://dx.doi.org/10.1002/pip.1160>.
- [12] North Arizona Wind and sun. What is maximum power point tracking (MPPT) n.d. (<https://www.solar-electric.com/mppt-solar-charge-controllers.html/>).
- [13] Jordan DC, Kurtz SR. Photovoltaic degradation rates – an analytical review. *Prog Photovolt Res Appl* 2013;21. <http://dx.doi.org/10.1002/pip.1182>.
- [14] Yahya HN, Sambo AS. Design and installation of solar photovoltaic powered water pumping system at Usmanu Danfodiyo University, Sokoto. 6; 1995. p. 311–2.
- [15] Hamidat A, Benyoucef B, Hartani T. Small-scale irrigation with photovoltaic water pumping system in Sahara regions. *Renew Energy* 2003;28:1081–96. [http://dx.doi.org/10.1016/S0960-1481\(02\)00058-7](http://dx.doi.org/10.1016/S0960-1481(02)00058-7).
- [16] Ali A, Hamza AZT. Performance of submersible PV solar pumping systems under conditions in the Sudan. *Sol Electr Photovolt Wind* 1995;6:491–5. [http://dx.doi.org/10.1016/0960-1481\(95\)00049-P](http://dx.doi.org/10.1016/0960-1481(95)00049-P).
- [17] Bucher W. Aspects of solar water pumping in remote regions. *Energy Sustain Dev* 1996;3:8–27. [http://dx.doi.org/10.1016/S0973-0826\(08\)60201-X](http://dx.doi.org/10.1016/S0973-0826(08)60201-X).
- [18] Vick BD, Clark RN. Determining the optimum solar water pumping system for domestic use. *Livest Watering Irrigation* 1992.
- [19] Merino GG, Lagos LO, Gontupil JE. Monitoring and evaluation of a direct coupled photovoltaic pumping system. *Appl Eng Agric* 2008;24:277–84. <http://dx.doi.org/10.13031/2013.24495>.
- [20] Taufik OiA, Anwari M, Taufik M. Modeling and simulation of photovoltaic water pumping system. In: Proceedings of – 2009 3rd Asia international conference model simulation, AMS 2009; 2009. p. 497–502. (<http://dx.doi.org/10.1109/AMS.2009.85>).
- [21] Mahmoud M, Mahmoud MM, Kukhun WR, Daud A. Efficiency improvement of a dual PV water pumping system on a desert well by solar matched load control. *Int J Energy Eng* 2013;3:151–7.
- [22] Deveci O, Onkol M, Unver HO, Ozturk Z. Design and development of a low-cost solar powered drip irrigation system using Systems Modeling Language. *J Clean Prod* 2015;102:529–44. <http://dx.doi.org/10.1016/j.jclepro.2015.04.124>.
- [23] Setiawan AA, Purwanto DH, Pamuji DS, Huda N. Development of a solar water pumping system in karsts rural area tepus, gunungkidul through student community services. *Energy Procedia* 2014;47:7–14. <http://dx.doi.org/10.1016/j.egypro.2014.01.190>.
- [24] Campana PE, Li H, Zhang J, Zhang R, Liu J, Yan J. Economic optimization of

- photovoltaic water pumping systems for irrigation. *Energy Convers Manag* 2015;95:32–41. <http://dx.doi.org/10.1016/j.enconman.2015.01.066>.
- [25] López-Luque R, Reza J, Martínez J. Optimal design of a standalone direct pumping photovoltaic system for deficit irrigation of olive orchards. *Appl Energy* 2015;149:13–23. <http://dx.doi.org/10.1016/j.apenergy.2015.03.107>.
- [26] Hossain MA, Hassan MS, Mottalib MA, Ahmmed S. Technical and economic feasibility of solar pump irrigations for eco-friendly environment. *Procedia Eng* 2015;105:670–8. <http://dx.doi.org/10.1016/j.proeng.2015.05.047>.
- [27] Kumar M, Reddy KS, Adake RV, Rao CVKN. Solar powered micro-irrigation system for small holders of dryland agriculture in India. *Agric Water Manag* 2015;158:112–9. <http://dx.doi.org/10.1016/j.agwat.2015.05.006>.
- [28] Srivastava RC, Bhatnagar PR. Gravity-fed Drip Irrigation System for Hilly Terraces of the Northwest Himalayas, 21. Springer-Verlag; 2002. p. 151–7. <http://dx.doi.org/10.1007/s00271-002-0058-y>.
- [29] Reza J, Torrente C, López-Luque R, Martínez J. Feasibility analysis of a standalone direct pumping photovoltaic system for irrigation in Mediterranean greenhouses. *Renew Energy* 2016;85:1143–54. <http://dx.doi.org/10.1016/j.renene.2015.07.056>.
- [30] Chandel SS, Nagaraju Naik M, Sharma V, Chandel R. Degradation analysis of 28 year field exposed mono-c-Si photovoltaic modules of a direct coupled solar water pumping system in western Himalayan region of India. *Renew Energy* 2015;78:193–202. <http://dx.doi.org/10.1016/j.renene.2015.01.015>.
- [31] Yahyaoui I, Tadeo F, Vieira M. Energy and water management for drip-irrigation of tomatoes in a semi-arid district. *Agric Water Manag* 2016. <http://dx.doi.org/10.1016/j.agwat.2016.08.003>.
- [32] Sami M, Shiekhdavoodi MJ, Pazhohanniya M, Pazhohanniya F. Environmental comprehensive assessment of agricultural systems at the farm level using fuzzy logic: a case study in cane farms in Iran. *Environ Model Softw* 2014;58:95–108. <http://dx.doi.org/10.1016/j.envsoft.2014.02.014>.
- [33] Rawat R, Kaushik SC, Lamba R. A review on modeling, design methodology and size optimization of photovoltaic based water pumping, standalone and grid connected system. *Renew Sustain Energy Rev* 2016;57:1506–19. <http://dx.doi.org/10.1016/j.rser.2015.12.228>.
- [34] Jones MA, Odeh I, Haddad M, Mohammad AH, Quinn JC. Economic analysis of photovoltaic (PV) powered water pumping and desalination without energy storage for agriculture. *Desalination* 2016;387:35–45. <http://dx.doi.org/10.1016/j.desal.2016.02.035>.
- [35] Vick BD, Clark RN. Experimental investigation of solar powered diaphragm and helical pumps. *Sol Energy* 2011;85:945–54. <http://dx.doi.org/10.1016/j.solener.2011.02.011>.
- [36] Mohammadi A, Mezzai N, Rekioua D, Rekioua T. Impact of shadow on the performances of a domestic photovoltaic pumping system incorporating an MPPT control: a case study in Bejaia, North Algeria. *Energy Convers Manag* 2014;84:20–9. <http://dx.doi.org/10.1016/j.enconman.2014.04.008>.
- [37] Posorski R. Photovoltaic water pumps, an attractive tool for rural drinking water supply. *Sol Energy* 1996;58:155–63. [http://dx.doi.org/10.1016/S0038-092X\(96\)00060-6](http://dx.doi.org/10.1016/S0038-092X(96)00060-6).
- [38] Campana PE, Leduc S, Kim M, Olsson A, Zhang J, Liu J, et al. Suitable and optimal locations for implementing photovoltaic water pumping systems for grassland irrigation in China. *Appl Energy* 2015;185:1879–89. <http://dx.doi.org/10.1016/j.apenergy.2016.01.004>.
- [39] Zhang C, Elia Campana P, Yang J, Yan J. Economic performance of photovoltaic water pumping systems with business model innovation in China. *Energy Convers Manag* 2016. <http://dx.doi.org/10.1016/j.enconman.2016.10.069>.
- [40] Elkholy MM, Fathy A. Optimization of a PV fed water pumping system without storage based on teaching-learning-based optimization algorithm and artificial neural network. *Sol Energy* 2016;139:199–212. <http://dx.doi.org/10.1016/j.solener.2016.09.022>.
- [41] Pawar PJ, Rao RV. Parameter optimization of machining processes using teaching-learning-based optimization algorithm. *Int J Adv Manuf Technol* 2013;1. <http://dx.doi.org/10.1007/s00170-013-4961-6>.
- [42] Closas A, Rap E. Solar-based groundwater pumping for irrigation: sustainability, policies, and limitations. *Energy Policy* 2017;104:33–7. <http://dx.doi.org/10.1016/j.enpol.2017.01.035>.
- [43] Campana PE, Li H, Yan J. Techno-economic feasibility of the irrigation system for the grassland and farmland conservation in China: photovoltaic vs. wind power water pumping. *Energy Convers Manag* 2015;103:311–20. <http://dx.doi.org/10.1016/j.enconman.2015.06.034>.
- [44] Allen RG, Rick G. Food and Agriculture Organization of the United Nations. Crop Evapotranspiration: Guidelines for Computing Crop Water Requirements. Food and Agriculture Organization of the United Nations; 1998.
- [45] Treephak K, Thongprong J, Somsak D, Saelao J, Patcharaprakiti N. An economic evaluation comparison of solar water pumping system with engine pumping system for rice cultivation. *Jpn J Appl Phys* 2015;54:08KH01.
- [46] Sarkar MNI, Ghosh HR. Techno-economic analysis and challenges of solar powered pumps dissemination in Bangladesh. *Sustain Energy Technol Assess* 2017;20:33–46. <http://dx.doi.org/10.1016/j.seta.2017.02.013>.
- [47] Meah K, Fletcher S, Ula S. Solar photovoltaic water pumping for remote locations. *Renew Sustain Energy Rev* 2008;12:472–87. <http://dx.doi.org/10.1016/j.rser.2006.10.008>.
- [48] De Wild-Scholten MJ. Energy payback time and carbon footprint of commercial photovoltaic systems. *Sol Energy Mater Sol Cells* 2013;119:296–305. <http://dx.doi.org/10.1016/j.solmat.2013.08.037>.
- [49] Sinha P. Life cycle materials and water management for CdTe photovoltaics. *Sol Energy Mater Sol Cells* 2013;119:271–5. <http://dx.doi.org/10.1016/j.solmat.2013.08.022>.
- [50] Laleman R, Albrecht J, Dewulf J. Life cycle analysis to estimate the environmental impact of residential photovoltaic systems in regions with a low solar irradiation. *Renew Sustain Energy Rev* 2011;15:267–71. <http://dx.doi.org/10.1016/j.rser.2010.09.025>.
- [51] Parikh MM, Bhattacharya AK. Wind data analysis for studying the feasibility of using windmills for irrigation. *Energy Agric* 1984;3:129–36. [http://dx.doi.org/10.1016/0167-5826\(84\)90015-9](http://dx.doi.org/10.1016/0167-5826(84)90015-9).
- [52] Das D, Ram Gopal M. Studies on a metal hydride based solar water pump. *Int J Hydrog Energy* 2004;29:103–12. [http://dx.doi.org/10.1016/S0360-3199\(03\)00044-2](http://dx.doi.org/10.1016/S0360-3199(03)00044-2).
- [53] Ferreira AC, Nunes ML, Teixeira JC, Martins LB, Teixeira SFCF. Thermodynamic and economic optimization of a solar-powered Stirling engine for micro-cogeneration purposes. In: Proceedings of Ecos 2015 – 28th international conference on efficiency, cost, optimization, simulation and environmental impact of energy systems 2015;111:13 pgs.
- [54] Felix A, Farret MGS. Appendix C the Stirling engine; 2006. (<http://dx.doi.org/10.1002/0471755621>).
- [55] Bagheri A, Bostanci H, Foster PR. Preliminary analysis of an innovative rotary displacer Stirling engine. *ASME Int Mech Eng Congr Expo Proc* 2015. <http://dx.doi.org/10.1115/IMECE2015-52455>, [6A–2015].
- [56] Ahmadi MH, Ahmadi M-A, Pourfayaz F. Thermal models for analysis of performance of Stirling engine: a review. *Renew Sustain Energy Rev* 2017;68:168–84. <http://dx.doi.org/10.1016/j.rser.2016.09.033>.
- [57] Delgado-Torres AM. Solar thermal heat engines for water pumping: an update. *Renew Sustain Energy Rev* 2009;13:462–72. <http://dx.doi.org/10.1016/j.rser.2007.11.004>.
- [58] Pytilinski JT. Solar energy installations for pumping irrigation water. *Sol Energy* 1978;21:255–62. [http://dx.doi.org/10.1016/0038-092X\(78\)90001-4](http://dx.doi.org/10.1016/0038-092X(78)90001-4).
- [59] Wong Y, Sumathy K. Solar thermal water pumping systems: a review. *Renew Sustain Energy Rev* 1999;3:185–217. [http://dx.doi.org/10.1016/S1364-0321\(98\)00018-5](http://dx.doi.org/10.1016/S1364-0321(98)00018-5).
- [60] Spencer LC. A comprehensive review of small solar-powered heat engines: Part II. research since 1950-“conventional” engines up to 100 kW. *Sol Energy* 1989;43:197–210. [http://dx.doi.org/10.1016/0038-092X\(89\)90020-0](http://dx.doi.org/10.1016/0038-092X(89)90020-0).
- [61] Wong YW, Sumathy K. Thermodynamic analysis and optimization of a solar thermal water pump. *Appl Therm Eng* 2001;21:613–27. [http://dx.doi.org/10.1016/S1359-4311\(00\)00065-X](http://dx.doi.org/10.1016/S1359-4311(00)00065-X).
- [62] Mahkamov K, Orda EP. Solar thermal water pumps: a preliminary analysis of the working process. *J Sol Energy Eng Trans ASME* 2005;127:29–36. <http://dx.doi.org/10.1115/1.1767191>.
- [63] Lakew AA, Bolland O, Ladam Y. Theoretical thermodynamic analysis of Rankine power cycle with thermal driven pump. *Appl Energy* 2011;88:3005–11. <http://dx.doi.org/10.1016/j.apenergy.2011.03.029>.
- [64] Tchanché BF, Lambrinos G, Frangoudakis A, Papadakis G. Low-grade heat conversion into power using organic Rankine cycles – a review of various applications. *Renew Sustain Energy Rev* 2011;15:3963–79. <http://dx.doi.org/10.1016/j.rser.2011.07.024>.
- [65] Nguyen VM, Doherty PS, Riffat SB. Development of a prototype low-temperature Rankine cycle electricity generation system. *Appl Therm Eng* 2001;21:169–81. [http://dx.doi.org/10.1016/S1359-4311\(00\)00052-1](http://dx.doi.org/10.1016/S1359-4311(00)00052-1).
- [66] Baral S, Kim D, Yun E, Kim K. Experimental and thermoeconomic analysis of small-scale solar organic Rankine cycle (SORC) system. *Entropy* 2015;17:2039–61. <http://dx.doi.org/10.3390/e17042039>.
- [67] Baral S, Kim KC. Stand-alone solar organic Rankine cycle water pumping system and its economic viability in Nepal. *Sustain* 2016;8:1–18. <http://dx.doi.org/10.3390/su8010018>.
- [68] Moonsri P, Kunchorrnat J, Namprakai P. Hybrid energy thermal water pump for producing hot water from a shallow well in Thailand. *J Energy Eng* 2015;4015023:4015023. [http://dx.doi.org/10.1061/\(ASCE\)EY.1943-7897.0000278](http://dx.doi.org/10.1061/(ASCE)EY.1943-7897.0000278).
- [69] Sitranon J, Lertsatithanakorn C, Namprakai P, Prathinthong N, Suparos T, Roomprasang N. Performance enhancement of solar water heater with a thermal water pump. *J Energy Eng* 2015;141:4014036. [http://dx.doi.org/10.1061/\(ASCE\)EY.1943-7897.0000216](http://dx.doi.org/10.1061/(ASCE)EY.1943-7897.0000216).
- [70] Bataineh KM. Optimization analysis of solar thermal water pump. *Renew Sustain Energy Rev* 2016;55:603–13. <http://dx.doi.org/10.1016/j.rser.2015.10.146>.
- [71] Kurhe N, Funde A, Gokhale P, Jadhav S, Ghaisas S, Date A. Development of low temperature heat engine for water pumping application. *Energy Procedia* 2017;110:292–7. <http://dx.doi.org/10.1016/j.egypro.2017.03.142>.
- [72] Joker H, Tavakolpour-Saleh AR. A novel solar-powered active low temperature differential Stirling pump. *Renew Energy* 2015;81:319–37. <http://dx.doi.org/10.1016/j.renene.2015.03.041>.
- [73] Date A, Akbarzadeh A. Theoretical study of a new thermodynamic power cycle for thermal water pumping application and its prospects when coupled to a solar pond. *Appl Therm Eng* 2013;58:511–21. <http://dx.doi.org/10.1016/j.applthermaeng.2013.05.004>.
- [74] Chandel SS, Naik MN, Chandel R. Review of performance studies of direct coupled photovoltaic water pumping systems and case study. *Renew Sustain Energy Rev* 2017;76:163–75. <http://dx.doi.org/10.1016/j.rser.2017.03.019>.
- [75] Benganem M, Daffallah KO, Alamri SN, Joraid AA. Effect of pumping head on solar water pumping system. *Energy Convers Manag* 2014;77:334–9. <http://dx.doi.org/10.1016/j.enconman.2013.09.043>.
- [76] Tiwari AK, Kalamkar VR. Performance investigations of solar water pumping system using helical pump under the outdoor condition of Nagpur, India. *Renew Energy* 2016;97:737–45. <http://dx.doi.org/10.1016/j.renene.2016.06.021>.
- [77] Kabalci Y, Kabalci E, Canbaz R, Calpiniaci A. Design and implementation of a solar

- plant and irrigation system with remote monitoring and remote control infra-structures. *Sol Energy* 2016;139:506–17. <http://dx.doi.org/10.1016/j.sol-ener.2016.10.026>.
- [78] Levidow L, Zaccaria D, Maia R, Vivas E, Todorovic M, Scardigno A. Improving water-efficient irrigation: prospects and difficulties of innovative practices. *Agric Water Manag* 2014;146:84–94. <http://dx.doi.org/10.1016/j.agwat.2014.07.012>.
- [79] Sunvention sunpulse. Sunvention stirling machine. vol. 0. n.d.
- [80] Coen Reith. Solar stirling engine water pump. JOVOTO; 2013. ([https://uploads1.jovo.to/idea\\_attachments/579121/solar-stirling-common-waterpump-1\\_big.jpg?1448775192](https://uploads1.jovo.to/idea_attachments/579121/solar-stirling-common-waterpump-1_big.jpg?1448775192)). [Accessed 20 January 2017].
- [81] Vineeth CS. *Beginners Guide to Stirling Engines*; 2011. ([https://books.google.com.sg/books?id=zTdzKxQaqNcC&pg=PT85&source=gbs\\_selected\\_pages&cad=2#v=onepage&q&f=false](https://books.google.com.sg/books?id=zTdzKxQaqNcC&pg=PT85&source=gbs_selected_pages&cad=2#v=onepage&q&f=false)).
- [82] Barreto G, Canhoto P. Modelling of a Stirling engine with parabolic dish for thermal to electric conversion of solar energy. *Energy Convers Manag* 2017;132:119–35. <http://dx.doi.org/10.1016/j.enconman.2016.11.011>.

### **8.5.2. Conference Proceedings**

Mohammed Wazed S, Hughes BR, O'Connor D, Calautit JK. Solar Driven Irrigation Systems for Remote Rural Farms, *International Conference on Applied Energy (ICAE)*, 2018, Impact Factor 5.746



9th International Conference on Applied Energy, ICAE2017, 21-24 August 2017, Cardiff, UK

## Solar Driven Irrigation Systems for Remote Rural Farms

Saeed Mohammed Wazed<sup>a\*</sup>, Ben Richard Hughes<sup>a</sup>, Dominic O'Connor<sup>a</sup>,  
John Kaiser Calautit<sup>b</sup>

<sup>a</sup> Energy2050, Mechanical Engineering, Faculty of Engineering, University of Sheffield,  
First Floor, Arts Tower, Sheffield, South Yorkshire, S10 2TN, United Kingdom

<sup>b</sup> Department of Architecture and Built Environment, University of Nottingham, Nottingham, NG7 2RD, United Kingdom

---

### Abstract

Solar powered irrigation technologies have developed significantly in the past decade assisted by the development of higher efficiency, low cost solar Photovoltaic (PV) panels. The technology has come so far as to be able to elapse diesel powered irrigation systems in terms of the payback period and reduction in greenhouse gasses. However, PV technologies are still not being used extensively due to their high initial investment costs and compared to other renewable energy technologies the carbon footprint is still comparatively large. On the other hand, solar thermal technologies are seen to be much cheaper, and have a much smaller carbon footprint, but are marred by low efficiencies. This paper investigates solar powered irrigation technologies (PV and solar thermal technologies) that can be utilised by independent farmers in small-scale remote rural farms in Sub-Saharan Africa. The focus is to be able to identify affordable solar powered irrigation systems that will make use of local resources effectively for drip irrigation.

© 2017 The Authors. Published by Elsevier Ltd.

Peer-review under responsibility of the scientific committee of the 9th International Conference on Applied Energy.

*Keywords:* Solar Energy; Solar Water Pumping, Photovoltaics, Concentrated Solar Thermal, Stirling Engine, Irrigation

---

### 1. Introduction

The world population is increasing exponentially and with this there is growing food insecurity that necessitates more farming, and hence, irrigation all over the world. As global temperatures continue to rise, the effort must not only be to boost production but to also do so in consideration of the environment. Furthermore, there is a social

---

\* Corresponding author. Tel.: +44-756-391-8961.

E-mail address: [SMohammedWazed1@sheffield.ac.uk](mailto:SMohammedWazed1@sheffield.ac.uk)

responsibility that must be addressed in the arid and semi-arid regions of the world where the conditions are getting worse and independent small-scale farmers are getting poorer still as they deal with long dry spells, unreliable safe water supply and polluted ground water reserves. This dictates the development of sustainable irrigation technology that not only serves the purpose of irrigation, but is environmentally friendly and can be afforded in rural areas.

The Sub Saharan Region of Africa has been dealing with inconsistent water supply issues for a long time. Their most reliable source is the abundant ground water supply. However, due to lack of economic incentives only 10% of the reserves are being used [1]. Small scale farms in this region are an average size of 1 hectare [2] and are often in remote rural areas. The farmers there can't cope with the high initial investments required for the purchase of generators and pumps. In addition to this, with the rising fuel costs and regular maintenance, the operation costs are also extremely high for local farmers using conventional technology [3]. The technology needs to improve, and emphasis must be put on renewable energy technologies to move forward in this regard. Solar power, in particular, has great potential in Africa receiving over 2000 kWh of global solar radiation annually, much greater than that received by the top countries implementing solar energy in the world [4].

With high potential in both photovoltaics and solar thermal energy [5], this study tracks the major technological developments made in PV and solar thermal power irrigation technologies and compared on the basis of cost, power output and flow generated. One of defining factors for the suitable technology also discussed, is the ability to make use of the local resources sustainably, this will help reduce the initial costs, maintenance costs as well as reduce the carbon footprint.

## 2. PV Irrigation Systems

PV irrigation systems use PV panels to produce electricity from solar energy which is then used in conjunction with an electric motor to drive a pump. This system can be further enhanced with the use of batteries for electricity storage, or incorporating a storage tank for water. The type of Pump (whether AC/DC) may also be considered which in turn dictates the type of motor to be used. For instance, in the case for AC powered pumps an AC motor will be required thus an inverter needs to be added to the system to convert the DC power from the solar panel to AC for the motor to utilize. With decreasing cost of PV panel technology, easy integration with available technology, reduction in price of Lithium Ion batteries and rapid commercialisation in recent times, PV irrigation systems have become more accessible for rural farms and a large amount of research has been undertaken on their performance, feasibility and economic viability. Fig. 3 shows performance data of various solar PV systems as per review by Saeed et al [6].

Multi-Junction PV panels are the most efficient form of PV panels but the environmental impact of these panels are higher than that of other renewable energy sources [7,8]. Cadmium telluride cells are a better option with a module efficiency of 19.1%, with the least greenhouse gas emissions and quickest payback period [7,9]. In terms of cost, PV systems fare better in the lifetime cost analysis when compared to diesel [8–10]. The initial investment cost for PV panels are however too high in comparison to Diesel and other renewable energy systems such as solar thermal and wind [8]. However, a PV system can have a payback period of under 6 years [9], which is unmatched by other types of irrigation solutions in remote rural areas.

Based on research by R. López-Luque et al. [11], to irrigate 1 hectare of land less than 1kW power is required and in such cases where the power system required is less than 5kW, the DC motor system is preferred over AC motors. The study further indicates that permanent magnet DC motors provide the highest efficiency, torque and fastest response in comparison to other DC systems. The Positive displacement pump is shown to be beneficial for higher heads while for lower heads the diaphragm pump is better suited both providing efficiencies of 70% [9,12–14].

The use of battery is subject to the location and type of irrigation requirement, the costs of the systems also vary likewise. While an overhead tank may suffice in certain scenarios, others demand the use of battery for on demand use of electricity and a more consistent electricity supply [12,13]. Research by D. H. Muhsen et al. [15], on the other hand, proposed an aluminium foil reflector to boost the solar radiation.

The Power output and costs associated with PV systems vary depending on the irrigation scenarios [14,16–21]. To optimise the design of the PV system and the associated costs, it is important to understand the requirements of the crop by performing site surveys and analysing the working conditions. Considering the high solar potential in sub Saharan Africa and a case for drip irrigation, Fig. 1 shows the proposed solution for retrieving underground water for irrigation. The system provides 13.65% over all thermal efficiency.

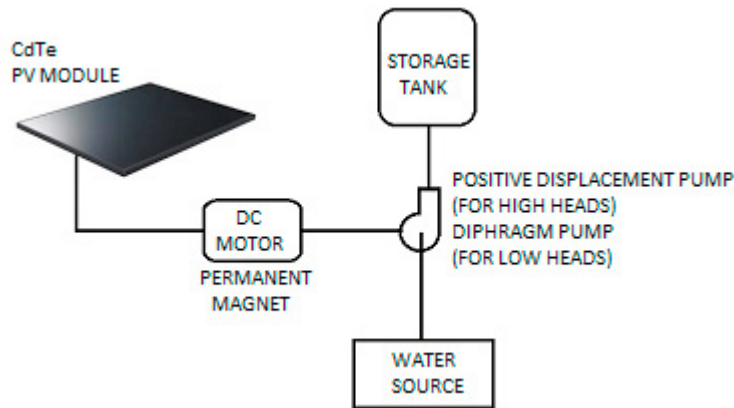


Fig. 1: Schematic of proposed PV water pumping system for remote rural areas of Sub Saharan Africa [6]

Drawback of PV technologies include, the degradation of power of PV cells due to long term exposure is 0.8% per year [22]. At the elevated temperatures and humidity expected in sub-Saharan Africa the issue may be more prevalent. To compensate for this, more intelligent systems may have to be incorporated which will further increase the cost. Another issue with PV technology is that it's manufacture process poses a higher threat to the environment in comparison to other Renewable Energy Technologies and about 4 times more harmful than Nuclear technology [8]. Using batteries and the transportation further elevate the carbon footprint of the technology. Finally, accumulation of dust is another issue associated with PV technology.

### 3. Solar Thermal Irrigation systems

Solar thermal systems utilize the energy from the sun using a solar collector or a solar concentrated surface to generate mechanical work via a Rankine, Brayton or Stirling Cycle engine. The work generated can be used directly or converted to electricity to power pumps for irrigation. While direct utilization of mechanical energy is desirable, storage of thermal energy is much more complicated when compared to storage of electricity. Location factors and irrigation scenario dictates the selection of direct mechanical drive or conversion to electrical power. There is a shortage of real life testing of solar thermal technologies for irrigation. Fig. 4 shows performance data of various solar thermal systems as per review by Saeed et al [6].

There are two types of solar thermal irrigation systems conventional technologies that use the Rankine Cycle and unconventional systems that use vapour cycle liquid pistons or metal hydride systems [23]. Conventional systems are much larger and more complex in comparison to unconventional systems but is the most widely tested solar thermal systems [8]. Conventional systems require high investment costs, maintenance costs and have very low efficiencies (around 1%) and hence aren't considered for wide scale use for irrigation[14]. Instead conventional solar thermal irrigation may be undertaken in conjunction with desalination, or power generation [15,23]. Standalone, conventional systems are large, expensive and immobile in comparison to PV.

Unconventional technologies include Stirling Engine systems, Two stroke piston systems which are similar to Stirling systems [24,25] and metal hydride systems. Unconventional solar thermal technologies, generally have low

pumping potential except for metal hydride systems that have flow of up to 2000 litres with a flat plate collector of just 1m<sup>2</sup> area. However, metal hydrides are expensive and not easily accessible in remote locations [8,23,26].

Stirling engines, are low cost systems, compact and easy to manufacture. Stirling engine irrigation systems are studied for low temperature operations 60 °C – 95 °C [23,27,28]. Due to the flexibility of Stirling systems in accommodating various heat sources and with the possibility of using better solar concentration techniques, higher temperature differences may be obtained which in turn will ensure a larger output from the system[23,25].

The dish type solar concentrator is relatively cheap and the most commonly used solar concentration system used capable of providing concentration up to 500 °C with a single axis tracker. Based on this system, cheaper and easier to manufacture concentration technologies have been designed such as the Linear Fresnel Reflector (400 °C concentration) [29]. Hence, the dish system is a good baseline for concentration technology that can be implemented with solar thermal irrigation systems. Local construction will further reduce the cost as well as carbon footprint of the system. Fig. 2 shows the proposed solution for retrieving underground water for irrigation in Sub Saharan Africa. A hybrid system comprising of Stirling pump with mechanical assist from an external system may be proposed to assist the displacer similar to work conducted by Jokar and Tavakolpour-Saleh [28].

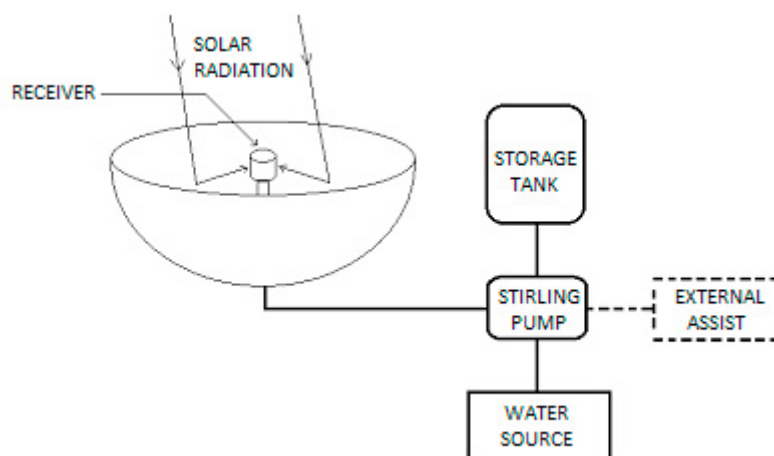


Fig. 2: Schematic of proposed solar thermal water pumping system for remote rural areas of Sub Saharan Africa [6]

#### 4. Comparing Solar PV and Thermal Technologies

Solar photovoltaic systems are far more developed in comparison to solar thermal systems. PV systems have been studied extensively (see fig. 3) and can provide wide range of capabilities ranging from small scale to large scale systems. One of the major issues of solar panels is the investment costs associated with the systems. Even though solar PV technology has seen a decline in costs, it is still very expensive for small scale, independent farmers. Based on the review, solar thermal technologies are not as flexible as PV technologies. Positive results have only been obtained in large scale Rankine systems. However, using the Stirling pump system, solar thermal technology could be utilised for small scale irrigation purposes. There is already a commercially available Stirling pump technology, SunPulse. However, the SunPulse system costs between US\$1250 – US\$2500 [30] which is still expensive for the Sub-Saharan Africa region. The research aims to develop a system that would be cheaper in comparison to the SunPulse system and this will be done by using locally available resources. Doing so will generate a source of income for the Sub-Saharan Africa region, reduce the cost of the technology, lower the carbon footprint and GHG emissions, and provide local, small-scale, independent farmers with a more affordable irrigation technology.





## 5. Conclusions

Various PV and solar thermal technologies have been discussed. Based on the literature review. The most effective PV system includes and CdTe PV module running a permanent magnet DC motor that drives a pump. The system only functions during ample sun hours and stores water in a storage tank instead of utilising a battery. The most effective solar thermal system utilises a solar concentrator powering a Stirling pump. Similar to the PV system there is no energy storage but instead the system functions at optimal sun hours and stores water.

There is a lot of research and real-life data for PV technology. PV systems require low maintenance and has almost no operational cost which has seen the system implemented abundantly in recent times. However, considering the Sub-Saharan African region, PV systems are still very expensive. Due to its simplicity, Stirling engines provide the opportunity of a solar thermal integrated irrigation system that can be locally produced. Furthermore, Stirling engines can be directly used as a pump thus reducing the number of components in the system. Local production also makes Stirling pumps more environmentally friendly with lower carbon footprint and greenhouse gas emissions when compared to PV systems.

## Acknowledgements

The Authors are grateful to the Grantham Institute for Sustainable Futures and the University of Sheffield for their support in sponsoring the PhD research program.

## References

- [1] Kashaigili JJ. Ground water Availability and Use in Sub-Saharan Africa. Srilanka: International Water Management Institute; 2012. doi:10.5337/2012.213.
- [2] FAO. Farm size | FAO | Food and Agriculture Organization of the United Nations 2012. <http://www.fao.org/family-farming/data-sources/dataportrait/farm-size/en/>.
- [3] Pavelic P, Villholth KG, Shu Y, Rebelo L-M, Smakhtin V. Smallholder groundwater irrigation in Sub-Saharan Africa: country-level estimates of development potential. *Water Int* 2013;38:392–407. doi:10.1080/02508060.2013.819601.
- [4] Quansah DA, Adaramola MS, Mensah LD. Solar Photovoltaics in sub-Saharan Africa – Addressing Barriers , Unlocking Potential. *Energy Procedia* 2016;106:97–110. doi:10.1016/j.egypro.2016.12.108.
- [5] International Renewable Energy Agency (IRENA). Africa 2030: Roadmap for a Renewable Energy Future. REMap 2030 Program 2015:72. doi:10.1017/CBO9781107415324.004.
- [6] Mohammed Wazed S, Hughes BR, O'Connor D, Calautit JK. A Review of Sustainable Solar Irrigation Systems for Developing Countries. 2017.
- [7] Martin A, Green, Keith Emery, Yoshihiro Hishikawa WW and EDD. Solar cell efficiency tables (Version 45). *Prog Photovolt Res Appl* 2007;23:659–76. doi:10.1002/pip.2573.
- [8] Gopal C, Mohanraj M, Chandramohan P, Chandrasekar P. Renewable energy source water pumping systems - A literature review. *Renew Sustain Energy Rev* 2013;25:351–70. doi:10.1016/j.rser.2013.04.012.
- [9] Chandel SS, Nagaraju Naik M, Chandel R. Review of solar photovoltaic water pumping system technology for irrigation and community drinking water supplies. *Renew Sustain Energy Rev* 2015;49:1084–99. doi:10.1016/j.rser.2015.04.083.
- [10] Jones MA, Odeh I, Haddad M, Mohammad AH, Quinn JC. Economic analysis of photovoltaic (PV) powered water pumping and desalination without energy storage for agriculture. *Desalination* 2016;387:35–45. doi:10.1016/j.desal.2016.02.035.
- [11] López-Luque R, Reca J, Martínez J. Optimal design of a standalone direct pumping photovoltaic system for deficit irrigation of olive orchards. *Appl Energy* 2015;149:13–23. doi:10.1016/j.apenergy.2015.03.107.
- [12] Deveci O, Onkol M, Unver HO, Ozturk Z. Design and development of a low-cost solar powered drip irrigation system using Systems Modeling Language. *J Clean Prod* 2015;102:529–44. doi:10.1016/j.jclepro.2015.04.124.
- [13] Treephak K, Thongpron J, Somsak D, Saelao J, Patcharaprakiti N. An economic evaluation comparison of solar water pumping system with engine pumping system for rice cultivation. *Jpn J Appl Phys* 2015;54:08KH01.
- [14] Sontake VC, Kalamkar VR. Solar photovoltaic water pumping system - A comprehensive review. *Renew Sustain Energy Rev* 2016;59:1038–67. doi:10.1016/j.rser.2016.01.021.
- [15] Muhsen DH, Khatib T, Nagi F. A review of photovoltaic water pumping system designing methods, control strategies and field performance. *Renew Sustain Energy Rev* 2017;68:70–86. doi:10.1016/j.rser.2016.09.129.
- [16] Campana PE, Li H, Yan J. Techno-economic feasibility of the irrigation system for the grassland and farmland conservation in China: Photovoltaic vs. wind power water pumping. *Energy Convers Manag* 2015;103:311–20. doi:10.1016/j.enconman.2015.06.034.
- [17] Campana PE, Li H, Zhang J, Zhang R, Liu J, Yan J. Economic optimization of photovoltaic water pumping systems for irrigation. *Energy Convers Manag* 2015;95:32–41. doi:10.1016/j.enconman.2015.01.066.
- [18] Kumar M, Reddy KS, Adake R V., Rao CVKN. Solar powered micro-irrigation system for small holders of dryland agriculture in India. *Agric Water Manag* 2015;158:112–9. doi:10.1016/j.agwat.2015.05.006.

- [19] Hossain MA, Hassan MS, Mottalib MA, Ahmmed S. Technical and economic feasibility of solar pump irrigations for eco-friendly environment. *Procedia Eng* 2015;105:670–8. doi:10.1016/j.proeng.2015.05.047.
- [20] Yahyaoui I, Tadeo F, Vieira M. Energy and water management for drip-irrigation of tomatoes in a semi- arid district. *Agric Water Manag* 2016. doi:10.1016/j.agwat.2016.08.003.
- [21] Reza J, Torrente C, López-Luque R, Martínez J. Feasibility analysis of a standalone direct pumping photovoltaic system for irrigation in Mediterranean greenhouses. *Renew Energy* 2016;85:1143–54. doi:10.1016/j.renene.2015.07.056.
- [22] Chandel SS, Nagaraju Naik M, Sharma V, Chandel R. Degradation analysis of 28 year field exposed mono-c-Si photovoltaic modules of a direct coupled solar water pumping system in western Himalayan region of India. *Renew Energy* 2015;78:193–202. doi:10.1016/j.renene.2015.01.015.
- [23] Delgado-Torres AM. Solar thermal heat engines for water pumping: An update. *Renew Sustain Energy Rev* 2009;13:462–72. doi:10.1016/j.rser.2007.11.004.
- [24] Date A, Akbarzadeh A. Theoretical study of a new thermodynamic power cycle for thermal water pumping application and its prospects when coupled to a solar pond. *Appl Therm Eng* 2013;58:511–21. doi:10.1016/j.applthermaleng.2013.05.004.
- [25] Sitranon J, Lertsatitthanakorn C, Namprakai P, Prathinthong N, Suparos T, Roonprasang N. Performance Enhancement of Solar Water Heater with a Thermal Water Pump. *J Energy Eng* 2015;141:4014036. doi:10.1061/(ASCE)EY.1943-7897.0000216.
- [26] Das D, Ram Gopal M. Studies on a metal hydride based solar water pump. *Int J Hydrogen Energy* 2004;29:103–12. doi:10.1016/S0360-3199(03)00044-2.
- [27] Mahkamov K, Orda EP. Solar thermal water pumps: A preliminary analysis of the working process. *J Sol Energy Eng Trans ASME* 2005;127:29–36. doi:10.1115/1.1767191.
- [28] Jokar H, Tavakolpour-Saleh AR. A novel solar-powered active low temperature differential Stirling pump. *Renew Energy* 2015;81:319–37. doi:10.1016/j.renene.2015.03.041.
- [29] Tchanche BF, Lambrinos G, Frangoudakis A, Papadakis G. Low-grade heat conversion into power using organic Rankine cycles - A review of various applications. *Renew Sustain Energy Rev* 2011;15:3963–79. doi:10.1016/j.rser.2011.07.024.
- [30] Sunvention Sunpulse. Sunvention Stirling Machine. vol. 0. n.d.

Mohammed Wazed S, Hughes BR, O'Connor D, Calautit JK. Development of Stirling Pump mechanism for Irrigation in remote rural farms. Global Conference on Energy and Sustainable Development, 18-20 December 2018 (Published) WEENTECH Proceedings in Energy 5 (2019) 26-36

2<sup>nd</sup> Global Conference on Energy and Sustainable Development, GCESD2018, 18-20 December 2018,  
John McIntyre Conference Centre, The University of Edinburgh, United Kingdom

## Development of Stirling Pump mechanism for Irrigation in remote rural farms

Saeed Mohammed Wazed <sup>a\*</sup>, Ben Richard Hughes <sup>a</sup>, Dominic O'Connor <sup>a</sup>, John Kaiser Calautit <sup>b</sup>

<sup>a</sup> Mechanical Engineering, Faculty of Engineering, University of Sheffield, Sheffield, South Yorkshire, S10 2TN. United Kingdom.

<sup>b</sup> Department of Architecture and Built Environment, University of Nottingham, Nottingham, NG7 2RD. United Kingdom

\*Corresponding author's Email: [SMohammedWazed1@sheffield.ac.uk](mailto:SMohammedWazed1@sheffield.ac.uk)

---

### Abstract

Inadequate supply of safe water, the requirement of food exports, Low GDP creates a scenario where 26% of the population in the Sub-Saharan Africa suffer from food insecurity. Cultivation of food locally is necessary to drive the cost of food down. This can be done using the abundant groundwater source in the region, however, the energy cost of harvesting the water supply is very high and hence not presently utilised. While solar PV technology is readily available, PV solutions are much too expensive for small scale rural farmers. This research aims at developing a solar thermal powered Stirling pump that can be produced locally, using local resources to reduce irrigation costs and provide income, food and energy security in the region, by promoting independent farming through small-scale farms. In order to develop the Stirling pump, a Low Temperature Differential (LTD) Stirling engine has been modelled in 3D, simulated and investigated with the help of Computational Fluid Dynamics with ANSYS 16.1 software. The Analysis is aimed at obtaining a true representation of the pressure, temperature and compression ratio that dictate the functioning of a Gamma type Stirling engine. This model developed can then be modified and improved upon to further boost the performance of the Stirling Engine to be integrated with a water pumping system to extract ground water for irrigation purposes.

*Keywords:* Irrigation; Solar energy; Solar irrigation; Solar Thermal; Stirling Pump; Stirling engine

Copyright © 2019 Published by WEENTECH Ltd. The peer-review process is under responsibility of the scientific committee of the 2<sup>nd</sup> Global Conference on Energy and Sustainable Development, GCESD2018

---

## Nomenclature

$z$	Displacement (mm – millimetre)
$z_p$	Piston Displacement (mm – millimetre)
$z_d$	Displacer Displacement (mm – millimetre)
$\theta$	Starting Crank Angle of Piston
$\beta$	Position of Displacer Crank in relation to Piston
$l_{c1}$	length from the centre of the crank wheel to the bottom of the engine (mm – millimetre)
$r_1$	piston crank radius (mm – millimetre)
$l_1$	Piston Crank shaft Length (mm – millimetre)
$r_2$	Displacer Crank Radius (mm – millimetre)
$l_2$	Length of Piston (mm – millimetre)
$l_3$	Displacer Crank shaft Length (mm – millimetre)
$l_4$	Length of Displacer connector Rod (mm – millimetre)
$l_d$	Length of displacer (mm – millimetre)
$u, v, w$	Velocity components in the x, y and z directions (m/s – meters per second)
$w_p$	Piston Velocity (m/s – meters per second)
$w_d$	Displacer Velocity (m/s – meters per second)
$\omega$	Engine rotation speed (rpm – Rotations per minute, rad/s – Radians per second)
$p$	Pressure (Pa – Pascals, kPa – Kilopascals)
$T$	Temperature ( $^{\circ}\text{C}$ – Degree Celsius, K - Kelvin)
$T_L$	Temperature at the cold surface ( $^{\circ}\text{C}$ – Degree Celsius, K - Kelvin)
$T_H$	Temperature at the hot surface ( $^{\circ}\text{C}$ – Degree Celsius, K - Kelvin)
$V$	Volume ( $\text{m}^3$ – cubic metre)

## 1. Introduction

Energy use is a matter of global importance and as the effects of global warming is being realised across the entire world, a conscience effort needs to be made to utilise renewable energy. However, the sub-Saharan African region is very much underdeveloped and to force them to implement costly renewable energy technologies would be inappropriate. The need is then to offer renewable energy at a low-cost than what is presently available [1].

The Sub-Saharan Africa region is marred by issues of draught and long dry spells which means that there isn't enough accessible portable water for the residents to drink let alone use for irrigation. [2]. There is however an abundant supply [3] of underground water reserves that could be used in the region, which if harvested cheaply could be utilised by the people in the region for irrigation.

Sub-Saharan Africa receives in excess of 2000 kWh global solar radiation annually. This is value is much higher than the value or global solar radiation received by the world's top solar energy implementing countries [4]. Due to the high cost of conventional energy supply in the region and the abundance of solar power, the Sub-Saharan Africa region offers an opportunity in the use of solar power for both solar Photovoltaic and Solar Thermal technologies [2].

## 2. Problem identification and basic principle

The purpose of this research work is to develop an independent, portable, low-cost solar powered irrigation system that assists in establishing a sustainable water-food-security nexus in developing nations. Based on the literature review performed by Saeed et al [1], solar thermal energy has been discussed to drive a Stirling pump to provide underground water and thus generate a farming prospect to small-scale remote rural inhabitants of the Sub-Saharan Africa region. In order to realise this solution, the solar energy system design should be such that it is portable, effective and cheap to manufacture. There is also a need to make use of the local infrastructure of the region While numerous expensive technologies exist, they can be expensive such as dish type or parabolic concentrators. In order to reduce the costs alternative manufacturing processes and materials will be proposed such that they can be locally sourced which not only reduces the cost but also substantially lowers the carbon footprint of the technology.

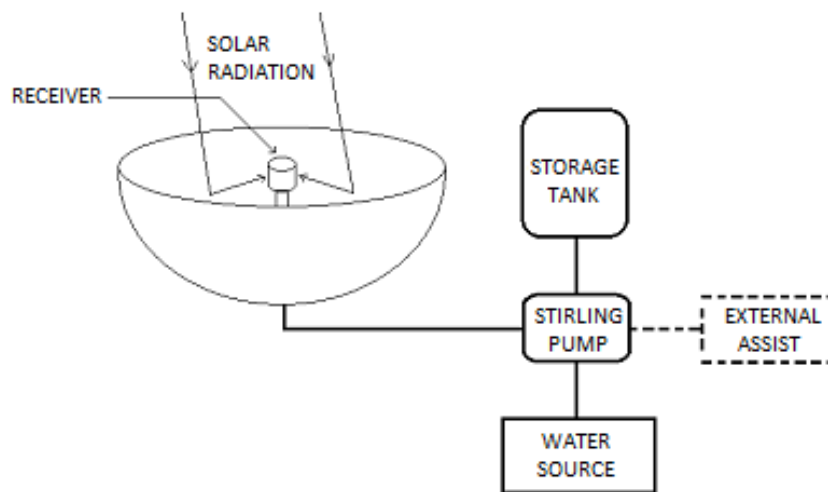


**Fig. 1: The proposed schematic of solar thermal powered Stirling pump for irrigation of small-scale rural farms in the Sub-Saharan Africa region [1].**

The goal is not to produce the most efficient but a system that will be the most effective in solving the issue. To make the best use of the energy obtained, the mechanical energy generated from the Stirling engine will be directly utilised to pump water instead of first producing electricity than then using a separate pump. The pump will function during the day when water will be pumped from the underground reserve to a storage tank for later irrigational use, preferably during the night time as the evaporation rate during the night is lower [5]. Fig. 1 demonstrates the proposed schematic of solar thermal powered Stirling pump for retrieving underground water for irrigation of small-scale rural farms in the Sub-Saharan Africa region. Similar to Jokar and Tavakolpour-Saleh [2], a hybrid energy system providing an external mechanical assist to the Stirling pump may be proposed for better output.

Stirling engines are easy to manufacture, quite compact, thus portable and can be built at a low cost. These solar thermal powered engines are also flexible in terms of the heat source that is needed. Numerous studies have been presented on low temperature Stirling Engines operating between 60 °C – 95 °C [3,4,5]. The larger the heat difference between the hot and cold regions the better the performance of the pump these higher temperatures can be obtained with the help of solar concentration techniques, however, it must be ensured that the materials used will be able to withstand the heat [7,8].

Mechanical work is produced by a Stirling Engine in an enclosed space subjected to a difference in temperature [9] through the cyclic expansion and compression of a working fluid such as nitrogen, helium, hydrogen or in the case of this research, air [10]. While efficiency is not paramount in achieving the goal for this research, the Stirling system is one of the closest in attaining ideal Carnot cycle efficiency in comparison to other thermal engines [11]. A well-constructed Stirling engine can provide an efficiency between 30-40% for operation temperatures up to 923-1073K at the hot end with an engine speed between 2000 – 4000 rpm [12].

### 3. CFD Analysis of Stirling Engines

Stirling Engines are analysed by qualifying the complicated procedures of heat and mass transference and the geometrical effects of the various multi-dimensional components of the engine. While Numerical methods have implemented to define the workings of the engine, an accurate representation of the performance is yet to be obtained. In such cases, advanced simulation approaches using CFD models can assist in mapping the geometrical features to accurately predict the heat and mass transference of the system.

The first instance of successful application of 3D simulation of Stirling Engine is attributed to K. Mahkamov [13] in 2006. In his work, he developed a prototype of an alpha type biomass Stirling engine based on mathematical analysis. Upon testing the power output of the system was appreciably lower than that predicted. This prompted the use of advanced 3D CFD analysis which provided numerical results that closely replicate the experimental data.

With the application of CFD becoming more common in recent times, due to CFD software becoming more accessible to researchers, numerous studies have been conducted covering both 2D and 3D simulations of Stirling engines. Due to the cyclic nature of the system, transient analysis is performed on a compressible fluid performing under the rules of the ideal gas.

Simulations made using 2D modelling are generally compiled within a short period of time when compared to 3D models. However, due to the non-uniform distribution temperature in Stirling Engines, the rate of heat transfer is not accurate. The same goes for fluid flow analysis in the Stirling engine. For both these parameters the geometry of the models need to be well defined and calls for a more complex 3D model analysis [12,13,14].

Both laminar and turbulent models for CFD analysis have been presented. To facilitate laminar flow conditions in the system the model prepared are very small [12,13,15,16,17,18,19]. Once again this is done to reduce the computational time and for the simulation of the Stirling engine but does not accurately represent the experimental parameters with which the results are compared. Furthermore, using a laminar flow model makes it difficult to obtain convergence as no unsteady term has been considered [22]. For an accurate representation of the fluid in the engine, turbulent modelling is required. In the research carried out, the k-epsilon turbulent model has been implemented for the analysis of the engine [11,14,20,21,22,23].

A number of software have been utilised for the production of the CFD models. Most of the early models were prepared using in-house software. While the principle of various software used by the researchers are the same, accessibility is the major factor determining the use of software. Among the software used include, USTREAM mesh [12,15,16,17,18,24], FORTRAN77 [22,24], COMSOL Multiphysics [15,27] and ANSYS FLUENT [16,23,25,28].

In the context of this research, the desired Stirling pump system is required to have simple construction. Analysis by Wen-Lih Chen et al. [17,20] demonstrates a simple geometry while lacking detailed modelling of the regenerator and using laminar flow modelling and thus provides a baseline for further

development. The model developed by Wen-Lih Chen et al. has been studied and further developed to demonstrate turbulent flows and a porous medium for the displacer to demonstrate the regenerator. Furthermore, the Wen-Lih Chen model used half the dimensions of the actual Stirling Engine to retain a laminar flow inside the engine by reducing the Reynolds number. For this research an even simpler Stirling system has been considered so that the model doesn't have to be simplified as dramatically as the Wen-Lih Chen model.

However, in order to carry further development of a piece of work it needs to first be replicated. Hence the work undertaken by Wen-Lih Chen has been replicated using ANSYS FLUENT software which is a much more accessible software for researchers and students. This model developed can then be further improved upon to achieve the ultimate goal for the simulation of Stirling engines.

#### 4. Stirling Engine CFD model

The schematic of the Stirling engine is based off of the model prepared by Wen-Lih Chen et al. [18,21]. See Fig. 2. The motion of the piston and displacer is simulated using a dynamic mesh generated by a User Defined Function (UDF) developed with C-Programming. The programme is formulated based on the motion dynamics equations of the piston and displacer.

The piston and displacer are connected to a crank shaft. The pistons are at a 90-degree phase angle to the displacer. The motion of the power piston ( $z_p$ ) and displacer ( $z_d$ ) are dictated by the equations below [17]:

$$z_p(\theta) = l_{c1} - \left( -r_1 \sin\theta + \sqrt{l_1^2 - r_1^2 \cos^2\theta} + l_2 \right) \quad (1)$$

$$z_d(\beta) = l_{c1} - \left( -r_2 \sin\beta + \sqrt{l_3^2 - r_2^2 \cos^2\beta} + l_4 + l_d \right) \quad (2)$$

The Velocities of the Piston ( $w_p$ ) and displacer ( $w_d$ ) are represented below [17]:

$$w_p(\theta) = r_1 \omega \cos\theta - \frac{r_1^2 \omega \cos\theta \sin\theta}{\sqrt{l_1^2 - r_1^2 \cos^2\theta}} \quad (3)$$

$$w_d(\beta) = r_2 \omega \cos\beta - \frac{r_2^2 \omega \cos\beta \sin\beta}{\sqrt{l_3^2 - r_2^2 \cos^2\beta}} \quad (4)$$

Where,

- $\theta$  is the starting crank angle determining the position of the power piston
- $\beta = \theta - 90^\circ$  determining the position of the displacer. The piston and displacer are at 90-degree phase angle to each other.
- 

The following modelling parameters were considered to model the Stirling Engine in Ansys FLUENT:

- The fluid viscosity of all materials is constant
- Constant thermal properties have been assumed.
- Air - working gas with properties defined by the ideal gas equation of state gas constant = 287.0 Jkg<sup>-1</sup>K<sup>-1</sup>
- Mechanical friction effects are ignored
- Thermal radiation effects are ignored.

- The displacer faces are set to porous medium
- A pressure Outlet is assigned into the piston chamber out of the displacer chamber
- 3D Transient model
- Laminar Flow
- Flow is modelled using compressible Navier-Stokes equations
- Heat Transfer is modelled using the Energy Equation
- Viscous dissipation has not been considered

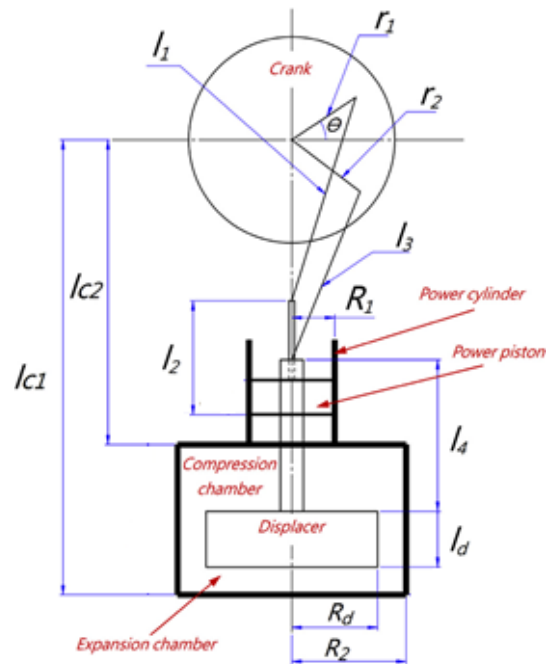


**Fig. 2: Stirling Engine Schematic**

Pressure-based SIMPLEC finite volume code is used to conduct the simulation on the USTREAM platform. The dynamic mesh method implemented involves the changing of the geometry of the cells by expanding or compressing the volumes. In Ansys 16.1 this corresponds to smoothing and remeshing technique.

The following Boundary conditions have been implemented:  $u$ ,  $v$  and  $w$  are velocity components in  $x$ ,  $y$  and  $z$  directions respectively.  $T_L$  is the Temperature at the cold surface,  $T_H$  is the Temperature at the Hot surface.

- Engine Rotation speed,  $\omega = 120$  rpm (clockwise)
- Initial Conditions:  $\theta = 0^\circ C$ ,  $u = v = w = 0$ ,  $p = 101.0$  kPa,  $T = T_L$
- Hot Surface ( $z = 0$ ):  $u = v = w = 0$ ,  $T = T_H = 400K$
- Cold Surface ( $z = l_{c1} - l_{c2}$ ):  $u = v = w = 0$ ,  $T = T_L = 300K$
- Displacer Surface (adiabatic):  $u = v = 0$ ,  $\frac{\delta T}{\delta n} = 0$  ( $n$  is normal to displacer wall)
- Power Piston Surface (adiabatic):  $u = v = 0$ ,  $w = w_d$ ,  $\frac{\delta T}{\delta z} = 0$
- displacer cylinder, lateral wall:  $u = v = w = 0$ ,  $T = T_L + \frac{z}{(l_{c1} - l_{c2})} (T_H - T_L)$

Since the design of the engine is symmetrical only half of the engine will be simulated. Four cycles were programmed to make the solution periodic.

### 5. 3D CFD Analysis

The 3D Stirling engine has been modelled based on the in order to simulate the motion of the displacer and piston, the motion dynamics was modelled using a user defined function (UDF) in C-programming using equ 1-4. The model simulated is presented in Fig. 3 is based on the model prepared by Wen-Lih Chen et al. [18,21]. The Mesh Statistics are provided in table1.

In FLUENT, the CFD model is then set-up in Transient mode, Laminar flow and the energy equation is turned on. In the material Properties, air is set as an Ideal gas, and boundary conditions are set for the Hot edge at the bottom at 400K and the cold edge at the top including the pistons as 300K. The UDF and the profiles for the piston and the displacer motion are then loaded using the FLUENT define function.

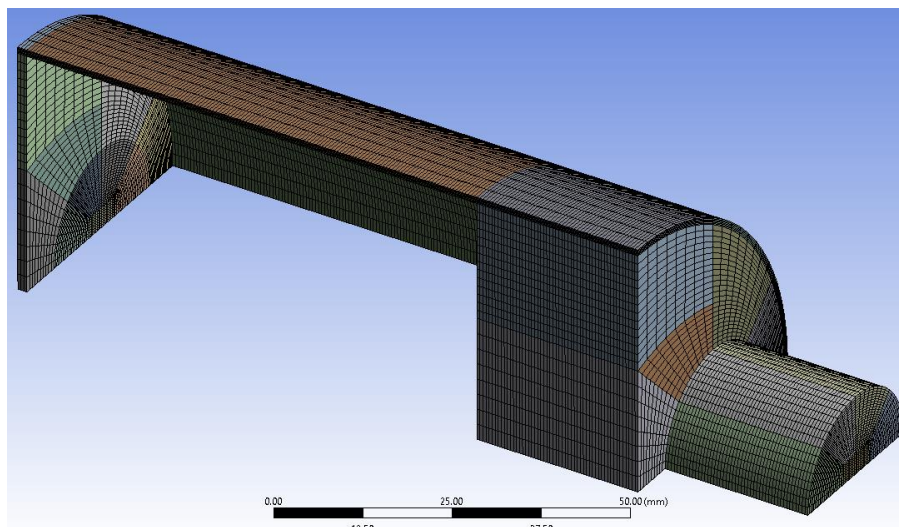


**Fig. 3: 3D model geometry and mesh**

**Table 1: Mesh Statistics 3D Model**

Nodes	173090	Average	5.17476227272727
Elements	158400	Standard Deviation	5.2136092539616
Mesh Metric	Aspect Ratio	Minimum Orthogonal	7.20906e-01
Min	1.25	Quality <sup>1</sup>	
Max	18.631	Maximum Ortho Skew <sup>2</sup>	2.79094e-01

<sup>1</sup> Orthogonal Quality value is between 0 and 1, close to 1 is high quality.

<sup>2</sup> Ortho Skew ranges value is between 0 and 1, close to 0 is high quality.

There are three types of dynamic mesh methods, Smoothing, Layering and Remeshing. The method used by Wen-Lih Chen et al. utilised smoothing and remeshing, however, using this method on ANSYS produced negative volumes and the simulation crashed. Hence, the layering method was used to conduct the simulation. The layering methods involves the adding and/or removing mesh cells to alter the computational domain’s volume.

The time-step size utilised was 0.001733908 seconds with 576 steps dictating the number of steps required to complete 4 complete cycles of the Stirling engine. A maximum 20 iterations were set with a report being saved every 4 iterations.

## 6. Results and discussions

The findings of the simulation are presented as per Fig. 4. The 3D mesh motion has been generated and it is similar to that produced by Wen-Lih Chen et al. The only difference is that the crank rotation has been set in the anti-clockwise direction in this model compared to the model by Wen-Lih Chen et al. The temperature modelling has not been set-up in the model and hence does not produce the results shown in the original work. The Pressure profile obtained for the Stirling engine simulation indicates a max and minimum pressure of 6.5 Pa and -6.5 Pa respectively. There is an issue with the calculation since the initial pressure of the Stirling engine was set to 101 kPa. Both the temperature and pressure set-up needs to be further studied as the values for both these parameters are incorrect. This will require further development of the UDF and or creation of temperature profiles based on the boundary conditions.

The chart for the volume variation and crank angle is demonstrated below in Fig. 5. The Graph obtained is a mirror image of the work by Wen-Lih Chen et al. since the rotation is considered as anti-clockwise, instead of clockwise as considered in the original work. The minimum and maximum values of the Total volume as obtained from the CFD analysis are:  $1.34 \times 10^{-4} \text{ m}^3$  ( $270^\circ$ ) and  $1.75 \times 10^{-4} \text{ m}^3$  ( $90^\circ$ ) respectively. This provides a compression ratio of 1.31.

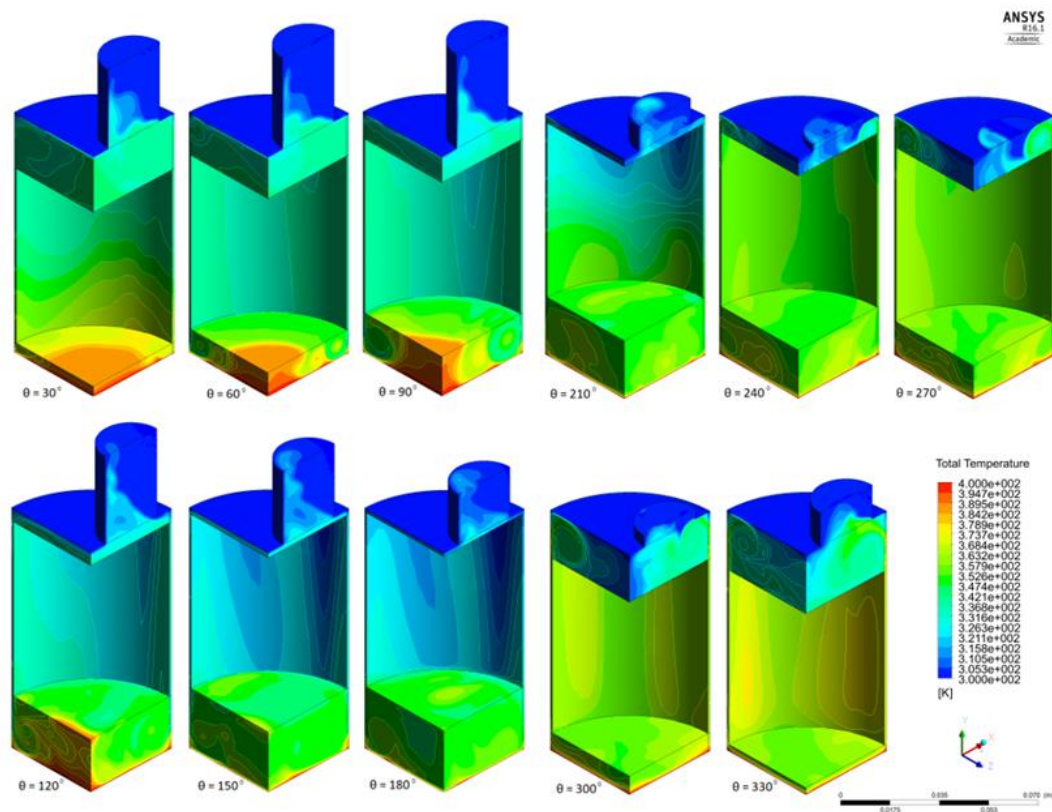


**Fig. 4: 3D Simulation of Wen-Lih Chen Stirling Engine model in ANSYS FLUENT.**

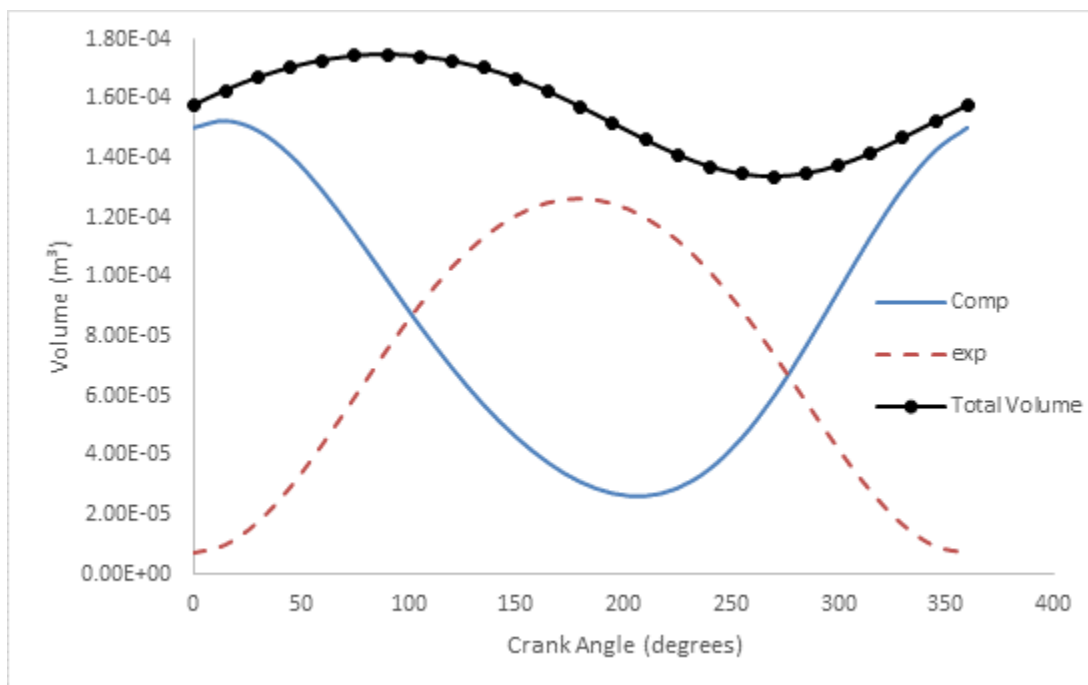


**Fig. 5: Variation of volume against Crank angle in the compression and expansion chambers**

## 7. Conclusions

Stirling engines hold the potential to be used for irrigation in the arid regions of Sub-Saharan Africa. In order to develop a cheap functional pump using Stirling Engine it is important to understand the working of the engine. The best way to do this, is using CFD. Various research has been conducted over the years utilising many CFD modelling tools however, they all produce different results and aren't comparable. Many times, the models developed are in-house and therefore very difficult to replicate and verify in the scientific community. An analysis has hence been initiated using ANSYS FLUENT, a software that is easily accessible for Researchers and students so that the work can be further improved.

The Wen-Lih Chen model developed in-house has been studied and a replication of the model has been attempted. While the motion of the engine and the compression ratio of the developed model matches that of the Wen-Lih Chen model, the temperature and pressure profiles do not match. However, The Wen-Lih Chen model has been scaled from the original test apparatus so the practicality of the Wen-Lih Chen model would be brought to question. The model developed here needs to be subjected to turbulent flows and a porous medium for the displacer to demonstrate the regenerator and a further prototype test is required of a full scale model to properly validate the CFD model.

## Acknowledgement

The Authors would like to thank the Grantham Institute for Sustainable Futures which is a collaboration between the Grantham Foundation for the Protection of the Environment and the University of Sheffield for finding this PhD research work.

## ORCID Id of authors

Mohammed Wazed, Saeed: <https://orcid.org/0000-0002-9136-9561>  
Hughes, Ben: <https://orcid.org/0000-0001-6314-4683>  
O'Connor, Dominic: <https://orcid.org/0000-0003-2861-1842>  
Calautit, John Kaiser: <https://orcid.org/0000-0001-7046-3308>

## References

- [1] Mohammed Wazed S, Hughes BR, O'Connor D, Kaiser Calautit J. A review of sustainable solar irrigation systems for Sub-Saharan Africa. *Renew Sustain Energy Rev* 2018;81:1206–25. doi:10.1016/j.rser.2017.08.039.
- [2] Jokar H, Tavakolpour-Saleh AR. A novel solar-powered active low temperature differential Stirling pump. *Renew Energy* 2015;81:319–37. doi:10.1016/j.renene.2015.03.041.
- [3] Kashaigili JJ. Ground water Availability and Use in Sub-Saharan Africa. Srilanka: International Water Management Institute; 2012. doi:10.5337/2012.213.
- [4] Quansah DA, Adaramola MS, Mensah LD. Solar Photovoltaics in sub-Saharan Africa – Addressing Barriers , Unlocking Potential. *Energy Procedia* 2016;106:97–110. doi:10.1016/j.egypro.2016.12.108.
- [5] FAO. Irrigation Techniques for Small-scale Farmers. 2016.
- [6] Mahkamov K, Orda EP. Solar thermal water pumps: A preliminary analysis of the working process. *J Sol Energy Eng Trans ASME* 2005;127:29–36. doi:10.1115/1.1767191.
- [7] Delgado-Torres AM. Solar thermal heat engines for water pumping: An update. *Renew Sustain Energy Rev* 2009;13:462–72. doi:10.1016/j.rser.2007.11.004.
- [8] Sitranon J, Lertsatitthanakorn C, Namprakai P, Prathinthong N, Suparos T, Roonprasang N. Performance Enhancement of Solar Water Heater with a Thermal Water Pump. *J Energy Eng* 2015;141:04014036. doi:10.1061/(ASCE)EY.1943-7897.0000216.
- [9] Felix A. Farret MGS. Appendix C the Stirling Engine. 2006. doi:10.1002/0471755621.
- [10] Ferreira AC, Nunes ML, Teixeira JC, Martins LB, Teixeira SFCF. Thermodynamic and Economic Optimization of a Solar-powered Stirling engine for Micro- Cogeneration Purposes. *Proc Ecos 2015 - 28Th Int Conf Effic Cost, Optim Simul Environ Impact Energy Syst* 2015;111:13 pgs.
- [11] Bagheri A, Bostanci H, Foster PR. Preliminary analysis of an innovative rotary displacer stirling engine. *ASME Int Mech Eng Congr Expo Proc* 2015;6A–2015. doi:10.1115/IMECE2015-52455.
- [12] Ahmadi MH, Ahmadi M-A, Pourfayaz F. Thermal models for analysis of performance of Stirling engine: A review. *Renew Sustain Energy Rev* 2017;68:168–84. doi:10.1016/j.rser.2016.09.033.
- [13] Mahkamov K. Design Improvements to a Biomass Stirling Engine Using Mathematical Analysis and 3D CFD Modeling 2013;128. doi:10.1115/1.2213273.
- [14] Leon J, Chen W. A computational fluid dynamics study on the heat transfer characteristics of the working cycle of a  $\beta$ -type Stirling engine. *Energy Convers Manag* 2014;88:177–88. doi:10.1016/j.enconman.2014.08.040.
- [15] Alfarawi S, Mahmoud S. Influence of phase angle and dead volume on gamma-type Stirling engine power using CFD simulation. *Energy Convers Manag* 2016;124:130–40. doi:10.1016/j.enconman.2016.07.016.
- [16] Cheng C, Chen Y. Numerical simulation of thermal and flow fields inside a 1-kW beta-type Stirling engine. *Appl Therm Eng* 2017;121:554–61. doi:10.1016/j.applthermaleng.2017.04.105.
- [17] Chen W-L, Wong K-L, Chang Y-F. A computational fluid dynamics study on the heat transfer

- characteristics of the working cycle of a low-temperature-differential  $\gamma$ -type Stirling engine. *Int J Heat Mass Transf* 2014;75:145–55. doi:10.1016/j.ijheatmasstransfer.2014.03.055.
- [18] Chen WL, Wong KL, Po LW. A numerical analysis on the performance of a pressurized twin power piston gamma-type Stirling engine. *Energy Convers Manag* 2012;62:84–92. doi:10.1016/j.enconman.2012.02.035.
- [19] Chen W, Wong K, Chang Y. International Journal of Heat and Mass Transfer A numerical study on the effects of moving regenerator to the performance of a  $\beta$ -type Stirling engine. *Int J Heat Mass Transf* 2015;83:499–508. doi:10.1016/j.ijheatmasstransfer.2014.12.035.
- [20] Chen W, Yang Y, Leon J. A CFD parametric study on the performance of a low-temperature-differential  $\gamma$ -type Stirling engine. *Energy Convers Manag* 2015;106:635–43. doi:10.1016/j.enconman.2015.10.007.
- [21] Chen WL, Wong KL, Chen HE. An experimental study on the performance of the moving regenerator for a  $\beta$ -type twin power piston Stirling engine. *Energy Convers Manag* 2014;77:118–28. doi:10.1016/j.enconman.2013.09.030.
- [22] Kato Y, Saitoh S, Ishimatsu K, Iwamoto M. Effect of geometry and speed on the temperatures estimated by CFD for an isothermal model of a gamma configuration low temperature differential Stirling engine with Flat-shaped heat exchangers. *Appl Therm Eng* 2017;115:111–22. doi:10.1016/j.applthermaleng.2016.12.070.
- [23] Xiao G, Sultan U, Ni M, Peng H, Zhou X, Wang S, et al. Design optimization with computational fluid dynamic analysis of  $\beta$ -type Stirling engine. *Appl Therm Eng* 2017;113:87–102. doi:10.1016/j.applthermaleng.2016.10.063.
- [24] Kato Y. Indicated diagrams of low temperature differential Stirling engines with channel-shaped heat exchangers Heat exchanger Magnification. *Renew Energy* 2017;103:30–7. doi:10.1016/j.renene.2016.11.026.
- [25] Tongdee N, Jandakaew M, Dolwichai T. Thermodynamics analysis for optimal geometrical parameters and influence of heat sink temperature of Gamma- configuration Stirling engine. *Energy Procedia* 2017;105:1782–8. doi:10.1016/j.egypro.2017.03.516.
- [26] Chen W. A study on the effects of geometric parameters in a low-temperature- differential  $\gamma$ -type Stirling engine using CFD. *Int J Heat Mass Transf* 2017;107:1002–13. doi:10.1016/j.ijheatmasstransfer.2016.11.007.
- [27] Almajri AK, Mahmoud S, Al-dadah R. Modelling and parametric study of an efficient Alpha type Stirling engine performance based on 3D CFD analysis. *Energy Convers Manag* 2017;145:93–106. doi:10.1016/j.enconman.2017.04.073.
- [28] Abuelyamen A, Abualhamayel H, Mokheimer EMA. Parametric study on beta-type Stirling engine. *Energy Convers Manag* 2017;145:53–63. doi:10.1016/j.enconman.2017.04.098.